Hadronic Spectral Functions in Nuclear Matter

Inaugural-Dissertation
zur
Erlangung des Doktorgrades
der Naturwissenschaftlichen Fakultät
der Justus-Liebig-Universität Gießen
Fachbereich 7 – Mathematik, Physik, Geographie

vorgelegt von
Marcus Post
aus Wetzlar

Gießen, 2003

D 26
Dekan: Prof. Dr. Volker Metag
I. Berichterstatter: Prof. Dr. Ulrich Mosel
II. Berichterstatter: Prof. Dr. Werner Scheid
Tag der mündlichen Prüfung: 06.02.2004

Contents

Chapter 1

Introduction

The goal of this thesis is a description of the properties of baryon resonances and mesons in nuclear matter. The issue of how mass and width of hadrons change in the medium is of interest for two reasons. First, various experiments have found indications for such medium modifications. Second, the change of hadron masses in a medium is related to the restoration of one of the fundamental symmetries of QCD, namely chiral symmetry, which is spontaneously broken in the vacuum.

Let us quickly review the current experimental status of in-medium modifications of hadrons. We begin with a discussion of the ρ meson, which is of particular interest. Its decay into dileptons, which travel nearly undisturbed in the nuclear medium and can carry information from hot and dense environments, makes it an ideal probe for in-medium studies. A much debated signal are the dilepton spectra measured in heavy-ion collisions. Whereas in the vacuum the $e^+ e^-$ cross section shows a clear peak around the ρ mass, this peak appears to be shifted to smaller invariant masses when created in heavy-ion collisions. This has been found in experiments of the NA45/CERES [3, 4, 129, 76] collaboration and of the HELIOS collaboration [92]. Complementary information can be obtained from photonuclear experiments [31], which are expected to take place in the near future at JLAB. Photonuclear reactions play also an important role for the investigation of baryon resonances in the nuclear medium. Here the most striking effect is seen in photoabsorption experiments, where the peak structure in the second resonance region is completely lost [14, 15, 43]. One possible explanation of this finding is that the $D_{13}(1520)$ resonance receives a significant broadening in nuclear matter. In [65] a broadening of about 300 MeV has been obtained for this resonance in a resonance fit to photoabsorption data. Also the analyses of [32, 73, 112] have corroborated the influence of a broadening of the $D_{13}(1520)$ on the photoabsorption data. An alternative explanation has been offered in the work of [55], which is based on a microscopic description of $\gamma N \to \pi N$ and $\gamma N \to 2\pi N$ reactions. There it has been found that the peak structure may already be lost by the change of interference patterns due to Fermi motion. Consequently, there a smaller broadening of only 100 MeV is required to describe the data. Photon- and pion induced reactions on nuclei have also unraveled the in-medium properties of the $P_{33}(1232)$ resonance [54, 99, 98]. The general consensus is that a broadening of that state of about 80 MeV relative to the Pauli-blocked width is required by the data. Due to its strong coupling to the $N\eta$ channel, the in-medium properties of the $S_{11}(1535)$ can be analyzed by means of photo induced η production on nuclei [133, 115]. These experiments suggest only mild modifications of the $S_{11}(1535)$. A prime source of information on pions and η mesons in nuclear matter is the

study of pionic [11] and η-mesic atoms [48].

We now turn to the connection of the restoration of chiral symmetry with hadron mass modifications. Chiral symmetry is a symmetry under vector and axial-vector transformations, which rotate states of opposite parity into each other. In the limit of vanishing quark masses, the Lagrangian of QCD is invariant under chiral transformations. Since it is generally believed that QCD is the fundamental theory of strong interactions, one would expect that the hadronic spectra display this symmetry, i.e. that states of different parity have the same mass. This is not the case, however. One finds for example, that the masses of ρ and a_1 mesons, having the quantum numbers 1^- and 1^+ respectively, are not even approximately the same, with $m_\rho = 0.77$ GeV and $m_{a_1} = 1.2$ GeV. The phenomenon that a symmetry of the underlying Lagrangian is not exhibited in the ground state of the theory, is called the spontaneous breaking of that symmetry. According to Goldstones theorem, the spontaneous breaking of chiral symmetry requires the existence of Goldstone bosons, which in the case of QCD are the pseudoscalar mesons π, η and K. The spontaneous breaking of chiral symmetry is also reflected in the non-vanishing expectation value of the chiral condensate $\langle \bar{\psi}\,\psi \rangle = -(240\,\mathrm{MeV})^3$, which is not invariant under chiral transformations and would therefore vanish in a chirally restored phase.

It is expected that in the vicinity of the deconfinement phase transition, i.e. at a few times normal nuclear matter density and/or temperatures around 170 MeV, chiral symmetry is restored. An indication for that are calculations of the chiral condensate within the NJL model and lattice QCD, which predict that the chiral condensate drops to zero at the corresponding temperatures and/or densities [113]. While a general consensus exists concerning the behaviour of the chiral condensate in the medium, the effects of the restoration of chiral symmetry on hadron masses are much less clear. The only thing one knows for sure is that in the chirally restored phase, the masses – or, more general, the spectral functions – of chiral partners have to be the same. This can be realized in different ways. Taking as an example ρ and a_1 meson, both spectral functions could have peaks of equal strength at the ρ and the a_1 masses or they could be smeared over the entire invariant mass range [60, 64]. More specific statements are model dependent. For baryon resonances the influence of chiral symmetry is not very transparent at all, here it is even difficult to clearly identify chiral partners. The Goldstone bosons, in particular the pion, are better controlled by chiral symmetry arguments, since their masses have to remain small in the broken phase.

In two approaches, Brown-Rho scaling and QCD sum rules, an attempt is made to relate the in-medium changes of condensates and the masses of hadrons. The Brown-Rho scaling hypothesis [21] is based on the assumption that the scale invariance of the QCD Lagrangian should also be respected by effective low-energy theories. This line of thought leads to the conclusion that the in-medium hadron masses display the same scaling as the chiral condensate itself, which results in typical mass reductions of about 20% at normal nuclear matter density. Historically, the Brown-Rho scaling has been a major stimulant for both the theoretical and the experimental search for medium modifications. However, it is not unanimously accepted within the community and has lead to controversial discussions. The QCD sum rules use a dispersion relation to relate an integral over a spectral function to quark and gluon condensates [106, 120]. This way in-medium changes of the condensates must be met by changes of the spectral function. Here most analyses have been concerned about the ρ meson [62, 47, 78]. As a general feature, the sum rules require a shift of spectral strength down to smaller invariant masses. On a quantitative level, this redistribution may

proceed in various ways: assuming a small width of the ρ meson, an attractive mass shift compatible with Brown-Rho scaling is predicted, which can be substantially weakened or even reversed into repulsion if the width of the ρ is sizeable [78]. On a quantitative level, one should be aware that uncertainties exist concerning the size and the in-medium behaviour of various condensates entering the sum rule analysis.

We have now elucidated that the in-medium properties of hadrons are in principle linked to a fundamental property of QCD, namely the spontaneous breaking of chiral symmetry and its (partial) restoration at finite temperatures and/or densities. While this serves certainly as a main motivation to study in-medium physics, one has to realize that modifications of mass and width are expected from standard many-body theoretical arguments as well. For example, in nuclear matter a hadron can scatter inelastically on a nucleon which results in a loss of that hadron. Formally this is described by the introduction of a complex in-medium self energy. The imaginary part of the self energy describes corrections to the lifetime of the particle and its real part changes of its mass. For sufficiently small densities, the in-medium self energy is related to the hadron-nucleon forward scattering amplitude by the low-density theorem [29]. Up to which extent a many-body theory – based essentially on vacuum hadron-nucleon scattering amplitudes – incorporates effects from the restoration of chiral symmetry, is an open question. Given an ideal hadronic theory which takes into account all our knowledge of hadron-nucleon scattering in the vacuum and of many-body effects like Pauli-blocking or 3-body absorption, a careful comparison with experimental data would help to decide whether additional mechanisms, which go beyond the standard many-body framework, have to be invoked. In any case, a sound many-body theory is required if one wants to make quantitative statements about the partial restoration of chiral symmetry in hot and dense matter.

Stimulated both from experiment and the findings of Brown-Rho scaling and QCD sum rules, a significant theoretical effort has been undertaken to construct hadronic models for the in-medium properties of ρ mesons, see for example [52, 111, 122, 62, 38, 107, 24, 84]. A comprehensive overview of these models is given in the report [113]. These models differ significantly in their setup and in their quantitative results, but they all predict that spectral strength is moved to smaller invariant masses in nuclear matter, as is suggested both from QCD sum rules and from dilepton spectra. However, at the moment the dilepton spectra do not allow for a discrimination of the hadronic models for the ρ meson. Maybe this situation can be improved by the forthcoming experiments with the HADES detector at GSI. Concerning the properties of the $P_{33}(1232)$ and the pion in nuclear matter, exhaustive studies have been carried out in the framework of the Δ-hole model or related models [33, 99, 98, 7, 49, 132, 61, 67, 126]. Less well studied are the baryon resonances $D_{13}(1520)$ and $S_{11}(1535)$. For the former, the broadening suggested from photoabsorption data can be generated dynamically by coupling this state either to the ρ meson [107] or to the pion [67]. In the works [26, 56] the in-medium properties of the $S_{11}(1535)$ have been found to be small, which is in agreement with experimental observations.

From a theoretical point of view it would be desirable to describe as many in-medium effects as possible within one model in order to arrive at a combined understanding of these phenomena. For example, reshuffling the spectral strength of the ρ meson (as suggested from dilepton spectra) might have an immediate impact on the width of the $D_{13}(1520)$ [107] and can help to explain the nuclear photoabsorption data [32, 73, 112]. Similarly, a quantitative analysis of the optical potential of the η meson is constrained from the fact that recent data on η photoproduction [115, 133] suggest that the in-medium modifications

experienced by the $S_{11}(1535)$ are relatively small. To this end we have set up a model which generates the in-medium modifications of mesons and baryon resonances within a self-consistent coupled channel analysis. The mesons are dressed by the excitation of resonance-hole loops and a remarkably complicated spectrum with various peak structures is found for the mesonic spectral functions. In a second step the in-medium self energy of the baryon resonances arising from the dressing of the mesons is calculated. The corresponding set of coupled-channel equations is then solved iteratively. In the course of the iterations one leaves the regime of the low-density theorem [29], which relates the in-medium self energy to vacuum scattering amplitudes. It is least reliable for systems close to threshold, where already small changes of the available phase space can lead to large modifications of the resonance and therefore the meson as well. A well-known example is the $\Lambda(1405)$ coupling to the $K\,N$ channel, see for example [63, 83]. Another case is the $\rho N D_{13}(1520)$ system: in a previous publication [107], a first step in this direction was done and strong effects from the interplay of ρ and $D_{13}(1520)$ were reported, modifying both the ρ spectral function and that of the baryon resonance. We have extended the model presented in [107] in several ways: in order to guarantee the normalization of the vacuum and the in-medium spectral functions, we employ dispersion relations to generate the real part of the self energies. Since most baryon resonances couple strongly to the pion, a complete analysis of their in-medium properties requires also a dressing of the pion. In order to obtain reliable estimates for the $S_{11}(1535)$, which couples dominantly to the ηN channel, the η meson is included as well. Finally, stimulated by the fact that the in-medium width of the $P_{33}(1232)$ needs to be protected by repulsive short-range terms, we have developed a framework that allows for the incorporation of such effects for resonances with negative parity, such as the $D_{13}(1520)$ and the $S_{11}(1535)$.

The thesis is organized in the following way. In Chapter 2, we study under some simplifying assumptions the pion and Δ in nuclear matter. This chapter is meant to introduce the main concepts that will be relevant for the rest of this work. It discusses the formation of particle-hole states from resonant pion-nucleon scattering and investigates how the Δ width is modified due to changes of the pion dispersion relation. Some emphasis is given to the role of short-range correlations.

Chapter 3 is concerned about the description of ρ meson and baryon resonances in the vacuum. There we explain how we calculate the vacuum self energy. Special care is taken with respect to the use of dispersion relations to obtain the real part of the self energy.

In Chapter 4 we discuss up to which extent our model is constrained from data on meson-nucleon data. In particular, we discuss problems connected with the experimental identification of the coupling of baryon resonances to the ρ meson. In Chapter 5, the basic theoretical ingredients of our model are laid out. We give explicit formulae for the in-medium self energies of mesons and baryon resonances and discuss their relation to the low-density theorem, i.e. we give an interpretation of the self energy in terms of scattering amplitudes. In Chapter 6 we discuss in some detail, how the nucleon-nucleon and the resonance-nucleon interaction receive contributions from short-range correlations, which modify the meson exchange picture at small distances. Here we also extend the formalism for the description of such correlations to the case of negative parity resonances and show how short-range correlations affect the in-medium self energies of mesons and baryon resonances.

The role of mean-field potentials of Walecka type for the in-medium properties of hadrons is discussed in Chapter 7. In particular, we explain that these potentials have

a large effect on the self energy of baryon resonances.

In Chapters 8, 9 and 10 we present the results of our model. In Chapter 8, we give the main results found for the in-medium properties of ρ mesons, pions and η mesons as well as the baryon resonances $D_{13}(1520)$, $P_{33}(1232)$ and $S_{11}(1535)$. Some general features of these results are studied in Chapter 9. There we comment on the density dependence of the self energies, on the influence of dispersion relations and the effect of mean field potentials. Also a systematic study concerning the momentum dependence of the ρ spectral function is carried out. In Chapter 10 the in-medium properties of the ω as obtained within a resonance-hole model are discussed.

In Chapter 11 we give a summary of the thesis and discuss in which way our model can be extended. In the Appendices we present some necessary details of the calculations, which have not been mentioned in the main text in order to enhance the readability of the thesis.

Chapter 2

The Pion in Nuclear Matter

In this Chapter we will discuss the propagation of pions in nuclear matter within the well known frame work of the Δ-hole model [99, 33, 100]. The aim is to introduce the main physical concepts that will be relevant for the rest of this work. Within the Δ-hole model, both the properties of pions and Δ resonances in nuclear matter are studied.

We will begin with a discussion of the formation of so called particle-hole states. These form an integral part of the pion self energy in nuclear matter and lead to a complicated multi-peak structure in the pion spectral function. Apart from the in-medium properties of the pion, the strong coupling in the $\pi N \Delta$ system determines also the shape of the Δ spectral function and leads to a finite width of $\Gamma = 120$ MeV already in the vacuum. This gives rise to the question of self-consistency, since the in-medium modifications of the pion which are due to the Δ will in turn influence the properties of the Δ in nuclear matter and so forth. The calculations carried out in this Chapter are of approximative nature only. This allows to furnish the discussion with analytical formulae, thus providing a qualitative understanding of the formalism.

2.1 Particle-Hole Formation

In this Section the basic ingredient of π propagation in nuclear matter, namely the formation of particle-hole states, will be discussed. The physical picture is that by scattering on a nucleon provided by nuclear matter the meson converts into a baryon resonance, thus creating a particle and a nucleon hole. Therefore one often refers to this process as the formation of a resonance-hole or particle-hole state. The formation can happen in two ways: either the resonance-hole pair is formed with an incoming or with an outgoing pion, corresponding to s and u channel scattering, respectively. The corresponding Feynman diagrams are depicted in Fig. 2.1. In the following we will concentrate on the excitation of Δ-hole pairs, where Δ stands for the $P_{33}(1232)$ resonance, which dominates the pion propagation in nuclear matter. Besides the Δ-hole mode in the pion propagation, there are further dominant particle-hole excitations, for example the $N^\star(1520)\, N^{-1}$ state coupled to the ρ meson or the $N^\star(1535)\, N^{-1}$ state coupled to the η meson. The discussion of the in-medium properties of ρ, π and η meson will form the central part of this work.

Let us now go into the details. To keep the expression as simple as possible, we neglect the decay width of the Δ resonance as well as Fermi motion and use non-relativistic vertex functions. Studies similar to ours have for example been performed in [50, 40]. At this stage, the reader should not worry about the numerical factors in the following formulae. They

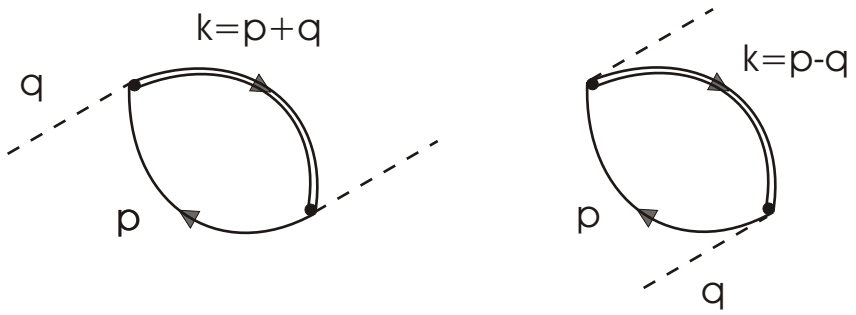

Figure 2.1: Feynman diagrams representing the resonance hole excitation. Left: s-channel contribution. Right: u-channel contribution.

are not essential for a qualitative understanding and will be explained in later Sections. We need to calculate the self energy of the pion, $\Pi_\Delta(q_0, \mathbf{q})$, in terms of which the in-medium propagator of the pion is defined as:

$$\mathcal{D}_\pi^{med}(q_0, \mathbf{q}) \;=\; \frac{1}{q_0^2 - \mathbf{q}^2 - m_\pi^2 - \Pi_\Delta(q_0, \mathbf{q})} \quad . \tag{2.1}$$

Within the above assumptions, the self energy of the pion, taken as the sum of s and u channel contributions, is given by (cf. [50] and Chapter 5.2.1):

$$\begin{aligned} \Pi_\Delta(q_0, \mathbf{q}) \;&=\; \frac{16}{9}\left(\frac{f}{m_\pi}\right)^2 \mathbf{q}^2 \int \frac{d^4p}{(2\,\pi)^4}\, \mathcal{G}_N^{med}(p)\; (\mathcal{G}_\Delta(p+q) + \mathcal{G}_\Delta(p-q)) \\ &=\; \frac{8}{9}\,\mathbf{q}^2 \left(\frac{f}{m_\pi}\right)^2 \rho\, \frac{\bar{E}}{q_0^2 - \bar{E}^2} \;=\; \frac{\mathbf{q}^2\,\rho\, C_\Delta}{q_0^2 - \bar{E}^2} \quad . \end{aligned} \tag{2.2}$$

Here $q = (q_0, \mathbf{q})$ denotes the four-momentum of the meson and p that of the nucleon. By

$$\bar{E} \;=\; \sqrt{m_\Delta^2 + \mathbf{q}^2} - m_N \tag{2.3}$$

we denote the energy, which is necessary for a pion with given momentum $\mathbf{q}$ to scatter on a nucleon at rest into an on-shell Δ and the factor C_Δ is given by:

$$C_\Delta \;=\; \frac{8}{9}\left(\frac{f}{m_\pi}\right)^2 \bar{E} \quad . \tag{2.4}$$

Neglecting the decay width, the non-relativistic Δ propagator $\mathcal{G}_\Delta$ has the form:

$$-\,i\,\mathcal{G}_\Delta(k_0, \mathbf{k}) \;=\; \frac{1}{k_0 - \sqrt{m_\Delta^2 + \mathbf{k}^2}} \quad . \tag{2.5}$$

Note that via the relativistic dispersion relation for the energy of the Δ kinematic corrections of the propagator are taken into account. By $\mathcal{G}_N^{med}(p)$ the non-relativistic nucleon propagator is denoted (cf. Appendix B.5):

$$-\,i\,\mathcal{G}_N^{med}(p) \;=\; \frac{1 - \theta(p_F - |\mathbf{p}|)}{p_0 - E(\mathbf{p}) + i\epsilon} + \frac{\theta(p_F - |\mathbf{p}|)}{p_0 - E(\mathbf{p}) - i\epsilon} \quad . \tag{2.6}$$

It contains two parts [33]: the first part represents the propagation of nucleons above the Fermi sphere, and the second part describes hole states. Since a meson can not decay into two baryons, only the hole propagation gives a contribution to the self energy and the nucleon momentum has to be smaller then the Fermi momentum p_F. In going to the second line, we have made the low-density approximation that the Fermi momentum p_F is small and that therefore the 4-vector of the nucleon momentum may be approximated by $p = (m_N, 0)$. Then the integrand can be pulled out of the integral. The remaining integral then yields a factor $\rho/4$ in spin-isospin symmetric nuclear matter. In principle, replacing the absolute value of the nucleon momentum by the Fermi momentum is a better approximation. However, when keeping the nucleon momentum finite, one needs to take into account Fermi motion and the simple form of the result of Eq. 2.2 is lost.

After iterating this self energy insertion by means of the Dyson-Schwinger equation (see Appendix D), one obtains for the full meson propagator:

$$\mathcal{D}_\pi^{med}(q_0, \mathbf{q}) = \frac{1}{q_0^2 - E_\pi^2 - \dfrac{\mathbf{q}^2\,\rho\,C_\Delta}{q_0^2 - \bar{E}^2}} \quad .$$

The meson energy E_π is given by $E_\pi = \sqrt{m_\pi^2 + \mathbf{q}^2}$, with m_π the meson mass. Let us now examine, where the pole(s) of $\mathcal{D}_\pi^{med}(q_0, \mathbf{q})$ is (are) located. To this end, the propagator is rewritten as:

$$\begin{aligned} \mathcal{D}_\pi^{med}(q_0, \mathbf{q}) &= \frac{q_0^2 - \bar{E}^2}{(q_0^2 - E_\pi^2)(q_0^2 - \bar{E}^2) - \mathbf{q}^2\,\rho\,C_\Delta} \\ &= \frac{q_0^2 - \bar{E}^2}{(q_0^2 - q_{01}^2)(q_0^2 - q_{02}^2)} \\ &= \frac{a_1}{q_0^2 - q_{01}^2} + \frac{a_2}{q_0^2 - q_{02}^2} \quad . \end{aligned} \tag{2.7}$$

The q_{0i} are solutions of the equation

$$\begin{aligned} (q_0^2 - E_\pi^2)(q_0^2 - \bar{E}^2) - \mathbf{q}^2\,\rho\,C_\Delta &= 0 \\ &\Rightarrow \\ q_{01}^2 &= \frac{\bar{E}^2 + E_\pi^2 + \sqrt{(\bar{E}^2 - E_\pi^2)^2 + 4\,\mathbf{q}^2\,\rho\,C_\Delta}}{2} \\ q_{02}^2 &= \frac{\bar{E}^2 + E_\pi^2 - \sqrt{(\bar{E}^2 - E_\pi^2)^2 + 4\,\mathbf{q}^2\,\rho\,C_\Delta}}{2} \quad . \end{aligned} \tag{2.8}$$

The strength factors a_i follow by means of the relation

$$a_i = \mathcal{D}_\pi^{med}(q_0, \mathbf{q})(q_0^2 - q_{0i}^2)|_{q_0 = q_{0i}} \quad ,$$

leading to

$$\begin{aligned} a_1 &= \frac{q_{01}^2 - \bar{E}^2}{q_{01}^2 - q_{02}^2} = \frac{1}{2} - \frac{\Delta E}{2\sqrt{\Delta E^2 + \mathbf{q}^2\,\rho\,C_\Delta}} \\ a_2 &= \frac{\bar{E}^2 - q_{02}^2}{q_{01}^2 - q_{02}^2} = \frac{1}{2} + \frac{\Delta E}{2\sqrt{\Delta E^2 + \mathbf{q}^2\,\rho\,C_\Delta}} \quad , \end{aligned} \tag{2.9}$$

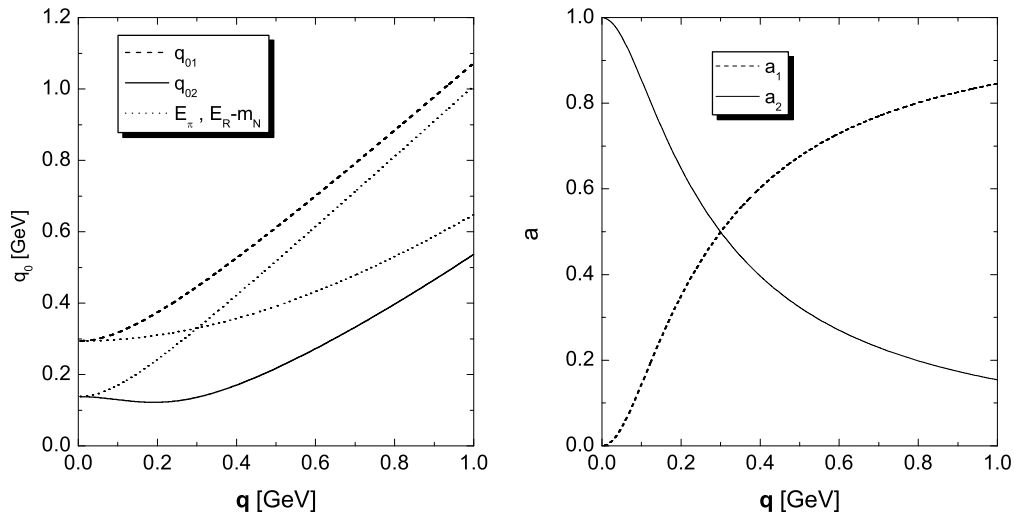

Figure 2.2: Left: Dispersion relation of the interacting (solid, dashed) and free (dotted) modes in the $\pi N\Delta$ system. Right: Strength of the interacting modes. The results are shown for density $\rho = \rho_0$.

where $\Delta E = \bar{E}^2 - E_\pi^2$ has been introduced. These formulae are identical to those obtained in [50].

This result can be interpreted in the following way: due to the existence of two poles, the pion propagates in nuclear matter in two different modes. One is related to the meson mode already present in the vacuum and the other one to the excitation of Δ hole states. The strength of both modes follows from Eq. 2.9. This scenario is easily extended to the case of the coupling to n resonances: then the propagator would have $n+1$ poles, corresponding to the propagation of $n+1$ modes.

Next we discuss the dispersion relations of Eq. 2.8 and the relative strength in both modes as given by Eq. 2.9. In the limit of a vanishing coupling ρC_Δ, the dispersion relations are given by $E_\pi(\mathbf{q})$ and $\bar{E}(\mathbf{q})$. After the coupling has been turned on, both modes repel each other, as can be seen by expanding Eq. 2.8 for small coupling C_Δ, i.e. $\frac{\mathbf{q}^2 \rho C_\Delta}{\Delta E^2} \ll 1$:

$$\begin{aligned} q_{01}^2 &= \frac{\bar{E}^2 + E_\pi^2}{2} + \left| \frac{\bar{E}^2 - E_\pi^2}{2} \right| + \epsilon \\ &= \begin{cases} \bar{E}^2 + \epsilon & \text{if } \bar{E}^2 > E_\pi^2 \\ E_\pi^2 + \epsilon & \text{if } \bar{E}^2 < E_\pi^2 \end{cases} \\ q_{02}^2 &= \frac{\bar{E}^2 + E_\pi^2}{2} - |\frac{\bar{E}^2 - E_\pi^2}{2}| - \epsilon \\ &= \begin{cases} E_\pi^2 - \epsilon & \text{if } \bar{E}^2 > E_\pi^2 \\ \bar{E}^2 - \epsilon & \text{if } \bar{E}^2 < E_\pi^2 \end{cases} , \end{aligned} \tag{2.10}$$

with $\epsilon = \frac{\mathbf{q}^2 \rho C_\Delta}{|\Delta E|} > 0$. Note that the repulsion gets weaker with increasing energy difference ΔE. If on the other hand ΔE becomes very small, then the above expansion of Eq. 2.8

does not hold any longer. In the limiting case $\Delta E = 0$ one obtains the following solutions:

$$\begin{aligned} q_{01}^2 &= E^2 + \sqrt{\mathbf{q}^2\,\rho\,C_\Delta} \\ q_{02}^2 &= E^2 - \sqrt{\mathbf{q}^2\,\rho\,C_\Delta} \quad , \end{aligned} \tag{2.11}$$

where $E^2 = \frac{\bar{E}^2 + E_\pi^2}{2}$.

In Fig. 2.2 we show the dispersion relation of the interacting system (solid and dashed line) together with the free dispersion relations (dotted lines). Here and for the remaining plots in this Chapter we take for the density $\rho = \rho_0 = 0.15\,\mathrm{fm}^{-3}$. These results are very interesting. They display effects from level repulsion and furthermore the full solutions q_{01} and q_{02} change their character as the momentum increases. This reflects the fact that the free dispersion relations E_π and $\bar{E}$ cross each other at momenta around $\mathbf{q} = 0.3$ GeV. The solution q_{02} (solid line) corresponds at small momenta to the pion mode, but at large momenta it resembles the Δ hole mode. Similarly, the solution q_{01} (dashed lined) switches from the Δ hole mode at small momenta to the pionic mode at large momenta. This behaviour of the solution is also seen in Eq. 2.10. The distribution of strength in both branches follows along these lines, see right panel of Fig. 2.2: At small momenta more strength sits in q_{02} (solid line) and at large momenta in q_{01} (dashed line), implying that in general more strength is accumulated in the meson branch compared to the particle-hole branch. There is a crossing point (at $E_\pi = \bar{E}$) where the strength in both branches is equal. At this point the solutions q_{01} and q_{02} switch from the pion to the Δ hole mode and vice versa.

As we have just seen, the full dispersion relations seem to repel each other as compared to the free case. This phenomenon is known as *level repulsion* and can be observed in any quantum mechanical two-level system with a perturbation coupling both levels. To see that, consider the following Hamiltonian:

$$\begin{aligned} H &= H_0 + V \\ &= \begin{pmatrix} E_1 & 0 \\ 0 & E_2 \end{pmatrix} + \begin{pmatrix} 0 & V \\ V & 0 \end{pmatrix} \quad . \end{aligned} \tag{2.12}$$

The *eigenvalues* $\lambda_{1/2}$ of H have the form

$$\lambda_{1/2} = \frac{E_1 + E_2}{2} \pm \sqrt{\left(\frac{E_1 - E_2}{2}\right)^2 + V^2} \quad . \tag{2.13}$$

Identifying $E_1 = E_\pi^2$, $E_2 = \bar{E}^2$ and $V = \sqrt{\mathbf{q}^2\,\rho\,C_\Delta}$, one recovers Eq. 2.8.

Let us now turn to the strength factors a_i of Eq. 2.9. They fulfill a sum rule $a_1 + a_2 = 1$. This fact suggests a probabilistic interpretation of the a_i: they give the probability that the meson is either in the mesonic mode or in the particle-hole mode. One can recast the sum rule in a more formal manner. Using that

$$\mathcal{I}\mathrm{m}\,\frac{1}{q_{0i}^2 - q_0^2 + i\,\epsilon} = -\pi\,\delta(q_{0i}^2 - q_0^2) \quad , \tag{2.14}$$

the following expression holds:

$$\begin{aligned} -\int_{-\infty}^{+\infty} \frac{dq_0\,q_0}{\pi}\,\mathcal{I}\mathrm{m}\,\mathcal{D}_\pi^{med}(q_0,\mathbf{q}) &= \int_{-\infty}^{+\infty} dq_0\,q_0\,\mathcal{A}_\pi^{med}(q_0,\mathbf{q}) = 1 \\ \mathcal{A}_\pi^{med}(q_0,\mathbf{q}) &= -\frac{1}{\pi}\,\mathcal{I}\mathrm{m}\,\mathcal{D}_\pi^{med}(q_0,\mathbf{q}) \quad . \end{aligned} \tag{2.15}$$

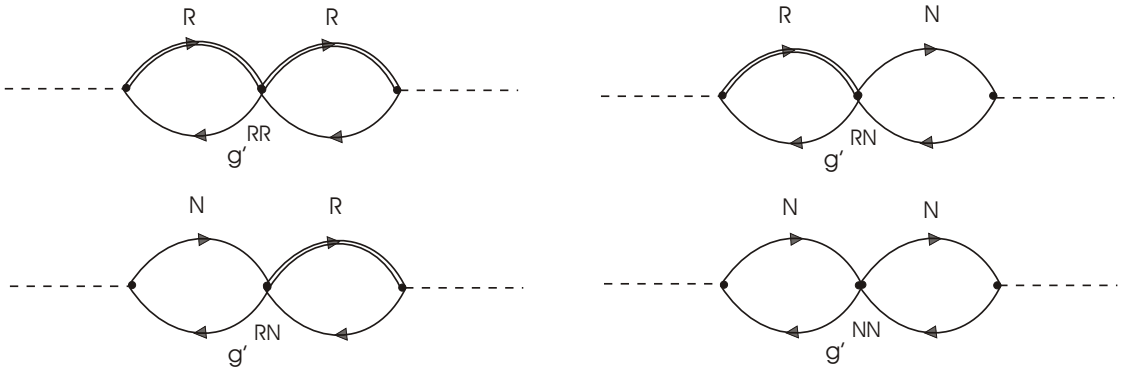

Figure 2.3: Contribution from short-range correlations to the pion self energy. Note that in principle one has independent parameters g' for the interaction of ΔN^{-1} and ΔN^{-1} loops, of ΔN^{-1} and NN^{-1} loops and of NN^{-1} and NN^{-1} loops. For simplicity we take these parameters to be the same in this Chapter.

The quantity $\mathcal{A}_\pi^{med}(q_0, \mathbf{q})$ is called *spectral function* and will play a central role in this work. One can indeed show, that the above sum rule for the spectral function is a very general statement and holds true for any spectral function obeying certain restrictions. Details can be found in Appendix E.

2.2 Short-Range Correlations and Meson Propagation

A modification of the above results arises from short-range correlations. In the context of meson propagation this means, that a particle-hole state, once it is produced, does not necessarily have to decay into a pion, but might rather form a complex multi-meson state. Phrased differently, this reflects the fact that the nucleon-nucleon or resonance-nucleon interaction is not exhausted by pion exchange contributions alone, see Chapter 6. As detailed there, the modifications of the pion exchange interaction are conveniently summarized in a point interaction with a strength parameter g', which is often called the Migdal parameter. The lowest order contribution of such short-range interactions to the pion self energy is shown in upper left diagram in Fig. 2.3.

After summing up the short-range corrections, one arrives at a modified expression for the propagator (cf. Eq. 2.7):

$$\mathcal{D}_\pi^{med}(q_0, \mathbf{q}) \;=\; \frac{1}{q_0^2 - E_\pi^2 - \dfrac{\mathbf{q}^2\,\chi_\Delta}{1 - g'\,\chi_\Delta}} \quad . \tag{2.16}$$

Here we have introduced the loop function

$$\chi_\Delta = \rho\, C_\Delta / (q_0^2 - \bar{E}^2) \quad . \tag{2.17}$$

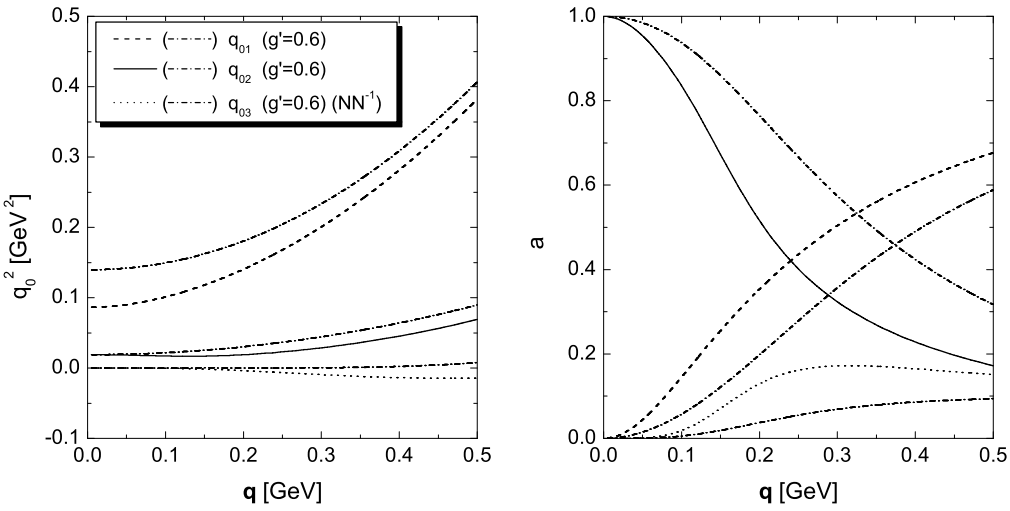

Figure 2.4: Influence of the short-range correlations. Left: Dispersion relations q_{01}, q_{02} and q_{03} of the interacting modes in the $\pi N\Delta$ system for $g' = 0.6$ (dash-dotted lines) and $g' = 0$. Right: Same for the strength in all three branches. q_{01} and q_{02} correspond to Δ-hole and pion mode, q_{03} is the nucleon-hole mode.

In order to understand the effect of g', let us consider the self energy:

$$\begin{aligned} \Pi_\Delta(q_0, \mathbf{q}) &= \frac{\mathbf{q}^2 \chi_\Delta}{1 - g' \chi_\Delta} \\ &= \frac{\mathbf{q}^2 \rho C_\Delta}{q_0^2 - \bar{E}^2} \frac{q_0^2 - \bar{E}^2}{q_0^2 - \bar{E}^2 - g' \rho C_\Delta} \\ &= \frac{\mathbf{q}^2 \rho C_\Delta}{q_0^2 - \bar{E}^2 - g' \rho C_\Delta} \quad . \end{aligned} \tag{2.18}$$

Apparently the self energy can be cast into a form similar to the case of $g' = 0$, if the replacement $\bar{E}^2 \to \bar{E}^2 + g' \rho C_\Delta$ is made. With this adjustment the results from Eqs. 2.8 and 2.9 are valid also if short-range correlations are included. This implies that through the short-range interactions an additional repulsion for the particle-hole branch is induced (cf. [50]). By level repulsion arguments then also the meson branch will be shifted upwards.

From now on we study a slightly extended version of the Δ hole model and include also the nucleon-hole loop, which leads to the self energy contribution:

$$\Pi_N(q_0, \mathbf{q}) = 2\,\mathbf{q}^2 \left(\frac{f_N}{m_\pi}\right)^2 \rho \frac{\bar{E}_N}{q_0^2 - \bar{E}_N^2} \tag{2.19}$$

$$\chi_N(q_0, \mathbf{q}) = 2 \left(\frac{f_N}{m_\pi}\right)^2 \rho \frac{\bar{E}_N}{q_0^2 - \bar{E}_N^2} \quad , \tag{2.20}$$

with $\bar{E}_N = \sqrt{m_N^2 + \mathbf{q}^2} - m_N$. The inclusion of the nucleon does not imply principal complications, but we refrain from giving analytical results for position and strength of

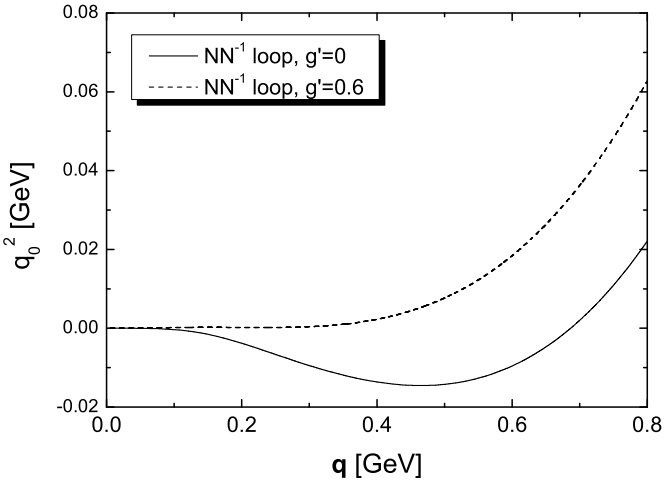

Figure 2.5: Influence of the short-range correlations on the dispersion relation of the NN^{-1} pair. Shown is the dispersion relation for $g' = 0$ (solid) and $g' = 0.6$ (dashed).

the individual poles of the pion propagator. Instead, numerical solutions will be presented. We also multiply the total self energy with a form factor:

$$F^2(\mathbf{q}) \;=\; \left(\frac{\Lambda^2 + q_\Delta^2}{\Lambda^2 + \mathbf{q}^2}\right)^2 \quad . \tag{2.21}$$

The parameter q_Δ is the momentum of an on-shell pion from the decay of an on-shell Δ. For the cutoff we take $\Lambda = 2$ GeV. This form factor is chosen for the following reason: in the following two Sections 2.3 and 2.4, we calculate the width of the Δ, which is also multiplied by the same form factor. For an on-shell Δ the form factor F is equal to unity and therefore does not change the on-shell width of the Δ. It is somewhat arbitrary to multiply Π_N with this form factor since it includes the momentum q_Δ. However, since the results presented here are only of qualitative nature, we have not chosen a different form factor for the πNN vertex.

If the nucleon-hole loop is added to the model, one needs to consider interactions between the following particle-hole loops: ΔN^{-1} with ΔN^{-1}, ΔN^{-1} with NN^{-1}, and NN^{-1} with NN^{-1}, see Fig. 2.3. This means, that one could in principle have three independent short-range parameters g' describing the strength of these interactions. For simplicity, we will assume a universal coupling for all particle-hole loops.

In Fig. 2.4 we show position and strength of the poles both for the case of no short-range correlations and and for a value of $g' = 0.6$. The calculations without short-range correlations are depicted by dotted lines (nucleon-hole, q_{03}), solid lines (q_{02}) and dashed lines (q_{01}). The results with short-range correlations are shown in dash-dotted lines. As expected there is a moderate repulsion of all three levels, when the short-range correlations are switched on. In addition, the strength of the branches is somewhat rearranged.

Historically, the effects of short-range correlations on the in-medium properties of pions have been of great interest since the possibility of pion condensation was pointed out in [93, 94]. Pion condensation occurs if the propagator has a pole at $q_0 = 0$, see for example

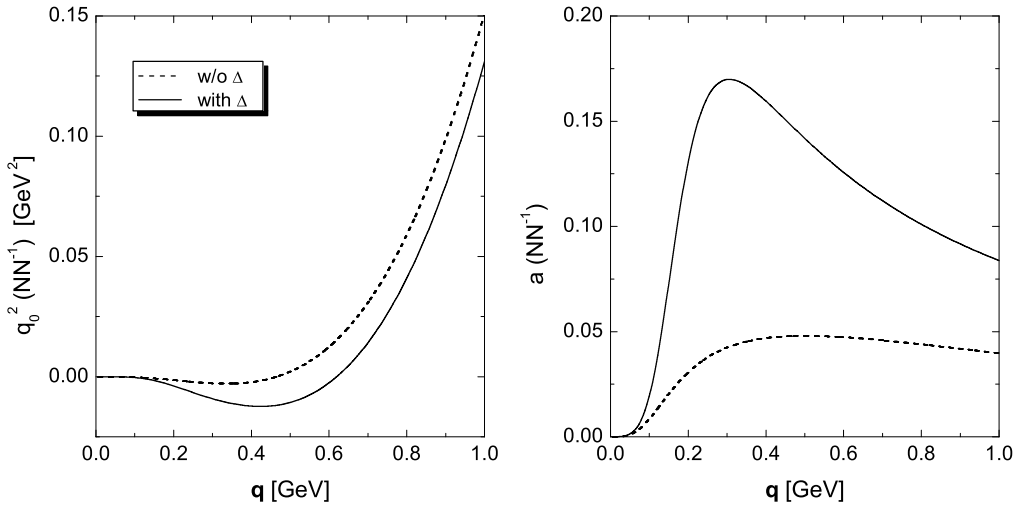

Figure 2.6: Influence of the Δ on position (left) and strength (right) of the nucleon branch. The calculation with (without) the Δ is indicated by solid (dashed) lines. In both calculations no short-range correlations are included.

[75, 94]. Let us now discuss how pion condensation is removed by short-range correlations. In Figs. 2.5 we show the nucleon-hole branch as arising from a full calculation with (dashed line) and without (solid line) short-range correlations. One finds that for $g' = 0$ the nucleon-hole branch dives into the region of negative q_0^2 at finite momenta ranging from $\mathbf{q} = 0.2$ GeV to $\mathbf{q} = 0.7$ GeV, where the strength in this branch is non-vanishing (cf. right plot in Fig. 2.4). This implies the existence of pion condensation for these momenta. The situation is remedied after the short-range correlations have been introduced, and the nucleon-hole branch is situated in the region of positive q_0^2 for all momenta. It is also interesting to understand the mechanism responsible for the downward shift of the NN^{-1} excitation. As can be seen in Fig. 2.6, it is the influence of the Δ which, by level repulsion, moves the nucleon branch into regions of negative q_0^2 (cf. [99, 33]). As shown on the right panel, the presence of the Δ enhances the strength in the nucleon branch by up to a factor of 3.

2.3 The Δ Properties in Medium

In this Chapter we discuss the properties of the Δ in nuclear matter. Due to its coupling to the $N\pi$ channel, the Δ resonance has a vacuum width of 120 MeV. In the medium there will be important corrections to this free space value from Pauli-blocking and collisional broadening. Due to Pauli-blocking, the phase space available for the nucleon is reduced since its momentum must be larger than the Fermi momentum. Collisional broadening acts in the opposite direction: by interacting with the surrounding nucleons in nuclear matter, the Δ can either be absorbed via the process $\Delta\, N \to N\, N$ or it can be scattered in a different phase space element via $\Delta\, N \to N\, \Delta$, which is often referred to as quasi-elastic scattering in the literature [100, 98]. Both processes shorten the lifetime of the Δ and thus increase its width. We mention that the numerical results presented in this Chapter aim

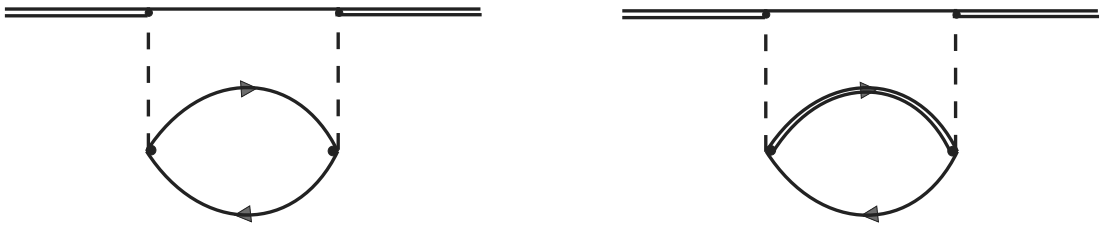

Figure 2.7: Contribution to collisional broadening. Left: absorptive ($\Delta\, N \to N\, N$) process. Right: quasi-elastic ($\Delta\, N \to N\, \Delta$) process.

at a qualitative understanding of the underlying mechanisms and should not be taken at face value.

To lowest order in the nuclear density ρ, the in-medium broadening follows from the formula [32, 65, 22]:

$$\Gamma_{coll} \;=\; \rho\, v\, \sigma_{\Delta}^{tot} \quad ,$$

where ρ is the density, v is the velocity of the Δ relative to nuclear matter and σ_{Δ}^{tot} denotes the total ΔN cross section. We will come back to this formula in Section 5.3.2, where we demonstrate explicitly that the Feynman diagrams shown in Fig. 2.7 – dressing the meson propagator with only one particle-hole loop – correspond to Γ_{coll}. Then the in-medium width is given as a sum of the Pauli-corrected vacuum width Γ_{Pauli} and collisional broadening:

$$\Gamma_{med} \;=\; \Gamma_{Pauli} + \Gamma_{coll} \quad . \tag{2.22}$$

In this Section as well as in the rest of this work we will go beyond this approximation and replace the vacuum pion propagator by the in-medium one, i.e. we resum the particle-hole loops in the pion propagator. In this Section, short-range correlations will only be taken into account for the pion self energy. As we will discuss in the following Section 2.4, the short-range correlations lead to additional diagrams for the Δ self energy, which are not considered in this Section.

In terms of the self energy $\Sigma_{\Delta}(k_0, \mathbf{k})$, the propagator of the Δ is defined as:

$$\mathcal{G}_{\Delta}(k_0, \mathbf{k}) \;=\; \frac{1}{k_0 - E_{\Delta}(\mathbf{k}) - \frac{\Sigma_{\Delta}}{2\sqrt{k^2}}} \quad . \tag{2.23}$$

Note that Σ_{Δ} is averaged over the spins of the Δ, which with our normalization leads to the additional factor $2\sqrt{k^2}$. For details concerning the averaging process see Appendix D.1.1. Keeping this in mind, Σ_{Δ} follows from the integral:

$$\Sigma_{\Delta}(k_0, \mathbf{k}) \;=\; -\left(\frac{f}{m_{\pi}}\right)^2 \frac{16}{3}\sqrt{k^2}\, m_N \int \frac{d^4p}{(2\pi)^4}\, F^2(\mathbf{k}-\mathbf{p})(\mathbf{k}-\mathbf{p})^2\, \mathcal{G}_N(p)\, \mathcal{D}_{\pi}(k-q) \tag{2.24}$$

Here $\mathcal{G}_N(p)$ and $\mathcal{D}_{\pi}(k-q)$ denote the propagator of pion and nucleon, respectively. As in Section 2.1, we assume a non-relativistic framework for nucleon and Δ. To obtain the imaginary part of the self energy, we use Cutkosky's cutting rules. They require to replace the propagators of nucleon and pion by their respective spectral functions.

Since the particles have no width, these spectral functions are proportional to δ functions multiplied with a strength factor a, which is the residue of the δ peak. When calculating the imaginary part of the vacuum self energy, both propagators have poles at the on-shell points, $p^2 = m_N^2$ and $q^2 = (k-p)^2 = m_\pi^2$. The residues at these poles are equal to unity. In the medium, Pauli-blocking of the nucleon has to be taken into account. Furthermore, as discussed before, the pion propagator now contains two additional poles from the excitation of nucleon-hole and Δ-hole states. Each of these three poles comes with a (momentum dependent) strength factor a_i. Taking this into account, we find for the width $\Gamma = -\mathcal{I}\mathrm{m}\,\Sigma_\Delta/\sqrt{k^2}$ of a Δ at rest:

$$\Gamma_{vac}(k^2) = \frac{1}{6}\left(\frac{f}{m_\pi}\right)^2 \frac{m_N}{\pi\sqrt{k^2}}\,\mathbf{q}^3\,F^2(\mathbf{q}) \tag{2.25}$$

$$\Gamma_{Pauli}(k_0, \mathbf{k}=0) = \frac{1}{6}\left(\frac{f}{m_\pi}\right)^2 \frac{m_N}{\pi\sqrt{k^2}}\,\mathbf{q}^3\,F^2(\mathbf{q})\,\theta(|\mathbf{q}| - p_F) \tag{2.26}$$

$$\Gamma_{med}(k_0, \mathbf{k}=0) = \frac{1}{6}\left(\frac{f}{m_\pi}\right)^2 \frac{m_N}{\pi\sqrt{k^2}} \sum_{q_i^2} a_i\,\mathbf{q}^3\,F^2(\mathbf{q})\,\theta(|\mathbf{q}| - p_F) \quad . \tag{2.27}$$

The sum in the third equation extends over all three poles of the in-medium pion propagator $q_i^2 = q_{0i}^2 - \mathbf{q}^2$. The 3-momentum $\mathbf{q} = \mathbf{q}(k^2, q_i^2)$ of the pion is a function of the invariant mass k^2 of the Δ and that of the pion mode q_i^2. The θ-function takes into account effects from Pauli-blocking and $p_F = 0.27$ GeV is the Fermi momentum at normal nuclear matter density. Also included is a form factor $F(\mathbf{q})$. The form of these results is very intuitive: the vacuum result contains phase space factors and a squared matrix element proportional to $\mathbf{q}^2$, evaluated at the kinematics corresponding to a decay into an on-shell pion. In the nuclear medium, the decay can happen into three different branches. The decay into any of those branches is of the same form as the vacuum width if one corrects for the (momentum dependent) mass of the branch. The total width is then given as a sum over these branches where each branch is weighted by the appropriate strength factor a_i.

In order to further illuminate this picture, we show in Fig. 2.8 the three dispersion relations q_i^2 of the interacting pion (solid lines) as well as the invariant mass available for the pion from the decay of an on-shell Δ (dashed line), which for a Δ at rest is given by $(\sqrt{k^2} - E_N)^2 - \mathbf{q}^2$, where $E_N = \sqrt{m_N^2 + \mathbf{q}^2}$. The points where the latter crosses the pion dispersion relations indicate the invariant mass q_i^2 of the individual branches in Eq. 2.25. Whereas a decay into the highest lying branch q_1^2 is not only possible for an on-shell Δ with invariant mass 1.232 GeV, the remaining two branches are easily accessible. For comparison, we also indicate the position of the vacuum pion (dotted lines) and the Fermi momentum (dash-dot-dotted line).

Let us now turn to a physical interpretation of Eq. 2.27. In light of Eq. 2.22 it is tempting to associate the decay into the individual branches either with the meson-nucleon decay (Γ_{vac}) or with ΔN scattering processes (Γ_{coll}). We will argue now, that such an interpretation is in general not possible. In our model, the mode q_3^2 always represents the NN^{-1} branch, and consequently we can identify this mode with the absorptive process $\Delta N \to NN$. Going beyond Eq. 2.22, which describes Δ absorption on a nucleon with the exchange of a vacuum pion, in the corresponding part of Eq. 2.27 the exchanged pion is medium modified by the coupling to NN^{-1} and ΔN^{-1} states. More complicated is the interpretation of the remaining two branches, since – as discussed in Section 2.1 – they

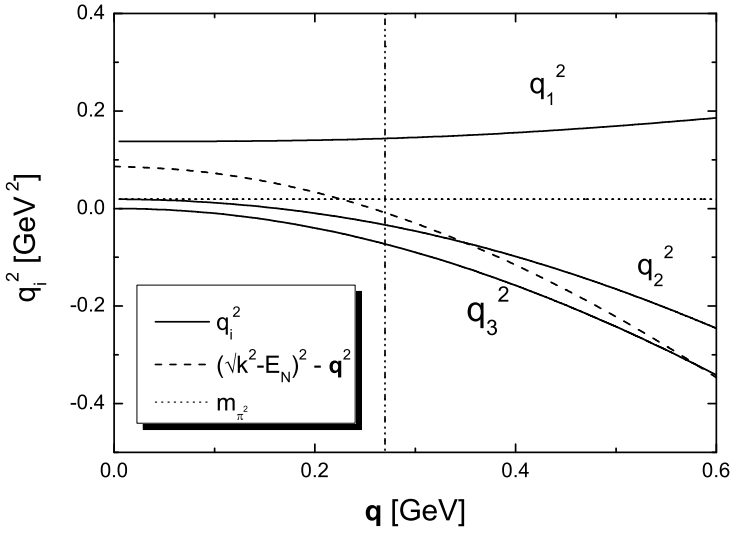

Figure 2.8: Shown are the three poles q_i^2 of the in-medium pion propagator (solid lines) together with the invariant mass available for the pion in the decay of an on-shell Δ at rest, which is given by $(\sqrt{k^2} - E_N)^2 - \mathbf{q}^2$ (dashed line). For comparison also the position of the free pion (dotted line) and the Fermi momentum (dash-dot-dotted line) are indicated.

correspond to different modes at different momenta. Thus, it is in general not possible to relate one of these branches to elastic scattering $\Delta N \to N\Delta$ or the decay $\Delta \to N\pi$. However, by inspecting Fig. 2.8 and Fig. 2.2 one sees, that the kinematics for the decay of an on-shell Δ at rest is such that it is legitimate to interpret branch q_2^2 as the Δ-hole branch and branch q_1^2 as the pion branch as both branches are tested for momenta $\mathbf{q} > 0.3$ GeV. Since the in-medium dispersion relations differ significantly from that of a pion in vacuum, the resulting decay width into the in-medium pion branch can differ significantly from the free vacuum width $\Delta \to N\pi$. For the kinematics described before, the in-medium pion branch is heavier than the vacuum one and thus we expect a smaller contribution from this branch. Also, the in-medium branches have strength factors $a_i < 1$, which leads to a further reduction of the decay into the pion branch relative to the vacuum decay. This suggests that a splitting of Γ_{med} according to Eq. 2.22 is not sensible when the particle-hole loops are resummed in the meson propagator.

The in-medium width Γ_{med} of a Δ at rest at normal nuclear matter density is shown by the dashed line in the left plot of Fig. 2.9 for a density $\rho = \rho_0$. For comparison also Γ_{Pauli} is displayed by the solid line. For the short-range correlations in the pion propagator we take $g' = 0.4$. For a Δ at rest, Γ_{Pauli} is either zero below a critical invariant mass or it is equal to its vacuum value, depending on whether the nucleon momentum is larger or smaller than the Fermi momentum. At normal nuclear matter density the width of an on-shell Δ is completely blocked and opens up only at invariant masses of about 1.27 GeV, as can be seen by the step in the solid line in Fig. 2.9 at this energy. After the interactions with the particle-hole loops have been switched on, the width increases dramatically, as indicated by the dashed line in the left plot of Fig. 2.9. This is due to phase space effects which allow for very large decay widths into the branches q_2^2 and q_3^2, whereas the branch q_1^2 is energetically not available for an on-shell Δ (cf. Fig. 2.8) and contributes only at energies above 1.45 GeV, thus explaining the step at this energy in Γ_{med}. The individual

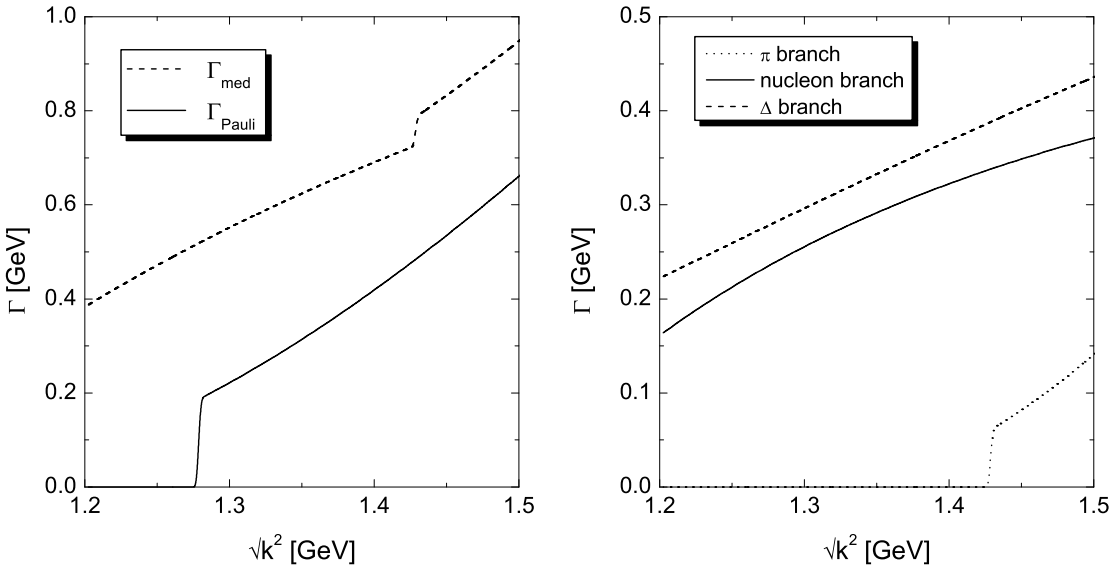

Figure 2.9: Left panel: Γ_{med} (dashed) and Γ_{Pauli} (solid) of the Δ at normal nuclear matter density with $g' = 0.4$. Right panel: Contribution of the individual poles q_i^2 to the total in-medium width. The sum of these contributions gives the in-medium width indicated by the dashed line in the left plot. The density is $\rho = \rho_0$.

contributions to Γ_{med} are shown in the right plot of Fig. 2.9.

The in-medium width Γ_{med} of the Δ is in the order of 400 MeV for an on-shell Δ, corresponding to a broadening of roughly 300 MeV, which is much larger than the empirical value of 80 MeV [54]. We will show in the next Section, that the vertex corrections introduced by the short-range interaction help to substantially reduce this number.

Let us make a general comment at this point: not always does the coupling to additional many-body states increase the width. Imagine a situation where the excitation of a resonance-hole state requires more energy than available from the decay of the resonance under consideration. Then only the meson pole will contribute, however with a reduced strength $a < 1$, since some strength is carried by the resonance-hole loop. As a result, the decay width in the medium could be smaller than in vacuum, if the reduced strength in the meson pole is not compensated for by enhanced phase space factors from level repulsion. This effect is entirely due to the summation of the resonance-hole loop insertion into the meson propagator according to the Dyson-Schwinger equation. By considering only the lowest diagram for the self energy, involving just one resonance-hole loop insertion, one would find that the width does not change at all, if the resonance can energetically not be reached.

2.4 Effect of Short Range Correlations

In Chapter 6 we discuss the influence of short-range correlations on the NR interaction in nuclear matter. As a result we will find that the correlations not only suggest an in-medium modification of the meson propagator, but also generate vertex corrections and additional contact terms in the NR interaction. We now study the effect of these terms on the width of the Δ. The formulae used in this Chapter will be derived in Chapter 6.

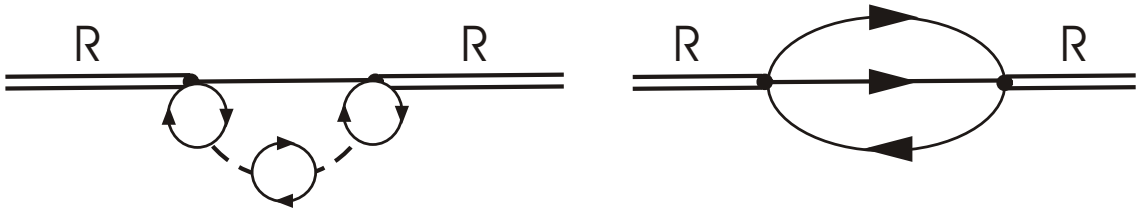

Figure 2.10: Diagrams illustrating the influence of short-range correlations on the decay width. Left panel: vertex corrections, right panel: direct contribution. Each loop represents a resummed nucleon-hole or resonance-hole bubble.

Taking into account the vertex corrections and the additional term from the short-range interactions, the in-medium Δ self energy is given by:

$$\Sigma_\Delta^{med}(k_0,\mathbf{k}) = -\left(\frac{f}{m_\pi}\right)^2 \frac{16}{3}\sqrt{k^2}\, m_N \int \frac{d^4p}{(2\pi)^4} \mathcal{G}_N(p)\, F^2(\mathbf{k}-\mathbf{p}) \times \tag{2.28}$$
$$\times \left[(\mathbf{k}-\mathbf{p})^2 \frac{\mathcal{D}_\pi^{med}(k-p)}{(1-g'\,\chi)^2} + \frac{g'}{1-g'\,\chi}\right] \quad .$$

The notation here is the same as in the previous Section, see Eq. 2.24. By $\mathcal{D}_\pi^{med}$ the in-medium propagator of the pion is denoted. For χ we have $\chi = \chi_N + \chi_\Delta$, see Eqs. 2.17 and 2.20.

Comparing this result with Eq. 2.24, two additional factors are found: a vertex correction factor $1/(1-g'\,\chi)^2$ and an additional term $g'/(1-g'\,\chi)$. The vertex correction factor $1/(1-g'\,\chi)^2$ can be motivated as follows: due to the short-range correlations, the Δ can not only couple to a pion but also to a particle-hole state. This is indicated by the bubbles at the left and right self energy vertices in the left graph of Fig. 2.10. Each bubble yields a factor $g'\,\chi$ and a resummation gives $1/(1-g'\,\chi)$. This factor appears squared since left and right vertex of the self energy are dressed. One can also have a term where the pion does not appear at all in the Δ self energy. This term, which is depicted by the right graph in Fig. 2.10, will be called "direct term" from now on. Again, the factor $1/(1-g'\,\chi)$ results from a resummation of particle-hole loops.

Let us assume for now that only Δ-hole states are included in the calculation. The numerical results shown later in this Section are obtained with inclusion of the nucleon-hole loop as well. When calculating the imaginary part of the self energy, one needs to locate the poles of the terms in the brackets. The residue of the poles then gives the strength with which these poles contribute to the width. Inspecting Eq. 2.28, one sees that the integrand has poles at the pion propagator $\mathcal{D}_\pi^{med}$. In addition, there is a new pole at

$$1 - g'\,\chi_\Delta \quad . \tag{2.29}$$

Taking this into account we find for the width $\Gamma_{med} = -\mathcal{I}\mathrm{m}\,\Sigma_\Delta^{med}/\sqrt{k^2}$ of a Δ at rest (cf. Eq. 2.25):

$$\Gamma_{med}(k_0,\mathbf{k}=0) = \frac{1}{6}\left(\frac{f}{m_\pi}\right)^2 \frac{m_N}{\pi\sqrt{k^2}} \sum_{q_i^2} \mathbf{q}^3\, a_i\, h_i\, F^2(\mathbf{q})\, \theta(|\mathbf{q}|-p_F) + X \quad . \tag{2.30}$$

	$a(g'=0)$	$a(g'=0.4)$	h	$\Gamma(g'=0)$[MeV]	$\Gamma(g'=0.4)$[MeV]
$\Delta\, N^{-1}$	0.21	0.39	0.42	138	92
$N\, N^{-1}$	0.15	0.12	0.35	462	86

Table 2.1: Values the strength factor a_i, the vertex correction h_i and the partial decay width of a Δ into the $\Delta\, N^{-1}$ and $N\, N^{-1}$ branches for various values of the short-range parameter g'.

This is very similar to the result of Eq. 2.25 with $F(\mathbf{q})$ denoting the form factor. The sum extends over both poles of the propagator (remember that the nucleon-hole loop is not considered for the moment) and the relative strength of the poles is given by the residue a_i. Again $\Gamma_{med} = -\mathcal{I}\mathrm{m}\,\Sigma_\Delta^{med}/\sqrt{k^2}$. There are two additional quantities, the vertex correction factor h_i and a term denoted by X. The factor h_i reads:

$$h_i \;=\; \frac{1}{(1-g'\,\chi_\Delta)^2} \quad ,$$

where χ_Δ is evaluated at the pole q_i^2 of the pion propagator. In X we have summarized the contributions to $\mathcal{I}\mathrm{m}\,\Sigma_\Delta^{med}$ originating from the new pole at

$$1-g'\,\chi_\Delta = 0 \quad . \tag{2.31}$$

Let us consider the contribution of X by evaluating the residue of the pole Eq. 2.31:

$$\begin{aligned}\frac{(\mathbf{k}-\mathbf{p})^2\,\mathcal{D}_\pi^{med}}{(1-g'\,\chi_\Delta)^2} + \frac{g'}{1-g'\,\chi_\Delta} \;&=\; \left[\frac{(\mathbf{k}-\mathbf{p})^2}{(q_0^2-E_\pi^2)(1-g'\,\chi_\Delta)-(\mathbf{k}-\mathbf{p})^2\,\chi_\Delta} + g'\right]\times \\ &\quad \times \left.\frac{1}{1-g'\,\chi_\Delta}\right|_{\chi_\Delta=1/g'} \quad .\end{aligned}$$

The term in brackets indicates the residue, which vanishes if one plugs in $\chi_\Delta = 1/g'$. Therefore there is no contribution from this pole to the width.

It is also interesting to study the factors h_i. According to Eq. 2.10, if the pion energy is larger than that of the $\Delta\, N^{-1}$ state, the location of these poles is given by:

$$\begin{aligned} q_{01}^2 \;&=\; E_\pi^2 + \epsilon \\ q_{02}^2 \;&=\; \bar{E}^2 - \epsilon \quad . \end{aligned}$$

One therefore finds the following results for the h_i:

$$h_1 \;=\; \left(1 - g'\frac{\rho\, C_\Delta}{E_\pi^2 - \bar{E}^2 + \epsilon}\right)^{-2} \quad , \quad h_2 \;=\; (1 + g'\rho\, C_\Delta/\epsilon)^{-2} \quad .$$

Clearly, $h_1 > 1$ and $h_2 < 1$. Since we have assumed that $q_{01} > q_{02}$, this means that more weight is given to the higher lying states through the short-range correlations. Since phase space favours low lying states, this means that the width decreases due to the influence of the short-range correlations. This qualitative feature does not depend on our choice $E_\pi > \bar{E}$ and holds also for $\bar{E} < E_\pi$.

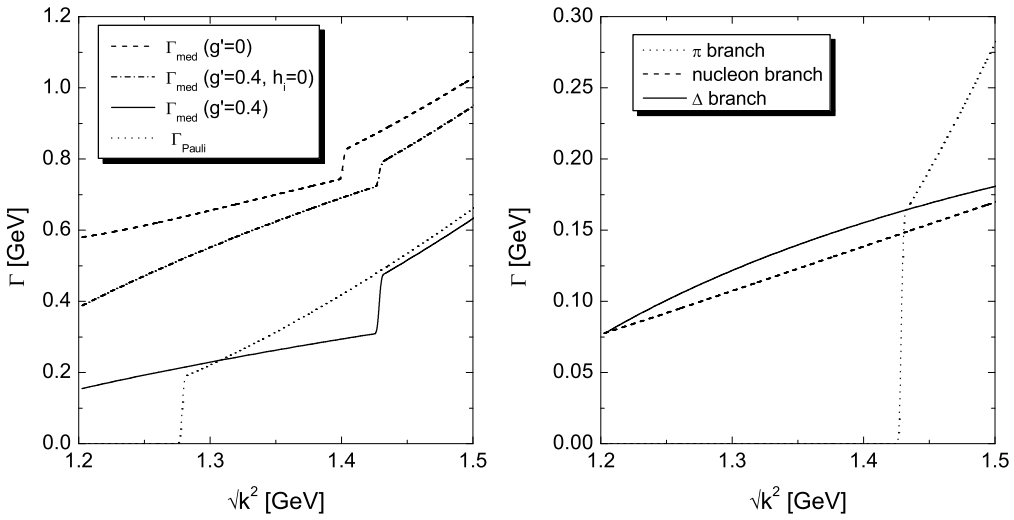

Figure 2.11: Left panel: In-medium width and Pauli-blocked width of the Δ at normal nuclear matter density. Short-range correlations are included in the pion propagator(dash-dotted), also in the vertex corrections (solid) and not at all (dashed). Right panel: Contribution of the individual poles to the total in-medium width.

We will now present some numerical results for the decay width of an on-shell Δ at rest in nuclear matter. Here the contribution from nucleon-hole loops is included. Then the decay into the pion branch is Pauli-blocked and we can identify the solution q_{02} with the ΔN^{-1} branch and solution q_{03} with the NN^{-1} branch, as already discussed in the previous Section 2.3. In the numerical calculations the nucleon-hole excitations are included. We have chosen $g' = 0.4$ for the Migdal parameter, assuming that the coupling of all particle-hole loops to each other is the same. In Table 2.1 we show results for the strength parameter a_i, the vertex correction h_i and the width for $g' = 0$ and $g' = 0.4$. One can see by considering the results for the h_i that the effect of the short-range correlations is to reduce the strength of the low-energy excitations (NN^{-1} and ΔN^{-1}). This leads to a reduction of the partial decay widths into the nucleon-hole branch and the Δ-hole branch. By looking at the numbers in Table 2.1, it becomes clear that the short-range correlations form an essential part of the theory, reducing the total decay width – given as the sum of NN^{-1} and ΔN^{-1} branch – from about 600 MeV to 180 MeV. A value of about 180 MeV is in good agreement with phenomenology, which requires a broadening of 80 MeV [54].

In the left plot of Fig. 2.11 we show the width as a function of the invariant mass of the Δ. Compared are different scenarios: the dashed line corresponds to a calculation where short-range correlations are not taken into account. For the dash-dotted curve short-range correlations only enter into the pion self energy, i.e. $h_i = 0$ and the solid curve represents a full calculation. The dash-dotted curve is identical to the dashed curve in the left panel of Fig. 2.9. By comparing the solid and the dash-dotted lines, one sees that the effect of the short-range correlations on the pion propagator is of much less importance for the Δ width than the vertex corrections. The right plot of Fig. 2.11 disentangles the individual contributions to the full width (solid line in the left plot). While nucleon-

hole (dashed line) and Δ-hole (solid line) branch produce similar contributions, the pion branch sets in only at large invariant masses. This explains the step found in the left plot of Fig. 2.11 at invariant masses around 1.4 GeV. Comparing this with the right plot of Fig. 2.9, where short-range correlations are taken into account only for the pion propagator, supports our finding that through the correlations strength is moved up to the highest lying state: whereas the contributions from nucleon-hole (dashed line) and Δ-hole (solid line) are strongly suppressed, the pion branch (dotted line) produces a much larger contribution if the short-range correlations are switched on. Thus at $\sqrt{k^2} \approx 1.45$ GeV the partial width from this branch is enhanced by a factor of two relative to the calculation with no vertex corrections.

In Fig. 2.12 we investigate the behaviour of the on-shell width as a function of g'. It does not come as a surprise that with increasing g' the width decreases. The results highlight again the sensitivity of the results on the strength of the correlations. This is both interesting and reason for concern since for most particle-hole loops information on g' is not available.

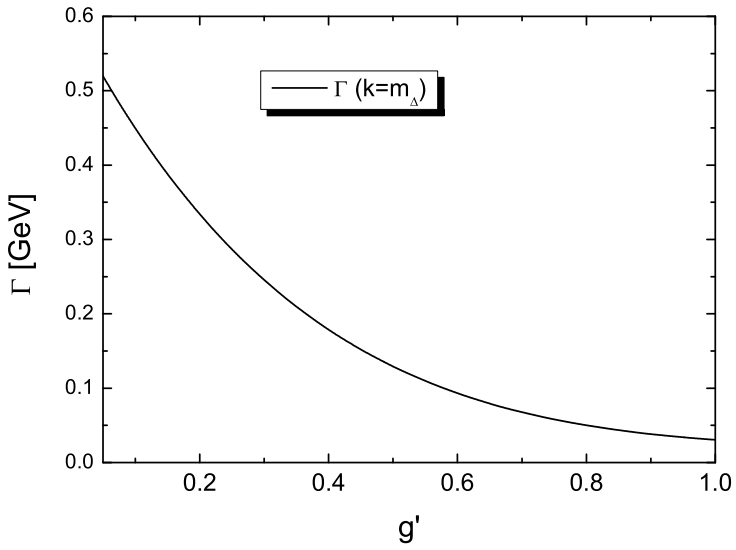

Figure 2.12: In-medium width of the Δ as a function of the strength of the short-range correlations.

Chapter 3

Mesons and Baryon Resonances in the Vacuum

In this Chapter we discuss the vacuum spectral functions of the ρ meson and baryon resonances, which are denoted by $\mathcal{A}(q)$ and $\rho(k)$, respectively. The spectral function is defined as the imaginary part of the retarded propagator, see Appendix E and [16]. In terms of the retarded self energies $\Pi^+_{vac}(q)$ and $\Sigma^+_{vac}(k)$ they are given by:

$$\begin{aligned} \mathcal{A}(q) &= -\frac{1}{\pi}\frac{\mathcal{I}\mathrm{m}\,\Pi^+_{vac}(q)}{(q^2 - m_M^2 - \mathcal{R}\mathrm{e}\,\Pi^+_{vac}(q))^2 + \mathcal{I}\mathrm{m}\,\Pi^{+\,2}_{vac}(q)} \\ \rho(k) &= -\frac{1}{\pi}\frac{\mathcal{I}\mathrm{m}\,\Sigma^+_{vac}(k)}{(k^2 - m_R^2 - \mathcal{R}\mathrm{e}\,\Sigma^+_{vac}(k))^2 + \mathcal{I}\mathrm{m}\,\Sigma^{+\,2}_{vac}(k)} \quad . \end{aligned} \tag{3.1}$$

In this work we will denote the four-momentum of meson M by $q = (q_0, \mathbf{q})$ and that of resonance R by $k = (k_0, \mathbf{k})$. Note that our ansatz for $\rho(k)$ does not take into account the full Dirac structure of the self energy. A detailed discussion of this topic can be found in Chapter 5.2.4 and in Appendix E.5. In Appendix E we also explain the relation between retarded and Feynman self energy and propagator. As shown there, retarded propagator and self energy are analytic in the upper half of the complex energy plane, whereas the Feynman quantities do not have this property. However, as detailed in Appendix E, there is a close relation between both retarded and Feynman quantities in the vacuum:

$$\begin{aligned} \mathcal{I}\mathrm{m}\,\mathcal{D}^+/\Pi^+(q_0,\mathbf{q}) &= \mathrm{sgn}(q_0)\,\mathcal{I}\mathrm{m}\,\mathcal{D}^F/\Pi^F(q_0,\mathbf{q}) \\ \mathcal{R}\mathrm{e}\,\mathcal{D}^+/\Pi^+(q_0,\mathbf{q}) &= \mathcal{R}\mathrm{e}\,\mathcal{D}^F/\Pi^F(q_0,\mathbf{q}) \quad . \end{aligned} \tag{3.2}$$

These relations hold both for bosons and fermions. Due to analyticity, the imaginary part and the real part of retarded propagator and self energy are connected by a dispersion relation.

Both $\mathcal{A}(q)$ and $\rho(k)$ are normalized quantities. In order to guarantee this within our model, we calculate the retarded self energies Π^+_{vac} and Σ^+_{vac} in the following way:

- for positive energies, the imaginary part of the Feynman self energy is identical to the imaginary part of the retarded self energy. We can therefore use Cutkosky's cutting rules to obtain $\mathcal{I}\mathrm{m}\,\Pi^+_{vac}$ and $\mathcal{I}\mathrm{m}\,\Sigma^+_{vac}$ for $q_0 > 0$.
- for mesons we use the antisymmetry of the imaginary part of the self energy

$$\mathcal{I}\mathrm{m}\,\Pi^+_{vac}(-q_0) = -\mathcal{I}\mathrm{m}\,\Pi^+_{vac}(q_0)$$

and apply a dispersion relation to obtain the real part of the self energy. A derivation of the antisymmetry in q_0 can be found in Appendix E.

- as outlined in Appendix E for baryons the antisymmetry of the imaginary part of the self energy holds in vacuum, but not in the nuclear medium. Therefore we neglect the contribution from negative energies to the dispersion integral already in the vacuum.

Calculating the real part of the self energy from a dispersion relation does not automatically produce a normalized spectral function. In addition, the high energy limit of the self energy must fulfill certain relations if the spectral function is to be normalized. A further discussion of this topic can be found in [77] and in Appendix E.

Having computed its self energy, the width Γ of the particle is given by (cf. Appendix D.2):

$$\Gamma = -\mathcal{I}\mathrm{m}\,\Pi^{+}_{vac}/\sqrt{k^2} \quad ,$$

and similarly for fermions.

The issue of how to obtain normalized spectral functions is of relevance to us when going to the nuclear medium. Then within our coupled channel analysis the spectral function of any state is allowed to influence the spectral function of any other state. This implies that even rather small violations of the normalization can lead to errors in the calculation, which are difficult to control. We will discuss this issue in detail in Chapter 9.3.

Let us make a purely technical note: throughout this work we will encounter various traces, arising from the spin summation at the meson-nucleon-resonance vertices. For most of the results presented in this thesis we keep only the leading non-relativistic contribution of these traces. This does not greatly affect the results in the vacuum presented in this Chapter, where effectively only the parametrization of the resonance decay width is modified. In Section 9.4 – which is based on the results reported in [109] – we will demonstrate that the non-relativistic approximation works also well for the in-medium self energies of mesons as long as the kinematical quantities are consistently evaluated in the rest frame of the resonance. The advantage of using non-relativistic expressions it that this way the expressions for the in-medium self energies are simplified, see Chapter 4. In particular, a consistent relativistic description of the short-range interactions is a formidable task [75, 82] and - albeit in principle desirable - beyond the scope of this work.

3.1 ρ Meson

In this Section we discuss the properties of the ρ meson in vacuum. We explain the Lorentz structure of propagator and self energy and discuss in detail how the self energy Π^{+}_{vac} is to be calculated. Our treatment follows that of [52].

The propagator of a non-interacting ρ meson in vacuum has both a four-transversal and a four-longitudinal part:

$$\begin{aligned} -i\,\mathcal{D}^{\mu\nu}_{\rho}(q) &= \frac{1}{q^2-(m^0_\rho)^2+i\epsilon}\left[g^{\mu\nu}-\frac{q^\mu\,q^\nu}{(m^0_\rho)^2}\right] \\ &= \frac{1}{q^2-(m^0_\rho)^2+i\epsilon}\,P^{\mu\nu}_T-\frac{q^\mu\,q^\nu}{q^2}\,\frac{1}{(m^0_\rho)^2} \\ &= \frac{1}{q^2-(m^0_\rho)^2+i\epsilon}\,P^{\mu\nu}_T-\frac{1}{(m^0_\rho)^2}\,P^{\mu\nu}_L(q) \quad . \end{aligned} \tag{3.3}$$

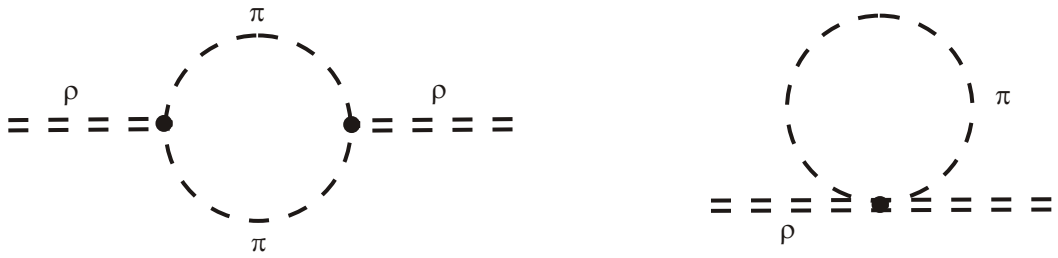

Figure 3.1: Self energy Π_{vac} resulting from the coupling of the ρ to pions. The diagram on the left corresponds to the usual decay of a ρ to two pions. The diagram on the right gives rise to an energy independent real mass shift.

Here $P_T^{\mu\nu}$ stands for the four-transverse projector introduced in Appendix B, Section B.3. The mass m_ρ^0 is the bare mass of the ρ.

Due to interactions with pions the ρ acquires a finite width and its bare mass is shifted to the physical mass. This is described by the following Lagrangian [16, 52]:

$$\begin{aligned} \mathcal{L}_{\rho\pi} &= (D_\mu \pi)^\star (D^\mu \pi) - m_\pi^2 \pi^\star \pi - \frac{1}{4}\rho_{\mu\nu}\rho^{\mu\nu} + \frac{1}{2}(m_\rho^0)^2 \rho_\mu \rho^\mu \\ \rho_{\mu\nu} &= \partial_\mu \rho_\nu - \partial_\nu \rho_\mu \quad , \quad D_\mu = \partial_\mu + i g_\rho \rho_\mu \quad . \end{aligned} \tag{3.4}$$

Note that the coupling of the ρ to the pions has been introduced via minimal substitution and contains $\rho\pi\pi$ and $\rho\rho\pi\pi$ vertices. By g_ρ we denote the coupling strength to pions and m_ρ^0 is the bare mass of the ρ, which is not equal to its physical mass $m_\rho = 0.77$ GeV as observed in experiments.

The coupling derived from Eq. 3.4 is current conserving (since it has been introduced via minimal substitution) and therefore proportional to the four-transverse projector $P_T^{\mu\nu}$. As a consequence, only the transverse part of the propagator is modified by the self energies. Also when coupling the ρ meson to baryon resonances, we use current conserving couplings, see Appendix C.1.1, and can therefore discard the four-longitudinal part of the propagator altogether since it does not contribute to physical quantities. After resumming the self energy according to the Dyson Schwinger equation (cf. Appendix D.1), one obtains for the transverse part of the propagator:

$$D_\rho^{\mu\nu}(q) = D_\rho^T(q)\, P_T^{\mu\nu} \quad \text{with} \quad D_\rho^T(q) = \frac{1}{q^2 - (m_\rho^0)^2 - \Pi_{vac}} \quad .$$

We now turn to the evaluation of the self energy Π_{vac}^+. To this end we first write down the Feynman self energy, which is determined from the two Feynman graphs depicted in Fig. 3.1, leading to the expression [52]:

$$\begin{aligned} -i\,\Pi_{vac}^{\mu\nu}(q^2) &= g_\rho^2 \int \frac{d^4l}{(2\pi)^4} \frac{(2l-q)^\mu (2l-q)^\nu}{[l^2 - m_\pi^2 + i\epsilon]\,[(l-q)^2 - m_\pi^2 + i\epsilon]} \\ &\quad - g_\rho^2 \int \frac{d^4l}{(2\pi)^4} \frac{2g^{\mu\nu}}{l^2 - m_\pi^2 + i\epsilon} \quad . \end{aligned} \tag{3.5}$$

The first expression is energy dependent and has a finite imaginary part, whereas the second one is purely real and energy independent. Both diagrams are needed to ensure

that the self energy is current conserving, i.e. $q_\mu \, \Pi^{\mu\nu}_{vac} = 0$. In order to see this we consider:

$$\begin{aligned} -\frac{i}{g_\rho^2} q_\mu \, \Pi^{\mu\nu}_{vac} &= \int \frac{d^4l}{(2\pi)^4} \left[\frac{(2lq - q^2)(2l - q)^\nu}{\big(l^2 - m_\pi^2 + i\epsilon\big)\big((l-q)^2 - m_\pi^2 + i\,\epsilon\big)} \right. \\ &\quad \left. -q^\nu \frac{2\big((l-q)^2 - m_\pi^2\big)}{\big(l^2 - m_\pi^2 + i\epsilon\big)\big((l-q)^2 - m_\pi^2 + i\,\epsilon\big)} \right] \\ &= \int \frac{d^4l}{(2\pi)^4} \left[\left\{ -\frac{2l^\nu}{l^2 - m_\pi^2 + i\epsilon} + \frac{2l^\nu}{(l-q)^2 - m_\pi^2 + i\epsilon} \right\} \right. \\ &\quad \left. -q^\nu \frac{2\big((l-q)^2 - m_\pi^2\big) + 2lq - q^2}{\big(l^2 - m_\pi^2 + i\epsilon\big)\big((l-q)^2 - m_\pi^2 + i\,\epsilon\big)} \right] \end{aligned} \tag{3.6}$$

With the substitution $l \to l + q$ in the second term of the curly brackets, this can be transformed to yield

$$\begin{aligned} -\frac{i}{g_\rho^2} q_\mu \, \Pi^{\mu\nu}_{vac} &= \int \frac{d^4l}{(2\pi)^4} (-q^\nu) \frac{2lq - q^2}{\big(l^2 - m_\pi^2 + i\epsilon\big)\big((l-q)^2 - m_\pi^2 + i\,\epsilon\big)} \\ &= \int \frac{d^4l}{(2\pi)^4} (-q^\nu) \left\{ \frac{-1}{l^2 - m_\pi^2 + i\epsilon} + \frac{1}{(l-q)^2 - m_\pi^2 + i\epsilon} \right\} \\ &= 0 \quad . \end{aligned} \tag{3.7}$$

In the last step again the above substitution has been made. However, these transformations are not allowed since the integral is divergent. By inspecting Eq. 3.5 one sees that the numerator in the first integral goes like l^6 whereas the denominator goes like l^4. Therefore the loop integral needs to be regularized. The regularization scheme needs to retain the symmetry properties of the self energy. For this reason, the self energy can not be regularized by introducing a cutoff at the vertices. As explained in [16] this would violate the transversality of the self energy.

Following the work of [52] we use Pauli-Villars regularization. The basic idea is to add terms to the Lagrangian, which are of the same form as Eq. 3.4 but where the pion field is replaced by a fictitious heavy particle of mass Λ. The new states do not affect the low energy ($q^2 < \Lambda^2$) behaviour of the theory. At large energies, however, a cancellation of divergent terms is achieved. The self energy can then be cast into the form [52]:

$$\Pi^{\mu\nu}_{vac}(q) \;\; \to \;\; \Pi^{\mu\nu}_{vac}(q;\, m_\pi) - \sum_{i=1}^{N} B_i \Pi^{\mu\nu}_{vac}(q;\, \Lambda_i) \quad . \tag{3.8}$$

The number of necessary subtractions N is determined by the degree of divergence of the loop integral, in our case we have $N = 2$. For further details of the Pauli-Villars regularization we refer to [52] or textbooks on quantum field theory [16, 106].

The expressions Eqs. 3.5 and 3.8 give the Feynman self energy. As discussed in Appendix E and in the introduction to this Chapter, the retarded self energy Π^+_{vac} is readily

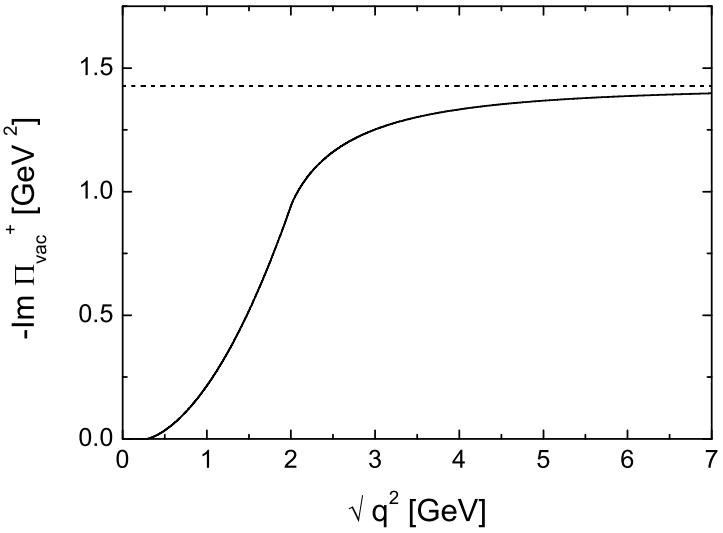

Figure 3.2: $\mathcal{I}\mathrm{m}\,\Pi^+_{vac}$ as a function of the invariant mass of the ρ meson (solid line). By the dashed line we have indicated the limiting value of Eq. 3.10.

obtained from the Feynman self energy with the result:

$$\begin{aligned}
\mathcal{R}\mathrm{e}\,\Pi^+_{vac}(q) &= -\frac{g_\rho^2}{24\pi^2}q^2\left[\mathcal{G}(q,m_\pi)-\mathcal{G}(q,\Lambda)+4\,(\Lambda^2-m_\pi^2)/q^2+ln\frac{\Lambda}{m_\pi}\right] \\
\mathcal{I}\mathrm{m}\,\Pi^+_{vac}(q) &= -\mathrm{sgn}(q_0)\,\frac{g_\rho^2}{48\pi}q^2\left[\theta(q^2-4\,m_\pi^2)\,\left(1-\frac{4\,m_\pi^2}{q^2}\right)^{3/2}-\right. \\
&\qquad \left.-\theta(q^2-4\,\Lambda^2)\,\left(1-\frac{4\,\Lambda^2}{q^2}\right)^{3/2}\right] \quad ,
\end{aligned} \tag{3.9}$$

where we have introduced the function

$$\begin{aligned}
\mathcal{G}(q,m) &= \begin{cases} y^{3/2}\arctan(1/\sqrt{y}) & \text{for } y\,>\,0 \\ -\dfrac{1}{2}(-y)^{3/2}\ln\left|\dfrac{\sqrt{-y}+1}{\sqrt{-y}-1}\right| & \text{for } y\,<\,0 \end{cases} \\
y &= \frac{4m^2}{q^2}-1 \quad .
\end{aligned}$$

The imaginary part $\mathcal{I}\mathrm{m}\,\Pi^+_{vac}$ nicely displays the effect of the Pauli-Villars regularization: it is the sum of two formally identical terms which differ in the mass ($m_\pi \to \Lambda$) and in the sign. Thus, effectively this regularization scheme acts as a form factor in q^2 and in the limit of $q^2 \to \infty$, $\mathcal{I}\mathrm{m}\,\Pi^+_{vac}$ approaches a constant value:

$$\lim_{q^2\to\infty}\mathcal{I}\mathrm{m}\,\Pi^+_{vac} = -\mathrm{sgn}(q_0)\frac{g_\rho^2}{8\pi}\left(\Lambda^2-m_\pi^2\right) \quad , \tag{3.10}$$

as can be seen by a Taylor expansion of Eq. 3.9. The width goes to zero for large invariant masses since

$$\Gamma_{vac} = -\mathcal{I}\mathrm{m}\,\Pi^+_{vac}/\sqrt{(q^2)} \quad .$$

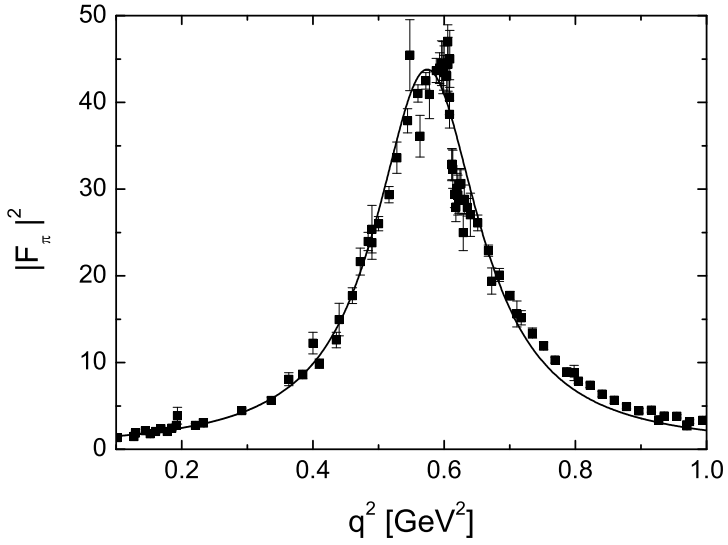

Figure 3.3: Comparison of our model for the pion electromagnetic form factor with experimental data from the analyses of [9, 5].

We have plotted $-\mathcal{I}\mathrm{m}\,\Pi^+_{vac}$ in Fig. 3.2. By the dashed line we have also indicated the limiting value of Eq. 3.10. Since $\mathcal{I}\mathrm{m}\,\Pi^+_{vac}$ approaches a constant at large invariant masses, real and imaginary part of the ρ self energy are related by a once subtracted dispersion relation:

$$\mathcal{R}\mathrm{e}\,\Pi^+_{vac}(q) \;=\; q^2\,\mathcal{P}\int_{4m_\pi^2}^{\infty}\frac{dq'^2}{\pi}\frac{\mathcal{I}\mathrm{m}\,\Pi^+_{vac}(q')}{q'^2(q^2-q'^2)} \quad . \tag{3.11}$$

The subtraction is made at the point $q=0$ in order to satisfy the condition $\mathcal{R}\mathrm{e}\,\Pi^+_{vac}(q=0)=0$ as required from gauge invariance [52, 62]. This condition is explained by the observation that the photon self energy from the coupling to pions is up to the coupling constant identical to that of the ρ meson. For the photon the condition that the self energy vanishes at $q^2=0$ is crucial since otherwise it would become massive. Introducing a mass term as a compensation for the self energy violates gauge invariance. In [116] it is shown that a cutoff regularization always leads to a finite mass term for the photon, which is related to the fact that the gauge invariance of the self energy is violated within such a scheme.

The three free parameters in Eq. 3.9, m_ρ^0, g_ρ and Λ, are determined by fitting the phase shift of $\pi\,\pi$ scattering in the vector-isovector channel and the pion electromagnetic form factor. One gets [52]:

$$m_\rho^0 = 0.875\mathrm{GeV}\ ,\ g_\rho = 6.05\ ,\ \Lambda = 1\mathrm{GeV} \quad . \tag{3.12}$$

In Fig. 3.3 we show the electromagnetic form factor $|F_\pi|^2$ of the pion, which is defined by [33]:

$$|F_\pi(q)|^2 \;=\; \frac{(m_\rho^0)^4}{\left[q^2-(m_\rho^0)^2-\mathcal{R}\mathrm{e}\,\Pi^+_{vac}(q)\right]^2+\mathcal{I}\mathrm{m}\,\Pi^{+\,2}_{vac}(q)} \quad , \tag{3.13}$$

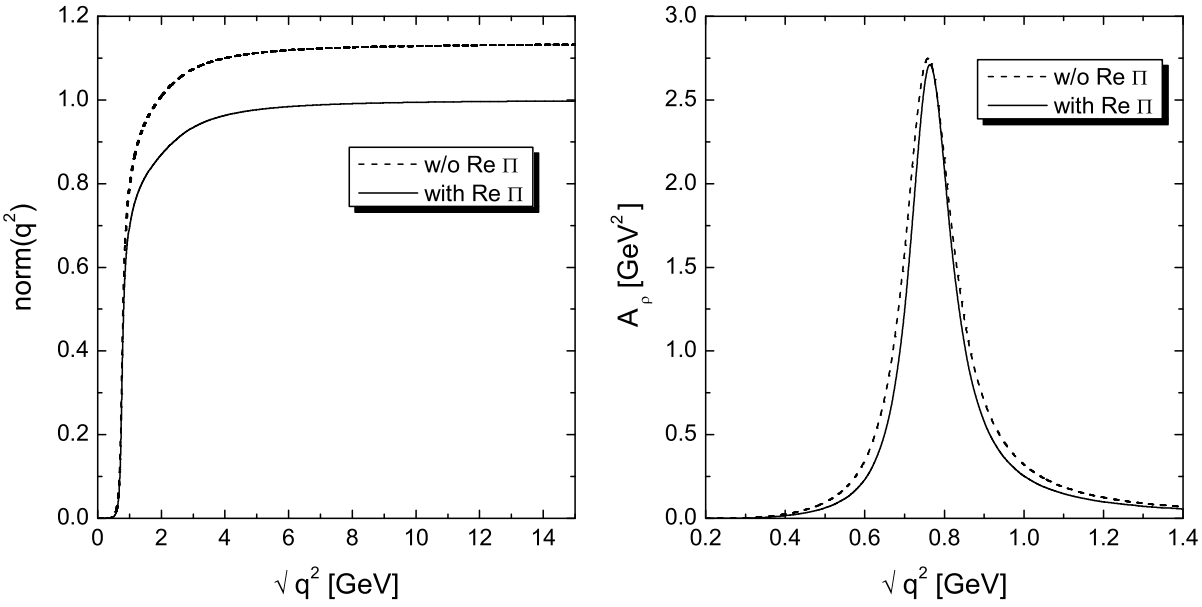

Figure 3.4: Normalization function $\mathrm{norm}(q^2)$ (left) and spectral function (right) with (solid) and without (dashed) $\mathcal{R}\mathrm{e}\,\Pi^+_{vac}(q)$.

in comparison with experimental data. The agreement with the data is of very good quality. Only the little structure near the peak, which results from $\rho - \omega$ mixing (see for example [97]), is missed since such effects are not taken into account in the model.

In Fig. 3.4 we plot the normalization of the spectral function of the ρ meson as a function of the upper integration limit, comparing a calculation with (solid line) and without (dashed lined) real part of the self energy:

$$\mathrm{norm}(q) \;=\; \int_0^q dq'^2\, \mathcal{A}_\rho^{vac}(q') \tag{3.14}$$

If $\mathcal{R}\mathrm{e}\,\Pi^+_{vac}$ is neglected, the bare mass has to be replaced by the physical mass. We find that the spectral function containing $\mathcal{R}\mathrm{e}\,\Pi^+_{vac}$ is normalized to unity, whereas neglecting $\mathcal{R}\mathrm{e}\,\Pi^+_{vac}$ leads to a violation of this constraint, which is mainly due to small differences around the pole region. Here the inclusion of $\mathcal{R}\mathrm{e}\,\Pi^+_{vac}$ leads to a somewhat squeezed spectral shape, hence the contribution to the normalization integral is a little bit smaller. When discussing baryon resonances we will encounter such a modification of the spectral shape again.

3.2 Baryon Resonances

3.2.1 Resonance Nomenclature

A resonance is labeled by a set of quantum numbers of the partial wave in which it appears in πN scattering experiments. This set comprises total spin and isospin as well as the

relative angular momentum of the πN system, which identifies the parity of the resonance. To be more specific, a partial wave amplitude where the πN system is in a relative l-wave, forming a state with total spin $J = \frac{j}{2}$ and isospin $I = \frac{i}{2}$ would be labeled by l_{ij}. The parity of the πN system is $P = +1$ for $l = 1, 3, 5 \ldots$ and $P = -1$ for $l = 0, 2, 4 \ldots$, since the parity is given by $P^\pi P^N (-1)^l = (-1)^{l+1}$. It follows, that the $\Delta(1232)$ resonance which shows up in the P_{33} partial wave has the quantum numbers $I = \frac{3}{2}$, $J = \frac{3}{2}$ and parity $P = +1$. The $N^\star(1520)$ resonance is observed in the D_{13} channel and consequently has the quantum numbers $I = \frac{1}{2}$, $J = \frac{3}{2}$ and $P = -1$. For a given partial wave also the lowest relative orbital angular momentum of any other 2-body state follows from the conservation of parity: for example, in the P_{33} partial wave, the ρN system is in a relative p-wave and for the D_{13} it is in a relative s-wave.

Around the decay threshold $\sqrt{k^2_{thr}}$, the energy dependence of the width is determined by the orbital angular momentum l:

$$\Gamma(\sqrt{k^2} \approx \sqrt{k^2_{thr}}) \quad \sim \quad p^{2l+1} \quad , \tag{3.15}$$

with p the cm momentum of the decay products. One power of p is due to the two-body phase space (Appendix B.6), the remaining powers follow from the dynamics of the interaction. Away from the threshold, higher orders of p modify the expansion.

3.2.2 Framework

The self energy of a baryon resonance arises from the coupling to meson-nucleon channels, see Fig. 3.5. After calculating the corresponding decay width, we obtain $\mathcal{R}\mathrm{e}\,\Sigma^+_{vac}$ by a dispersion analysis. Following standard Feynman rules, the decay width of a nucleon resonance with invariant mass $\sqrt{k^2}$ and spin-$\frac{1}{2}$ into a pseudoscalar meson $\varphi = \pi$, η of mass m_φ and a nucleon is in the resonance rest frame given by:

$$\begin{aligned}
\Gamma_\varphi(k) &= I_\Sigma \frac{q}{8\pi k^2} \frac{1}{2} \sum_{s\,r} \bar{u}_s(p_N)\, \mathcal{V}\, u_{R,r}(k)\, \bar{u}_{R,r}(k)\, \mathcal{V}^\dagger\, u_s(p_N) \\
&= \frac{1}{2} I_\Sigma \frac{p_{cm}}{8\pi k^2} Tr\left[\mathcal{V}\,(\not{k} + \sqrt{k^2})\,\mathcal{V}^\dagger\,(\not{p}_N + m_N)\right] \\
&= \frac{1}{2} I_\Sigma \left(\frac{f}{m_\varphi}\right)^2 F(k,q)^2 \frac{p_{cm}}{8\pi k^2}\,\Omega_\varphi \\
&= \frac{1}{2} I_\Sigma \frac{1}{\sqrt{k^2}} Tr\left[(\not{k} + \sqrt{k^2})\,\mathcal{I}\mathrm{m}\,\Sigma(k)\right] \quad .
\end{aligned} \tag{3.16}$$

The last line follows if Cutkoskys cutting rules (Appendix D.2.1) are employed to calculate $\Gamma_\varphi(k)$. It shows explicitly how the decay width is related to the averaged self energy $\langle\Sigma\rangle$ (cf. Appendix D.1.1). By p_{cm} the momentum of the meson in the rest frame of the decaying resonance is denoted and p_N is the four-momentum of an on-shell nucleon. The vertex function $\mathcal{V}$ is derived from the interaction Lagrangians given in the Appendices C.1.1 and C.2. In Appendix C.1.2 we give a formal definition of $\mathcal{V}$ as well as a few illustrating examples. Performing a summation over the spins of nucleon and resonance leads to the traces Ω_φ. Explicit expressions (both relativistic and non-relativistic) are found in Appendix C.1.2, Table C.5 and Table C.6 and in Appendix C.2, Table C.2. The coupling constants f are obtained by fits to the corresponding hadronic partial decay

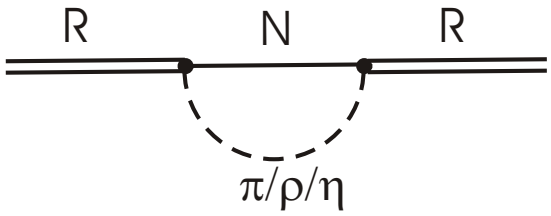

Figure 3.5: Self energy of a baryon resonance from the decay into a π, η or ρ meson.

widths given in Table A.2. The isospin factor I_Σ is 1 for Δ resonances with isospin $\frac{3}{2}$ and 3 for N^* resonances with isospin $\frac{1}{2}$ if the decay into an isovector π meson is considered. For the isoscalar η this factor is 1 and there is no coupling to Δ resonances. The two-fold degeneracy of a spin-$\frac{1}{2}$ field is taken into account with a factor $\frac{1}{2}$. The form factor $F(k,q)$ will be discussed in the paragraphs following Eq. 3.20. Note that an on-shell spinor for the decaying particle of mass k^2 has been employed, such that the completeness relation reads $\not{k} + \sqrt{k^2}$ rather than $\not{k} + M$, see Appendix B.2, Eq. B.15.

In analogy with Eq. 3.16, one obtains for spin-$\frac{3}{2}$ resonances:

$$\begin{aligned} \Gamma(k) &= \frac{1}{4}\, I_\Sigma \left(\frac{f}{m_M}\right)^2 \frac{p_{cm}}{8\pi k^2}\, \Omega_\varphi \\ &= \frac{1}{4}\, I_\Sigma \frac{1}{\sqrt{k^2}}\, Tr\left[(\not{k} + \sqrt{k^2})\, P^{\mu\nu}_{3/2}\, \mathcal{I}\mathrm{m}\, \Sigma_{\mu\nu}(k)\right] \quad , \end{aligned} \tag{3.17}$$

where the trace Ω_φ now results from the coupling of spin-$\frac{3}{2}$ resonances. By p_{cm} the momentum of the meson in the rest frame of the resonance is denoted. Spin averaging is taken into account with a factor of $\frac{1}{4}$.

When considering the decay into one stable and one unstable particle, an integration over the spectral function of the unstable particle is necessary. For a resonance with fixed mass $\sqrt{k^2}$ and spin j decaying into the $N\rho$ channel, for example, one finds:

$$\begin{aligned} \Gamma_{N\rho}(k) &= \int\limits_{4m_\pi^2}^{\left(\sqrt{k^2}-m_N\right)^2} dq^2\, \Gamma_{N\rho}(k,q)\, \mathcal{A}_\rho(q) \\ \Gamma_{N\rho}(k,q) &= \frac{1}{2\,j+1}\, I_\Sigma \left(\frac{f}{m_\rho}\right)^2 F^2(k,q)\, \frac{p_{cm}}{8\pi k^2}\, (2\,\Omega^T + \Omega^L) \quad , \end{aligned} \tag{3.18}$$

where $\Gamma_{N\rho}(k,q)$ stands for the width of a resonance for decay into a ρ meson with invariant mass $\sqrt{q^2}$. The isospin factor I_Σ is the same as for the pions. Explicit expressions for the spin-traces $\Omega^{T/L}$ are found in Table C.2, Appendix C. Again p_{cm} is the momentum of the meson in the rest frame of the resonance. Note that $\Omega^{T/L}$ and p_{cm} depend implicitly on the invariant mass $\sqrt{q^2}$ of the ρ meson.

In Table A.2 on page 193 we give a list of all resonances and their decay channels. For most states the sum $\Gamma_{\pi N} + \Gamma_{\eta N} + \Gamma_{\rho N}$ does not exhaust the total width. As an approximation we put the remaining width into the $\Delta\pi$ channel and take the energy dependence to be s-wave for negative parity states and p-wave for positive parity states. In contrast to the other decay channels we do not modify $\Gamma_{\Delta\pi}$ when going to the nuclear

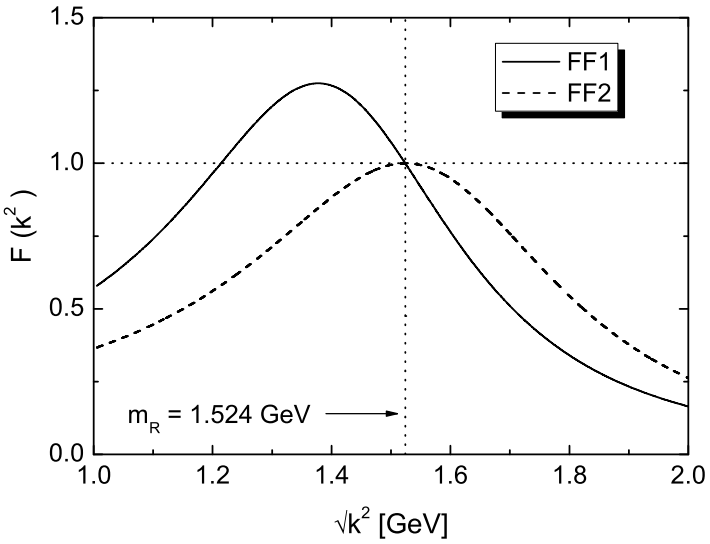

Figure 3.6: Form factor $FF1$ of Eq. 3.22 (solid line) and form factor $FF2$ of Eq. 3.23 (dashed line) for the $D_{13}(1520)$ resonance. The cutoff parameter in $FF2$ is taken to be $\Lambda = 1$ GeV, the parameters s_0 and Λ of form factor $FF1$ are listed in Table A.2.

medium. The corresponding Lagrangians are given in Appendix C.2 and lead to traces Ω^{Δ}, which are given explicitly in Table C.2. In analogy to the $N\,\rho$ width, we find for $\Gamma_{\Delta\pi}$:

$$\begin{aligned} \Gamma_{\Delta\pi}(k) &= \int\limits_{(m_N+m_\pi)^2}^{(\sqrt{k^2}-m_\pi)^2} dm^2\, \Gamma_{\Delta\pi}(k,m)\, \rho_{\Delta}(m) \qquad (3.19) \\ \Gamma_{\Delta\pi}(k,m) &= \frac{1}{2\,j+1}\, I_\Sigma \left(\frac{f}{m_\Delta}\right)^2 F^2(k,m)\, \frac{p_{cm}}{8\pi k^2}\, \Omega^{\Delta} \quad . \end{aligned}$$

The isospin factor I_Σ is 1 both for the decay of isospin-$\frac{3}{2}$ and isospin-$\frac{1}{2}$ states and $\Gamma_{\Delta\pi}(k,m)$ stands for the decay into a pion and a Δ with invariant mass m. Since the Δ resonance is a broad particle, we need to integrate over its spectral function $\rho_\Delta(m)$. As in the case of the $N\rho$ decay, the spin trace Ω^{Δ} and the cm momentum p_{cm} depend implicitly on in the invariant mass m of the pion.

We discussed before the threshold behaviour of the decay width. By inspecting the results for the traces Ω^{φ}, $\Omega^{T/L}$ and Ω^{Δ} as given in Appendix C, one can see that the correct threshold behaviour emerges in our formalism.

We write the form factor $F(k,q)$ at the resonance-meson-nucleon vertex in the following form:

$$F(k,q) \equiv F_s(k)\, F_t(q) \quad . \qquad (3.20)$$

The form factor $F_t(q)$ is a usual monopole form factor:

$$F_t(q) = \frac{\Lambda_M^2 - m_M^2}{\Lambda_M^2 - q^2} \quad . \qquad (3.21)$$

The values taken for Λ_M are listed in Table A.1. We multiply the resonance-nucleon-meson vertex with a monopole type form factor since this vertex is also used in baryon-baryon interactions, where the large space-like 4-momenta acquired by the exchange particle need to be cut off. For the decay of a resonance into a stable final state we have $q^2 = m_M^2$ and therefore $F_t(q) = 1$. For $F_s(k)$ we take different parameterizations at the $RN\rho$ and the $RN\varphi$ vertices. When considering an $RN\rho$ vertex we choose [104]

$$F_s(k) = \frac{\Lambda^4 + \frac{1}{4}(s_0 - m_R^2)^2}{\Lambda^4 + (k^2 - \frac{1}{2}(s_0 + m_R^2))^2} \quad , \tag{3.22}$$

while at the $RN\varphi$ vertex we take [104, 123]:

$$F_s(k) = \frac{\Lambda^4}{\Lambda^4 + (k^2 - m_R^2)^2} \quad . \tag{3.23}$$

In the following we will refer to the form factor of Eq. 3.22 as $FF1$ and to the form factor of Eq. 3.23 as $FF2$.

We have plotted both $FF1$ (solid line) and $FF2$ (dashed line) in Fig. 3.6. As a function of k^2 the form factor of Eq. 3.22 is asymmetric with respect to the resonance mass m_R. It is equal to unity both at $k^2 = m_R^2$ and at the decay threshold $k^2 = s_0 < m_R^2$, larger than unity within the interval $\{s_0, m_R^2\}$ and smaller outside. The exact shape depends on the cutoff Λ and the threshold parameter s_0. We give values for the cutoff Λ in Table A.2 and take $s_0 = (m_N + 2m_\pi)^2$. In the following Section we will support the somewhat unconventional form factor Eq. 3.22.

For positive energies, the imaginary part of the self energy $\mathcal{I}\mathrm{m}\,\Sigma^+_{vac}$ is obtained from the decay width via (cf. Appendix D.2.2)

$$\mathcal{I}\mathrm{m}\,\Sigma^+_{vac}(k^2) = -\sqrt{k^2}\,\Gamma(k^2) \quad . \tag{3.24}$$

Note that this self energy is averaged over the spin of the resonance, see Appendix D.1.1. The reader will have noticed that the baryon resonances are treated on a different level than the ρ meson. There we had to worry about current conservation which made it mandatory to regularize the self energy loops by means of the symmetry preserving Pauli-Villars regularization scheme. For baryon resonances these problems do not arise: this is obvious for the contribution from the pseudoscalar mesons π and η, and also the contribution from the ρN channel produces no problems, since we use current conserving couplings involving the structure $\rho_{\mu\nu} = \partial_\mu \rho_\nu - \partial_\nu \rho_\mu$, see Appendix C.1.1. Therefore we can follow a more straightforward strategy and calculate the width (which is always finite) first and furnish it with a form factor. The real part of the self energy is obtained using a dispersion integral:

$$\mathcal{R}\mathrm{e}\,\Sigma^+_{vac}(k) = \mathcal{P}\int_{\omega_{min}}^{\infty} \frac{d\omega}{\pi} \frac{\mathcal{I}\mathrm{m}\,\Sigma^+(\omega, \mathbf{k})}{\omega - k_0} - c_{vac}(\mathbf{k}) \tag{3.25}$$

with

$$c_{vac}(\mathbf{k}) = \mathcal{P}\int_{\omega_{min}}^{\infty} \frac{d\omega}{\pi} \frac{\mathcal{I}\mathrm{m}\,\Sigma^+(\omega, \mathbf{k})}{\omega - \sqrt{m_R^2 + \mathbf{k}^2}} \quad .$$

Here $\mathcal{P}$ denotes the principal value. The energy $\omega_{min} = \sqrt{(m_N + m_\pi)^2 + \mathbf{k}^2}$ follows from the threshold for the decay into $N\pi$. By m_R the mass of the resonance is denoted. As

can be inferred from Fig. 3.7, the suppression from the form factor $F(k,q)$ is sufficient to produce a decreasing width, such that the dispersion integral converges. Had we not used a form factor here, we would have had to consider multiple subtracted dispersion relations, thus potentially spoiling the normalization of the spectral function: Taking as an example the $P_{33}(1232)$, the leading subtraction would have been proportional to k_0^4, since $\mathcal{I}\mathrm{m}\,\Sigma \sim k_0^4$. According to Appendix E.2.3 the spectral function would not have been normalized any more. The subtraction $c_{vac}(\mathbf{k})$ is convenient to ensure that the physical mass of the resonance is recovered, but it is not necessary to ensure convergence of the dispersion integral.

In principle the dispersion integral extends over negative energies as well. We omit this contribution since in the nuclear medium no symmetry exists which relates $\mathcal{I}\mathrm{m}\,\Sigma^+(k_0)$ to $\mathcal{I}\mathrm{m}\,\Sigma^+(-k_0)$. This issue is addressed in Appendix E.2.3. We have checked that in the vacuum the contributions from negative energies to the dispersion integral can safely be neglected. Also in cold nuclear matter we do not expect that antibaryons are important.

3.2.3 Results for $\mathcal{R}\mathrm{e}\,\Sigma$ and $\mathcal{I}\mathrm{m}\,\Sigma$

In this Section we present results for the self energy and the propagator of baryon resonances. We start with a discussion of the $P_{33}(1232)$ and the $D_{13}(1520)$ resonances, both of which have according to the PDG [46] an on-shell width of about 120 MeV. We will see that a strong energy dependence of $\Gamma_{N\rho}$ leads to unexpected results for the spectral function. We will then discuss two more resonances, the $P_{13}(1720)$ and the $F_{35}(1905)$, both of which have a large coupling to the $N\rho$ channel.

In Fig. 3.7 we show the decay width of the $P_{33}(1232)$ and the $D_{13}(1520)$ resonances as a function of their invariant mass. Note the different scales on the y axes. The $N\rho$ width (solid line) of the D_{13} state displays a strong energy dependence, which is of kinematical origin. The resonance is below the nominal threshold for the decay at $m_N + m_\rho = 0.938 + 0.77 \approx 1.7$ GeV. Therefore the decay into this channel can only proceed via the low mass tail of the ρ meson, which in turn generates a steep increase of the width as the available phase space opens up. Since the maximum width achieved in this channel is much larger than the on-shell width we will refer to this state as subthreshold, even though this is strictly speaking incorrect.

Let us now turn to the results for the self energy and the spectral function, which are depicted in Figs. 3.8 and 3.9. From Fig. 3.8 we find that around the resonance peak the spectral functions of the $D_{13}(1520)$ and the $P_{33}(1232)$ (solid lines) obtained by a full calculation including the real part of the self energy do not differ much from those obtained by neglecting $\mathcal{R}\mathrm{e}\,\Sigma$ (dashed lines). In both cases we observe a slight squeezing of the resonance peak in the spectral function, which is more pronounced for the $D_{13}(1520)$. Going away from the resonance peak, we observe an additional shoulder for the $D_{13}(1520)$. Since this shoulder has most probably no direct influence on observables due to the large off-shellness, we are not concerned about this. The real part of the self energy of both states – indicated by the solid and the dashed lines in Fig. 3.9 – is comparable around resonance, with a slightly larger energy variation for the $D_{13}(1520)$. Away from the resonance peak we observe a strong energy variation in the real part of the self energy of the $D_{13}(1520)$ which is responsible for the additional shoulder found in the spectral function. The change of curvature at $\sqrt{k^2} - m_R \approx 0.2$ is due to the Breit-Wigner like behaviour of the imaginary part of the self energy – with a peak at roughly $\sqrt{k^2} - m_R \approx 0.3$ both for $P_{33}(1232)$

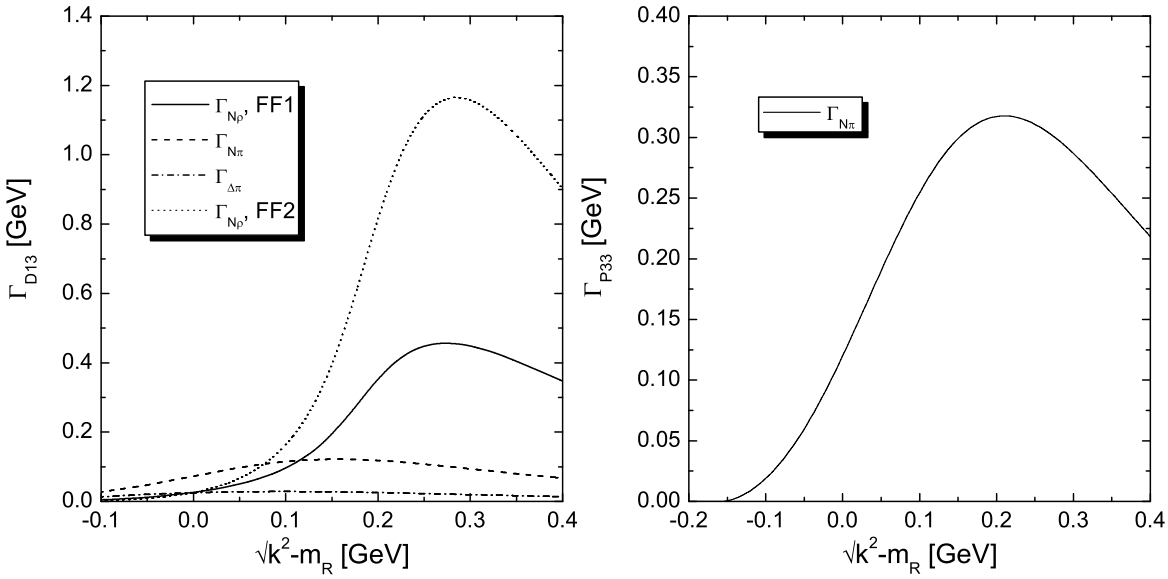

Figure 3.7: Left: Partial decay widths of the $D_{13}(1520)$. The $N\rho$ width $\Gamma_{N\rho}$ as following from form factor $FF1$ of Eq. 3.22 is indicated by the solid line, the result from form factor $FF2$ of Eq. 3.23 by the dotted line. Right: Width of the $P_{33}(1232)$ resonance in vacuum. The ρ component is negligible over the energy interval shown here and has not been plotted.

and $D_{13}(1520)$ – which has to translate into a Breit-Wigner type real part, i.e. it has to vanish around the peak. The dashed-dotted line in Fig. 3.8 shows the spectral function of the $D_{13}(1520)$ as resulting from the use of a smaller partial decay width $\Gamma_{N\rho} = 12$ MeV instead of $\Gamma_{N\rho} = 26$ MeV. Using the smaller width the shoulder nearly disappears whereas the resonance peak becomes a little bit broader. In the next paragraph we link both effects. We will come back to the issue of the proper choice for $\Gamma_{N\rho}$ in Chapter 4.

Next we address the question as to why form factor $FF2$ should be discarded at the $RN\rho$ vertex. Therefore consider the results for $\mathcal{I}\mathrm{m}\,\Sigma$, $\mathcal{R}\mathrm{e}\,\Sigma$ and the spectral function ρ, which are depicted by the dotted lines in Figs. 3.7, 3.8 and 3.9. All three curves display unsatisfying features: the $N\rho$ decay width rises very quickly to values above 1 GeV, around the resonance peak the real part of the self energy has a strong energy dependence $\partial\mathcal{R}\mathrm{e}\,\Sigma/\partial k^2$ and we observe a significant squeezing of the resonance peak in the spectral function ρ. The sum of these effects provides enough evidence to abandon form factor $FF2$ and take form factor $FF1$ instead.

These three effects are connected to each other in the following way: the rapid increase of $\Gamma_{N\rho}$ translates into a strong energy dependence of $\mathcal{R}\mathrm{e}\,\Sigma$: if $\mathcal{I}\mathrm{m}\,\Sigma$ is nearly constant around the pole of the resonance, one expects $\mathcal{R}\mathrm{e}\,\Sigma$ to be small since the contributions from below and above the pole approximately cancel. Turning this argument around implies that a rapid variation with energy leads to a sizeable $\mathcal{R}\mathrm{e}\,\Sigma$. A squeezing of the peak results which can be understood by expanding $\mathcal{R}\mathrm{e}\,\Sigma$ to first order in k^2. One gets for

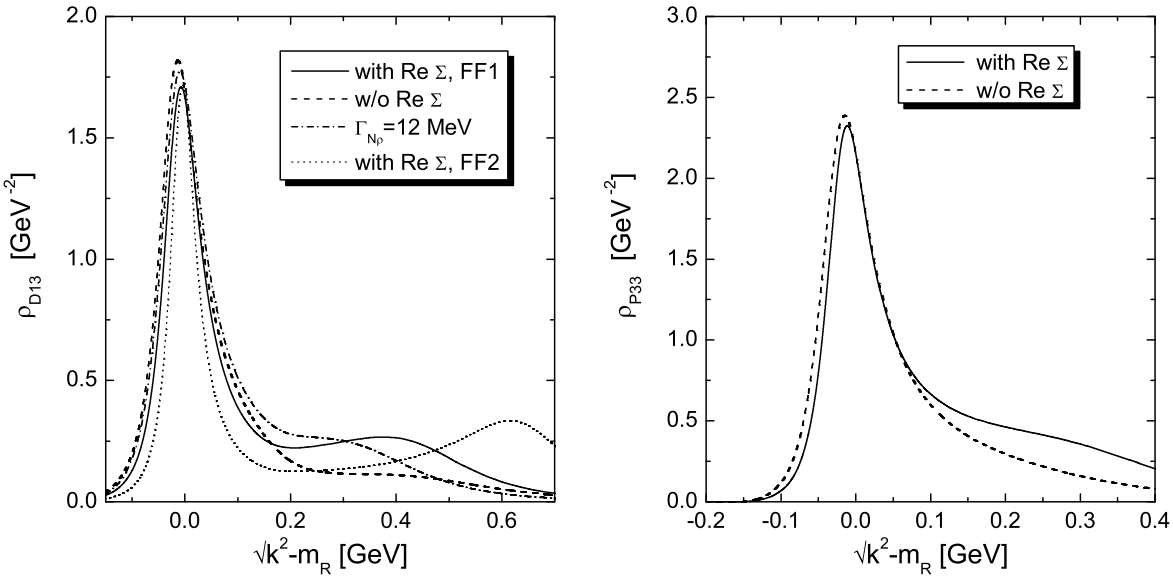

Figure 3.8: Spectral function ρ of the $D_{13}(1520)$ (left) and the $P_{33}(1232)$ resonances. In both cases the solid lines indicate the results as following from using $FF1$ for $\Gamma_{N\rho}$. The dashed line shows the spectral function without $\mathcal{R}\mathrm{e}\,\Sigma$. In the left figure, the dash-dotted curve is the spectral function of the $D_{13}(1520)$ if a value of 12 MeV for $\Gamma_{N\rho}$ is used. In the dotted curve the form factor $FF2$ of Eq. 3.23 is taken at the $RN\rho$ vertex.

the spectral function (cf. Section 3.2.4):

$$\begin{aligned} \rho(k) &\approx \frac{-1}{\pi}\frac{z^2\mathcal{I}\mathrm{m}\,\Sigma(k)}{(k^2-m_R^2)^2+z^2\mathcal{I}\mathrm{m}\,\Sigma(k)^2} \\ z &= \left(1-\frac{\partial\mathcal{R}\mathrm{e}\,\Sigma(k)}{\partial k^2}\right)^{-1}\Bigg|_{k^2=m_R^2}. \end{aligned} \tag{3.26}$$

One can infer from all three curves in Fig. 3.9 that $\partial\mathcal{R}\mathrm{e}\,\Sigma(k)/\partial k^2 < 0$ and therefore $z < 1$. This factor effectively measures the influence of $\mathcal{R}\mathrm{e}\,\Sigma$ and indicates that – depending on the energy variation of $\mathcal{R}\mathrm{e}\,\Sigma$ – strength is shifted away from the resonance peak to larger invariant masses. This explains the pronounced peak at energies around 2 GeV. Now one can also understand why form factor $FF1$ can cure this problem: its functional form restricts the energy variation of the $N\rho$ width of the $D_{13}(1520)$, which we have identified as the main source of trouble, and weakens the subthreshold character of this state. Similarly, when the smaller width of $\Gamma_{N\rho} = 12$ MeV (dash-dotted line in the left plot of Fig. 3.8) is used, the energy variation is smaller resulting in a broader peak. In the following Section 3.2.4 we will discuss the z factor in more detail. There we will also make the relation between the energy dependence of the imaginary part and the real part of the self energy more explicit. Since we do not observe significant modifications of the spectral function from the decay into a pseudoscalar meson and a nucleon, we prefer to use the more conventional form factor $FF2$ at the $RN\varphi$ vertices.

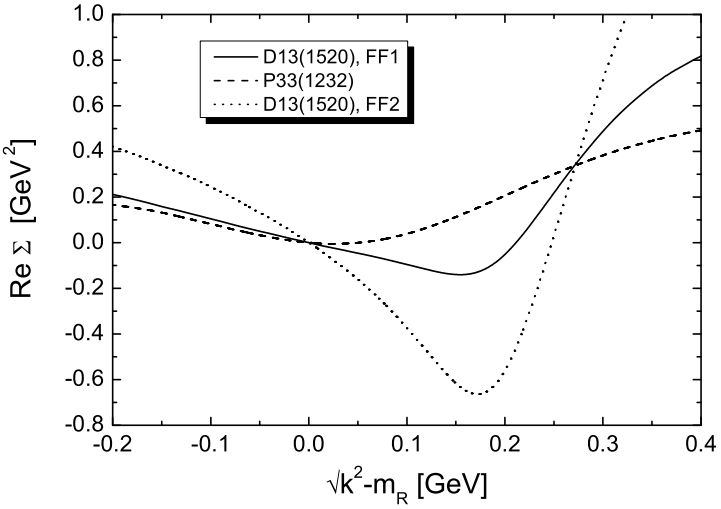

Figure 3.9: Real part of the self energy of the $D_{13}(1520)$ resonance (solid and dotted lines) and the $P_{33}(1232)$ resonance (dashed line). The solid line is obtained using form factor $FF1$ of Eq. 3.22 and the dotted line follows from form factor $FF2$ of Eq. 3.23.

Let us now turn to the other two resonances to be discussed, the $P_{13}(1720)$ and the $F_{35}(1905)$. The large decay width of $\Gamma_{N\rho} = 300$ MeV for the $P_{13}(1720)$ given in [89] also leads to problems when calculating $\mathcal{R}\mathrm{e}\,\Sigma$. Since such a large decay width seems questionable for a resonance close to the nominal $N\rho$ threshold and coupling in a p-wave to this channel, we instead use the PDG estimate $\Gamma_{N\rho} = 110$ MeV for this resonance. For a further discussion of the parameters of this resonances see Chapter 4. Like the $D_{13}(1520)$, the $P_{13}(1720)$ state is essentially subthreshold with respect to $N\rho$. In Fig. 3.10 we show the spectral function of the $P_{13}(1720)$ (left) and the $F_{35}(1905)$ (right). The latter has a large partial decay width of $\Gamma_{N\rho} = 282$ MeV, but is already far above the nominal $N\rho$ threshold. We compare a calculation with and without $\mathcal{R}\mathrm{e}\,\Sigma$. The results without $\mathcal{R}\mathrm{e}\,\Sigma$ are indicated by the dashed lines, those obtained with inclusion of $\mathcal{R}\mathrm{e}\,\Sigma$ with form factor $FF1$ ($FF2$) are shown by the solid (dotted) line. For both resonances the form factor $FF2$ leads to pronounced resonant structures away from resonance, and for the $P_{13}(1720)$ we observe a squeezing of the resonance peak, which is more or less absent for the $F_{35}(1905)$. By using the asymmetric form factor $FF1$ the resonant structures are softened into shoulders, see solid lines. In comparison to a calculation without $\mathcal{R}\mathrm{e}\,\Sigma$ (dotted lines) substantially more strength sits a invariant masses above resonance. Since the $F_{35}(1905)$ has by no means subthreshold character, the large effects from $\mathcal{R}\mathrm{e}\,\Sigma$ must be of a different origin than for the $D_{13}(1520)$. We will now address this issue by considering the normalization of the spectral functions.

In Fig. 3.11 we show the normalization integral for the four resonances discussed so far as a function of the upper integration limit k^2:

$$\mathrm{norm}(k) \;=\; \int_0^{k^2} ds\, \rho(s) \quad . \tag{3.27}$$

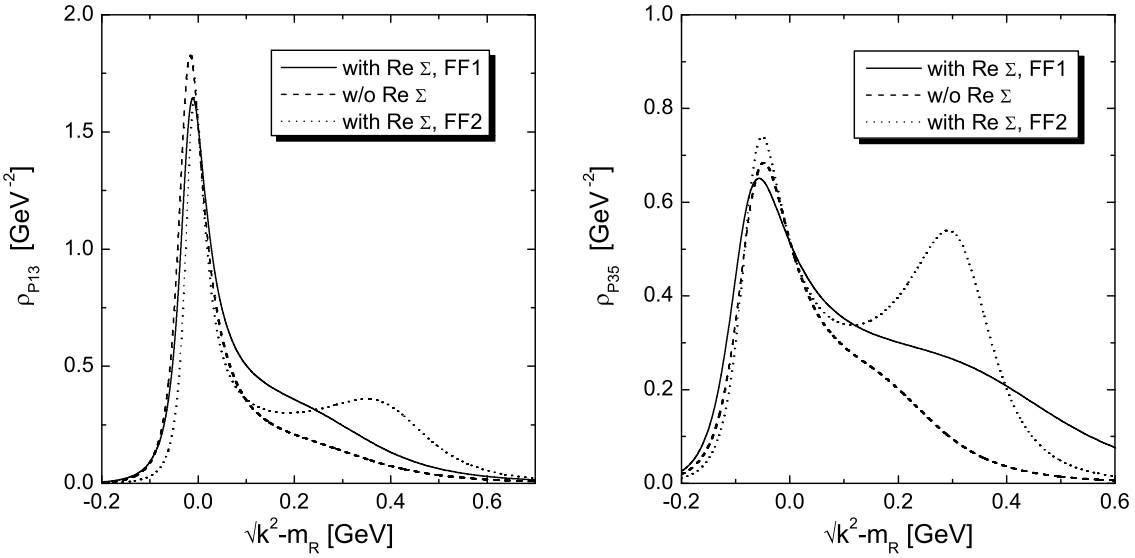

Figure 3.10: Strength function ρ of the $P_{13}(1720)$ (left) and the $F_{35}(1905)$ (right). The dashed line corresponds to a calculation w/o $\mathcal{R}\mathrm{e}\,\Sigma$, in the solid (using form factor Eq. 3.22) and dotted (using form factor Eq. 3.23) lines $\mathcal{R}\mathrm{e}\,\Sigma$ is included.

According to the discussion in Appendix E, for $k^2 \to \infty$ the normalization integral should approach unity. As can be seen, this is the case for the calculations including $\mathcal{R}\mathrm{e}\,\Sigma$ (solid lines). Neglecting $\mathcal{R}\mathrm{e}\,\Sigma$ leads to typical deviations from unity of about 15%. For the $F_{35}(1905)$ state the normalization is violated even more, if $\mathcal{R}\mathrm{e}\,\Sigma$ is not taken into account. The normalization integral converges independent of $\mathcal{R}\mathrm{e}\,\Sigma$ since the width decreases sufficiently fast at large momenta.

Let us now study the relation between the normalization integral and the cutoff parameter Λ in the form factor F_s. The value of the normalization integral depends on the form factor in the following way: increasing the cutoff parameter leads to larger values for the imaginary part of the self energy away from resonance. In this region the spectral function can be approximated by neglecting the self energy in the denominator:

$$\rho(k) \;\approx\; \frac{\mathcal{I}\mathrm{m}\,\Sigma}{(k^2 - m_R^2)^2} \quad . \tag{3.28}$$

Clearly, a larger $\mathcal{I}\mathrm{m}\,\Sigma$ away from resonances increases the value of the normalization integral.

Having established this relation between the energy dependence of $\mathcal{I}\mathrm{m}\,\Sigma$ and the normalization of the spectral function, one can interpret the results obtained for the spectral function in a new light: if without $\mathcal{R}\mathrm{e}\,\Sigma$ the normalization is smaller than one, inclusion of the real part mainly leads to the build up of a shoulder at larger invariant masses, which is necessary to bring the normalization up to unity. The best examples for this behaviour are the spectral functions of the $F_{35}(1905)$ (Fig. 3.10) and also of the $P_{33}(1232)$ (Fig. 3.8). Both states are relatively far above the respective thresholds for decay into πN or ρN. For

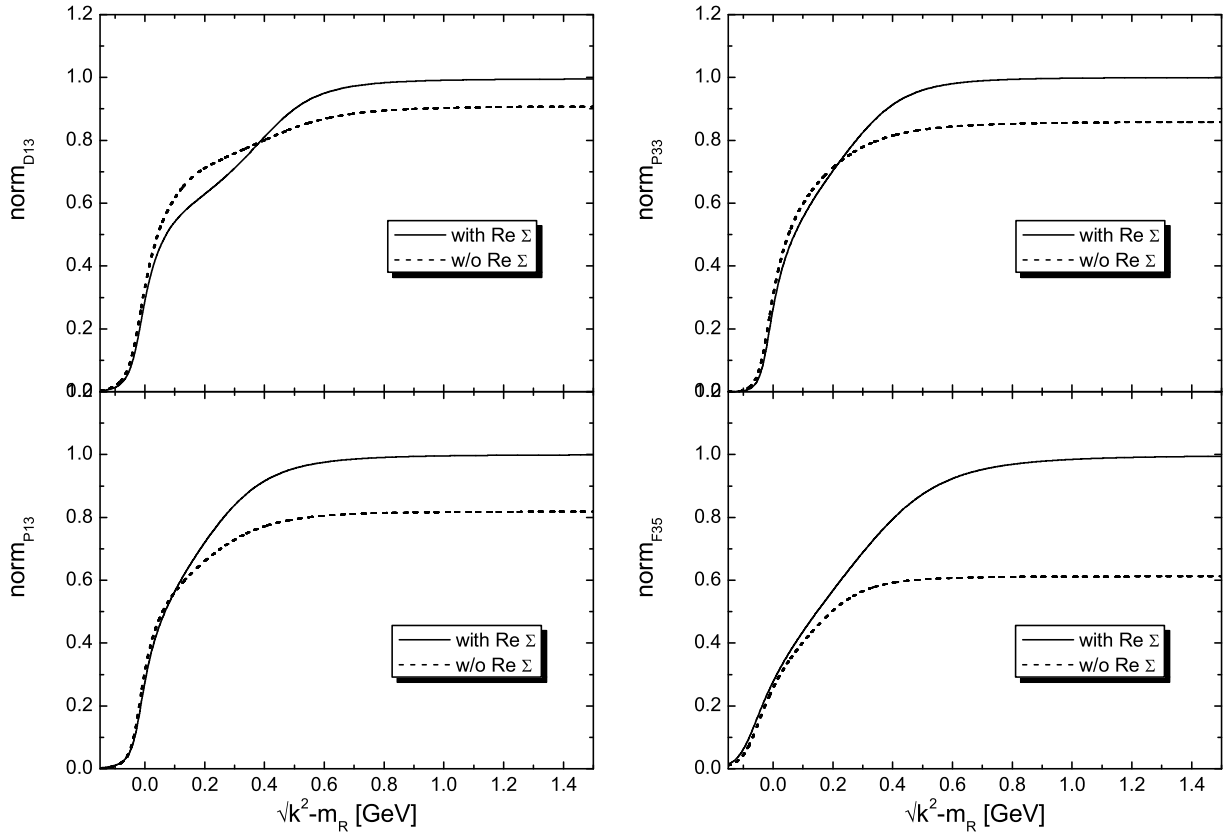

Figure 3.11: Normalization of the spectral function for different states. In the upper line the normalization of the $D_{13}(1520)$ (left) and the $P_{33}(1232)$ are depicted, in the lower line we show the normalization of the $P_{13}(1720)$ (left) and the $F_{35}(1905)$. The dashed lines correspond to a calculation neglecting $\mathcal{R}\mathrm{e}\,\Sigma$, in the dashed line $\mathcal{R}\mathrm{e}\,\Sigma$ is included and we use the form factor $FF1$ of Eq. 3.22.

the $D_{13}(1520)$ and the $P_{13}(1720)$ this build up of an additional peak is accompanied by a squeezing of the resonance peak owing to the subthreshold character of both resonances, which as we argued before leads to a strong energy dependence around the resonance pole and induces the squeezing.

If on the other hand, the normalization integral gives values larger than unity, the main effect of $\mathcal{R}\mathrm{e}\,\Sigma$ is to squeeze the resonance peak. An example of that we have already seen: the spectral function of the ρ meson in vacuum, see the dashed curve in Fig. 3.4. This observation indicates also why we find in our analysis form factors that lead to a fast decrease of the width and therefore to a spectral function, which without $\mathcal{R}\mathrm{e}\,\Sigma$ is normalized to a value smaller than one: The corresponding peaks/shoulders at larger invariant masses are not of great concern since they are probably hard to detect. On the other hand, a squeezing of the resonance peak – that would follow from larger cutoffs – is more likely to be in conflict with established properties of the resonances (for example from phase shifts).

In Fig. 3.12 we display the impact of the form factor on $\mathcal{R}\mathrm{e}\,\Sigma$ and spectral function.

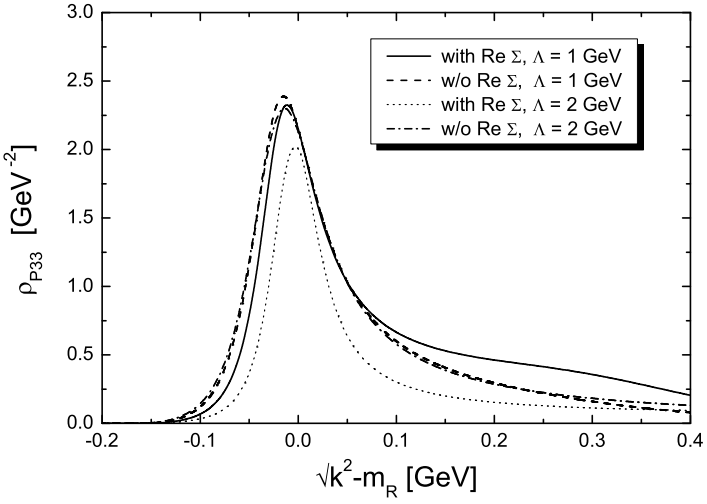

Figure 3.12: Spectral function of the $P_{33}(1232)$ in four different calculations. The solid and dashed lines indicate results obtained with $\Lambda = 1$ GeV, whereas the dotted and dash-dotted lines result from $\Lambda = 2$ GeV.

Shown are four results for the spectral function of the $P_{33}(1232)$: the solid (with $\mathcal{R}\mathrm{e}\,\Sigma$) and and the dashed lines (without $\mathcal{R}\mathrm{e}\,\Sigma$) correspond to calculations using for the cutoff $\Lambda = 1$ GeV. The same curves are shown in Fig. 3.8. For dotted (with $\mathcal{R}\mathrm{e}\,\Sigma$) and dash-dotted (without $\mathcal{R}\mathrm{e}\,\Sigma$) lines we used a larger cutoff $\Lambda = 2$ GeV, which leads to a normalization larger than unity if $\mathcal{R}\mathrm{e}\,\Sigma$ is not taken into account. One can see that the spectral functions are nearly identical if the real part of the self energy is neglected. If included, however, very different results are obtained: the smaller cutoff produces a shoulder and the larger cutoff produces a squeezing of the peak.

Finally a note on the values chosen for the cutoff parameter Λ in form factor $FF1$, Eq. 3.22: If we were interested only in a description of the spectral function in the vacuum, we could in principle use arbitrarily small values for the cutoff Λ in form factor Eq. 3.22 and thus suppress the effect from $\mathcal{R}\mathrm{e}\,\Sigma$. Due to the asymmetry in the form factor, the price to pay for a small cutoff is a large enhancement in the region $s_0 < s < m_R^2$. As a compromise, we fix the cutoff such that the enhancement induced by the squared cutoff remains smaller than 2 and if possible, i.e. if the effects on the spectral function ρ are comparatively small, we relax the cutoff even further. This way we keep some control on the effects of the form factor on the in-medium self energies of both mesons and baryons.

3.2.4 Toy Model

In this Subsection we analyse the previous results in some more detail. First we will discuss the z factor, which is most useful for the discussion of subthreshold resonances. Then we will set up a toy model that allows for the analytic evaluation of the dispersion integral and makes the relation between the imaginary part of the self energy and real part more explicit.

z Factor

Consider the spectral function ρ of a baryon resonance. Assume that around the peak of the resonance $\mathcal{R}\mathrm{e}\,\Sigma$ can be approximated by a linear Taylor expansion:

$$\begin{aligned} \mathcal{R}\mathrm{e}\,\Sigma(k) &\approx \mathcal{R}\mathrm{e}\,\Sigma(m_R^2) + (k^2 - m_R^2)\,\frac{\partial \mathcal{R}\mathrm{e}\,\Sigma(k)}{\partial k^2}\bigg|_{k^2=m_R^2} \\ &= (k^2 - m_R^2)\,\mathcal{R}\mathrm{e}\,\Sigma'(k)\big|_{k^2=m_R^2} \quad . \end{aligned} \tag{3.29}$$

The second line follows if one performs a subtraction of the self energy such that the physical mass is not shifted. With this approximation the spectral function ρ reads:

$$\begin{aligned} \rho(k) &= -\frac{1}{\pi}\,\frac{\mathcal{I}\mathrm{m}\,\Sigma(k)}{(k^2 - m_R^2 - \mathcal{R}\mathrm{e}\,\Sigma(k))^2 + \mathcal{I}\mathrm{m}\,\Sigma(k)^2} \\ &= -\frac{1}{\pi}\,\frac{z^2\,\mathcal{I}\mathrm{m}\,\Sigma(k)}{(k^2 - m_R^2)^2 + z^2\,\mathcal{I}\mathrm{m}\,\Sigma^2(k)} \quad . \end{aligned} \tag{3.30}$$

The z factor has been introduced around Eq. 3.26. For an interpretation of this quantity consider the case of a subthreshold resonance, which couples to a continuum of states above the threshold s_0 [16, 106]. Then we have for the propagator around the pole:

$$\mathcal{G}(k) = 1/(k^2 - m_R^2 - \mathcal{R}\mathrm{e}\,\Sigma(k) + i\,\epsilon) \approx z/(k^2 - m_R^2 + i\,\epsilon) \quad , \tag{3.31}$$

such that the spectral function around the pole is given by:

$$\rho(k) \approx z\,\delta(k^2 - m_R^2) \quad . \tag{3.32}$$

This situation is schematically presented in Fig. 3.13. Here the z factor gives the strength of the quasi-particle peak. Since the total strength is normalized to unity, we must have $z < 1$. This can be confirmed explicitly by calculating the derivative from a dispersion relation:

$$\mathcal{R}\mathrm{e}\,\Sigma(m_R) = \frac{1}{\pi}\,\mathcal{P}\int_{s_0}^{\infty} dl^2\,\frac{\mathcal{I}\mathrm{m}\,\Sigma(l^2)}{l^2 - m_R^2} \quad ,$$

leading to

$$\begin{aligned} \frac{\partial \mathcal{R}\mathrm{e}\,\Sigma(k)}{\partial k^2}\bigg|_{k^2=m_R^2} &= \frac{\mathcal{R}\mathrm{e}\,\Sigma(m_R^2 + \Delta) - \mathcal{R}\mathrm{e}\,\Sigma(m_R^2)}{\Delta} \\ &= \frac{1}{\pi\Delta}\int_{s_0}^{\infty} dl^2\,\mathcal{I}\mathrm{m}\,\Sigma(l)\left(\frac{1}{l^2 - m_R^2 - \Delta} - \frac{1}{l^2 - m_R^2}\right) \\ &= \frac{1}{\pi}\int_{s_0}^{\infty} dl^2\,\frac{\mathcal{I}\mathrm{m}\,\Sigma(l)}{(l^2 - m_R^2)^2} \quad . \end{aligned} \tag{3.33}$$

We have assumed that $m_R^2 < s_0$, so that there is no singularity in the integrand and the principal value integral reduces to a normal one. Since $\mathcal{I}\mathrm{m}\,\Sigma < 0$, the derivative is negative and $z < 1$.

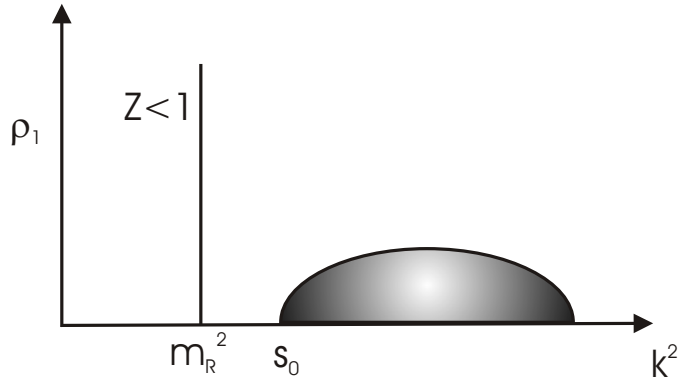

Figure 3.13: Schematic plot of the spectral function ρ in the case of a subthreshold resonance with $s_0 > m_R^2$. Besides a quasi-particle peak with strength $z < 1$ there is a continuum of states above the threshold s_0.

For broad resonances above the threshold the direct interpretation of z is lost. Somewhere in between both extremes are resonances which are subthreshold with respect to only one of their decay channels, but above the threshold for the other channels. An example is the $D_{13}(1520)$ which is (nearly) subthreshold with respect to the $N\rho$ channel, but above the decay thresholds for $N\pi$ and $\Delta\pi$.

Let us relate the findings of this Section to the case of the $D_{13}(1520)$. Applying the derivation of Eq. 3.33 to calculate the contribution of the high energy tail of the width – which we define by the condition that it sets in above resonance – to the z factor of the resonance, shows that this part of $\mathcal{I}\mathrm{m}\,\Sigma$ leads to a depletion of strength in the quasiparticle peak. The strength of the depletion scales directly with $\mathcal{I}\mathrm{m}\,\Sigma$. This is line with our findings that using the asymmetric form factor $FF1$ of Eq. 3.22 leads to less squeezing of the resonance peak: this form factor leads to smaller values of $\mathcal{I}\mathrm{m}\,\Sigma$ far away from resonance. We have now found two arguments as to why $\mathcal{R}\mathrm{e}\,\Sigma$ affects the spectral shape of the $D_{13}(1520)$, namely the energy dependence of $\mathcal{I}\mathrm{m}\,\Sigma$ around resonance and its high energy behaviour. In fact, both quantities are closely related to each other: a strong energy dependence around resonance directly imposes large values far off-shell. In the next Section we will see that indeed both effects work hand in hand in producing a small z factor.

3.2.5 Analytic Expressions

Let us now consider a model allowing to study the effects of the energy dependence of $\mathcal{I}\mathrm{m}\,\Sigma$ on $\mathcal{R}\mathrm{e}\,\Sigma$ in some detail. To this end we set up a simple parameterization of $\mathcal{I}\mathrm{m}\,\Sigma$ such that the dispersion integrals can be solved analytically. We assume that the mass of the resonance be $s_0 = 1.5\,\mathrm{GeV}^2$ GeV and the *on-shell* width $\mathcal{I}\mathrm{m}\,\Sigma(s_0) = 0.2\,\mathrm{GeV}^2$. The parameterization of the width as a function of $k^2 = s$ is split up into two intervals:

$$\mathcal{I}\mathrm{m}\,\Sigma(s) \;=\; \Theta(s-a)\Theta(b-s)\,\mathcal{I}\mathrm{m}\,\Sigma_1(s) + \Theta(s-b)\,\mathcal{I}\mathrm{m}\,\Sigma_2(s) \quad . \tag{3.34}$$

The upper and lower bounds of the interval are taken to be $a = 1\,\mathrm{GeV}^2$ and $b = 6.25\,\mathrm{GeV}^2$. We assume that in the interval $\{a, b\}$ the width is given either by a quadratic or a linear

polynomial:

$$\mathcal{I}\mathrm{m}\,\Sigma_1(s) \;=\; \begin{cases} a_1\,(s-a) & (I) \\ \\ a_2\,(s-a)^2 & (II) \end{cases} \quad . \tag{3.35}$$

The constants a_1 and a_2 are chosen such that they reproduce the *on-shell* width $\mathcal{I}\mathrm{m}\,\Sigma(s_0)$. If one assumes that the decay products are both massless, then $p_{cm} \sim s^{1/2}$ and the above polynomials correspond to a s-wave (I) or a p-wave (II) decay.

For the high energy tail $s > b$ we study two different parameterizations:

$$\mathcal{I}\mathrm{m}\,\Sigma_2(s) \;=\; \begin{cases} c_1 & (a) \\ \\ \dfrac{2\,c_1\,b}{s+b} & (b) \end{cases} \quad , \tag{3.36}$$

where $c_1 = \mathcal{I}\mathrm{m}\,\Sigma_1(b)$.

We calculate $\mathcal{R}\mathrm{e}\,\Sigma$ in the interval $\{a,b\}$ from a dispersion integral:

$$\begin{aligned} \mathcal{R}\mathrm{e}\,\Sigma(s) \;&=\; \frac{s-s_0}{\pi}\,\mathcal{P}\int_a^\infty ds' \frac{\mathcal{I}\mathrm{m}\,\Sigma(s')}{(s'-s)(s'-s_0)} \qquad (3.37) \\ &=\; \underbrace{\frac{1}{\pi}\left[\mathcal{P}\int_a^b ds' \frac{\mathcal{I}\mathrm{m}\,\Sigma_1(s')}{s'-s} - \mathcal{P}\int_a^b ds' \frac{\mathcal{I}\mathrm{m}\,\Sigma_1(s')}{s'-s_0}\right]}_{\mathcal{R}\mathrm{e}\,\Sigma_1} + \underbrace{\frac{s-s_0}{\pi}\int_b^\infty ds' \frac{\mathcal{I}\mathrm{m}\,\Sigma_2(s')}{(s'-s)(s'-s_0)}}_{\mathcal{R}\mathrm{e}\,\Sigma_2} \quad . \end{aligned}$$

Here we have split the dispersion integral into two regions. Note that the second integral is not a principal value integral since s, $s_0 < b$. The advantage of this splitting is that it allows for a Taylor expansion of $\mathcal{I}\mathrm{m}\,\Sigma_1(s)$ in the finite interval $\{a,b\}$, and all contributions except for the leading term lead to trivial polynomial integrals:

$$\mathcal{I}\mathrm{m}\,\Sigma_1(s') \;=\; \mathcal{I}\mathrm{m}\,\Sigma_1(s) + \mathcal{I}\mathrm{m}\,\Sigma_1'(s)(s'-s) + \frac{1}{2}\mathcal{I}\mathrm{m}\,\Sigma_1''(s)(s'-s)^2 \quad ,$$

$$\begin{aligned} \mathcal{R}\mathrm{e}\,\Sigma_1(s) \;&=\; \frac{1}{\pi}\,\mathcal{P}\int_a^b ds' \left[\frac{\mathcal{I}\mathrm{m}\,\Sigma_1(s)}{s'-s} + \mathcal{I}\mathrm{m}\,\Sigma_1'(s) + \frac{1}{2}\mathcal{I}\mathrm{m}\,\Sigma_1''(s)(s'-s)\right] - (s \to s_0) \\ &=\; \frac{1}{\pi}\left[\mathcal{I}\mathrm{m}\,\Sigma_1(s)\ln\left|\frac{b-s}{a-s}\right| + \mathcal{I}\mathrm{m}\,\Sigma_1'(s)\times(b-a) + \right. \qquad (3.38) \\ &\quad \left. + \frac{1}{4}\,\mathcal{I}\mathrm{m}\,\Sigma_1''(s)\times[(b-s)^2-(a-s)^2]\right] - (s \to s_0) \quad . \end{aligned}$$

The derivatives of $\mathcal{I}\mathrm{m}\,\Sigma$ follow from the parametrization I and II in Eq. 3.34. For the contribution of the high energy tail we find

$$\mathcal{R}\mathrm{e}\,\Sigma_2(s) \;=\; \begin{cases} \dfrac{c_1}{\pi}\ln\left|\dfrac{b-s_0}{b-s}\right| & (a) \\ \\ \dfrac{c_1}{\pi}\dfrac{2b}{s+b}\ln\left|\dfrac{2b}{b-s}\right| - (s \to s_0) & (b) \end{cases} \quad . \tag{3.39}$$

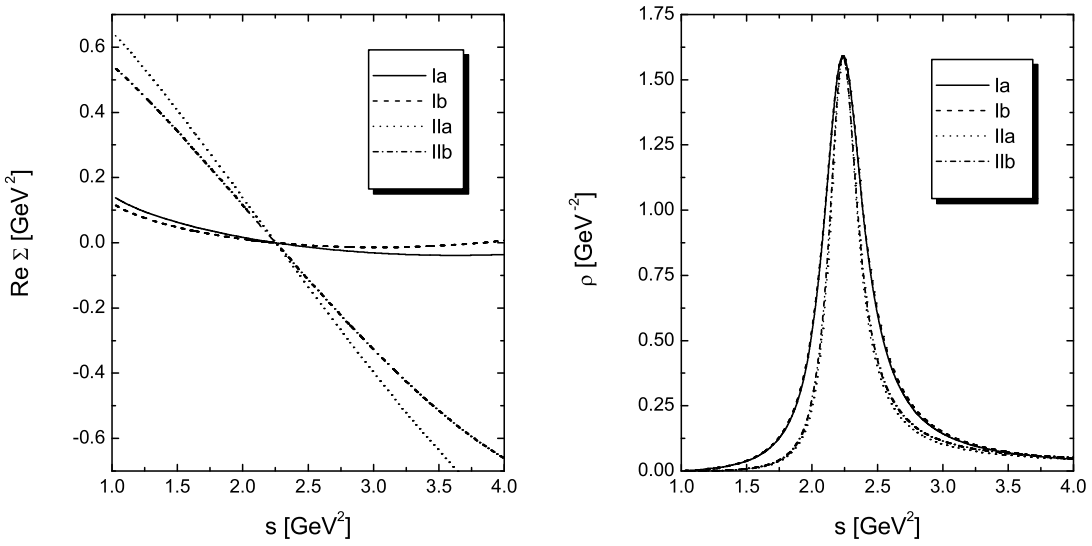

Figure 3.14: Left: real part of the self energy $\mathcal{R}\mathrm{e}\,\Sigma(s)$ for the four cases as discussed in the text. For example, the label Ia indicates that $\mathcal{I}\mathrm{m}\,\Sigma$ has been calculated using formula I in Eq. 3.34 and formula a in Eq. 3.35 and similar for the other curves. Right: Same for the spectral function $\rho(s)$.

As already discussed, it is the first derivative of $\mathcal{R}\mathrm{e}\,\Sigma$ which is responsible for the modification of the spectral shape. Within our model, we find for this quantity from Eqs. 3.38 and 3.39:

$$\begin{aligned}
\frac{\partial \mathcal{R}\mathrm{e}\,\Sigma_1(s)}{\partial s} &= \frac{1}{\pi}\left[-\mathcal{I}\mathrm{m}\,\Sigma_1(s)\frac{b-a}{(s-a)(b-s)} + \mathcal{I}\mathrm{m}\,\Sigma_1'(s)\ln\frac{b-s}{s-a} + \mathcal{I}\mathrm{m}\,\Sigma_1''(s)\frac{b-a}{2}\right] \\
&\equiv \mathcal{R}\mathrm{e}\,\Sigma_1^{0\prime} + \mathcal{R}\mathrm{e}\,\Sigma_1^{1\prime} + \mathcal{R}\mathrm{e}\,\Sigma_1^{2\prime} \qquad (3.40)
\end{aligned}$$

$$\frac{\partial \mathcal{R}\mathrm{e}\,\Sigma_2(s)}{\partial s} = \begin{cases} \dfrac{c_1}{\pi}\dfrac{1}{b-s} & (a) \\ \dfrac{c_1}{\pi}\dfrac{2b}{s+b}\left[-\dfrac{1}{s+b}\ln\dfrac{2b}{b-s} + \dfrac{1}{b-s}\right] & (b) \end{cases} \equiv \mathcal{R}\mathrm{e}\,\Sigma_2' \quad .$$

In the left plot of Fig. 3.14 we display results for $\mathcal{R}\mathrm{e}\,\Sigma(s)$ for the four scenarios $Ia - IIb$ discussed in the text. Note that around resonance the energy dependence of $\mathcal{R}\mathrm{e}\,\Sigma$ is essentially determined by the energy variation of the imaginary part, i.e. those curves using a linear s dependence (solid and dashed lines) and those using a quadratic s dependence (dotted and dashed-dotted lines) deliver very similar results, whereas the parametrization of the high energy tail, Eq. 3.35, does not have a great influence. This behaviour is also reflected in the spectral shape of $\rho(s)$, which is shown in the right plot of Fig. 3.14. Again, the differences in the results are due to the linear or quadratic s dependence of $\mathcal{I}\mathrm{m}\,\Sigma(s)$. If a quadratic s dependence is used (corresponding to parameter sets IIa and IIb), we find the normalization of ρ to be larger than one, when the real part of the self energy is neglected. This is mirrored in the squeezing of the resonance peak once $\mathcal{R}\mathrm{e}\,\Sigma$ is switched on (see dotted and dash-dotted lines in the right plot of Fig. 3.14).

In order to analyze this finding in more detail, we have calculated the z factor for each of the four combinations. Also, since our concern is to establish a direct connection between

	z	$\mathcal{R}\mathrm{e}\,\Sigma_2'$	$\mathcal{R}\mathrm{e}\,\Sigma_1^{0\prime}$	$\mathcal{R}\mathrm{e}\,\Sigma_1^{1\prime}$	$\mathcal{R}\mathrm{e}\,\Sigma_1^{2\prime}$
Ia	0.94	0.06	-0.06	0.059	0
Ib	0.96	0.046	-0.06	0.059	0
IIa	0.65	0.28	-0.06	0.12	0.21
IIb	0.69	0.19	-0.06	0.12	0.21

Table 3.1: Numerical values for the parameter z as obtained within the four models discussed in the text. Also given are the contributions to the derivative $\partial\mathcal{R}\mathrm{e}\,\Sigma(s)/\partial s$ taken at $s = m_R^2$ from the individual moments of $\mathcal{I}\mathrm{m}\,\Sigma(s)$.

the energy variation of $\mathcal{I}\mathrm{m}\,\Sigma(s)$ and that of $\mathcal{R}\mathrm{e}\,\Sigma(s)$, we give the individual contributions to $\partial\mathcal{R}\mathrm{e}\,\Sigma/\partial s$ as defined in Eq. 3.40. The results are given in Table 3.1.

The z factors confirm the conclusions from the discussion of $\mathcal{R}\mathrm{e}\,\Sigma$ and ρ: a linear s dependence of $\mathcal{I}\mathrm{m}\,\Sigma\,(s)$ produces a z factor much closer to unity as compared to a quadratic s dependence. The results for the individual contributions of the moments of $\mathcal{R}\mathrm{e}\,\Sigma(s)$ nicely confirm our assumption that it is mainly the energy variation which is responsible for the z factor. The result for $\mathcal{R}\mathrm{e}\,\Sigma_1^{0\prime}(s)$ is small and independent of the choice of the parametrization. This is understandable since only the global parameters on-shell width and the intervall limits a and b enter.Much larger contributions are derived from the derivatives of $\mathcal{I}\mathrm{m}\,\Sigma_1(s)$. In particular, the contribution from the second derivative, $\mathcal{R}\mathrm{e}\,\Sigma_1^{2\prime}$, is sizeable. The high energy tail $\mathcal{R}\mathrm{e}\,\Sigma_2(s)$ adds sizeably to the total derivative if parametrization II is employed, whereas it is rather small for parametrization I. This is due to the much higher value of $\mathcal{I}\mathrm{m}\,\Sigma(s)$ at $s = b$, which sets the overall scale for the contribution of $\mathcal{R}\mathrm{e}\,\Sigma_2(s)$ to the dispersion integral. Thus the relation between the z factor and the energy dependence of $\mathcal{I}\mathrm{m}\,\Sigma\,(s)$ is enhanced by the influence of the high energy tail. The functional form of $\mathcal{I}\mathrm{m}\,\Sigma_2(s)$ has only a moderate influence on the z factor, parametrization (a) giving a somewhat smaller result for z than parametrization (b) as $\mathcal{I}\mathrm{m}\,\Sigma_2\,(s)$ is larger in this case and - as pointed out in the discussion around Eq. 3.33 - the high energy tail per se decreases the z factor. Since all four spectral functions are normalized, for parameter sets IIa and IIb, a large amount of strength sits in the high energy tail.

In Fig. 3.15 we compare results for the spectral function obtained with and without $\mathcal{R}\mathrm{e}\,\Sigma(s)$. This is done for two parameter sets, Ia and IIa. Expect for the dotted line – corresponding to parameter set IIa with $\mathcal{R}\mathrm{e}\,\Sigma$– all calculations produce essentially identical results. Switching the real part on or off has no great impact on parametrization Ia. On the other hand, using parameter set IIa, which produces a stronger energy dependence of the imaginary part of the self energy, a substantial squeezing is introduced from $\mathcal{R}\mathrm{e}\,\Sigma$. This implies that for this curve the missing strength sits in the high energy tail. If $\mathcal{R}\mathrm{e}\,\Sigma$ is neglected the spectral function is not very sensitive on the parametrization of $\mathcal{I}\mathrm{m}\,\Sigma$.

Summarizing, in this Section we have found from a simple model that the energy dependence of the width has a significant effect on the spectral function via the real part of the self energy. By comparing a linear and a quadratic s-dependence of $\mathcal{I}\mathrm{m}\,\Sigma$ we have found that the latter leads to a substantial squeezing of the peak. Although our parametrization has not assumed a subthreshold character of the resonance, the effects of the real part of the self energy are approximated by the z factor. Analyzing the various contributions to the z factor, it turns out that both the derivatives of $\mathcal{I}\mathrm{m}\,\Sigma$ and its high

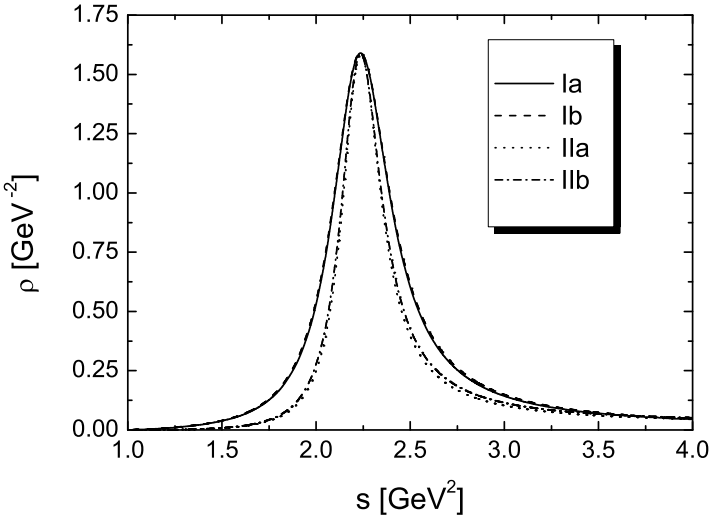

Figure 3.15: Influence of the real part of the self energy on the spectral function ρ.

energy tail give important contributions to the z factor. This analysis therefore supports our previous conjecture that the strong energy dependence of $\Gamma_{N\rho}$ is responsible for the reshaping of the spectral functions of the $D_{13}(1520)$ and the $P_{13}(1720)$.

Chapter 4

Meson Nucleon Scattering - Input from Experiment

In the low density limit, the meson self energy is proportional to the meson-nucleon forward scattering amplitude as is detailed in Chapter 5.2. Via the optical theorem (see Eq. B.38 in Appendixs B.6), the imaginary part of the forward scattering amplitude is related to the total meson nucleon cross section. Concentrating on the ρ meson we thus obtain:

$$\mathcal{I}\mathrm{m}\,\Pi_\rho \;\propto\; \sigma_{\rho N} \;=\; \sum_X \sigma_{\rho N \to X N} \quad . \tag{4.1}$$

Via detailed balance the in-medium properties of the ρ are thus partially constrained from hadronic data on the reaction $\pi N \to \rho N$. In the context of the properties of vector mesons in nuclear matter, this line of thought was first put forward in [39] and used to critically examine the results proposed in [62, 111] and has led to a readjustment of cutoff parameters in those works. Let us now discuss in how far experimental constraints are built into our model and to what extent uncertainties in the model parameters prevail.

In our model the meson self energy consists of resonance-hole loops corresponding to the assumption that meson-nucleon scattering is dominated by the excitation of intermediate resonances. In fact, it is well known that $\pi\,N$ scattering can be approximately exhausted by resonance contributions, i.e. the non-resonant background terms are comparatively small. For a demonstration we show Fig. 4.1, where total cross sections of pion induced reactions are plotted. The calculations include only resonance contributions and are taken from the PhD thesis of M. Effenberger [30]. We use this as a motivation to neglect background contributions altogether and, consequently, accept some uncertainty on the level of the scattering amplitude. While being suitable for πN scattering and possibly also ηN scattering [104, 57], a resonance picture is much less appropriate for γN reactions. There non-resonant background terms build up the main part of the amplitudes [105, 40, 95].

Experimental information enters into our model via the determination of the coupling constants at the meson-nucleon-resonance vertices. These are obtained by fitting analytical expressions for the decay widths $\Gamma_{N\pi}$, $\Gamma_{N\eta}$ and $\Gamma_{N\rho}$ to the experimentally observed values. For the coupling strength of π, η and ρ to the nucleon and at the $\Delta\,N\,\rho$ vertex we take standard values based on NN scattering, see Appendix A.

Whereas π and η are stable under the strong interaction, the ρ has a large decay width of 150 MeV. Also, the η and π_0 mesons decay electromagnetically, making them unsuitable as beam particles. This leads to the following experimental situation: information on the

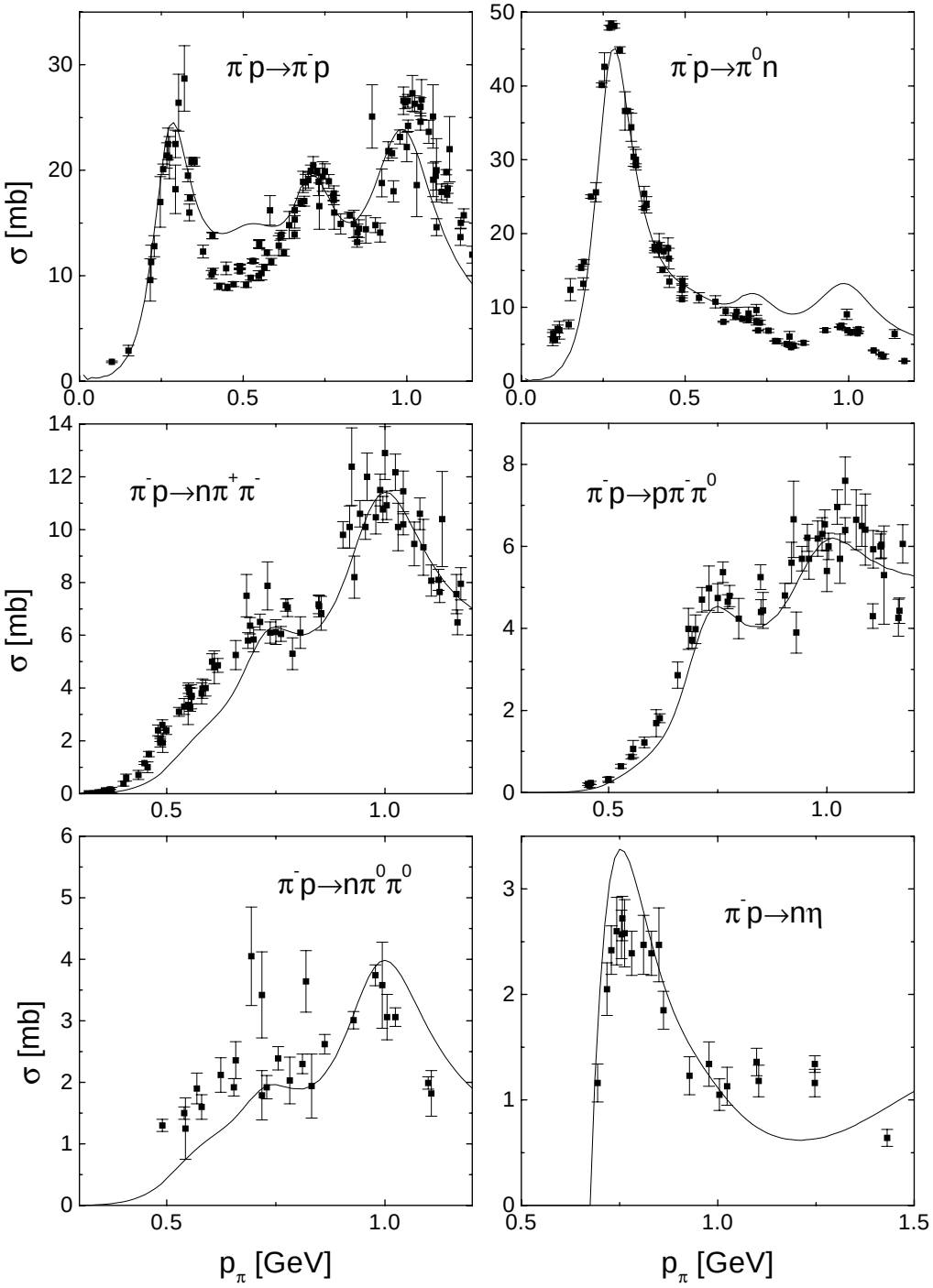

Figure 4.1: Description of pion induced reactions on the nucleon with a resonance model. The plot is taken from the PhD Thesis [30].

pion coupling to baryon resonances exists in abundance and is rather well under control, owing to the existence of π beams and the fact that a pion in the final state can easily be tracked down. Also, the η couplings are rather well established. Information of the partial decay width of resonances to these channels is obtained by fits to partial wave amplitudes as well as total and differential cross sections.

The situation is more involved for the ρ meson. Information on the coupling of baryon resonances to the $N\,\rho$ channel originates mainly from an analysis of the reaction $\pi\,N \to 2\,\pi\,N$ [90, 89, 124]. This is a formidable task as the available data base comprises several 10.000 events [90]. To simplify the problem, it is assumed that the 3-body $2\,\pi\,N$ final state may be decomposed into various 2-body isobar states, such as $\rho\,N$, $\Delta\,\pi$ or $N\,\epsilon$, which in the last step of the reaction then decay to form the $2\,\pi\,N$ state. If the total energy of the reaction is sufficiently large ($\sqrt{s} > 1.8$ GeV) to produce a ρ meson above the threshold of $m_N + m_\rho = 1.7$ GeV, the ρN contribution can safely be separated from the other isobars by means of the $2\,\pi$ invariant mass spectra. At smaller energies the ρ is identified from its angular distribution. To this end a partial anaylsis of the reaction $\pi\,N \to 2\,\pi\,N$ is carried out for the individual isobar states [90, 51, 28, 20]. These amplitude together with the well-known decay properties of the isobar states determines the angular distribution of the $2\pi N$ final state. Once a good partial wave analysis is at hand, one can proceed along the same lines as in the $\pi N \to \pi N$ case and perform a resonance fit to the partial wave amplitudes, thus determining the properties of the resonance [89, 124]. In the following we discuss the uncertainties arising in various partial wave amplitudes concerning the coupling of resonances to the $N\rho$ channel.

4.1 The D_{13} Amplitude

As it will turn out, a significant part of this work hinges on the coupling of the $D_{13}(1520)$ resonance to the $N\rho$ channel. According to the PDG, this resonance has a total width of about 120 MeV, with roughly 70 MeV decay width to the $\pi\,N$ channel and the remaining 50 MeV being split up in equal parts between the $\rho\,N$ and the $\Delta\,\pi$ isobar states (cf. Table A.2). In this work we use a value of $\Gamma_{N\rho} = 26$ MeV, as suggested by Manley *et al*[89]. In the following we give a short motivation for this choice.

Obviously, it is hopeless to determine the coupling to $\rho\,N$ by considering the invariant mass distribution, because the energy available for the ρ is at maximum $m_R - m_N \approx 580$ MeV, roughly 200 MeV less than the pole mass of the ρ. This implies, that the decay is strongly suppressed from phase space and may only happen through the low mass tail of

	data points in 1.5-1.55 GeV	isobar states considered
Manley *et al*[90]	35796	$\Delta\pi$, $N\rho$, $N\sigma$, $N^\star\pi$
Herndon *et al*[51]	25203	$\Delta\pi$, $N\rho$, $N\sigma$
Dolbeau *et al*[28]	22492	$\Delta\pi$, $N\rho$, $N\sigma$
Brody *et al*[20]	5017	$\Delta\pi$, $N\rho(\sqrt{s} > 1.6\,\text{GeV})$ + phase space

Table 4.1: Parameters of the partial wave analyses discussed in the text. Given are the number of events in the relevant energy range and the included isobar states.

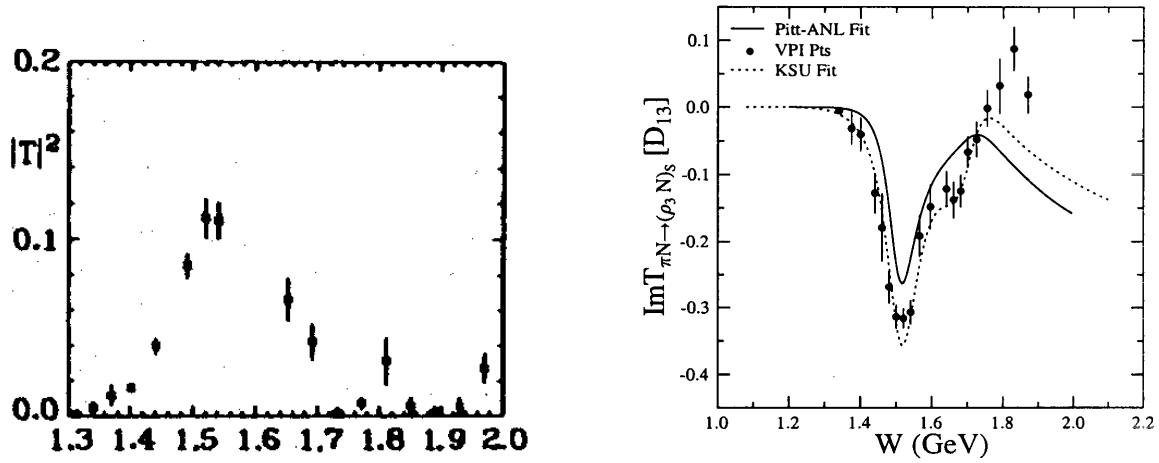

Figure 4.2: D_{13} partial wave amplitude of the reaction $\pi N \to \rho N$. Left: Squared amplitude from [51]. Right: Imaginary part from [90]. Also shown are the resonance fits from [89] and [124].

the ρ distribution. In this light it is surprising that the partial wave amplitudes show a rather clear resonant shape in the $\pi N \to \rho N$ channel in the D_{13} partial wave amplitude around the energy of this resonance, see Fig. 4.2. This is found in the works of Manley *et al*[90], Herndon *et al*[51] and Dolbeau *et al* [28]. Only in the work of Brody [20] - the oldest analysis and also the one comprising the smallest data set - no coupling is found, since below $\sqrt{s} = 1.6$ GeV the $N\rho$ contribution is set to zero and what - besides $\Delta\pi$ - remains below that threshold value is attributed to phase space. A list of the included isobar states and the size of the underlying data set of each analysis is shown in Table 4.1. Thus the picture emerging from the analysis of πN scattering is that the $D_{13}(1520)$ couples to a state with the quantum numbers of the $N\rho$ channel. However, it may be possible that some of that strength is not due to the physical ρ meson state, but to pure phase space as is suggested by the work of [20]. A clean discrimination of these two channels is not easily achieved since they lead to the same angular distribution. In spite of this ambiguity, one should keep in mind that the more quantitative analyses of [90, 28, 51] have opted to assign the full strength to the ρ meson and that the results of [20] have not been confirmed by the follow-up experiment of [28]. This is demonstrated in Fig. 4.3, where the results for the total cross section of the reaction $\pi^- p \to \rho^0 n$ as found in both works are shown together with a resonance fit resulting from the parameters as extracted by [90].

As can be inferred from Fig. 4.2, where the results of both the resonance fits of Manley *et al* [89] and Vrana *et al*[124] are displayed, a reasonable fit of the partial wave amplitudes from [90] - which does not assume any phase space contributions - can be achieved. As a result a relatively large decay width (in view of the available phase space) of the $D_{13}(1520)$ into $N\rho$ emerges. Thus, both in [89] and in [80] a partial width of 26 MeV is found, a value that we use throughout this work and that is very close to what is given in the PDG [46]. In contrast, the analysis of [124] yields a somewhat smaller value of 11 MeV. In Table A.2 and Table A.3 we give a detailed listing of the resonance parameters as found in the analyses [89] and [124].

Further support for a rather large value for $\Gamma_{N\rho}$ comes from a complementary experiment, where photo production of pion pairs on the nucleon has been measured [70]. There

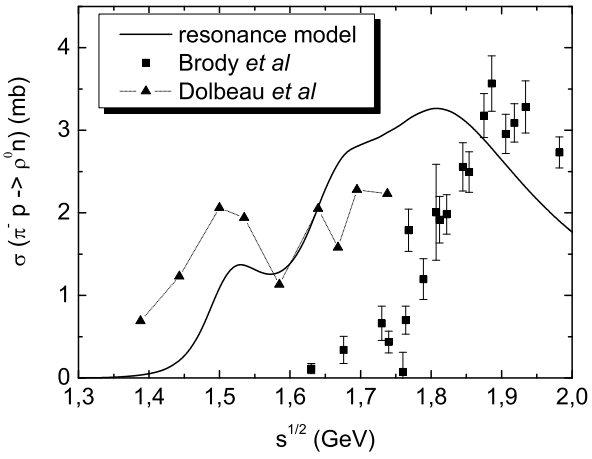

Figure 4.3: Total cross section for the reaction $\pi^- p \to \rho^0 n$. Shown are the results from the analyses of [20] and [28] in comparison to a resonance fit with the parameters of [89].

the 2π invariant mass spectra - measured at photon energies just below the nominal threshold for ρ production - follow the expected phase space distribution in the isoscalar channel ($\pi^0\pi^0$). On the other hand, in the isovector channel a systematic asymmetry, favouring larger invariant masses, is reported. An appealing interpretation of this finding assigns this asymmetry to the ρ meson, which does not couple to the isoscalar channel. In the subsequent theoretical work of [95], this conjecture has been put on a more solid basis. There a coupling of the $D_{13}(1520)$ to the $N\rho$ channel is necessary for a succesful description of two pion photo production in all isospin channels.

In [37, 84] meson-nucleon scattering is described in terms of 4-point interactions. After iterating the interaction, the resonant structures seen in experiment emerge dynamically. Fitting these structures with a Breit-Wigner type ansatz, width and mass can be compared with what is obtained in other analyses. For the decay width of the $D_{13}(1520)$ to $N\,\rho$ a value of about 6 MeV is found, smaller than the results from [89, 124]. We would like to stress the point that these different findings are not due to the different model input (resonances versus contact interactions) but result from fitting to different parameter sets. As mentioned in [37] the small width found for the $D_{13}(1520)$ is due to the fact that a direct fit of $\pi\,N \to \rho\,N$ data from [20] is performed, thus leaving the region around this resonance essentially unconstrained, whereas the larger values for $\Gamma_{N\rho}$ found in [89, 124] are derived from fits to the more exhaustive database of [90]. In [84] an even smaller coupling is obtained after the inclusion of photo-induced data to the coupled channel analysis. There the direct constraint of photo data to the hadronic $\rho\,N$ vertex results from the assumption of strict vector meson dominance (VMD). The ρ coupling strength is then essentially determined by the isovector part of the photon coupling and not from the hadronic data, which reduces the values obtained for $\Gamma_{N\rho}$ again. In principle, this in line with our finding concerning VMD as published in [110]. As we will discuss in detail in Chapter 10, already the electromagnetic and hadronic decay branching ratios hint that VMD leads to smaller predictions for $\Gamma_{N\rho}$ compared to hadronic analyses. The difference between our approach and that of [84] is whether one prefers the VMD predictions or argues that this mismatch

hints primarily on a failure of VMD on a quantitative level.

Although we cannot exclude the possibility of such a weak coupling to the $N\rho$ channel, we believe that there is enough experimental evidence supporting a rather large width $\Gamma_{N\rho}$ of the $D_{13}(1520)$. We base our calculations on $\Gamma_{N\rho} = 26$ MeV as suggested in [89]. In order to get some feeling for the sensitivity of our results on $\Gamma_{N\rho}$ we present also calculations using $\Gamma_{N\rho} = 12$ MeV reported in [124].

4.2 Other Partial Waves

Uncertainties concerning resonance parameters not only exist for the $D_{13}(1520)$ state, but for many of the high lying resonances included in this work. Fortunately, in most cases it turns out that the results are not too sensitive to changes in the parameters. This is not true, however, for the $P_{13}(1720)$ and the $D_{33}(1700)$ states, which have a large energy overlap with the $N\rho$ system.

For both resonances a large branching ratio into the $2\pi N$ final state is well established in the literature, see for example [89, 124, 104, 105]. However, so far no agreement has been reached both for the total width of the resonance and for the relative strength of $N\rho$ and $\Delta\pi$ contributions. Note first, that the decay of the $P_{13}(1720)$ to $N\,\rho$ is strongly suppressed from phase space, if one takes into account that the coupling is p-wave. In this light, the huge partial decay width assigned in [89] of about 300 MeV seems questionable. Therefore we have opted to take the PDG value $\Gamma_{N\rho} = 110$ MeV [46] for this channel, which is in agreement with the findings in [124]. For the $D_{33}(1700)$ in [89] a value of 46 MeV is found, whereas the PDG suggests a value of 120 MeV. Here we follow the results of [89]. This way we arrive at a conservative estimate concerning the influence of both states for in-medium effects.

Chapter 5

The Physics Program - Low Density Theorem and Beyond

In this work we discuss the properties of π, η and ρ mesons as well as baryon resonances in nuclear matter within a self-consistent coupled channel approach. The in-medium properties of these states are determined by their spectral functions, which in analogy to the vacuum (see Chapter 3) are given by:

$$\begin{aligned} \mathcal{A}_{med}(q) &= -\frac{1}{\pi}\mathcal{I}\mathrm{m}\,\frac{1}{q^2 - m_M^2 - \Pi^+_{vac}(q) - \Pi^+_{med}(q)} \\ \rho_{med}(k) &= -\frac{1}{\pi}\mathcal{I}\mathrm{m}\,\frac{1}{k^2 - m_R^2 - \left\langle \Sigma^+_{med}(k)\right\rangle} \quad , \quad . \end{aligned} \tag{5.1}$$

where m_M and m_R stand for the mass of the meson or baryon resonance, respectively. The notation for meson and baryon self energies is different: while within our model in the meson sector a clear separation of vacuum and in-medium contributions is possible, the in-medium self energy of baryon resonances is based on the same Feynman diagrams as in the vacuum, thus not allowing for a clear separation of both contributions. We therefore denote by $\left\langle \Sigma^+_{med}\right\rangle$ the full self energy in the medium. The brackets denote that we consider an averaged self energy as explained in Appendix D.1. From now it is understood that the baryon self energy is always obtained in an averaged sense even when not explicitly mentioned.

Similar to the vacuum case, the calculation of the in-medium self energy proceeds in three steps: we first obtain the imaginary part of the self energy for positive energies, using Cutkoskys cutting rules. By implying anti-symmetry of $\mathcal{I}\mathrm{m}\,\Pi$ we are able to write down a dispersion relation, yielding $\mathcal{R}\mathrm{e}\,\Pi$. As already mentioned in the introduction of Chapter 3 and as further detailed in Appendix E, for baryon resonances the antisymmetry of $\mathcal{I}\mathrm{m}\,\Sigma$ found in the vacuum does not carry over to the nuclear medium. Therefore we neglect there the negative energy contribution to the dispersion integral. In the remainder of this Chapter we will lay out the details of these calculations.

5.1 Breaking of Lorentz invariance

In this section we discuss two properties of the in-medium self energy of baryons and mesons. Whereas in the vacuum a meson is by a four-vector $q_\mu = (q_0, \mathbf{q})$, the description

of mesons in nuclear matter requires another four-vector, n_μ, characterizing the medium. As a consequence, the self energy depends in general not only on q^2, but also on two other Lorentz invariant structures which can be build up from q_μ and n_μ: $q.n$ and $n.n$. A convenient choice is to evaluate n_μ in the rest frame of nuclear matter

$$n_\mu = (m_N, 0) \quad . \tag{5.2}$$

Then $q.n = q_0\, m_N$ and the self energy is a function of both energy q_0 and the invariant mass q^2. Alternatively, one can formulate the self energy as a function of energy q_0 and 3-momentum $\mathbf{q}$ as measured in the rest frame of nuclear matter, $\Pi_{med} = \Pi_{med}(q_0, \mathbf{q})$. The same argument holds for baryons and we have $\Sigma_{med} = \Sigma_{med}(k_0, \mathbf{k})$.

In the case of particles with spin, there is a further implication due to the presence of nuclear matter. In the vacuum the self-energy does not depend on the polarization, i.e. the projection of the spin onto the 3-momentum. An intuitive explanation is that one may always perform a Lorentz boost to the rest frame of the particle, where all polarizations coincide. In nuclear matter, the situation is more complicated and the self energy depends also on the polarization. Boosting to the rest frame of the particle does not help any more, since a polarization can be defined with help of the 4-vector n_μ. As a result, at finite 3-momenta one has to consider several self energies and spectral functions. For a particle at rest in nuclear matter these quantities become degenerate.

For vector mesons the existence of several spectral functions is related to the fact that with the 4-vectors q_μ and n_μ two current conserving projectors can be constructed [16, 106], whereas in the vacuum only one such structure exists. These projectors are given in Appendix B.3. Therefore we have to calculate two independent self energies and spectral functions for vector mesons, which become degenerate in the limit $\mathbf{q} = 0$.

In the case of baryon resonance, we average the self energy as detailed in Appendix D.1. Therefore we loose the information on the spin-dependence of the self energy and the spectral function. Since both the realization of a polarized resonance state in a nuclear medium and its detection are impossible, however, this approximation does not lead to a loss of important information.

5.2 Mesons

Let us now calculate the contribution to the meson self energy in nuclear matter due to the excitation of a resonance. This process is depicted in Fig. 5.1. A qualitative analysis of the underlying physical processes can be found in Chapter 2. Before presenting the final formulae used for the numerical calculations, we will start with a simple model, showing the general philosophy of the framework. As a result, the *low density theorem* [29, 81] will emerge.

5.2.1 The Low Density Theorem

Assume that the coupling of a pseudoscalar meson φ of mass m_M to a baryon resonance is described by the relativistic Lagrangian:

$$\mathcal{L} = g\, \bar{\psi}_R\, \psi_N\, \varphi + h.c. \quad . \tag{5.3}$$

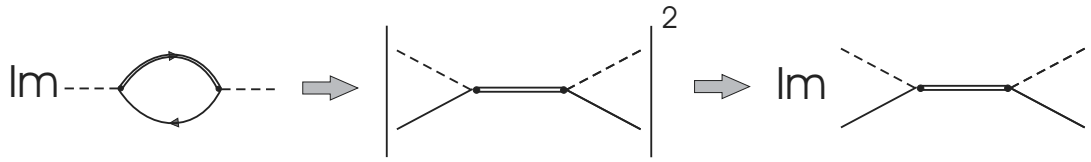

Figure 5.1: Going from the self energy (left) via the total cross section (right) to the imaginary part of the forward scattering amplitude.

Such a Lagrangian is appropriate for the coupling of a resonance with the quantum numbers $J^\pi = \frac{1}{2}^-$ to pions. The isospin coupling is of the form $\chi^\dagger \sigma \chi \varphi$, yielding an additional factor $I_\Pi = 2$ for the self energy if an isovector meson is considered.

We use relativistic propagators for nucleon-hole and resonance (cf. Appendix B.5):

$$\begin{aligned} -i\,\mathcal{G}_N(p) &= \frac{n(\mathbf{p})}{2E_N(\mathbf{p})}\,\frac{\not{p}+m_N}{p_0 - E_N(\mathbf{p}) - i\epsilon} \\ -i\,\mathcal{G}_R(k) &= \frac{\not{k}+\sqrt{k^2}}{k_0^2 - E_R^2(\mathbf{k}) - \Sigma(k)} \quad . \end{aligned}$$

The on-shell energies of nucleon and resonances are given by $E_N(\mathbf{p})$ and $E_R(\mathbf{k})$. The factor $\sqrt{k^2}$ (instead of m_R) in the numerator of $\mathcal{G}_R(k)$ will be explained in Section 5.2.4 and $\Sigma(k)$ is the averaged vacuum self energy of the resonance, calculated according to the results of Chapter 3 and Appendix D.1.1. For the Fermi distribution function one has $n(\mathbf{p}) = \theta(p_F - |\mathbf{p}|)$. Note that for the nucleon we only keep the hole-propagator. The contribution from the particle part vanishes and the antiparticle contribution becomes relevant only at meson masses around the threshold for decay into $N\bar{N}$ pairs.

With p the 4-momentum of the nucleon, q that of the meson and $k = p + q$ the 4-momentum of the resonance, the application of Feynman rules, Appendix B, leads to the following expression for the meson self energy:

$$\begin{aligned} -i\,\Pi(q_0,\mathbf{q}) &= I_\Pi \int \frac{d^4p}{(2\,\pi)^4}\,(-i\,g)^2\,Tr\left[\mathcal{G}_N(p)\mathbb{1}\,\mathcal{G}_R(k)\mathbb{1}\right]\,(-1) \qquad (5.4) \\ \Pi(q_0,\mathbf{q}) &= -i\,I_\Pi\,g^2 \int \frac{d^4p}{(2\,\pi)^4}\,\frac{n(\mathbf{p})}{2E_N(\mathbf{p})}\,\frac{\Omega}{(p_0 - E_N(\mathbf{p}))(k_0^2 - E_R^2(\mathbf{k}) - \Sigma(k))} \quad . \end{aligned}$$

The factor (-1) in the first line is due to the fact that one has a fermion loop. By Ω we denote the trace arising from the spin-summation, which is necessary since the Dirac indices form a closed loop and the vertex factor $\mathbb{1}$ is derived from the Lagrangian of Eq. 5.3:

$$\Omega \;=\; Tr\left[(\not{p}_N + m_N)(\not{k} + \sqrt{k^2})\right] \;=\; 4\,\sqrt{k^2}(E_N^{cm} + m_N) \quad ,$$

where $E_N^{cm} = \sqrt{m_N^2 + p_{cm}^2}$ is calculated in the rest frame of the resonance. For the remainder of this Section we will only keep the leading non-relativistic term

$$\Omega \;\rightarrow\; 8\,\sqrt{k^2}\,m_N \quad ,$$

where corrections of the order p_{cm}/m_N have been neglected. It can be derived from the non-relativistic Lagrangian:

$$\mathcal{L} = g\,\psi_R^\dagger\,\psi_N\,\varphi + h.c. \quad .$$

Using Cutkoskys cutting rules (cf. Appendix D.2), the imaginary part of the self energy is given by:

$$\begin{aligned}
\mathcal{I}\mathrm{m}\,\Pi(q_0,\mathbf{q}) &= -\frac{1}{2}\,I_\Pi\,g^2\int\frac{d^4p}{(2\,\pi)^4}\,\frac{n(\mathbf{p})}{2E_N(\mathbf{p})}\,(2\pi\,i)\,\delta(p_0-E_N)\,(-2\pi\,i)\,\rho(k)\,\Omega \\
&= I_\Pi\,g^2\int\frac{d^3p}{(2\,\pi)^3}\,\frac{n(\mathbf{p})}{2\,E_N(\mathbf{p})}\,\mathcal{I}\mathrm{m}\,\frac{\Omega}{k_0^2-E_R^2(\mathbf{k})-\Sigma(k)} \qquad (5.5)\\
&\approx \frac{1}{2m_N}\,I_\Pi\,g^2\,\frac{\rho}{4}\,\mathcal{I}\mathrm{m}\,\frac{\Omega}{k_0^2-E_R^2(\mathbf{k})-\Sigma(k)} \quad .
\end{aligned}$$

Here $\rho(k)=-\frac{1}{\pi}\mathcal{I}\mathrm{m}\,\frac{1}{k_0^2-E_R^2(\mathbf{k})-\Sigma(k)}$. In the last step we have made the approximation – valid at small densities – that the dependence of the integrand on the nucleon momentum $\mathbf{p}$ can be neglected such that it can be pulled out of the integral. In spin-isospin symmetric nuclear matter – to which we will confine ourselves throughout this work – the remaining integral then gives a factor of $\rho/4$. As demonstrated in Appendix D.1.1, the imaginary part of the resonance self energy from the decay into $N\,M$ is given by:

$$-\mathcal{I}\mathrm{m}\,\Sigma/\sqrt{k^2} \;=\; \Gamma_R(k^2) \;=\; \frac{q_{cm}}{8\,\pi\,k^2}\,\frac{1}{2}\,|\mathcal{M}^2| \;=\; \frac{q_{cm}}{8\,\pi\,k^2}\,g^2\,4\,m_N\,\sqrt{k^2}\,I_\Gamma \quad .$$

For the isospin factor we have $I_\Gamma=3$ and q_{cm} is the cm momentum of the final states. The factor $4\,m_N\,\sqrt{k^2}$ is a remnant of the non-relativistic reduction.

Let us now discuss how this formula translates into the well known collisional broadening, relating the width to the total cross section of that particle on a nucleon [32, 65]:

$$\Gamma_{coll} \;=\; \rho\,v\,\sigma_{MN} \quad .$$

Assuming again that the MN interaction is exhausted by a single resonance, we get:

$$\begin{aligned}
\sigma_{MN} &= \frac{1}{\text{flux}}\,\frac{1}{4}\,|\mathcal{M}|^2\;\Phi_2 \\
&= I_\sigma\,\frac{1}{4\,q_{cm}\,\sqrt{s}}\,2\,g^4\;|G_R|^2\;4\,m_N^2\,\frac{q_{cm}}{4\,\pi\,\sqrt{s}} \;=\; I_\sigma\,\frac{m_N^2}{2\,s\,\pi}\,g^4\;|G_R|^2 \\
&\Rightarrow \qquad (5.6)\\
\mathcal{I}\mathrm{m}\,\Pi(q_0,\mathbf{q}) &= -\rho\,\sigma_{\pi N}\,q_{cm}\,\frac{\sqrt{s}}{m_N} \;=\; -\rho\,\sigma_{\pi N}\;q_{lab} \quad .
\end{aligned}$$

Here, Φ_2 stands for the 2-body phase space, Appendix B.6. The isospin factor for the squared matrix element is $I_\sigma=6$. Identifying $\mathcal{I}\mathrm{m}\,\Pi=-q_0\,\Gamma$ (see Appendix D.2.2), the desired result for Γ_{coll} is obtained. From this derivation it is clear that one thus obtains the width of the meson in the rest frame of nuclear matter. If one needs the width in the rest frame of the meson, one has to multiply the above formula for Γ by a factor $q_0/\sqrt{q^2}$. The relation between self energy and total cross section is shown in the left and middle diagram of Fig. 5.1. The Eq. 5.6 has the intuitive interpretation that by scattering processes – elastic or inelastic – the meson is converted into another state, which is akin to saying that is has decayed.

The same expression could have been obtained by using the optical theorem:

$$\sigma \;=\; \frac{1}{2\,q_{cm}\,\sqrt{s}}\,\mathcal{I}\mathrm{m}\,\mathcal{M}_{forward} \quad ,$$

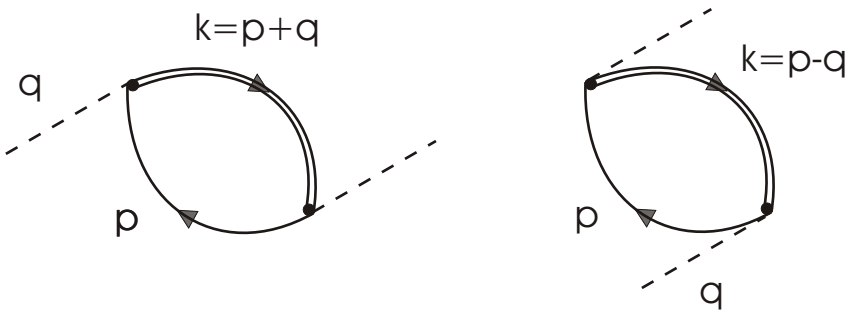

Figure 5.2: Feynman diagram representing the resonance hole excitation. Left: s-channel contribution. Right: u-channel contribution. The double-line stands for any of the resonances or a nucleon. The meson lines represent any of π, η or ρ meson.

which implies a relation between the spin/isospin averaged forward scattering amplitude $\mathcal{M}$ and the self energy (see also right diagram in Fig. 5.1)

$$\mathcal{I}\mathrm{m}\,\Pi \;=\; -\rho\,\frac{1}{2\,m_N}\,\mathcal{I}\mathrm{m}\,\mathcal{M}_{forward} \quad . \tag{5.7}$$

The last equation also explains why the *low density theorem* is sometimes referred to as the $\rho\,\mathcal{T}$ approximation (with $\mathcal{T}$ rather than $\mathcal{M}$ being the forward scattering amplitude). In an alternative derivation of the *low density theorem* one would calculate the forward scattering amplitude and compare it directly to the self energy.

5.2.2 Full Expressions for Π_{med}

In this Section we give the full expressions for the contributions to the self energy of ρ, π and η mesons as following from the excitation of one resonance. The corresponding Feynman graphs are depicted in Fig. 5.2, where the left graph is the s-channel contribution and the right graph is the u-channel contribution.

Let us begin with the calculation of the s-channel contribution, left diagram in Fig. 5.2. We will first show in detail, how the calculation is done for a pseudoscalar meson φ coupling to a resonance with the quantum numbers $J^\pi = \frac{1}{2}^+$. The interaction Lagrangian is given by:

$$\mathcal{L} \;=\; \frac{f}{m_\varphi}\,\bar{\psi}_R\,i\,\gamma^5\,\gamma^\mu\,\psi_N\,\partial_\mu\varphi \quad ,$$

leading to the vertex factor (see Appendix C.1.2)

$$\mathcal{V} \;=\; \pm\gamma^5\,\gamma^\mu\,q_\mu \quad .$$

The sign depends on whether an incoming or an outgoing meson is considered.

As usual, we denote the 4-momentum of meson, nucleon and resonance by q, p and k, respectively. Momentum conservation requires that $q + p = k$. Using standard Feynman

rules, we get in agreement with Eq. 5.4 for the self energy:

$$\begin{aligned}\Pi_\varphi(q_0,\mathbf{q}) &= -i\,I_\Pi\left(\frac{f}{m_\varphi}\right)^2\int\frac{d^4p}{(2\,\pi)^4}\,\frac{n(\mathbf{p})}{2\,E_N(\mathbf{p})}\,\frac{Tr\left[\mathcal{V}(\not{p}_N+m_N)\,\mathcal{V}^\dagger\,(\not{k}+\sqrt{k^2})\right]}{(p_0-E_N(\mathbf{p}))(k_0^2-E_R^2(\mathbf{k})-\Sigma(k))} \qquad (5.8)\\ &= -i\,I_\Pi\left(\frac{f}{m_\varphi}\right)^2\int\frac{d^4p}{(2\,\pi)^4}\,\frac{n(\mathbf{p})}{2\,E_N(\mathbf{p})}\,\frac{\Omega^\varphi}{(p_0-E_N(\mathbf{p}))(k_0^2-E_R^2(\mathbf{k})-\Sigma(k))} \quad .\end{aligned}$$

Applying Cutkosky's cutting rules to this expression, we obtain for the imaginary part of the self energy:

$$\mathcal{I}\mathrm{m}\,\Pi_\varphi(q_0,\mathbf{q}) = I_\Pi\left(\frac{f}{m_\varphi}\right)^2\int\frac{d^3p}{(2\,\pi)^3}\,\frac{n(\mathbf{p})}{2\,E_N(\mathbf{p})}\mathcal{I}\mathrm{m}\,\frac{\Omega^\varphi}{k_0^2-E_R^2(\mathbf{k})-\Sigma(k)} \quad .$$

The isospin factor I_Π is calculated from the isospin part of the Lagrangian and is $I_\Pi = 2$ for isospin-$\frac{1}{2}$ and $I_\Pi = 4/3$ for isospin-$\frac{3}{2}$ resonances if pions or are considered. For the isoscalar η we have $I_\Pi = 2$. In addition we multiply the self energy with the form factor $F(k,q)$ (not shown explicitly) of Eq. 3.20, Chapter 3.2. When considering the coupling of meson φ to other resonances, only the corresponding interaction Lagrangians – leading to the spin traces Ω^φ – and resonance propagators have to be modified. When we refer to a non-relativistic calculation of the meson self energy, a calculation is meant where the traces Ω^φ are obtained from non-relativistic Lagrangians. We have given an explicit example for that in the previous Section. Explicit expressions for Ω^φ are given in Appendix C.

The transverse and the longitudinal self energy of the ρ meson, Π_ρ^T and Π_ρ^L, are obtained by contracting the three-transverse and three-longitudinal projectors $T^{\mu\nu}$ and $L^{\mu\nu}$, respectively, with the self energy tensor $\Pi_{\mu\nu}$ (cf. Appendix D.1.1):

$$\begin{aligned}\Pi_\rho^T &= \frac{1}{2}\,T^{\mu\nu}\,\Pi_{\mu\nu} \qquad (5.9)\\ \Pi_\rho^L &= L^{\mu\nu}\,\Pi_{\mu\nu} \quad .\end{aligned}$$

The projectors are given explicitly in Appendix B.3. We then find for the self energy of the ρ meson:

$$\Pi_\rho^{T/L}(q_0,\mathbf{q}) = -i\,I_\Pi\left(\frac{f}{m_\rho}\right)^2\int\frac{d^4p}{(2\,\pi)^4}\,\frac{n(\mathbf{p})}{2\,E_N(\mathbf{p})}\,\frac{\Omega^{T/L}}{(p_0-E_N(\mathbf{p}))(k_0^2-E_R^2(\mathbf{k})-\Sigma(k))} \quad ,$$

$$\mathcal{I}\mathrm{m}\,\Pi_\rho^{T/L}(q_0,\mathbf{q}) = I_\Pi\left(\frac{f}{m_\rho}\right)^2\int\frac{d^3p}{(2\,\pi)^3}\,\frac{n(\mathbf{p})}{2\,E_N(\mathbf{p})}\,\mathcal{I}\mathrm{m}\,\frac{\Omega^{T/L}}{k_0^2-E_R^2(\mathbf{k})-\Sigma(k)} \quad . \qquad (5.10)$$

The isospin factor I_Π is calculated from the isospin part of the Lagrangian and is $I_\Pi = 2$ for isospin-$\frac{1}{2}$ and $I_\Pi = 4/3$ for an isospin $\frac{3}{2}$ resonance. As for the pseudoscalar mesons, we multiply the form factor $F(k,q)$ (not displayed explicitly 5.10), see Chapter 3, Eq. 3.20. The spin traces $\Omega^{T/L}$ are given in Appendix C.

We do not explicitly calculate the u-channel diagram. It does not have an imaginary part for positive meson energies $q_0 > 0$ and we will show later in this Section that its real part is generated automatically when a dispersion relation is used to obtain the real part of the self energy. In order to see that the imaginary part of the u-channel diagram is zero

for positive energies, we calculate the invariant mass k_u^2 of the intermediate resonance for a u-channel process. We get for k_u^2:

$$k_u^2 \;=\; (p-q)^2 \;=\; m_N^2 + q^2 - 2\,m_N\,q_0 \;=\; (m_N - q_0)^2 - \mathbf{q}^2 \;\leq\; m_N^2 \quad . \tag{5.11}$$

The imaginary part of the self energy only opens up above the threshold of $\mathcal{I}\mathrm{m}\,\Sigma(k)$, i.e. for invariant masses $> (m_N + m_\pi)^2$. Since $k_u^2 < m_N^2$, it follows that the contribution from the u-channel to the imaginary part of the self energy is zero.

The complete self energy is given as the sum of these individual contributions. A complete list of the resonances which are taken into account is given in Table A.2. We include all resonances which have a sizeable coupling to either of the mesons that are considered in this work. As for the parameters mass and decay width we follow with one exception the parametrization of Manley *et al* [89]. This exception is the $P_{13}(1720)$ resonance, for details see Section 4. The coupling constants f are fitted to reproduce the partial decay widths.

Apart from the resonance excitations, we also take into account the conversion of mesons into nucleon-hole loops. This is done in a strictly non-relativistic manner. The non-relativistic interaction Lagrangian is given in Appendix C.2, Eq. C.17. Since the nucleon is stable, the integration over the Fermi distribution can be performed analytically and one finds [33]:

$$\Pi_M^N(q_0, \mathbf{q}) \;=\; 4\,\mathbf{q}^2 \left(\frac{f_{NNM}}{m_M}\right)^2 U_N(q)\, F_t^2(q) \quad . \tag{5.12}$$

Here M stands for either π, η or ρ meson and the coupling constants f_{NNM} are given in Table A.1 in Appendix A. The form factor $F_t(q)$ is defined in Eq. 3.21 in Chapter 3.2, the corresponding cutoff parameters are listed in Table A.1. The Lindhart function $U_N(q)$, consisting of s and u channel contributions, is given explicitly by [33, 119]:

$$\begin{aligned} U_N(q) \;&=\; \int \frac{d^3p}{(2\pi)^3} \left\{ \frac{n(\mathbf{p})(1-n(\mathbf{p}+\mathbf{q}))}{q_0 - E(\mathbf{p}+\mathbf{q}) + E(\mathbf{p}) + i\epsilon} + \frac{n(\mathbf{p}+\mathbf{q})(1-n(\mathbf{p}))}{-q_0 - E(\mathbf{p}) + E(\mathbf{p}+\mathbf{q}) + i\epsilon} \right\} \\ &=\; \frac{m\,p_F}{\pi^2} \left\{ -1 + \frac{1}{2q}\left[1 - (\nu/q - \frac{1}{2}q)^2\right] \ln\left(\frac{\nu/q - \frac{1}{2}q + 1}{\nu/q - \frac{1}{2}q - 1}\right) - \right. \\ &\quad \left. \frac{1}{2q}\left[1 - (\nu/q + \frac{1}{2}q)^2\right] \ln\left(\frac{\nu/q + \frac{1}{2}q + 1}{\nu/q + \frac{1}{2}q - 1}\right) \right\} \end{aligned} \tag{5.13}$$

$$\mathcal{I}\mathrm{m}\,U_N(q) \;=\; \begin{cases} -\dfrac{2\,m_N\,p_F}{4\pi q}\left[1 - \left(\dfrac{\nu}{q} - \dfrac{1}{2}q\right)^2\right] & \text{for} \quad q > 2\ ,\ \frac{1}{2}q^2 + q \geq \nu \geq \frac{1}{2}q^2 - q \\ -\dfrac{2\,m_N\,p_F}{4\pi q}\left[1 - \left(\dfrac{\nu}{q} - \dfrac{1}{2}q\right)^2\right] & \text{for} \quad q < 2\ ,\ \frac{1}{2}q^2 + q \geq \nu \geq q - \frac{1}{2}q^2 \\ -\dfrac{2\,m_N\,p_F}{4\pi q}\,2\,\nu & \text{for} \quad q < 2\ ,\ 0 \leq \nu \leq q - \frac{1}{2}q^2 \end{cases} \quad . \tag{5.14}$$

Here we have defined the variables $\nu = q_0 m_N / p_F^2$ and $q = |\mathbf{q}|/p_F$. The real part of the self energy follows by replacing the argument in the logarithms of U_N by its absolute value,

the imaginary part is due to negative arguments in the logarithm. Following a suggestion made in [56], for the case of η and π mesons, we multiply U_N with a recoil factor:

$$U_N(q_0,\mathbf{q}) \;\rightarrow\; U_N(q_0,\mathbf{q})\left(1-\frac{q_0}{2m_N}\right)^2 \quad , \tag{5.14}$$

which is a $\mathcal{O}\left(\frac{p}{m_N}\right)$ correction from the relativistic pseudo-vector coupling [33].

The Eqs. 5.8 and 5.10 can not only be used to obtain the imaginary part of the self energy, but they also yield its real part. In the actual calculations, however, we obtain the real part by means of an unsubtracted dispersion relation, thus making sure that the self energy remains an analytic function in the upper half of the complex energy plane and that the spectral function of the meson remains normalized. In Chapter 9 we investigate to which extent both approaches differ. The dispersion relation reads:

$$\mathcal{R}\mathrm{e}\,\Pi_M^+(q_0,\mathbf{q}) \;=\; \mathcal{P}\int_0^\infty \frac{d\omega^2}{\pi}\frac{\mathcal{I}\mathrm{m}\,\Pi_M^+(\omega,\mathbf{q})}{\omega^2-q_0^2} \quad . \tag{5.15}$$

The index + indicates that the dispersion relation produces the retarded self energy. By writing the dispersion relation as an integral over positive energies only, we have made use of the antisymmetry of $\mathcal{I}\mathrm{m}\,\Pi_M^+(q_0,\mathbf{q})$, see Appendix 9.9. The unsubtracted dispersion relation converges due to the influence of the form factors, which cut off the high energy tail.

Note that due to the antisymmetry of $\mathcal{I}\mathrm{m}\,\Pi^+$, in this way we also generate the u channel contribution: changing the meson energy from q_0 to $-q_0$ in an s-channel diagram yields exactly the corresponding u-channel diagram since an incoming meson with negative energy $-q_0$ is nothing but an outgoing meson with positive energy q_0. As an example, consider the excitation of a sharp resonance with quantum numbers $J^\pi=\frac{3}{2}^+$ and compare a direct calculation of the self energy including s- and u-channel (yielding the Feynman self energy) with a dispersive calculation into which only the s-channel enters (this way the retarded self energy is generated). Fermi motion is neglected. If our assertion is correct we expect that both approaches give the same real part and up to a sign the same imaginary part as well (cf. Appendix E.2). Summing up s- and u-channel contributions from Fig. 5.2 gives from a direct calculation (compare with Eq. 2.2 in Chapter 2.1):

$$\begin{aligned}
\mathcal{R}\mathrm{e}\,\Pi_M^F(q_0,\mathbf{q}) &= \frac{4}{9}\rho\,\mathbf{q}^2\left(\frac{f}{m_M}\right)^2\left[\underbrace{\frac{1}{q_0+m_N-E_R(\mathbf{q})}}_{s-channel}+\underbrace{\frac{1}{-q_0+m_N-E_R(\mathbf{q})}}_{u-channel}\right] \\
&= \frac{8}{9}\rho\,\mathbf{q}^2\left(\frac{f}{m_M}\right)^2\frac{E_R(\mathbf{q})-m_N}{q_0^2-[m_N-E_R(\mathbf{q})]^2} \qquad (5.16)\\
\mathcal{I}\mathrm{m}\,\Pi_M^F(q_0,\mathbf{q}) &= \frac{4}{9}\rho\,\mathbf{q}^2\left(\frac{f}{m_M}\right)^2\Big\{\,\theta(q_0)\,\delta[q_0+m_N-E_R(\mathbf{q})]+ \\
&\qquad\qquad \theta(q_0)\,\delta[-q_0+m_N-E_R(\mathbf{q})]\,\Big\} \qquad (5.17)
\end{aligned}$$

The imaginary part is proportional to δ functions since we neglect finite width effects as

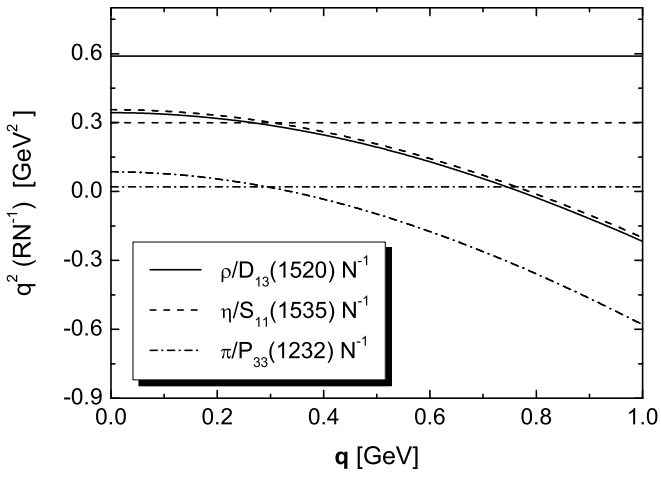

Figure 5.3: Invariant mass q^2 Eq. 5.20 as function of the 3-momentum $\mathbf{q}$ of the following resonance-hole excitations: $D_{13}(1520)N^{-1}$ (solid), $S_{11}(1535)N^{-1}$ (dashed) and $P_{33}(1232)N^{-1}$ (dashed-dotted). Also indicated are the masses of ρ, η and pion (straight).

well as Fermi motion. The dispersion integral

$$\mathcal{R}\mathrm{e}\,\Pi_M^+(q_0,\mathbf{q}) \;=\; \mathcal{P}\int_{-\infty}^{\infty}\frac{d\omega}{\pi}\frac{\mathcal{I}\mathrm{m}\,\Pi_M^+(\omega,\mathbf{q})}{\omega-q_0} \tag{5.18}$$

is easily solved:

$$\begin{aligned}\mathcal{I}\mathrm{m}\,\Pi_M^+(q_0,\mathbf{q}) &= -\pi\,\frac{4}{9}\,\rho\,\mathbf{q}^2\,\left(\frac{f}{m_M}\right)^2\,\Big\{\,\theta(q_0)\,\delta[q_0+m_N-E_R(\mathbf{q})]\,-\\ &\qquad\qquad \theta(q_0)\,\delta[-q_0+m_N-E_R(\mathbf{q})]\,\Big\}\\ \mathcal{R}\mathrm{e}\,\Pi_M^+(q_0,\mathbf{q}) &= \frac{4}{9}\,\rho\,\mathbf{q}^2\,\left(\frac{f}{m_M}\right)^2\,\Bigg[\underbrace{\frac{1}{q_0+m_N-E_R(\mathbf{q})}}_{q_0>0}+\underbrace{\frac{1}{-q_0+m_N-E_R(\mathbf{q})}}_{q_0<0}\Bigg]\end{aligned} \tag{5.19}$$

This makes the relation between the u-channel contribution and the antisymmetry of $\mathcal{I}\mathrm{m}\,\Pi_M^+(q)$ explicit: the real part obtained by summing up s and u-channel contributions is identical to the real part resulting from a dispersion relation. The imaginary parts are up to a sign identical.

Throughout this work the coupling of the ρ meson to baryon resonances is described by current conserving interaction Lagrangians, see Appendix C.1.1. This is strictly speaking not mandatory as long as massive ρ mesons are considered. However, in our in-medium calculations we will have to cover the complete 4-momentum range, in particular also the photon point $q^2 = 0$. Choosing an interaction Lagrangian which is not current conserving then leads to unphysical results in the vicinity of the photon point for longitudinal degrees of freedom, for which the coupling to the photon has to vanish.

Let us finally discuss the physics contained in the particle-hole excitations. The meson spectral function generated by the self energies of Eqs. 5.8, 5.10, 5.14 and 5.15 is characterized by the formation of additional peaks arising from the excitation of particle-hole loops. This has been discussed already in the introductory Chapter 2. At a given 3-momentum the energy of a resonance-hole state with resonance mass m_R is approximately determined by the equation:

$$q_0^2 - \mathbf{q}^2 + m_N^2 + 2m_N q_0 \;=\; m_R^2 \quad , \tag{5.20}$$

which does not take into account effects from level repulsion. In Fig. 5.3 we have indicated the solution of this equation for the most interesting particle-hole states. Also indicated are the meson peaks. Similar pictures are shown in Figs. 2.2 and 2.4. The actual position of the particle-hole peaks is only approximately determined by Eq. 5.20 and is modified by effects from level-repulsion, see disucssion around Eq. 2.10 in Chapter 2 for more details. The invariant mass q^2 of this branch moves down to smaller values as the 3-momentum increases, eventually reaching space-like kinematics $q_0^2 < \mathbf{q}^2$ [107]. This in-medium shift of spectral strength to the space-like region is not only encountered in resonance-hole models such as ours. Quite generally, the threshold for the conversion of a meson M into a pion is determined by the requirement that the invariant energy of the $M\,N$ system must exceed $(m_N + m_\pi)$. As a function of momentum, the corresponding q^2 of the meson M decreases and becomes finally space-like. Whereas for these conversion processes the space-like region is reached only for finite 3-momentum $\mathbf{q}$, one can on top have Landau damping, i.e. the absorption of a meson on a nucleon. This process is confined to space-like mesons for all 3-momenta considered. One can therefore expect that the spectral strength available for physical final states like – for vector mesons – e^+e^- or $\pi^+\pi^-$ pairs decreases as a function of the momentum, since more strength is shifted to regions which cannot be reached by the time-like physical final states.

5.2.3 Nonrelativistic Reduction, Lindhardt Functions and Susceptibilities

The Eqs. 5.8 and 5.10 are valid both within a relativistic and a non-relativistic framework. In the actual calculations we will often use a non-relativistic formalism, where only the leading non-relativistic terms of the traces Ω^φ and $\Omega^{T/L}$ are kept. A detailed derivation of the non-relativistic reduction is given in Appendix C.2. In a systematic study [109], which forms part of this work, it was demonstrated that the non-relativistic reduction produces satisfying results when performed in the cm frame of the resonance. For details see Chapter 9.4. A particularly convincing example for that is the $\pi N\Delta$ vertex. Comparing the results obtained from the fully relativistic Lagrangian and a non-relativistic reduction one finds (cf. Tables C.1 and C.2):

$$\begin{aligned} \mathcal{L}_{rel} &= \frac{f}{m_\pi}\,\bar\psi^\mu\,\psi\,\partial_\mu\pi \quad\rightarrow\quad \Omega_{rel} \;=\; \frac{8}{3}\,\sqrt{k^2}\,(E_N^{cm}+m_N)\,\mathbf{q}_{cm}^2 \\ \mathcal{L}_{nrel} &= \frac{f}{m_\pi}\,\psi^{\dagger,i}\,\psi\,\partial_i\pi \quad\rightarrow\quad \Omega_{nrel} \;=\; \frac{16}{3}\,\sqrt{k^2}\,m_N\,\mathbf{q}^2 \quad . \end{aligned} \tag{5.21}$$

Here we have replaced the rest mass m_Δ by the invariant mass $\sqrt{k^2}$. The relativistic trace Ω_{rel} has been evaluated in the cm-frame. One finds that when taking $\mathbf{q}^2 = \mathbf{q}_{cm}^2$

for Ω_{nrel}, Ω_{rel} is obtained from Ω_{nrel} by the replacement $m_N \to E_N^{cm}$ which only for very large momenta induces some corrections. The numerical results shown in Chapter 9.4.1 indicate, that using cm kinematics in the non-relativistic reduction provides consistently convincing results also for the vector mesons. In Chapter 9.4.1 we also stress that in a non-relativistic formalism the same kinematics have to be used for the self energy and for the determination of the coupling constants.

Let us introduce at this point some quantities which are often found in non-relativistic works (for example in [33, 7, 98]) and to which we will refer in later parts of this work (Section 5.3.2 and 6.6). The Lindhardt function $U_R(q)$ for resonance-hole states is defined in analogy to the nucleon-hole excitation as the momentum integral over the product of nucleon and resonance propagator:

$$U_R(q) \;=\; \int \frac{d^3p}{(2\,\pi)^3}\frac{n(\mathbf{p})}{2\,E_N(\mathbf{p})}\frac{1}{k_0^2 - E_R^2(\mathbf{k}) - \Sigma_{vac}(k)} \quad .$$

Here we have $k = q + p$. If one takes into account the energy dependence of $\Sigma_{vac}(k)$, it is not possible to find an analytic solution of the integral. A second function that is often encountered in the discussion of particle-hole excitations is the so called susceptibility χ, defined as:

$$\chi_M(q) \;=\; I_\Pi \left(\frac{f}{m_M}\right)^2 \Omega^{red}\, U_R(q) \quad , \tag{5.22}$$

where M refers to the meson under consideration. The quantity Ω^{red} is obtained from Ω by dividing out the squared meson energy or momentum. For example, for particle-hole loops coupling in a p-wave to a meson, the relation between Ω and Ω^{red} reads:

$$\Omega \;=\; \mathbf{q}^2\,\Omega^{red} \quad , \tag{5.23}$$

as can be inferred by considering the expressions listed in Table C.2 and Table C.3. Having explained U_R, χ and Ω^{red}, we can write down the self energy in the following factorized ways:

$$\Pi_M(q) \;=\; I_\Pi \left(\frac{f}{m_M}\right)^2 F_t(q)\Omega\, U_R(q) \;=\; \mathbf{q}^2\,(q_0^2,\, q^2)\, F_t(q)\chi_M(q) \quad .$$

Here the factors q_0^2 and q^2 arise for resonance-hole states coupling in a relative s-wave to the mesons. In order to write down the self energy $\Pi_M(q)$ in this way one needs to pull the trace Ω out of the integral. This is not exact because the cm momentum depends on the invariant mass $\sqrt{k^2}$ of the resonance and is therefore implicitly also a function of the nucleon momentum p. However, the deviations from a full calculation are small.

5.2.4 Comments on the Relativistic Calculation

In the first part of this Section we discuss a problem that arises in the calculation of the meson self energy when working with relativistic expressions for the traces Ω^φ and $\Omega^{T/L}$. This discussion has initially been published in [109], but here we are able to explore the origin of the problem in some more detail. As a result the reason for the replacement $\not{k} + M \to \not{k} + \sqrt{k^2}$ in the relativistic propagator of spin-$\frac{1}{2}$ and spin-$\frac{3}{2}$ states (cf. Appendix D.1.1) within our frame work will emerge. The second part of this Section is devoted to a short discussion of the coupling scheme for spin-$\frac{3}{2}$ resonances suggested in [101].

A Sign Problem

In Section 5.2.1 we have related the imaginary part of the in-medium meson self energy to the total meson-nucleon cross section. Within our sign conventions this requires $\mathcal{I}\mathrm{m}\,\Pi_M$ to be negative. Naively, we would expect that the self energy calculated according to Eqs. 5.8 and 5.10 obeys this constraint. In the following we will investigate this issue with a simple relativistic Lagrangian describing the coupling of pions to resonances with positive or negative parity:

$$\mathcal{L} \;=\; g\,\bar{\psi}_R \left\{ \begin{array}{c} i\,\gamma^5 \\ \mathbb{1} \end{array} \right\} \psi_N\,\varphi + h.c. \tag{5.24}$$

From this Lagrangian the self energy can be calculated according to Eq. 5.8. Neglecting Fermi motion, i.e. taking $p = (m_N, 0)$, 4-momentum conservation takes on the form

$$\begin{aligned} q_\mu &= (q_0, \mathbf{q}) \\ p_\mu &= (m_N, 0) \\ k_\mu &= q_\mu + p_\mu \;=\; (q_0 + m_N, \mathbf{q}) \quad . \end{aligned} \tag{5.25}$$

Thus we get for the self energy:

$$\begin{aligned} \mathcal{I}\mathrm{m}\,\Pi_\pi(q_0,\mathbf{q}) &= I_\Pi\, g^2 \frac{\rho}{8m_N} Tr\left[(\not{p} + m_N) \left\{ \begin{array}{c} i\,\gamma^5 \\ \mathbb{1} \end{array} \right\} (\not{k} + m_R) \left\{ \begin{array}{c} -i\,\gamma^5 \\ \mathbb{1} \end{array} \right\} \right] \times \\ &\quad \times \mathcal{I}\mathrm{m}\,\frac{1}{k_0^2 - E_R^2(\mathbf{k}) - \langle\Sigma(k)\rangle} \\ &= I_\Pi\, g^2 \frac{\rho}{8m_N} \mathcal{I}\mathrm{m}\,\frac{4\,m_N\,[m_N + q_0 \mp m_R]}{k_0^2 - E_R^2(\mathbf{k}) - \langle\Sigma(k)\rangle} \quad . \end{aligned} \tag{5.26}$$

The isospin coefficient I_Π is either 2 or 4/3, depending on whether nucleon or Δ resonances are considered. Here $\langle\Sigma(k)\rangle$ is the averaged vacuum self energy – see Appendix D.1.1 – in contrast to $\Sigma(k)$, which is full self energy containing a Dirac structure.

Since it will be needed in a moment, let us give an explicit expression for the vacuum resonance self energy $\Sigma(k) = 2\,(k^2\,\mathcal{I}\mathrm{m}\,I_1 + m_R\,\mathcal{I}\mathrm{m}\,I_2)$ as arising from the Lagrangian Eq. 5.24, see Appendix D.1.1:

$$\begin{aligned} -i\Sigma(k) &= (-i\,g)^2 \int \frac{d^4p}{(2\pi)^4} \frac{i}{\not{p} - m_N} \left\{ \begin{array}{c} i\,\gamma^5 \\ \mathbb{1} \end{array} \right\} \frac{i}{(k-p)^2 - m_\pi^2} \left\{ \begin{array}{c} -i\,\gamma^5 \\ \mathbb{1} \end{array} \right\} \\ &= i\,(\not{k}\,I_1(k) + I_2(k)) \\ \mathcal{I}\mathrm{m}\,I_1(k) &= \frac{1}{4k^2} Tr\,[\not{k}\,\mathcal{I}\mathrm{m}\,\Sigma(k)] \;= -\alpha\,p\,\frac{E_N(p)}{k^2} \\ \mathcal{I}\mathrm{m}\,I_2(k) &= \frac{1}{4} Tr\,[\mathcal{I}\mathrm{m}\,\Sigma(k)] \;= \pm\alpha\,p\,\frac{E_N(p)}{\sqrt{k^2}} \quad . \end{aligned} \tag{5.27}$$

Here α denotes a common factor and p is the momentum of the nucleon in the rest frame of the resonance. The upper/lower sign refers to a positive/negative parity resonance.

Coming back to the meson self energy, we see from Eq. 5.26, that its imaginary part undergoes a change of sign for resonances with positive parity (upper sign) at $q_0 = m_R - m_N$. This means that for $q_0 < m_R - m_N$, $\mathcal{I}\mathrm{m}\,\Pi_\pi$ is positive, which is wrong.

As we will see in a moment, this problem is due to the resonance propagator entering into Eq. 5.26:

$$\mathcal{G}_F(k) \;=\; \frac{\not{k} + m_R}{k^2 - m_R^2 - \langle \Sigma(k^2) \rangle} \quad . \tag{5.28}$$

This is an approximation to the exact propagator, which is commonly found in the literature. It violates an important relation of the strength functions ρ_1 and ρ_2 [16], which are defined via (see Appendix E.1.2):

$$\begin{aligned} \rho_1(k) &= -\frac{1}{4\pi\, k^2} Tr\left[\not{k}\, \mathcal{I}\mathrm{m}\, \mathcal{G}_F(k)\right] \\ \rho_2(k) &= -\frac{1}{4\pi} Tr\left[\mathcal{I}\mathrm{m}\, \mathcal{G}_F(k)\right] \quad . \end{aligned} \tag{5.29}$$

As detailed in Appendix E.1.2, they have to obey the relation:

$$\sqrt{k^2}\rho_1(k) - \rho_2(k) \;\geq\; 0 \quad . \tag{5.30}$$

A direct calculation of ρ_1 and ρ_2 from propagator Eq. 5.28 exhibits that for $k^2 > m_R^2$ this constraint is not fulfilled:

$$\rho_1(k) \;=\; -\frac{1}{\pi} \frac{\langle \mathcal{I}\mathrm{m}\, \Sigma(k) \rangle}{(k^2 - m_R^2 - \langle \mathcal{R}\mathrm{e}\, \Sigma(k) \rangle)^2 + \langle \mathcal{I}\mathrm{m}\, \Sigma^2(k) \rangle} \;=\; \frac{\rho_2(k)}{m_R} \quad .$$

Before we found that the self energy changes sign for $q_0 + m_N < m_R$. In order to relate this to $k^2 < m_R^2$, we write

$$\begin{aligned} (q_0 + m_N)^2 &= m_N^2 + q^2 + 2\, m_N\, q_0 + \mathbf{q}^2 \;=\; k^2 + \mathbf{q}^2 \;\leq\; m_R^2 \\ &\Rightarrow\; k^2 \;< m_R^2 - \mathbf{q}^2 \quad . \end{aligned}$$

Thus, we have reason to hope that using a correct propagator will solve the sign problem of the self energy.

In order to confirm this, let us recalculate $\mathcal{I}\mathrm{m}\, \Pi_\pi$ by assuming the most general form for $\mathcal{I}\mathrm{m}\, \tilde{\mathcal{G}}_F$, as it follows from the Lehmann representation Eq. E.5:

$$\begin{aligned} \mathcal{I}\mathrm{m}\, \tilde{\mathcal{G}}_F(k) &= -\pi \left(\not{k}\rho_1(k) + \rho_2(k)\right) \\ \mathcal{I}\mathrm{m}\, \Pi_\pi(q_0, \mathbf{q}) &= -\pi\, I_\Pi\, g^2 \frac{\rho}{8 m_N} 4\, m_N\, \left[(m_N + q_0)\rho_1(k) - \rho_2(k)\right] \\ &\leq -\pi\, I_\Pi\, g^2 \frac{\rho}{8 m_N} 4\, m_N\, \rho_1(k) \left[(m_N + q_0) - \sqrt{k^2}\right] \;\leq\; 0 \quad , \end{aligned} \tag{5.31}$$

where in going from the second to the last line we have used relation Eq. 5.30 and

$$(q_0 + m_N)^2 \;=\; m_N^2 + q^2 + 2\, m_N\, q_0 + \mathbf{q}^2 \;=\; k^2 + \mathbf{q}^2 \;\geq\; k^2 \quad .$$

We demonstrate now that the exact propagator fulfills constraint Eq. 5.30 and that therefore the sign problem is due to a bad approximation of the full propagator. Without approximations we have for $\bar{\mathcal{G}}_F(k)$:

$$\bar{\mathcal{G}}_F(k) \;=\; \frac{\not{k}\,(1 - I_1) + (m_R + I_2)}{k^2(1 - I_1)^2 - (m_R + I_2)^2} \quad . \tag{5.32}$$

with the self energies I_1 and I_2 as given above. Obtaining ρ_1 and ρ_2 from Eq. 5.29 yields:

$$\begin{aligned} \rho_1(k) &= -\frac{1}{\pi D}\left[\langle \mathcal{I}\mathrm{m}\,\Sigma(k)\rangle - \mathcal{I}\mathrm{m}\,I_1(k)(k^2-m_R^2)\right] \\ \rho_2(k) &= -\frac{1}{\pi D}\left[\langle \mathcal{I}\mathrm{m}\,\Sigma(k)\rangle\; m_R - \mathcal{I}\mathrm{m}\,I_2(k)(k^2-m_R^2)\right] \quad . \end{aligned} \tag{5.33}$$

Here we have neglected the real part of the self energy, for which analytic expressions are not available. By D we denote the squared absolute value of the denominator of the propagator. Plugging in explicit expressions for I_1 and I_2, one finds after some algebra that

$$\sqrt{k^2}\,\rho_1(k) - \rho_2(k) = \alpha\,\frac{p}{\pi D}\,(\sqrt{k^2}-m_R)^2\,\frac{E_N \pm m_N}{\sqrt{k^2}} > 0$$

for all energies and momenta, independent of the parity of the resonance. Thus, when using a consistent propagator the sign problem of the meson self energy is avoided.

In the actual calculations we do not keep the full Dirac structure of the propagator but make an approximation to it which simultaneously retains the simplicity of Eq. 5.28 and satisfies the constraint of Eq. 5.30:

$$\begin{aligned} \mathcal{G}_F(k) &= \frac{\not{k}+m_R}{k^2-m_R^2-\langle\Sigma(k)\rangle} \to \frac{\not{k}+\sqrt{k^2}}{k^2-m_R^2-\langle\Sigma(k)\rangle} \\ & \sqrt{k^2}\rho_1(k) - \rho_2(k) = 0 \quad . \end{aligned} \tag{5.34}$$

Using this expression for the propagator, the self energy is given by:

$$\mathcal{I}\mathrm{m}\,\Pi_\pi(q_0,\mathbf{q}) = I_\Pi\, g^2 \frac{\rho}{8m_N}\mathcal{I}\mathrm{m}\,\frac{4\,m_N\left[m_N+q_0\mp\sqrt{k^2}\right]}{k_0^2-E_R^2(\mathbf{k})-\langle\Sigma(k)\rangle} \quad . \tag{5.35}$$

While the imaginary part of the propagator Eq. 5.34 is correct in the sense that it fulfills the fundamental constraints listed in Appendix D.1.1, the real part of the propagator should strictly speaking be obtained by means of a dispersion relation as follows from the Lehman representation of Eq. E.5 in Appendix E.1.2. We have checked explicitly that the differences between the (approximated) real part of Eq. 5.34 and a full solution using dispersion relations are small. When using a dispersion relation for the self energy Σ_{vac}, the Lehmann representation for the propagator is automatically respected.

For spin-$\frac{3}{2}$ states the same problem arises. We cure it as in the spin-$\frac{1}{2}$ case by replacing $m_R^2 \to \sqrt{k^2}$ in the original Rarita-Schwinger propagator, Eq. B.27 in Appendix B.4 and end up with the expression:

$$\mathcal{G}_F^{\mu\nu\,new}(k) = \frac{\not{k}+\sqrt{k^2}}{k^2-m_R^2-\langle\Sigma(k)\rangle}\,P_{3/2}^{\mu\nu}(k^2) \quad . \tag{5.36}$$

Some remarks about this propagator are in order. First we note that it is directly proportional to the spin-$\frac{3}{2}$ projector $P_{3/2}^{\mu\nu}$. Second, in analogy to the case of spin-$\frac{1}{2}$ resonances this expression is – strictly speaking – not correct for the real part, but again we expect the deviations to be negligible for our purposes. Finally, Eq. 5.36 and variants thereof have already been discussed in the literature [12, 2, 118, 130]. In [2] it is introduced to insure

gauge invariance of photon-nucleon amplitudes. This is not necessary in our case as the vector mesons are introduced via the gauge invariant field tensor $V^{\mu\nu}$. On the other hand, in [12] it was shown that Eq. 5.36 is incorrect in the limit of a small decay width Γ, since it does not contain an inverse. This observation is in full agreement with our previous statements about the real part of Eqs. 5.34 and 5.36. Also, as pointed out in [12, 118], the propagator Eq. 5.36 displays a pole at $k^2 = 0$, which is never reached when considering the imaginary part of the meson self energy Eqs. 5.8 and 5.10. Therefore the relativistic results presented in this work do not suffer from these poles. One should also be aware of the fact that the use of gauge-invariant couplings for the spin-$\frac{3}{2}$ field – which introduce additional orders of the resonance momentum – as suggested in [101] avoids these poles, see following Subsection.

The Pascalutsa Coupling for Spin-$\frac{3}{2}$ Resonances

In Appendix C.1.1 we give explicit expressions for standard Lagrangians describing the coupling of baryon resonances to several meson-nucleon channels. Lagrangians like this can be found in various places, see for example [35, 36, 104, 105, 123, 12, 2, 118, 130] and references therein. For resonances with spin $j \geq \frac{3}{2}$, in [101] an alternative way of describing the resonance physics has been proposed. We will shortly comment on this method and consider its effect on our results.

The propagation of spin-$\frac{3}{2}$ resonances away from their mass shell involves on top of the expected spin-$\frac{3}{2}$ components also spin-$\frac{1}{2}$ contributions. This is seen explicitly in the decomposition of the Rarita-Schwinger propagator in Appendix B.4, Eq. B.27. A similar phenomenon is encountered in the propagation of spin-1 states, where away from the on-shell point the propagator contains modes which are not 4-transverse (see Eq. B.22 in Appendix B.3. In [101] it has been suggested that in order to propagate only spin-$\frac{3}{2}$ modes, a special type of Lagrangians describing the coupling of the resonance should be employed. The idea is that a properly chosen Lagrangian projects onto the spin-$\frac{3}{2}$ sector exclusively and does not admit off-shell contributions with spin-$\frac{1}{2}$. Lagrangians satisfying this requirement are constructed by means of the antiysymmetric tensor

$$\psi_{\mu\nu} \;=\; \partial_\mu \psi_\nu - \partial_\nu \psi_\mu$$

or its dual $\tilde{\psi}_{\mu\nu} = \frac{1}{2}\epsilon_{\mu\nu\alpha\beta}\,\psi^{\alpha\beta}$. In a Feynman diagram this quantity leads to the tensor

$$\Gamma_{\mu\nu} \;=\; g_{\alpha\nu}k_\mu - g_{\alpha\mu}k_\nu$$

multiplying the Rarita propagator. The crucial observation is that $k^\mu \Gamma_{\mu\nu} = 0$. By inspecting the decomposition of the Rarita-Schwinger propagator in Eq. B.27, Appendix B.4, one realizes that only its spin-$\frac{3}{2}$ contribution is going to give finite contributions, if at both vertices, which are contracted with the propagator, the tensor $\psi_{\mu\nu}$ is employed. The situation is akin to that of spin-1 fields, where by using Lagrangians containing the field tensor $F_{\mu\nu}$ only the 4-transverse part of the propagator yields finite contributions.

As suggested in [103] a close relation exists between the conventional coupling and Pascalutsa type couplings, which are obtained from the conventional ones by the replacement:

$$\mathcal{V}^\mu\,\psi_\mu \;\;\rightarrow\;\; \mathcal{V}^\mu \gamma_5 \gamma^\nu \tilde{\psi}_{\mu\nu} \quad .$$

Here $\mathcal{V}^\mu$ is the vertex factor derived from the conventional Lagrangian. Following the argument in [103], apart from a normalization factor, the scattering amplitude obtained

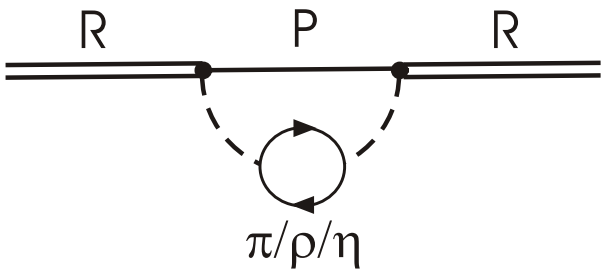

Figure 5.4: Feynman diagram representing the in-medium decay of a baryon resonance into a nucleon and a dressed meson. The particle-hole loops stands both for nucleon and resonance excitations and it is understood that it represents a complete resummation of particle-hole insertions. The symbol P indicates that Pauli blocking is taken into account.

from the Pascalutsa coupling is up to a factor k^2/m_R^2 identical to the standard one. We checked this conjecture for all the traces appearing in our framework and always found it to be valid. This finding implies that by using Pascalutsa type Lagrangians the unphysical pole at $k^2 = 0$ mentioned above is avoided.

In this work we do not present results arising from the Pascalutsa coupling. The extra factor k^2/m_R^2 only affects the off-shell behaviour of the self energy, while leaving the on-shell point (and therefore the determination of the coupling constants) untouched. The small effects in the off-shell behaviour are easily overshadowed by the uncertainties in the form factor (functional form, cutoff) and therefore a systematic comparison of Pascalutsa and standard Lagrangians will not provide any new insight.

5.3 Resonances

We will now turn to a discussion of the in-medium properties of baryon resonances. There two competing mechanisms have to be considered. Pauli blocking will reduce the decay width. This affects mostly resonances which are close to one of the meson-nucleon thresholds and have a considerable branching ratio into this channel. For example, at normal nuclear matter density the width of a $\Delta(1232)$ at rest vanishes. A second source of in-medium modifications is resonance-nucleon scattering: due to the scattering process the resonance is converted into a different state and therefore its decay width increases. We generate these processes by replacing the vacuum meson propagator with the in-medium one, see Fig. 5.4. The connection between the imaginary part of the self energy diagram thus obtained and collisional broadening will be made explicit in Section 5.3.2. As in the case of Pauli blocking, we expect these effects to be most important for those resonances with decay channels that are suppressed from phase space. Then already slight modifications of the spectral function can result in relatively large effects. On a qualitative level these phenomena have been studied in Chapter 2.

5.3.1 The in-medium self energy of baryon resonances

We calculate the in-medium broadening of baryon resonances by replacing the vacuum meson propagator by the in-medium one. The corresponding Feynman diagram is shown in Fig. 5.4. Applying Cutkosky's cutting rules, one finds for the width of a nucleon

resonance with spin-$\frac{j}{2}$ and invariant mass $\sqrt{k^2}$ decaying into a pseudoscalar meson φ or a ρ meson:

$$\begin{aligned}
\mathcal{I}\mathrm{m}\,\Sigma^{+}_{\varphi,med}(k_0,\mathbf{k}) &= -\frac{I_\Sigma}{2j+1}\left(\frac{f}{m_\varphi}\right)^2 \int\limits_{k_F}^{2\sqrt{k_0^2-m_N^2}} \frac{dp\,p^2}{8\,\pi\,E_N} \times \\
&\quad \times \int\limits_{-1}^{+1} dx\, F^2(k,(k-p))\,\Omega^{\varphi}\,\mathcal{A}^{med}_{\varphi}(k-p) \qquad (5.37) \\
\mathcal{I}\mathrm{m}\,\Sigma^{+}_{\rho,med}(k_0,\mathbf{k}) &= -\frac{I_\Sigma}{2j+1}\left(\frac{f}{m_\rho}\right)^2 \int\limits_{k_F}^{2\sqrt{k_0^2-m_N^2}} \frac{dp\,p^2}{8\,\pi\,E_N} \times \\
&\quad \times \int\limits_{-1}^{+1} dx\, F^2(k,(k-p))\,(2\,\Omega^{T}\,\mathcal{A}^{med}_{\rho,T}(k-p) + \Omega^{L}\,\mathcal{A}^{med}_{\rho,L}(k-p)) \quad .
\end{aligned}$$

Here the integration variable x – defined as $\cos\,\angle(\mathbf{k},\mathbf{p})$ – is implicitly contained in $(k-p)^2 = (k_0-E_N)^2-(\mathbf{k}-\mathbf{p})^2$. Propagator and spectral function of meson M are denoted by D^{med}_M and $\mathcal{A}^{med}_M$, respectively. The isospin factor I_Σ is 1 for Δ resonances with isospin $\frac{3}{2}$ and 3 for N^* resonances with isospin $\frac{1}{2}$. For the decay into $N\eta$ $I_\Sigma = 1$. The integration variable p refers to the nucleon momentum with respect to the rest frame of nuclear matter, E_N is the on-shell energy of a nucleon and we have $E_F = \sqrt{m_N^2+p_F^2}$. This explains the lower integration bound, reflecting Pauli blocking. The upper integration limit follows from the condition that the meson energy $q_0 > 0$. These expressions are similar to what one obtains in the vacuum for the decay into one stable and one unstable particle, see Eqs. 3.18 and 3.19 in Chapter 3.2. For practical reasons we perform the phase space integration in Eq. 5.37 in the rest frame of nuclear matter and not in the rest frame of the resonance. In passing we mention that there is an additional contribution to the imaginary part of the resonance self energy which is due to the decay of a nucleon from the Fermi sphere into a resonance and a meson. For details see Appendix D.3. Since the energy of the resonance involved in this process is necessarily smaller than the Fermi energy and therefore much smaller than the on-shell energy of the resonance, this term does not change the imaginary part of the self energy in the vicinity of the resonance and should also have a small impact on the real part which is obtained via a dispersion relation (see Section 5.3.3).

We do not modify the $\Delta\pi$ decay channel. For the $D_{13}(1520)$ we do not expect this channel to be important since the partial decay width of 25 MeV is quite small in view of the available phase space, resulting in a small coupling constant. For some of the higher lying resonances, the situation is not as clear since they have a sizeable coupling to this channel. Here and in particular for the $P_{11}(1440)$ a modification of the $\Delta\pi$ channel would be interesting, though it probably will not affect the central results of this work.

5.3.2 Relation to Resonance Nucleon Scattering

In this Section we discuss the physical interpretation of the imaginary part of the resonance self energy Eq. 5.37. By cutting diagram 5.4 one generates two diagrams which are shown

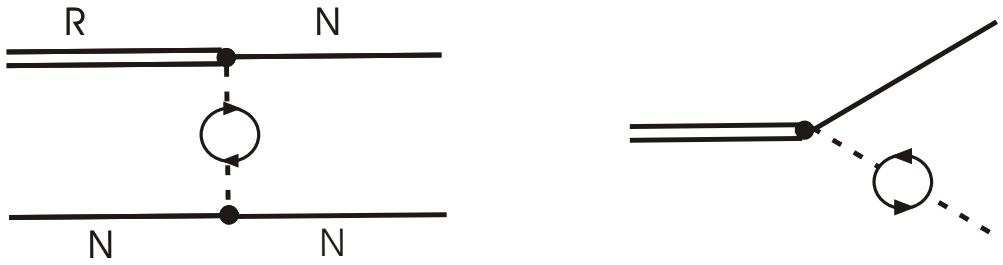

Figure 5.5: Interpretation of the in-medium self energy as a sum of a collision term and the decay into a nucleon and a dressed meson.

in Fig. 5.5: the diagram on the left stands for resonance-nucleon scattering processes and the diagram on the right describes the resonance decay into a nucleon (with Pauli-blocking) and a dressed meson. Such a separation is intuitive: when dressing a meson with one resonance-hole excitation, its spectral function contains two branches, a particle-hole branch and a meson branch. Resonance-nucleon scattering (or the decay $R \to N(N^{-1}R)$) is related to the particle-hole branch, the resonance decay into meson and nucleon is related to the meson branch.

For illustrative purposes we study now the contribution of the particle-hole branch. Therefore we consider Eq. 5.37 for the decay $R \to NM$ in the low density limit. The resonance is supposed to have the quantum numbers $J^\pi = \frac{3}{2}^+$ and the meson is a pseudoscalar, such that the decay is p-wave. Furthermore, we assume that the position of the free resonance-hole pair is below the meson, i.e. $m_R - m_N < m_M$. The calculation is done non-relativistically and we obtain the following expressions for propagator, self energy and spin-trace Ω (see also Section 5.2.3):

$$\begin{aligned} \mathcal{I}\mathrm{m}\, D_M^{med} &= \mathcal{I}\mathrm{m}\, D_M^{vac} + |D_M^{vac}|^2\, \mathcal{I}\mathrm{m}\, \Pi_M \\ \Pi_M &= I_\Pi \left(\frac{f}{m_M}\right)^2 \Omega^\varphi\, U_R \quad , \quad \Omega^\varphi = 16/3\, m_N\, m_R\, \mathbf{q}^2 \quad . \end{aligned}$$

Here $I_\Pi = \frac{4}{3}$ is an isospin factor and $\mathbf{q}$ stands for the 3-momentum of the meson. In terms of these quantities the imaginary part of the in-medium resonance self energy can be written in the low density limit as a sum of the vacuum width and an in-medium contribution:

$$\begin{aligned} \mathcal{I}\mathrm{m}\, \Sigma(k_0, \mathbf{k}) &= \mathcal{I}\mathrm{m}\, \Sigma_{vac}(k) + \mathcal{I}\mathrm{m}\, \Sigma_{coll}(k_0, \mathbf{k}) \qquad (5.38) \\ &= \mathcal{I}\mathrm{m}\, \Sigma_{vac}(k) + \frac{1}{4} \int \frac{d^3p}{(2\pi)^3 2\, E_N(\mathbf{p})} \underbrace{|D_M^{vac}|^2\, I_\Pi\, I_\Sigma \left(\frac{f}{m_M}\right)^4 \Omega^{\varphi\,2}\, \mathcal{I}\mathrm{m}\, U_R}_{I} \quad . \end{aligned}$$

The integrand I is related to the scattering amplitude $RN \to NR$, which reads

$$\mathcal{M} = -\left(\frac{f}{m_M}\right)^2 4\, m_N\, m_R\, (\mathbf{S}_1 \cdot \mathbf{q})\, D_M^{vac}\, (\mathbf{S}_2^\dagger \cdot \mathbf{q}) \quad .$$

The squared and spin/isospin averaged amplitude $|\bar{\mathcal{M}}|^2$ is:

$$\frac{1}{2j_R+1}\frac{1}{2j_N+1}\frac{1}{2I_N+1} \sum_{spins} |\mathcal{M}|^2 = \frac{1}{16} \left(\frac{f}{m_M}\right)^4 \Omega^\varphi\, 2\, |D_M^{vac}|^2\, I_\sigma = |\bar{\mathcal{M}}|^2 \quad .$$

One readily calculates $I_\sigma = 4/3$ and remembering that $I_\Sigma\, I_\Pi = 4/3$, $\mathcal{I}\mathrm{m}\,\Sigma$ is expressed in terms of $|\bar{\mathcal{M}}|^2$ as follows:

$$\mathcal{I}\mathrm{m}\,\Sigma_{coll}(k_0,\mathbf{k}) \;=\; 4\int \frac{d^3p}{(2\pi)^3 2\,E_N(\mathbf{p})}\,|\bar{\mathcal{M}}|^2\,\mathcal{I}\mathrm{m}\,U_R \quad , \tag{5.39}$$

Assuming that the vacuum width of the R vanishes, $\mathcal{I}\mathrm{m}\,U_R$ is proportional to a δ function which puts the RN^{-1} state on-shell. This generates the low density limit of the left diagram of Fig. 5.5:

$$\begin{aligned}
\mathcal{I}\mathrm{m}\,U_R(k_0,\mathbf{k}) &= -\frac{\rho}{8\,m_N}\,\pi\,\delta(k^2-m_R^2) \qquad (5.40)\\
\mathcal{I}\mathrm{m}\,\Sigma_{coll}(k_0,\mathbf{k}) &= -\frac{\rho}{4\,m_N}\int d\Phi_2\,|\bar{\mathcal{M}}|^2 \;=\; -\,\rho\,|\mathbf{k}|\,\sigma \quad .
\end{aligned}$$

Here we have used expressions for the 2-body phase space Φ_2 and the total cross section σ listed in Appendix B.6. By relating the total cross section to the forward scattering amplitude, the low density theorem Eq. 5.7 is recovered and we have shown, that in the low density limit the excitation of particle-hole pairs in the meson spectral function generates resonance-nucleon scattering terms in the resonance self energy.

If the resonance is allowed to scatter into additional final states, then the above formula for collisional broadening is extended to

$$\mathcal{I}\mathrm{m}\,\Sigma_{coll}(k_0,\mathbf{k}) \;=\; -\,\rho\,|\mathbf{k}| \sum_{X=\{R',N\}} \sigma_{RN\to NX} \quad ,$$

where R' stands for any of the involved resonances and N is the nucleon. For the meson self energy the appearance of various final states translates into the excitation of additional particle-hole states:

$$\mathcal{I}\mathrm{m}\,\Pi_M \;=\; \sum_{X=\{R',N\}} \mathcal{I}\mathrm{m}\,\Pi_M^X \quad . \tag{5.41}$$

If one is interested in the collisional broadening from scattering into final state X, one only takes into account the particle-hole excitation due to this state, Π_M^X, in the self energy Π_M.

We now discuss the question, up to which extent one can identify collision terms, if a resummation of particle-hole loops in the propagator is performed, leading to:

$$\mathcal{I}\mathrm{m}\,D_M^{med} \;=\; \mathcal{I}\mathrm{m}\,\Pi_M \left|\frac{1}{q^2-m_M^2-\Pi_M}\right|^2 \tag{5.42}$$

We showed above, that in the low density limit the collision into state X is obtained by considering only the corresponding piece of the self energy, Π_M^X. This suggests that with the replacement

$$\mathcal{A}_M^{med} \;=\; -\frac{1}{\pi}\mathcal{I}\mathrm{m}\,\Pi_M^X \left|\frac{1}{q^2-m_M^2-\Pi_M}\right|^2 \tag{5.43}$$

in Eq. 5.37, one can trigger on the individual scattering process $RN \to NX$ [7, 98]. As compared to the low-density limit of Eq. 5.40, now the collision term contains medium

modifications resulting from the dressing of the meson propagator. A further difference to the low-density limit is that a decomposition of the self energy into vacuum part and collision term as in Eq. 5.38 can not be sensibly achieved anymore. The reason is that the decay mode meson-nucleon is modified: the dispersion of the meson branch differs from the free dispersion relation and the meson branch has strength factor $z < 1$.

What has been said so far applies only if the resonance under consideration lies below the meson, i.e. if $m_R - m_N < m_M$. The situation becomes much more involved when the resonance state R lies above the meson mass. A typical example for that is the coupling of pions to the Δ-hole state. We have detailed in Chapter 2, Sections 2.1 and 2.3, that then the free dispersion relations of meson and particle-hole cross each other at a finite 3-momentum and that the interpretation of the branches of the spectral function in terms of meson and particle-hole modes becomes more complicated. Also the low density limit, Eq. 5.40, is difficult to obtain if $m_R - m_N > m_M$. The reason is that then in the collisional term, Eq. 5.40, the exchange meson can be on shell, since the decay $R \to NM$ is possible.

We conclude from the above discussion that in a full calculation the absorptive processes $RN \to NN$ can always be obtained from Eq. 5.43. Another scattering process which will be of interest to us is the scattering $D_{13}(1520)N \to ND_{13}(1520)$ with ρ exchange. Since the $D_{13}(1520)N^{-1}$ excitation is below the ρ meson, Eq. 5.43 is applicable.

5.3.3 Mass Shift and Level Repulsion

As in the vacuum case, we calculate the real part of the self energy in the medium by means of a dispersion relation, which guarantees that the spectral function of the resonance remains normalized:

$$\mathcal{R}\mathrm{e}\,\Sigma^+_{med}(k_0,\mathbf{k}) \;=\; \mathcal{P}\int\limits_{E_F}^{\infty}\frac{d\omega}{\pi}\frac{\mathcal{I}\mathrm{m}\,\Sigma^+_{med}(\omega,\mathbf{k})}{\omega-k_0} - c_{vac}(\mathbf{k}) \quad . \tag{5.44}$$

The lower integration bound is the Fermi energy E_F below which $\mathcal{I}\mathrm{m}\,\Sigma^+_{med}(\omega,\mathbf{k})$ vanishes, see Eq. 5.37. We generate the main body of the dispersive mass shift in our approach. Processes like $RN \to R'R''$, which are not considered in this work, are on-shell either closed or suppressed from phase space and should give comparatively small attractive corrections as detailed below. Non-relativistic corrections from relativistic nuclear mean fields can be sizeable [71], but large uncertainties arise since their size is only poorly known for the baryon resonances. In Chapters 7 and 9 we will discuss effects from mean fields under the assumption that they are identical for nucleon and resonance.

The Eq. 5.44 has a nice physical interpretation which relates the dispersion integral to effects from level repulsion. To see this, we rewrite the dispersion integral in the following way:

$$\begin{aligned}\mathcal{R}\mathrm{e}\,\Sigma^+_{med}(k_0,\mathbf{k}) \;&=\; \mathcal{P}\int\limits_{E_F}^{\infty}\frac{d\omega}{\pi}\frac{\mathcal{I}\mathrm{m}\,\Sigma^+_{vac}(\omega,\mathbf{k})+\Delta\mathcal{I}\mathrm{m}\,\Sigma^+(\omega,\mathbf{k})}{\omega-k_0} - c_{vac}(\mathbf{k}) \\ &=\; \mathcal{R}\mathrm{e}\,\Sigma^+_{vac}(k)+\Delta\mathcal{R}\mathrm{e}\,\Sigma^+(k_0,\mathbf{k}) \quad .\end{aligned} \tag{5.45}$$

The quantities $\Delta\mathcal{R}\mathrm{e}\,\Sigma^+_{vac}$ and $\Delta\mathcal{I}\mathrm{m}\,\Sigma^+_{vac}$ are defined via:

$$\Delta\Sigma^+(k_0,\mathbf{k}) \;=\; \Sigma^+_{med}(k_0,\mathbf{k}) - \Sigma^+_{vac}(k) \quad .$$

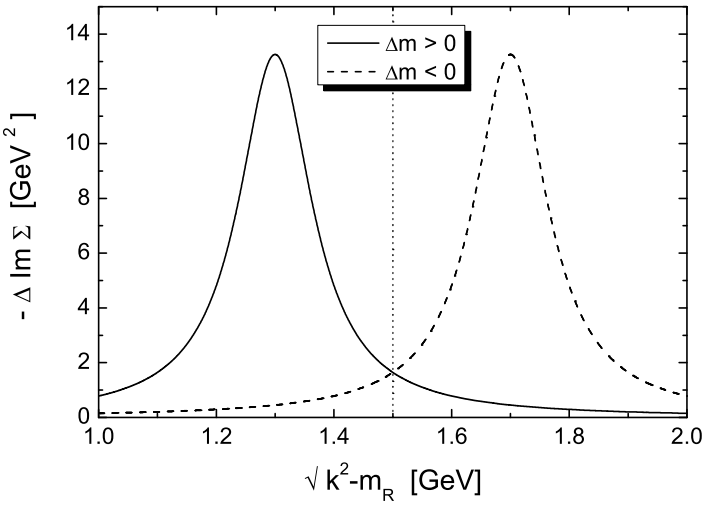

Figure 5.6: Schematic plot indicating the relationship between the imaginary part of the self energy and a mass shift. The vertical line indicates the position of the resonance.

If evaluated on the mass shell $k^2 = m_R^2$, $\Delta\mathcal{R}\mathrm{e}\,\Sigma^+$ gives a direct measure of the mass shift induced by the in-medium corrections. Let us now consider two limiting cases:

$$(I)\ \Delta\mathcal{I}\mathrm{m}\,\Sigma^+ \begin{cases} < 0 \quad , \quad k^2 < m_R^2 \\ \\ \approx 0 \quad , \quad k^2 > m_R^2 \end{cases} \quad \text{and} \quad (II)\ \Delta\mathcal{I}\mathrm{m}\,\Sigma^+ \begin{cases} \approx 0 \quad , \quad k^2 < m_R^2 \\ \\ < 0 \quad , \quad k^2 > m_R^2 \end{cases} \tag{5.46}$$

This situation is depicted in Fig. 5.6 by the solid (case I) and dashed (case II) lines. The dotted line indicates the position of the resonance, which is supposed to have mass of 1.5 GeV. In scenario (I) the dispersion integral produces a repulsive mass shift, i.e. $\Delta\mathcal{R}\mathrm{e}\,\Sigma^+ > 0$. This follows since in the region of a non-vanishing $\Delta\mathcal{I}\mathrm{m}\,\Sigma^+$ one has $\omega < k_0$ and $\Delta\mathcal{I}\mathrm{m}\,\Sigma^+ < 0$. On the other hand, in scenario (II) an attractive mass shift is generated from the dispersion integral.

This finding can be interpreted in terms of level repulsion. Think of a broad baryon resonance as a sharp resonance state coupling to a continuum of meson-nucleon states. Scenario (I) corresponds to a situation where in the nuclear medium states are polarized below resonance but none are affected above resonance. Due to level repulsion the interacting states move the resonance peak up to larger invariant masses. In scenario (II) the situation is reversed: now the additional states are added above the resonance, pushing the resonance peak down. We have noted in the discussion of Eq. 5.44 that the contribution from scattering into two (different) resonances gives presumably small and attractive corrections. Within the picture of level repulsion this is understood as follows: the imaginary part belonging to such processes opens up only for invariant masses above the resonance and attraction results. The only exception is the that the incoming resonance R has enough energy such that the invariant mass of the incoming RN system exceeds $m'_R + m''_R$. In any case, the main effect of such processes will be the population of continuum states above the resonance and as a result they will act as an attraction.

This picture relating the size of the real part of the self energy to the effects from level repulsion, allows also for an estimate of the effects of form factors on the results. When comparing calculations using form factor $FF1$ (Eq. 3.22 in Chapter 3.2.2) with calculations using form factor $FF2$ (Eq. 3.23 in Chapter 3.2.2), level repulsion suggests that more repulsion is provided by the form factor $FF1$. This is due to the asymmetry of $FF1$, which leads to a relative enhancement of strength below resonance and to a depletion of strength above resonance. This way a repulsion relative to a calculation using $FF2$ is achieved.

In practical calculations, $\Delta\mathcal{I}\mathrm{m}\,\Sigma^+$ populates the region around resonance more symmetrically and clear predictions about the sign of the mass shift are not possible (note also that in a symmetric case the absolute size of the mass shift is smaller). One example, where the above arguments can be applied, is the $\Lambda(1405)$ resonance which couples to the KN channel. Here the effects from Pauli-blocking can be related to scenario (II). Since the $\Lambda(1405)$ is below the KN threshold, Pauli blocking removes states from above the resonance. This means that in comparison to the vacuum less repulsion is experienced by the resonance peak which therefore moves up. Such a behaviour is indeed found in various many-body calculations, see for example [83, 63].

Before closing this Section we discuss a particular effect concerning an in-medium shift of the peak of the spectral function. Let us therefore introduce the notions "in-medium mass" and "peak position". The in-medium mass is determined by the real part of the in-medium self energy of the resonance via the equation:

$$k^2 - m_R^2 - \mathcal{R}\mathrm{e}\,\Sigma^+_{med}(k_0, \mathbf{k}) \;=\; 0 \quad . \tag{5.47}$$

In contrast to that, the peak position describes the actual peak of the spectral function ρ (and is therefore more closely related to observables). Both quantities are only identical when the imaginary part of the self energy is not energy dependent. To be more quantitative, let us calculate the derivative of the spectral function taken at the in-medium mass. Remembering the general Breit-Wigner like form of the spectral function ρ, it follows that a positive value for the derivative at this point corresponds to a repulsive shift of the peak, while attraction is indicated by a negative derivative. One finds:

$$\begin{aligned}
\pi\frac{\partial\rho}{\partial k^2} \;&=\; -\frac{\mathcal{I}\mathrm{m}\,\Sigma^{+\prime}_{med}}{(k^2 - m_R^2 - \mathcal{R}\mathrm{e}\,\Sigma^+_{med})^2 + \mathcal{I}\mathrm{m}\,\Sigma^{+\,2}_{med}} + \frac{\mathcal{I}\mathrm{m}\,\Sigma^+_{med}}{[(k^2 - m_R^2 - \mathcal{R}\mathrm{e}\,\Sigma^+_{med})^2 + \mathcal{I}\mathrm{m}\,\Sigma^{+\,2}_{med}]^2} \\
&\quad \times 2\,[(k^2 - m_R^2 - \mathcal{R}\mathrm{e}\,\Sigma^+_{med})(1 - \mathcal{R}\mathrm{e}\,\Sigma^{+\prime}_{med}) + \mathcal{I}\mathrm{m}\,\Sigma^+_{med}\,\mathcal{I}\mathrm{m}\,\Sigma^{+\prime}_{med}] \\
&=\; \frac{\mathcal{I}\mathrm{m}\,\Sigma^{+\prime}_{med}}{\mathcal{I}\mathrm{m}\,\Sigma^{+\,2}_{med}} \quad .
\end{aligned}$$

Here the second step follows from using the defining equation Eq. 5.47 for the in-medium mass. This result indicates that the mass shift is directly proportional to the derivative of the imaginary part of the self energy. For all cases discussed in this work the resonance width is increasing around the in-medium mass. Since the imaginary part of the self energy is proportional to $-\Gamma$, this implies that $\partial\rho/\partial k^2$ is negative and that therefore a shift of the peak of the spectral function down to smaller invariant masses is expected.

This finding allows us to give a qualitative estimate concerning the influence of form factors on the observed of the peak position: a form factor that flattens the width around resonance will lead to more conservative estimates concerning the in-medium shift of the peak position. In particular, the form factor $FF1$ of Eq. 3.22 in Chapter 3.2 leads to smaller peak shifts than form factor $FF2$ of Eq. 3.23.

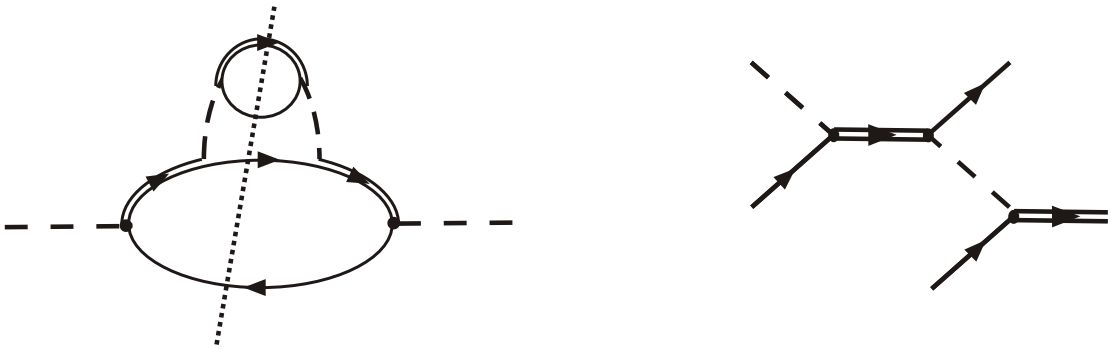

Figure 5.7: Feynman diagram corresponding to the improved meson self energy $\mathcal{I}\mathrm{m}\,\Pi^1$ (left). The right diagram shows that by cutting the self energy diagram, a scattering process on two nucleons is generated.

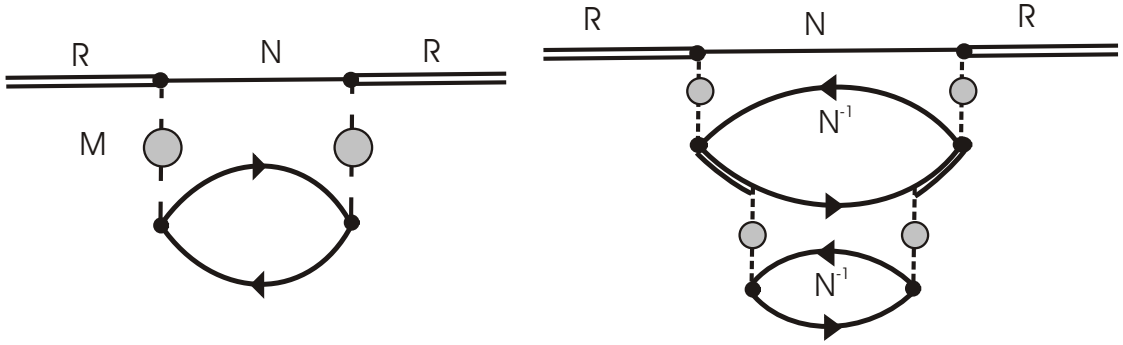

Figure 5.8: Baryon resonance self energies as generated in our scheme. Left: Self energy in the first iteration (Eq. 5.37). Right: Self energy in the second iteration.

5.4 Iteration Scheme

We have now set the stage for a typical self consistency problem. Starting with a model for the in-medium self energy of mesons, we are led to modify also the resonance self energy, which in turn serves as input for an improved calculation of the meson self energy and so forth.

In the actual calculation we proceed as follows: Having calculated the in-medium self energy of the resonances according to Eqs. 5.37 and 5.44, we can improve the meson self energy by replacing $\Sigma^+_{vac} \to \Sigma^+_{med}$ in Eqs. 5.8 and 5.10:

$$\mathcal{I}\mathrm{m}\,\Pi^{(1)}_{\pi/\eta}(q_0,\mathbf{q}) = I_\Pi \left(\frac{f}{m_\varphi}\right)^2 \int \frac{d^3p}{(2\,\pi)^3}\frac{n(\mathbf{p})}{2\,E_N(\mathbf{p})}\mathcal{I}\mathrm{m}\,\frac{\Omega^\varphi}{k_0^2 - E_R^2(\mathbf{k}) - \Sigma^+_{med}(k)} \quad (5.48)$$

$$\mathcal{I}\mathrm{m}\,\Pi^{T/L,(1)}_{\rho}(q_0,\mathbf{q}) = I_\Pi \left(\frac{f}{m_\rho}\right)^2 \int \frac{d^3p}{(2\,\pi)^3}\frac{n(\mathbf{p})}{2\,E_N(\mathbf{p})}\mathcal{I}\mathrm{m}\,\frac{\Omega^{T/L}}{k_0^2 - E_R^2(\mathbf{k}) - \Sigma^+_{med}(k)} \quad .$$

Thus an improved meson spectral function $\mathcal{A}^1_{med}$ is generated, leading to a new guess for the resonance self energy. We iterate this scheme until convergence is reaches. As it will turn out in the result section, this is the case after at most three iterations.

In Fig. 5.7 we show the Feynman diagram corresponding to the improved meson self energy of Eq. 5.48. The diagram on the left is the self energy as generated by plugging in the in-medium width of the resonance. The diagram on the right is obtained by cutting the self energy diagram and displays the physical scattering amplitude leading to the imaginary part of the meson self energy. One sees that the iteration generates reactions of the incoming meson with more than one nucleon.

In Fig. 5.8 we show the resonance self energy as obtained after the first iteration (Eq. 5.37) – this is just a different way of drawing diagram Fig. 5.4 – and after the second iteration. One sees that the diagrams of the first iteration involve at least one nucleon and those after the second iteration involve at least two nucleons. As in the case of the mesons, the iterative procedure generates diagrams that are related to scattering processes on more than one nucleon.

5.5 What Is Not in The Model ?

In this Section we will briefly comment on physical processes that are not included in the calculations.

Let us begin with the meson self energies, which in lowest order in the nuclear density are determined by the meson-nucleon forward scattering amplitude. We saturate this quantity by the assumption that meson-nucleon scattering proceeds only via intermediate baryon resonances. As argued in Chapter 4, this is a reasonable approximation for pions and η mesons, whose scattering amplitudes are dominated from the $P_{33}(1232)$ and the $S_{11}(1535)$ resonances, respectively. However, for small momenta we are missing the s-wave component of the pion-nucleon scattering amplitude, which is responsible for the repulsive mass shift of the pion observed in pionic atoms.

More complicated is the situation for the ρ meson. Here a lot of theoretical work has been devoted to the calculation of effects arising from the dressing of the pions in the pion cloud [24, 52, 62, 113, 111, 122], which forms the self energy of the ρ meson in the vacuum. The corresponding Feynman diagram is depicted in the left digram of Fig. 5.9. As shown in the right diagram of Fig. 5.9, it corresponds to non-resonant contributions to the ρN forward scattering amplitude. Such terms are not present in our calculation. However, their effects are found to be rather small, when the ρN scattering amplitude is subjected to constraints from pion-nucleon scattering and photoabsorption on the nucleon [113].

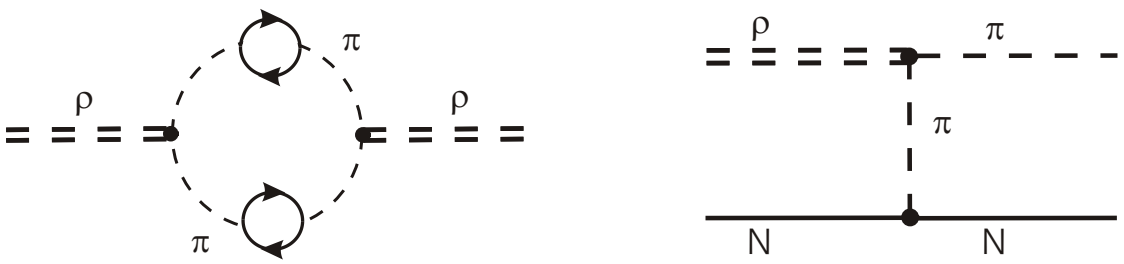

Figure 5.9: Left: In-medium contribution to the ρ self energy arising from dressing the pions in the pion cloud. Right: Corresponding non-resonant contribution to the ρN scattering amplitude.

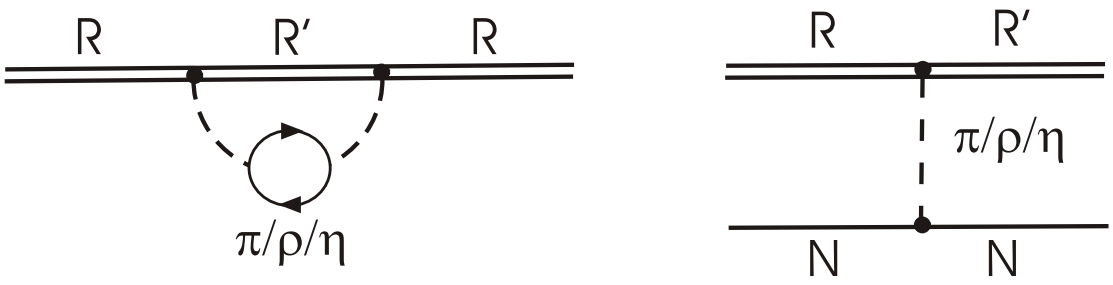

Figure 5.10: Contribution to the baryon resonance self energy (left) arising from the scattering process $RN \to R'N$.

Let us now turn to baryon resonances. There exist many diagrams which are not included in our scheme. For example, scattering processes of the type $RN \to R'N$ as depicted in Fig. 5.10 are not taken into account. Here the main problem is the determination of the coupling constants at the $RR'M$ vertex. Information from phenomenology exists at most for the decay $R \to P_{33}(1232)\pi$ and quark models give estimates for the vertex $P_{33}(1232)P_{33}(1232)\pi$ [33]. For other vertices, information about the coupling constant is very scarce.

Further examples of diagrams not taken into account are shown in Fig. 5.11. The diagram on the left corresponds to an exchange diagram in RN scattering. The right diagram is a higher order correction to the left diagram of Fig. 5.10.

Let us finally mention, that we do not dress the nucleon, i.e. except for Pauli-blocking no medium modifications of the intermediate nucleons are taken into account. Since it is generally acknowledged that the nucleon undergoes a broadening of at most $20 - 30$ MeV at normal nuclear matter density [42], we expect such effects to be small.

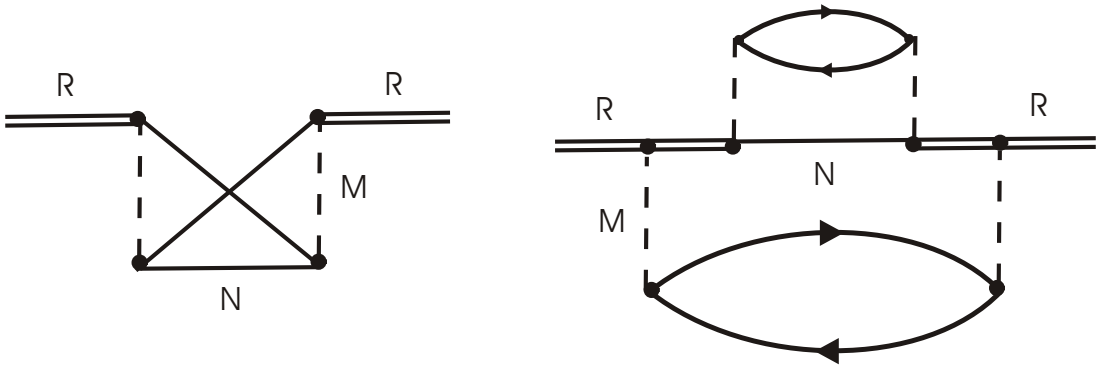

Figure 5.11: Examples of Feynman graphs that are not considered in this work.

5.6 Mixing of Different Meson and Resonance States

In this Section we discuss a phenomenon that is directly related to this work, but that we find interesting enough for a short discussion. In nuclear matter, one can think of various Feynman diagrams corresponding to mixing processes of meson or resonance states

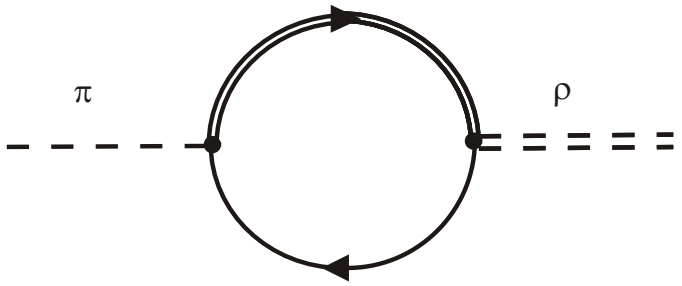

Figure 5.12: Feynman diagram representing the mixing of different mesons.

by scattering on a nucleon, for example $\pi N \leftrightarrow \rho N$ or $D_{13}(1520)N \leftrightarrow S_{11}(1535)N$. A Feynman diagram representing such a mixing process in shown in Fig. 5.12. Such mixing is of great interest if the masses of the states under consideration are reasonably close. In this Section we show that after the usual summation over the spins of the nucleons has been carried out, sharp conditions on the quantum numbers of the states that can mix with each other arise.

Starting point is the following relation between scattering amplitudes of states with definite helicity, which is a consequence of parity conservation [103]:

$$\begin{aligned} \mathcal{T}^{fi}_{-\lambda',-\lambda}(\theta) &= \eta(\eta')^{-1}(-1)^{\lambda-\lambda'}\,\mathcal{T}^{fi}_{\lambda',\lambda}(\theta) \\ \eta &\equiv \eta_k\eta_p(-1)^{s_k+s_p+1/2} \quad , \end{aligned} \tag{5.49}$$

where we have introduced η_q and s_q denoting parity and spin of the particle with momentum q. The helicity λ of the initial or final state is defined the difference of the projections of the angular momentum on the axis of the incoming particles (meson or resonance) in the cm frame of the reaction. Since the self energy is determined from the forward scattering amplitude, we can consider the case $\lambda = \lambda'$. If the forward scattering amplitude changes sign under $\lambda \to -\lambda$, the self energy vanishes.

Let us first discuss the mixing of (pseudo)scalar and (axial)vector states. Here mixing can occur between longitudinal spin-1 meson and spin-0 mesons, since the z component of the angular momentum is to be conserved. It follows that switching the nucleon helicity amounts to switching the total helicity. Thus, if the factor η changes sign when going from (pseudo)scalar to (axial)vector states, no mixing occurs. This implies, that a change of the spin must be followed by a change of the internal parity. Therefore, one can have $\sigma - \omega$ mixing [131], but pions can not mix with ρ mesons.

Of particular interest with respect to the restoration of chiral symmetry are the so called chiral partners, states which have the same quantum numbers except for the parity. In a chirally restored phase their spectral functions have to be identical. Examples are $\rho - a_1$ or $\pi - \sigma$. From the above discussion it follows that mixing of the chiral partners is not possible since they have the same spin but different parity.

Similarly, one can argue for the mixing of baryon resonances. If in addition to summing over the nucleon spin, also a summation over the spin of the resonance is performed, mixing only occurs for certain quantum numbers. In total we can 4 different helicity constellations if the scattering of a spin-$\frac{1}{2}$ resonance is considered, leading to a total helicity of -1, 0 or $+1$. Through the optical theorem the total cross section is proportional to the sum of the imaginary parts of these amplitudes. Using the same arguments as above, it follows that

mixing is only possible if the parity does not change. Similarly, if mixing of spin-$\frac{1}{2}$ and spin-$\frac{3}{2}$ is considered, a change of parity has to be accompanied by a change of the spin.

Chapter 6

The Resonance-Nucleon Interaction

In this Chapter we discuss the modifications of the nucleon-nucleon and the resonance-nucleon interaction at small distances. We start by considering the NN potential. As we will see, the pion exchange part of the NN potential contains a δ-type contribution in position space. Since due to its small mass, pion exchange is not expected to be appropriate at small distances, additional terms are added to the potential which simulate the physics at short short-distances. Similar terms are needed for the ρ exchange contribution. These correction terms are commonly called short-range correlations (SRC).

The δ-type pathologies are not restricted to the NN potential alone. They show up for any potential where the exchanged meson couples in a p-wave to the baryon current. The most prominent example is the $P_{33}(1232)N$ potential. There it is well known that a successful description of $NN \to NN\pi$ scattering requires the introduction of short-range terms [71, 7, 49, 58]. More important for us, it turns out that a realistic model for the in-medium properties of the $P_{33}(1232)$ state needs to take into account such short-range corrections. We have already discussed this issue in Chapter 2 and will show further results in Chapter 8. Since we are interested in the in-medium properties of both positive and negative parity states, we also have to address the question of how to incorporate short-range corrections for those states. In contrast to the $P = +1$ sector, recipes are hardly available at the moment. The development of a framework allowing for a realistic description of short-range effects for $P = -1$ states is one of the major novelties of this thesis.

This Chapter is organized as follows. We start with a discussion of the NN potential and explain the appearance of δ terms in position space. The correction terms are then introduced in two different ways. On the one hand we follow the approach of [100], where short-range correlations are introduced on the basis of a correlation function in position space. This ansatz is contrasted with a formulation where the SRC are generated from contact interactions. These contact interactions are provided by relativistic Lagrangians which respect the quantum numbers of the states under consideration. They contain a priori unknown parameters, describing the strength of the interaction. By matching both approaches we can derive acceptable ranges for those strength parameters.

6.1 The NN potential

In this short introduction to the NN potential we will closely follow the arguments presented in [33, 99]. Within the One Boson Exchange model, the NN interaction is written

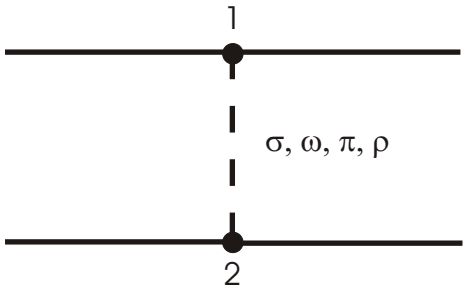

Figure 6.1: One-Boson-Exchange model for the NN interaction.

down in terms of meson exchange contributions. For many applications it is sufficient to consider the exchange of four mesons, σ, ω, π and ρ. The potential is depicted in Fig. 6.1. The corresponding interaction terms read in a relativistic formulation:

$$\begin{aligned}
\mathcal{L}_\sigma &= g_\sigma \, \bar{\psi}_N \, \psi_N \, \sigma \\
\mathcal{L}_\pi &= i \, \frac{f_{NN\pi}}{m_\pi} \, \bar{\psi}_N \, \gamma^\mu \, \gamma^5 \, \psi_N \, \partial_\mu \, \pi \\
\mathcal{L}_\rho &= g_\rho \left(\bar{\psi}_N \, \gamma^\mu \, \psi_N \, \rho_\mu + \frac{\kappa_\rho}{2 \, m_N} \bar{\psi}_N \, \sigma^{\mu\nu} \psi_N \, \rho_{\mu\nu} \right) \\
\mathcal{L}_\omega &= g_\omega \left(\bar{\psi}_N \, \gamma^\mu \, \psi_N \, \omega_\mu + \frac{\kappa_\omega}{2 \, m_N} \, \bar{\psi}_N \, \sigma^{\mu\nu} \psi_N \, \omega_{\mu\nu} \right) \quad .
\end{aligned} \tag{6.1}$$

Here σ, π, ρ and ω denote the respective meson fields, $\rho_{\mu\nu}$ and $\omega_{\mu\nu}$ are the corresponding field tensors. For the pion, we have chosen a pseudovector coupling $\propto \gamma^\mu \gamma^5$. The quantum numbers of the pion allow also for a pseudoscalar Lagrangian,

$$\mathcal{L}_\pi = i \, g \, \bar{\psi}_N \, \gamma^5 \, \psi_N \, \pi \quad .$$

By using the Dirac equation, it is readily shown that for on-shell nucleons both Lagrangians give the same results, if one properly relates the coupling constants $f_{NN\pi}$ and g. When considering off-shell nucleons this equivalences is lost, however. From chiral symmetry arguments the pseudovector coupling is generally preferred. We will not discuss this question in more detail, since in the remainder of this work we will work in the non-relativistic limit, where both couplings lead to identical results.

Note that the Lagrangians describing the coupling of the isovector mesons π and ρ contain also an isospin part, which reads:

$$\chi^\dagger \, \tau \, \chi \, \pi \quad \text{and} \quad \chi^\dagger \, \tau \, \chi \, \rho \quad ,$$

where χ denotes the nucleon isopin spinor. For simplicity we will omit the isospin part in the following discussion.

Taking the non-relativistic reduction of these expressions allows to disentangle the NN-potential into a spin-independent, a spin-longitudinal $(\boldsymbol{\sigma} \cdot \mathbf{q})$ and a spin-transverse $(\boldsymbol{\sigma} \times \mathbf{q})$

piece:

$$\begin{aligned}
\mathcal{L}_\sigma &= g_\sigma\, \psi_N^\dagger\, \psi_N\, \sigma \\
\mathcal{L}_\pi &= i\, \frac{f_{NN\pi}}{m_\pi}\, \psi_N^\dagger\, \sigma_k\, \psi_N\, \partial^k\, \pi \\
\mathcal{L}_\rho &= g_\rho \left[\psi_N^\dagger\, \psi_N\, \rho_0 + \left(\frac{1+\kappa_\rho}{2\, m_N} \right)\, \psi_N^\dagger\, \sigma_j\, \psi_N\, \epsilon_{jkl}\, \partial_k\, \rho_l \right] \\
\mathcal{L}_\omega &= g_\omega \left[\psi_N^\dagger\, \psi_N\, \omega_0 + \left(\frac{1+\kappa_\omega}{2\, m_N} \right)\, \psi_N^\dagger\, \sigma_j\, \psi_N\, \epsilon_{jkl}\, \partial_k\, \omega_l \right] \quad .
\end{aligned} \tag{6.2}$$

Since $g_\omega/g_\rho \approx 3$ whereas $\kappa_\rho \approx 6$ and $\kappa_\omega \approx 0$ [33], one sees that the ω meson mainly contributes to the spin-independent term, whereas the ρ is important in the spin-transverse channel.

The meson exchange potential is given as the product of vertex factor – for example, for pions one obtains $f_{NN\pi}/m_\pi\, \boldsymbol{\sigma} \cdot \mathbf{q}$ from the above Lagrangians – and propagator of the exchanged meson. In addition, we multiply each vertex with a form factor $F(q)$, where q is the 4-momentum of the meson. The exact form of $F(q)$ is not important at this point and will be specified later. One therefore arrives at the following non-relativistic potentials:

$$\begin{aligned}
V^\sigma(q_0, \mathbf{q}) &= g_\sigma^2\, \frac{1}{q_0^2 - \mathbf{q}^2 - m_\sigma^2}\, F_\sigma^2(q_0, \mathbf{q}) \\
V^\omega(q_0, \mathbf{q}) &= g_\omega^2\, \frac{1}{q_0^2 - \mathbf{q}^2 - m_\omega^2}\, F_\omega^2(q_0, \mathbf{q}) \\
V^\pi(q_0, \mathbf{q}) &= \left(\frac{f_{NN\pi}}{m_\pi} \right)^2\, \frac{(\boldsymbol{\sigma}_1 \cdot \mathbf{q})\, (\boldsymbol{\sigma_2} \cdot \mathbf{q})}{q_0^2 - \mathbf{q}^2 - m_\pi^2}\, F_\pi^2(q_0, \mathbf{q}) \\
V^\rho(q_0, \mathbf{q}) &= \left(\frac{f_{NN\rho}}{m_\rho} \right)^2\, \frac{(\boldsymbol{\sigma}_1 \times \mathbf{q})\, (\boldsymbol{\sigma_2} \times \mathbf{q})}{q_0^2 - \mathbf{q}^2 - m_\rho^2}\, F_\rho^2(q_0, \mathbf{q}) \quad .
\end{aligned} \tag{6.3}$$

Here the indizes 1 and 2 refer to the upper and lower vertex of the potential as shown in Fig. 6.1 and we have introduced $f_{NN\rho}/m_\rho = g_\rho/(2\, m_N)(1+\kappa_\rho)$. In a next step we express the spin-dependent π and ρ contributions in terms of spin-central $(\boldsymbol{\sigma}_1 \cdot \boldsymbol{\sigma}_2)$ and spin-tensor $S_{12} = 3\, (\boldsymbol{\sigma}_1 \cdot \hat{\mathbf{q}})\, (\boldsymbol{\sigma}_2 \cdot \hat{\mathbf{q}}) - (\boldsymbol{\sigma}_1 \cdot \boldsymbol{\sigma}_2)$ terms. One easily verifies that

$$\begin{aligned}
(\boldsymbol{\sigma}_1 \times \hat{\mathbf{q}})\, (\boldsymbol{\sigma}_2 \times \hat{\mathbf{q}}) &= \frac{2}{3}\, \boldsymbol{\sigma}_1 \cdot \boldsymbol{\sigma}_2 - \frac{1}{3}\, S_{12} \\
(\boldsymbol{\sigma}_1 \cdot \hat{\mathbf{q}})\, (\boldsymbol{\sigma}_2 \cdot \hat{\mathbf{q}}) &= \frac{1}{3}\, \boldsymbol{\sigma}_1 \cdot \boldsymbol{\sigma}_2 + \frac{1}{3}\, S_{12} \quad .
\end{aligned} \tag{6.4}$$

Here $\hat{\mathbf{q}}$ stands for a unit vector in $\mathbf{q}$ direction. The spin-dependent potentials then read:

$$\begin{aligned}
V^\pi(q_0, \mathbf{q}) &= \left(\frac{f_{NN\pi}}{m_\pi} \right)^2\, \frac{\mathbf{q}^2}{q_0^2 - \mathbf{q}^2 - m_\pi^2}\, \left(\frac{1}{3}\, \boldsymbol{\sigma}_1 \cdot \boldsymbol{\sigma}_2 + \frac{1}{3}\, S_{12} \right) \\
V^\rho(q_0, \mathbf{q}) &= \left(\frac{f_{NN\rho}}{m_\rho} \right)^2\, \frac{\mathbf{q}^2}{q_0^2 - \mathbf{q}^2 - m_\rho^2}\, \left(\frac{2}{3}\, \boldsymbol{\sigma}_1 \cdot \boldsymbol{\sigma}_2 - \frac{1}{3}\, S_{12} \right) \quad .
\end{aligned} \tag{6.5}$$

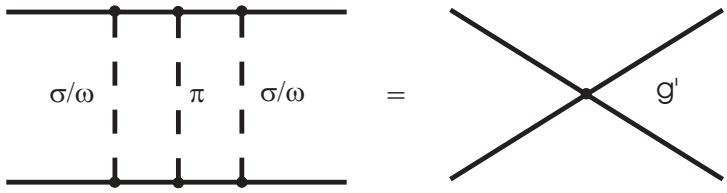

Figure 6.2: Diagrammatic interpretation of the short-range correlations and the parameter g'. There exist similar diagrams, where the pion is replaced by a ρ meson.

6.1.1 The Correlation Potential

For the remainder of this chapter we will concentrate on how the meson-exchange picture is modified at small distances due to the presence of so called short-range correlations. Consider the static limit, i.e. the limit $q_0 \to 0$, of $V^\pi(q_0, \mathbf{q})$. Concentrating on the spin-central term exhibits a very peculiar result:

$$\begin{aligned} V_C^\pi(q_0 = 0, \mathbf{q}) &= -\frac{1}{3}\left(\frac{f_{NN\pi}}{m_\pi}\right)^2 \frac{\mathbf{q}^2}{\mathbf{q}^2 + m_\pi^2}\,\boldsymbol{\sigma}_1 \cdot \boldsymbol{\sigma}_2 \\ &= -\frac{1}{3}\left(\frac{f_{NN\pi}}{m_\pi}\right)^2 \left(1 - \frac{m_\pi^2}{\mathbf{q}^2 + m_\pi^2}\right)\boldsymbol{\sigma}_1 \cdot \boldsymbol{\sigma}_2 \quad . \end{aligned}$$

Obviously, upon Fourier transformation, the central part of the π potential will be proportional to $\delta(r)$ in position space. The same argument holds for the ρ meson exchange potential. Introducing a form factor for the potential will formally get rid of the δ function, but it does not solve the problem that there are large contributions from π and ρ exchange at small distances, where at least the pion exchange is not very reliable.

In order to remedy this situation, one introduces an additional repulsive term $V_{corr}^\pi(q_0, \mathbf{q})$ which is supposed to cancel the δ function. This must be a constant term in momentum space and upon comparison with the central part of the pion potential, one finds

$$V_{corr}^\pi(q_0, \mathbf{q}) = g\left(\frac{f_{NN\pi}}{m_\pi}\right)^2 \boldsymbol{\sigma}_1 \cdot \boldsymbol{\sigma}_2 \quad , \tag{6.6}$$

with $g = \frac{1}{3}$. The physical interpretation of this term is that it resembles more complicated physical processes, like for example the simultaneous exchange of a π and several σ and/or ω mesons, as indicated in Fig. 6.2 [33, 99]. Diagrams like that are expected to be important at small distances and form the origin of short-range correlations. We would like to add here, that the ω exchange can not play the role of the repulsive short-range potential, since the ω is an isoscalar, whereas pion and ρ meson are isovector (remember that we omit the isospin part of the potential for notational convenience).

6.1.2 Contact Interactions

We now start with a more quantitative analysis of short-range correlations. A reliable direct computation of multiple meson exchange diagrams such as the one shown in Fig. 6.2 is not possible, because there is a large number of diagrams which can contribute. Since these diagrams are expected to be important at small distances, it is natural to parametrize

them either in terms of contact interactions or in terms of the exchange of a single, very heavy meson (which is not necessarily identified as a physical meson).

The contact interactions have to be chosen such that they become active in the same spin and isospin structures as the original pion and ρ exchange terms, whose behaviour at small distances has to be improved by the contact terms. In order to achieve this, we obtain them by contracting the hadronic currents coupling to pion and ρ meson. Depending on whether this current is taken from the relativistic $\pi\,N\,N$ or $\rho\,N\,N$ Lagrangian of Eq. 6.1, we denote the Lagrangian describing the contact interaction by $\mathcal{L}_C^\pi$ and $\mathcal{L}_C^\rho$, respectively:

$$\mathcal{L}_C^\pi = c_\pi\, J^\mu\, J_\mu \tag{6.7}$$

$$\mathcal{L}_C^\rho = c_\rho\, B^{\mu\,\nu}\, B_{\mu\,\nu} \quad . \tag{6.8}$$

We stress that these contact interactions do not describe the exchange of a pion or a ρ meson, the index π and ρ refers to the interaction from which the hadronic currents J^μ and $B^{\mu\nu}$ are obtained. The strength parameters c_π and c_ρ are at this point unknown. We will come back to their determination in Section 6.1.4. The tensor $B_{\mu\nu}$ is defined by rewriting the $NN\rho$ Lagrangian of Eq. 6.1 as:

$$\mathcal{L} = B^{\mu\,\nu}\,\partial_\mu\,\rho_\nu \quad . \tag{6.9}$$

More explicitly, the current J_μ and the tensor $B_{\mu\nu}$ read:

$$\begin{aligned} J^\mu &= i\,\frac{f}{m_\pi}\bar{\psi}_N\,\gamma^\mu\,\gamma^5\,\psi_N \\ B^{\mu\nu} &= \frac{f}{m_\rho}\,\bar{\psi}_N\,\sigma^{\mu\nu}\,\psi_N \quad . \end{aligned}$$

An alternative way of deriving these contact interactions is to consider the exchange of a heavy meson with the quantum numbers $J^\pi = 1^+$ ($\mathcal{L}_C^\pi$) or $J^\pi = 2^+$ ($\mathcal{L}_C^\rho$). Also in this picture the multiple meson exchange mechanisms of Fig. 6.2 are parametrized. Sending the mass of the exchange particle to infinity, the contact interactions of Eqs. 6.7 and 6.8 result [118]. More explicitly, the Lagrangian describing the coupling of an axial vector meson (the a_1 meson for example) with $J^\pi = 1^+$ to nucleons has the following form:

$$\mathcal{L} = g\,\bar{\psi}_N\,\gamma_5\,\gamma_\mu\,\psi_N\,a_1^\mu \quad .$$

The nucleon-nucleon scattering amplitude derived from this Lagrangian is proportional to:

$$\mathcal{M} \propto g^2\,\left(\bar{\psi}_N\,\gamma_5\,\gamma_\mu\,\psi_N\right)\frac{g^{\mu\nu} - q^\mu\,q^\nu/m_{a_1}^2}{q^2 - m_{a_1}^2}\left(\bar{\psi}_N\,\gamma_5\,\gamma_\nu\,\psi_N\right) \quad .$$

Taking the limit $m_{a_1} \to \infty$ of this expression yields the same result for the scattering amplitude that would have been obtained by employing the Lagrangian of Eq. 6.7. This procedure does not correspond to the exchange of a physical meson since the mass is not the physical one.

We have now explained the general relativistic form of the Lagrangians of Eqs. 6.7 and 6.8 describing the contact interaction. In our calculations we will only be interested in the leading non-relativistic terms of these Lagrangian. We present now details of the

non-relativistic reduction. As a result we will find that in the non-relativistic limit they lead to the spin-structure $\propto \boldsymbol{\sigma}_1 \cdot \boldsymbol{\sigma}_2$ as required from Eq. 6.6.

Starting from Eq. 6.7 and performing a non-relativistic reduction of $\mathcal{L}_C^\pi$, i.e. dropping terms in p_N/m_N, we find for the contact interaction:

$$\begin{aligned} \mathcal{L}_C^\pi &= c_\pi \left(\frac{f_{NN\pi}}{m_\pi}\right)^2 \left(\bar{\psi}_N \gamma_5 \gamma^\mu \psi_N\right)\left(\bar{\psi}_N \gamma_5 \gamma_\mu \psi_N\right) \qquad (6.10) \\ &\Rightarrow c_\pi \left(\frac{f_{NN\pi}}{m_\pi}\right)^2 \left(\psi_N^\dagger \sigma^i \psi_N\right)\left(\psi_N^\dagger \sigma_i \psi_N\right) \quad , \end{aligned}$$

Note that in the lower line of each of the equations ψ_N denotes the non-relativistic two-component spinor fields.

In order to build $\mathcal{L}_C^\rho$, we first decompose the baryonic tensor $B^{\mu\nu}$ into its spatial (j,k) and time $(j,0)$, $(0,k)$ components. The non-relativistic interaction is then obtained by keeping only the leading terms in p_N/m_N of $B^{\mu\nu}$:

$$\bar{\psi}_N \sigma^{\mu\nu} \psi_N = \left\{ \begin{array}{lcl} (j,k) & : & \epsilon^{jkl} \psi_N^\dagger \sigma_l \psi_N \\ (j,0) & : & -i \psi_N^\dagger \sigma^j \dfrac{\boldsymbol{\sigma}\cdot\boldsymbol{\partial}}{2m_N} \psi_N \\ (0,k) & : & -(j,0) \end{array} \right\} \qquad (6.11)$$

In the derivation we have used that the leading component of σ^{ij} – i.e. the component that leads to the leading non-relativistic term of $B^{\mu\nu}$ – is given by (cf. Appendix B.1):

$$\sigma^{ij} = \frac{i}{2}\left[\gamma^i, \gamma^j\right] \rightarrow -\frac{i}{2}\left[\sigma^i, \sigma^j\right] = \epsilon^{ijk}\sigma_k \quad .$$

Dropping now the terms $\frac{\boldsymbol{\sigma}\cdot\mathbf{p}_N}{2m_N}$ gives:

$$\mathcal{L}_C^\rho = 2\, c_\rho \left(\frac{f}{m_\rho}\right)^2 \left(\psi_N^\dagger \sigma^i \psi_N\right)\left(\psi_N^\dagger \sigma_i \psi_N\right) \quad . \qquad (6.12)$$

Both π and ρ induced interactions have the same spin-structure $\propto \boldsymbol{\sigma}_1 \cdot \boldsymbol{\sigma}_2$, as required from Eq. 6.6. The form of $\mathcal{L}_C^\pi$ and $\mathcal{L}_C^\rho$ implies, that in any calculation where $\mathcal{L}_C^\pi$ contributes, also $\mathcal{L}_C^\rho$ has to be considered. Therefore it is advisable to consider the sum of both terms with a new parameter g^p, where the index p refers to the p-wave coupling of the underlying interaction. The short-range terms of the NN interaction read then:

$$g^p \left(\frac{f_{NN\pi}}{m_\pi}\right)^2 \boldsymbol{\sigma}_1 \cdot \boldsymbol{\sigma}_2 = \left[c_\pi \left(\frac{f_{NN\pi}}{m_\pi}\right)^2 + 2\, c_\rho \left(\frac{f_{NN\rho}}{m_\rho}\right)^2\right] \boldsymbol{\sigma}_1 \cdot \boldsymbol{\sigma}_2 \quad . \qquad (6.13)$$

Keeping terms of higher order in the non-relativistic expansion, the contributions from $\mathcal{L}_C^\pi$ and $\mathcal{L}_C^\rho$ are presumably different. It is therefore hard to find an argument based on the quantum numbers of the involved states, that explains why in the non-relativistic limit both interactions yield formally the same results.

Now we need to determine the strength parameter g^p. In the next Subsection we will show how this can be done.

6.1.3 Correlation Integral

In this Section we explain a method to generated short-range correlations that was originally introduced in [100]. The aim is to find a way to obtain estimates for the so far unknown strength parameter c_π and c_ρ of the Eqs. 6.7 and 6.8. This is done by comparing the approach presented in this Section with the contact interactions of the previous Section.

Consider a typical meson exchange potential in position space, $V(q_0, \mathbf{r})$, defined as

$$V(q_0, \mathbf{q}) \;=\; \int d^3r\, e^{i\,\mathbf{q}\mathbf{r}} V(q_0, \mathbf{r}) \quad .$$

In order to model the short-range correlations, which are not present in V, we introduce the correlation function $C(\mathbf{r})$, such that $V(q_0, \mathbf{r}) \to V(q_0, \mathbf{r})\, C(\mathbf{r})$. Therefore, also the exchange potential in momentum space will be modified:

$$\tilde{V}(q_0, \mathbf{q}) \;=\; \int d^3r\, e^{i\,\mathbf{q}\mathbf{r}}\, V(q_0, \mathbf{r})\, C(\mathbf{r}) \quad . \tag{6.14}$$

The crucial question now is how to choose the correlation function $C(\mathbf{r})$. A popular choice consists of setting $C(r) = 1 - j_0(q_C r)$, with $j_0(q_C r)$ the lowest order Bessel function. This can be motivated by observing that $C(0) = 0$ and $C(r \to \infty) = 1$, which is in accordance with our expectation that the correlations cancel the singularity of the potential at zero distance, whereas at large distances they hardly affect the physics. For the correlation parameter q_C we adopt the usual value of $q_C = m_\omega$ [100]. Loosely speaking this reflects that the correlations are driven by multiple ω exchange. This choice for $C(r)$ has the advantage that its Fourier transform is simply a δ function:

$$\int d^3r\, e^{i\,\mathbf{q}\mathbf{r}}\, j_0(q_C r) \;=\; \frac{2\,\pi^2}{q_C^2}\,\delta(q - q_C) \quad ,$$

thus making an analytical evaluation of the integral Eq. 6.14 feasible. Using this relation and the well-known folding theorem, the full exchange potential including correlations can be cast into the form:

$$\begin{aligned} V(q_0, \mathbf{q}) \;\to\; \tilde{V}(q_0, \mathbf{q}) \;&=\; V(q_0, \mathbf{q}) - \frac{2\,\pi^2}{q_C^2} \int \frac{d^3k}{(2\pi)^3} \delta(|q-k| - q_C)\, V(q_0, \mathbf{k}) \\ &=\; V(q_0, \mathbf{q}) - V_{corr}(q_0, \mathbf{q}) \quad . \end{aligned} \tag{6.15}$$

Let us now subject the π and ρ exchange parts of the NN potential (see Eq. 6.3) to

the correlation integral. The contribution from π exchange leads to:

$$\begin{aligned} V^{\pi}_{corr}(q_0,\mathbf{q}) &= \frac{2\,\pi^2}{q_C^2}\int\frac{d^3k}{(2\pi)^3}\delta(|\mathbf{q}-\mathbf{k}|-q_C)\left(\frac{f_{NN\pi}}{m_\pi}\right)^2 F_\pi^2(q_0,\mathbf{k})\,k_ik_j\,\frac{\sigma_1^i\,\sigma_2^j}{q_0^2-\mathbf{k}^2-m_\pi^2} \\ &= \frac{2\,\pi^2}{q_C^2}\int\frac{d\Omega}{(2\pi)^3}\,q_C^2\left(\frac{f_{NN\pi}}{m_\pi}\right)^2 F_\pi^2(q_0,\mathbf{k}'+\mathbf{q})\frac{\sigma_1^i\,\sigma_2^j}{q_0^2-(\mathbf{k}'+\mathbf{q})^2-m_\pi^2}\;\times \\ &\quad\times\left[\underbrace{q_i\,q_j}_{I}+\underbrace{k_i'\,k_j'}_{II}+\underbrace{k_i'\,q_j+k_j'\,q_i}_{III}\right]_{|\mathbf{k}'|=q_C} \qquad (6.16) \\ &\approx \left(\frac{f_{NN\pi}}{m_\pi}\right)^2\tilde{F}_\pi^2(q_0,\mathbf{q})\frac{\sigma_1^i\,\sigma_2^j}{q_0^2-\mathbf{q}^2-q_C^2-m_\pi^2}\left[\underbrace{q_i\,q_j}_{I}+\underbrace{\int\frac{d\Omega}{4\pi}k_i'k_j'|_{|\mathbf{k}'|=q_C}}_{II}\right] \\ &= \left(\frac{f_{NN\pi}}{m_\pi}\right)^2\tilde{F}_\pi^2(q_0,\mathbf{q})\,\tilde{D}_\pi(q_0,\mathbf{q})\,\sigma_1^i\,\sigma_2^j\,(q_iq_j+\frac{1}{3}\,q_C^2\,\delta_{ij}) \quad . \end{aligned}$$

Here the quantities $\tilde{D}_\pi(q_0,\mathbf{q})$ and $\tilde{F}_\pi(q_0,\mathbf{q})$ stand for the usual meson propagator and monopole form factors with the replacement $\mathbf{q}^2\to\mathbf{q}^2+q_C^2$:

$$\tilde{D}_\pi(q_0,\mathbf{q}) = \frac{1}{q_0^2-\mathbf{q}^2-q_C^2-m_\pi^2} \quad , \quad \tilde{F}_\pi(q_0,\mathbf{q}) = \frac{\Lambda^2}{\Lambda^2-q_0^2+\mathbf{q}^2+q_C^2} \quad .$$

The second line follows from the first line via the variable substitution $\mathbf{k}\to\mathbf{k}'=\mathbf{k}-\mathbf{q}$. In order to arrive at the third line an approximation has been made [100]: There are three terms depending on the angle $x=\cos\theta$ between the vectors $\mathbf{k}$ and $\mathbf{q}$, namely the form factor F, the propagator and the terms in square brackets. Instead of performing the dx integration over the product of these three terms, the integration is done for each term individually. This procedure implies that all terms linear in x vanish. For example, for the integral over the propagator we get:

$$\int dx\,\frac{1}{q_0^2-\mathbf{k}^2-\mathbf{q}^2-2\,|\mathbf{q}||\mathbf{k}|x-m_\pi^2}\bigg|_{|\mathbf{k}|=q_C} \approx \frac{1}{q_0^2-q_C^2-\mathbf{q}^2-m_\pi^2}$$

As a further consequence of this approximation the therm denoted by III does not contribute to the correlation potential. One might worry about the quality of these approximations. Since in the remainder we will only consider the case $\mathbf{q}=0$ GeV, where the integrand does not depend on x, this needs not to be of concern to us.

The contribution of term II can either be checked explicitly or by realizing that

$$\int\frac{d\Omega}{4\,\pi}k_ik_j = a\,\delta_{ij} \quad .$$

Taking the trace of this expression yields:

$$\delta_{ij}\int\frac{d\Omega}{4\,\pi}k_ik_j = \mathbf{k}^2 = 3\,a \;\Rightarrow\; \int\frac{d\Omega}{4\,\pi}\,k_ik_j|_{|\mathbf{k}|=q_C} = \frac{1}{3}\,q_C^2\,\delta_{ij} \quad ,$$

which explains the result for term II.

The important point of the result of Eq. 6.16 is that the leading term in the 3-momentum of $V^{\pi}_{corr}(q_0, \mathbf{q})$ is a constant proportional to q_C^2, whereas the original potential $V^{\pi}(q_0, \mathbf{q})$ is in leading order proportional to $\mathbf{q}^2$.

The ρ exchange potential is treated along the same lines. The final result for the correlation part of both the π and ρ exchange potentials reads therefore:

$$\begin{aligned} V^{\pi}_{corr}(q_0, \mathbf{q}) &= \left(\frac{f_{NN\pi}}{m_\pi}\right)^2 \tilde{F}^2_\pi(q_0, \mathbf{q})\, \sigma_1^i\, \sigma_2^j\, \tilde{D}_\pi(q_0, \mathbf{q})\, \left(q_i q_j + \frac{1}{3}\, q_C^2 \delta_{ij}\right) \\ V^{\rho}_{corr}(q_0, \mathbf{q}) &= \left(\frac{f_{NN\rho}}{m_\rho}\right)^2 \tilde{F}^2_\rho(q_0, \mathbf{q})\, \sigma_1^i\, \sigma_2^j\, \tilde{D}_\rho(q_0, \mathbf{q})\, \left(-q_i q_j + (\mathbf{q}^2 + \frac{2}{3}\, q_C^2) \delta_{ij}\right) \quad . \end{aligned} \tag{6.17}$$

These equations show that the short-range correlations mix the spin-longitudinal and the spin-transverse channel. It is therefore rewarding, to write out the sum of both $V^{\pi}_{corr}(q_0, \mathbf{q})$ and $V^{\rho}_{corr}(q_0, \mathbf{q})$ in terms of the spin-longitudinal and spin-transverse channels. Using Eq. 6.4 yields:

$$\begin{aligned} &V^{\pi}_{corr}(q_0, \mathbf{q}) + V^{\rho}_{corr}(q_0, \mathbf{q}) = \\ &\left[\left(\frac{f_{NN\pi}}{m_\pi}\right)^2 (\mathbf{q}^2 + \frac{1}{3} q_C^2) \tilde{D}_\pi\, \tilde{F}^2_\pi + \left(\frac{f_{NN\rho}}{m_\rho}\right)^2 \frac{2}{3} q_C^2\, \tilde{D}_\rho\, \tilde{F}^2_\rho\right]\, (\boldsymbol{\sigma}_1 \cdot \hat{\mathbf{q}})(\boldsymbol{\sigma}_2 \cdot \hat{\mathbf{q}}) + \\ &\left[\left(\frac{f_{NN\pi}}{m_\pi}\right)^2 \frac{1}{3} q_C^2\, \tilde{D}_\pi\, \tilde{F}^2_\pi + \left(\frac{f_{NN\rho}}{m_\rho}\right)^2 (\mathbf{q}^2 + \frac{2}{3} q_C^2)\, \tilde{D}_\rho\, \tilde{F}^2_\rho\right]\, (\boldsymbol{\sigma}_1 \times \hat{\mathbf{q}})(\boldsymbol{\sigma}_2 \times \hat{\mathbf{q}}) \ . \end{aligned} \tag{6.18}$$

Here we have suppressed the arguments in propagator and form factor. In the limit $\mathbf{q} = 0$, the contributions to both the spin-longitudinal and spin-transverse potential are identical and proportional to the central part only:

$$\begin{aligned} &V^{\pi}_{corr}(q_0, \mathbf{q} = 0) + V^{\rho}_{corr}(q_0, \mathbf{q} = 0) = \\ &\frac{q_C^2}{3}\left[\left(\frac{f_{NN\pi}}{m_\pi}\right)^2 \tilde{D}_\pi\, \tilde{F}^2_\pi + 2\left(\frac{f_{NN\rho}}{m_\rho}\right)^2 \tilde{D}_\rho\, \tilde{F}^2_\rho\right]\, (\boldsymbol{\sigma}_1 \cdot \hat{\mathbf{q}})(\boldsymbol{\sigma}_2 \cdot \hat{\mathbf{q}}) \\ &+ \frac{q_C^2}{3}\left[\left(\frac{f_{NN\pi}}{m_\pi}\right)^2 \tilde{D}_\pi\, \tilde{F}^2_\pi + 2\left(\frac{f_{NN\rho}}{m_\rho}\right)^2 \tilde{D}_\rho\, \tilde{F}^2_\rho\right]\, (\boldsymbol{\sigma}_1 \times \hat{\mathbf{q}})(\boldsymbol{\sigma}_2 \times \hat{\mathbf{q}}) \\ = \quad &\frac{q_C^2}{3}\left[\left(\frac{f_{NN\pi}}{m_\pi}\right)^2 \tilde{D}_\pi\, \tilde{F}^2_\pi + 2\left(\frac{f_{NN\rho}}{m_\rho}\right)^2 \tilde{D}_\rho\, \tilde{F}^2_\rho\right]\, \boldsymbol{\sigma}_1 \cdot \boldsymbol{\sigma}_2 \quad . \end{aligned} \tag{6.19}$$

Keeping the 3-momentum $\mathbf{q}$ finite, the contributions of pion and ρ exchange to the central part of the potential are not identical any more. This reflects the observation made at the end of Section 6.1.2 that the next-to-leading order contributions of $\mathcal{L}^{\pi}_C$ and $\mathcal{L}^{\rho}_C$ generate different structures.

6.1.4 Matching

We will now obtain estimates for g^p by matching the Eqs. 6.19 and 6.13. Our contact interactions produce only terms proportional to $\boldsymbol{\sigma}_1 \cdot \boldsymbol{\sigma}_2$ and for the matching we keep only

the central part of the correlation potential taken at $\mathbf{q} = 0$ GeV. Comparing the correlation potential Eq. 6.19 and the contact interaction Eq. 6.13, yields the following result for g^p:

$$g^p \left(\frac{f_{NN\pi}}{m_\pi}\right)^2 = \frac{q_C^2}{3}\left[\left(\frac{f_{NN\pi}}{m_\pi}\right)^2 \tilde{F}_\pi^2\,\tilde{D}_\pi + 2\left(\frac{f_{NN\rho}}{m_\rho}\right)^2 \tilde{F}_\rho^2\,\tilde{D}_\rho\right] \quad . \tag{6.20}$$

It has been known for a long time that this way reasonable guesses for g^p are obtained, if one takes $q_0 \approx 0$ GeV and $q_C = 0.782$ GeV [99, 100]. Phenomenology requires values for g^p to be in the order of 0.6 for the NN potential, see for example [99, 100, 7, 49, 71, 58] and references therein. With the parameters used in this work for the coupling constants and the cutoff parameters (given in Table A.1 in Appendix A) we obtain a value of 0.35 which is somewhat smaller than what is required by phenomenology. One should note, however, that the results are quite sensitive to the precise value of the cutoff parameters Λ_π and Λ_ρ. Taking $\Lambda_\pi = 1.2$ GeV instead of $\Lambda_\pi = 1$ GeV and $\Lambda_\rho = 2$ GeV instead of $\Lambda_\rho = 1.5$ GeV, a significantly larger value of $g^p = 0.51$ is derived (cf. [99]). Due to these sensitivities we take phenomenological values for g^p rather than relying on the precise value of the correlation integral. Note that g^p is larger than $\frac{1}{3}$, a value suggested in the discussion following Eq. 6.6. Apart from rather small effects coming from the form factor, which in fact decrease the value of g^p, both the correlation integral approach and the contact interactions explain this effect with the ρ admixture in the π potential, see Eqs. 6.19 and 6.20.

Let us summarize the results: we have shown that starting from two different sides – the contact interactions of Eqs. 6.7 and 6.8 and the correlation integral Eq. 6.14 – one arrives at the same non-relativistic description of the short-range correlations. Furthermore, matching both results allows for a reasonable computation of the strength parameter g^p. In the practical calculations we will not use values for g^p as following from the correlation approach, but vary them freely within commonly accepted boundaries in order to obtain a decent fit of the in-medium properties of the $P_{33}(1232)$. The reader may now rightly ask himself why we had to go through the lengthy formalism of Section 6.1.1, if its results are discarded at the end. The reason is that later on we want to discuss the effects of short-range terms for $P = -1$ states. There we will again encounter parameters characterizing the strength of the short-range correlations. In contrast to the case of $P = +1$ states, there no accepted boundaries for these parameters exist, in fact not much work has been done on this field at all except for a study in [117]. We use the correlation integral method to obtain estimates for the strength of the short-range correlations. However, in order to do so we first had to demonstrate that this way the better known potentials for states with positive parity are well described.

6.2 Positive Parity Resonances

In the previous Section we have discussed the appearance of short-range correlations in the NN interaction. However, such correlations are also present in resonance-nucleon processes like those shown in Fig. 6.3. We first discuss the case of positive parity $P = +1$ states. For $J^\pi = \frac{1}{2}^+$ resonances the results from the NN interaction can be translated piece by piece, only obvious adjustments concerning the coupling constant f and isospin factors have to be made. In this work we are also interested in a few resonances with the quantum numbers $J^\pi = \frac{3}{2}^+$. In particular, the $P_{33}(1232)$ and the $P_{13}(1720)$ play an important role

in the discussion of pions and ρ mesons in nuclear matter. We will see that one can treat the corresponding RN transition potentials in exactly the same way as the NN potential.

6.2.1 Contact Interactions

The contact interactions $\mathcal{L}_C^\pi$ and $\mathcal{L}_C^\rho$ for $J^\pi = \frac{3}{2}^+$ states are obtained similarly to the NN case. Based on the relativistic Lagrangian given in Appendix C, Eq. C.1, we obtain the non-relativistic contact interaction by dropping terms of the order p_N/m_N:

$$\begin{aligned} \mathcal{L}_C^\pi &= c_\pi \left(\frac{f_{RN\pi}}{m_\pi}\right)^2 \left(\bar\psi_R^\mu \psi_N\right)\left(\bar\psi_N \psi_{R,\mu}\right) \\ &\Rightarrow c_\pi \left(\frac{f_{RN\pi}}{m_\pi}\right)^2 \left(\psi_R^\dagger\, S^{i\,\dagger}\, \psi_N\right)\left(\psi_N^\dagger\, S_i\, \psi_R\right) \quad , \end{aligned} \tag{6.21}$$

Here the spin-$\frac{3}{2}$ transition matrix S has been introduced, which contains the Clebsch-Gordan coefficients for the spin coupling $\frac{1}{2} \oplus 1 = \frac{3}{2}$, see Eq. B.25 in Appendix B.4. In the ρ sector we find for the spatial (j,k) and the time $(j,0)\,,\,(0,k)$ components of the tensor $B_{\mu\nu}$ of Eq. 6.9

$$i\left(\bar\psi_R^\mu \gamma^\nu - \bar\psi_R^\nu \gamma^\mu\right)\gamma^5\,\psi_N = \begin{cases} (j,k) & : \quad \psi_R^\dagger\, \epsilon^{jkl}\, S_l^\dagger\, \psi_N \\ (j,0) & : \quad i\,\psi_R^\dagger\, S^{j\,\dagger}\, \dfrac{\boldsymbol{\sigma}\cdot\boldsymbol{\partial}}{2m_N}\,\psi_N \\ (0,k) & : \quad -(j,0) \end{cases} \tag{6.22}$$

Since the derivation of B^{ij} is a somewhat tricky, let us give some details. First of all, we need the relation $\sigma_i\,\sigma_j = \delta_{ij} + i\,\epsilon_{ijk}\,\sigma_k$ (cf. Appendix B.1). Keeping only the leading non-relativistic terms we find:

$$\begin{aligned} B^{jk} &= i\left(\bar\psi_R^j \gamma^k - \bar\psi_R^k \gamma^j\right)\gamma^5\,\psi_N \;\rightarrow\; i\left(\psi_R^\dagger\, S^{j\,\dagger}\,\sigma^k - \psi_R^\dagger\, S^{k\,\dagger}\,\sigma^j\right)\psi_N \\ &= i\left(\psi_R^\dagger\, \mathbf{S}^\dagger \times \boldsymbol{\sigma}\right)_l \epsilon^{jkl}\,\psi_N \;=\; i\,\psi_R^\dagger\, S^{j'}\,\sigma^{k'}\,\epsilon_{j'k'l}\,\epsilon^{jkl}\,\psi_N \\ &= \psi_R^\dagger\, S^{j'}\,\delta_{j'\,l}\,\epsilon^{jkl}\,\psi_N \;=\; \psi_R^\dagger\, S_l\,\epsilon^{jkl}\,\psi_N \end{aligned}$$

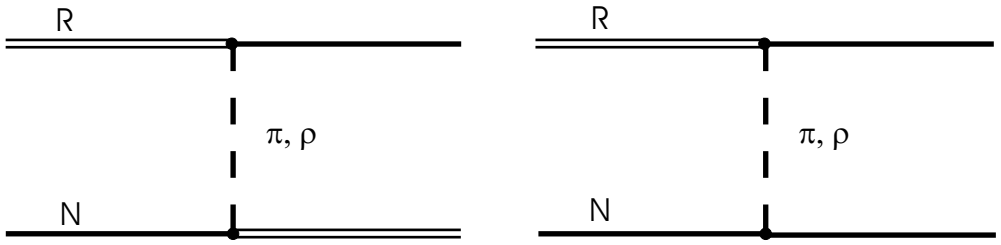

Figure 6.3: π and ρ meson contribution to the transition potential $RN \to NR$ and $RN \to NN$.

Whereas the spinor ψ_N in the first equation is a relativistic one, in the remaining equations it stands for a non-relativistic spinor. In going from the forth to the fifth equation we have used that $\sigma_i\,\sigma_j\,S^j = 0$ since $\sigma_i\,\sigma_j$ is proportional to the non-relativistic spin-$\frac{1}{2}$ projector, see Eq. C.13 in Appendix C.2. Dropping terms $\frac{\boldsymbol{\sigma}\cdot\mathbf{p}_N}{2m_N}$ leads to the contact interaction:

$$\mathcal{L}_C^\rho \;=\; 2\,c_\rho\,\left(\frac{f_{RN\rho}}{m_\rho}\right)^2\,\left(\psi_R^\dagger\,S^{i\,\dagger}\,\psi_N\right)\left(\psi_N^\dagger\,S_i\,\psi_R\right) \quad . \tag{6.23}$$

The results obtained here are – apart from the replacement $\sigma_i \to S_i$ – identical to those for the NN interaction. Both π and ρ exchange lead in the non-relativistic limit to the same structure and they can be combined to give:

$$g^p\,\left(\frac{f_{RN\pi}}{m_\pi}\right)^2\,\mathbf{S}_1\cdot\mathbf{S}_2 \;=\; \left[c_\pi\,\left(\frac{f_{RN\pi}}{m_\pi}\right)^2 + 2\,c_\rho\,\left(\frac{f_{RN\rho}}{m_\rho}\right)^2\right]\mathbf{S}_1\cdot\mathbf{S}_2 \quad . \tag{6.24}$$

6.2.2 Correlation Integral and Matching

The π and ρ exchange pieces of the RN potential are obtained from the corresponding pieces in the NN potential by letting $\sigma_i \to S_i$ in Eqs. 6.5 and 6.19. Also the coupling constants and – in the case isospin-$\frac{3}{2}$ resonances – isospin factors have to be changed. One thus gets for the correlation part of the RN transition potential:

$$\begin{aligned} &V_{corr}^\pi(q_0,\mathbf{q}=0) + V_{corr}^\rho(q_0,\mathbf{q}=0) = \\ &\frac{q_C^2}{3}\left[\left(\frac{f_{NN\pi}}{m_\pi}\right)^2\,\tilde{D}_\pi\,\tilde{F}_\pi^2 + 2\,\left(\frac{f_{NN\rho}}{m_\rho}\right)^2\,\tilde{D}_\rho\,\tilde{F}_\rho^2\right]\mathbf{S_1}\cdot\mathbf{S_2} \quad . \end{aligned} \tag{6.25}$$

As for the NN potential, we can now obtain estimates for g^p by matching Eqs. 6.24 and 6.25. For the $P_{33}(1232)$ resonance we find – depending on the form factor – values in the range of $g^p = 0.2 - 0.3$. Note that the short-range strength in this channel is somewhat smaller compared to the NN channel, where we found values around 0.35. This is explained by the fact that the ρ contribution – measured by the ratio $(f_\rho/f_\pi)^2\,(m_\pi/m_\rho)^2$ – is larger in the NN channel. It is interesting to note that similar results are reported from phenomenology [71, 49, 58]. The values for g^p taken in this work respect this finding, see Table A.1. This shows again that the results obtained via the correlation integral approach Eq. 6.14 are reasonable at least on a qualitative level and are therefore a good starting point for the discussion of negative parity resonances.

Spin-$\frac{5}{2}$ resonances are treated in a more phenomenological manner: we have not attempted a construction of contact interactions from pion or from ρ meson exchange. For the pion propagation in nuclear matter we neglect the effects from short-range correlations in the $J^\pi = \frac{5}{2}^+$ sector altogether. For the ρ meson we carry over the results obtained in the $J^\pi = \frac{1}{2}^+$ and $J^\pi = \frac{3}{2}^+$ sectors. This ad-hoc prescription is motivated from the fact that subjecting the ρ meson part of the exchange potential to the correlation integral leads to exactly the same results in all three sectors. This is due to the fact that the potentials are p-wave.

6.3 Negative Parity Resonances

In the previous Sections we have discussed the correlation potential for the nucleon and resonances with positive parity. Although the quantum numbers of the particles are not the same, we obtained similar contact interactions owing to the fact that the underlying meson-nucleon-resonance interaction is p-wave. We will now turn to states with negative parity. Here the coupling to pions and ρ mesons is either s-wave or d-wave.

Before going into details, let us first present a basic argument concerning the relative importance of the correlations for s-wave potentials. As detailed in Subsection 6.1.1, p-wave potentials contain a contribution proportional to unity in momentum space, thus producing a δ type interaction in position space. We show now that for s-wave potentials this does not hold. A typical non-relativistic Lagrangian appropriate for the coupling of negative parity resonances to the πN system is of the form:

$$\mathcal{L} \;=\; f\,\psi_R^\dagger\,\psi\,\pi \quad , \tag{6.26}$$

The potential derived from this Lagrangian is given by:

$$V(q_0,\mathbf{q}) \;=\; f^2\,\frac{F_\pi^2}{q_0^2-q^2-M^2} \quad , \tag{6.27}$$

where F_π is a form factor. This potential does not produce a $\delta(r)$ contribution. It follows that there is no immediate need to introduce short-range correlation. Nonetheless, correlations such as those generated from the approach in Eq. 6.14 do exist. Performing the correlation integral leads to the following potential:

$$V(q_0,\mathbf{q}) \;=\; f^2\,\frac{F_\pi^2}{q_0^2-\mathbf{q}^2-M^2} - f^2\,\frac{\tilde{F}_\pi^2}{q_0^2-\mathbf{q}^2-q_C^2-M^2} \quad . \tag{6.28}$$

The function $\tilde{F}_\pi$ is introduced after Eq. 6.16. The correlations manifest themselves in the replacement $\mathbf{q}^2 \to \mathbf{q}^2+q_C^2$ in the second term. Comparing this with the result from Eq. 6.17 for p-wave resonances, we find an important difference: whereas at small momenta the leading term of the correlations there is a constant, the uncorrelated potential is proportional to $\mathbf{q}^2$. Thus, a large correction is induced for small momenta. For s-wave states, on the other hand, both the uncorrelated potential and the correlation correction start off with the same momentum dependence and the relative effect of correlations is much reduced. Since the potential and scattering amplitudes are directly related, this means that short-range correlations are presumably not an important ingredient for an analysis of NN scattering involving s-wave states.

On the other hand, when going to the nuclear medium effects from short-range terms might become more sizeable. As we will detail in Section 6.5, these terms are iterated and one is sensitive to the absolute size of the short-range correlations which in part is determined by the coupling constant f. It follows that if f is sufficiently large, important corrections from the short-range correlations can be expected.

6.3.1 Contact Interactions

Let us now turn to the discussion of negative parity states. We proceed along the same lines as for $P=+1$ states. For the contact interactions derived in the π sector the following Lagrangians are obtained.

$J^\pi = \frac{1}{2}^-$:

$$\begin{aligned} \mathcal{L}_C^\pi &= c_\pi \left(\frac{f}{m_\pi}\right)^2 \left(\bar\psi_R\,\gamma^\mu\,\psi_N\right)\left(\bar\psi_N\,\gamma_\mu\,\psi_R\right) \\ &\Rightarrow\ c_\pi \left(\frac{f}{m_\pi}\right)^2 \left(\psi_R^\dagger\,\psi_N\right)\left(\psi_N^\dagger\,\psi_R\right) \quad . \end{aligned} \tag{6.29}$$

$J^\pi = \frac{3}{2}^-$:

$$\begin{aligned} \mathcal{L}_C^\pi &= c_\pi \left(\frac{f}{m_\pi}\right)^2 \left(\bar\psi_R^\mu\,\gamma^5\,\psi_N\right)\left(\bar\psi_N\,\gamma^5\,\psi_{R,\mu}\right) \\ &\Rightarrow\ c_\pi \left(\frac{f}{m_\pi}\right)^2 \left(\psi_R^\dagger\,S^{i\,\dagger}\,\frac{\sigma_k\,\partial_k}{2m_N}\,\psi_N\right)\left(\psi_N^\dagger\,\frac{\overleftarrow{\partial}_k\ \sigma_k}{2m_N}\,S_i\,\psi_R\right) \quad . \end{aligned} \tag{6.30}$$

For $J^\pi = \frac{3}{2}^-$ resonances, the contact interaction is of the order $\frac{\boldsymbol{\sigma}\cdot\mathbf{p_N}}{2m_N}$ and up to now we have dropped such terms. Here these terms should be kept for consistency, since they also arise in the non-relativistic reduction of the πNR interaction (see Eqs. C.1 and C.15 in Appendix C), where they produce the necessary d-wave coupling.

In order to obtain the non-relativistic contact interaction $\mathcal{L}_C^\rho$, we first decompose the tensor $B_{\mu\nu}$ into spatial (j,k) and time $(j,0)$, $(0,k)$ components. Keeping only the leading non-relativistic terms, this leads to the following expressions for the nucleon-resonance interaction:

$J^\pi = \frac{1}{2}^-$:

$$i\,\bar\psi_R\,\sigma^{\mu\,\nu}\,\gamma^5\,\psi_N = \begin{cases} (j,k) & : \quad i\,\psi_R^\dagger\,\epsilon^{ijl}\,\sigma_l\,\dfrac{\boldsymbol{\sigma}\cdot\boldsymbol{\partial}}{2m_N}\,\psi_N \\ (j,0) & : \quad \psi_R^\dagger\,\sigma^j\,\psi_N \\ (0,k) & : \quad -(j,0) \end{cases} \tag{6.31}$$

$$\mathcal{L}_C^\rho = 2\,c_\rho \left(\frac{f}{m_\rho}\right)^2 \left(\psi_R^\dagger\,\sigma^i\,\psi_N\right)\left(\psi_N^\dagger\,\sigma_i\,\psi_R\right) \quad .$$

$J^\pi = \frac{3}{2}^-$:

$$\left(\bar\psi_R^\mu\,\gamma^\nu - \bar\psi_R^\nu\,\gamma^\mu\right)\,\psi_N = \begin{cases} (j,k) & : \quad -i\,\psi_R^\dagger\,\epsilon^{jkl}\,S_l^\dagger\,\dfrac{\boldsymbol{\sigma}\cdot\boldsymbol{\partial}}{2m_N}\,\psi_N \\ (j,0) & : \quad \psi_R^\dagger\,S^{j\,\dagger}\,\psi_N \\ (0,k) & : \quad -(j,0) \end{cases} \tag{6.32}$$

$$\mathcal{L}_C^\rho = 2\,c_\rho \left(\frac{f}{m_\rho}\right)^2 \left(\psi_R^\dagger\,S^{i\,\dagger}\,\psi_N\right)\left(\psi_N^\dagger\,S_i\,\psi_R\right) \quad .$$

As in the $P = +1$ case, these interactions are the simplest contact interactions leading to non-vanishing contributions in typical diagrams such as Fig. 6.4. The technical steps

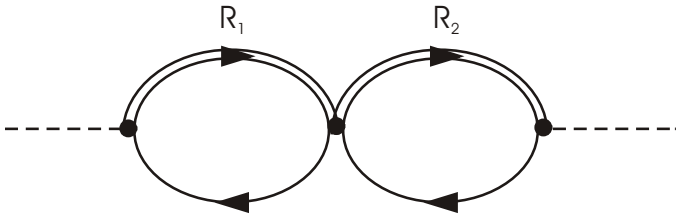

Figure 6.4: Lowest order correction of the self energy from the contact interaction. The double-line stands for any of the resonances or the nucleon and does not need to represent the same state in both loops.

involved in the non-relativistic reduction are similar to those encountered in the $P = +1$ sector, which are discussed in detail around Eqs. 6.12 and 6.23.

As mentioned already in the introduction of this Chapter, there is a clear difference between the contact interactions for $P = +1$ and those for $P = -1$ states. In the negative parity sector $\mathcal{L}_C^\pi$ and $\mathcal{L}_C^\rho$ are not equivalent. Considering, for example, a correction to the meson self energy according to Fig. 6.4, the pion self energy will not receive contributions from $\mathcal{L}_C^\rho$ and neither will the ρ self energy receive contributions form $\mathcal{L}_C^\pi$. For spin-$\frac{1}{2}$ resonances this can be motivated as follows: since the coupling to pions is s-wave and the pion is a pseudoscalar particle, there is no vector available that could couple to a σ matrix and consequently the leading non-relativistic term of J_μ contains no spin-flip terms. For the ρ meson, albeit coupling an s-wave as well, there is still the polarization vector $\boldsymbol{\rho}$ and the therefore the leading non-relativistic terms of $B_{\mu\nu}$ produce spin-flip contributions. Doing the spin-summation as appropriate for calculations in nuclear matter, the decoupling of π and ρ sector follows. To be more explicit, let us consider the diagram Fig. 6.4. Assuming that the external meson is a pion and that the contact interaction is derived from $\mathcal{L}_C^\rho$, we find for the self energy contribution of a $J^\pi = \frac{1}{2}^-$ state:

$$\Pi_\pi(q_0, \mathbf{q}) \;\propto\; Tr\left[\sigma_i\right] Tr\left[\sigma_j\right] \;=\; 0 \quad . \tag{6.33}$$

A similar argument holds for $J^\pi = \frac{3}{2}^-$ states. It is therefore necessary to keep both $\mathcal{L}_C^\pi$ and $\mathcal{L}_C^\rho$ independently and fix the respective parameters c_π and c_ρ. We will from now on denote c_π and c_ρ by g_π^d, g_π^s and g_ρ^s, where s and d indicate the angular momentum of the underlying meson-nucleon interaction.

6.3.2 Correlation Integral and Matching

We now subject the π and ρ exchange potentials to the correlation integral Eqs. 6.14 and 6.15, which allows us to determine the strength of the contact interaction. Let us start off with the ρ exchange for $J^\pi = \frac{3}{2}^-$ states. Constructing the potential from the corresponding non-relativistic Lagrangian as given in the Appendix C, Eq. C.15, leads to the following

result:

$$\begin{aligned} V_\rho^s(q_0,\mathbf{q}) &= -\left(\frac{f}{m_\rho}\right)^2 F_\rho^2\, V^{\mu\nu}\, g_{\mu\nu}\, D_\rho(q_0,\mathbf{q}) \\ &= \left(\frac{f}{m_\rho}\right)^2 F_\rho^2\, D_\rho(q_0,\mathbf{q})\, \left(q_0^2\, \mathbf{S}_1\cdot\mathbf{S}_2 - (\mathbf{S}_1\cdot\mathbf{q})\,(\mathbf{S}_2\cdot\mathbf{q})\right) \qquad (6.34) \\ &\Rightarrow \left(\frac{f}{m_\rho}\right)^2 F_\rho^2\, D_\rho(q_0,\mathbf{q})\, \left(q_0^2-\mathbf{q}^2\right)\, \mathbf{S}_1\cdot\mathbf{S}_2 \end{aligned}$$

with

$$V^{\mu\nu} = S_1^i\, S_2^j \begin{pmatrix} q_i\, q_j & q_0\, q_j \\ q_i\, q_0 & q_0^2 \end{pmatrix} \quad .$$

Here we have projected out the spin-central part $\mathbf{S}_1\cdot\mathbf{S}_2$, which is generated by the contact interactions. The energy dependence of the s-wave potential is a direct consequence of current conservation, which we impose on the coupling of the baryon resonances to the vector meson-nucleon channel.

The correlation potential V_{corr} obtained via Eq. 6.15 reads:

$$V_{corr}^\rho(q_0,\mathbf{q}) = \left(\frac{f}{m_\rho}\right)^2 \tilde{F}_\rho^2\, \tilde{D}_\rho(q_0,\mathbf{q})\, \left(q_0^2 - \frac{1}{3}\, q_C^2\right)\, \mathbf{S}_1\cdot\mathbf{S}_2 \quad . \qquad (6.35)$$

By matching this with Eq. 6.32, we can estimate the strength of the contact interaction to be

$$g_\rho^s \equiv 2\, c_\rho = \left(q_0^2 - \frac{1}{3}\, q_C^2\right)\, \tilde{F}_\rho^2\, \tilde{D}_\rho(q_0,\mathbf{q}) \quad . \qquad (6.36)$$

Here it becomes crucial at which energy one evaluates this expression. Usually the non-relativistic potential is written down in the limit $q_0 \to 0$. This is a reasonable reference frames for usual exchange potentials, where the squared 4-momentum transfer is negative. This is not necessarily a good approximation when heavy resonances like the $D_{13}(1520)$ are considered, where also timelike mesons can be exchanged. This is the case when the resonance is above the threshold for decay into meson-nucleon. Also in the meson self energy – which is also modified by short-range correlations – one often has the case that the dominant part of the interaction takes place of time like mesons. For example, in order to form a resonance in a scattering reaction on a nucleon at rest (as typical in the discussion of in-medium properties of ρ mesons), the energy of the ρ is determined by the requirement $(p+q)^2 = m_R^2$, leading to:

$$q_0(\mathbf{q}) = \sqrt{m_R^2 + \mathbf{q}^2} - m_N \quad . \qquad (6.37)$$

Comparable energies are also dominant in the elastic reaction $RN \to NR$. For the $D_{13}(1520)$ this amounts to an energy of $q_0 \approx 0.5$ GeV at vanishing 3-momentum. Plugging this value into Eq. 6.36 we find $g_\rho^s \approx 0.05 - 0.1$. On the other hand, taking $q_0 = 0$ GeV, one obtains $g_\rho^s \approx -0.05$. The negative sign follows since the $\mathbf{q}^2$ dependent part in the potential Eq. 6.34 comes with a relative minus sign. In the discussion of the results in Chapter 8

we will discard the effects from a negative g_ρ^s. We believe that the matching point defined in Eq. 6.37 leads to a realistic estimate of the strength of the short-range correlations and that the point $(0,0)$ is not of particular relevance for the interaction of a ρ meson and a $D_{13}(1520)$.

A second arguments for rejecting a negative g_ρ^s goes like this: as will be discussed in detail in Chapter 8, we find a strong broadening of the $D_{13}(1520)$ due to its coupling to $N\rho$. The main motivation for the study of repulsive short-range correlations for $P=-1$ states is the question in how far these terms affect the broadening. By considering negative short-range terms, however, we would enhance the broadening. In a handwaving way this can be understood by realizing that the short-range terms are supposed to remove strength from the interaction (in the case of p-wave interactions the δ-type contribution). If, however, these terms come with the opposite sign, strength is added and an increase of the broadening is expected.

We take the uncertainties in g_ρ^s into account by varying this parameter within the boundaries $(0, 0.1)$ in our calculations. For simplicity we take the same g_ρ^s for all other $\frac{3}{2}^-$ states.

The non-relativistic Lagrangian describing the coupling of $J^\pi = \frac{3}{2}^-$ states to $N\pi$ is given in Appendix C, Eq. C.15, and leads to a d-wave potential:

$$V^\pi(q_0,\mathbf{q}) \;=\; \left(\frac{f}{m_\pi}\right)^2 F_\pi^2 \,\frac{1}{4\,m_N^2}\,\frac{(\boldsymbol{S}_1\cdot\mathbf{q})\,(\boldsymbol{\sigma}_1\cdot\mathbf{p_N})\,(\boldsymbol{S}_2\cdot\mathbf{q})\,(\boldsymbol{\sigma}_2\cdot\mathbf{p_N})}{q_0^2-\mathbf{q}^2-m_\pi^2} \quad . \tag{6.38}$$

Just as for the Δ, the interaction of pions and nucleons is spin-longitudinal in the D_{13} channel. The only difference is an additional momentum dependence from the nucleon. From Eq. 6.15 we obtain for the central part of the correlation potential:

$$V^\pi_{corr}(q_0,\mathbf{q}) \;=\; \frac{1}{3}\,q_C^2\,\tilde{F}_\pi^2\,\frac{(\boldsymbol{\sigma}_1\cdot\mathbf{p_N})\,(\boldsymbol{\sigma}_2\cdot\mathbf{p_N})}{4\,m_N^2}\left(\frac{f}{m_\pi}\right)^2(\mathbf{S}_1\cdot\mathbf{S}_2)\,\tilde{D}_\pi(q_0,\mathbf{q}) \quad . \tag{6.39}$$

This result is similar to that of p-wave potentials, see Eq. 6.16. While the correction of the potential induced by the correlations, V^π_{corr}, scales with $\frac{1}{3}\,q_C^2\,\frac{\mathbf{p}_N^2}{4\,m_N^2}$ and seems to be suppressed by a factor $\frac{\mathbf{p}_N^2}{4m_N^2}$, comparison with Eq. 6.38 shows that the original meson exchange potential V^π scales like $\mathbf{q}^2\,\frac{\mathbf{p}_N^2}{4\,m_N^2}$. Therefore the relative correction from V^π_{corr} is as large as for p-wave states. The spin-structure of V^π_{corr} is the same as found in $\mathcal{L}^\pi_C$, Eq. 6.30, which in principle allows for the matching:

$$g_\pi^d \;=\; \frac{1}{3}\,q_C^2\,\tilde{F}_\pi^2\,\tilde{D}_\pi(q_0,\mathbf{q}) \quad . \tag{6.40}$$

If one determines the matching energy q_0 via Eq. 6.37, a large value of about 0.6 for g_π^d results since one approaches the (unphysical) pole of $\tilde{D}_\pi$ when $q_0^2-\mathbf{q}^2-q_C^2=m_\pi^2$. Such a pole is also found in scattering processes in the vacuum where the exchange particle can go on-shell, as detailed in [10, 102, 98]. From that point of view its appearance is not a complete surprise in our formalism. It is worthwhile checking whether the pole is due to the angular averaging that is used to obtain the correlation integral, see discussion around Eq. 6.16. To see this, just consider the angular integral over the denominator in Eq. 6.16:

$$\int_{-1}^{+1}\frac{dx}{q_0^2-\mathbf{q}^2-q_C^2-2\,|\mathbf{q}|\,q_C\,x} \;=\; \frac{1}{2|\mathbf{q}|\,q_C}\ln\left[1+\frac{4|\mathbf{q}|\,q_C}{q_0^2-m_\pi^2-(|\mathbf{q}|+q_C)^2}\right] \quad . \tag{6.41}$$

Since the argument of the logarithm contains two zeros at finite $\mathbf{q}$ the problem of poles persists independently of the angular average.

For energies up to about 0.4 GeV the results for g_π^d do not vary much. This suggests that one might consider a matching point at these smaller energies. Following this procedure results around $g_\pi^d \propto 0.2$ follow, which is smaller than for p-waves since no corrections from the ρ meson enter into the expressions. Another option to obtain a reasonable estimate for g_π^d is to utilize the above mentioned similarity of d-wave potentials Eq. 6.39 and the p-wave potentials Eq. 6.25, and assume that the strength of the respective short-range correlation terms is comparable. This would lead to $g_\pi^d \approx 0.4$. Taking into account the uncertainties for g_π^d, we vary this parameter in the interval $(0, 0.4)$. Note that due to the larger mass of the ρ meson the pole problem does not arise when matching g_ρ^s.

Turning to $J^\pi = \frac{1}{2}^-$ states, not much changes in the ρ sector. With the usual replacement $\mathbf{S} \to \boldsymbol{\sigma}$, we find exactly the same expressions as for $J^\pi = \frac{3}{2}^-$ states, Eqs. 6.35 and 6.36. Here the state we are most interested in is the $S_{11}(1535)$ and we take the same value for g_ρ^s as for $J^\pi = \frac{3}{2}^-$ resonances. This is suggested from Eqs. 6.36, 6.37 and the fact that the $S_{11}(1535)$ and the $D_{13}(1520)$ have similar masses. We take this value also for all other $\frac{1}{2}^-$ resonances, thus reducing the amount of parameters.

Last we discuss the pion sector for $J^\pi = \frac{1}{2}^-$ states. As can be inferred from Appendix C, the pion potential is s-wave with a trivial spin-structure:

$$V(q_0, \mathbf{q}) \;=\; \left(\frac{f}{m_\pi}\right)^2 \frac{q_0^2}{q_0^2 - \mathbf{q}^2 - m_\pi^2} \quad , \tag{6.42}$$

producing for the correlation part:

$$V_{corr}^\pi(q_0, \mathbf{q}) \;=\; \left(\frac{f}{m_\pi}\right)^2 \frac{q_0^2}{q_0^2 - \mathbf{q}^2 - q_C^2 - m_\pi^2} \quad . \tag{6.43}$$

Here the q_0 dependence follows from the vector coupling employed to describe $\pi\, N\, R$ dynamics. Concerning the calculation of the short-range parameter g_π^s, one could in principle follow the argument as before and take:

$$g_\pi^s \;=\; q_0^2\, \tilde{F}_\pi^2\, \tilde{D}_\pi \quad , \tag{6.44}$$

with q_0 determined from Eq. 6.37. Clearly, one runs again into the pole problem. We therefore take $g_\pi^s = 0.1$ as in the ρ sector. As it will turn out, our results are not sensitive on this parameter, since there are no s-wave states with a large coupling to $N\,\pi$ and consequently the effects from the contact interactions are small regardless of the precise value for g_π^s.

In our model only $J^\pi = \frac{1}{2}^-$ states couple to the η meson. For the corresponding short-range parameter g_η^s we take in accordance to the pion a value of $g_\eta^s = 0.1$.

6.4 Mixing Terms

Up to now we have considered processes of the type $RN \to NR$. An interesting question is whether the contact interactions allow for mixing of different resonance states. On the

level of Feynman diagrams this corresponds to a situation where in Fig. 6.4 R_1 and R_2 stand for different states. These terms are driven by the following contact Lagrangians:

$$\begin{aligned} \mathcal{L}_C^{\pi} &= c_\pi \, J_{R1}^{\mu} \, J_{\mu,R2} \\ \mathcal{L}_C^{\rho} &= c_\rho \, B_{R1}^{\mu\nu} \, B_{\mu\nu,R2} \quad . \end{aligned} \tag{6.45}$$

Clearly, processes like $R_1 N \to N R_2$ are possible if R_2 has the same quantum numbers as R_1. The situation is more complicated if resonance R_2 has different quantum numbers. While in a fully relativistic framework mixing is always possible regardless of the quantum numbers of the involved states, certain restrictions arise in the non-relativistic limit. For pions, mixing is allowed in the non-relativistic reduction, if the leading terms of both J_{R1}^{μ} and J_{R2}^{μ} are derived either from the vector (i) or the time (0) component. Similarly, in $\mathcal{L}_C^{\rho}$ the leading terms of both $B_{R1}^{\mu\nu}$ and $B_{R2}^{\mu\nu}$ must be either the spatial (k,j) or the time $(k,0)$, $(0,j)$ components. Since these restrictions are present only in the non-relativistic reduction, they can not be due to the conservation of quantum numbers.

For the pion sector, these considerations lead to the conclusion that mixing is allowed between $J^{\pi} = \frac{3}{2}^{+}$, $J^{\pi} = \frac{3}{2}^{-}$ and $J^{\pi} = \frac{1}{2}^{+}$ states. In all three cases the leading non-relativistic contributions come from the vector components of J_μ. In contrast, there is no mixing to $J^{\pi} = \frac{1}{2}^{-}$ states, which derive their leading behaviour from the 0-th component of J_μ. For the remainder of this work the most important finding is the possibility that nucleon, $P_{33}(1232)$ and $D_{13}(1520)$ states can mix.

In the ρ sector the situation is slightly different. For positive parity states the leading components come from the spatial (j,k) components and for negative states from the time $(j,0)$ or $(0,k)$ components of $B^{\mu\nu}$, such that the contraction vanishes if states of different parity are considered. This implies, that unlike the pion case, there is no mixing of the $D_{13}(1520)$ state to the $P_{33}(1232)$ or the nucleon. However, mixing between states of the same parity is possible and taken into account in this work.

Let us now write down the Lagrangians describing the mixing phenomena. They are obtained from Eq. 6.45. For example, the mixing of $J^{\pi} = \frac{1}{2}^{+}$ or $J^{\pi} = \frac{3}{2}^{+}$ states and $J^{\pi} = \frac{3}{2}^{-}$ states is described by:

$$\begin{aligned} \mathcal{L}_C &= g_\pi^{dp} \left(\frac{f}{m_\pi}\right)^2 \left(\psi_{R1}^{\dagger} \, S^{i\,\dagger} \, \frac{\sigma_k \, \partial_k}{2m_N} \, \psi_N\right) \left(\psi_N^{\dagger} \, S_i \, \psi_{R2}\right) \; + \; h.c. \\ \mathcal{L}_C &= g_\pi^{dp} \left(\frac{f}{m_\pi}\right)^2 \left(\psi_{R1}^{\dagger} \, S^{i\,\dagger} \, \frac{\sigma_k \, \partial_k}{2m_N} \, \psi_N\right) \left(\psi_N^{\dagger} \, \sigma_i \, \psi_{R2}\right) \; + \; h.c. \end{aligned} \tag{6.46}$$

Here dp indicates that the Lagrangian describes the mixing of p and d waves and the index π implies that mixing takes place only in the pion sector. The coupling f^2 stands for the product of the coupling constants of both involved resonances. Similarly, the mixing of $J^{\pi} = \frac{1}{2}^{+}$ and $J^{\pi} = \frac{3}{2}^{+}$ states as well as the mixing in the ρ sector of $J^{\pi} = \frac{1}{2}^{-}$ and $J^{\pi} = \frac{3}{2}^{-}$ states follows from the Lagrangian:

$$\mathcal{L}_C = g \left(\frac{f}{m_\pi}\right)^2 \left(\psi_{R1}^{\dagger} \, \sigma^i \, \psi_N\right) \left(\psi_N^{\dagger} \, S_i \, \psi_{R2}\right) \; + \; h.c. \tag{6.47}$$

Here g stands either for g^p (positive parity states) or for g_ρ^s (negative parity states). Values for g and g_π^{dp} can be found in Table A.1.

The mixing of negative parity and positive parity states in the pion sector is proportional to the momentum $\mathbf{p}_N$ as is evident from Eq. 6.46. This is to be expected from parity conservation: consider a scattering process of a $P = +1$ state and a nucleon into a $P = -1$ state and a nucleon. The switch in the internal parities of the involved states must then be compensated by an odd angular momentum, leading to the observed momentum dependence.

Let us clarify that by the terminology "mixing" we do not imply the existence of self energy diagrams where one resonance converts into another resonance in the nuclear medium (this would correspond to diagrams like that of Fig. 6.5, where different resonances are meant by R). We have discussed in Chapter 5.6, that rather sharp conditions must be met by the quantum numbers of the involved resonances for that to happen. In particular, the mixing of spin-$\frac{1}{2}$ and spin-$\frac{3}{2}$ states is only allowed if the parity of the resonance changes. In this Chapter we mean by mixing the possibility that different resonance-hole loops can couple directly to each other. As has been pointed out, here restrictions only arise in the non-relativistic reduction.

6.5 Effect on the self energies Π_{med} and Σ_{med}

In this Section we discuss how the previous results for the in-medium self energies of mesons and baryon resonances, Eqs. 5.37 and 5.48, are modified in the presence of short range interactions.

For notational convenience, let us first recall the definition of the susceptibility χ_M from Chapter 5.2.3:

$$\chi_M^R(q_0, \mathbf{q}) \;=\; I_\Pi \left(\frac{f}{m_M}\right)^2 \int \frac{d^3p}{(2\,\pi)^3} \frac{n(\mathbf{p})}{2\,E_N(\mathbf{p})} \frac{F_s^2(k)\,\Omega^{red}}{k_0^2 - E_R^2(\mathbf{k}) - \Sigma_{med}(k^2)} \quad , \tag{6.48}$$

where $k = p + q$ is the resonance 4-vector. The form factor $F_s(k)$ has been introduced around Eq. 3.22. The trace Ω^{red} arises from a spin trace of the contact interactions. Results for Ω^{red} are given in Appendix C in Table C.3. For the nucleon we define in analogy:

$$\chi_M^N(q_0, \mathbf{q}) \;=\; 4 \left(\frac{f_{NNM}}{m_M}\right)^2 U_N(q) \quad . \tag{6.49}$$

Since the short-range interactions couple resonances of various quantum numbers to each other, the resulting coupled channel problem ought to be written down in a matrix formulation. Before proceeding we define the quantities

$$\begin{aligned} g_\pi^p &\equiv g^p \\ g_\rho^p &\equiv \frac{f_{RN\pi}^2}{f_{RN\rho}^2} \frac{m_\rho^2}{m_\pi^2}\, g^p \quad . \end{aligned} \tag{6.50}$$

and similarly if the interaction of two different resonances is considered. Then we can

introduce the following matrices:

$$\boldsymbol{\chi}_\pi = \begin{pmatrix} \boldsymbol{\chi}_\pi^p & 0 & 0 & 0 \\ 0 & \boldsymbol{\chi}_\pi^d & 0 & 0 \\ 0 & 0 & \boldsymbol{\chi}_\pi^s & 0 \\ 0 & 0 & 0 & \boldsymbol{\chi}_\pi^f \end{pmatrix} \tag{6.51}$$

$$\mathbf{g}_\pi = \begin{pmatrix} \mathbf{g}_\pi^p & \mathbf{g}_\pi^{dp} & 0 & 0 \\ \mathbf{g}_\pi^{dp} & \mathbf{g}_\pi^d & 0 & 0 \\ 0 & 0 & \mathbf{g}_\pi^s & 0 \\ 0 & 0 & 0 & 0 \end{pmatrix} \tag{6.52}$$

$$\boldsymbol{\Pi}_\pi^0 = \begin{pmatrix} \boldsymbol{\Pi}_\pi^p & 0 & 0 & 0 \\ 0 & \boldsymbol{\Pi}_\pi^d & 0 & 0 \\ 0 & 0 & \boldsymbol{\Pi}_\pi^s & 0 \\ 0 & 0 & 0 & \boldsymbol{\Pi}_\pi^f \end{pmatrix} \tag{6.53}$$

Each entry is a matrix itself. For example, $\boldsymbol{\chi}_\pi^p$ is a diagonal matrix consisting of all the states to which the pion couples in a p-wave and similarly for $\boldsymbol{\chi}_\pi^d$ and $\boldsymbol{\chi}_\pi^s$. The diagonal elements of the matrix $\boldsymbol{\Pi}_\pi^0$ contain the self energies, Eqs. 5.48 and 5.15, grouped in the same order as in the matrix $\boldsymbol{\chi}_\pi$. Since we allow for different g_π^p parameters, we find for the matrix $\mathbf{g}_\pi^p$ assuming that n resonances couple in a p-wave:

$$\mathbf{g}_\pi^p = \begin{pmatrix} g_\pi^{p,NN} & g_\pi^{p,R_1N} & \cdots & g_\pi^{p,R_nN} \\ g_\pi^{p,R_1N} & g_\pi^{p,R_1R_1} & & \\ \vdots & & \ddots & \\ g_\pi^{p,R_nN} & & & g_\pi^{p,R_nR_n} \end{pmatrix} . \tag{6.54}$$

In the following we take all entries but g_π^{NN} to be the same, see Table A.1. The matrices $\mathbf{g}_\pi^s$ and $\mathbf{g}_\pi^d$ describe the coupling of s- and d-wave states to themselves. The structure of the matrix $\mathbf{g}_\pi$ indicates the mixing of resonances with different quantum numbers as discussed in Chapter 6.45. Thus, we have a coupling of p- and d-wave states represented by $\mathbf{g}_\pi^{dp}$, whereas the s-wave states couple only to themselves. We take the same entries for g_π^d and g_π^{dp}. For spin-$\frac{5}{2}$ states, which couple in an f-wave to $N\pi$, we have no short range correlations, which is indicated by the entry 0 in the field of the f-wave resonances. In Table A.1 we give explicit values for the short-range parameters.

For the ρ meson one can introduce similar matrices $\boldsymbol{\chi}_\rho$ and $\mathbf{g}_\rho$ which are constructed

in exactly the same way:

$$\boldsymbol{\chi}_\rho = \begin{pmatrix} \boldsymbol{\chi}_\rho^p & 0 \\ 0 & \boldsymbol{\chi}_\rho^s \end{pmatrix} \tag{6.55}$$

$$\mathbf{g}_\rho = \begin{pmatrix} \mathbf{g}_\rho^p & 0 \\ 0 & \mathbf{g}_\rho^s \end{pmatrix} \tag{6.56}$$

$$\boldsymbol{\Pi}_\rho^{0,T/L} = \begin{pmatrix} \boldsymbol{\Pi}_\rho^{p,T/L} & 0 \\ 0 & \boldsymbol{\Pi}_\rho^{s,T/L} \end{pmatrix} \tag{6.57}$$

The matrix $\mathbf{g}_\rho^p$ looks formally identical to $\mathbf{g}_\pi^p$. For simplicity, we relax the relation between g_π^p and g_ρ^p Eq. 6.50 for the two $J^\pi = \frac{3}{2}^+$ states $P_{13}(1720)$ and $P_{13}(1878)$ and take the same values g_ρ^p as for the $P_{33}(1232)$. This is reasonable, since the vacuum properties of these states are only poorly known. In the case of the $P_{11}(1440)$, which is a $J^\pi = \frac{1}{2}^+$ state, we would in principle face the same problem, if it would couple to both pion and the ρ meson. Since this is not the case in our model, we do not to worry about this state. For $J^\pi = \frac{5}{2}^+$ states we take $g_\rho^p = g_\rho^{p,\Delta N}$. To be more explicit, if there was only the $P_{33}(1232\ (\Delta)$, one more $J^\pi = \frac{3}{2}^+$ state and one more $J^\pi = \frac{5}{2}^+$ state, the matrix $\mathbf{g}_\rho^p$ would have the following form:

$$\mathbf{g}_\rho^p = \begin{pmatrix} g_\rho^{p,NN} & g_\rho^{p,\Delta N} & g_\rho^{p,\Delta N} & g_\rho^{p,\Delta N} \\ g_\rho^{p,\Delta N} & g_\rho^{p,\Delta\Delta} & g_\rho^{p,\Delta\Delta} & g_\rho^{p,\Delta N} \\ g_\rho^{p,\Delta N} & g_\rho^{p,\Delta\Delta} & g_\rho^{p,\Delta\Delta} & g_\rho^{p,\Delta N} \\ g_\rho^{p,\Delta N} & g_\rho^{p,\Delta N} & g_\rho^{p,\Delta N} & g_\rho^{p,\Delta N} \end{pmatrix} \quad . \tag{6.58}$$

The matrix ${\boldsymbol{\Pi}_\rho}^{0,T/L}$ contains the self energies from Eqs. 5.48 and 5.15.

For the η meson the corresponding matrices $\boldsymbol{\chi}_\eta$, $\mathbf{g}_\eta$ and $\boldsymbol{\Pi}_\eta^0$ have the same form as for the ρ. Here the only state coupling in a p-wave is the nucleon, all other resonances couple in an s-wave, see also Table A.2.

Let us finally introduce the vector $\mathbf{v}$ as

$$\mathbf{v}^T = \underbrace{\begin{pmatrix} 1 & 1 & \dots & 1 \end{pmatrix}}_{N\times} \quad , \tag{6.59}$$

where N is number of resonances included in the calculation.

Having defined these quantities, we can now proceed and present the results for the self energy. We first the full expressions before motivating the results in more detail. In Fig. 6.4 we display the lowest order correction to the meson self energy. Summing up to all orders leads to the following result for the self energy of meson M [7]:

$$\Pi_M(q_0, \mathbf{q}) = F^2(k,q)\, \mathbf{v}^T \frac{1}{1 - \boldsymbol{\chi}_M\, \mathbf{g}_M}\, \boldsymbol{\Pi}_M^0\, \mathbf{v} \quad . \tag{6.60}$$

Taking into account the contact interactions, the resonance self energy consists of two diagrams, see Fig. 6.5. In terms of scattering processes these diagrams correspond to the

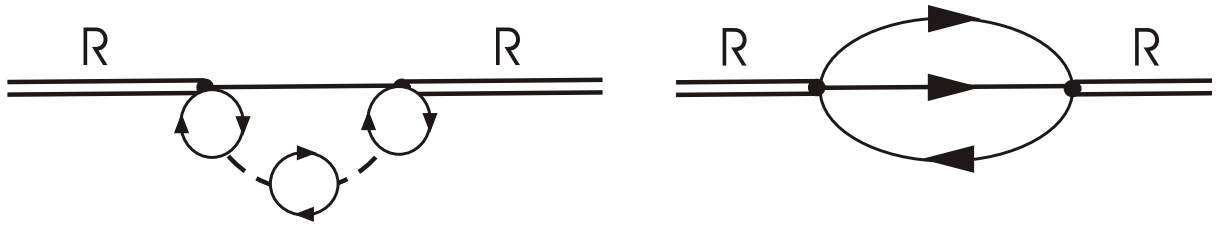

Figure 6.5: The resonance self energy in the presence of short-range correlations. The loop insertion stands for any particle-hole state discussed in the text. Note that any loop as a representative of the full vertex correction $1/(1-g\chi)$ or the resummed and renormalized self energy.

coherent sum of a scattering with meson exchange and scattering via a contact interaction as we will show in Section 6.6. Iterating the particle-hole insertions generates vertex corrections at the resonance-nucleon-meson vertices. We split the resonance self energy into three parts:

$$\mathcal{I}\mathrm{m}\,\Sigma(k_0,\mathbf{k}) \;=\; \mathcal{I}\mathrm{m}\,\Sigma_\pi(k_0,\mathbf{k}) + \mathcal{I}\mathrm{m}\,\Sigma_\rho(k_0,\mathbf{k}) + \mathcal{I}\mathrm{m}\,\Sigma_\eta(k_0,\mathbf{k}) \tag{6.61}$$

according to whether the resonance has decayed into a medium-modified pion, η or ρ meson. Throughout the following formulae Ω_φ and $\Omega_{T/L}$ as well as Ω^{red} have to be chosen according to the quantum numbers of the resonance.

For the imaginary part of the resonance self energy one obtains a matrix [7]. The diagonal elements of this matrix yield the imaginary part of the self energy for the individual resonances. Thus we obtain for the pionic decay mode:

$$\begin{aligned}\mathcal{I}\mathrm{m}\,\mathbf{\Sigma}_\pi(k_0,\mathbf{k}) \;&=\; -\frac{I_\Sigma}{2j+1}\left(\frac{f}{m_\pi}\right)^2 \int\frac{dp\,p^2}{8\pi^2}\int_{-1}^{+1}dx\,\frac{1}{E_N}\times \\ &\times\mathcal{I}m\,\left[\Omega^\varphi\,D_\pi\,F^2(k,(k-p))\frac{1}{1-\mathbf{g}_\pi\,\boldsymbol{\chi}_\pi}\,\mathbf{v}\,\mathbf{v}^T\,\frac{1}{1-\boldsymbol{\chi}_\pi\,\mathbf{g}_\pi}+\Omega^{red}\,F_s^2(k)\,\mathbf{g}_\pi\,\frac{1}{1-\boldsymbol{\chi}_\pi\,\mathbf{g}_\pi}\right]\quad .\end{aligned} \tag{6.62}$$

For the decay into an η meson one obtains the same result, if the appropriate matrices are chosen:

$$\begin{aligned}\mathcal{I}\mathrm{m}\,\mathbf{\Sigma}_\eta(k_0,\mathbf{k}) \;&=\; -\frac{I_\Sigma}{2j+1}\left(\frac{f}{m_\eta}\right)^2 \int\frac{dp\,p^2}{8\pi^2}\int_{-1}^{+1}dx\,\frac{1}{E_N}\times \\ &\times\mathcal{I}m\,\left[\Omega^\varphi\,D_\eta\,F^2(k,(k-p))\frac{1}{1-\mathbf{g}_\eta\,\boldsymbol{\chi}_\eta}\,\mathbf{v}\,\mathbf{v}^T\,\frac{1}{1-\boldsymbol{\chi}_\eta\,\mathbf{g}_\eta}+\Omega^{red}\,F_s^2(k)\,\mathbf{g}_\eta\,\frac{1}{1-\boldsymbol{\chi}_\eta\,\mathbf{g}_\eta}\right]\quad .\end{aligned} \tag{6.63}$$

Finally, for the decay into a ρ meson we find:

$$\begin{aligned}\mathcal{I}\mathrm{m}\,\mathbf{\Sigma}_\rho(k_0,\mathbf{k}) &= -\frac{I_\Sigma}{2j+1}\left(\frac{f}{m_\rho}\right)^2 \int \frac{dp\,p^2}{8\pi^2}\int_{-1}^{+1} dx\,\frac{1}{E_N}\times \\ &\times\mathcal{I}m\left[(2\,\Omega^T\,D_\rho^T+\Omega^L\,D_\rho^L)\,F^2(k,(k-p))\,\frac{1}{1-\mathbf{g}_\rho\,\boldsymbol{\chi}_\rho}\,\mathbf{v}\,\mathbf{v}^T\,\frac{1}{1-\boldsymbol{\chi}_\rho\,\mathbf{g}_\rho}+\right. \\ &\left.+\,3\,(2)\Omega^{red}\,F_s^2(k)\,\mathbf{g}_\rho\,\frac{1}{1-\boldsymbol{\chi}_\rho\,\mathbf{g}_\rho}\right] \quad .\end{aligned} \tag{6.64}$$

Since a longitudinal ρ meson does not couple to $P=+1$ resonances, we have a factor of 2 in the second term for these states. In the above formulae, the meson propagator D_M is obtained with the self energy of Eq. 6.60, containing short-range correlations.

Let us now discuss the above formulae of Eqs. 6.60, 6.62, 6.63 and 6.64 in some more detail. We begin by studying the case of a pion coupling to the $P_{33}(1232)$. In a subsequent step, we will add the nucleon to the system. We add a remark concerning the notation: by Π_π^R and χ_π^R we refer to the pion self energy and susceptibility due to the excitation of resonance R and similar for χ_π^N and Π_π^N. The upper index $(0,1)$ refers to the order in the short-range parameter g, in which the calculation is done.

If only one resonance is taken into account, the self energy Eq. 6.60 reduces to the following expression (here form factors are suppressed for the sake of simplicity):

$$\Pi_\pi^R = \frac{\Pi_\pi^{0,R}}{1-g_\pi^{p,RR}\,\chi_\pi^R} \quad , \tag{6.65}$$

where $\Pi_\pi^{0,R}$ is the self energy containing no short-range correlations. We will now show how this expression is obtained.

The non-relativistic Lagrangians describing the dynamics of pions and resonance-hole states are given by (cf. Appendix C.2 and Eq. 6.21):

$$\begin{aligned}\mathcal{L}_C &= g_\pi^{p,RR}\left(\frac{f_R}{m_\pi}\right)^2\left(\psi_R^\dagger\,S^{i\,\dagger}\,\psi_N\right)\left(\psi_N^\dagger\,S_i\,\psi_R\right) \\ \mathcal{L} &= \frac{f_R}{m_\pi}\,\psi_R^\dagger\,S^{i\,\dagger}\,\psi_N\,\partial_i\,\varphi+h.c. \quad .\end{aligned}$$

Remembering the definition of Lindhardt function U_R and susceptibility χ_π^R as given in Chapter 5.2.3, we can write $\Pi_\pi^{0,R}$ in the following form:

$$\begin{aligned}\Pi_\pi^{0,R} &= I_\Pi\,U_R\left(\frac{f_R}{m_\pi}\right)^2 4\,m_N\,\sqrt{k^2}\,q_i\,q_j\,Tr\,[S_i\,S_j] \\ &= I_\Pi\,U_R\left(\frac{f_R}{m_\pi}\right)^2\frac{4}{3}\,\mathbf{q}^2\,4\,m_N\,\sqrt{k^2} \\ &= I_\Pi\,U_R\left(\frac{f_R}{m_\pi}\right)^2\Omega^\varphi \;=\; \mathbf{q}^2\,\chi_\pi^R \quad .\end{aligned}$$

Here k^2 is the invariant mass of the $P_{33}(1232)$ and I_Π is an isospin factor. Let us now cal-

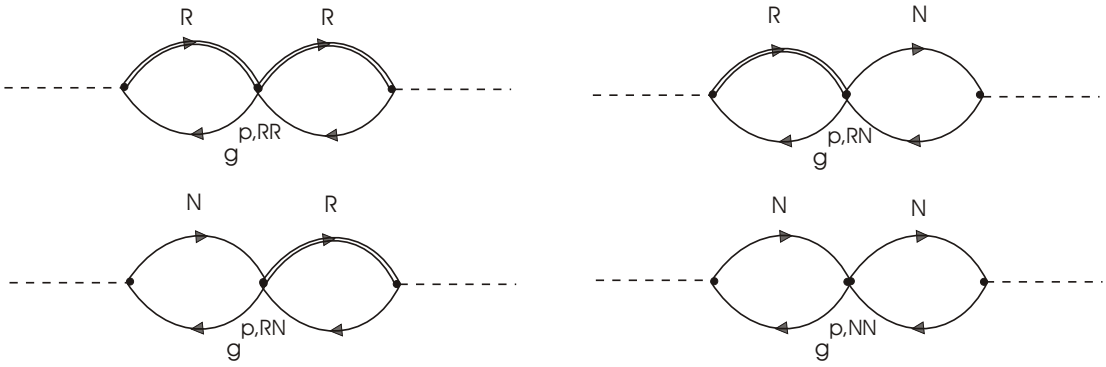

Figure 6.6: Lowest order short-range correlation corrections to the meson self energy.

culate the first order correction in the short-range parameter $g_\pi^{p,RR}$, see upper left diagram in Fig. 6.6:

$$\begin{aligned}
\Pi_\pi^{1,R} &= g_\pi^{p,RR}\, I_\Pi^2\, U_R^2 \left(\frac{f_R}{m_\pi}\right)^4 16\, m_N^2\, k^2\, q_i\, q_j\, Tr\left[S_i\, S_k\right]\, Tr\left[S_k\, S_j\right] \\
&= I_\Pi\, U_R \left(\frac{f_R}{m_\pi}\right)^2 4\, m_N \sqrt{k^2}\, \frac{4}{3}\, \mathbf{q}^2 \times g_\pi^{p,RR}\, I_\Pi\, U_R \left(\frac{f_R}{m_\pi}\right)^2 4\, m_N \sqrt{k^2}\, \frac{4}{3} \\
&= I_\Pi\, U_R \left(\frac{f_R}{m_\pi}\right)^2 \Omega^\varphi \times g_\pi^{p,RR}\, I_\Pi\, U_R \left(\frac{f_R}{m_\pi}\right)^2 \Omega^{red} \\
&= \Pi_\pi^{0,R} \times g_\pi^{p,RR}\, \chi_\pi^R \quad .
\end{aligned}$$

Apparently each additional resonance-hole bubble generates a factor $g_\pi^{p,RR}\,\chi_\pi^R$, leading to a geometric series which is readily summed up to give the result of Eq. 6.65.

This important result will help us to explain the effect of short-range correlations on the baryon resonance self energy as well, see Eqs. 6.62, 6.63 and 6.64. With the above Lagrangians we get for $\mathcal{I}\mathrm{m}\,\Sigma_\pi$, (neglecting form factors):

$$\begin{aligned}
\mathcal{I}\mathrm{m}\,\Sigma_\pi &= -\frac{I_\Sigma}{2j+1}\left(\frac{f_R}{m_\pi}\right)^2 \int \frac{dp\, p^2}{8\pi^2} \int_{-1}^{+1} dx\, \frac{1}{E_N} \times \\
&\qquad \times \mathcal{I}m \left[\Omega^\varphi\, D_\pi \left(\frac{1}{1 - g_\pi^{p,RR}\,\chi_\pi^R}\right)^2 + \Omega^{red}\, \frac{g_\pi^{p,RR}}{1 - \chi_\pi^R\, g_\pi^{p,RR}}\right] \quad .
\end{aligned}$$

The first term in brackets corresponds to the left diagram of Fig. 6.5. Apart from the correction of the pion propagator, which is implicitly encoded in D_π, it contains a vertex correction factor $1/(1 - g_\pi^{p,RR}\,\chi_\pi^R)^2$. This follows from the above observation that each bubble yields a factor $g_\pi^{p,RR}\,\chi_\pi$. The second term in the brackets corresponds to the right diagram in Fig. 6.5, and describes the decay of the resonance exclusively into particle-hole states. We find again the characteristic factor $g_\pi^{p,RR}\,\chi_\pi^R$, which after the resummation gives $1/(1 - g_\pi^{p,RR}\,\chi_\pi^R)$.

Let us now discuss the case that the pion can couple both to the nucleon and the $P_{33}(1232)$ resonance. For the pion self energy this leads to the remaining three diagrams

in Fig. 6.6 not yet considered so far. In order to calculate them, the following Lagrangians need to be included in our formalism (cf. Appendix C.2, Eqs. 6.10, 6.12 and 6.47):

$$\begin{aligned}
\mathcal{L}_C &= g_\pi^{p,RN} \frac{f_R}{m_\pi} \frac{f_N}{m_\pi} \left(\psi_R^\dagger S^{i\,\dagger} \psi_N\right) \left(\psi_N^\dagger \sigma_i \psi_N\right) + h.c. \\
\mathcal{L}_C &= g_\pi^{p,NN} \left(\frac{f_N}{m_\pi}\right)^2 \left(\psi_N^\dagger \sigma^{i\,\dagger} \psi_N\right) \left(\psi_N^\dagger \sigma_i \psi_N\right) \\
\mathcal{L} &= \frac{f_N}{m_\pi} \psi_N^\dagger \sigma^{i\,\dagger} \psi_N \partial_i \varphi \quad .
\end{aligned}$$

The first Lagrangian describes the coupling of resonance-hole to nucleon-hole loops, the second the coupling of nucleon-hole to nucleon-hole loops and the last one the coupling of pions to nucleons. One checks straightforwardly that the first order (in the short-range parameter g) self energy is given by:

$$\Pi_\pi^{1,R} = \Pi_\pi^{0,R} \times g^{p,RR} \chi_\pi^R + \Pi_\pi^{0,R} \times g^{p,RN} \chi_\pi^N + \Pi_\pi^{0,N} \times g^{p,RN} \chi_\pi^R + \Pi_\pi^{0,N} \times g^{p,NN} \chi_\pi^N \quad .$$

This is exactly the same result that one gets by explicitly calculating Π_π from equation Eq. 6.60 in lowest order in g:

$$\Pi_\pi = \mathbf{v}^T \boldsymbol{\chi}_\pi \mathbf{g}_\pi \boldsymbol{\Pi}_\pi^0 \mathbf{v} \quad ,$$

where

$$\begin{aligned}
\mathbf{v}^T &= \begin{pmatrix} 1 & 1 \end{pmatrix} \\
\mathbf{g}_\pi &= \begin{pmatrix} g^{p,RR} & g^{p,RN} \\ g^{p,RN} & g^{p,NN} \end{pmatrix} \\
\boldsymbol{\chi}_\pi &= \begin{pmatrix} \chi_\pi^R & 0 \\ 0 & \chi_\pi^N \end{pmatrix} \\
\boldsymbol{\Pi}_\pi^0 &= \begin{pmatrix} \Pi_\pi^{0,R} & 0 \\ 0 & \Pi_\pi^{0,N} \end{pmatrix}
\end{aligned}$$

One thus sees how the matrix notation takes care of the coupling between different particle-hole states to each other as generated by the short-range correlations.

6.6 Relation of Resonance Self Energy to Scattering Amplitudes

In this Section we extend the discussion of Chapter 5.3.2 concerning the relation between the resonance self energy and the resonance-nucleon scattering amplitudes in the presence of short-range correlations. Again the resonance has the quantum numbers $J^\pi = \frac{3}{2}^+$ and the meson is pseudoscalar such that the decay is p-wave. Then $\Sigma_{coll}(k_0, \mathbf{k})$ – the in-medium correction to the self energy (cf. Eq. 5.38) in the low density limit – takes on the following

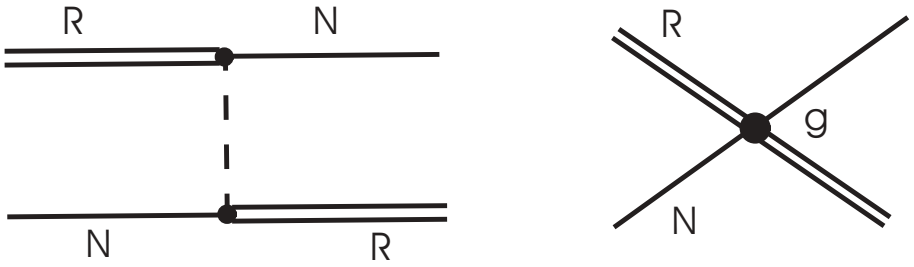

Figure 6.7: Interpretation of the self energy in terms of scattering diagrams. On the left: meson exchange amplitude $\mathcal{M}_1$. On the right: contact term $\mathcal{M}_2$.

form (neglecting the form factors):

$$\begin{aligned}
\mathcal{I}\mathrm{m}\,\Sigma_{coll}(k_0,\mathbf{k}) &= -\frac{I_\Sigma}{4}\left(\frac{f}{m_M}\right)^2 \int \frac{d^3p}{(2\pi)^3}\frac{1}{2\,E_N}\times \\
&\quad \times \mathcal{I}m\left[\Omega^\varphi\, D_M\left(\frac{1}{1-g_M^p\,\chi_M^p}\right)^2 + \Omega^{red}\, g_M^p\,\frac{1}{1-g_M^p\chi_M^p}\right] \qquad (6.66)\\
&\overset{\rho\to 0}{\to} -\frac{I_\Sigma}{4}\left(\frac{f}{m_M}\right)^2 \int \frac{d^3p}{(2\pi)^3}\frac{1}{2\,E_N}\left[\Omega^\varphi\,|D_M^{vac}|^2\,\mathcal{I}\mathrm{m}\,\Pi_M^{med} + \right.\\
&\quad \left. + 2\,\Omega^\varphi\, g_M^p\, D_M^{vac}\,\mathcal{I}\mathrm{m}\,\chi_M^p + \Omega^{red}\, g_M^{p\,2}\,\mathcal{I}\mathrm{m}\,\chi_M^p\right] \quad ,
\end{aligned}$$

where we have made a low-density expansion in the last line. In order to facilitate the notation we will omit in the following the indices M and p as well as the form factors and write $f/m_M \to f_R$.

Let us now consider the coherent sum of the scattering amplitudes $\mathcal{M}_1$ and $\mathcal{M}_2$, depicted in Fig. 6.7. They describe resonance-nucleon scattering in terms of a meson exchange diagram and a diagram generated by contact interactions. Using non-relativistic Lagrangians one obtains the following expressions for the scattering amplitudes:

$$\begin{aligned}
\mathcal{M}_1 &= -f_R^2\,(\mathbf{S}_1\cdot\mathbf{q})\,(\mathbf{S}_2\cdot\mathbf{q})\,D_M^{vac}\,4\,m_N\,m_R \\
\mathcal{M}_2 &= -g\,f_R^2\,(\mathbf{S}_1\cdot\mathbf{S}_2)\,4\,m_N\,m_R \quad .
\end{aligned}$$

In terms of the quantities Ω and Ω^{red}, introduced in Chapter 5.2.3

$$\begin{aligned}
\Pi_M &= I_\Pi\, f_R^2\,\Omega^\varphi\, U_R \quad , \quad \chi = I_\Pi\, f_R^2\,\Omega^{red}\,U_R \\
\Omega^\varphi &= 16/3\,m_N\,m_R\,\mathbf{q}^2 \quad , \quad \Omega^{red} = 16/3\,m_N\,m_R \quad ,
\end{aligned} \qquad (6.67)$$

one finds for the spin-averaged squared matrix element:

$$\begin{aligned}
|\mathcal{M}_1+\mathcal{M}_2|^2 &= |\mathcal{M}_1|^2 + |\mathcal{M}_2|^2 + 2\,\mathcal{R}\mathrm{e}\,(\mathcal{M}_1\,\mathcal{M}_2^\star) \\
&= f_R^4\,\Omega^{red\,2}\left[\mathbf{q}^4\,|D_M^{vac}|^2 + g^2 + 2\,g\,\mathbf{q}^2\,D_M^{vac}\right] \quad .
\end{aligned}$$

Note that we have kept only the spin-longitudinal part of the contact interaction. The spin-transverse part corresponds to the exchange of ρ mesons, which we do not discuss in this Section.

A straightforward calculation along the same lines as in Section 5.3.2 shows that the self energy may be expressed in terms of the squared matrix element as (cf. Eq. 5.39):

$$\mathcal{I}\mathrm{m}\,\Sigma_{coll}(k_0,\mathbf{k}) \;=\; \frac{1}{4}\int \frac{d^3p}{(2\pi)^3\,2E_N(\mathbf{p})}\,|\mathcal{M}_1+\mathcal{M}_2|^2\;\mathcal{I}\mathrm{m}\,U_R \quad . \tag{6.68}$$

This equation makes the relation between the scattering processes and the imaginary part of the self energy explicit. The first term of $\mathcal{I}\mathrm{m}\,\Sigma_{coll}(k_0,\mathbf{k})$ corresponds to the sum of the squared amplitude $|\mathcal{M}_1|^2$ and the interference term of $\mathcal{M}_1$ and $\mathcal{M}_2$, the second term of $\mathcal{I}\mathrm{m}\,\Sigma_{coll}(k_0,\mathbf{k})$ corresponds to $|\mathcal{M}_2|^2$. In analogy to the steps around Eq. 5.40 in Section 5.3.2 the interpretation of Eq. 6.68 is the following: The imaginary part of the meson self energy as obtained in the presence of short-range correlations is related to the resonance-nucleon cross section σ via $\mathcal{I}\mathrm{m}\,\Sigma_{coll} = -\rho\,|\mathbf{k}|\,\sigma$, where the cross section is generated from a meson exchange and a short-range term. This is depicted in Fig. 6.7.

We close this Section by commenting on a problem due to the non-relativistic framework. As we will see in Chapter 9.4, the non-relativistic reduction is a good approximation when calculating the meson self energy, if the kinematical variables are evaluated in the rest frame of the resonance under consideration. In the above expressions we have so far not taken this into account and the same momentum $\mathbf{q}$ was taken at both vertices, though the invariant mass and therefore the corresponding cm momentum formed at each vertex are different.

Taking the kinematical cm corrections into account, the amplitudes $\mathcal{M}_1$ and $\mathcal{M}_2$ are modified:

$$\begin{aligned}\mathcal{M}_1 &= -f_R^2\,(\mathbf{S}_1\cdot\mathbf{q}_{cm,a})\,(\mathbf{S}_2\cdot\mathbf{q}_{cm,b})\,D_M^{vac}\,4\,m_N\,\sqrt{m_a\,m_b} \\ \mathcal{M}_2 &= -g\,f_R^2\,(\mathbf{S}_1\cdot\mathbf{S}_2)\,4\,m_N\,\sqrt{m_a\,m_b} \quad ,\end{aligned} \tag{6.69}$$

where the indices a and b refer to the upper and lower vertex of the diagrams in Fig. 6.7, respectively. The invariant masses of the meson-nucleon system at the upper and lower vertices are denoted by m_a and m_b, respectively. The relativistically improved squared matrix element is given by:

$$|\mathcal{M}_1+\mathcal{M}_2|^2 \;=\; f_R^4\,\Omega_1^{red}\,\Omega_2^{red}\,\left[q_{cm,a}^2\,q_{cm,b}^2\,|D_M^{vac}|^2 \;+\; g^2 \;+\; 2\,g\,q_{cm,a}\,q_{cm,b}\,D_M^{vac}\right] \quad .$$

Here the quantities Ω_1^{red} and Ω_2^{red} are obtained from the Ω^{red} of Eq. 6.67 by replacing $m_R \to m_a\,(m_b)$. There is no problem with the terms $|\mathcal{M}_1|^2$ and $|\mathcal{M}_2|^2$. The different momenta $q_{cm,a}^2$ and $q_{cm,b}^2$ correspond to the different momenta at the $N\,M$ decay vertex and at the meson self energy, see Eq. 6.66. Problematic is only the interference term, which should be proportional to $q_{cm,a}\,q_{cm,b}$. This momentum dependence is not found in Eq. 6.66. The origin of the problem is the fact that the instruction to choose appropriate cm kinematics is not easily translated into Feynman rules. This argument does not depend on the low density limit taken in the above expressions and we therefore make the following replacement in the self energy of meson M of p-wave resonances (taking the pion part of

the self energy as an example) :

$$\begin{aligned}
\mathcal{I}\mathrm{m}\,\mathbf{\Sigma}_\pi(k_0,\mathbf{k}) &= -\frac{I_\Sigma}{2j+1}\left(\frac{f}{m_\pi}\right)^2 \int \frac{dp\,p^2}{8\pi^2}\int_{-1}^{+1} dx\,\frac{1}{E_N}\times \\
\times\mathcal{I}m\,&\left[\Omega^\varphi\,D_\pi\,F^2(k,(k-p))\left|\frac{1}{1-\mathbf{g}_\pi\,\boldsymbol{\chi}_\pi}\,\mathbf{v}\,\mathbf{v}^T\,\frac{1}{1-\boldsymbol{\chi}_\pi\,\mathbf{g}_\pi}\right|+\right. \\
+\Omega^\varphi\,&\frac{q_{cm,b}\,m_b}{q_{cm,a}\,m_a}\,D_\pi\,F^2(k,(k-p))\left(\frac{1}{1-\mathbf{g}_\pi\,\boldsymbol{\chi}_\pi}\,\mathbf{v}\,\mathbf{v}^T\,\frac{1}{1-\boldsymbol{\chi}_\pi\,\mathbf{g}_\pi}-\right. \\
-&\left.\left.\left|\frac{1}{1-\mathbf{g}_\pi\,\boldsymbol{\chi}_\pi}\,\mathbf{v}\,\mathbf{v}^T\,\frac{1}{1-\boldsymbol{\chi}_\pi\,\mathbf{g}_\pi}\right|\right)+\Omega^{red}\,F_s^2(k)\,\mathbf{g}_\pi\,\frac{1}{1-\boldsymbol{\chi}_\pi\,\mathbf{g}_\pi}\right] \quad .
\end{aligned} \tag{6.70}$$

Without these modifications one is in danger to produce negative values for the imaginary part of the self energy, since one does not calculate a quantity proportional to a squared matrix element any more and the interference term is overestimated. In the calculations, we correct only the decay of p-wave resonances. For s-wave resonances, the leading term of the squared matrix element goes with the energy of the meson and the mistakes made in the momenta are not as serious.

6.7 Relativistic Formalism

Our description of short-range correlations is non-relativistic. A relativistic extension of the model would be of great interest, in particular when considering the resonance-nucleon interaction for heavy resonances, where the exchanged 4-momenta can become sizeable. For positive parity states first attempts towards a fully relativistic description, based on Lagrangians of the type $\mathcal{L}_C^\pi$, have recently been proposed in [75, 82]. The results presented there indicate that the non-relativistic limit is only recovered for vanishing 3-momenta and energies. Therefore the quality of the non-relativistic frame work should be worse here than for the case of meson-nucleon scattering, where only the 3-momentum of the meson is required to be small. In the discussion of negative parity resonances we have already encountered possible short-comings of the non-relativistic frame wok when discussing the ambiguity concerning the matching point of contact interactions and correlation integral. Also the discussion presented at the end of the previous Section indicates problems with a non-relativistic scheme.

However, a complete and relativistic description of short-range correlations forms a task of high complexity. Already when considering only the contact interactions as derived from $\mathcal{L}_C^\pi$, the formalism is significantly complicated [82]. It is to be expected that the complex structures generated from $\mathcal{L}_C^\rho$ will lead to even more involved structures. A consistent treatment is furthermore complicated by the fact that the accepted phenomenological range for values of g^p needs to be rejected if the relativistic corrections are sizeable. Then new appropriate values for the short-range parameters have to be obtained from fits to observables.

Chapter 7

Mean Field Potentials

Up to now we have discussed the NN and RN interactions resulting from π and ρ exchange as well as from short-range correlations. In the resonance self energy those terms lead to both real and imaginary parts. We now turn to a different class of diagrams. Starting point is the QHD-I model, originally introduced by Walecka [119]. This model accounts for the empirically observed large scalar and vector components in the NN interaction on the basis of a meson exchange picture. Nuclear systems are described by means of the exchange of the scalar σ meson and the ω vector meson. The corresponding Feynman diagrams are shown in Fig. 7.1. Only the diagrams of lowest order in the coupling constant, which generate Hartree or tadpole contributions, are taken into account. This suffices for a description of the bulk properties of nuclear matter and of nuclei. For the pion and ρ meson, the Hartree contributions vanish in isospin symmetric nuclear matter due to the isospin of both mesons.

7.1 The Underlying Theory

Let us write down the Lagrangian of the QHD-I model [119]:

$$\mathcal{L}_I = \bar{\psi}\left[\gamma_\mu(i\partial^\mu - g_v V^\mu) - (m_N - g_s\varphi)\right]\psi + \frac{1}{2}(\partial_\mu\partial^\mu\varphi - m_s^2\varphi^2) - \frac{1}{4}F_{\mu\nu}F^{\mu\nu} \quad . \quad (7.1)$$

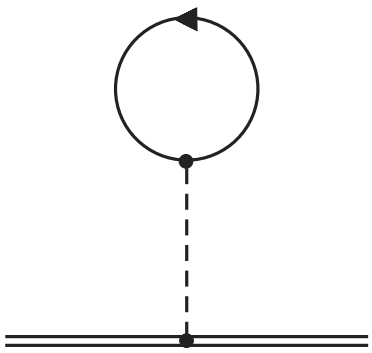

Figure 7.1: σ and ω exchange generating a scalar self energy $\Sigma_s = g_s\rho_s$ and a vector self energy $\Sigma_v = g_v\rho_B$.

Here, φ stands for the scalar field, V_μ is the free vector field and $F_{\mu\nu}$ is the usual antisymmetric field tensor. From this Lagrangian the equations of motion are readily obtained:

$$\begin{aligned} (\partial_\mu \partial^\mu + m_s^2)\varphi &= g_s \bar{\psi}\,\psi \\ \partial_\mu F^{\mu\nu} + m_v^2 V^\nu &= g_v \bar{\psi}\gamma^\nu \psi \\ [\gamma^\mu (i\partial_\mu - g_v V_\mu) - (m_N - g_s\varphi)]\,\psi &= 0 \quad . \end{aligned} \tag{7.2}$$

This constitutes a coupled set of quantum field equations, a solution of which is not easily obtained. Also, in the light of the large coupling constants g_s and g_v perturbative approximations are not appropriate. An alternative approach considers the limit of large densities. Then the source terms on the right hand side of the above equations become very large and the meson field operators can be replaced by their constant expectation values:

$$\begin{aligned} \varphi &\rightarrow \langle\varphi\rangle \equiv \varphi_0 \\ V_\mu &\rightarrow \langle V_\mu\rangle \equiv V_0\,\delta_{\mu 0} \quad . \end{aligned}$$

Note that for a particle (nucleon or resonance) at rest in nuclear matter rotational invariance requires that the space components of the vector field vanish as long as infinite nuclear matter is considered and one averages over the spin of the particle. If the particle has a finite momentum, this is not true any more and finite components $\langle V_i\rangle$ are in principle allowed. In this work we will not be concerned about such terms. In the mean field approximation, the equations for the meson fields reduce to:

$$\begin{aligned} m_s^2\varphi_0 &= g_s\bar{\psi}\,\psi \equiv g_s\,\rho_s \\ m_v^2 V_0 &= g_v\psi^\dagger\psi \equiv g_v\,\rho_B \quad , \end{aligned} \tag{7.3}$$

where we have introduced the scalar density ρ_s and the baryon density ρ_B:

$$\begin{aligned} \rho_s &= \gamma \int_0^{k_F} \frac{d^3p}{(2\pi)^3}\frac{m_N}{E_N(p)} \\ \rho_B &= \gamma \int_0^{k_F} \frac{d^3p}{(2\pi)^3} \quad . \end{aligned} \tag{7.4}$$

Here γ denotes the spin/isopin degeneracy of the system. Within these approximations also the field equations for the nucleon can be solved analytically:

$$[i\gamma^\mu\partial_\mu - g_v V_0 - (m_N - g_s\varphi_0)]\,\psi = 0 \quad . \tag{7.5}$$

This is the free Dirac equation with a shifted energy $p_0^\star$ and effective mass $m_N^\star$:

$$\begin{aligned} p_0^\star &= p_0 - g_v V_0 \equiv p_0 - \Sigma_v \\ m_N^\star &= m_N - g_s\varphi_0 \equiv m_N - \Sigma_s \quad , \end{aligned} \tag{7.6}$$

with the scalar and vector self energies Σ_s and Σ_v, respectively. By directly calculating the self energy from the tadpole diagrams in Fig. 7.1, the same results for Σ_s and Σ_v would be obtained, which shows that the mean field approach and the tadpole self energies are equivalent. For a further discussion see [119]. We mentioned before that the spatial components of the vector field are not taken into account in this work. Explicit calculations

show that the corresponding self energy is relatively small [27, 121]. Had we kept these terms, also the 3-momentum of the nucleon (or the resonance) would have to be modified.

We turn now to the solution of the Dirac equation. Neglecting the potentials, the Dirac equation and its solution read in momentum space [106]:

$$\begin{aligned} (\not{p} - m_N)\, u_s(p) &= 0 \qquad (7.7) \\ u_s(p) &= \sqrt{E_p + m_N} \begin{pmatrix} \mathbb{1} \\ \dfrac{\boldsymbol{\sigma}\cdot\mathbf{p}}{E_p + m_N} \end{pmatrix} \chi_s \quad . \end{aligned}$$

For the eigenvalue one has $E_p = \sqrt{\mathbf{p}^2 + m_N^2}$, as can be checked by plugging $u_s(p)$ into the Dirac equation. Taking care of the coupling to the mean fields modifies the Dirac equation and one obtains:

$$\begin{aligned} (\not{p}^\star - m_N^\star)\, u_s(p^\star) &= 0 \qquad (7.8) \\ u_s(p^\star) &= \sqrt{E_p^\star + m_N^\star} \begin{pmatrix} \mathbb{1} \\ \dfrac{\boldsymbol{\sigma}\cdot\mathbf{p}}{E_p^\star + m_N^\star} \end{pmatrix} \chi_s \quad , \end{aligned}$$

with the notation:

$$\begin{aligned} p^\star &= (p_0^\star, \mathbf{p}) \qquad (7.9) \\ E_p^\star &= \sqrt{m_N^{\star\,2} + \mathbf{p}^2} \quad . \end{aligned}$$

Into the eigenvalue both Σ_s and Σ_v enter via $p_0 = \sqrt{m_N^2 + \mathbf{p}^2} \to p_0^\star = \sqrt{m_N^{\star\,2} + \mathbf{p}^2}$, while the eigenvector $u_s(p)$ is only modified from the scalar self energy Σ_s. The normalization of the spinors changes in the nuclear medium according to:

$$\begin{aligned} \bar{u}_s(p)\, u_{s'}(p) &= 2\, m_N\, \delta_{ss'} \to 2\, m_N^\star\, \delta_{ss'} \qquad (7.10) \\ u_s^\dagger(p)\, u_{s'}(p) &= 2\, E_p\, \delta_{ss'} \to 2\, E_p^\star\, \delta_{ss'} \quad . \end{aligned}$$

Before proceeding, let us mention that in the literature various extensions of the QHD-I model exist. In order to describe asymmetric nuclei, additional fields carrying isospin like π or the ρ have to be introduced. As is turns out, the quality of the Hartree mean-field model can be substantially improved by allowing for non-linear self interactions of the sigma field [72, 69, 53]. The resulting Lagrangian is similar in form to that of Eq. 7.1, but contains additional self interactions terms for the σ meson [72, 69]:

$$\begin{aligned} \mathcal{L}_I &= \bar{\psi}\left[\gamma_\mu(i\partial^\mu - g_v V^\mu) - (m_N - g_s\varphi)\right]\psi + \frac{1}{2}(\partial_\mu\partial^\mu\varphi - m_s^2\varphi^2) + \\ &\quad + \frac{1}{3}g_2\varphi^3 - \frac{1}{4}g_3\varphi^4 - \frac{1}{4}F_{\mu\nu}F^{\mu\nu} \quad . \qquad (7.11) \end{aligned}$$

The modified equation of motion for the sigma field read in the mean field approximation:

$$m_s^2\varphi_0 - g_2\varphi_0^2 + g_3\varphi_0^3 = g_s\rho_s \quad . \qquad (7.12)$$

This leads to a different effective mass for the nucleon, as the expectation value φ_0 and therefore the scalar self energy $\Sigma_s = g_s\varphi_0$ are different in this picture. We will discuss this issue in some detail in the following Subsection.

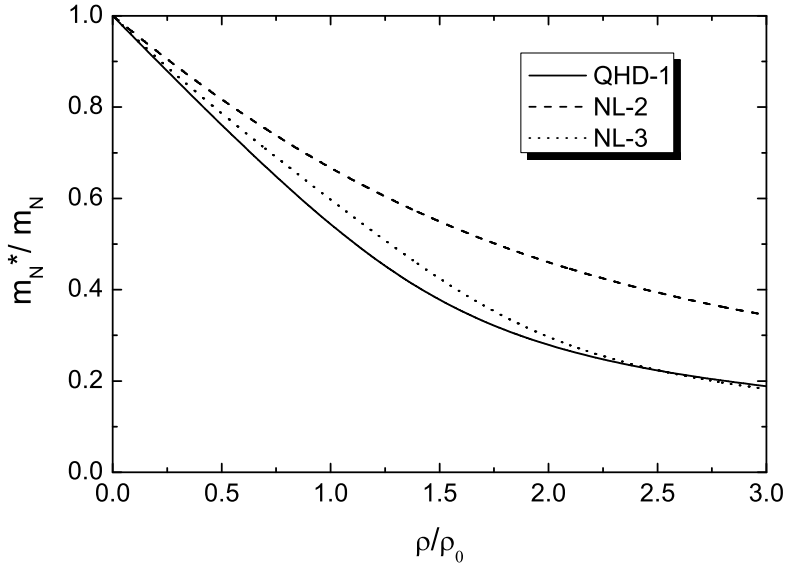

Figure 7.2: Ratio $m_N^\star/m_N$ in nuclear matter as a function of the nuclear density. Shown are the results for the QHD-1 [119], the NL-2 [72] and the NL-3 [69] model. The parameters of these models are given in Table 7.1.

7.2 Numerical Results: The Effective Mass

The baryonic current $\bar{\psi}\,\gamma^\mu\,\psi$ is a conserved quantity. Therefore, the baryon density, which is the 0-th component of the current, is time independent. It follows, that for a given coupling constant g_v the value of the vector self energy Σ_v can be immediately obtained. For example, with the parameter set of QHD-I (see Table 7.1)one obtains $\Sigma_v = 350.24$ MeV.

For the scalar self energy Σ_s, the situation is more complicated. The φ_0 field is generated by the scalar density, which in turns depends on φ_0. This leads to a transcendental equation for φ_0:

$$\begin{aligned} \varphi_0 &= \frac{g_s}{m_s^2}\,\rho_s \qquad (7.13)\\ &= \frac{g_s}{m_s^2}\gamma \int_0^{k_F} \frac{d^3p}{(2\pi)^3} \frac{m_N - g_s\varphi_0}{\sqrt{(m_N - g_s\varphi_0)^2 + \mathbf{p}^2}} \quad . \end{aligned}$$

For spin/isospin symmetric nuclear matter we have $\gamma = 4$. Using QHD-I, we get for the scalar self energy $\Sigma_s = 430$ MeV.

Taking into account the non-linear self interactions of the scalar field modifies this GAP equation according to [72, 69]:

$$\varphi_0 = \frac{g_s}{m_s^2}\,\rho_s + \frac{g_2}{m_s^2}\,\varphi_0^2 - \frac{g_3}{m_s^2}\,\varphi_0^3 \qquad (7.14)$$

It turns out that the self interactions somewhat screen the scalar field, leading to a larger value for the effective nucleon mass, see Table 7.1. This screening effect is reflected in the

	$m_s[MeV]$	$m_V[MeV]$	g_s	g_v	$g_2[\frac{1}{fm}]$	g_3	$m_N^\star/m_N$	$\rho_0[\frac{1}{fm}]$
QHD-I	520	783	10.47	13.78	–	–	0.541	0.148
NL-2	504.89	780	9.111	11.493	−2.304	13.783	0.67	0.1483
NL-3	508.194	782.501	10.217	12.868	−10.431	−28.885	0.60	0.1483

Table 7.1: Parameters of the three mean field models discussed in this Section. Given are different parameter sets and results for the effective mass and the saturation density.

ratios $m_N^\star/m_N$ as shown in Fig. 7.2. One sees that for a given density the QHD-1 model [119] produces the smallest values for these ratios and the NL-2 model [72] the largest ones. Note that in the medium the nucleon mass is very strongly reduced, up to a factor of 1/2 at normal nuclear matter density. In Table 7.1 we give explicit values for the ratio $m_N^\star/m_N$ at saturation density ρ_0. The values given there correspond to self energies Σ_s ranging from $310 - 430$ MeV.

Let us now introduce two interesting functionals of Σ_v and Σ_s. First, consider the expectation value of the full Hamilton operator, yielding the single-particle energy:

$$\begin{aligned} H &= \gamma^0 \boldsymbol{\gamma}\mathbf{p} + \gamma^0 m_N - \gamma^0 \Sigma_s + \Sigma_v \qquad (7.15) \\ \langle u| \gamma^0 \Sigma_s + \Sigma_v |u\rangle &= 2E_p^\star \left(-\frac{m_N^\star}{E_p^\star} \Sigma_s + \Sigma_v \right) \quad . \end{aligned}$$

This demonstrates how Σ_s and Σ_v conspire to produce the well known binding energy of about -70 MeV in nuclear matter. Also, for larger momenta the binding is weakened, since the attractive scalar part gets suppressed by a factor $m_N^\star/E_N^\star$. Such a momentum dependence is also found in various non-relativistic parameterizations of the NN potential [128]. This phenomenon is recovered by considering the so called Schrödinger equivalent potential [79]. It is derived from the dispersion relation

$$\mathbf{p}^2 + (m_N - \Sigma_s)^2 = (\epsilon + m_N - \Sigma_v)^2 \quad , \qquad (7.16)$$

where $\epsilon \equiv E_p^\star + \Sigma_v - m_N$ denotes the single particle energy of the nucleon. These terms can be rearranged to yield the Schrödinger equivalent potential $U_{S.e.}$:

$$\begin{aligned} \frac{\mathbf{p}^2}{2m_N} + U_{S.e.} &= \epsilon + \frac{\epsilon^2}{2m_N} \qquad (7.17) \\ U_{S.e.} &= -\Sigma_s + \frac{\epsilon + m_N}{m_N}\Sigma_v + \frac{1}{2m_N}\left(\Sigma_s^2 - \Sigma_v^2\right) \quad . \end{aligned}$$

The potential $U_{S.e.}$ has a similar momentum dependence as the single particle energy, implying a reduced attraction as the momentum increases.

The results presented here for Σ_s are based on the Walecka model QHD-I [119] and modifications thereof [72, 69]. These models allow for a succesful description of nuclear properties. It is important to realize that the large values for Σ_s found in such models are not a consequence of specific model ingredients. In our opinion this is demonstrated by

the fact that similar values for Σ_s are obtained by starting from a realistic description of NN scattering as achieved by the Bonn potential(s) [87]. In [79] it has been demonstrated explicitly that a self consistent calculation of Σ_s from solving the in-medium NN scattering problem leads to comparable results.

In the present work we consider the effect of potentials not only for the nucleon, but also for baryon resonances. While the corresponding self energies are based on the same diagrams, no information exists about the coupling constants to σ and ω meson. Therefore we assume some sort of universality, implying that the scalar and vector self energies are the same for both nucleon and baryon resonances. This assumption has to be taken with some care, since explicit calculations for the $P_{33}(1232)$ resonance [121, 27] find much smaller values for both Σ_s and Σ_v. Unfortunately, referring to the known non-relativistic mean-field potential of the $P_{33}(1232)$ [33] does not help, since this potential is the difference of the relativistic scalar and vector potentials, see Eqs. 7.15 and 7.17. It does therefore not provide information about the size of the underlying relativistic potentials Σ_s and Σ_v.

7.3 Effect on Observables

As we have just established, the Walecka model leads to an effective mass (from the scalar potential) and energy (from the vector potential) of the nucleon or resonance in nuclear matter. We now establish how this affects the calculation of observables. The result will be that the shift of the energy does not appear in the final expressions as long as the vector potential is taken to be the same for all particles involved. We prove this assertion by constructing the normal mode expansion of the Dirac field, allowing for an ab initio calculation of in-medium matrix elements.

7.3.1 The Normal Mode Expansion: Vacuum

Let us begin by reviewing the normal mode expansion in the vacuum. For simplicity, we keep only the positive energy part. All the steps are straightforwardly extended to the negative energy sector as well. One finds [106]:

$$\psi(x) \;=\; \int \frac{d^3p}{(2\,\pi)^3}\,\frac{1}{\sqrt{2\,E_p}}\,\sum_s a_s(\mathbf{p})\,u_s(E_p,\mathbf{p})\,e^{i\,\mathbf{p}\,\mathbf{x}} \quad . \tag{7.18}$$

The factor $1/\sqrt{2\,E_p}$ is introduced to guarantee the anti-commutation relation:

$$[\psi(\mathbf{x}),\pi(\mathbf{y})] \;=\; i\,\delta^3(\mathbf{x}-\mathbf{y}) \quad , \tag{7.19}$$

and is a direct reflection of the normalization of the spinors $u^\dagger(p)\,u(p) = 2\,E_p$.

The time dependence of the field is obtained from the commutator of the field and the Hamilton operator. In terms of creation and annihilation operators, the Hamilton operator

reads:

$$\begin{aligned} \mathcal{H} &= \int d^3x\, \bar{\psi}(x)\, (-i\,\boldsymbol{\gamma}\,\nabla + m)\, \psi(\mathbf{x}) \\ &= \int \frac{d^3p}{(2\,\pi)^3} \sum_s E_p\, a_s^\dagger(\mathbf{p})\, a_s(\mathbf{p}) \end{aligned} \tag{7.20}$$

and

$$[\mathcal{H}, a_s(\mathbf{p})] = -E_p\, a_s(\mathbf{p}) \quad .$$

The steps leading to the second line clarify that the energy E_p enters as the eigenvalue of the Dirac equation into the final expression. With the commutator of the Hamilton operator and the creation/annihilation operator, the time dependence of the Dirac field is found to be:

$$\psi(\mathbf{x}, t) = \int \frac{d^3p}{(2\,\pi)^3} \frac{1}{\sqrt{2\,E_p}} \sum_s a_s(\mathbf{p})\, u_s(E_p, \mathbf{p})\, e^{-i\,(E_p\,t - \mathbf{p}\,\mathbf{x})} \quad . \tag{7.21}$$

7.3.2 The Normal Mode Expansion: Medium

If one wants to write the corresponding expression in the presence of scalar and vector potentials, one needs to find out if the energies E_p in the expansion Eq. 7.21 have to be replaced by $E_p^\star = \sqrt{m^{\star\,2} + \mathbf{p}^2}$ or by the new eigenvalue $E_p^\star + \Sigma_v$. The energy appears at three places: in the spinor u_s, as normalization factor $1/\sqrt{2E_p}$ and in the phase determining the time evolution of $\psi(\mathbf{x}, t)$. We have already demonstrated that in the spinor the replacement reads $E_p \to E_p^\star$. The factor $1/\sqrt{2\,E_p}$ has been introduced for normalization reasons. According to Eq. 7.10 the normalization of the spinors changes to $2\,E_p^\star$, thus suggesting the replacement $1/\sqrt{2\,E_p} \to 1/\sqrt{2\,E_p^\star}$.

This leaves us with the time dependence of $\psi(\mathbf{x})$, which is governed by the commutator of $\psi(\mathbf{x})$ and the Hamilton operator $\mathcal{H}$. We therefore construct $\mathcal{H}$ in nuclear matter. In steps analogous to those in the vacuum and remembering that it is the eigenvalue that shows up in the expression, one finds

$$\mathcal{H} = \int \frac{d^3p}{(2\,\pi)^3} \sum_s (E_p^\star + \Sigma_v)\, a_s^\dagger(\mathbf{p})\, a_s(\mathbf{p}) \quad . \tag{7.22}$$

Therefore the in-medium mode expansion of the Dirac field reads as follows:

$$\psi(t, \mathbf{x}) = \int \frac{d^3p}{(2\,\pi)^3} \frac{1}{\sqrt{2\,E_p^\star}} \sum_s a_s(\mathbf{p})\, u_s(E_p^\star, \mathbf{p})\, e^{-i\,((E_p^\star + \Sigma_v)\,t - \mathbf{p}\,\mathbf{x})} \quad . \tag{7.23}$$

7.3.3 Calculation of Matrix Elements: Resonance Decay

We now give one explicit example that demonstrates how the mean-field potentials show up in matrix elements. As an example, we describe the decay of a resonance R into a nucleon and a meson φ. Since the exact form of the Lagrangian is not relevant for our discussion, we pick a simple one:

$$\mathcal{L} = g\, \bar{\psi}_R\, \psi_N\, \varphi \quad . \tag{7.24}$$

Using the normalization conditions:

$$|p\rangle = \sqrt{2\,E_p}\,a_p^\dagger\,|0\rangle \quad , \quad \left\{a_p, a_{p'}^\dagger\right\} = (2\pi)^3\delta^3\left(\mathbf{p}-\mathbf{p}'\right) \quad , \tag{7.25}$$

such that

$$\int \frac{d^3p}{(2\pi)^3}\,\frac{a_p}{\sqrt{2E_p}}\,|p\rangle = 1 \quad , \tag{7.26}$$

one obtains in lowest order perturbation theory for the matrix element describing the decay of the resonance with momentum k into nucleon (momentum p) and meson (momentum q):

$$\begin{aligned}
\langle p;q|\,i\mathcal{T}\,|k\rangle &= -i\int d^4x\,\langle p;q|\,\bar\psi(x)\,\varphi(x)\,\psi_R(x)\,|k\rangle \\
&= -i\int d^4x\,\frac{d^3p'}{(2\pi)^3}\,\frac{d^3q'}{(2\pi)^3}\,\frac{d^3k'}{(2\pi)^3}\,\frac{1}{2E_{p'}2E_{q'}2E_{k'}}\,\times \\
&\quad \times\,\langle p,q|\,a_s^\dagger(\mathbf{p}')\,\bar u_s(E^\star_{p'},\mathbf{p}')\,a^\dagger(\mathbf{q}')\,a_{s'}(\mathbf{k}')\,u_s(E^\star_{k'},\mathbf{k}')\;|k\rangle\;\times \\
&\quad \times\,e^{-i(E^\star_{k'}+\Sigma_V^R-E^\star_{p'}-\Sigma_V^N-E_{q'})\,x_0}\;e^{i(\mathbf{k}'-\mathbf{p}'-\mathbf{q}')\,\mathbf{x}} \\
&= -i\,(2\pi)^4\,\delta(E^\star_k-E^\star_p+E_q+\Sigma_V^R-\Sigma_V^N)\,\delta^3(\mathbf{k}-\mathbf{p}-\mathbf{q})\,\bar u(E^\star_p,\mathbf{p})\,u(E^\star_k,\mathbf{k}) \quad .
\end{aligned} \tag{7.27}$$

The energies E_p, E_k and E_q stand for the energy of nucleon, resonance and meson, respectively. Note that in the final expression the vector potential only shows up in the energy conserving δ-function. Taking it to be the same for both nucleon and resonance, it drops completely out of the expression. On the other hand, the spinors of nucleon and resonance appear with the modified on-shell energy $E^\star_p$ and $E^\star_k$. In particular, they contain the effective masses $m^\star_N$ and $m^\star_R$. These corrections will also be present in a non-relativistic frame work, despite the fact that in the non-relativistic reduction of the Dirac equation the size of the potential is essentially determined by the difference of Σ_s and Σ_v. This is the case since the non-relativistic reduction of matrix elements is determined by the leading components of the nucleon/resonance spinors, which in turn are only modified by Σ_s and cancellations between Σ_s and Σ_v are not possible.

We have now established in which way the matrix elements have to be adjusted in the presence of mean-field potentials. Throughout this work we will assume that the vector potentials of nucleon and resonance are the same and can therefore neglect them from our considerations.

Chapter 8

Results

In this Chapter we present the results of our coupled channel analysis. In the Sections 8.1 and 8.2 we give the main results obtained for pion, η and ρ meson as well as for the resonances $P_{33}(1232)$, $D_{13}(1520)$ and $S_{11}(1535)$. Both Sections represent slightly extended versions of our publication [108] and are obtained within the self-consistent coupled channel approach. In Chapter 9 we study certain aspects of the results in more detail.

8.1 Mesons

8.1.1 ρ Meson

In Fig. 8.1 we show the spectral functions A_ρ^T and A_ρ^L for momenta 0, 0.4 and 0.8 GeV at density $\rho_0 = 0.15\,\mathrm{fm}^{-3}$. Let us first discuss the general features of the results before turning to the details. We begin with the transverse channel A_ρ^T. Due to the large width of many of the involved resonances and their close overlap with the broad ρ meson, the individual particle-hole peaks cannot be identified for all resonances. However, the structure coming from the $D_{13}(1520)$ is clearly seen. This state couples in a relative s-wave and is responsible for the peak at invariant masses below the ρ seen at small momenta. If the momentum increases, the relative importance of this state is reduced due to the fact that it moves away from the ρ pole. Then it is the sum of a few higher lying p-wave states like the $F_{35}(1905)$ or the $P_{13}(1720)$ which mostly affects A_ρ [38, 109]. Because they couple in a p-wave, these resonances are not seen at small momenta. Thus in the transverse channel the following general picture emerges: at small momenta the spectrum is dominated by the excitation of the $D_{13}(1520)$ state, leading to a pronounced double-peak structure. Increasing the momentum, the additional peak diminishes, but a sizeable broadening of the original ρ peak persists, which varies from $\Gamma_{med} = \mathcal{I}\mathrm{m}\,\Pi_\rho^T(q^2 = m_\rho^2)/m_\rho \approx 130$ MeV at $\mathbf{q} \approx 0.4$ GeV to $\Gamma_{med} = 250$ MeV at $\mathbf{q} = 0.8$ GeV. One should not conclude that the broadening keeps increasing with momentum. Within our model, there is a certain momentum above which all the resonances have passed the point $q^2 = m_\rho^2$. Beyond that momentum the particle-hole excitations move away from the resonance and their influence on the ρ spectral function becomes less important.

The different momentum dependence of A_ρ^T and A_ρ^L, which is expected from the breaking of Lorentz invariance in nuclear matter (see Chapter 5.1), is nicely displayed in the Fig. 8.2 where the transverse (left) and the longitudinal (right) spectral functions are shown as functions of momentum $\mathbf{q}$ and invariant mass $m = \sqrt{q^2}$. Whereas at small momenta both

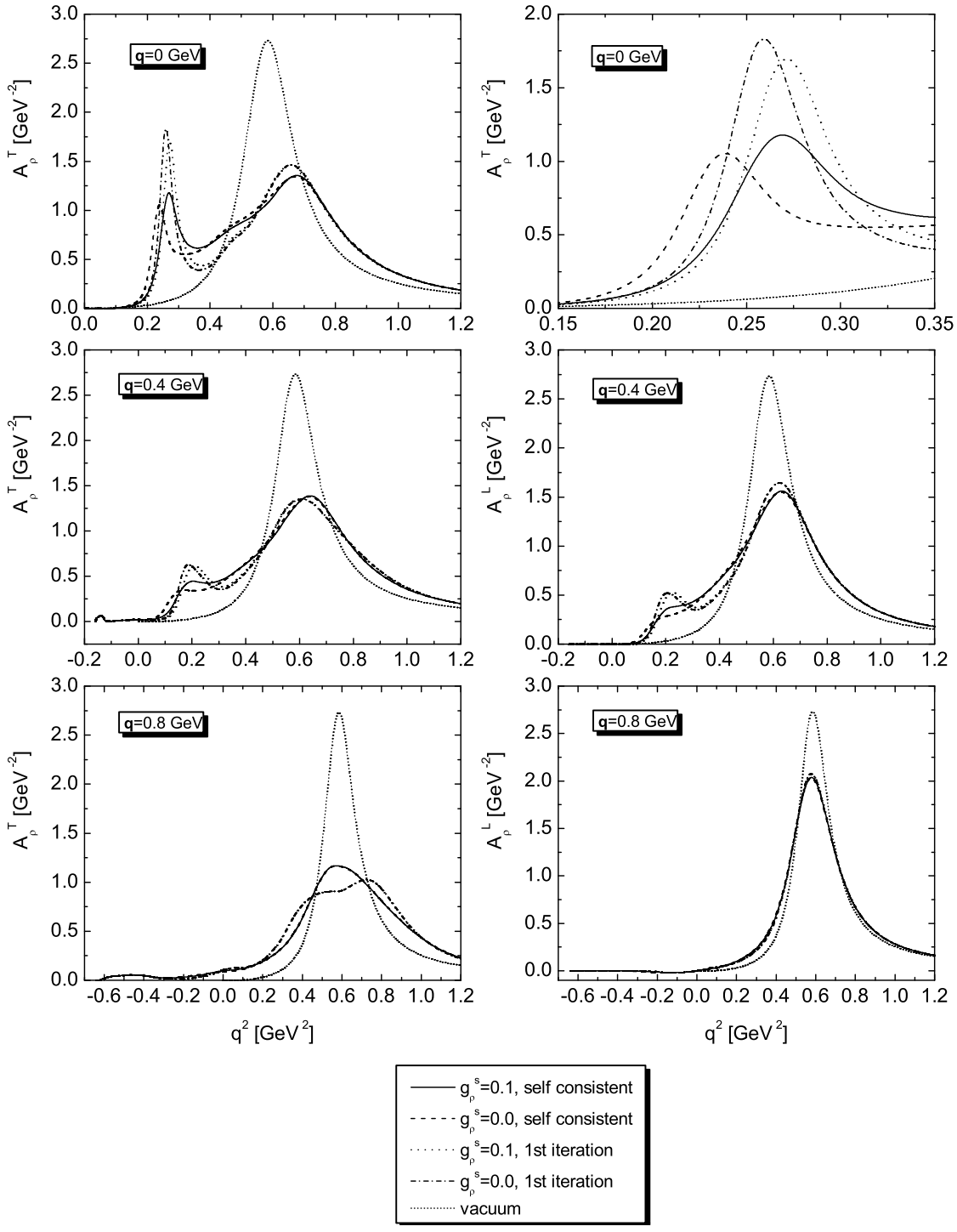

Figure 8.1: Spectral function of the ρ meson at normal nuclear matter density. Shown are the transverse and longitudinal spectral functions A_ρ^T and A_ρ^L, which are degenerate at $\mathbf{q} = 0$ GeV. Shown are the effects of iterating the spectral function and of varying the short-range parameter g_ρ^s. The picture in upper right corner represents a zoom around the $D_{13}(1520)N^{-1}$ peak for $\mathbf{q} = 0$ GeV.

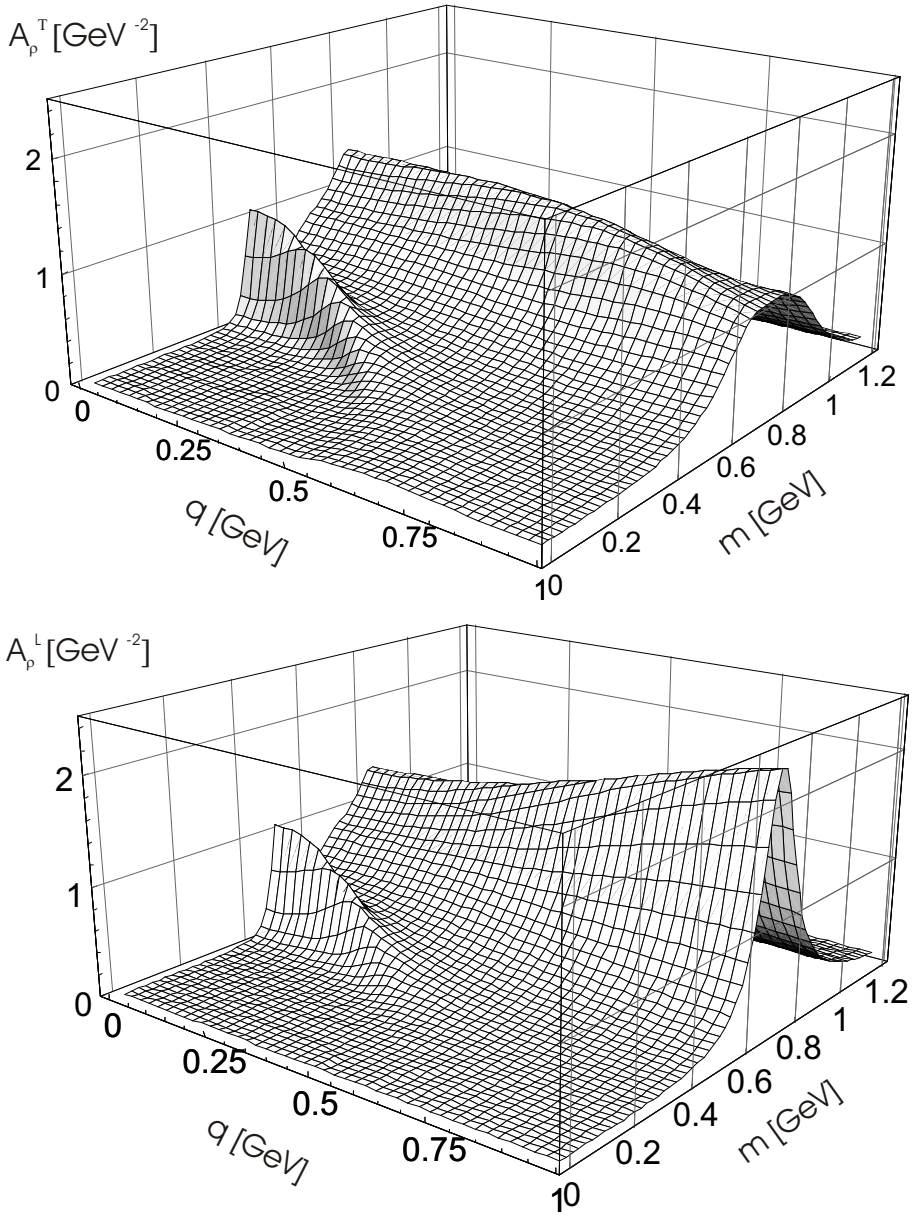

Figure 8.2: Spectral function of the ρ meson at normal nuclear matter density as a function of three momentum $\mathbf{q}$ and invariant mass $m = \sqrt{q^2}$. In the upper graph the transverse spectral function is shown and in the lower one the longitudinal spectral function is shown.

spectral functions are very similar and dominated by the $D_{13}(1520)$ excitation, at larger momenta we observe a different behaviour. For a more detailed discussion let us return to Fig. 8.1. Whereas at small momenta up to 0.4 GeV both spectral functions develop a similar behaviour, for large momenta around 0.8 GeV A_ρ^L is much less modified and starts resembling the vacuum spectral function. This is due to the fact that the p-wave resonances - responsible for the broadening of the meson peak in A_ρ^T - do not couple to a longitudinal ρ meson and that - apart from the $D_{13}(1520)$ - the s-wave states do not couple strongly enough to cause a large effect. Furthermore, their coupling is proportional to q^2 and gets therefore smaller when the momentum increases until it eventually vanishes in the vicinity of the photon point $q^2 = 0$, which is approached by states with a mass around 1.5 GeV at a momentum of 0.8 GeV.

In Fig. 8.1 we also compare the effects from higher order corrections in the density and from inclusion of the short-range correlations (SRC) for s-wave states. For p-waves, the SRC are always taken into account. Concerning the iterations, we obtain good convergence after maximal four iterations. At low momenta the main effect of the iterations is to smear out the region around the peak generated by the $D_{13}(1520)$ (see especially top right plot in Fig. 8.1). This is due to a broadening of that state, which is discussed below in Section 8.2.2. The strength sitting in the ρ peak remains stable. At larger momenta one observes a minor shift of the ρ peak down to smaller invariant masses. This shift is due to a combined effect of the in-medium modifications of the higher lying resonances and is therefore not easily disentangled. In our previous publication [107], the iterations led to a structureless ρ spectral function due to a large in-medium broadening of the baryon resonances. We find that this discrepancy results from the use of different form factors. In the previous publication the form factor did not depend on the invariant energy k^2 of the baryon resonance, but on the 3-momentum $\mathbf{q}$ of the ρ meson relative to nuclear matter, leading to much larger self energies away from the resonance-hole peak. This way the in-medium broadening of baryon resonances was allowed to generate large effects far away from the resonance peak, in particular in the vicinity of the ρ peak. Using an k^2 dependent form factor, the effects of resonance broadening are confined to the region around the resonance peak. Thus the width of the ρ peak remains smaller than before and at large momenta the ρ regains a quasi-particle structure. This effect does not depend on whether one uses form factor $FF1$ of Eq. 3.22 or $FF2$ of Eq. 3.23. The form factor at the meson-nucleon-resonance vertex does not only affect the meson self energy $\Pi_\rho^{T/L}$, but also the resonance self energy. In order to prevent the resonance width from exploding away from the on-shell point, a form factor like Eq. 3.22 or Eq. 3.23, producing the necessary suppression, is mandatory. We conclude that with the new form factor the effects from self-consistency are estimated more reliably. The effect of the form factor on the first iteration is discussed in Chapter 9.4.

The SRC for s-wave states have mainly the effect of moving the D_{13} peak slightly up, leaving the gross structure of the results untouched (see again top right plot in Fig. 8.1). The repulsive nature of the SRC is well known. In analogy to the discussion in Chapter 2.2, this can be seen by putting the resonance width to zero. Then the contribution of the

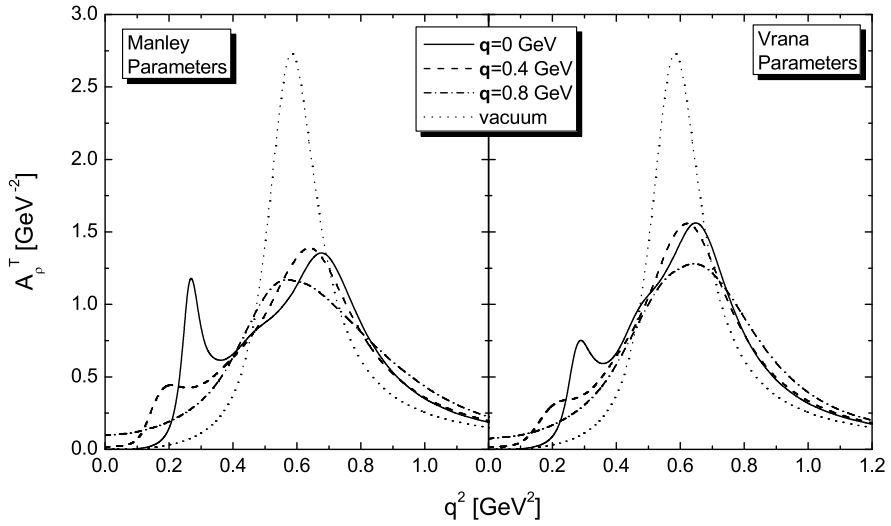

Figure 8.3: Comparison of a calculation of A_ρ^T employing the parameter set of Manley [90](left) and that of Vrana [124] (right). The calculations are done at a density $\rho = \rho_0$. Note that we only show the timelike part of the spectrum since there are no differences in the parameter sets for the $P_{33}(1232)$ and the nucleon. For the SRC in the s-wave sector we take $g_\rho^s = 0.1$.

$D_{13}(1520)$ to the transverse self energy can be cast into the form (cf. also [50]):

$$\begin{aligned} \Pi_\rho^T(q_0, \mathbf{q}) &= q_0^2 \frac{\chi_s}{1 - g_\rho^s \chi_s} \\ &= q_0^2 \frac{C}{q_0^2 - \bar{E}^2 - g_\rho^s C} \quad , \end{aligned} \tag{8.1}$$

where we have introduced $\bar{E} = E_R - m_N$, simulating the kinematical situation of a ρ meson scattering on a nucleon at rest. The constant $C > 0$ is proportional to the density and the coupling constant. One sees that the inclusion of SRC acts like a repulsive mass shift of the resonance. This effect is enhanced by the fact that the attractive in-medium shift of the peak of the spectral function of the $D_{13}(1520)$ is less pronounced once the short-range interactions are switched on, see Section 8.2.2. Since s-wave states are less important at large momenta, we find virtually no influence of g_ρ^s on the results. Therefore only three curves (instead of five) can be distinguished in the bottom of Fig. 8.1. Summarizing, the spectral function is rather stable with respect to SRC in the s-wave sector, which mainly influence the details around the D_{13} peak at small momenta.

In Fig. 8.3 we study the influence of the resonance parameters as extracted from [90] and [124]. As explained in Chapter 4, those analyses differ in that they assign different strength to the $N\rho$ channel, the analysis [90] favouring larger values for the partial decay widths. As can be seen, the differences between both results are most pronounced around the $D_{13}(1520)$ peak, where the smaller coupling leads to a reduced influence of that state. However, at lot of strength is still removed from the ρ peak. At larger momenta the differences are quite small and the broadening of the ρ peak remains untouched.

Comparison with other models: Let us now compare our results with those obtained from other models for the ρ meson. In the works of [111, 24] the main source of in-medium modifications is due to the renormalization of the $\rho\pi\pi$ decay in the nuclear medium, generated by the coupling of pions to nucleon-hole and Δ-hole states. On the level of scattering amplitudes this corresponds to a consideration of background terms of the ρN scattering amplitude. The overall picture emerging from such works is a substantial broadening of the ρ peak, accompanied by a slight repulsion. In addition, the effects from coupling the ρ to $D_{13}(1520)N^{-1}$ holes have been estimated in [24] and the peak structure reported here and in our previous publications has been qualitatively confirmed. In [122] the momentum dependence of the spectral function inherent to such models has been studied and found to be small. This is in clear contrast to the finding in our work. As shown in Fig. 8.1 the resonance-hole loops create a sizeable dependence on $\mathbf{q}$, which is a direct consequence of the condition that the invariant mass of the meson-nucleon system equals that of the excited resonance. Such kinematical constraints are absent for the decay of a ρ meson into pions in nuclear matter, where the corresponding self energy is build up from background terms of the ρN scattering amplitude (cf. Section 5.5). Therefore the small momentum dependence found in [122] is reasonable. In the work of [62] the ρN forward scattering amplitude has been calculated based on a combination of vector meson dominance (VMD) and heavy baryon chiral perturbation theory. There a strong broadening of the ρ in combination with attractive mass shift is reported. As compared to our scheme the models [111, 24, 62, 122] are clearly more elaborate concerning the in-medium $\rho\pi\pi$ decay. Qualitatively, however, such effects only lead to an additional broadening and shift of the ρ peak. On the other hand, the gross features of the spectral function – especially the rich peak structure – is given by the resonance-hole excitations studied here with great sophistication.

Closer in spirit to our approach are the works of [38, 84, 37]. In [38] the effects of coupling the ρ to two p-wave resonances, the $P_{13}(1720)$ and the $F_{35}(1905)$, are considered, which only contribute at finite momenta. This model predicts the existence of additional peaks in the spectral function and a broadening of the original ρ peak. In [84, 37] the ρN scattering amplitude is generated as a solution of a coupled-channel Bethe-Salpeter equation. This way resonant structures are formed dynamically. This analysis is restricted to small momenta since no p-wave states are incorporated in the model. For a ρ at rest the in-medium modifications are found to be much smaller than in our work, owing to a much smaller coupling of ρN in the D_{13} channel (see also discussion in Section 4.1). For a more detailed overview of the different models we refer the reader to [111].

While differing in many details, the results have one general feature in common: all of them predict a sizeable shift of spectral strength down to smaller invariant masses of the ρ. This is required by the QCD sum rules [47, 62, 78] and offers a possible explanation for the apparent shift in the dilepton spectra measured in heavy ion collisions.

Dilepton Spectra: Much of the interest in the in-medium properties of the ρ meson has been triggered by dilepton spectra of the CERES/NA45 [3, 4, 76, 129] and the HELIOS [92] collaboration, indicating an enhancement of spectral strength below the free ρ mass. We turn therefore to a computation of momentum integrated dilepton rates as resulting from our model for the ρ meson. This rate is defined as [44, 113]:

$$\frac{dR_{e^+e^-}}{dq^2}(q) \;=\; \int \frac{d^3q}{2q_0}\,\frac{dR_{e^+e^-}(q_0,\mathbf{q})}{dq^4} \quad . \tag{8.2}$$

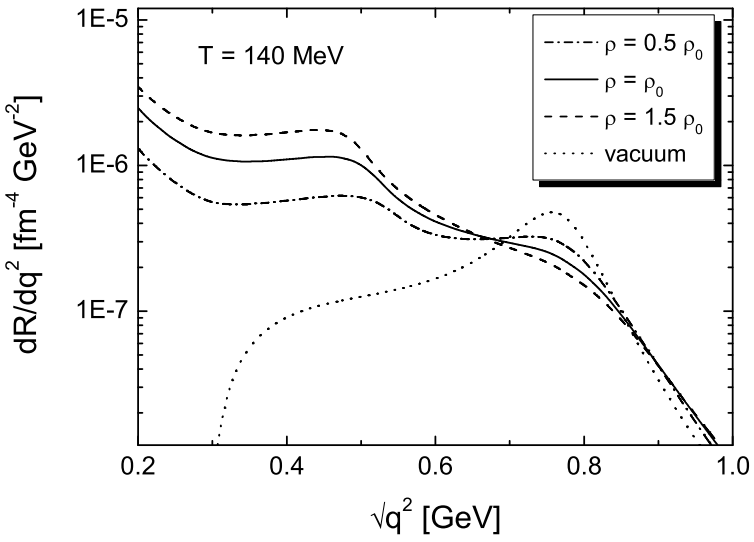

Figure 8.4: Momentum integrated dilepton rates at a temperature $T = 140$ MeV for three different densities, $0.5\,\rho_0$ (dashed-dotted), ρ_0 (solid) and $1.5\,\rho_0$ (dashed). In all curves SRC with $g_\rho^s = 0.1$ and $g_\pi^d = 0.4$ are included.

Using the assumption of strict Vector Meson Dominance (VMD), the four-fold momentum differential rate is directly related to the transverse and longitudinal spectral functions of the ρ meson:

$$\frac{dR_{e^+e^-}}{dq^4} \;=\; \frac{\alpha^2}{\pi^2\,q^2}\,n_B(q_0,T)\,\frac{m_\rho^{0,4}}{g_\rho^2}\,\left[\frac{2}{3}\,\mathcal{A}_\rho^T(q_0,\mathbf{q})+\frac{1}{3}\,\mathcal{A}_\rho^L(q_0,\mathbf{q})\right] \quad . \tag{8.3}$$

Here α is the electromagnetic fine-structure constant and $g_\rho = 6.05$ denotes the coupling strength of the ρ to the photon. The thermal Bose occupation factor reads:

$$n_B(q_0,T) \;=\; \frac{1}{e^{q_0/T}-1} \quad . \tag{8.4}$$

The formula Eq. 8.3 is derived in [44]. Without repeating this derivation here, one can nonetheless motivate the terms appearing in this equation: The underlying concept is the optical theorem, relating the total cross section to the imaginary part of the $e^+\,e^-$ forward scattering amplitude. This amplitude contains a photon propagator, which explains the factor $1/q^2$. Within the VMD picture the photon then couples to hadrons via a ρ meson. This leads to the appearance of the ρ spectral function in Eq. 8.3. The factor $m_\rho^{0,4}/g_\rho^2$ comes from the coupling of the photon to the ρ meson. Finally, the Bose distribution n_B characterizes the distribution of states with energy q_0 at a given temperature T.

In Fig. 8.4 we present results for the momentum integrated dilepton rates $\frac{dR_{e^+e^-}}{dq^2}(q)$ for the densities $\rho = 0.5\,\rho_0$, $\rho = \rho_0$ and $\rho = 1.5\,\rho_0$. For the temperature we take $T = 140$ MeV, which should be typical for SPS energies [113, 38]. For comparison we have also plotted the dilepton spectrum as resulting from using the vacuum ρ propagator in Eq. 8.3. No experimental acceptance cuts are taken into account.

The overall picture is that our model produces a substantial reduction of strength around the free ρ peak and leads to a strong enhancement of the dilepton yield at small invariant masses around $300 - 600$ MeV, where the resonance-hole contributions dominate the dilepton spectrum. The strong population of small invariant masses is due to the excitation of the resonance-hole pairs, for example the $D_{13}(1520)$ and the $P_{13}(1720)$ states. It is further enhanced by the factor $1/q^2$ as well as the thermal Bose distribution factor in Eq. 8.3. The $D_{13}(1520)N^{-1}$ excitation leaves a clear trace in the peak structure seen at invariant masses of about 500 MeV. Probably we overestimate the effects resulting from dressing the ρ meson by using the strict VMD picture where the photon coupling of hadrons is directly related to the hadronic coupling. In Chapter 10 we will show explicitly, that within such an approach the electromagnetic coupling of the baryon resonances is overestimated by about a factor of 2. Still the qualitative picture remains valid also with more elaborate versions of VMD.

The spectral function $\mathcal{A}_\rho^{T/L}$ is calculated at zero temperature. This is a reasonable approximation for resonance-hole states. Finite temperature effects only slightly rearrange the nucleon distribution function and also the small overestimation of Pauli-blocking – which is not important for the $D_{13}(1520)$ – should leave the results shown in Fig. 8.4 qualitatively intact. We do not consider scattering processes of the ρ meson on pions present at finite temperatures lead to a further broadening of the ρ peak of about 80 MeV at $T = 140$ MeV [113]. Albeit non-negligible, inclusion of this effect would not lead to qualitative changes of the results in Fig. 8.4.

8.1.2 π Meson

The properties of the pion in nuclear matter have been exhaustively studied within the Δ-hole model, see for example [99], where the pion is allowed to couple to the $P_{33}(1232)$ resonance and the nucleon. Our model goes beyond that by explicitly including resonances with higher mass, like the $P_{11}(1440)$ or the s-wave states $S_{11}(1535)$ and $S_{11}(1650)$. In addition, we generate corrections which are due to the self-consistent iteration of resonance and meson spectral functions. In that way different mesons influence each other to some extent.

In Fig. 8.5 we show results for the spectral function $\mathcal{A}_\pi$ at three momenta, 0.4 GeV 0.5 GeV and 0.6 GeV, after the first (dashed lined) and the fourth (solid line) iteration at density ρ_0. One can clearly see the multi-peak structure of the spectral function due to the excitation of nucleon-hole (left most peak) and $P_{33}(1232)$-hole states (peak in the middle). In the momentum range under consideration the kinematics are such that the pion branch is above the $P_{33}(1232)$ and the nucleon branches, see also Fig. 5.3. Due to level repulsion the position of the pion peak is therefore shifted to larger invariant masses. In Fig. 8.5 this is indicated by the dotted vertical line at the invariant mass of the free pion. Note that a substantial amount of spectral strength is sitting at space-like four-momenta. For momenta $\mathbf{q} \geq 0.6$ GeV the additional peaks from nucleon and $P_{33}(1232)$ become much less pronounced since they are too far away from the pion pole and the pion starts resembling a good quasi-particle. The results presented here are in qualitative agreement with those of other analyses, see for example the results presented in [56], where on the basis of a model that is close to ours after the first iteration the spectral function is plotted for a momentum of $\mathbf{q} = 0.5$ GeV.

The effects of the iteration (solid line) lead to a smearing of pion and the $P_{33}(1232)$

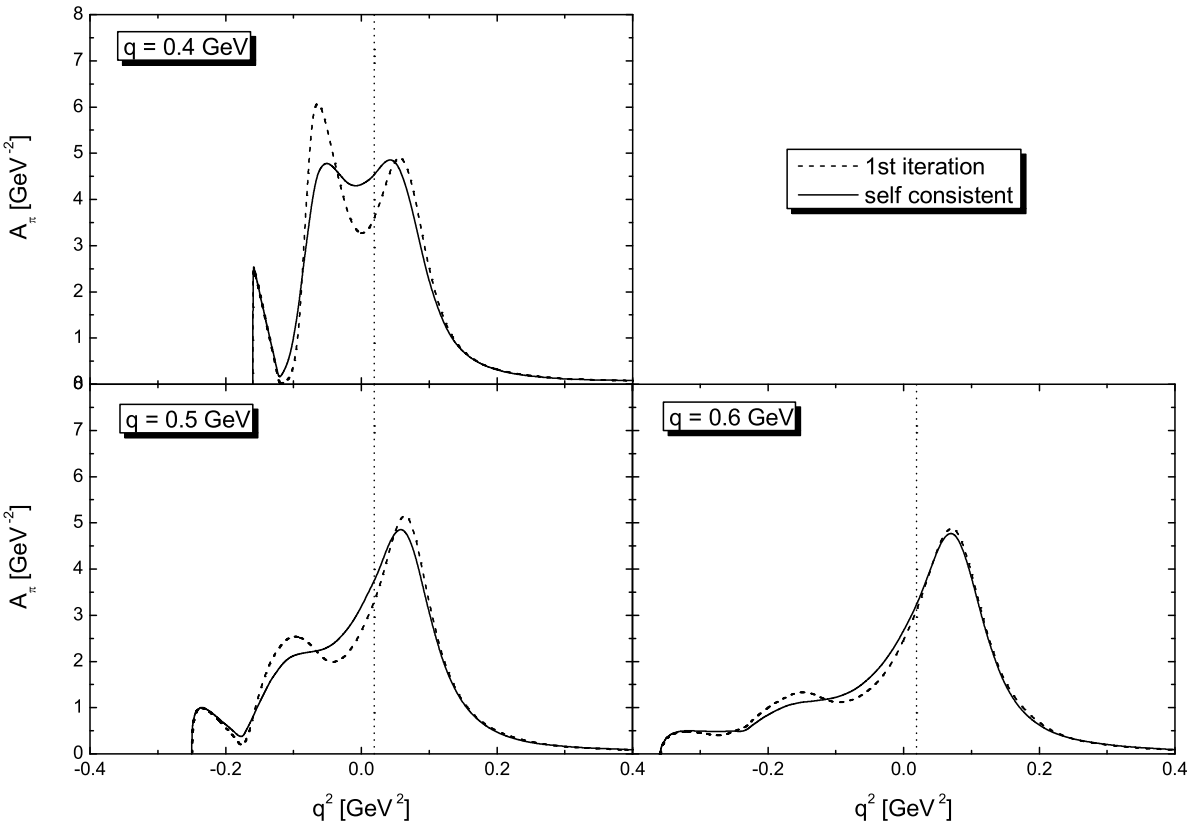

Figure 8.5: Spectral function of the pion at $\rho = \rho_0$. Shown is the spectral function at three momenta, 0.4 GeV, 0.5 GeV and 0.6 GeV after the first (dashed line) and fourth (solid line) iteration. Also indicated is the position of the free pion peak (dotted vertical line).

peaks, while leaving the nucleon contribution unchanged. More importantly, however, there is no significant shift of spectral strength down to smaller invariant masses by the iterations. This point will become important when we discuss the properties of the $P_{33}(1232)$ in nuclear matter.

In Fig. 8.6 we display the influence of the remaining resonances besides the $P_{33}(1232)$ on the pion spectral function. We show the results after the first iteration in order to avoid mixing up effects from the inclusion of these additional states and from the iterations. We find a modest influence of two s-wave states, the $S_{11}(1535)$ and the $S_{11}(1650)$, and the $P_{11}(1440)$, coupling in a p-wave. Although these states have sizeable decay widths into the $N\pi$ channel, the large available phase space prevents a strong coupling of these resonances and the coupling is not sufficient to produce distinct peaks in the spectral function. Nonetheless, these states serve as a background contribution and smear out the pion peak. The somewhat smaller repulsion in the pion peak is due to the attractive interaction generated by heavy resonance-hole states due to level repulsion. Their impact is most pronounced at 3-momenta $\mathbf{q} \geq 0.6$ GeV where the energy of the corresponding resonance-hole states is close to that of the pion, see Fig. 5.3. Effects from the $D_{13}(1520)$ state are suppressed by the d-wave coupling. Thus only at large momenta we see the influence of that state.

At very small 3-momenta $\mathbf{q}$, the πN scattering amplitude receives contributions from non-resonant s-wave terms [13], which are not included in our model. Therefore our results

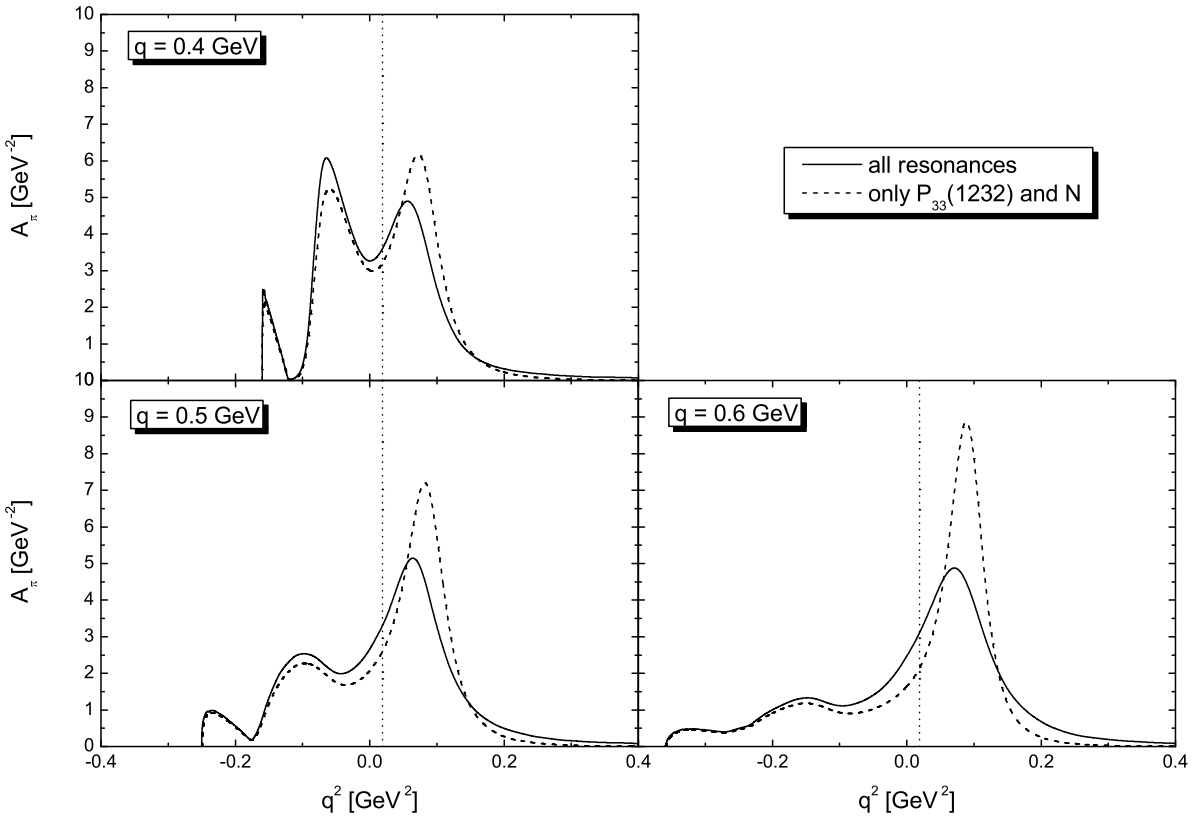

Figure 8.6: Spectral function of the pion at $\rho = \rho_0$. Shown is the spectral function at thee momenta, 0.4 GeV, 0.5 GeV and 0.6 GeV after the first iteration. The solid line indicates the results if all resonances are included, for the dashed line only the $P_{33}(1232)$ and the nucleon are coupled to the pion. Also indicated is the position of the free pion peak (dotted vertical line).

are not completely reliable in this kinematical regime and we cannot comment on the problem of s-wave repulsion demanded by data on pionic atoms [11]. Due to level repulsion, our model gives a small attraction of the pion since all the s-wave resonance-hole pairs have energies larger than m_π. This shortcoming at small momenta has no sizeable effects on the results of the iterative scheme presented in this work, however, since the regime of small 3-momenta is hardly tested in the decay of baryon resonances due to Pauli-blocking. Apart from these details, the spectral function of the pion is at low momenta dominated by the pion peak since both the nucleon-hole and the $P_{33}(1232)$-hole excitation are p-wave and open up only at finite momenta.

8.1.3 η Meson

In the discussion of the in-medium properties of the η meson we focus on the question of η-mesic nuclei, where the ηN interaction is tested at small relative momenta. It is well known from coupled-channel analyses of πN scattering, that close to threshold the ηN interaction is dominated by the $S_{11}(1535)$ resonance, see for example [104, 57]. As was already pointed out in e. g. [56, 125, 96], the presence of the $S_{11}(1535)$ in the ηN interaction provides an attractive optical potential U_η since the resonance pole is about 50

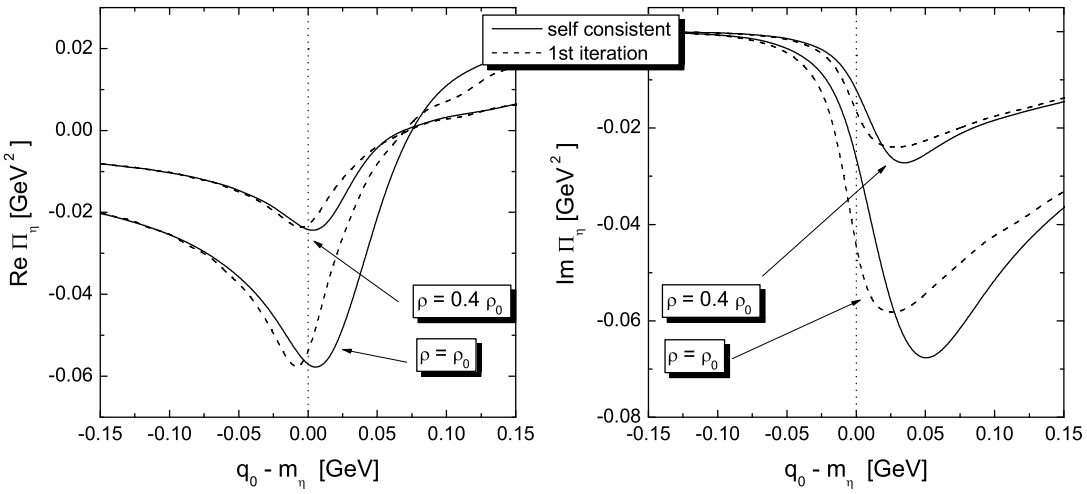

Figure 8.7: Real (left) and imaginary (right) part of the in-medium self energy of the η meson. Shown are calculations at densities $\rho = \rho_0$ and $\rho = 0.4\,\rho_0$. The dashed lines indicate the results following from the first iteration Eq. 5.8 and the solid incorporate all the effects from dressing the $S_{11}(1535)$.

MeV above the ηN threshold. In terms of the self energy Π_η, the optical potential reads close to threshold:

$$U_\eta(m_\eta, \mathbf{0}, \rho) \;=\; \frac{\Pi_\eta(q_0, \mathbf{0}, \rho)}{2\, m_\eta} \quad . \tag{8.5}$$

Let us first focus on the vacuum scattering amplitude, which via the low-density theorem Eq. 5.8 yields a first estimate for Π_η. In our model the $S_{11}(1535)$ resonance has a total width of about 151 MeV with $\Gamma_{N\eta} = 66$ MeV, corresponding to a branching ratio of 44%. In the approach described in [56] this state is generated dynamically and the resulting resonance parameters are quite different [57]: for the total width a value of 94 MeV is found whereas the partial width $\Gamma_{N\eta}$ is the same as in our model. To be more quantitative, let us compare results for the scattering length $a_{\eta N}$: we find $a_{\eta N} = (0.43 + i\,0.32)$ fm. The model of [57] produces $a_{\eta N} = (0.26 + i\,0.24)$ fm, whereas in [104] a value of $a_{\eta N} = (0.991 + i\,0.347)$ fm is reported and in [84] a scattering length $a_{\eta N} = (0.43 + i\,0.21)$ fm results. We conclude that our model and that of [56] yield results for the elementary ηN amplitude, which – albeit different – are well within the commonly accepted range.

The different resonance parameters have a direct effect on the self energy Π_η of the η meson calculated via Eq. 5.8, which is indicated with dashed lines in Fig. 8.7 for the densities $0.4\,\rho_0$ and ρ_0, where ρ_0 is the normal nuclear matter density ρ_0. Comparing our results with those obtained in [56], one finds that for the imaginary part the peak value is smaller in our case whereas off-shell we obtain larger values. Both findings are an immediate consequence of the larger total width in our model.

The most important in-medium correction is generated from Pauli-blocking the $N\eta$ width of the $S_{11}(1535)$. At normal nuclear matter density and for a resonance at rest the

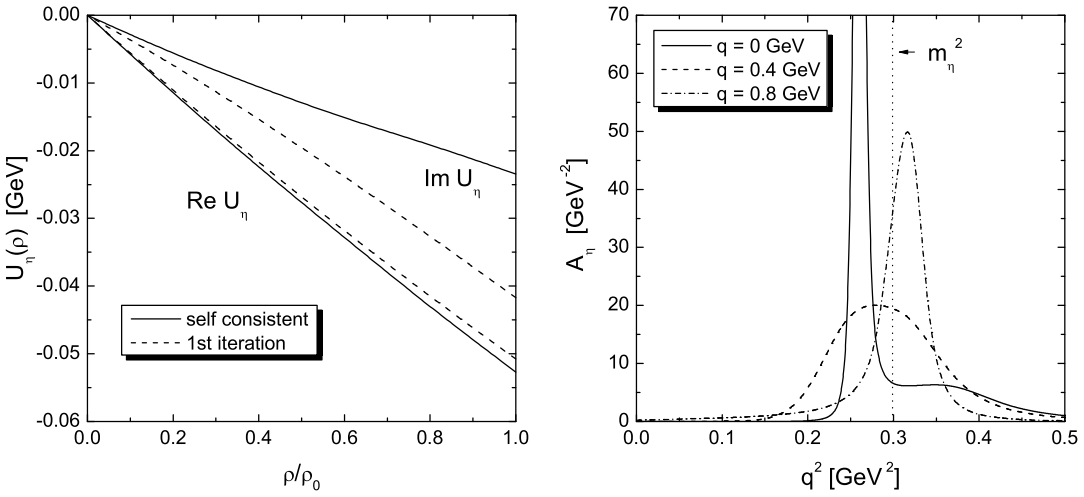

Figure 8.8: Left: Optical potential U_η of the η meson at $\mathbf{q} = 0$ GeV as a function of the nuclear density ρ. The solid lines indicate the results including in-medium corrections, for the dashed lines the vacuum scattering amplitude has been used. Right: Spectral function $\mathcal{A}_\eta$ of the η meson in nuclear matter at $\rho = \rho_0$. Shown are the results for three momenta: $\mathbf{q} = 0$ GeV, $\mathbf{q} = 0.4$ GeV and $\mathbf{q} = 0.8$ GeV.

Pauli-blocked width is zero, however even if excited by a η meson at rest the resonance has a finite 3-momentum $\mathbf{k} \approx 0.2$ GeV due to the Fermi motion of the nucleons. This weakens the effects of Pauli-blocking and the approximation to put $\Gamma_{N\eta} = 0$ as done in [96] is not accurate. On top of Pauli-blocking there are additional mechanisms that influence mass and width of the $S_{11}(1535)$. This is discussed in Section 8.2.3 and we find an additional broadening of about 30 MeV for the $S_{11}(1535)$ relative to the Pauli-blocked width at these small momenta, accompanied by a small repulsive mass shift of the $S_{11}(1535)$. Concentrating on the point $q_0 = m_\eta$ (indicated by the dotted vertical line in Fig. 8.7) as appropriate for the optical potential, we find that the mass shift leads to a depletion of $\mathcal{I}\mathrm{m}\,\Pi_\eta$ while leaving $\mathcal{R}\mathrm{e}\,\Pi_\eta$ nearly unaffected. The peak of $\mathcal{I}\mathrm{m}\,\Pi_\eta$ is shifted upwards whereas the height of the peak remains essentially the same. In the analysis of [56] this is different since the relative weight of Pauli-blocking is enhanced due to the larger branching ratio for this channel and an enhancement of the peak of the self energy in the nuclear medium results.

In Fig. 8.8 we plot the optical potential as a function of the density. As expected, the low-density approximation Eq. 5.8 shows a linear behaviour in the density both for the real and imaginary part of U_η. When the in-medium corrections are included, we find deviations from this linearity for the imaginary part, which is strongly reduced as was already indicated in the discussion in the preceding paragraph. At normal nuclear matter density we find $U_\eta = (-50 - i\,43)$ MeV in the low density approximation and $U_\eta = (-52 - i\,24)$ MeV in the full calculation. The SRC have no big effect on the potential, neglecting the SRC in the s-wave sector one obtains $U_\eta = (-49 - i\,29)$ MeV. It follows that the iterations lead to a strong reduction of the imaginary part while hardly affecting

the real part of the optical potential. This behaviour is a direct reflection of the results found for the self energy, see Fig. 8.7. It is interesting that the analysis of [56] leads to a comparable final result, $U_\eta = (-54 - i\,29)$ MeV, despite the fact that the scattering lengths in both models are different. In [125] $U_\eta = (-20 - i\,22)$ MeV is found, i.e. the attraction provided by U_η is found to be only half of our value, whereas the width is comparable. Summarizing these results, most models seem to predict similar results for the imaginary part of the optical potential while uncertainties on the level of a factor of two persist for the real part. As far as the existence of η-mesic nuclei is concerned, the strong attraction found in our approach and in that of [26] is certainly encouraging.

We close the discussion of the properties of the η meson in nuclear matter by inspecting the spectral function $\mathcal{A}_\eta$ shown in Fig. 8.8. There the spectral function is displayed for three momenta $\mathbf{q} = 0$ GeV (solid line), $\mathbf{q} = 0.4$ GeV (dashed line) and $\mathbf{q} = 0.8$ GeV (dashed-dotted line). Also indicated is the position of the free η peak. In the calculations SRC are taken into account, they have however only a small effect. One observes that at $\mathbf{q} = 0$ GeV the coupling of the η to $S_{11}(1535)N^{-1}$ loops is not sufficient to generate a distinct peak in the spectral function. Only a shoulder arises at invariant masses slightly above the η peak, which is located at $q^2 = 0.25\,\mathrm{GeV}^2$. This is in contrast to the findings both of [56] and [125] and is probably explained by the substantially smaller peak value of $\mathcal{I}\mathrm{m}\,\Pi_\eta$ found in our work, which – as mentioned above – is due to a larger total width and a smaller branching ratio into $N\eta$. The position of the η peak is shifted downwards as expected from the attractive nature of the interaction at small momenta. Going to larger momenta we find that at 0.4 GeV the η peak is substantially broadened. Around this momentum the energies of the η branch and the $S_{11}(1535)N^{-1}$ are comparable (see also Fig. 5.3), leading to a strong mixing and broadening of both states. At even larger momenta the resonance-hole excitation is below the η. This induces a small repulsion of the η peak, whereas only a moderate broadening occurs.

8.2 Baryonic Resonances

8.2.1 $P_{33}(1232)$

It is well known that the in-medium broadening of the $P_{33}(1232)$ state is in the order of 100 MeV at normal nuclear matter density. This value has been extracted a long time ago in an analysis of pion-nucleus scattering, [54]. From the same analysis a slight repulsion of the $P_{33}(1232)$ of about 20 MeV relative to the nucleon is reported. Certainly, any model trying to describe the $P_{33}(1232)$ state in nuclear matter should arrive at comparable results. We thus use this resonance as a testing ground for our model: a reasonable description of its in-medium properties suggests that no major mechanisms are missing in our approach.

We have adjusted the parameters of the $\pi N \Delta$ system - cutoffs, SRC - such as to achieve a reasonable description of the in-medium properties. In the right graph of Fig. 8.9 we plot the spreading potential V_{sp} defined by:

$$\mathcal{I}\mathrm{m}\,V_{sp}(k_0, \mathbf{k}) \;=\; \frac{\mathcal{I}\mathrm{m}\,\Sigma_{med}(k_0, \mathbf{k}) - \mathcal{I}\mathrm{m}\,\Sigma_{pauli}(k_0, \mathbf{k})}{2\sqrt{k^2}} \tag{8.6}$$

and compare to the experimental data found in [54]. Following an argument in [98] that the effective density felt in a nucleus is $0.75\,\rho_0$ rather than ρ_0, we perform the comparison

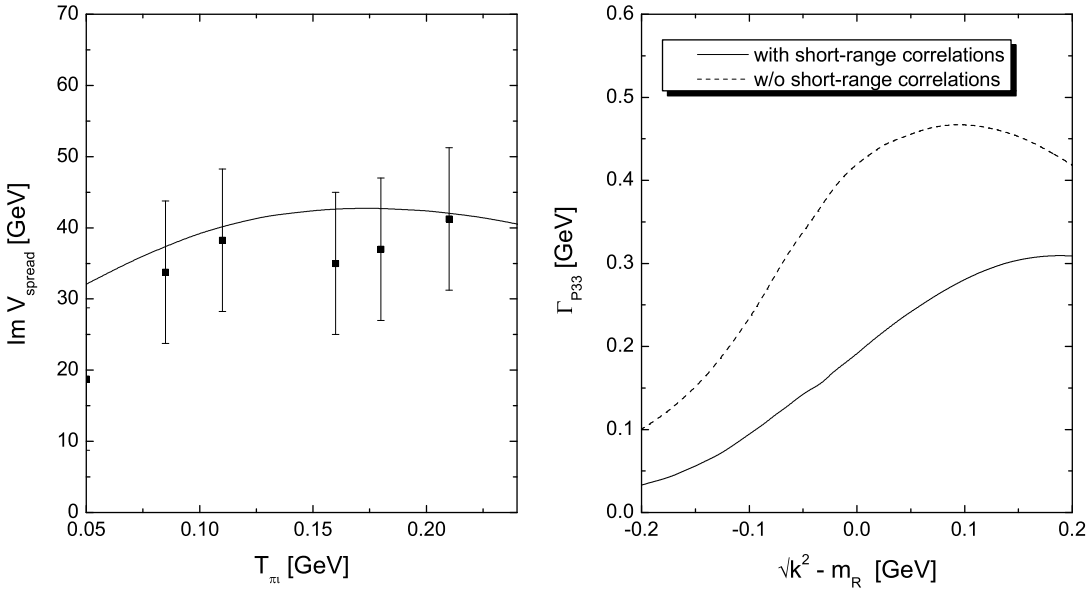

Figure 8.9: Left: Comparison of our model with the phenomenological spreading potential V_{sp} of [54]. The density is taken to be $\rho = 0.75\,\rho_0$. Right: Influence of the SRC on the width of the $P_{33}(1232)$ at $\rho = \rho_0$. Compared are a calculation with (solid line) and w/o (dashed line) SRC.

at this density. The kinematics corresponds to that of a pion, which hits a nucleon with an average momentum of $\frac{3}{5}\,\mathbf{p}_F$ and forms a Δ of energy k_0 and momentum $\mathbf{k}$:

$$k_0 \;=\; q_0 + \sqrt{m_N^2 + \frac{3}{5}\,\frac{\mathbf{p}_F^2}{2\,m_N}} \quad , \quad \mathbf{k}^2 \;=\; \mathbf{q}^2 + \frac{3}{5}\,\mathbf{p}_F^2 \quad , \quad T_\pi = q_0 - m_\pi \quad . \tag{8.7}$$

As shown in the left plot of Fig. 8.9, we achieve a reasonable description of $\mathcal{I}\mathrm{m}\,V_{sp}$ in our model. The values needed for cutoff and short-range parameter – given in Table A.1– lie well within the commonly accepted range, see for example [7, 49, 98]. In Fig. 8.10 we show width and spectral function of the $P_{33}(1232)$ state for a fixed momentum of 0.4 GeV. The width at $k^2 = m_R^2$ is found to be roughly 190 MeV, leading to broadening of the in-medium spectral function. In our model the peak position of the spectral function of the $P_{33}(1232)$ remains more or less unchanged, while $\mathcal{R}\mathrm{e}\,\Sigma(k^2 = m_R^2)/(2m_R) \approx 15$ MeV, indicating a slight repulsion of the resonance. The reason that this repulsion is not observed in the spectral function is due to the energy dependent width as outlined in the introduction to this Section.

If one calculates the baryon self energy according to Eq. 5.37 and constructs the in-medium spectral function of the π by coupling the pion to nucleon-hole and resonance-hole states, a dramatic overestimate of the in-medium width of the $P_{33}(1232)$ state results. Only after the inclusion of SRC according to Eq. 6.62 and 6.64, one arrives at satisfying results for the broadening [98, 7, 49]. This is shown in the right graph in Fig. 8.9. The effect of the correlations is to systematically move strength up to the higher branches of the spectral

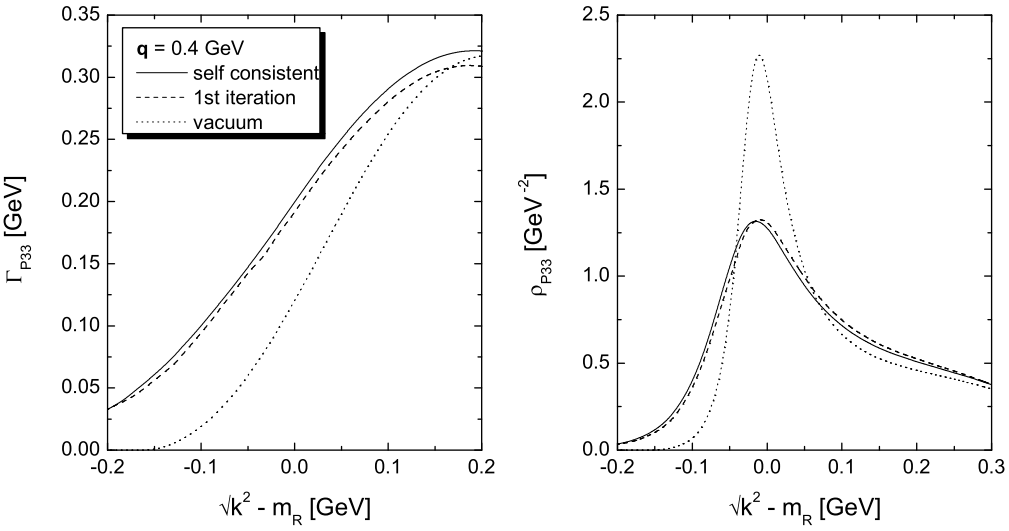

Figure 8.10: Width (left) and spectral function (right) of the $P_{33}(1232)$ moving with a relative momentum of 0.4 GeV. The solid line indicates the result obtained after four iterations whereas the dashed lined is the result after the first iteration. The density is $\rho = \rho_0$.

function. Then the available phase space is reduced and a reduction of the width results. A similar argument was put forward in [67]. In Chapter 2.4 we have systematically studied this effect within a simplified toy model. As pointed out there, the crucial effect from the short-range correlations is not the modification of the pion propagator but the induced vertex corrections.

In both plots of Fig. 8.11 we analyze the findings of the right plot of Fig. 8.9 in more detail. The left plot shows a decomposition of the results obtained without SRC. By comparing the solid and the dashed line one finds that the main body of the in-medium width is due to the inclusion of nucleon and $P_{33}(1232)$. Furthermore, we show the results for the absorptive channel $P_{33}(1232)N \to NN$ by the dotted and dash-dotted lines. These curves are obtained by multiplying the integrand of Eq. 5.37 in Chapter 5.3.1 by a factor $\mathcal{I}\mathrm{m}\,\Pi^{\pi}_{NN}/\mathcal{I}\mathrm{m}\,\Pi^{\pi}_{tot}$ as suggested by the discussion around Eq. 5.43 in Chapter 5.3.2. Not contained is the $\Delta \to N\pi$ decay contribution, therefore these results should not be directly compared with the solid and the dashed lines which give the total in-medium width. It is interesting to note that the dash-dotted curve gives a broadening which is already in the right order of magnitude before SRC are included. Indeed, in the literature some calculations exist [61, 123] where the in-medium properties are obtained just from dressing the pion with nucleon-hole loops. As discussed in Chapter 9.2, by considering nuclear mean fields – as done in these works – a further reduction of the broadening is achieved. In the light of our results, it should be clear, however, that this is not satisfying. By simply adding the $P_{33}(1232)$ to the pion self energy, the absorptive broadening goes already up by 50 MeV (compare dash-dotted and dotted lines). This qualitatively confirms that the results of the toy model presented in Chapter 2. There we argued at the end of Section 2.2

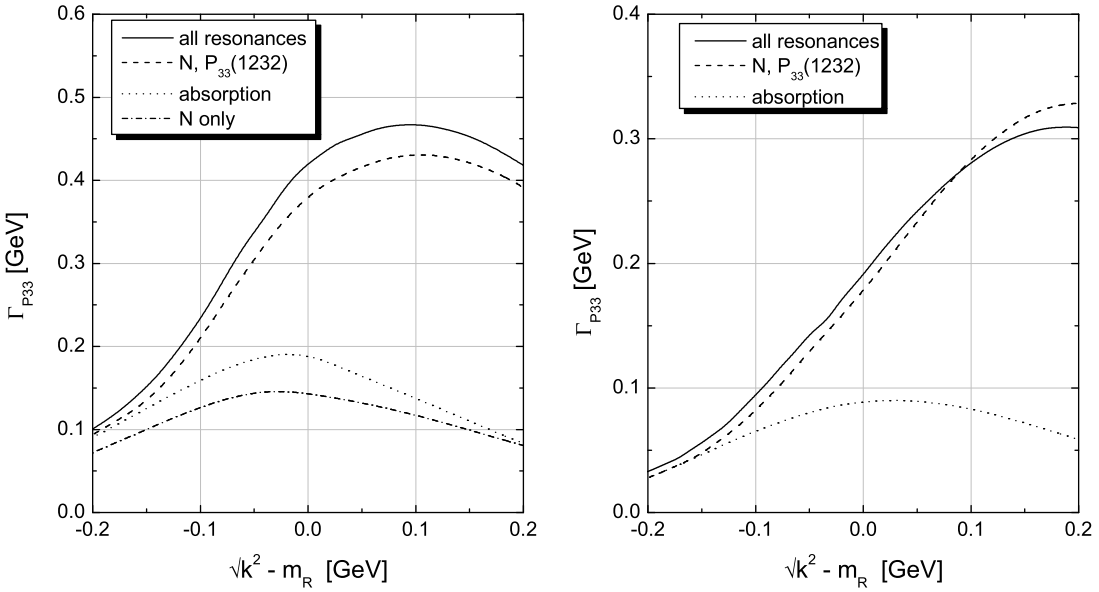

Figure 8.11: Width of the $P_{33}(1232)$ moving with a relative momentum of 0.4 GeV at $\rho = \rho_0$ as found after the first iteration. In the left plot we show results obtained w/o SRC. The solid line is the result obtained when all resonances are included, in the dashed line only N and $P_{33}(1232)$ are taken into account. The dotted line projects onto the nucleon-hole channel, while the dash-dotted line indicates the results when the pion is dressed only by nucleon-hole loops. In the right plot the same curves obtained with SRC are shown.

that due to the influence of the $P_{33}(1232)$ more strength is shifted into the nucleon-hole branch. Without explicitly showing the corresponding results, we note that by increasing the cutoff in form factor F_t of Eq. 3.21, Chapter 3.2, mainly the absorptive width, which is generated at relatively large pion momenta, is enhanced. This is line with the results for the width presented in Chapter 2.4, Table 2.1, where a large partial width into the NN channel is reported.

In the right plot of Fig. 8.11 we show the in-medium width with inclusion of SRC. Again, the in-medium width is nearly entirely generated from the dressing of the pion with the $P_{33}(1232)$ and the nucleon as can be inferred by comparing the solid and the dashed line. The dotted line shows that the absorptive part of the broadening is only about half the size as compared to the calculation without SRC. Note that in order to obtain that curve, both $\mathcal{I}\mathrm{m}\,\Sigma_\pi$ and $\mathcal{I}\mathrm{m}\,\Sigma_\rho$ have are multiplied by a factor $\mathcal{I}\mathrm{m}\,\Pi^{\pi/\rho}_{NN}/\mathcal{I}\mathrm{m}\,\Pi^{\pi/\rho}_{tot}$, since the short-range correlations give also contributions to the $N\rho$ channel (cf. Eq. 6.62 in Chapter 6.6).

In [98] it was found that 3-body absorption of the $P_{33}(1232)$ contributes significantly to the total width. There the 3-body contribution was calculated based on the same diagrams that we generate in the second iteration step, i.e. $\mathcal{I}\mathrm{m}\,\Sigma^2_{med}$ is the sum of 2-body and 3-body processes. Also an additional diagram was calculated, which we do not consider here and which was claimed to be comparatively small by the authors of [98]. In contrast to that work, we find only small effects of about 10 MeV from the iterations, i.e. our total

broadening is essentially due to 2-body processes contained in $\mathcal{I}\mathrm{m}\,\Sigma^1_{med}$. A significant modification of $\mathcal{I}\mathrm{m}\,\Sigma^2_{med}$ relative to $\mathcal{I}\mathrm{m}\,\Sigma^1_{med}$ can only follow if also the in-medium spectral function of the meson undergoes sizeable corrections, i.e. if $\mathcal{A}^1_\pi$ and $\mathcal{A}^2_\pi$ are very different. In particular, due to phase space arguments a large 3-body contribution for the $P_{33}(1232)$ can only result from a substantial shift of spectral strength down to smaller invariant masses in the pion spectral function when going from $\mathcal{A}^1_\pi$ to $\mathcal{A}^2_\pi$. Such a rearrangement is not produced by the moderate resonance broadening obtained after the first iteration, see also Fig. 8.5, where the effect of iterations on the pion spectral function is explicitly displayed. Therefore only a large additional attraction of the $P_{33}(1232)$ relative to the nucleon might help. This however is at variance with the phenomenological spreading potential [54]. We add that 3-body physics also plays no important role in the iterative scheme of [49].

We close the discussion of the $P_{33}(1232)$ with a comment on the absolute size of the absorptive channel as shown in Fig. 8.11. This channel of the in-medium width of the $P_{33}(1232)$ is constrained from data on the reaction $NN \to P_{33}(1232)N$ via the low density theorem $\Gamma = \rho\, v\, \sigma_{P_{33}(1232)N\to NN}$. In [73] it has been estimated that these data suggest an absorptive broadening of about 40 MeV. This is less than what we find in our model, which – in approximate agreement with the results of [7] – gives a value of roughly 80 MeV (see right plot of Fig.8.11). We have checked that these differences can not be explained from the resummation of particle-hole loops in the pion propagator. This demonstrates that in principle our model should be constrained from scattering data. A fit of these data would probably have lead to different model parameters. For example, in [73] a much smaller cutoff at the $NN\pi$ of $\Lambda = 0.6$ GeV has been used. We have decided not to fit our model to scattering data for the following reasons: 1) Only absorptive processes are constrained from data. Whereas they are important for the $P_{33}(1232)$, the heavier resonances can easily scatter into various final states according to the process $RN \to NR'$ with $m_{R'} \leq m_R$. These reactions and elastic scattering are, however, not directly accessible in NN scattering and we expect much weaker – if any at all – constraints for the model. When discussing the broadening of the $D_{13}(1520)$ in Chapter 8.2.2, we will see that there the main body of the broadening is due to such inelastic processes. 2) For the $P_{33}(1232)$ we are mainly concerned about a qualitative description of its global properties, i.e. a description of the spreading potential as shown in the left plot of Fig. 8.9. The main lesson learned from the $P_{33}(1232)$ is the necessity to include short-range correlations.

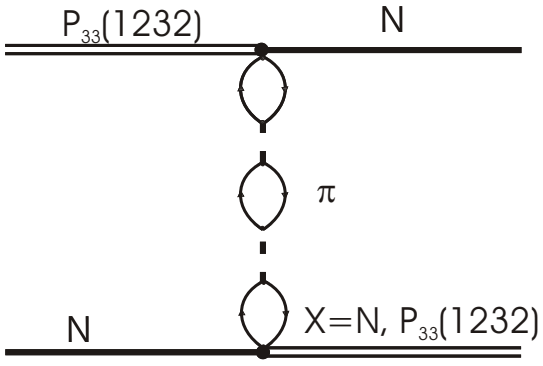

Figure 8.12: Main contribution to the self energy of the $P_{33}(1232)$ in nuclear matter.

We summarize the results of this Section by showing the most important diagram

contributing to the self energy of the $P_{33}(1232)$ in nuclear matter in Fig. 8.12: the scattering processes $P_{33}(1232)N \to NX$, where $X = N$, $P_{33}(1232)$. Important is the pion exchange term and the corrections induced from short-range correlations.

8.2.2 $D_{13}(1520)$

Our previous calculation [107] of the in-medium properties of the $D_{13}(1520)$ has been based on the effects induced by the in-medium spectral function of the ρ meson. As a result a large broadening of the $D_{13}(1520)$ state was reported. The origin of this broadening is easily explained: due to the coupling to particle-hole states, spectral strength is moved down to smaller invariant masses in the ρ spectral function, thus opening up the phase space for the decay of the $D_{13}(1520)$.

This model has now been extended in three ways. On top of considering the effects of modifications in the ρ spectral function - corresponding to RN scattering with ρ exchange - the in-medium spectral information of the pion is taken into account. Furthermore, guided by the experience with the $P_{33}(1232)$ state, effects from short-range correlations (SRC) are considered. Finally, we calculate the dispersive in-medium mass shifts.

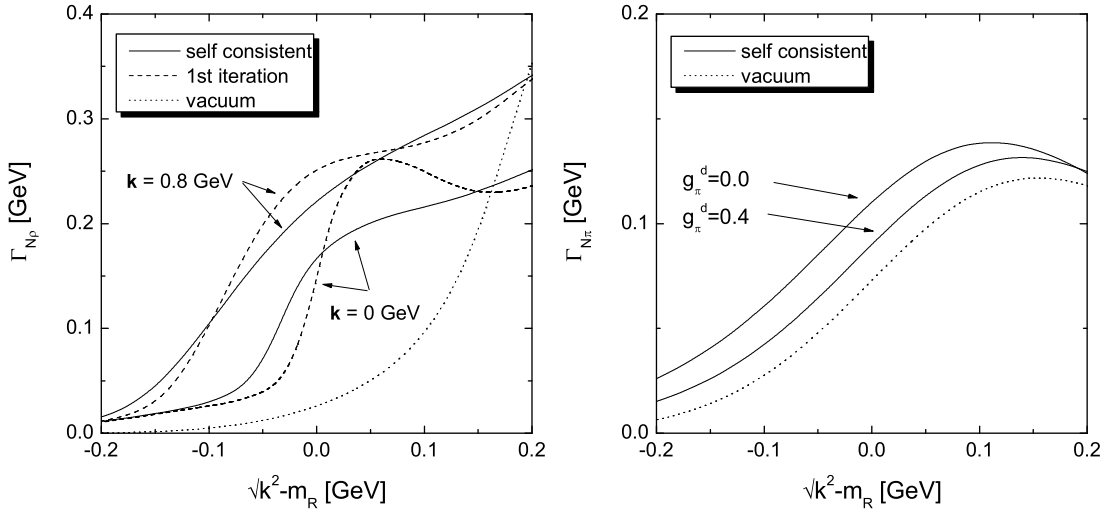

Figure 8.13: Decay width $\Gamma_{N\rho}$ (left) and $\Gamma_{N\pi}$(right) of the $D_{13}(1520)$. For the $N\rho$ width we show results w/o SRC at two different momenta, 0 and 0.8 GeV. Also indicated is the effect of the iterations. The $N\pi$ width $\Gamma_{N\pi}$ is shown for a momentum $\mathbf{k} = 0.8$ GeV. Here the effects for SRC are indicated. All results are obtained at $\rho = \rho_0$.

Neglecting the SRC for the moment, the following picture emerges: the broadening induced from the ρ meson is in the order of $200 - 250$ MeV at $k^2 = m_R^2$, i.e. at the vacuum pole of the propagator for momenta around $\mathbf{k} = 0.8$ GeV, see left plot in Fig. 8.13. In the same figure we also show that for a $D_{13}(1520)$ at rest the broadening is about 150 MeV only in this channel. These numbers are in approximate agreement with the results of our previous calculation [107]. In the language of scattering processes, most of this broadening is due to scattering $RN \to RN$ with a D_{13} in the final state, which explains the smaller

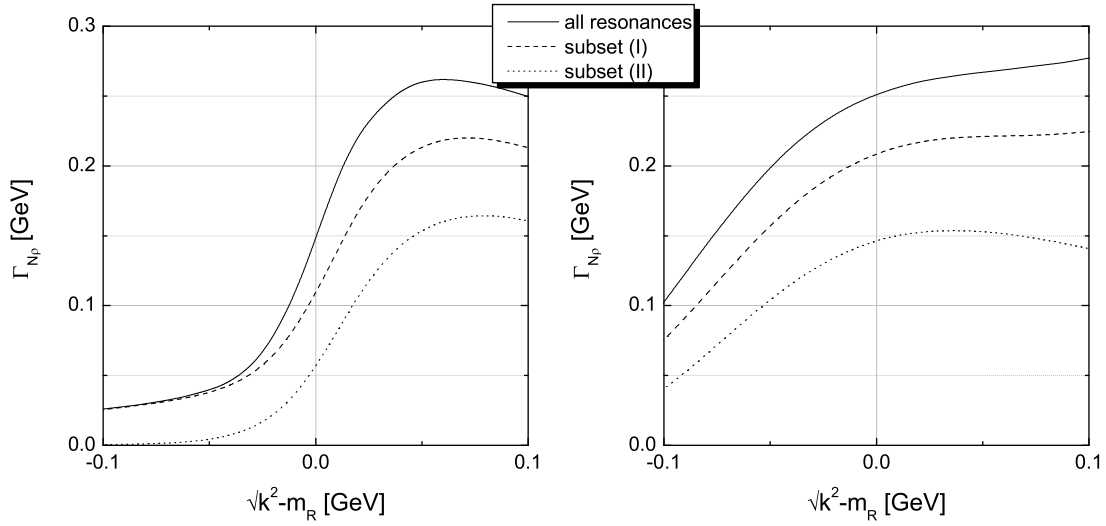

Figure 8.14: In-medium $N\rho$ width of the $D_{13}(1520)$ for resonance momenta of $\mathbf{k} = 0$ GeV (left) and $\mathbf{k} = 0.8$ GeV (right). The different curves are explained in the text.

broadening observed for small momenta $\mathbf{k}$: the available phase space for the scattering process opens up with increasing 3-momentum of the resonance. The inelastic processes $D_{13}N \to NN$ and $D_{13}N \to NP_{33}(1232)$ play only a moderate role, accounting in total for at maximum $30 - 40\%$ of the total broadening. Unfortunately, this makes it difficult to obtain reliable constraints on our model from the consideration of inelastic NN scattering.

From the in-medium pion decay we find from the right plot of Fig. 8.13 a broadening of about 40 MeV – difference between full calculation (solid line, $g'^{d}_{\pi} = 0$) and vacuum result (dotted line) – when SRC are neglected. The momentum dependence is small, therefore we show results for only one momentum $\mathbf{k} = 0.8$ GeV, appropriate in photonuclear reactions. In contrast to the ρ, here most of the broadening comes from decay into the $P_{33}(1232)$ or from absorption on the nucleon. The $D_{13}(1520)$ as a final state plays only a minor role since it couples in a d-wave, thus reducing the effectively available phase space. This relatively small broadening is at variance with the findings of [67] where a strong broadening of several hundred MeV from this channel is reported. We recall that in [67] the $D_{13}(1520)$ is dynamically generated in a coupled channel approach. Even though our results are quite sensitive to the value of the cutoff parameter Λ, we would have to relax Λ from 1.0 GeV - as appropriate in $\pi N \Delta$ dynamics - to a value of at least 2 GeV in order to generate a broadening of about 200 MeV. We conclude that within our approach a substantial softening of the $D_{13}(1520)$ state due to the decay into an in-medium pion seems unlikely. The decay mode $D_{13}(1520) \to \Delta\pi$ is not modified in the nuclear medium in our model.

We mentioned before that the in-medium $N\rho$ width of the $D_{13}(1520)$ is mainly built up of elastic resonance nucleon scattering $D_{13}(1520)N \to ND_{13}(1520)$. For the in-medium width in the $N\pi$ channel the claim was that only the scattering processes into nucleon and $P_{33}(1232)$ are important whereas elastic scattering or inelastic scattering into higher lying states is negligible.

In order to support these statements we have calculated the $N\rho$ width in two simplified frame works, where only the $D_{13}(1520)$, the $P_{33}(1232)$ and the nucleon couple to the ρ meson. These are denoted by subset (I) and subset (II). The difference between both frame works is that in the calculation (II) we have multiplied the integrand of Eq. 5.37 by

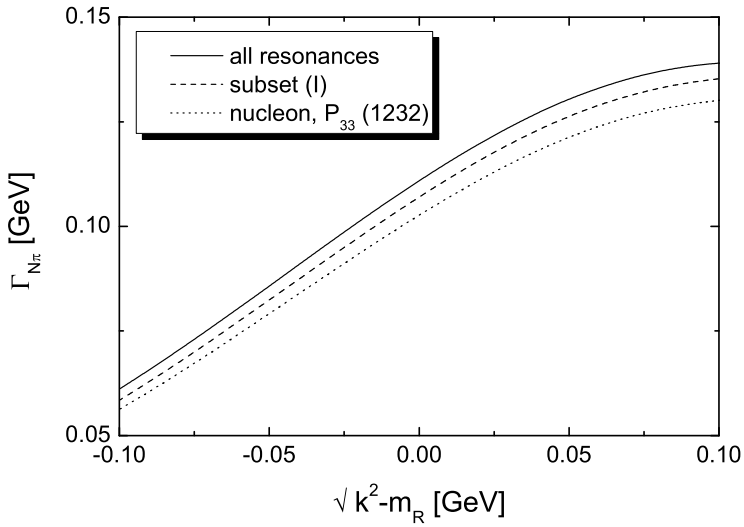

Figure 8.15: In-medium $N\pi$ width of the $D_{13}(1520)$ for a resonance momentum of $\mathbf{k} = 0.8$ GeV. The different curves are explained in the text.

a factor

$$\frac{\mathcal{I}\mathrm{m}\,\Pi_\rho^{D13(1520)}}{\mathcal{I}\mathrm{m}\,\Pi_\rho^{tot} + \mathcal{I}\mathrm{m}\,\Pi_{vac}} \quad , \tag{8.8}$$

where $\mathcal{I}\mathrm{m}\,\Pi_\rho^{tot}$ denotes the sum of nucleon, $D_{13}(1520)$ and $P_{33}(1232)$ contributions to the self energy of the ρ meson. This way we can trigger on the elastic scattering contribution, see also discussion around Eq. 5.43 in Chapter 5.3.2. In calculation (I) such a factor is not multiplied. It follows that the difference between both curves indicates the effects from inelastic scattering processes $D_{13}(1520)N \to NN$ and $D_{13}(1520)N \to P_{33}(1232)N$ and from the decay into $D_{13}(1520) \to N\rho$. In Fig. 8.14 the results of our calculation are shown for two resonance momenta, $\mathbf{k} = 0$ GeV (left) and $\mathbf{k} = 0.8$ GeV (right). The results from subset (I) are displayed by dashed lines and those from subset (II) by dotted lines. Also shown are results including all resonances (solid lines), which allows for all reactions of the type $D_{13}(1520)N \to NR$ and the $N\rho$ decay. The overall picture emerging from both plots in Fig. 8.14 is the following: Scattering into a nucleon or a $P_{33}(1232)$ amounts to a broadening of about 50 MeV (see difference between subset (I) and subset(II)). Another 50 MeV are due to the inclusion of all remaining resonances (see difference between solid line and subset (I)). The main effect of these higher lying states is to enhance the $D_{13}(1520)$ peak in the ρ spectral function (cf. Figs. 9.8 and 9.9 in the following Chapter 9). The contribution from elastic resonance-nucleon scattering on the other hand (see subset (II)) is very momentum dependent and of the order of 50 MeV at $\mathbf{k} = 0$ GeV and 150 MeV for a momentum of $\mathbf{k} = 0.8$ GeV, which can be motivated by the increase of available phase space.

For the pion we have carried out a similar analysis and compare in Fig. 8.15 three calculations: the solid line corresponds to a full calculation as obtained after the first iteration, the dashed curve shows the results when just using subset (II) and for the dotted lines the in-medium $N\pi$ width is obtained without including the $D_{13}(1520)$. One sees that all three curves show only very little difference. We conclude that the in-medium

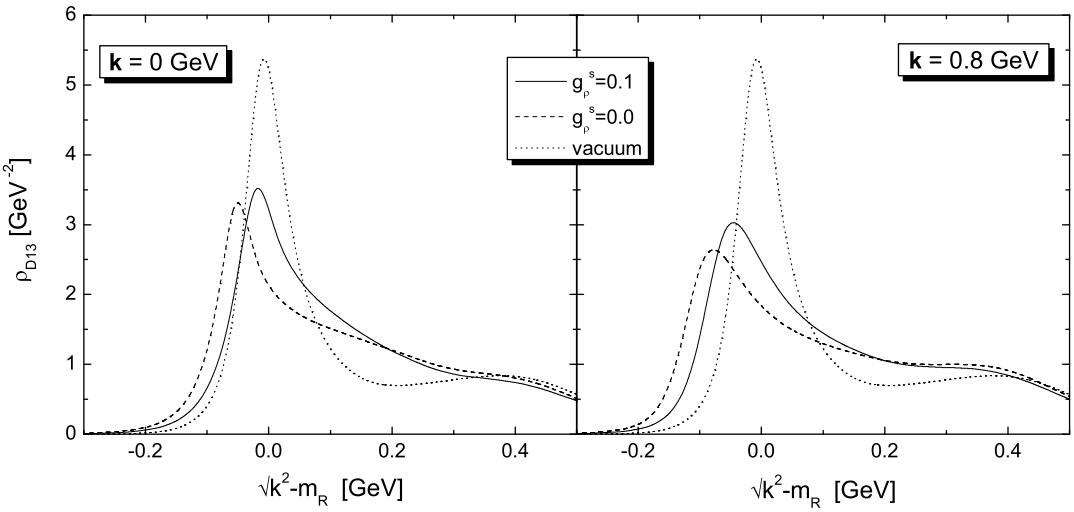

Figure 8.16: Spectral function of the $D_{13}(1520)$ resonance at momenta $\mathbf{k} = 0$ GeV and $\mathbf{k} = 0.8$ GeV. The solid lines are obtained with SRC, in the dashed lines effects from SRC are not included. The results are shown for $\rho = \rho_0$.

broadening is nearly entirely driven by the inelastic scattering processes $D_{13}(1520)N \to NN$ and $D_{13}(1520)N \to NP_{33}(1232)$.

The spectral function is shown in Fig. 8.16 in the dashed lines for two different momenta $\mathbf{k} = 0$ (left) GeV and $\mathbf{k} = 0.8$ GeV (right). In comparison to the vacuum spectral function (dotted line) the main modifications are a shift of the peak to smaller invariant masses accompanied by a smearing of the peak. Concerning the peak shift, we obtain an attraction of about $50 - 100$ MeV within our scheme. This is demonstrated in Fig. 8.18 where the dashed line shows the peak as a function of the 3-momentum of the resonance. The major part of this shift is not due to the influence of $\mathcal{R}\mathrm{e}\,\Sigma$, however. In the left plot of Fig. 8.17 (dashed line) we show $\mathcal{R}\mathrm{e}\,\Sigma_{med}$ for a momentum of $\mathbf{k} = 0.8$ GeV, where the peak shift is larger than at small momenta (see Fig. 8.16). At $k^2 = m_R^2$ one finds an attractive mass shift of $\mathcal{R}\mathrm{e}\,\Sigma_{med}/(2m_R) \approx 10$ MeV. The remaining larger part of the peak shift is due to the energy dependence of the width as outlined in Chapter 5.3.3: Owing to the large absolute size and energy dependence of $\mathcal{I}\mathrm{m}\,\Sigma_{med}$ as shown in Fig. 8.13, the maximum of the spectral function is shifted to smaller energies. As a consequence the resonant peak is not as broad as one might expect from the large in-medium widths at $k^2 = m_R^2$. We have visualized this effect by plotting the width of the $D_{13}(1520)$ not at $k^2 = m_R^2$ but rather at the true maximum of the spectral function in the right graph of Fig. 8.18 (dashed line). Note that the fluctuations in the curves shown in Fig. 8.18 are due to finite grid size effects. As explained in more detail in Chapter 5.3.3, the use of the asymmetric form factor $FF1$ of Eq. 3.22 in Chapter 3.2.2 leads to conservative estimates for the shift of the peak position and as long as a broadening of the $D_{13}(1520)$ is generated by the mechanisms discussed in this work, such a shift is inevitable. By considering the shape of the spectral function shown in Fig. 8.16, it becomes clear that a Breit-Wigner type parametrization in terms of mass and width is not possible, a tendency that is already visible in the vacuum. Instead,

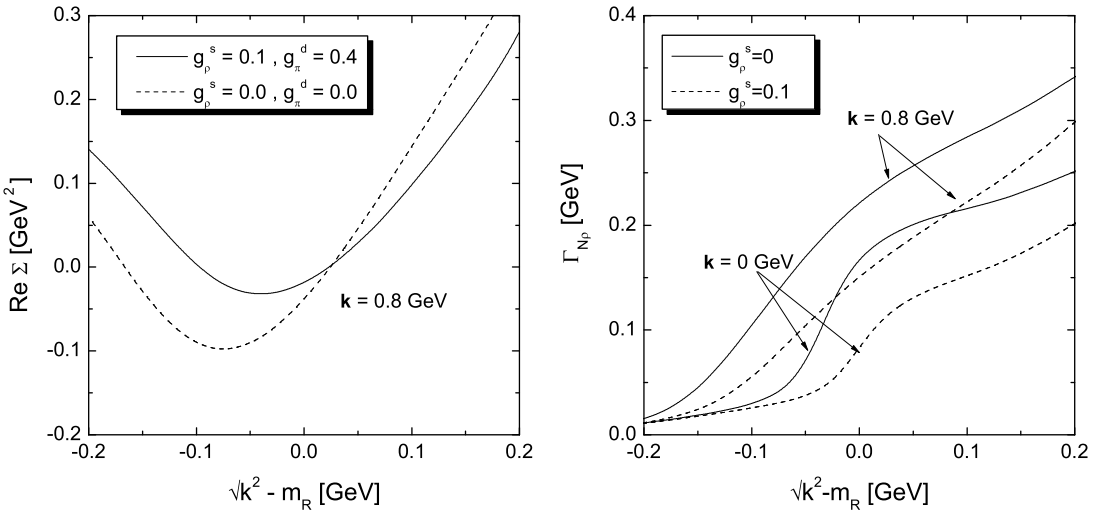

Figure 8.17: Effect of SRC on $\Gamma_{N\rho}$ (left) and $\mathcal{R}\mathrm{e}\,\Sigma$ (right). The solid lines indicate the results with SRC, the dashed lines obtained w/o SRC.

we find a structure with a rather narrow peak, but a large tail for $k^2 > m_R^2$. In comparison to the vacuum curve, the overall picture is that of a smearing of spectral strength over a much larger energy interval. In that sense the qualitative picture of a broadening of the resonance as advocated in [107] is not changed, although the calculations have been refined in many details.

The effect of the iterations is found to be quite small both for pion and ρ meson. This we have shown in Fig. 8.13 for $\Gamma_{N\rho}$, where the solid lines represent the results obtained after convergence has been reached. A tendency persists that in the second iteration the width gets somewhat reduced. This results from the effect of resonance broadening on the ρ spectral function: there the D_{13} peak "dies out" and less spectral strength sits at low invariant masses, leading to a relative suppression of the ρ decay mode. Since the $D_{13}(1520)$ decouples more or less completely from the pion spectral function, we do not find any effects from the iterations in this sector and we do not show explicit results for this channel. Higher iterations then change only very little in the actual results.

Let us now switch on the SRC. In connection Chapter 6.3, we have already argued that for s-wave potentials these effects are supposedly small, since unlike the p-wave case no big additional scale (like q_c) is introduced. However, in a full in-medium calculation the contact interactions are iterated to all orders, see Chapter 6.5. This produces a correction of the form $1/(1 - g_\rho^s \chi_s)$ for the resonance width, which is large if either g_ρ^s or the coupling constant at the meson-nucleon-resonance vertex are large. Due to the large coupling of the $D_{13}(1520)$ to $N\,\rho$, a sizeable reduction might result.

Using for the strength of the contact interaction $g_\rho^s = 0.1$ as advocated in Chapter 6.3, a reduction of the broadening from the $N\,\rho$ channel from 250 MeV down to around 150 MeV results, see right plot in Fig. 8.17. This result is quite sensitive on the value chosen for g_ρ^s, similar to the case of the $P_{33}(1232)$. Unfortunately g_ρ^s is completely unconstrained from experiment. Since in our model positive and negative parity states do not couple

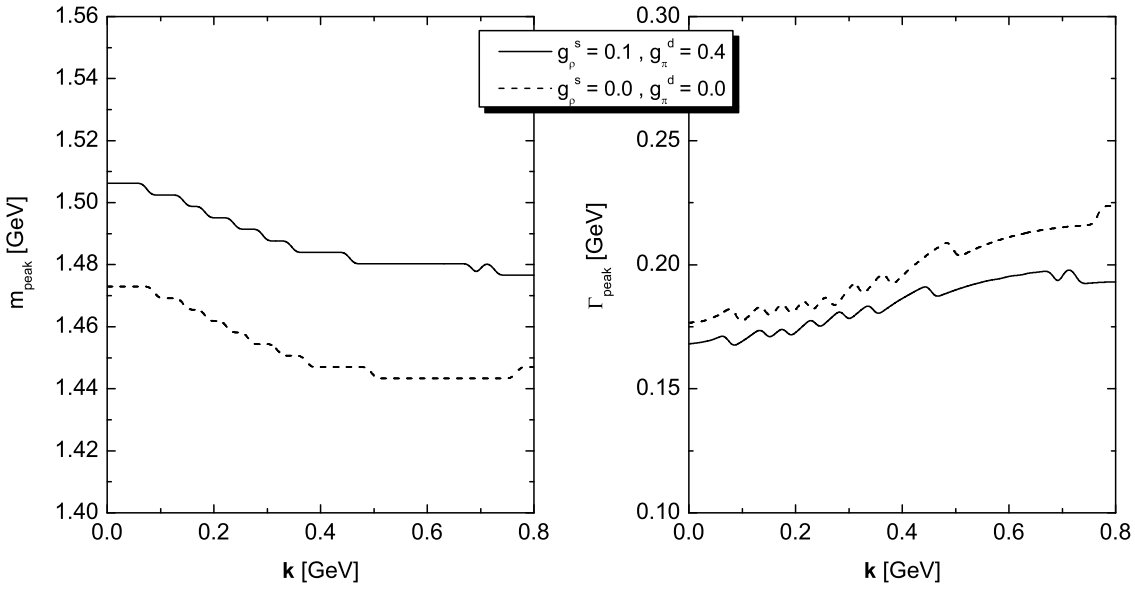

Figure 8.18: Left: Peak position of the spectral function of the $D_{13}(1520)$. Right: Width of the $D_{13}(1520)$ taken at the peak position. Shown are calculations with $g_\rho^s = 0.1$ (solid line) and $g_\rho^s = 0.0$ (dashed line). The density is $\rho = \rho_0$.

directly to each other via SRC, the decay width into $N\Delta$ or NN is left untouched and the reduction happens primarily in the channel $D_{13}N \to ND_{13}$. The effect of the correlations on the pionic decay mode, for which the results are shown in the right plot of Fig. 8.13, is just the opposite. Since the channel $D_{13}N \to ND_{13}$ is not important, it is the mixing to nucleon- and $P_{33}(1232)$ states that leads to a reduction of the width. Again there exists some uncertainty about the correlation strength. Using $g_\pi^d = 0.4$, the broadening is reduced and the width into $N\pi$ is about 20 MeV larger than the Pauli-blocked width.

The pole of the spectral function is less shifted once the correlations are switched on, compare solid and dashed curves in the left plot of Fig. 8.16. The total broadening is smaller and therefore the kinematic effect leading to a shift of the peak of the spectral function is reduced. Furthermore, as can be seen in the left plot of Fig. 8.17, $\mathcal{R}\mathrm{e}\,\Sigma$ itself is a little bit more repulsive when the short-range interactions are switched on. The effect of the correlations on the width of the peak is not as strong as one might have expected by comparing the width at equal values of k^2 as shown in Fig. 8.18. This is easy to understand: due to the smaller attraction, with SRC the width is tested at larger invariant masses, leading to a relative increase. Comparing both scenarios, even though the in-medium effects are somewhat reduced if the SRC are taken into account, the overall picture of a strongly broadened resonance structure survives.

We close this discussion by considering the spectral function as following from the parameter set of [124], where the branching ratio into $N\rho$ is only about half the size as compared to what is found in [90]. In the discussion concerning the ρ in-medium properties we were able to conclude that the gross features of the in-medium spectrum are

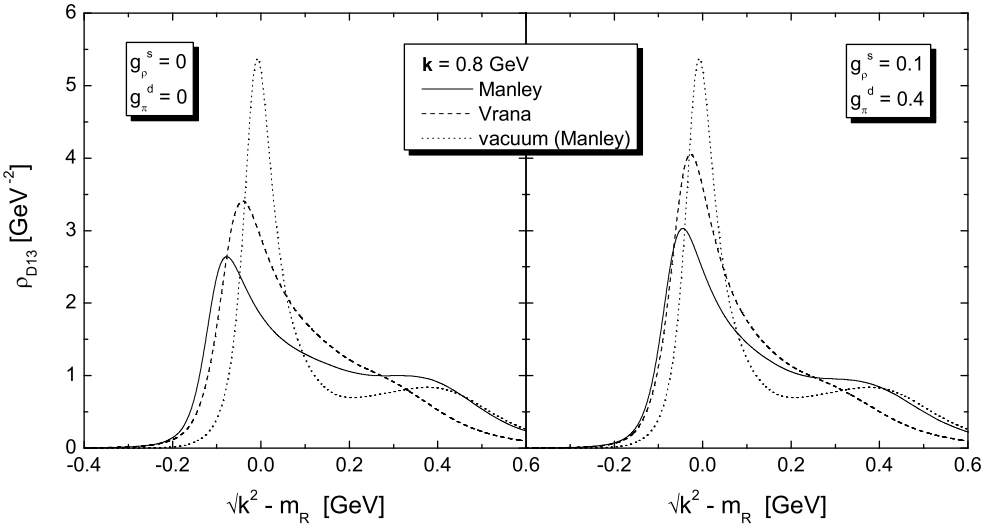

Figure 8.19: The spectral function ρ of the $D_{13}(1520)$ as obtained using the parameters from [90](solid line) and [124] (dashed lined). Left: no SRC are included. Right: SRC are switched on with the parameters $g_\rho^s = 0.1$ and $g_\pi^d = 0.4$. The density is $\rho = \rho_0$.

left untouched by considering this parameter set. For the $D_{13}(1520)$ this statement does not necessarily hold any more. In Fig. 8.19, we compare the results as following from the parameter sets of [90] (solid line) and [124] (dashed line) for two values of the short-range parameters g_π^d and g_ρ^s. The momentum of the resonance is $\mathbf{k} = 0.8$ GeV. As shown in the right graph of Fig. 8.19, if one chooses the parameters of [124] together with maximal suppression from SRC, i.e. $g_\rho^s = 0.1$ and $g_\pi^d = 0.4$, a spectral function results which is already rather close to the vacuum one. In that case the total broadening does not exceed 50 MeV, which is a small value as compared to the vacuum width of 120 MeV. Also the the shift of the peak position is very modest. Taking the parameters of [124] with $g_\rho^s = 0 = g_\pi^d$ as shown in the left plot of Fig. 8.19, a considerable broadening of more than 100 MeV remains at $k^2 = m_R^2$ remains.

The main result of this Section is that the self energy of the $D_{13}(1520)$ is dominated by the process $D_{13}(1520)N \to ND_{13}(1520)$ with ρ exchange. Possibly also effects from short-range correlations are important. The corresponding Feynman diagram is shown in Fig. 8.20.

8.2.3 $S_{11}(1535)$

In this Section we discuss the results for the $S_{11}(1535)$ resonance. It will turn out that the main part of the medium modifications is due to Pauli-blocking in the $N\eta$ channel and to the coupling of the $D_{13}(1520)$ resonance to the ρ meson.

In the left plot of Fig. 8.21 we show the in-medium width of a $S_{11}(1535)$ with relative 3-momentum $\mathbf{k} = 0.8$ GeV, which is approximately the momentum of an $S_{11}(1535)$ if produced from a photon scattering on a nucleon at rest. Shown is the decay width after

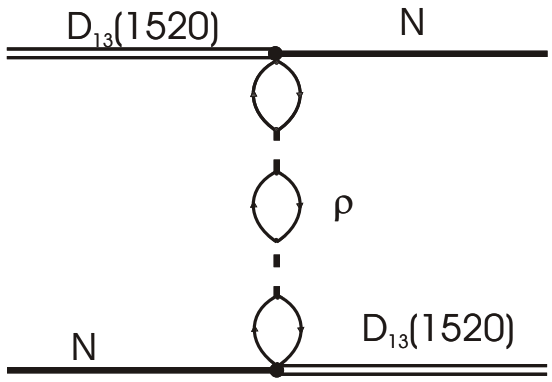

Figure 8.20: Main contribution to the self energy of the $D_{13}(1520)$ in nuclear matter.

the fourth iteration (dashed line) in comparison with a Pauli-blocked vacuum width (dotted line), which is calculated on the basis of the Feynman graph Fig. 3.5, taking into account Pauli-blocking of the nucleon. We find a broadening of about 30 MeV at the point $k^2 = m_R^2$ relative to the Pauli-blocked width. Although πN and ηN produce the main part of the total width, the in-medium modifications of π and η mesons do not lead to a broadening of the $S_{11}(1535)$. In fact, for these two channels we find even a reduction of the width below the Pauli-blocked width. The main effect comes from the in-medium modification of the ρ meson. The origin of this broadening is the same as found for the $D_{13}(1520)$ state: in the nuclear medium the ρ meson couples to the $D_{13}(1520)N^{-1}$ state and various other particle-hole states which leads to shift of spectral strength to smaller invariant masses. Therefore the phase space available for decay opens up, thus enhancing the 5 MeV partial decay width as found in [90] to values around $20-30$ MeV. This is a typical coupled channel effect: the coupling of the $D_{13}(1520)$ to $N\rho$ generates a broadening of the $S_{11}(1535)$ state.

In the work of [26] a qualitatively similar picture emerges. There the S_{11} is considered to be at rest. In that formalism the particle-hole loops are not iterated and the 2π channel is treated as pure phase space with a partial decay width of 10 MeV. Again, the broadening found from πN and ηN is small. The broadening from the 2π channel is somewhat larger that found in our work, but this is partly due to the fact that the total $2\pi N$ width is taken to be larger than our $N\rho$ width.

The spectral function is only slightly modified as can be inferred from the right plot in Fig. 8.21 by comparing the spectral function in the vacuum (dash-dotted line), with Pauli-blocking only (dotted line) and the full results without SRC (dashed line). The peak of the spectral function is shifted upwards relative to the nucleon by about $10 - 20$ MeV. Such a small (dispersive) mass shift is found also in other theoretical works on the $S_{11}(1535)$ [56, 125].

In Fig. 8.22 we show the position of the peak (left) and the width of the peak (right) as a function of the 3-momentum $\mathbf{k}$. The peak position varies only very little. The width taken at the peak position displays some momentum dependence. This is mostly due to Pauli-blocking of the $N\eta$ channel, which completely prohibits the decay into this channel at vanishing 3-momentum. At finite momenta the effects of Pauli-blocking are reduced, leading to an increase of the the width, which is enhanced by the fact that – as in the case of the $D_{13}(1520)$ – the $N\rho$ broadening receives additional support from the opening of phase space. As in the case of the $D_{13}(1520)$ the numerical fluctuations in the curves

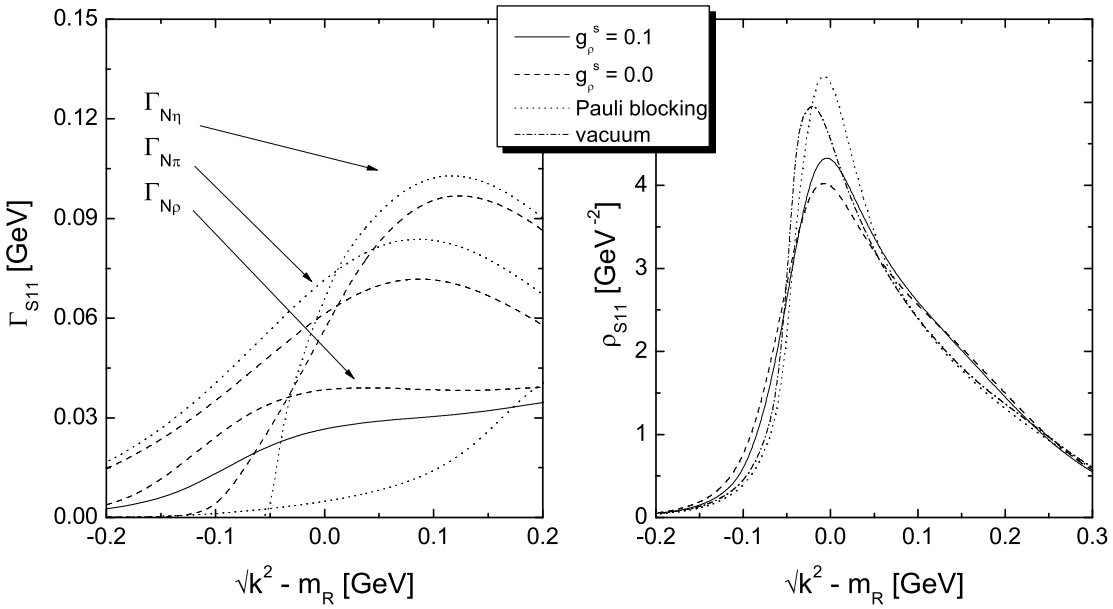

Figure 8.21: Left: Partial decay widths of the $S_{11}(1535)$ at a momentum of $\mathbf{k} = 0.8$ GeV. We compare results obtained from Pauli-blocking and our full in-medium calculations with and w/o SRC. For the $N\pi$ and $N\eta$ channels the effect of SRC is very small, therefore the in-medium width is represented by the full lines only. Right: spectral function ρ of the $S_{11}(1535)$ at the same momentum. The density is $\rho = \rho_0$.

are due to finite grid effects.

Switching on the SRC reduces the broadening, see Figs. 8.21 and 8.22. Just as in the case of the $D_{13}(1520)$ we find a reduction of the broadening in the ρN channel, whereas the other two channels remain essentially untouched. The insensitivity of the πN and ηN channels to effects from SRC is explained from the comparatively small coupling constants at the respective resonance-nucleon-meson vertices, which prevent large corrections terms of the form $1/(1 - g\chi)$. This substantiates our statement made in the introduction of Chapter 6 that for s-wave states the SRC become only sizeable in the presence of large coupling constants. The effects from the iteration are also similar to those observed for the $D_{13}(1520)$. The strong broadening of that state leads to a reduction of strength at small invariant masses and therefore the in-medium width of the $S_{11}(1535)$ slightly decreases.

We conclude from our results and those obtained in [26, 56, 125] that some consensus exists in the literature concerning the in-medium properties of the $S_{11}(1535)$. A small broadening relative to the Pauli-blocked width is expected, accompanied by a slight repulsive mass shift. In [74] is has been demonstrated that such medium modifications lead to a natural explanation of experimental data on η photoproduction [115, 133]. There the relatively large observed mass shift hinted in the data [133] is generated by the assumption that resonance and nucleon feel the same momentum dependent mean-field potential. As pointed out in [74], a small collisional broadening of the $S_{11}(1535)$ has also been found in [32] based on estimates of resonance-nucleon cross sections.

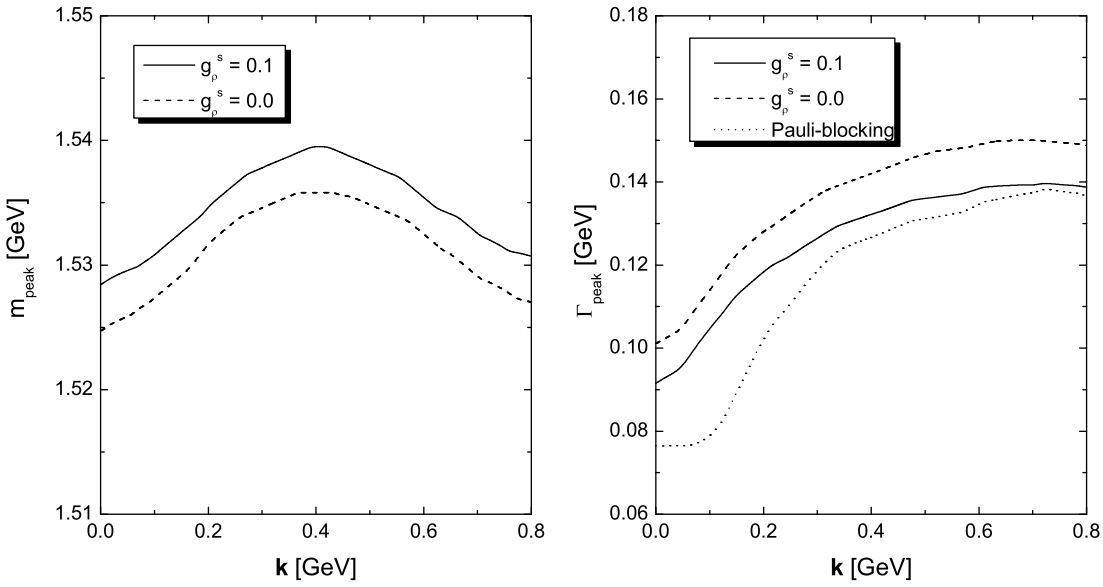

Figure 8.22: Left: Peak position of the spectral function ρ of the $S_{11}(1535)$. Right: Width of this state taken at the peak position. Shown are calculations with $g_\rho^s = 0.1$ and $g_\rho^s = 0.0$. For the width we also show the results from Pauli-blocking. The calculations are carried out at normal nuclear matter density.

Summarizing, the broadening of the $S_{11}(1535)$ is a typical example of a coupled-channel effect. The main physical effects are generated by the $D_{13}(1520)$ via the process $S_{11}(1535)\, N \rightarrow N\, D_{13}(1520)$. The corresponding Feynman diagram is shown in Fig. 8.23. Whereas we do not claim that the broadening found is accurate within 10 MeV, we can exclude a significant in-medium modification of the $S_{11}(1535)$ within the mechanisms discussed in this work. A strong broadening would either require a much larger coupling to $N\rho$ – which is unlikely since the total 2π width $\Gamma_{2\pi N}$ is estimated to be around 10 MeV in the vacuum [89, 46] – or effects from nuclear mean fields, which might increase the mass difference between nucleon and $S_{11}(1535)$ and thus enhance the phase space available for the decay.

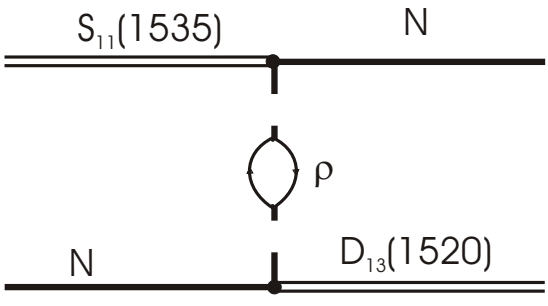

Figure 8.23: Main contribution to the self energy of the $S_{11}(1535)$ in nuclear matter.

Chapter 9

Results 2

This Chapter is concerned with some general aspects of our analysis. In Section 9.1 we study the density dependence of our results. This Section forms part of the publication [108]. In Section 9.2 the effect of nuclear mean fields is investigated and in Section 9.3 the influence of applying dispersion relations to the meson and resonance self energies is discussed. All these calculations are performed in our self-consistent non-relativistic framework. The aim of Section 9.4 is to examine the quality of the non-relativistic approximation in some detail. This study is concerned exclusively about the ρ meson and no self consistent iterations are attempted. In this Section also the influence arising from further uncertainties concerning the choice of the proper interaction Lagrangian or the parameter set is considered. The results shown in Section 9.4 are published in [109].

9.1 Density Dependence

In this Section we analyze the density dependence of our results. Within the low density expansion the in-medium self energies of mesons and baryon resonances are directly proportional to the nuclear density ρ. Deviations from this linear scaling are already introduced from Pauli blocking and Fermi motion. More importantly, within our self-consistent scheme meson and resonance interactions with more than one nucleon are generated. They correspond to terms of higher order in the nuclear density. Finally, short-range correlations (SRC) exhibit terms of the from $1/(1-g\chi)$ which also produce deviations from a linear density dependence. It is therefore interesting to study our results as a function of the nuclear density and determine a critical density above which the low density expansion becomes unreliable.

We begin with a study of the density dependence of our results for baryon resonances and will restrict ourselves to the case of the $N\rho$ decay of the $D_{13}(1520)$. In Fig. 9.1 we show the collisional broadening defined as

$$\Gamma_{coll} \;=\; \frac{\mathcal{I}\mathrm{m}\,\Sigma_{med} - \mathcal{I}\mathrm{m}\,\Sigma_{pauli}}{\sqrt{k^2}}, \tag{9.1}$$

in the $N\rho$ channel of the $D_{13}(1520)$ as a function of the nuclear density for two momenta, $\mathbf{k} = 0.4$ GeV (left) and $\mathbf{k} = 0.8$ GeV (right). The broadening is evaluated at $k^2 = m_R^2$. The dotted lines indicate the results from a calculation where the particle-hole loops have

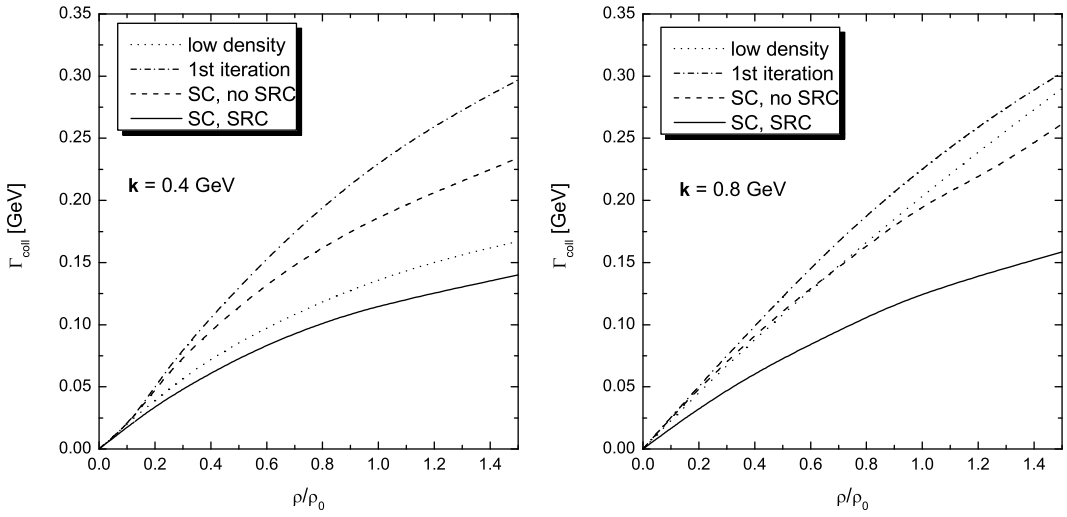

Figure 9.1: Collisional broadening of a $D_{13}(1520)$ with momenta $\mathbf{k} = 0.4$ GeV (left) and $\mathbf{k} = 0.8$ GeV (right) as a function of the nuclear density ρ. Compared are four calculations: low-density limit with Pauli blocking and Fermi motion (dotted), results of the first iteration (dash-dotted) and the self-consistent (SC) calculation (dashed). By the solid line we indicate the results from a self-consistent calculation where also effects from SRC are taken into account.

not been iterated. It has been obtained by the replacement

$$\mathcal{A}_\rho^{T/L}(q_0, \mathbf{q}) \to -\frac{1}{\pi} |D_\rho^{vac}(q)|^2 \, \mathcal{I}\mathrm{m} \, \Pi_\rho^{T/L}(q_0, \mathbf{q}) \tag{9.2}$$

in Eq. 5.37. This expression already goes beyond the low density theorem $\Gamma_{coll} = \rho \, v \, \sigma_{vac}$ [32, 65, 22] by including Pauli-blocking and Fermi motion. Here σ_{vac} is the total resonance-nucleon cross section and v the velocity of the resonance in nuclear matter. The effects from resumming the particle-hole loops are shown by the dash-dotted lines and the impact of the self-consistent (SC) scheme is shown by the dashed line. The solid line shows the results from a self-consistent calculation which contains also the effects from SRC.

As one can see in the left plot of Fig. 9.1, already the low density curve (dotted line) shows sizeable deviations from a linear density dependence (for $\rho > .4\,\rho_0$) for a resonance with momentum $\mathbf{k} = 0.4$ GeV. This is due to Pauli blocking, which becomes more active as the density increases. The resummation of particle-hole loops in the ρ propagator leads to a sizeable enhancement of the broadening already at small densities around $0.25\rho_0$. This is a direct consequence of the fact that due to level repulsion this resummation leads to an attractive shift of the position of the $D_{13}(1520)$ excitation in the ρ spectral function. Due to this shift the phase space available for the reaction $D_{13}(1520)N \to ND_{13}(1520)$ is enhanced. The effect of self consistency (dashed line) and short-range correlations (solid line) is to reduce the width as has been discussed in Section 8.2.2. One should not compare the results obtained with SRC and the low density curve, because the SRC change the resonance-nucleon cross section.

At $\mathbf{k} = 0.8$ GeV (see right plot in Fig. 9.1) the low density calculation (dotted line) displays a nearly linear density dependence, which is due to the smaller impact of Pauli-blocking at large momenta. The effect of resumming the particle-hole excitations is smaller

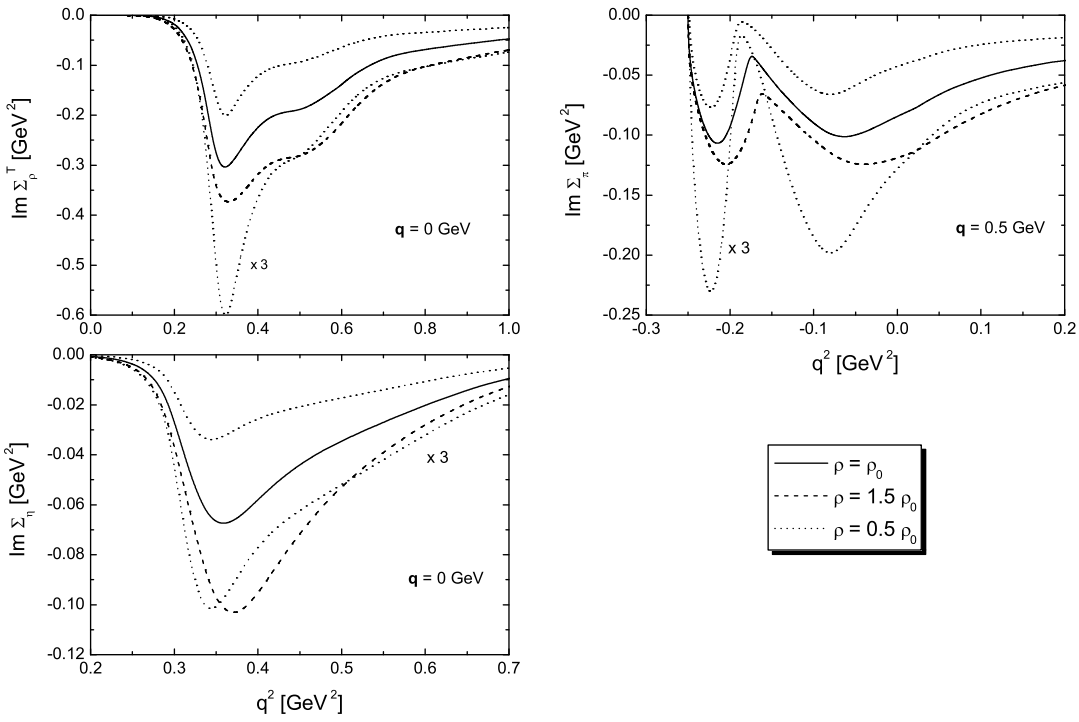

Figure 9.2: Influence of the density on the imaginary part of the in-medium self energy of ρ meson (left, top), pion (right) and η meson (left, bottom). The ρ meson and η meson are taken to be at rest while for the pion is moving with a momentum of $\mathbf{q} = 0.5$ GeV. The results are shown for three different densities. In order to facilitate the comparison we have rescaled the result obtained for $\rho = 0.5\,\rho_0$ by a factor of 3. In all calculations the SRC have been taken into account.

at $\mathbf{k} = 0.8$ GeV than at $\mathbf{k} = 0.4$ GeV as can be seen by comparing the dotted and dash-dotted lines. This is explained as follows: The resummation is important when the particle-hole excitation and the ρ peak have comparable energies. This is the case for a $D_{13}(1520)N^{-1}$ excitation at low resonance momenta. However, when calculating the in-medium width of a fast moving $D_{13}(1520)$ the spectral function is tested at large momenta, where the particle-hole excitation is far away from the ρ peak (cf. Fig. 5.3) and a smaller effect of the resummation is to be expected. The effects of self-consistency (dashed line) and SRC (solid line) are similar for both resonance momenta, both leading to a reduction of the resonance width. The different slope found already at very small densities for the calculation with SRC is due to a modification of the resonance-nucleon cross section from the short-range terms. Summarizing these results, we find for the $D_{13}(1520)$ strong deviations from a low density expansion. In particular for smaller momenta the low density results are found to be unreliable already at densities around $0.25\,\rho_0$, whereas at larger momenta the low density expansion starts to work better. This has an interesting effect on the momentum dependence of the width: in the low density limit the collisional broadening is proportional to the resonance velocity v and rises therefore nearly linearly with the momentum. Since the resummation of particle-hole loops leads to an enhancement of the

broadening at smaller momenta while having only a small influence on the results at large momenta, a flatter momentum dependence is expected (compare also right plot of Fig. 8.18).

Next we discuss the self energy of pion, η and ρ meson. Due to the complicated peak structure arising from the resonance-hole excitations it is difficult to summarize the information contained in the self energy at given density and momentum in one number. Therefore we show the self energy as a function of the invariant mass in Fig. 9.2. There the imaginary part of the self energy of the ρ meson (left, top), the pion (right) and the η meson (left, botttom) are displayed for three densities $\rho = 0.5\,\rho_0$ (dotted lines), $\rho = \rho_0$ (solid lines) and $\rho = 1.5\,\rho_0$ (dashed lines). In order to facilitate the comparison we also show with dotted lines the result obtained at $\rho = 0.5\,\rho_0$ multiplied by a factor of 3, which would equal the result at $\rho = 1.5\,\rho_0$ if the self energies would scale linearly with the density. We observe that for the pion and the ρ meson a linear scaling with the density is badly violated. A more detailed investigation shows that higher order corrections are already important for densities $\leq 0.5\,\rho_0$. This is not shown in Fig. 9.2. For the η meson we find that the height of the peak scales nearly directly with the density whereas the position of the peak is slightly shifted. As discussed in Section 8.1.3, this shift of the peak leads to the observed strong non-linearities of the optical potential (cf. Fig. 8.8). We already mentioned that the following sources act against a linear density dependence: Fermi-motion, Pauli-blocking, self-consistent iterations and short-range correlations. It is interesting to note that for each meson the most important deviation is generated by a different mechanism: For η and ρ the iterations act against the low density theorem by inducing a strong broadening for the $D_{13}(1520)$ and a slight repulsive mass shift for the $S_{11}(1535)$. In contrast, for the pion it is mainly the sum of Fermi motion and short-range interactions which is responsible for the non linear density dependence.

Let us make some comments about the applicability of the low density theorem. As we have just demonstrated for the $D_{13}(1520)$, its range of validity can be rather small. This is due to the combined effect of a large coupling constant to the $N\rho$ channel and the fact that the $D_{13}(1520)$ is essentially subthreshold with respect to this channel. Clearly, if the coupling constant is small one does not expect a large correction of the self energy in the medium anyway and it hardly matters whether one employs the low density theorem or takes into account higher order corrections in the density.

A second criterion involves the mass difference $\Delta_m = m_R - m_N - m_M$, which gives an indication for the phase space available for the resonance decay into the meson-nucleon channel. We expect a strong sensitivity of the results on higher order effects in the density when Δ_m is small. Then the decay $R \to N\,M$ is suppressed from phase space and one becomes very sensitive to small changes of the mesonic spectral function. One example of that we have discussed in the previous Chapter when disentangling the in-medium broadening of the $D_{13}(1520)$ into its individual contributions. There it turned out that the largest contribution to the broadening comes from the channel $D_{13}(1520)N \to N D_{13}(1520)$. We also noted that the impact of higher lying resonances is mainly to add strength to the $D_{13}(1520)$ peak of the ρ spectral function. This means that by iterating the particle-hole loops in the ρ propagator more strength is moved to small invariant masses by resonances, which within the low density approximation could not contribute to the broadening of the $D_{13}(1520)$ due to phase space arguments. If on the other hand Δ_m is large, such effects would be completely absent, indicating that for large Δ_m the low density theorem might work better. We want to add that the size of the coupling constant and of Δ_m are not

independent: in general, large coupling constants are encountered for small values of Δ_m, since the combination of large coupling constants and large phase space factors leads to unreasonably broad resonances.

The question of how to quantify what "large coupling constant" and "small Δ_m" mean in an actual physical problem will in general be difficult to answer. Further complications arise when one is dealing with a coupled-channel problem which is not confined to one resonance coupling to one meson and a nucleon. To quantify non-linearities arising from the coupled-channel effects is in general not possible. Therefore one probably has to check the validity of the low density theorem explicitly in each individual case.

In this work we have analyzed only the density dependence of the $N\rho$ contribution to the self energy of the $D_{13}(1520)$. The reason for this limitation is a problem arising when calculating the amplitude for the scattering processes $RN \to NR$ or $RN \to NR'$ in the vacuum: if the exchanged meson is allowed to go on-shell, the scattering amplitude contains a pole [10, 102, 98]. We have already discussed this in the Section 5.3.2. To be more specific, this affects the pion exchange contribution of the amplitudes $P_{33}(1232)N \to NP_{33}(1232)$, $D_{13}(1520)N \to NP_{33}(1232)$ or $S_{11}(1535)N \to ND_{13}(1520)$. Also the η exchange part of the amplitude $S_{11}(1535)N \to NS_{11}(1535)$ is troubled by such a pole. Only for ρ exchange amplitudes one is free of the pole problem due to the finite vacuum width of the ρ meson. Since the ρ amplitude is dominant for the $D_{13}(1520)$, it made sense to discuss this resonance neglecting the pion exchange part.

9.2 Influence of the Scalar Potentials

In this Section we discuss the influence of nuclear mean fields on the in-medium properties of mesons and baryon resonances. The underlying theoretical concepts have been introduced in Chapter 7. Let us repeat the main results found there: For the nucleon both the vector self energy Σ_v and the scalar self energy Σ_s are found to be large and in the order of $300 - 400$ MeV. Under the assumption that Σ_v is the same for all baryons (nucleon and resonances) this quantity drops out of the calculations. In contrast, the scalar self energy Σ_s enters into the calculations by modifying the spinors. We will touch on three topics

- modification of the resonance decay diagram, where the meson spectral function is unmodified and Pauli-blocking is neglected
- the effect of mean field potentials on the meson self energy
- full results, obtained by dressing the mesons and adding the mean field potentials.

Let us first discuss the effects on the baryon resonance width induced by the mean fields. Neglecting in a first step the dressing of the mesons and Pauli-blocking, the only medium modification taken into account is the effect of mean field potentials.

Concerning the magnitude of the potentials for the resonances, we make a universality assumption [126], meaning that both Σ_s and Σ_v are identical for nucleon and baryon resonance. Then Σ_v drops out of the calculation. Naively one might think that with this assumption the influence of Σ_s is quite small, since the phase space available for decay is not greatly changed. However, this argument is not complete. The squared matrix element for the resonance decay is proportional to the normalization of nucleon and resonance spinor:

$$|\mathcal{M}|^2 \quad \sim \quad (\bar{u}\, u)_N \, (\bar{u}\, u)_R \quad . \tag{9.3}$$

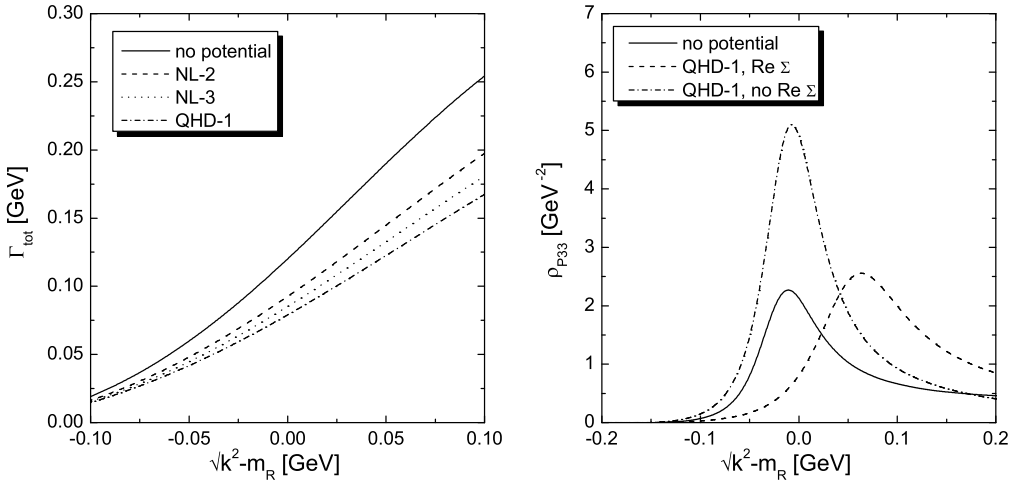

Figure 9.3: Total decay width (left) and spectral function (right) of the $P_{33}(1232)$. The decay width is shown for a calculation where the masses of resonance and nucleon have been shifted according to the results of various nuclear structure models: NL-2(dashed), NL-3 (dotted) and QHD-1 (dash-dotted). For the spectral function we have indicated the additional dispersive mass shift (dotted line). The results are shown for $\rho = \rho_0$.

As discussed in Chapter 7.1, the normalization of the spinors is proportional to the effective mass and is therefore reduced in the presence of scalar potentials. Roughly speaking one would expect from this argument that the in-medium decay width is reduced by a relative factor of $(m_N^\star\, m_R^\star)/(m_N\, m_R)$, which is large in view of the small effective masses reached in the nuclear medium, where $m_N/m_N^\star \sim 0.5 - 0.6$ (this ratio is closer to one for resonances since they are heavier). On the other hand, the decay width scales with

$$\Gamma \;\propto\; \frac{1}{m_R^2}\,|\mathcal{M}|^2 \quad , \tag{9.4}$$

such that the effects from the mean fields are reduced by the replacement $1/m_R^2 \to 1/m_R^{\star 2}$. After a little calculation one finds for the ratio of the width obtained with mean field potentials, Γ_{pot}, and the vacuum width, Γ_{vac}, the approximate scaling behaviour:

$$\Gamma_{vac}/\Gamma_{pot} \;=\; \frac{m_R\, m_N^\star}{m_R^\star\, m_N} \quad . \tag{9.5}$$

Here both quantities are evaluated at the respective on shell point, i.e. at m_R in the vacuum and at $m_R^\star$ in the medium.

In Figs. 9.3 and 9.4 we show width (left) and spectral function (right) of the $P_{33}(1232)$ and $D_{13}(1520)$ resonances. For the $P_{33}(1232)$ we observe a clear reduction of the vacuum width. Depending on the nuclear structure model, the on-shell width taken at $s = m_R^{\star 2}$ is reduced by values ranging from 25 MeV (NL-2, dashed line) to 40 MeV (QHD-1, dash-dotted line). For the sake of comparison also the vacuum result (solid line) and the width obtained by using the parameters of NL-3 (dotted line) are indicated. This reduction is

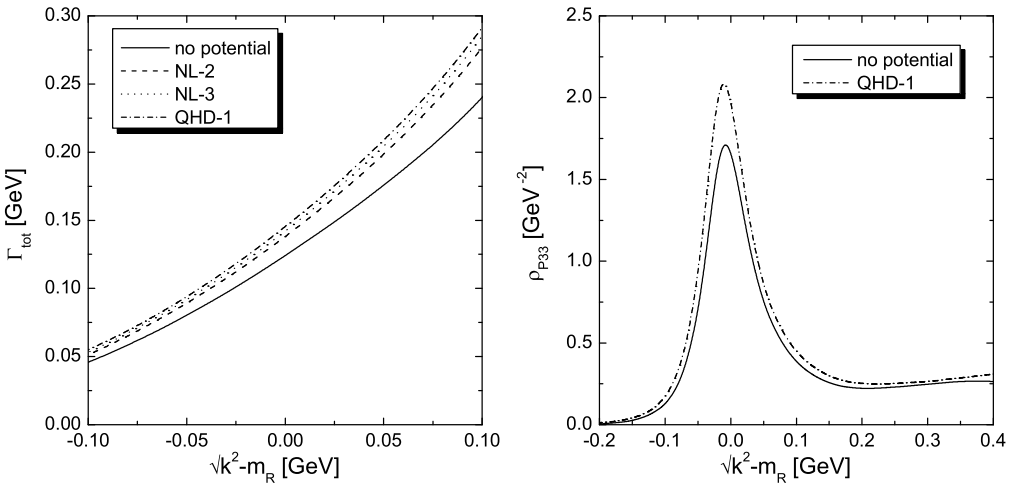

Figure 9.4: Same as Fig. 9.3, but for the $D_{13}(1520)$.

a direct consequence of the rescaling discussed above: using the potential QHD-1, one obtains $\Gamma_{pot}/\Gamma_{vac} \approx 0.8$ from Eq. 9.5, corresponding to $\Gamma_{pot} \approx 95$ MeV. This is in qualitative aggrement with the numerical results. Similar calculations have been performed in [126, 61, 123]. The results presented in these works are in qualitative agreement with our findings and a reduction of the decay width in nuclear matter due to mean field potentials is reported. Let us now turn to the spectral function, shown on the right plot of Fig. 9.3. There we have indicated three calculations: the vacuum result (solid line) and two results obtained from the QHD-1 model, which delivers the largest medium modification. The dashed line is obtained by including $\mathcal{R}\mathrm{e}\,\Sigma$ whereas for the dotted line $\mathcal{R}\mathrm{e}\,\Sigma$ has not been taken into account. As one can see, the mass shift induced by the energy dependence of the width is substantial and leads to a repulsion of more than 50 MeV for this state. The much higher peak values of the in-medium spectral functions (compare solid and dotted lines) are explained from the fact that in the normalization integral the spectral function is multiplied by the invariant mass, which – on an absolute scale – is much smaller around the resonance peak in the case that potentials are included.

Width and spectral function of the $D_{13}(1520)$ are shown in Fig. 9.4. Here the width is actually slightly enhanced in the presence of scalar potentials as indicated by the dashed (NL-2), dotted (NL-3) and dash-dotted (QHD-I) lines in the left plot. For comparison, we show again the vacuum result (solid line). This enhancement is due to the $N\pi$ channel. There the matrix element contains an additional factor $1/m_N^2$(see traces given in Table C.2,Appendix C.2), enhancing the width. For the other two decay channels, $N\rho$ and $\Delta\pi$, the expected reduction of the width is found in the medium. As a net effect the total width of this resonance is not greatly changed and the in-medium spectral functions are very similar to the vacuum ones. This is shown in the right plot of Fig. 9.4.

Let us now turn to the full in-medium results for the baryon resonances as obtained by adding the mean field potentials to the self-consistent iteration scheme. The results are shown in Figs. 9.5 and 9.6. There the abbreviation SC stands for self-consistent. We have taken the parameter set NL-2, which predicts the smallest mean fields and therefore gives

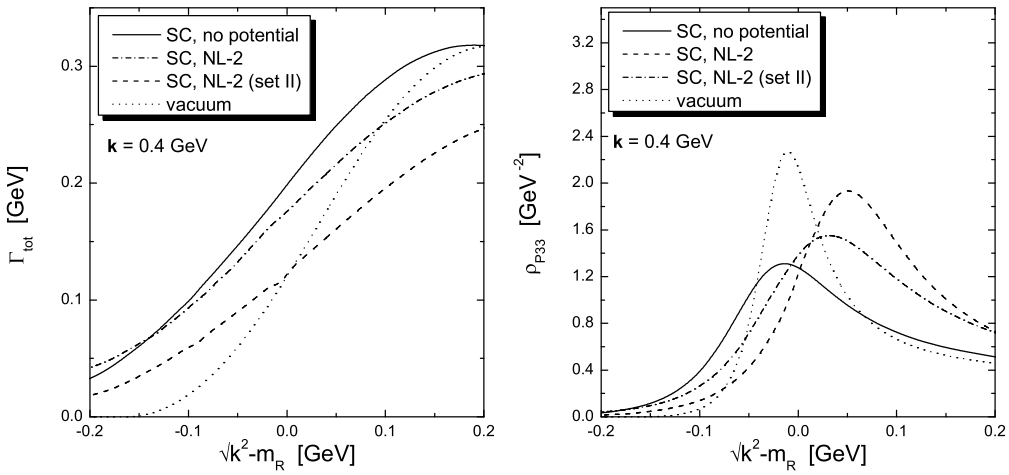

Figure 9.5: Total decay width (left) and spectral function (right) of the $P_{33}(1232)$ in nuclear matter at $\rho = \rho_0$. Shown is the effect of mean field potentials (dashed, dash-dotted) in comparison to a full calculation without these potentials (solid) and the vacuum curves. The dashed and dash-dotted curves differ by the used parameter set. The results are shown for $\rho = \rho_0$.

a lower bound for the effects induced by the mean fields. As is indicated by the dashed curves in Fig. 9.5, the tendency that for the $P_{33}(1232)$ the mean field potential leads to an increased repulsion and to a reduction of the broadening persists also in the iterated scheme. For comparison we have indicated the results obtained without potentials by the solid lines and the vacuum curves by the dotted lines. For the $P_{33}(1232)$ the inclusion of mean field potentials leads to a very small broadening of this state and a large repulsion. This is in conflict with phenomenology, which requires a larger broadening and less repulsion [54], see also Chapter 8.2.1. We therefore also present a calculation with a larger cutoff in the form factor F_t and smaller values for the correlation parameters g'. Specifically we take $\Lambda = 1.5$ GeV (instead of 1 GeV) and $g'_\pi = 0.3$ (instead of 0.6/0.45). The results corresponding to this parameter set (set II) are shown by the dash-dotted curves. One sees that they are in better agreement with the expectations one has from the phenomenological spreading potential. However, in set II the values for the short-range parameters are quite small, whereas the cutoff parameter is relatively large.

The results for the $D_{13}(1520)$ are indicated in Fig. 9.6. Shown are results from the full self-consistent approach with (dashed line) and without (solid line) mean field potentials as well as the vacuum result (dotted line). For the calculations the effects of short-range correlations for negative parity states have been included. In comparison to the $P_{33}(1232)$ we find a moderate influence of the nuclear mean fields on the results. This is akin to the situation encountered when considering only mean-field potentials in the in-medium calculations (cf. Figs. 9.3 and 9.4). Compared to a calculation without potentials the main difference is due to the $N\rho$ channel, where the mean fields reduce the broadening by 50 MeV. The $N\pi$ channel on the other hand comes out nearly identical, regardless whether potentials are switched on or switched off. This means that the enhancement due to the

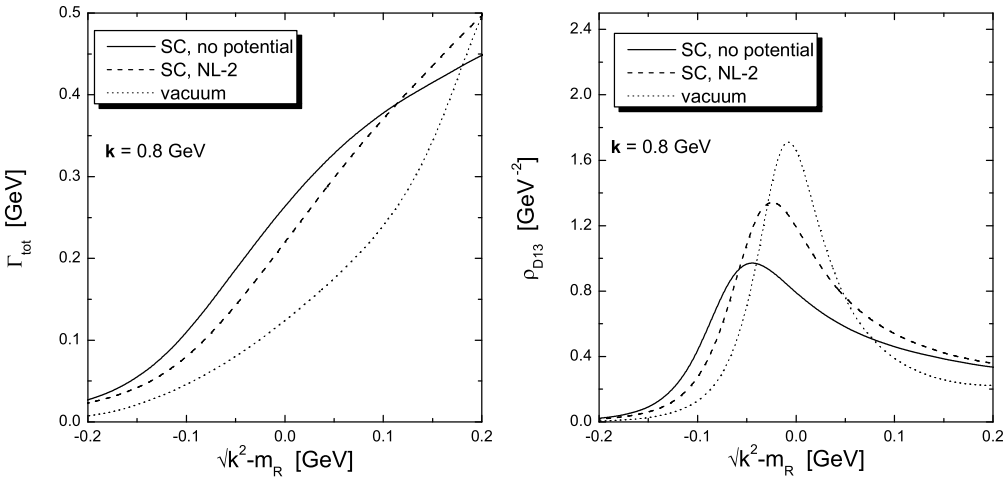

Figure 9.6: Same as Fig. 9.3 but for the $D_{13}(1520)$.

factor $1/m_N^2$ in this channel is counteracted by smaller effects from the iteration. We will come back to this point when discussing the in-medium spectral function of the pion. As a net effect, the total in-medium width of this state is smaller when nuclear mean fields are taken into account (compare dashed and solid line in left plot of Fig. 9.6). Since the shift of the peak position of the spectral function is essentially due to the in-medium broadening (cf. Chapter 8.2.2), the shift of the resonance peak is smaller in the presence of potentials, see dashed and solid lines in the right plot of Fig. 9.6.

Let us finally discuss the results for the in-medium spectral function of pions and ρ mesons. They are depicted in Fig. 9.7 for a ρ meson (left) at rest and pion moving with a relative momentum of 0.5 GeV (right). For comparison we show results of the self-consistent framework with (dashed line) and without (solid line) inclusion of nuclear mean fields. Concerning the meson self energies there is no such scaling behaviour as previously encountered for the baryon resonances. This follows since there are no external baryon lines in the self energy diagram that would introduce a scaling with the effective baryon masses. We therefore do not expect a sizeable reduction of the self energy. However, at finite momenta the position of the resonance peaks is shifted upwards due to the larger recoil that can be taken by a lighter resonance. This is seen by calculating the meson energy necessary to excite a resonance:

$$q_0 \;=\; \sqrt{m_R^2+\mathbf{q}^2}-m_N \;\approx\; m_R-m_N+\frac{\mathbf{q}^2}{2m_R} \quad . \tag{9.6}$$

Whereas the mass difference $m_R - m_N$ remains unchanged if Σ_s is the same for nucleon and resonance, the kinetic energy term is larger if the resonance mass is reduced by the mean fields.

As one can see in the left plot of Fig. 9.7, the effects on the spectral function of the ρ meson are relatively small. In comparison to a calculation without mean fields (solid line) the dashed curve, where potentials according to the parameter set NL-2 are included, displays an additional peak structure located in between the peaks of the $D_{13}(1520)$ excitation

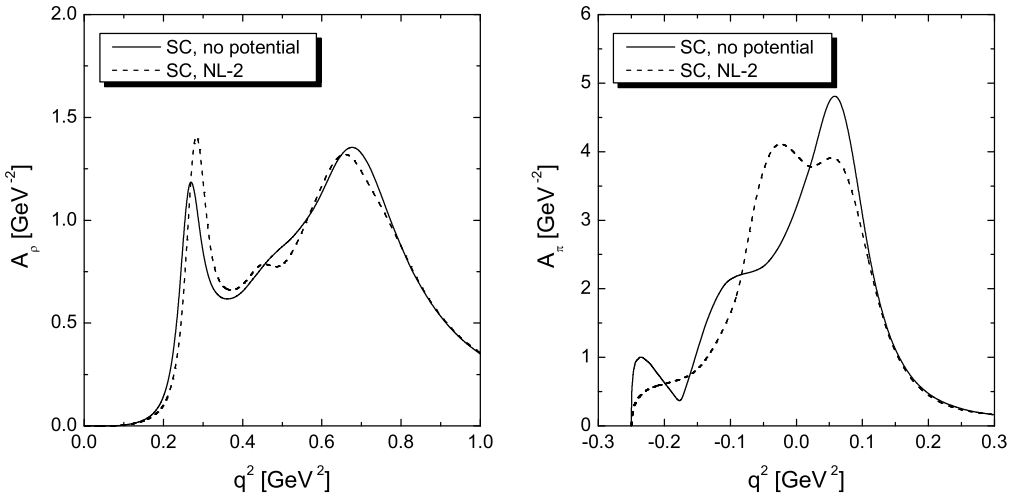

Figure 9.7: Spectral function of the ρ meson at $\mathbf{q} = 0$ GeV and the pion at $\mathbf{q} = 0.5$ GeV at $\rho = \rho_0$. Compared are calculations obtained within the self consistent scheme with (dashed) and without (solid) mean fields potentials. The parameters for the mean field potential are taken from the NL-2 model.

and the ρ peak, which is due to the $D_{33}(1700)$ state. This peak is visible in the presence of mean fields since the width of this resonance is reduced. As expected we also find a small repulsive shift of the $D_{13}(1520)$ excitation. Turning to the pion, the effects of nuclear mean fields are much stronger. Note in particular the sizeable shift of the $P_{33}(1232)$ state (located between nucleon-hole and pion peak). The shift is larger than for the $D_{13}(1520)$ since the $P_{33}(1232)$ is lighter and therefore the recoil effect of Eq. 9.6 is more pronounced. As a net effect, the inclusion of potentials leads to a rearrangement of strength in the pion spectral function up to larger invariant masses and thus adds to the found reduction of the in-medium width of the $P_{33}(1232)$. Also the fact that the in-medium $N\pi$ width of the $D_{13}(1520)$ is – despite the factor $1/m_N^2$ from the matrix element – in total not greatly affected from the potentials is due to this shift of spectral strength in the pion spectral function.

As we have just seen the inclusion of nuclear mean fields as found both from nuclear structure models [119, 72, 69] and from NN scattering [79], has sizeable effects on hadronic spectral functions. In particular, the pion and the $P_{33}(1232)$ are found to be sensitive on these potentials, whereas the $D_{13}(1520)$ is up to some extent protected by the fact that a decrease of the $N\rho$ and $\Delta\pi$ channels is counteracted by an increase of the $N\pi$ channel, owing to a factor of $1/m_N^2$ in the matrix element for the $N\pi$ decay. We are, however, sceptical about the reliability of these results. The most obvious open problem concerns the size of the resonance potential. For example, already minor shifts of the resonances relative to the nucleon can lead to large phase space effects which either further enhance or act against the reduction of matrix elements from the normalization of the spinors [126]. Also, for baryon resonances the absolute scale of Σ_s and Σ_v could be significantly smaller than for the nucleon, without affecting the peak position of this state, which is sensitive

only to the difference of both potentials. In [27] it was found that for the $P_{33}(1232)$ both Σ_s and Σ_v are much smaller (≤ 10 MeV at ρ_0) than for the nucleon. With such small self energies the scaling effects discussed in this Section would be suppressed. In order to arrive at a more reliable conclusion, systematic studies in this direction would be necessary.

9.3 Dispersion Relations

The real part of the in-medium meson self energy generated by the excitation of particle-hole loops, can be computed either directly or by means of dispersion relations. When dispersion relations are applied, a self energy energy results which is analytic in the upper complex energy half plane. As detailed in Appendix E, this leads to a normalized spectral function. Therefore we use dispersion relations in our iterative scheme. On the other hand, by computing the self energy directly from Feynman diagrams, analyticity is destroyed when the vertices are multiplied by form factors having bad analytical properties. Using a simple model for the self energy, we will study the differences arising from calculating the real part of the meson self energy in either way. In a second step also the importance of including the real part of the resonance self energy is discussed.

We work in the low-density approximation, i.e. $\Pi = \rho\,\mathcal{M}/(2\,m_N)$ (cf. Chapter 5.8). The particle-hole excitations are to be modeled by resonant scattering amplitudes. If analytic, the forward scattering amplitude $\mathcal{M}$ obeys the dispersion relation:

$$\mathcal{R}\mathrm{e}\,\mathcal{M}(\omega) \;=\; \mathcal{P}\int_{-\infty}^{+\infty}\frac{d\omega'}{\pi}\,\frac{\mathcal{I}\mathrm{m}\,\mathcal{M}(\omega')}{\omega'-\omega} \quad . \tag{9.7}$$

For the resonant scattering amplitude $\mathcal{M}$ we compare two different parameterizations. Both are based on a Breit-Wigner ansatz:

$$\begin{aligned}\mathcal{M}_1(\omega) &= \frac{2\,m_N}{\omega-\omega_R+i\,\gamma} \\ \mathcal{M}_2(\omega) &= \frac{2\,m_N}{\omega-\omega_R+i\,\gamma}\,\frac{\lambda^2}{\lambda^2+(\omega-\omega_R)^2} \quad .\end{aligned} \tag{9.8}$$

Here γ stands for the constant width of the resonance excitation and the additional factor in $\mathcal{M}_2$ is a form factor with cutoff parameter λ (note the similarity with the form factor $FF2$ of Eq. 3.23, Chapter 3.2.2). The factor $2\,m_N$ is due to the normalization of the nucleon spinor. Whereas $\mathcal{M}_1$ is analytic in the upper half of the complex energy plane, the form factor in $\mathcal{M}_2$ destroys analyticity due to an additional pole in the complex energy plane at $\omega = \omega_R \pm i\,\lambda$. This means that when we compare a direct calculation of $\mathcal{R}\mathrm{e}\,\mathcal{M}_{1/2}$ from Eq. 9.8 with a calculation via the dispersion integral Eq. 9.7, we expect to find the same result for amplitude $\mathcal{M}_1$, but different results for amplitude $\mathcal{M}_2$. This we will show in the following paragraph.

Let us subject both models for the scattering amplitude to the dispersion integral Eq. 9.7. Due to the simple form of the scattering amplitude, analytical solutions can be found in both cases. For $\mathcal{M}_1$ one obtains:

$$\mathcal{R}\mathrm{e}\,\mathcal{M}_1(\omega) \;=\; 2\,m_N\,\frac{\omega-\omega_R}{(\omega-\omega_R)^2+\gamma^2} \quad . \tag{9.9}$$

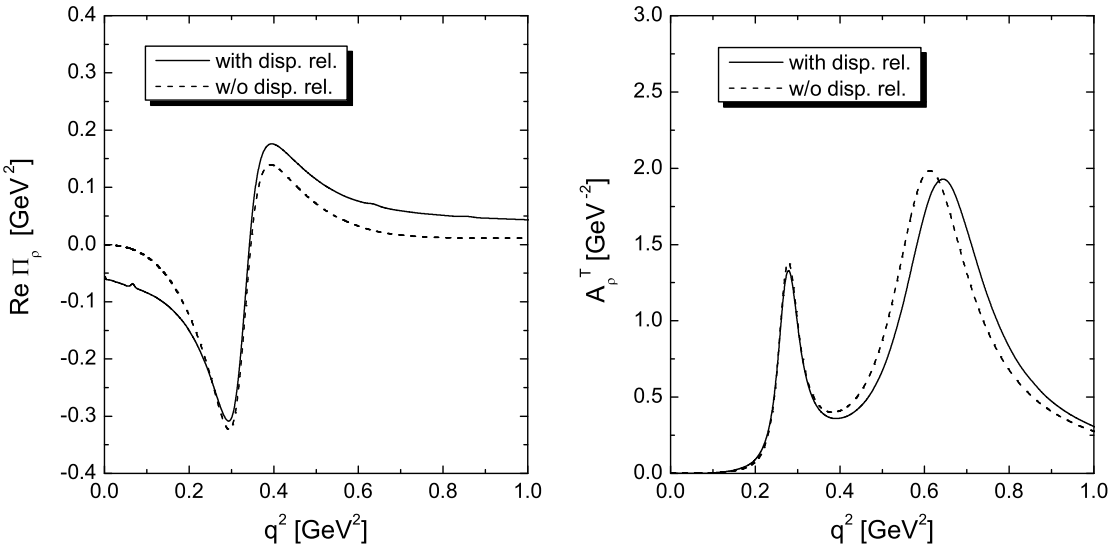

Figure 9.8: Real part of the self energy (left) and spectral function (right) of a ρ meson at rest. In this calculation the in-medium self energy consists of a $D_{13}(1520)N^{-1}$ excitation only. The solid lines indicate a result obtained from a dispersion relation and the dashed lines stand for a direct computation of the real part.

This is the same result that a direct computation of this quantity from Eq. 9.8 would deliver and demonstrates that a resonant scattering amplitude which is described by a Breit-Wigner with a constant width is analytic. On the other hand, for the scattering amplitude $\mathcal{M}_2$ one obtains the following result:

$$\begin{aligned} \mathcal{R}\mathrm{e}\,\mathcal{M}_2(\omega) &= 2\,m_N\,\frac{(\omega-\omega_R)\,\lambda^2}{[(\omega^2-\omega_R^2)+\gamma^2]\,[(\omega^2-\omega_R^2)+\lambda^2]}\,F \\ F &= \frac{\gamma^2+\gamma\,\lambda+\lambda^2+(\omega-\omega_R)^2}{\lambda\,(\lambda+\gamma)} \quad . \end{aligned} \tag{9.10}$$

Comparing with Eq. 9.8 demonstrates that a dispersion produces a different result for $\mathcal{R}\mathrm{e}\,\mathcal{M}_2$ than a direct computation. The difference between both approaches can be summarized in the factor F.

Let us give an interpretation of F. Remembering that typical values for the cutoff parameter λ are in the order of 1 GeV whereas the width $\gamma \approx 0.1$ GeV, it is tempting to make a Taylor expansion of F in the variable $\epsilon = \gamma/\lambda$:

$$\begin{aligned} F &= (\omega-\omega_R)^2\frac{1}{\lambda^2(1+\epsilon)} + \frac{\lambda^2\,(1+\epsilon+\epsilon^2)}{\lambda^2(1+\epsilon)} \\ &\approx \frac{(\omega-\omega_R)^2+\lambda^2}{\lambda^2} \quad . \end{aligned} \tag{9.11}$$

The last expression is identified as the inverse form factor, cf. Eq. 9.8. This is an interesting result as it suggests, that $\mathcal{R}\mathrm{e}\,\mathcal{M}_2$ as obtained from a dispersion integral equals that following from a direct computation except for the form factor. This result is actually quite intuitive: neglecting the form factor, the imaginary part of $\mathcal{M}_2$ is a Breit-Wigner with width γ. The form factor itself looks also like a Breit-Wigner centered around ω_R with width λ. Since

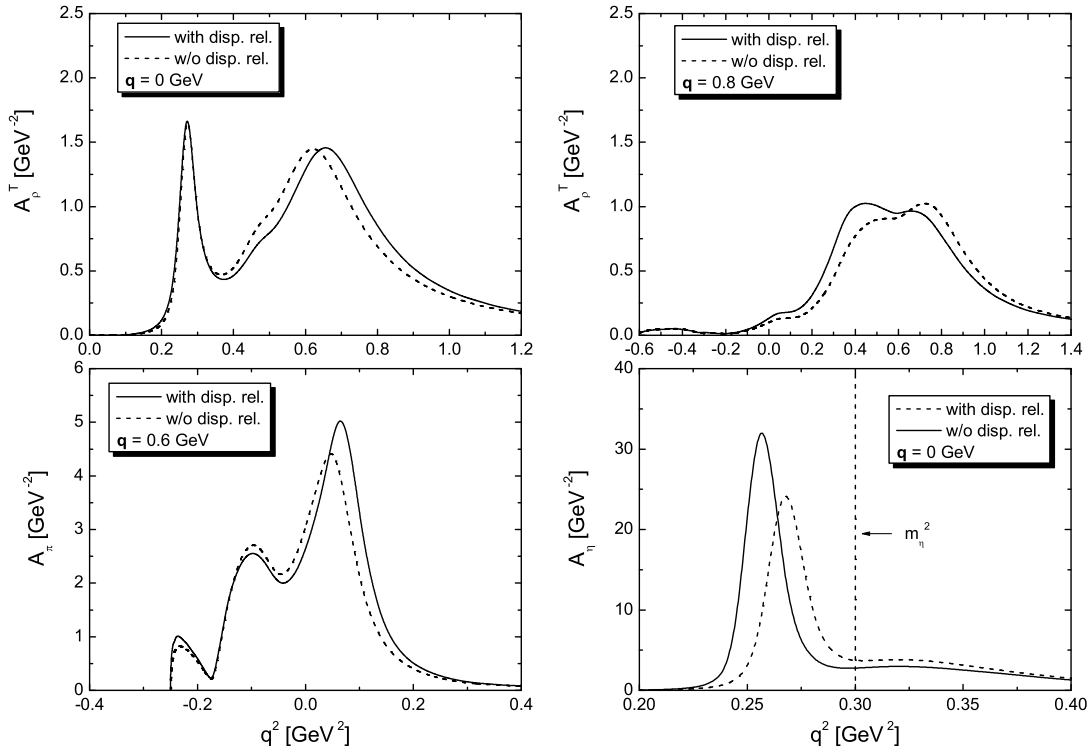

Figure 9.9: Spectral function of ρ meson (upper panel), pion (left, bottom) and η meson (right, bottom). Shown are the results of the first iteration as obtained by using a dispersion relation (solid line) or a direct computation (dashed line) to obtain $\mathcal{R}\mathrm{e}\,\Pi$. The vertical line in the bottom right plot indicates the position of the η meson in the vacuum.

we have assumed that $\lambda \gg \gamma$, the imaginary part is in a first approximation not influenced from the form factor. Via the dispersion integral this translates into a real part which does not know much of the form factor. The physical implications of this finding are clear: when dispersion relations are used, one expects larger real parts away from the resonance position. Due to level repulsion this implies a shift of the peaks in the meson spectral functions.

In the left plot of Fig. 9.8 we show the real part of the ρ self energy as obtained from a dispersion relation (solid line) and from a direct calculation (dashed line). The momentum of the ρ meson is taken to be $\mathbf{q} = 0$ GeV. For both calculations the imaginary part of the self energy is the same and it is due to the excitation of $D_{13}(1520)N^{-1}$ states. One can nicely identify the feature discussed before: in the off-shell region the dispersion relation leads to larger values for the real part of the self energy. In the right plot of Fig. 9.8 we show the spectral function of the ρ meson as resulting from both approaches: here one sees how the larger values of $\mathcal{R}\mathrm{e}\,\Pi_\rho$ away from the resonance-hole branch affects the position of the ρ peak, which is shifted upwards due to the enhanced level repulsion.

In Fig. 9.9 we show the full in-medium spectral function of ρ meson (upper panel), pion (left, bottom) and η meson (right, bottom) as obtained after the first iteration, comparing two calculations. The solid line is obtained using dispersion relations for $\mathcal{R}\mathrm{e}\,\Pi$, whereas the dashed lines follow from a direct computation of this quantity. While on a qualitative level both approaches lead to similar results, quantitatively they are characterized by the observation that by using a dispersion relation the effects of level repulsion on the original

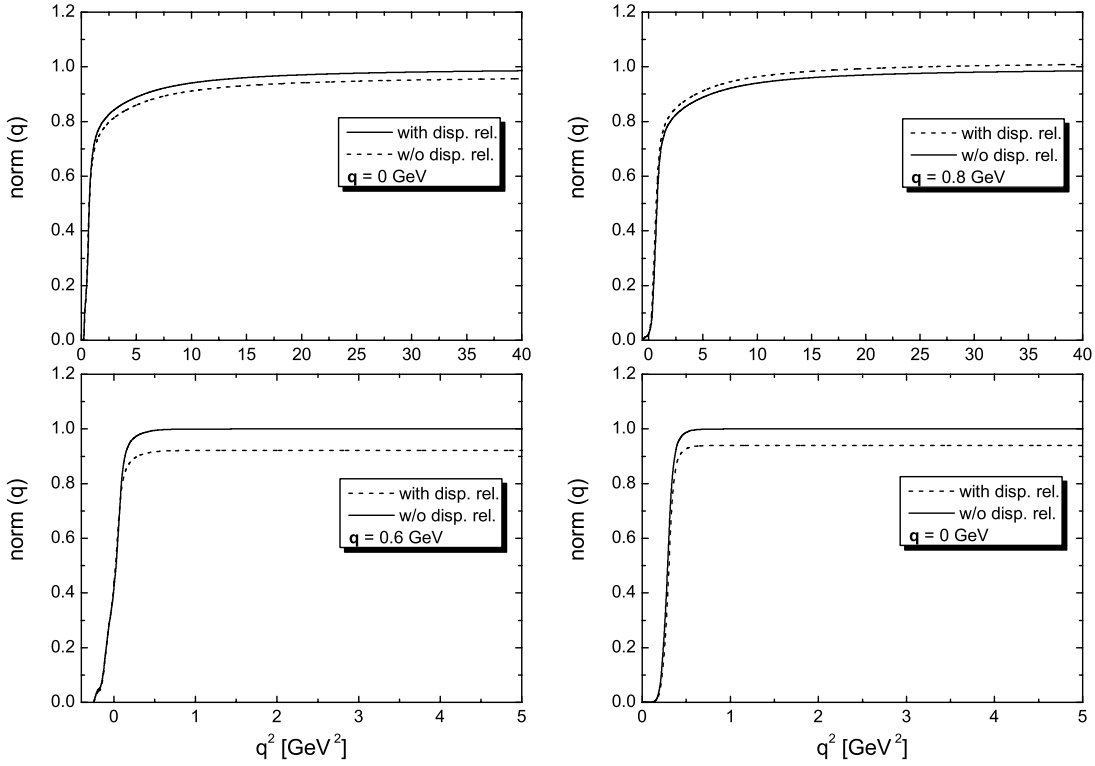

Figure 9.10: Same as Fig. 9.9 for the normalization.

meson peak are enhanced: for a ρ meson (upper panel) and a pion at $\mathbf{q} = 0.6$ GeV the meson peak is above the particle-hole excitations and is therefore moved upwards. On the contrary, the η at rest sits below the $S_{11}(1535)N^{-1}$ excitation and is therefore moved downwards. In call cases these effects are enhanced by the dispersion relations. This is a direct consequence of the larger self energy contribution away from the resonance-hole branch that was discussed before.

When using dispersion relations to obtain $\mathcal{R}\mathrm{e}\,\Pi$, normalized spectral functions should result. In Fig. 9.10 we have plotted the normalization integral

$$\mathrm{norm}(q) \;=\; \int_0^q dq'^{\,2}\, \mathcal{A}^{med}(q') \tag{9.12}$$

as a function of the upper integration variable q. The solid (dashed) line shows a calculation with (without) dispersion relations. Results are shown for the ρ meson (upper panel), the pion (bottom, left) and the η meson (bottom, right). In all cases normalized spectral functions are obtained when using dispersion relations. For the ρ meson a (nearly) normalized spectral function is also obtained when the real part of the self energy is obtained directly from Feynman graphs. Note the slow convergence of the ρ spectral function which is already seen in the vacuum (cf. Fig. 3.4 in Chapter 3.1). For pion and η meson the differences are more pronounced and a direct computation of $\mathcal{R}\mathrm{e}\,\Pi$ violates the normalization by up to 10%.

Let us now turn to the baryon resonances. In the Figs. 9.11 and 9.12 we show results for spectral function and normalization of the $D_{13}(1520)$ (top, left), the $P_{33}(1232)$ (bottom, left) and the $S_{11}(1535)$ (bottom, right). Compared are calculations where the real part of

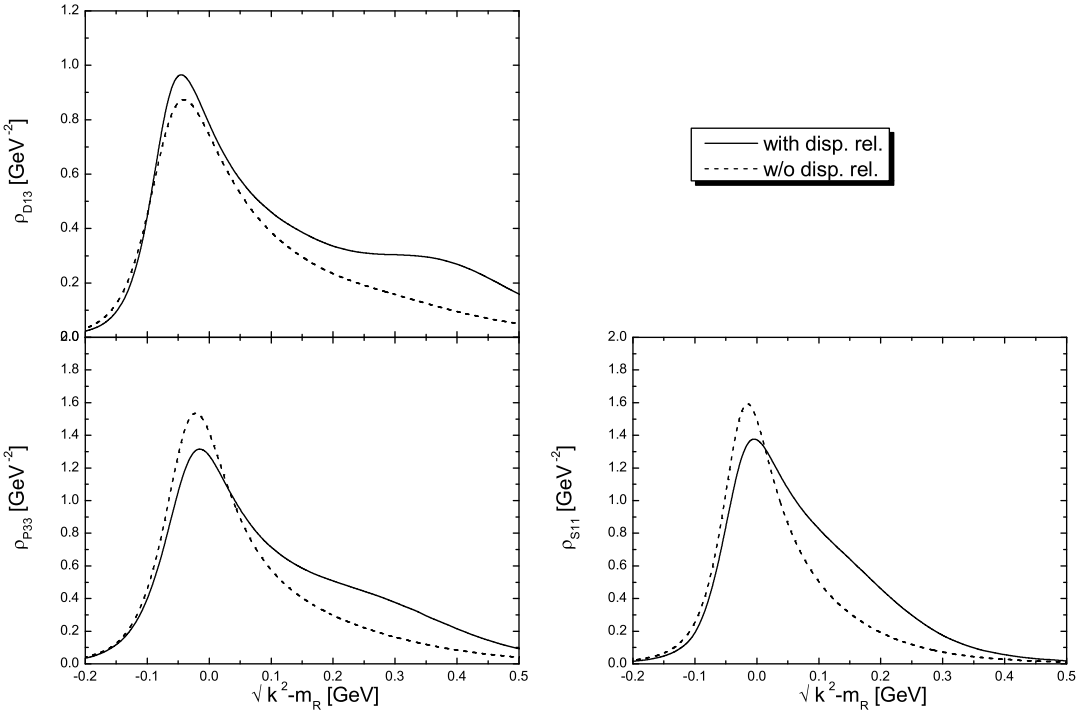

Figure 9.11: Spectral function of the $D_{13}(1520)$ (top, left), the $P_{33}(1232)$ (bottom, left) and the $S_{11}(1535)$ (bottom, right) resonances. Compared are calculations with (solid) and without (dashed) taking into account $\mathcal{R}\mathrm{e}\,\Sigma$.

the baryon resonance self energy is obtained with (solid line) dispersion relations and where it is neglected (dashed lined). In the latter case also the real part of the meson self energy is directly computed, corresponding to the dashed lines in Fig. 9.9. The normalization in the vacuum (w/o $\mathcal{R}\mathrm{e}\,\Sigma$) is also shown (dotted lines). Effects from short-range correlations are taken into account and we show the self consistent results.

The differences of the spectral function (Fig. 9.11) are of quantitative rather than of qualitative nature. The global attributes peak position and peak width remain essentially the same and the main differences are found in the high energy tails of the spectral function. Without explicitly showing it, we assure that the in-medium decay width is not sensitive to the use of dispersion relations for the self energy of baryon resonances or mesons. This is understandable since we do not find large mass shifts of the baryon resonances induced from $\mathcal{R}\mathrm{e}\,\Sigma$ (remember that the substantial shift of the peak position found for the $D_{13}(1520)$ is due to the energy dependence of the decay width) and consequently the meson spectral functions are not qualitatively changed by $\mathcal{R}\mathrm{e}\,\Sigma$. As already discussed before, the meson spectral functions are also not very sensitive on how the meson self energy $\mathcal{R}\mathrm{e}\,\Pi$ is computed. This implies that the resonance width, which is obtained by integrating over the meson spectral functions, is only weakly dependent on how $\mathcal{R}\mathrm{e}\,\Sigma/\mathcal{R}\mathrm{e}\,\Pi$ is obtained. On a quantitative level, the differences for the spectral function are more pronounced than for the mesons. This is not surprising since for the baryon resonances we are considering the total impact of the real part of the self energy and not just differences arising from a different way of calculating this quantity. Turning to the normalization shown in Fig. 9.12, we find that in particular for the $D_{13}(1520)$ the inclusion of the real part is important,

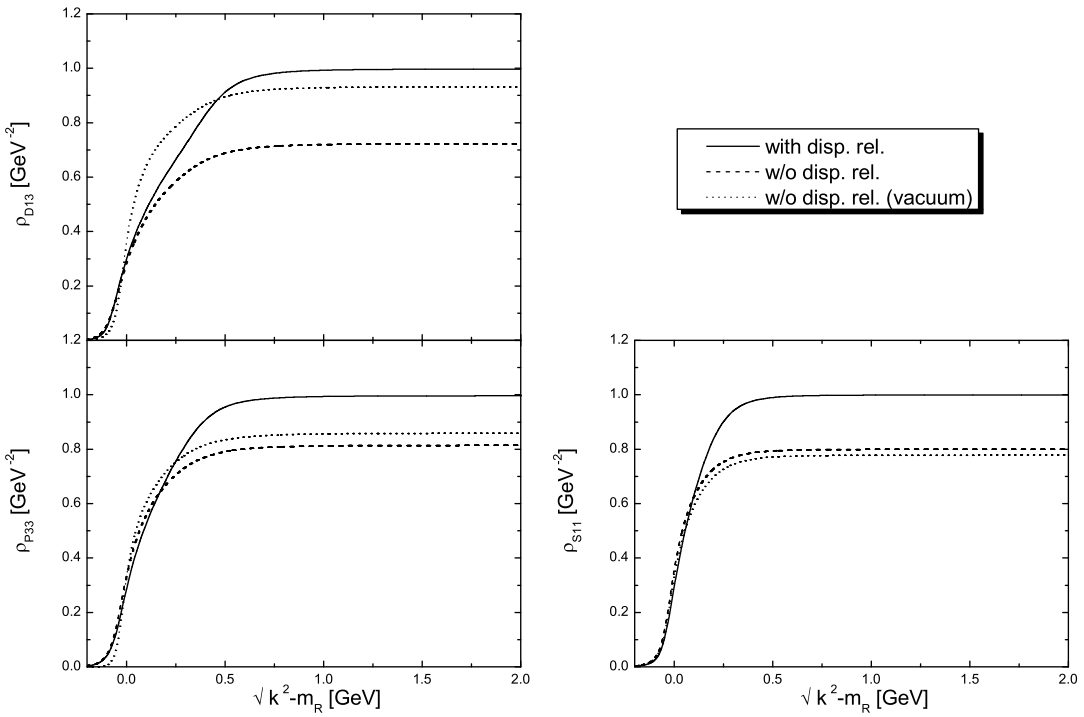

Figure 9.12: Same as Fig. 9.11 but for the normalization integral. The dotted lines show the normalization of the vacuum spectral functions if $\mathcal{R}\mathrm{e}\,\Sigma$ is neglected.

since otherwise the normalization is badly violated. It also changes sizeably in comparison to the vacuum case. For the other two states the deviation of the normalization from unity is non-negligible (on the level of 20%), but the normalization is only mildly affected from the in-medium modifications.

9.4 Momentum Dependence

This Section is based on the publication [109] and addresses the question of how reliable the momentum dependence of the ρ spectral function can be determined within a resonance model. To that end various sources of uncertainties have been considered: we have compared relativistic and non-relativistic calculations and we have studied how different relativistic couplings affect the ρ spectral function at large momenta.

Let us make a technical remark: all the results presented in this Section are based on calculations where the ρ spectral function has not been iterated. The real part of the ρ self energy $\Pi_\rho^{T/L}$ has been obtained directly from expression Eq. 5.10, i.e. a dispersion relation has not been applied. The real part of the baryon resonance self energy Σ is neglected. The traces $\Omega^{T/L}$ appearing this equation are obtained from relativistic and non-relativistic Lagrangians. Both the Lagrangians and the traces can either be found in the Appendices C.1.1 and C.2 or in Section 9.4.3. For the form factor we take the functional form suggested in Chapter 3.2, Eq. 3.23:

$$F(s) \;=\; \frac{\Lambda^4}{\Lambda^4 + (s - m_R^2)^2} \quad . \tag{9.13}$$

This is contrasted with a calculation using as done in [107]:

$$F(\mathbf{q}) \;=\; \frac{\Lambda^2}{\Lambda^2+\mathbf{q}^2} \quad . \tag{9.14}$$

9.4.1 Relativistic Versus Non-Relativistic

Many calculations of the in-medium properties of the ρ meson within a resonance model have considered a non-relativistic reduction of Eq. 5.4 [38, 107, 111, 122]. Whereas, at low momenta, the main uncertainty of the results comes from the values of the coupling constants, at large momenta an additional model dependence is introduced by the momentum dependence of the self energy and the question arises up to which extent the following findings of resonance models are model independent: In a non-relativistic calculation p-wave resonances do not couple to longitudinal ρ mesons. Furthermore, A_ρ^T and A_ρ^L display a completely different behaviour at high momenta. For A_ρ^L the effects from resonance excitation are rather small and the spectral function is strongly peaked at the ρ mass. A_ρ^T, in contrast, is completely smeared out in this kinematic regime.

We will demonstrate now that the momentum dependence of the self energy can not be reliably determined within a non-relativistic calculation and we argue that therefore a relativistic framework is imperative in order to put the results on a more solid basis.

Within the low density theorem the self energy is proportional to $f^2\,\Omega^{T/L}$, see Eqs. 5.8 and 5.10 in Chapter 5.2.2. From Eqs. 3.16 and 3.17 in Chapter 3.2 it is clear that $\Omega^{T/L}$ enters also into the determination of the the coupling constant f. It thus appears twice in the forward scattering amplitude and in the in-medium self energy. An ambiguity now arises for the choice of the reference frame in which the non-relativistic reduction leading to $\Omega^{T/L}$ is performed. In the works of [38, 107, 111, 122] the following choice was made: the coupling constant was obtained by evaluating the matrix element in the cm frame (rest frame of the resonance) whereas the self energy was calculated in the lab frame (rest frame of nuclear matter). This is a suggestive choice since the decay width is usually defined in the rest frame of the decaying particle whereas a nuclear matter calculation is preferably performed in the rest frame of nuclear matter. The non-relativistic reduction itself does not uniquely determine the reference frame, as it assumes that both the resonance and nucleon momentum are small compared to their mass. This condition is equally well met in the cm frame and in the lab frame.

As shown in [38, 107], for a resonance of positive parity both the resonance decay width and the forward scattering amplitude are proportional to $\mathbf{q}^2$. For a given invariant energy $\sqrt{s}$ the three momenta in lab frame and cm frame are easily related (see Appendix Eq. B.34 in Appendix B.6):

$$q_{lab} = q_{cm}\,\frac{\sqrt{s}}{m_N} \quad . \tag{9.15}$$

The coupling constant f is adjusted to the decay width. Computing the vertex function either in the cm frame or in the lab frame leads to the following relation between the resulting coupling constants:

$$f_{lab}^2 = f_{cm}^2\,\frac{m_N^2}{m_R^2} \quad . \tag{9.16}$$

The most relevant contribution from each resonance to the self energy comes from the

kinematical region $\sqrt{s} \approx m_R$ where the forward scattering amplitude obeys

$$T^2_{lab} = T^2_{cm} \frac{m_R^2}{m_N^2} \quad . \tag{9.17}$$

It is evident that the consistent use of either lab frame or cm frame kinematics for both the determination of the coupling constant and the forward scattering amplitude leads to the same results. In contrast, the previously applied method of mixed kinematics [38, 107, 111, 122] produces an in-medium self energy which is larger by a factor of $\left(\frac{m_R}{m_N}\right)^2$. Typically, the resonance masses vary between 1.5 and 2 GeV. Thus for p-wave resonances the ambiguity in the non-relativistic reduction leads to uncertainties which can be as large as a factor of four. For s-wave resonances the effects are less pronounced. Here the transverse and the longitudinal channel are proportional to the energy ω^2 and the invariant mass q^2 of the ρ meson respectively. Thus only the transverse channel will be affected by the ambiguity of the reference frame at momenta comparable to its invariant mass. Altogether, this is clearly not a satisfying situation which can only be resolved within a relativistic approach.

In a resonance model the spectral function A_ρ is most sensitive to the behaviour of the scattering amplitude in the vicinity of $s = m_R^2$, i.e. along the lines depicted in Fig. 5.3. In order to get a feeling for the differences between a relativistic and the different non-relativistic descriptions, it is therefore rewarding to compare the results from both approaches for the quantity $\Omega^{T/L}$. Explicit expression for relativistic and non-relativistic traces are given in Appendices C.1.2 (Table C.1)and C.2.2 (Table C.2).

In Fig. 9.13 we show Ω^T for two of the most prominent resonances in the non-relativistic analysis, the $D_{13}(1520)$ and the $P_{13}(1720)$. It is plotted as a function of the invariant mass of the ρ meson, the momentum being fixed by the condition $s = m_R^2$. We compare the relativistic results with three non-relativistic versions of Π^{med}:

i) relativistic (solid line)

ii) non-relativistic, self energy lab-frame, coupling constant cm-frame (dotted line)

iii) non-relativistic, both quantities cm-frame (dashed line)

iv) non-relativistic, both quantities lab-frame (dash-dotted line) .

Up to now, in the literature only calculations performed within kinematics ii) can be found [107, 38, 111].

We first remark that the results are not degenerate at threshold, since in each case the coupling constant has been adjusted to the measured partial decay width. As expected from the above discussion, the calculations reveal large differences between the different non-relativistic approaches ii)-iv) in the transverse channel. This effect is – as already discussed – more pronounced for p-wave resonances, see right graph of Fig. 9.13. Here, especially at low invariant masses, the commonly used non-relativistic version ii) is not reliable at all, overestimating the results by a factor of $2-3$, whereas both version iii) and iv) yield a surprisingly good agreement with the fully relativistic calculation i). In the s-wave channel – left graph of Fig. 9.13 – it is again the non-relativistic version ii) displaying a considerable disagreement with the relativistic calculation. Both versions iii) and iv)

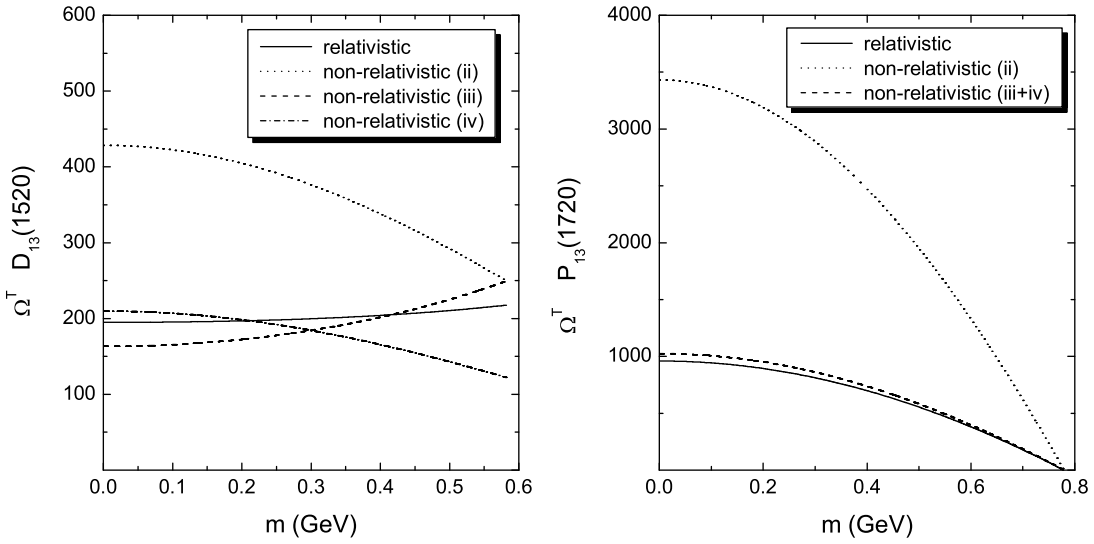

Figure 9.13: Ω^T for the $D_{13}(1520)$ resonance (left) and the $P_{13}(1720)$ (right). Shown are three different calculations, which are explained in Sect. 8.

yield better approximations. The exact form of the momentum dependence, however, is not well reproduced in version iv).

We do not show results for Ω^L. Here the effect from a relativistic calculation is rather small, since the momentum dependence of Ω^L is mainly determined from physical constraints at $\mathbf{q} = 0$ and at the photon point: at small momenta a relativistic calculation and its non-relativistic reduction must display a similar behaviour, whilst at the photon point Ω^L has to vanish in either version. Thus, both calculations do not have much room to develop differently. There is a finite contribution to Ω^L from p-wave resonances, which, however, is small as compared to the transverse coupling. In the spin-$\frac{1}{2}$ sector, one obtains qualitatively similar results for $\Omega^{T/L}$.

Summarizing these results, we find that the previously used non-relativistic version ii) is not a good approximation of a fully relativistic calculation. In contrast, using cm-kinematics for both the determination of the coupling constant and the self energy leads to a very reasonable agreement with the relativistic approach.

For this reason we argue also that the contribution from spin-$\frac{5}{2}$ particles — for which a relativistic theory is very complicated — should be evaluated within kinematics iii). Since in a non-relativistic calculation the vertex factors of both the spin-$\frac{3}{2}$ and spin-$\frac{5}{2}$ resonances are proportional to $\mathbf{q}^2$, we expect from Fig. 9.13 that at high momenta the contribution from spin-$\frac{5}{2}$ resonances is reduced as compared to previous works [38, 107, 111], where $\mathbf{q}^2$ was evaluated in the lab-frame.

9.4.2 Parameters and Form Factors

Turning now to the discussion of the results for the spectral function, we start with a comparison between a relativistic calculation and the non-relativistic approach with kinematics iii). The good agreement for the results of $\Omega^{T/L}$ translates into very similar results

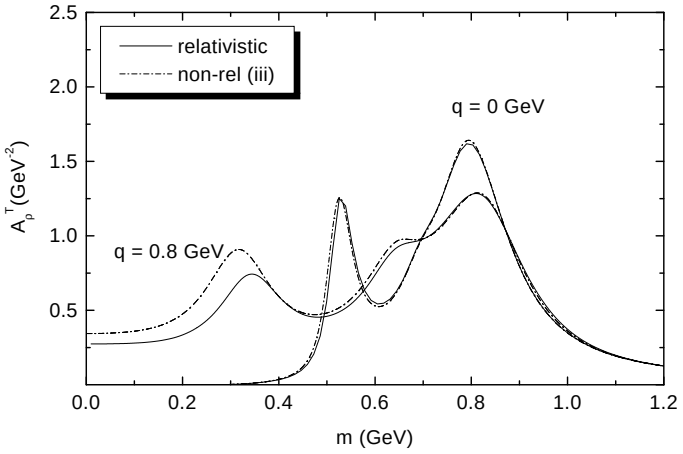

Figure 9.14: The transverse spectral function A_ρ^T at 0 GeV and 0.8 GeV. Shown is a comparison between a relativistic calculation and and a non-relativistic one using cm-kinematics iii).

for the spectral function $A_\rho^{T/L}$, see Fig. 9.14. There the transverse spectral function is plotted at momenta $\mathbf{q} = 0$ GeV and $\mathbf{q} = 0.8$ GeV. The resonance parameters are taken from Manley *et al*, only the resonances with a $\star$ in Table A.3 are included. We do not present a comparison for the longitudinal channel as there the differences are even smaller.

We have now demonstrated that calculations of the spectral function, which differ only in whether relativistic or consistent non-relativistic vertex functions (i.e. according to kinematics iii) are used, yield nearly identical results. On the other hand, we have shown in the previous Section that an inconsistent non-relativistic calculation (i.e. kinematics ii) does not provide a good approximation of the traces $\Omega^{T/L}$ and therefore the in-medium self energy of the ρ meson. Aim of the remainder of this Section is to analyze, in which way this and the use of different resonance parameters as well as form factors influences the results for the spectral function in comparison with our first publication [107]. Anticipating the results, we will find that in particular at large momenta the new results change substantially relative to [107].

First we concentrate on a comparison of our non-relativistic calculation [107] (dotted line) with a relativistic one (dashed line), where the same resonances as in the non-relativistic case have been employed, but with resonance parameters taken from the analysis of [89] rather than from the PDG. Now consider Fig. 9.15. At $\mathbf{q} = 0$ the non-relativistic calculation with PDG parameters shows a stronger depletion of the ρ peak than the relativistic approach with Manleys parameters. The form factor $F(s)$ Eq. 9.13 suppresses off-shell contributions ($s \neq m_R^2$) of resonances much stronger than the previously used one (9.14). This effects in general both the tail of the resonance excitation as, due to level repulsion, the strength in the resonance peak. Thus, due to the form factor, the impact of the excitation of the $D_{13}(1520)$ in the region of the ρ peak is noticeably reduced. This effect is enhanced by the small partial ρN decay width of the $D_{33}(1700)$ found in the Manley analysis as compared to PDG (ct. Table A.3). Its small coupling makes this resonance play a merely negligible role in the relativistic calculation.

At larger momenta both approaches lead to very different results for A_ρ^T, see the plots

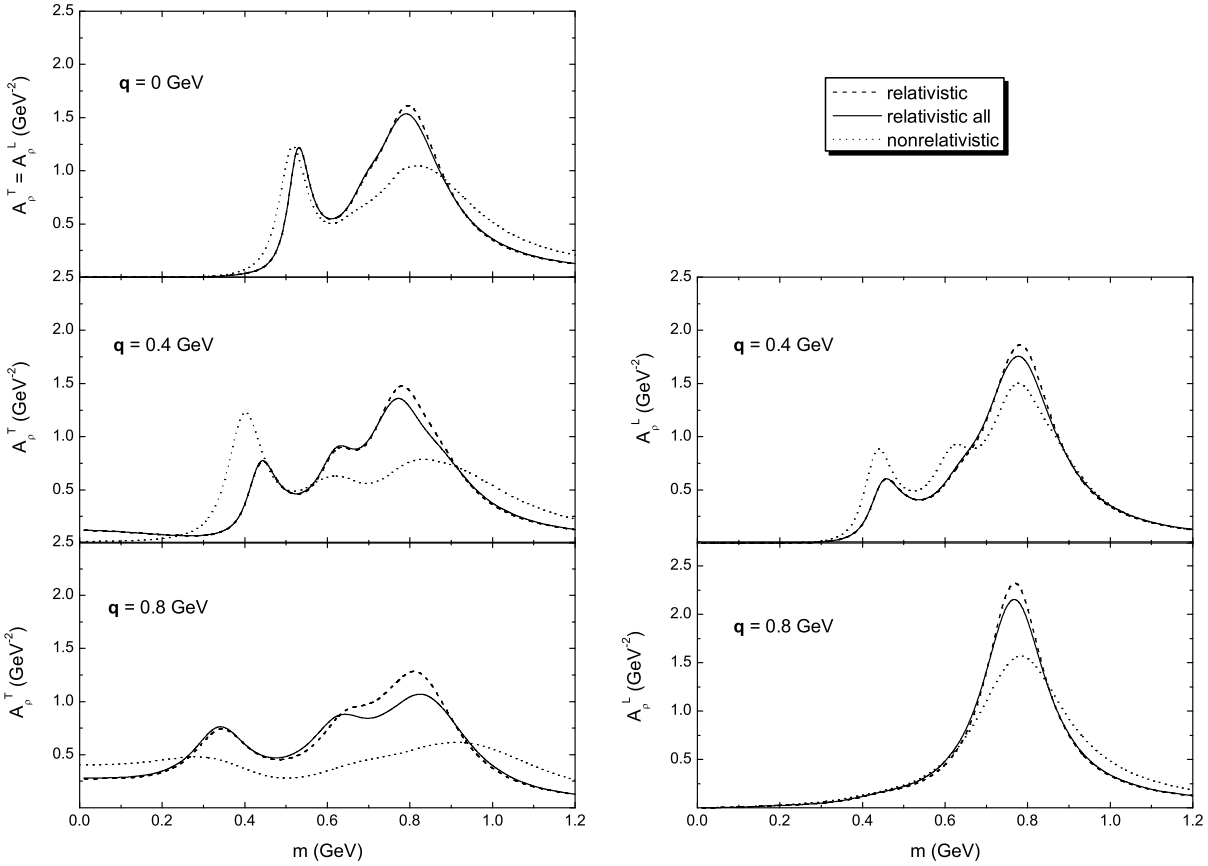

Figure 9.15: $A_\rho^{T/L}$ for three different momenta. Compared are relativistic (solid line, dashed line) and a non-relativistic calculation according to kinematics ii) (dotted line). For the relativistic calculation the resonance parameters of Manley *et al* [89] are employed, for the non-relativistic one the parameters of PDG [46]. For the solid curve all resonances listed in Table A.3 are included, for the dashed line only those with a $\star$ are taken into account.

on the left in the middle and the bottom panel of Fig. 9.15, where the spectral function is shown for momenta of $\mathbf{q} = 0.4$ GeV and $\mathbf{q} = 0.8$ GeV, respectively. As a general tendency, much more strength is centered around the original ρ peak. This behaviour can be retraced to various sources. As follows from the properties of $\Omega^{T/L}$, for a given branching ratio, a relativistic calculation produces a much smaller Π_ρ^T than a non-relativistic one. The resonance contribution is further suppressed by the form factor $F(s)$, thus producing a more conservative estimate of the resonance contribution. In addition, at higher momenta, Π_ρ^T is reduced by the smaller branching ratio of the $D_{33}(1700)$. These depletion mechanisms are only counteracted by the strongly increased branching ratio of the $P_{13}(1720)$. Overall, at high momenta A_ρ^T is dominated by the $D_{13}(1520)$ and the $P_{13}(1720)$ as well as, to some extent, by the spin-$\frac{5}{2}$ resonances $F_{15}(1680)$ and $F_{35}(1905)$. Still the transverse spectral function receives significant broadening with increasing 3-momentum in a relativistic calculation, but this effect is not as pronounced as in the non-relativistic case.

Whereas A_ρ^T receives strong qualitative modifications in a relativistic calculation, changes in A^L are only of a quantitative nature. This is shown in plots on the right of the middle and bottom panels of Fig. 9.15. As already mentioned, the momentum dependence is dom-

inated — both in a relativistic and a non-relativistic approach — by physical constraints at $\mathbf{q} = 0$ and $q^2 = 0$. Consequently, the $D_{13}(1520)$ peak at $\mathbf{q} = 0.4$ GeV contains nearly the same strength in both approaches. The depletion of resonance strength around the ρ peak is, as in the case of $\mathbf{q} = 0$, due to the form factor and the small coupling of the $D_{33}(1700)$. In the longitudinal channel the only sizeable contribution comes from the $D_{13}(1520)$.

The impact of the new, high lying resonances on our results – indicated by the solid lines – is small and noticeable only at high momenta. This is easily understood for the following reasons: Despite their large branching ratio, the coupling strength is relatively small, since their mass is far above the ρN threshold and consequently the phase space is very large. In addition, they have a very large total decay width, leading to a further suppression of the contribution. At low momenta, these resonances can only be excited from ρ mesons far above their pole mass. Correspondingly, their contribution to the imaginary part of $\Pi_\rho^{T/L}$ is drowned by the imaginary part of the vacuum self energy, the $2\,\pi$ decay width. It is only at momenta around 0.8 GeV (bottom panel of Fig. 9.15), that the resonance excitation occurs at invariant masses around the pole mass of the ρ meson. At this point resonance scattering becomes important. This explains why in Fig. 9.15 differences between both relativistic calculations (solid and dashed line) are only seen at momenta around $\mathbf{q} = 0.8$ GeV.

9.4.3 Influence of Couplings

So far, we discussed the differences between a relativistic and a non-relativistic calculation of $\Pi_\rho^{T/L}$ and their consequences for A_ρ. There are, in addition, various ways for a resonance to couple to the ρN system. In order to draw safe conclusions on the momentum dependence of the ρN scattering amplitude, it is important to study the influence of the chosen coupling on the results.

In this analysis we confine ourselves to the case of spin-$\frac{3}{2}$ resonances of both positive and negative parity. In addition to the Lagrangians given in Appendix C.1.1, Eq. C.2, we also consider:

$$\mathcal{L}_{RN\rho} = \begin{cases} \dfrac{f}{m_\rho^2}\,\bar{\psi}^\mu\,\gamma^5\,\partial^\nu\psi\,\rho_{\mu\nu} \\ \\ \dfrac{f}{m_\rho^2}\,\bar{\psi}^\mu\,\gamma^5\,\psi\,\partial^\nu\rho_{\mu\nu} \qquad . \end{cases} \tag{9.18}$$

In the spin-$\frac{1}{2}$ sector there is no resonance which has a sizeable coupling to ρN and a strong dependence of the final results on the coupling of spin-$\frac{1}{2}$ resonances is not expected. In the following discussion we will use some shorthand notations to distinguish between the different vertex functions. The standard coupling from Eq. C.2 will be referred to as coupling (i), to the first vertex function from Eq. 9.18 we refer as coupling (ii) and to the second one as coupling (iii).

The self energy contribution is characterized by traces $\Omega^{T/L}$, see Eq. 5.10 in Chapter 4. Here we give these quantities as following from the Lagrangians of Eq. 9.18. Using the

coupling denoted by ii) one derives:

$$\begin{array}{|ll|}\hline J^\pi = \frac{3}{2}^+ \quad : & \Omega^L = \frac{8}{3}\, m_N^3\, q^2\, (m_N + \omega - \sqrt{s})\, \left(1 - \frac{\mathbf{q^2}}{s}\right) \\ & \Omega^T = \frac{8}{3}\, m_N^3\, \omega^2\, (m_N + \omega - \sqrt{s}) \\ \hline J^\pi = \frac{3}{2}^- \quad : & \Omega^L = \frac{8}{3}\, m_N^3\, q^2\, (m_N + \omega + \sqrt{s})\, \left(1 - \frac{\mathbf{q^2}}{s}\right) \\ & \Omega^T = \frac{8}{3}\, m_N^3\, \omega^2\, (m_N + \omega + \sqrt{s}) \\ \hline \end{array} \tag{9.19}$$

The coupling denoted by iii) leads to:

$$\begin{array}{|ll|}\hline J^\pi = \frac{3}{2}^+ \quad : & \Omega^L = \frac{8}{3}\, m_N\, q^4\, (m_N + \omega - \sqrt{s})\, \left(1 - \left(\frac{m_N^2}{q^2}\right) \frac{\mathbf{q^2}}{s}\right) \\ & \Omega^T = \frac{8}{3}\, m_N\, q^4\, (m_N + \omega - \sqrt{s}) \\ \hline J^\pi = \frac{3}{2}^- \quad : & \Omega^L = \frac{8}{3}\, m_N\, q^4\, (m_N + \omega + \sqrt{s})\, \left(1 - \left(\frac{m_N^2}{q^2}\right) \frac{\mathbf{q^2}}{s}\right) \\ & \Omega^T = \frac{8}{3}\, m_N\, q^4\, (m_N + \omega + \sqrt{s}) \\ \hline \end{array} \tag{9.20}$$

To get a feeling for the changes, we present first $\Omega^{T/L}$ in Fig. 9.16 and 9.17. The results are shown for the $D_{13}(1520)$ and the $P_{13}(1720)$ resonances. The coupling constants f are adjusted to the $\rho\, N$ branching ratios. The most distinct behaviour is exhibited by coupling (iii). At the photon point, it enforces a vanishing contribution not only in the longitudinal, but also in the transverse channel. This behaviour can be read off from the Lagrangian $\mathcal{L}_{RN\rho}$ and is due to the derivative acting on the field tensor:

$$\partial^\nu\, F_{\mu\nu} = -q^2\, A^\nu \qquad . \tag{9.21}$$

Clearly, the vertex function has to vanish at $q^2 = 0$, regardless of the polarization of the ρ meson. Consequently, Π_ρ^T has to fulfill the same constraints as Π_ρ^L and both quantities become more or less identical. Thus, the coupling (iii) mostly affects the transverse channel, as can be seen in the left plots of Figs. 9.16 and 9.17. Noteworthy is also the much larger contribution from p-wave resonances to Ω^L, which is due to the larger coupling constant f required from this Lagrangian. This is explained as follows: In the determination of the coupling strength the quantity $2\,\Omega^T + \Omega^L$ enters, averaged over the ρ mass distribution. Since this expression has to vanish at $q^2 = 0$ in coupling (iii), its size is much reduced at low invariant masses. This behaviour can only be compensated by a large coupling constant. For p-wave resonances this effect is most evident, since in this case the matrix element becomes sizeable mostly near the photon point for the couplings (i) and (ii). As an example, we obtain a value of $f = 36$ for the $P_{13}(1720)$ in coupling (iii) as compared to $f = 10$ in coupling (i). Clearly, the increased values for the coupling constants are responsible for the enhanced resonance contribution in the longitudinal channel.

For coupling (iii) the coupling strength for the $P_{33}(1232)$ can not be obtained from VMD since the matrix element vanishes at the photon point. We take an *ad hoc* value of

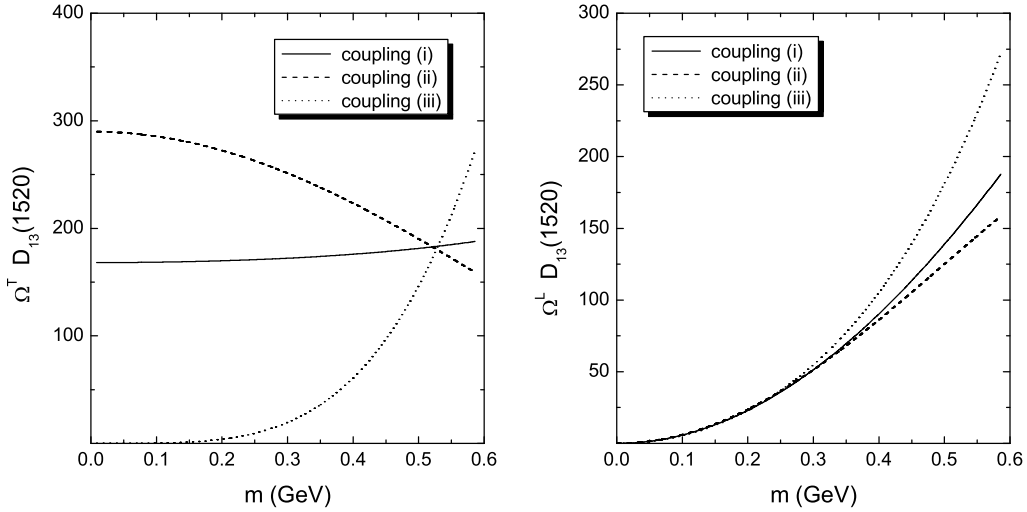

Figure 9.16: Ω^T (left) and Ω^L (right) for the $D_{13}(1520)$. Shown is the influence of different coupling schemes on the results. The couplings are explained in Sect. 9.4.3.

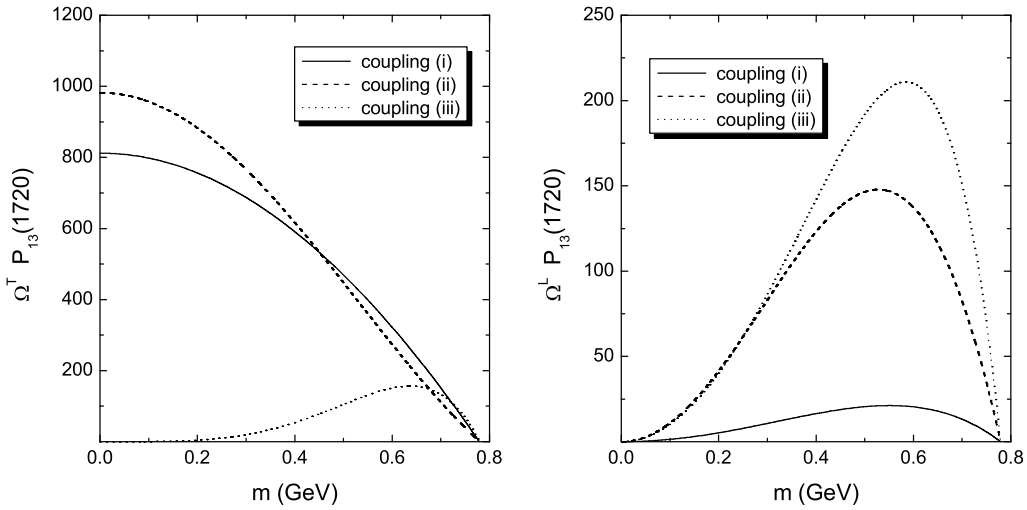

Figure 9.17: Same as Fig. 9.16 but for the $P_{13}(1720)$.

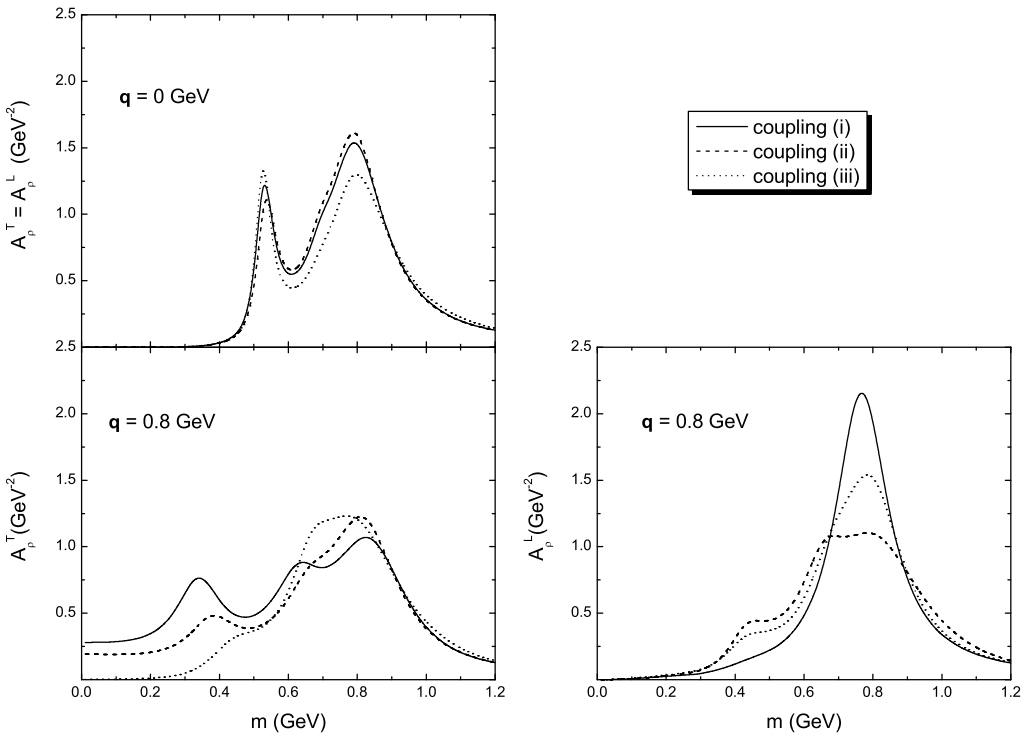

Figure 9.18: Results for the ρ spectral function at $\mathbf{q} = \mathbf{0}$ GeV (top) and at $\mathbf{q} = 0.8$ GeV (bottom). The couplings employed for the calculations are explained in Sect. 9.4.3.

$f = 30$ for the coupling constant, which is twice as much as obtained from coupling (i). Varying f between values of $15 - 30$ has only negligible influence on the results.

Coupling (ii) produces much less dramatic effects then coupling (iii) when compared to coupling (i) and the general properties of $\Omega^{T/L}$ do not change much in comparison. An exception is the coupling of p-wave resonances to longitudinal ρ mesons, where coupling (ii) generates a much larger contribution than coupling (i). This is shown in the left plot of Fig. 9.17. Quantitatively, also the coupling of s-wave resonances to transverse ρ mesons change up to some extent. Nearly identical results are achieved for both remaining channels.

Turning now to the results for the spectral function, at $\mathbf{q} = 0$ no significant modification is observed, see graph in the upper panel of Fig. 9.18. However, at higher momenta around $\mathbf{q} = 0.8$ GeV (shown in the lower panel of Fig. 9.18), the distinct character of coupling (iii) becomes apparent, reducing the resonance contribution at low invariant masses for transverse ρ mesons. At the same time, a stronger modification of A_ρ^L is exhibited. Thus, coupling (iii) induces a qualitatively different behaviour for A_ρ^{med}, removing much of the distinction between transverse and longitudinal ρ mesons at large momenta. In this kinematical region spin-$\frac{5}{2}$ resonances, for which we have only a non-relativistic coupling at hand, have noticeable influence on the results. Therefore, by changing the interaction in the spin-$\frac{3}{2}$ sector and leaving the spin-$\frac{5}{2}$ sector unchanged, the effect of the coupling scheme on the spectral function is underestimated. In order to obtain an upper limit for this effect, we treat the spin-$\frac{5}{2}$ resonances the same way as spin-$\frac{3}{2}$ resonances, correcting for the different spins of the states by a factor of 3/2. This procedure is reasonable, since

— except for the multiplicity — the spin of the resonance affects mostly the angular dependence of the matrix element. We checked that for the transition from spin-$\frac{1}{2}$ to spin-$\frac{3}{2}$ resonances our prescription works fine within 10%.

The most distinct feature of coupling (ii) is an increased resonance contribution to A_ρ^L at large momenta relative to coupling (i). The transverse channel, however, does not undergo large modifications as compared to coupling (i). This behaviour is expected from the results for the traces shown in Figs. 9.16 and 9.17.

One should keep in mind, that in general the actual coupling of a resonance to the ρN channel might contain contributions from all three couplings. Naturally this will smear out the differences. One expects from the above discussion, that the general tendency will go towards a less modified transverse ρ meson than predicted from coupling (i), whereas in the longitudinal channel a stronger modification is likely. It is beyond the scope of this work, however, to find realistic weighting factors for each coupling. This can only be achieved by a complete relativistic partial wave analysis of $\pi N \to \pi \pi N$ data.

Chapter 10

Results 3 – The ω Meson

This Chapter is based on the publication [110] and is concerned about the coupling of ω mesons to baryon resonances as following from a Vector Meson Dominance (VMD) analysis. In a second step, the resonance couplings have been used to determine the in-medium properties of the ω. The ω meson has not been included in our coupled channel analysis, i.e. self consistency effects for the in-medium spectral function have not been considered. This is motivated from the fact that the modifications that this states experiences in nuclear matter are rather weak. After the publication, some models [104, 105, 84, 34] have emerged which have tried to obtain information on the coupling of baryon resonances to $N\omega$. We have added a few comments concerning the results of these analyses.

10.1 Motivation

For a long time a satisfactory understanding of baryon resonances in the $N\,\omega$ channel has been a unsolved problem. While many quark models predict resonances with a coupling to this channel, for example [135, 134, 25], their experimental identification is very involved. Only the advent of sophisticated coupled channel analyses [104, 105, 84] as well as more precise data close to the threshold from the SAPHIR detector have allowed to shed some light on this issue. Thus, in the analysis of [104, 105] in particular the resonances $P_{11}(1710)$ and $P_{13}(1720)$ have been found to couple strongly to the $N\,\omega$ channel. In the model of [84] – where resonances with positive parity are not included – mainly the $D_{13}(1520)$ shows up in this channel.

An understanding of baryon resonances in the $N\,\omega$ channel is not only important for a description of scattering experiments, but might also be of interest for the properties of ω mesons in nuclear matter. This conjecture is guided from the experience with the ρ meson, which has been shown to undergo significant modification in the nuclear medium due to the excitation of resonance-hole loops. In this scenario a central role is played by the subthreshold resonance $D_{13}(1520)$ [107, 109, 37], suggesting that especially information on the coupling strength of subthreshold resonances to the $N\,\omega$ system would be very valuable for a determination of the in-medium properties of the ω meson.

In this Chapter we present estimates for the coupling strength of baryon resonances to the $\omega\,N$ channel $f_{RN\omega}$. Vector Meson Dominance (VMD) is utilized to relate $f_{RN\omega}$ to the isoscalar strength of the electromagnetic decay of the respective resonance, which is extracted from helicity amplitudes. The analysis covers all resonances for which helicity amplitudes are currently available [6, 46], most of which are below the nominal $\omega\,N$

threshold. Though the applicability of VMD in the resonance region is far from obvious, we believe that even in the light of the more refined analyses of [105, 104, 84], such an approach retains its value, since for resonances which are clearly subthreshold, a clear experimental evidence for a strong coupling will always be hard to achieve. Consequently, in [105, 104] no strong evidence for a coupling of the $D_{13}(1520)$ is found, whereas the resonances which are most important – the $P_{11}(1710)$ and $P_{13}(1720)$ states – are close to the threshold. On the other hand, in [84] constraints from VMD enter into the analysis, thus giving rise to presence of the $D_{13}(1520)$ in this channel. A coupling of subthreshold resonances to the $N\,\omega$ system has also been reported in [114]. The authors of [114] derive the coupling strength within a quark-model approach. We will compare our results with those of [105, 104, 114, 84, 37].

The paper is organized as follows. The details of the extraction of $f_{RN\omega}$ are presented in Sect. 10.2. In Sect. 10.3 we examine if our model gives reasonable results by comparing the VMD prediction for the isovector strength with fits to the hadronic decay width into the $N\,\rho$ channel. Sect. 10.4 is devoted to a presentation of the results for $f_{RN\omega}$ and a discussion of their compatibility with experimental information on the reactions $\pi\,N \to \omega\,N$ and $\gamma\,N \to \omega\,N$. Finally, in Sect. 10.5 the implications of excitations of resonance-hole loops for the in-medium properties of ω mesons are examined.

10.2 Determination of $f_{RN\omega}$

In this section we explain how we obtain an estimate for the magnitude of the coupling strength of a baryonic resonance to the $N\,\omega$ channel. Before going into the details of the calculation, we outline the basic idea of our approach.

Vector Meson Dominance (VMD) [130], a theory which describes photon-hadron interactions exclusively in terms of vector meson-hadron interactions, relates the hadronic coupling strength of resonances to vector mesons $f_{RN\rho(\omega)}$ and the isoscalar and isovector part of the photon-coupling, see Fig. 10.1:

$$\begin{aligned} f_{RN\omega} &= g_s\, m_\omega\, \frac{2\,g_\omega}{e} \\ f_{RN\rho} &= g_v\, m_\rho\, \frac{2\,g_\rho}{e} \quad . \end{aligned} \tag{10.1}$$

As values for g_ρ and g_ω – the coupling strengths of ρ and ω meson to the photon – we take $g_\rho = 2.5$ and $g_\omega = 8.7$ [130]. The isoscalar and isovector coupling strength of the resonance to the $N\,\gamma$ system is given by g_s and g_v, respectively, see Eq. 10.3.

Thus VMD gives access to both $f_{RN\omega}$ and $f_{RN\rho}$, if it is possible to obtain g_s and g_v from experimental data. In order to achieve this goal, it is clearly not sufficient to consider merely the total electromagnetic decay width of the resonance. Rather, the coupling has to be decomposed into an isoscalar and an isovector part, which is readily done by constructing suitable linear combinations of proton- and neutron-amplitudes. These amplitudes are known from experiment [6, 46], thus allowing to deduce numerical values for g_s and g_v.

In a nonrelativistic framework, the coupling of baryon resonances to the photon-nucleon system can be formulated as [107, 38]:

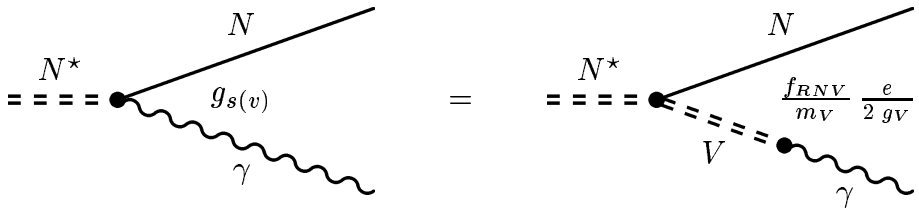

Figure 10.1: Diagrammatic description of the electromagnetic decay of a resonance in the VMD approach. The diagrams correspond to Eq. 10.1.

$$\mathcal{L}_{RN\gamma} = \begin{cases} \chi_R^\dagger\, \epsilon_{ijk}\, \sigma^i\, q^j\, \epsilon_\lambda^k\, \chi_N\, I + h.c. & \text{for} \quad J^P = \frac{1}{2}^+ \\ \chi_R^\dagger\, \epsilon_{ijk}\, S^i\, q^j\, \epsilon_\lambda^k\, \chi_N\, I + h.c. & \text{for} \quad J^P = \frac{3}{2}^+ \\ \chi_R^\dagger\, R_{ij}\, F_\lambda^{ij}\, \chi_N\, I + h.c. & \text{for} \quad J^P = \frac{5}{2}^+ \\ \chi_R^\dagger\, (\sigma_k\, \epsilon_\lambda^k\, q_0 - \sigma_k\, q^k\, \epsilon_\lambda^0)\, \chi_N\, I + h.c. & \text{for} \quad J^P = \frac{1}{2}^- \\ \chi_R^\dagger\, (S_k\, \epsilon_\lambda^k\, q_0 - S_k\, q^k\, \epsilon_\lambda^0)\, \chi_N\, I + h.c. & \text{for} \quad J^P = \frac{3}{2}^- \quad . \end{cases} \tag{10.2}$$

Here $\chi_R^\dagger$ and χ_N denote resonance and nucleon spinors respectively. The σ^i are the Pauli matrices, S^i denotes the spin-$\frac{3}{2}$ and R^{ij} the spin-$\frac{5}{2}$ transition operator. q is the c.m. momentum of the photon, q_0 its energy and ϵ_λ its polarization vector. F_λ^{ij} denotes the spatial components of the electromagnetic field strength tensor $F_\lambda^{\mu\nu}$ with $F_\lambda^{ij} = q^i\, \epsilon_\lambda^j - q^j\, \epsilon_\lambda^i$. By I we denote the isospin part of the coupling which is given as:

$$I = \chi_R^{I\,\dagger} \left(g_s + g_v \left\{ \begin{array}{c} \sigma^3 \\ S^3 \end{array} \right\} \right) \chi_N^I \quad \text{for} \quad \begin{cases} I_R = \frac{1}{2} \\ I_R = \frac{3}{2} \end{cases} \quad . \tag{10.3}$$

The spinors χ_R^I and χ_N^I represent resonance and nucleon isospinors and I_R denotes the isopin of the resonance. σ^3 and S^3 are defined as above. Note that owing to the VMD hypothesis these Lagrangians are identical to the $RN\rho$ couplings (cf. Appendix C.2).

Note that the invariant amplitude – as derived from (10.2) and (10.3) – for the decay of a resonance into a proton, $\mathcal{M}_p$, is proportional to $g_p = g_s + \alpha\, g_v$, whereas for the neutron the amplitude $\mathcal{M}_n$ is proportional to $g_n = g_s - \alpha\, g_v$. The factor α is defined as:

$$\alpha = \chi_R^{I\,\dagger} \left\{ \begin{array}{c} \sigma^3 \\ S^3 \end{array} \right\} \chi_N^I \quad . \tag{10.4}$$

For nucleon resonances it is 1 and for Δ resonances it is exactly the Clebsch-Gordan coefficient for the respective transition, in this case $\alpha = \sqrt{\frac{2}{3}}$ [33].

Thus, the linear combinations

$$\begin{aligned} \mathcal{M}_s &= \frac{1}{2}\left(\mathcal{M}_p + \mathcal{M}_n\right) \\ \mathcal{M}_v &= \frac{1}{2}\left(\mathcal{M}_p - \mathcal{M}_n\right) \begin{cases} 1 & \text{for} \quad I_R = \frac{1}{2} \\ \frac{1}{\alpha} & \text{for} \quad I_R = \frac{3}{2} \end{cases} \end{aligned} \tag{10.5}$$

are proportional to g_s and g_v respectively. $\mathcal{M}_s$ and $\mathcal{M}_v$ describe the $RN\gamma$ system in terms of the isospin of the photon rather than the isospin of the nucleon.

Experimental information on the decay amplitudes $\mathcal{M}_p$ and $\mathcal{M}_n$ exists in form the of measured helicity amplitudes $A^{p/n}_{\frac{1}{2}}$ and $A^{p/n}_{\frac{3}{2}}$. They describe the transition of the photon-proton and the photon-neutron system to a resonance state with $j_z = \frac{1}{2}$ or $\frac{3}{2}$, where the quantization axis is defined along the direction of the photon momentum. From the helicity amplitudes the isoscalar and isovector part of the coupling are constructed in exactly the same way as shown in Eq. 10.5 for the Feynman amplitudes. The helicity amplitudes are known from experiment at the pole-mass of the resonance, allowing the determination of g_s and g_v.

To this end we introduce the γ-width $\Gamma^{\gamma}_{s/v}$, which – using the normalization from [46] – is defined in terms of the helicity amplitudes $A_{s/v}$ in the following way:

$$\Gamma^{\gamma}_{s/v}(m_R) = \frac{q^2}{\pi}\,\frac{2m_N}{(2j_R+1)m_R}\left(|A^{s/v}_{\frac{1}{2}}|^2 + |A^{s/v}_{\frac{3}{2}}|^2\right) \quad , \tag{10.6}$$

with j_R and m_R denoting spin and pole-mass of the resonance. Note that after the angular integration has been performed no interference terms between $A^{\frac{1}{2}}$ and $A^{\frac{3}{2}}$ appears in Eq. 10.6.

Clearly, $\Gamma^{\gamma}_{s/v}$ can also be expressed using Feynman amplitudes:

$$\Gamma^{\gamma}_{s/v}(k^2) = \frac{1}{(2j_R+1)}\,\frac{q}{8\,\pi\,k^2}\,|\mathcal{M}_{s/v}|^2 \quad , \tag{10.7}$$

where $\sqrt{k^2}$ is the invariant mass of the resonance and q the momentum of the photon in the rest frame of the resonance. After summing over the photon polarizations, $|\mathcal{M}_s|^2$ assumes the following form:

$$|\mathcal{M}_s|^2 = 4\,m_N\,m_R\,\kappa\,g_s^2\,q^2\,F(k^2) \quad . \tag{10.8}$$

The same relation holds for $|\mathcal{M}_v|^2$ with g_s replaced by g_v. For the formfactor $F(k^2)$ at the $RN\gamma$ vertex we assume the following functional dependence as given by Eq. 3.23 in Chapter 3. For the cutoff parameter we take $\Lambda = 1$. If we consider on-resonance decays ($\sqrt{k^2} = m_R$) this formfactor is equal to 1. The numerical factor κ depends on the quantum numbers of the resonance. For isospin-$\frac{1}{2}$ resonances the values for κ are listed in Table 10.2. In the case of Δ resonances they need to be multiplied by a factor of $F^2 = \frac{2}{3}$ due to isospin. The two expressions Eqs. 10.6 and 10.7 can now be equated allowing to solve for $g_{s/v}$:

$$g^2_{s/v} = \frac{4}{\kappa}\,\frac{|A^{s/v}_{\frac{1}{2}}|^2 + |A^{s/v}_{\frac{3}{2}}|^2}{q} \begin{cases} 1 & \text{for} \quad I_R = \frac{1}{2} \\ \frac{1}{F^2} & \text{for} \quad I_R = \frac{3}{2} \end{cases} \quad . \tag{10.9}$$

	$f_{RN\rho}$ Arndt	$f_{RN\rho}$ Feuster	$f_{RN\rho}$ PDG	$f_{RN\rho}$ Manley1	$f_{RN\rho}$ Manley2	$f_{RN\rho}$ PDG
$D_{13}(1520)$	3.44±0.18	2.67	3.42±0.20	6.67±0.78	5.79±0.68	6.66±1.26
$S_{31}(1620)$	0.89±0.42	0.10	0.69±0.23	2.14±0.30	2.06±0.28	2.61±1.01
$S_{11}(1650)$	0.70±0.08	0.59	0.57±0.31	0.47±0.19	0.45±0.18	0.79±0.31
$F_{15}(1680)$	3.48±0.39	—	3.14±0.37	6.87±1.57	6.36±1.45	7.33±2.29
$D_{33}(1700)$	3.96±0.77	3.68	4.02±0.62	1.96±0.67	1.93±0.67	4.91±1.57
$P_{13}(1720)$	0.25±0.42	0.93	0.19±0.79	13.17±3.35	12.09±3.17	7.42±1.64
$F_{35}(1905)$	2.47±0.55	—	2.56±0.75	17.97±1.14	17.57±1.12	14.19±3.10
$P_{33}(1232)$	13.40±0.2	11.96	13.29±0.28	—	—	—-

Table 10.1: Listed are the hadronic coupling constants $f_{RN\rho}$ obtained from the isovector electromagnetic amplitudes through a VMD analysis. The first column shows the results employing the helicity amplitudes from Arndt *et al* [6]. In the second column the helicity amplitudes from Feuster *et al* [36] are used instead and the third column shows the results obtained from the PDG estimates [46]. For comparison we show also the values for $f_{RN\rho}$ resulting from direct fits to the partial decay width $\Gamma_{RN\rho}$. The values for $\Gamma_{RN\rho}$ are taken from Manley *et al* [89] (4th column) and PDG (6th column), the ρ decay is parameterized according to Eq. 10.12. To point out further inherent uncertainties in the analysis, we show in the 5th column the results from a fit to Manley's values for the partial width, using the parameterization from Eq. 10.13 of the ρ spectral function.

Again, in the case of Δ resonances an additional factor α^2 needs to be introduced.

Thus it is possible to obtain $g_{s/v}$ from helicity amplitudes. The hadronic couplings $f_{RN\omega(\rho)}$ are then readily deduced from the VMD relation Eq. 10.1. The corresponding values are listed in Tables 10.1 and 10.2.

A modified version of VMD (called VMD1 in [130]) contains also a direct coupling between hadrons – in our case baryon resonances – and the photon. In particular, at the photon point $q^2 = 0$ the photon-resonance interaction proceeds without intermediate vector mesons, whereas the decay into a massive photon consists of both a direct coupling term and a term with an intermediate vector meson. In principle, it would be preferable to perform an analysis such as ours within the framework of the modified version of VMD by studying – currently unavailable – dilepton production data on the nucleon. This process involves massive photons and would, in combination with the data for real photons, allow for a separation of the direct photon and vector meson contributions. As a further advantage, the coupling strength of the vector mesons then does not need to be extrapolated over the large mass range from the photon point to the on-shell mass of ρ and ω meson.

10.3 Results for the ρ: How Reliable is VMD ?

In this section we study the applicability of VMD in the resonance region. This is done for the isovector part of the analysis, where the VMD predictions for $f_{RN\rho}$ can be compared with the measured resonance decay width into the $N\,\rho$ channel.

We consider all resonances with $j_R < \frac{7}{2}$, for which both the hadronic decay widths into $N\,\rho$ and the helicity amplitudes are known. This excludes a few light resonances like the $S_{11}(1535)$ and the $P_{33}(1600)$, for which only upper limits for the $N\,\rho$ branching ratio exist

[46]. For both the helicity amplitudes and for the partial $N\rho$ decay width we use different parameter sets in order to provide an estimate for the experimental uncertainties entering this analysis. The helicity amplitudes are taken from Arndt *et al* [6] and the PDG [46]. Furthermore we use the values obtained in the work of [36], which is of particular interest as it represents the only available approach which describes simultaneously hadronic-and electromagnetic reactions over the full energy region of interest here. The ρ decay widths are taken from the analysis of Manley *et al* [90, 89] and the PDG [46]. Furthermore, we study the additional model dependence introduced by different parameterizations of the spectral function of the ρ meson.

The hadronic coupling constant $f_{RN\rho}$ is obtained via the following expression for the $R \to N\rho$ decay width (taken on the pole mass of the resonance), see also Eq. 3.18 in Chapter 3.2:

$$\Gamma_{R\to N\rho} = \frac{1}{8\pi m_R^2}\,\frac{1}{2j_R+1}\int\limits_{2m_\pi}^{m_R-m_N} dm\, 2m\, A_\rho(m)\,|\mathcal{M}_{R\to N\rho}|^2\, q \quad . \tag{10.10}$$

The decay amplitude $\mathcal{M}_{R\to N\rho}$ is obtained from the same Lagrangians as in the electromagnetic case and is proportional to $f_{RN\rho}$ [107]. q is the three momentum of the ρ meson in the rest frame of the resonance. Note that there is no formfactor in Eq. 10.10 because we consider the on-resonance decay.

The spectral function of the ρ meson $A_\rho(m)$ is taken as:

$$A_\rho(m) = \frac{1}{\pi}\,\frac{m\,\Gamma(m)}{(m^2-m_\rho^2)^2+m^2\,\Gamma^2(m)} \quad . \tag{10.11}$$

The decay into $N\rho$ of low-lying resonances, for example the $D_{13}(1520)$, proceeds mainly through the low-mass tail of A_ρ. The shape of the tail is quite sensitive to the parameterization of the ρ decay width. To study the effect on $f_{RN\rho}$ we compare two different parameterizations of the ρ decay width:

$$\Gamma(m) \;=\; \left(\frac{m_\rho}{m}\right)^2 \Gamma_0 \left(\frac{\mathbf{p}_m}{\mathbf{p}_{m_\rho}}\right)^3 \tag{10.12}$$

and

$$\Gamma(m) \;=\; \left(\frac{m_\rho}{m}\right) \Gamma_0 \left(\frac{\mathbf{p}_m}{\mathbf{p}_{m_\rho}}\right)^3 \frac{1+r^2\,\mathbf{p}_{m_\rho}^2}{1+r^2\,\mathbf{p}_m^2} \quad . \tag{10.13}$$

The first version follows from a one-loop approximation of the self energy of the ρ meson [107, 62], the second one is taken from the PDG [46]. m is the invariant mass of the ρ meson, $m_\rho = 0.768$ GeV its pole mass and $\Gamma_0 = 150$ MeV its decay width on the pole mass. $\mathbf{p}_{m_\rho}\,(\mathbf{p}_m)$ denotes the 3-momentum of the pions measured in the rest frame of a decaying ρ meson with mass $m_\rho\,(m)$. The range parameter r, appearing in the second expression has the numerical value $r = 5.3/\text{GeV}$ [46].

In Table 10.1 the results for the coupling constants and the corresponding error-bars - which are calculated from the error-bars assigned to the partial decay width and the helicity amplitude in the respective analysis - are given. As a general tendency, our finding is that VMD works well within a factor of two. It tends to somewhat underestimate the coupling constants, leaving some room for an additional direct coupling of the resonance

to the photon. This can be seen particularly well in the case of the $D_{13}(1520)$ and the $F_{15}(1680)$, which are the most prominent resonances in photon-nucleon reactions, and whose ρ decay widths are also well under control. Note that in the case of the $S_{31}(1620)$ and the $P_{13}(1720)$ large discrepancies occur between the VMD predictions based on different sets of helicity amplitudes, thus reflecting the uncertainties inherent in this analysis. The helicity amplitudes from Arndt [6] and PDG [46] produce nearly identical results for the ρ coupling of the $P_{13}(1720)$, which might seem suprising as the helicity amplitudes from both works are very different. However, most of these differences cancel out in the isovector channel after proton- and neutron- amplitudes have been subtracted from each other (see Eq. 10.5). In the isoscalar sector this cancellation does not occur and both sets lead to very different predictions for $f_{RN\omega}$, see Sect. 10.4.

For the $P_{13}(1720)$ and the $F_{35}(1905)$ VMD is off by an order of magnitude. We argue that this mismatch does not hint to a failure of VMD, but has to be attributed to the unsatisfactory experimental information on these two resonances. Comparing the helicity amplitudes of the $P_{13}(1720)$ obtained from different analyses [46, 36] reveals that neither their sign nor their magnitude are under control at all. Also the partial decay width into the ρN channel is subject to large uncertainties, here the PDG and Manley differ by about a factor of three [46, 90, 89]. Obviously, the experimental observation of this resonance is very complicated and its parameters might be sensitive to the details of the underlying theoretical model, such as the treatment of the non-resonant background. For a conclusive VMD analysis of these resonances it is therefore mandatory to enlarge the data base and to describe hadronic- and photoinduced reactions within one model. In [38] a VMD analysis for exactly these resonances was performed, leading to the general conclusion - in contradiction to this work - that VMD is not at all reliable in the resonance region.

Different parameterizations of the ρ decay width mainly influence the coupling constants of low-lying resonances. Since the PDG parameterization of the ρ decay (see Eq. 10.13) distributes more strength at invariant mass below the ρ meson pole mass, it leads to smaller values for the coupling constant, thus leading to an improved agreement between VMD and the hadronic fits. This effect is most notable for the $D_{13}(1520)$ (see fourth and fifth column in Table 10.1).

In [34] it has been proposed that the discrepancy of VMD and hadronic models concerning the extraction of the ρ coupling constant can be resolved by extending the VMD model. Within this model the coupling of the (isovector) photon to hadronic currents proceeds not only via the ρ meson, but also via the excited ρ' states. This process involves the unknown coupling constants of the ρ' states to the hadronic current. By extending the their VMD model to large space-like 4-momenta Q^2, constraints on these coupling constants are derived from the requirement that the resulting electromagnetic form factor scales like $1/Q^6$ as motivated from quark models. This requires a cancellation of terms which is only possible when the coupling constants are related to each other. Ultimately improved predictions from the VMD model are generated. For example, the discrepancy factor of 2 for the $D_{13}(1520)$ resonance is explained this way. While this sound in principle quite appealing, one should realize that a certain arbitrariness arises from the fact that only two excited ρ meson states are considered in [34] and that their scheme looses any predictive power if more ρ states included. Then the large Q^2 limit does not yield enough constraints on the coupling constants any more.

At this point we also want to comment (again) on the work published in [84]. There

the applicability of VMD has been elevated as a guiding principle for the description of hadronic processes involving vector mesons. As mentioned in Chapter 4.1, there a very small coupling of the ρ meson to the $D_{13}(1520)$ is found. To be more quantitative, a value of $\Gamma_{N\rho} \approx 2$ MeV is reported. This is actually in reasonable agreement with our VMD prediction, which would give a value $\Gamma_{N\rho} \approx 5$ MeV, since within VMD the coupling constant comes out to be roughly half the size as compared to the hadronic fit. This shows that in [84] the $N\rho$ coupling is nearly entirely constrained from photon data.

Summarizing the results, we conclude that VMD can be applied in the resonance region on a phenomenological basis. We have shown that for the coupling constants $f_{RN\rho}$ it leads to an approximate agreement with values adjusted to the hadronic decay width $\Gamma_{RN\rho}$ with a tendency to somewhat underestimate these values. Therefore, our approach should yield reasonable predictions – at least for the lower limits – of the unknown coupling constants $f_{RN\omega}$.

10.4 Results for the ω: Strong Coupling of Subthreshold Resonances

In this section we present our results for the coupling constants $f_{RN\omega}$ following from the VMD analysis and discuss their compatibility with experimental information obtained from pion- and photon-induced ω-production cross sections.

All nucleon resonances with $j_R < \frac{7}{2}$, for which helicity amplitudes have been extracted, are included. Thus we consider only one resonance above the $N\,\omega$ threshold in our analysis, namely the $D_{13}(2080)$. Three different parameter sets for the helicity amplitudes are used, the results from the analysis of Arndt *et al* [6] and Feuster *et al* [36] as well as the values listed in the PDG [46]. The corresponding results for $f_{RN\omega}$ together with the error-bars are given in Table 10.2. We find a strong coupling to the $N\,\omega$ channel in the S_{11}, D_{13} and F_{15} partial waves; especially the $S_{11}(1650)$, the $D_{13}(1520)$ and the $F_{15}(1680)$ resonances show a sizeable coupling strength to this channel. In most cases the three parameter sets for the helicity amplitudes lead to similar results. As in the case of the ρ meson, however, for some resonances ($P_{11}(1440)$, $S_{11}(1650)$, $P_{11}(1710)$ and $P_{13}(1720)$) the differences are more pronounced. In particular, for the $P_{13}(1720)$ and the $P_{11}(1710)$ the poor experimental situation does not allow for a reliable extraction of the coupling strength, thus emphasizing the difficulties concerning the $P_{13}(1720)$, which were already discussed in the previous section. The relatively large coupling constant for the $D_{13}(1520)$ might at first seem surprising as the helicity amplitudes suggest that its electromagnetic decay is mainly an isovector one, corresponding to a small value for g_s. However, $f_{RN\omega}$ is proportional to g_ω (see Eq. 10.1), which is about three times larger than g_ρ. As a result, the ρ and ω coupling are of the same size, but with a much larger error-bar for the ω coupling.

It is noteworthy that the resonances with the largest coupling are well below the $N\,\omega$ threshold. Subthreshold resonances in the $N\,\omega$ channel are also reported elsewhere [84, 37, 114, 34]. In [37, 84] it is shown that within a coupled-channel analysis the description of $\pi\,N$ scattering enforces resonant structures in the $N\,\omega$ channel. As in our work, strong contributions from the S_{11} and D_{13} partial waves are found. Quantitatively, both approaches yield quite different predictions for the coupling strength of the $D_{13}(1520)$, however. Whereas our VMD analysis predicts a coupling strength of about 3 (see Table

	κ	Arndt	Feuster	PDG
$S_{11}(1535)$	4	1.27±1.58	1.36	0.76±1.23
$S_{11}(1650)$	4	1.59±0.29	0.56	1.12±1.09
$D_{13}(1520)$	8/3	2.87±0.76	2.28	3.42±0.87
$D_{13}(1700)$	8/3	− − −	1.88	0.65±2.76
$D_{13}(2080)$	8/3	− − −	− − −	1.13±1.46
$P_{11}(1440)$	4	0.61±0.68	1.26	0.85±0.48
$P_{11}(1710)$	4	0.14±0.85	0	0.20±1.02
$P_{13}(1720)$	8/3	0.29±1.30	2.18	1.79±3.18
$F_{15}(1680)$	4/5	6.89±1.38	− − −−	6.52±1.49

Table 10.2: The coupling constants $f_{RN\omega}$ as extracted from the helicity amplitudes from the Arndt *et al* [6](2nd column), Feuster *et al* [36] (3rd column) and the PDG group [46] (4th column). In the first column we give the values for κ (see Eq. 10.9).

10.2), in [37] a value of $f_{RN\omega} \approx 6.5$ is given. This value is confirmed in the subsequent analysis in [84]. At the same time it is found in a quark model calculation [114] that the coupling constant of this resonance should be $f_{RN\omega} \approx 2.6$, which is surprisingly close to our result. However, from their quark model calculation the authors of [114] obtain initially coupling constants for hadronic Lagrangians which display very different energy dependences compared to ours. To be specific, in the case of the $D_{13}(1520)$ close to threshold ω and nucleon couple in a relative d-wave in their formalism, rather than forming an s-wave state as following from our Lagrangian, see Eq. 10.2 (which for example has also been employed in [37]). Thus a direct comparison of the results as done in [114] is possible only after simplifying assumptions, if at all.

A complete coupled-channel analysis of pion and photo induced ω production has been carried out in the coupled channel K-matrix analysis presented in [105, 104]. There the resonance coupling to $N\omega$ is determined directly from a fit pion- and photoinduced ω production data. Besides direct constraints from ω data, further constraints arise from unitarity, i.e. from the fact that via the inelasticity $\pi N \to \pi N$ amplitude upper bounds exist for the $\pi N \to \omega N$ amplitude. As a result, the two resonance with the largest coupling to $N\omega$ are found to be the $P_{11}(1710)$ and the $P_{13}(1720)$, both of which couple only weakly in the VMD approach, which in addition yields large uncertainties for these two states (cf. Table 10.2). Therefore the VMD predictions for these resonances should be considered with great care. On the other hand, states that within VMD are found to couple substantially to $N\omega$ like the $D_{13}(1520)$ or the $S_{11}(1535)$ play only a negligible role in the analysis of [105, 104]. This may indicate a failure of VMD also for these states. It is however not clear up to which extent any description of ω data is able to pin down the contribution from resonances that are so far below the threshold.

A direct experimental observation of a resonant coupling of subthreshold resonances is very complex, since the resonances can add to the cross-sections only through the high-mass tails of their mass distribution and are therefore hard to disentangle from background effects. Sensitivity to the contribution of subthreshold resonances in ω production experiments can probably only be achieved by studying polarization observables. The current data do not permit such a project, however. As was pointed out in various previous works [19, 18, 85], an analysis of dilepton production on the nucleon in combination with VMD might provide further insight on this issue.

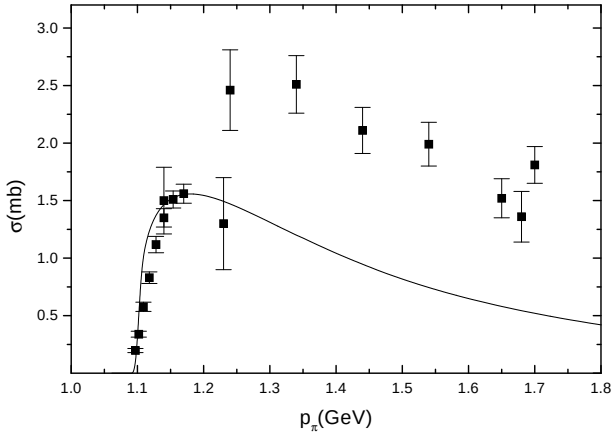

Figure 10.2: Total cross-section for the reaction $\pi^- p \to \omega n$. The data are taken from [8].

In spite of these difficulties, it is still rewarding to compare the VMD predictions with existing data on the reactions $\pi^- p \to \omega n$ and $\gamma p \to \omega p$. Thus it is possible to infer if the predicted coupling constants of the subthreshold resonances produce a satisfactory overall agreement with data above the threshold. Comparison with data allows also to discuss the results for the $D_{13}(2080)$, the only resonance in our analysis above threshold. Based on recent data from photoproduction experiments, which display a richer structure than expected within a simple meson-exchange model, the search for resonances in the $N\omega$ channel has so far concentrated on the mass range of approximately $1.8 - 2$ GeV. At the current stage the data do not allow to pin down the quantum numbers of the involved resonances, however, and a variety of predictions exist [23, 135, 134, 25]. The $D_{13}(2080)$ is not amongst them. In contrast to the photoproduction data, no experimental signature of a coupling of baryon resonances to the $N\omega$ channel above the threshold has been detected in pion induced reactions [8]. We find for the $D_{13}(2080)$ an ω decay width of about 70 MeV and argue that its contribution to both reactions is too small to be seen in experiment.

As a first approximation, we take the full production amplitude as an incoherent sum of *Breit-Wigner* type amplitudes, describing s-channel contributions:

$$\sigma_{ab} = \sum_R \frac{2j_R+1}{(2j_N+1)\Omega_a} \frac{\pi}{k_a^2} \frac{\Gamma_a \Gamma_b}{(E_a - E_R)^2 + \Gamma_{tot}^2/4} \quad . \tag{10.14}$$

Here a stands for the incoming channel ($\pi^- p$ or γp) and b for the ωN channel. $\Gamma_{a(b)}$ denote the respective partial decay width of the resonance and Γ_{tot} its total decay width, taking into account the ωN decay as well. The energy dependence of the photon and the ω decay amplitudes is obtained from the Lagrangians given in Eq. 10.2 and the formfactor of Eq. 3.23 with $\Lambda = 1.0$. Whenever possible, $f_{RN\omega}$ is obtained from the helicity amplitudes from Arndt *et al*, otherwise the PDG estimates are used. For the remaining channels we take the parameterization from Manley *et al*. In Eq. 10.14 Ω_a is 1 for the pion and 2 for the photon. k_a is the cm-momentum of the particles in channel a and E_a denotes their cm-energy. All resonances listed in Table 10.2 are included. We stress that the only free parameter is the cutoff parameter Λ.

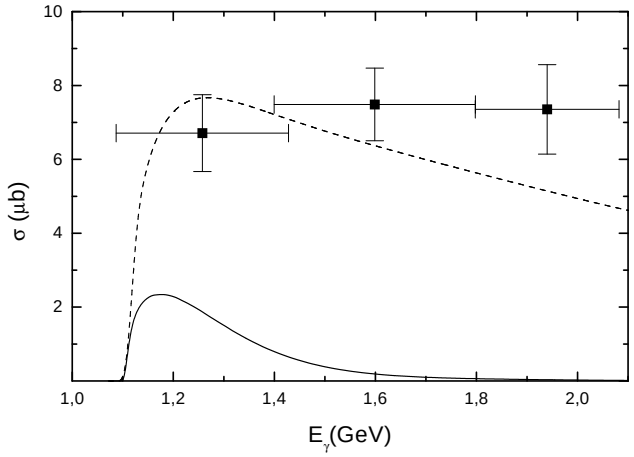

Figure 10.3: Total cross-section for the reaction $\gamma\, p \to \omega\, p$. The data are taken from [1].The straight line shows the cross-section resulting from the resonance model, where the dashed line indicates the sum of resonance and pion-exchange contributions.

The results for both reactions are shown in Fig. 10.2 and Fig. 10.3. The data for the π-induced reaction are taken from [8] and we use the photoproduction data of [1]. The cross-section for $\pi^-\, p \to \omega\, n$ is reproduced rather well, especially near threshold, whereas at high energies some strength is missing. This is in approximate agreement with the findings of the authors of [37], who are able to give a satisfactory description of this process around threshold in terms of subthreshold resonances. One can therefore conclude that the excitation of subthreshold resonances constitutes an essential ingredient to the production mechanism. This interpretation is confirmed by the fact that it is hard to understand this process in terms of non-resonant amplitudes only. Already the contribution from ρ_0 exchange overestimates the data; only by suppressing the amplitudes by the introduction of very restrictive form factors a rough agreement with experimental data can be achieved [86]. Similar problems have been reported in [62] in a model that includes all Born terms. The contribution coming from the only resonance above threshold – the $D_{13}(2080)$ – is about 0.1 mb, roughly 10% of the total cross-section. This is certainly too small to produce a distinguishable resonant structure in the total cross-section.

On the other hand, the photoproduction data can not be saturated within the resonance model. In particular, it seems futile to look for the $D_{13}(2080)$ in this reaction. It is commonly assumed that the π^0-exchange as invoked in [40] plays a key role in the photoproduction. In the coupled channel analysis of [105], the same conclusions concerning the importance of that diagram are drawn. Therefore we – incoherently – added π_0 exchange to the resonance contribution, using the same parameters as given in [40]. As shown in Fig. 10.3 the sum of both mechanisms yields a qualitative explaination of the data over the energy range under consideration.

It is not surprising that the resonance contribution is more likely to produce lower bounds for the cross-sections. We already discussed in Sect. 10.3, that the VMD analysis tends to underestimate the hadronic coupling constants. Also, at energies above the ωN threshold, the helicity amplitudes of only a few resonances are known and the experimentally observed cross-sections have to be explained by additional production mechanisms, such as the π-exchange in the photoproduction. Keeping this in mind, the predictions of

the resonance model are in reasonable agreement with the data and can be viewed as a first confirmation of the VMD analysis. Up to which extent the findings of [104, 105] – predicting a strong coupling of $P_{11}(1710)$ and $P_{13}(1720)$ to $N\,\omega$ and therefore indicating that at least these two resonances can not reliably be determined from VMD – would spoil this conclusion also for the other resonances is not clear.

10.5 The ω Meson in Nuclear Matter

In the previous section we discussed the relevance of resonances in the $\omega\,N$ channel for an understanding of ω production data. Here we study up to which extent the existence of these resonant states affects the properties of ω mesons in nuclear matter. Of particular interest in this context is the fact that the VMD analysis predicts a strong coupling of subthreshold resonances, since in the case of the ρ meson it is widely acknowledged that its in-medium properties are dominated by low lying resonances, especially the $D_{13}(1520)$.

The in-medium properties of the ω meson can be read off its spectral function, which is defined as:

$$A_\omega^{med}(q_0,\mathbf{q}) = \frac{1}{\pi}\,\frac{\mathrm{Im}\,\Pi_{tot}(q_0,\mathbf{q})}{(q_0^2-\mathbf{q}^2-m_\omega^2-\mathrm{Re}\,\Pi_{med}(q_0,\mathbf{q}))^2+\mathrm{Im}\,\Pi_{tot}(q_0,\mathbf{q})^2}. \tag{10.15}$$

Energy and three-momentum of the ω meson are denoted by q_0 and $\mathbf{q}$. The total self energy of the ω meson Π_{tot} is the sum of the vacuum and the in-medium self energies Π_{vac} and Π_{med}. In this work we neglect $\mathrm{Re}\,\Pi_{vac}$ and approximate $\mathrm{Im}\,\Pi_{vac}$ with the dominating $3\,\pi$ decay width. We assume that this decay may only proceed via an intermediate ρ meson. The coupling constant $f_{\omega\rho\pi}$ is adjusted to reproduce the vacuum decay width of 8.41 MeV [46].

To lowest order in the nuclear density ρ_N, the in-medium self energy of the ω meson Π_{med} in symmetric nuclear matter is given by:

$$\Pi_{med} = \rho_N\,T_{\omega\,N}, \tag{10.16}$$

where $T_{\omega\,N}$ is the spin/isospin averaged $\omega\,N$ forward scattering amplitude. We approximate the scattering amplitude as a sum over all resonances which are discussed in this work and determine the resonance contributions in a non-relativistic approach.

For further details of the calculation the reader may consult our previous publication on the ρ meson [107, 109]. Both calculations are carried out within the same framework, differences appearing only in some minor points: First, the explicit values for the coupling constants and isospin factors are different. More crucial, we now evaluate the self energy in the cm-frame rather than in the rest frame of the nucleon. We do so since it has been demonstrated in [109] that thus a much better approximation of a relativistic calculation is achieved. As explained in [109], this leads in general to a reduction of the results. Finally, at the $\omega\,N\,R$ vertex the same formfactor is taken as in Eq. 3.23, in contrast to the choice in [107].

In Fig. 10.4 we show the spectral function for both an ω meson at rest and moving with a momentum of 0.4 GeV with respect to the nuclear medium. The most obvious observation is that our model predicts an in-medium ω meson which survives very well as a quasi-particle. At rest, its peak position is slightly shifted upwards by about 20 MeV, due to level-repulsion. The in-medium width is roughly 40 MeV as can be read off Fig. 10.5,

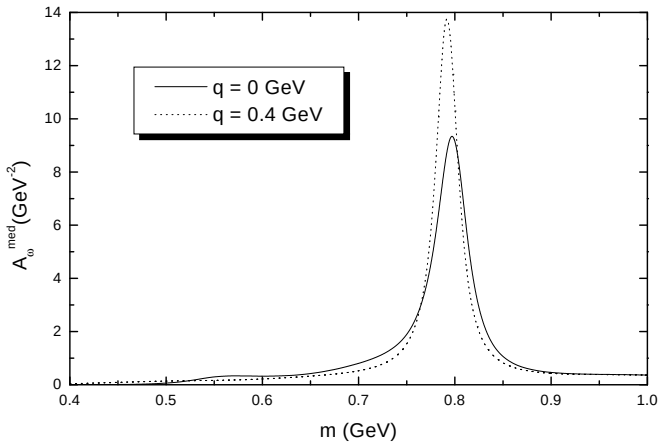

Figure 10.4: The spectral function of an ω meson in nuclear matter versus its the invariant mass m. Shown are results at $q = 0$ GeV (solid line) and at $q = 0.4$ GeV (dotted line). Only the transverse part is displayed. As discussed in the text, there is virtually no difference between transverse and longitudinal spectral function at 0.4 GeV.

where Π_{med} is depicted for an ω at rest. The ωN forward scattering amplitude contains all elastic and inelastic channels. In the previous section we demonstrated that our model can give a good description of the important πN channel close to threshold. This enhances our belief that the VMD approach yields reasonable results for the in-medium properties of the ω meson, especially for an ω at rest.

By construction, the in-medium self energy develops resonant structures in the subthreshold region. The most important contributions come from the $D_{13}(1520)$ and the $S_{11}(1650)$ resonances. In contrast to the case of the ρ meson, these structures translate only into small bumps in the spectral function, reflecting - as follows from the coupling constants - that the ω self energy is substantially smaller than that of the ρ meson.

Our value for the in-medium broadening of the ω meson is in approximate agreement with that obtained in [62] and – in a dynamical simulation – in [127] and [31]. Also in the coupled channel analysis of [37] an in-medium broadening of 40 MeV for the ω meson is reported. However, in this work the authors find that the ω spectrum displays a richer structure in the subthreshold region, which is not surprising since their coupling constant for the $D_{13}(1520)$ is much larger.

At higher momenta the influence of resonance-hole excitations gets reduced, see Fig. 10.4. Also, the longitudinal and transverse channel display a very similar behaviour (we therefore only show the results for the transverse channel). This is different from the case of the ρ meson, whose spectral function at large momenta receives a strong broadening in the transverse channel from the the coupling of p-wave resonances, for example the $P_{13}(1720)$, whilst the longitudinal mode is only slightly modified. In the case of the ω meson however, only the $F_{15}(1680)$ shows a sizeable coupling strength.

In light of the results from [104, 105] predicting a strong coupling of the p-wave resonances $P_{11}(1710)$ and $P_{11}(1720)$, the results at finite momenta are to be taken with some care. In particular, we expect a larger broadening of the ω. For an ω at rest, however, the p-wave states do not contribute to the self energy and therefore our results are not affected.

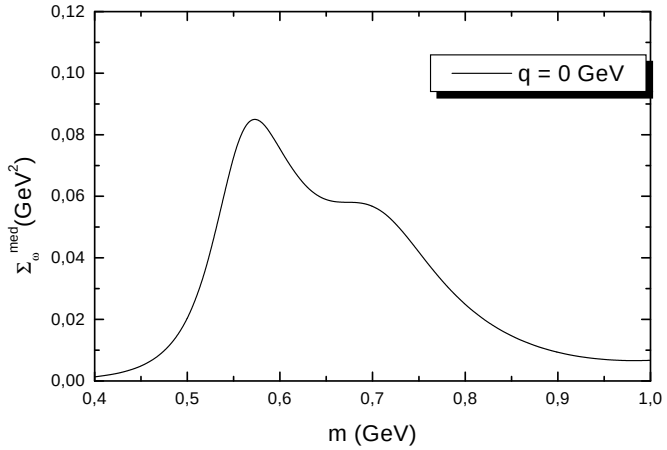

Figure 10.5: In-medium self energy of an ω meson at rest as a function of its invariant mass m. One clearly sees resonant structures from the excitation of the $D_{13}(1520)$ and the $S_{11}(1650)$.

We have already mentioned that the ω decay in vacuum proceeds mainly via an intermediate ρ meson. Due to kinematics, only the low-mass tail of the ρ mass spectrum is involved in this process. Consequently, if a lot of ρ strength is shifted to smaller invariant masses in the nuclear medium – as is generally believed, see for example [107, 109, 122] – the ω meson will receive additional broadening. We have estimated this effect by replacing the vacuum spectral function of the ρ with the in-medium one as given in [109] for the calculation of the ω decay. To lowest order in the density, this corresponds to scattering processes like $\omega N \to \pi R$, where R stands for any baryon resonance included in the calculation in [109]; such processes have so far not been included in any calculation. We find an additional in-medium width for the ω of about 40 MeV at the ω mass from this process. It has to be pointed out, however, that we did not take into account the corresponding mass-shift of the ω meson. Since the ω decay width varies rapidly as a function of its mass, this is a strong simplification.

Chapter 11

Summary & Outlook

We have constructed a model that allows for a combined description of in-medium modifications of hadrons. The constituents of the model are on the meson sector the pion, η meson and ρ meson and on the baryonic sector all resonances that couple at least to one of these states and the nucleon. Our previous work in this direction [107] has been extended and improved in several ways: The basis space of included states has been significantly enlarged. Due to the use of dispersion relations the spectral functions of all states are guaranteed to remain normalized both in the nuclear medium and in the vacuum. Special care has been taken with respect to the (non-relativistic) treatment of short-range correlations (SRC), in particular in the s-wave sector. This was motivated by the fact that a realistic description of the in-medium properties of the $P_{33}(1232)$ requires such repulsive mechanisms.

For the ρ meson we find a significant shift of spectral strength down to smaller invariant masses generated by its coupling to the $D_{13}(1520)N^{-1}$ state. In particular at smaller momenta, the coupling to this state leads to a pronounced double-peak structure in the spectral function. In order to corroborate this finding we have tested it against variations of the coupling strength and against possible effects from SRC. As a result we find that the results remain quite stable when varying the width within ranges suggested by different analyses of pion-nucleon scattering. Also SRC do not qualitatively change the results. At finite momenta, the in-medium properties of the ρ meson are influenced not only by the $D_{13}(1520)$ but also by some other higher lying resonances and our model predicts a different momentum dependence of transverse and longitudinal modes. In the transverse channel we find that the spectral function is characterized by a substantially broadened peak, whereas in the longitudinal channel the medium modifications get weaker and at momenta $\mathbf{q} \geq 0.8$ GeV the vacuum spectral function is recovered in this channel. The self-consistent iteration scheme mainly affects the results at low momenta and smears out the $D_{13}(1520)N^{-1}$ peak. Thus, by and large the central findings from our previous calculation [107] can be confirmed, while in particular at finite momenta the effects from the iterations are weakened. We have also calculated the momentum integrated dilepton rate at densities and temperatures typically encountered at SPS energies. The results suggest that our model is able to generate the observed shift of spectral strength down to smaller invariant masses.

For the pion we reproduce the essential features of the Δ-hole model, i.e. at finite momenta around $0.3 - 0.6$ MeV the pion spectral function is dominated by a complicated peak structure which is derived from the coupling of the pion to NN^{-1} and $P_{33}(1232)N^{-1}$

states. Going beyond the usual Δ-hole model we have also investigated the effects of coupling the pion to other resonance-hole states. The coupling of these states is not sufficient to generate distinct peaks, but it nonetheless produces a smooth background that influences the detailed structure of the pion spectral function. Turning to the η meson, we have calculated both the optical potential – which is of relevance for a quantitative analysis of η-mesic nuclei – and its spectral function. Based on reasonable predictions for the ηN scattering length, we arrive at a potential that provides rather strong binding relative to the life-time of the η. On a quantitative level the inclusion of medium modifications of the $S_{11}(1535)$ is found to be important. The spectral function of the η meson exhibits an interesting momentum dependence, receiving attraction at small momenta and repulsion at large momenta ($\mathbf{q} \approx 0.8$ GeV), while in the intermediate momentum region we observe a significant broadening of the η meson.

Turning to the baryon resonances, our model is able to reproduce the in-medium properties of the $P_{33}(1232)$ resonance and we obtain a reasonable fit of the phenomenological spreading potential. Here the inclusion of SRC turns out to be absolutely crucial. We have tried to explain this finding in some detail. The contribution from three-body processes is found to be very small. Our results for the $D_{13}(1520)$ show some sensitivity on coupling parameters and the effects of SRC. Assuming both a large coupling of this resonance to the $N\rho$ channel (corresponding to $\Gamma_{N\rho} = 26$ MeV), and small effects from SRC leads to a significant total broadening of about $250 - 300$ MeV. If, on the other hand, $\Gamma_{N\rho} = 12$ MeV is taken in combination with a rather large value for the SRC, the in-medium broadening of the $D_{13}(1520)$ is much reduced. We do not find large contributions to the broadening from the pion sector. With these uncertainties in mind, the experimental and theoretical challenge is to pin down the unsettled parameters in more detail. Finally, for the $S_{11}(1535)$ we find only modest medium effects. Even though there is some uncertainty concerning the resonance parameters and the strength of SRC, we can exclude the appearance of large medium modifications on the basis of our model. It is interesting to mention that the main body of the broadening found for the $S_{11}(1535)$ is due to typical coupled channel effect: without the rearrangement of spectral strength in the ρ spectral function due to the $D_{13}(1520)$, the observed broadening would have been even smaller.

We have investigated the differences between a relativistic and a non-relativistic calculation of the ρ spectral function. Here the essential finding is that a properly performed non-relativistic reduction leads to very reasonable results for the meson self energies. The uncertainties due to relativistic effects are certainly much smaller than those related to poorly known resonance parameters. These results directly carry over to the other mesons. Also investigated was the effect of various relativistic couplings on the momentum dependence of the ρ spectral function. On a quantitative level, some dependency on the employed coupling was found. For more conclusive statements detailed information on the relative weight of these coupling schemes would be needed.

Some care has been taken to set up a self-consistent coupled channel analysis with normalized spectral functions. The effects of self-consistency should clearly have an influence on the density dependence of the in-medium properties. We have investigated this issue and found that for the $D_{13}(1520)$ already at small densities around $0.25\,\rho_0$ the low density expansion breaks down and terms of higher order become important. Also the in-medium properties of the mesons deviate from a low density expansion, which is either due to effects from self consistency (ρ meson, η meson) or the effects of SRC (pion). Such effects are already important at small densities $0.25\,\rho_0 - 0.5\,\rho_0$. Applying dispersion relations to

obtain the real part of the in-medium self energies turns out to induce only comparatively small corrections to the meson spectral functions. There also the normalization is essentially fulfilled already if the real part of the self energy is directly obtained from Feynman diagram. More important are the real parts of resonance self energies, where otherwise violations of the normalization condition in the order of $30 - 40\%$ can be found.

We have shortly discussed the effects of dropping baryon resonance masses resulting from nuclear mean fields. Those are found to be sizeable, which can be explained by the induced change of the normalization of the wave functions. In particular, the in-medium width of the baryon resonances tends to be reduced by such effects. One should, however, be aware of the large theoretical uncertainties related to this topic. In particular, one knows nearly nothing about the size of the relativistic mean field potentials for the baryon resonances.

Motivated by the fact that the ρ meson properties are strongly affected by the excitation of resonance-hole states, we have set up a resonance-hole model for the ω meson as well. No attempt has been made to consider effects from self consistency here. Since a coupling of baryon resonances to the $N\omega$ channel is not established experimentally, we have used helicity amplitudes in connection with VMD in order to generate estimates for the coupling strength. The resonance-hole excitations lead to a much weaker modification of the ω spectral function compared to the ρ meson, owing to smaller coupling constants which are not sufficient to produce distinct particle-hole branches. The resulting broadening of the ω meson is found to be in qualitative agreement with several other analyses.

Let us now turn to possible extensions of the model.

- In-medium decay $\omega \to \rho\pi$ and $\varphi \to \rho\pi$
  An interesting project would consist in a calculation of the in-medium decay $\omega \to \rho\pi$, using in medium spectral functions both for the pion and the ρ meson. Since in the vacuum this decay is suppressed from phase space, large effects can be expected in the medium due to the rearrangement of spectral strength in both channels. Similarly, one might also study the decay $\varphi \to \rho\pi$. These calculations could be carried out in a rather straightforward way.

- Testing the model
  In order to test the predictions of this model for ρ meson and $D_{13}(1520)$ it might be interesting to calculate some observables: Using a reliable description of $\gamma N \to \pi N$ and $\gamma N \to 2\pi N$, a calculation of nuclear photoabsorption could help to decide on the in-medium properties of the $D_{13}(1520)$. It would also be interesting to compare the results obtained with different parameter sets. By using a simple fireball model one might try to calculate dilepton spectra from heavy ion collisions. Last but not least, a QCD sum rule analysis could provide additional constraints on the size of coupling constants.

- Finite Temperature Effects
  An extension of our model to finite temperature involves two steps: 1) The diagrams considered so far are modified since the Fermi distribution function changes with temperature and since at finite temperature the nuclear ground state is also populated by resonances. 2) Whereas at finite density the hadron properties are driven by hadron-nucleon scattering processes, at finite temperature one has to consider hadron-pion scattering. The corresponding diagrams would have to be added to the

model. Whereas both points have – at least to some degree – been considered in the literature for the ρ meson, not much work has been done for the baryon resonances. When going to finite temperature, also the nucleon spectral function should be modified.

- $\Delta\pi$ decay channel
  For the sake of completeness one could modify the $\Delta\pi$ decay channel of the baryon resonances. This might have some effect on higher lying states, while it probably leaves the results for the $D_{13}(1520)$ more or less untouched.

- Relativistic Short-Range Correlations
  On a more theoretical level, it might be interesting to consider a relativistic extension of our model for short-range correlation. This is a very demanding exercise and has not been attempted in this thesis. Nonetheless, existing relativistic model for $P = +1$ states show that the non-relativistic limit is only recoved for both small momenta and energies. This is critical in particular when considering heavy resonances. Thus one can not expect that for SRC the non-relativistic reduction works as well as for the meson-nucleon scattering amplitudes.

- Model for NN scattering
  In an attempt to pin down uncertainties concerning the cutoff and short-range parameters, one might attempt a description of NN scattering. Reactions like $NN \to NN\pi$ or $NN \to NN\eta$ might help to find reasonable ranges for these parameters.

The first three points are likely to be the most interesting ones. A calculation of the in-medium width of the ω and ϕ meson would be interesting and could be quite easily done. Also finite temperature effects for baryon resonances would be an interesting object to study. However, here the technical complications are considerable. The most promising way to test the model parameters is a combined consideration of nuclear photoabsorption, heavy ion collisions and QCD sum rules. Ideally one can find one parameter which is in reasonable agreement with all three quantities, which support the predictive power of our model.

The last three points are less interesting. The implementation of the decay $R \to \Delta\pi$ can be easily done, but it will most likely not greatly affect the results. The other points are interesting from a theoretical point of view. They involve, however, a large effort and it is not guaranteed that at the end the model will be more quantitative.

Appendix A

Parameters

We use the following parameters:

coupling constant	$f_{NN\pi} = 1.0$	$f_{NN\eta} = 2.34$	$f_{NN\rho} = 7.8$	$f_{\Delta N\rho} = 10.5$
cutoffs [GeV]	$\Lambda_\pi = 1.0$	$\Lambda_\eta = 1.5$	$\Lambda_\rho = 1.5$	$\Lambda_g = 1.5$
short range	$g_\pi^{p,NN} = 0.6$	$g_\pi^{p,R_N R_M} = 0.45$	$g_\eta^{p,NN} = 0.6$	
	$g_\pi^s = (0, 0.1)$	$g_\rho^s = (0, 0.1)$	$g_\pi^d = (0, 0.4) = g_\pi^{pd}$	$g_\eta^s = (0, 0.1)$

Table A.1: Parameters used in the calculations.

Here the brackets denote the range within which we allow the respective parameter to vary. Note that at each vertex corresponding to short-range interactions we multiply a monopole form factor [7, 49]:

$$F_g(q^2) \;=\; \left(\frac{\Lambda_g^2}{\Lambda_g^2 - q^2}\right)^2 \quad . \tag{A.1}$$

The value for also Λ_g is also taken from this reference. Let us comment on theses choices for coupling constants and cutoff parameters. For the coupling constant $f_{\pi NN}$ hardly any uncertainties exist and a value of $f_{\pi NN} = 1$ can be found in various places, for example in [99, 7]. For $f_{NN\eta}$ and the cutoff Λ_η we take the values given in the work of [26], which was originally suggested in [88]. The values for $f_{\rho NN}$ and $f_{\rho N\Delta}$ lie within the ranges suggested in for example [49, 17, 99] and are a obtained by a mix of quark model considerations and fits to NN scattering. These fits also determine the approximately the values of the cutoff parameters, in particular the rather large value for Λ_ρ is suggested from those data, see for example [49].

The cutoff used in the form factor $F(k^2)$ of Eq. 3.23 for pseudoscalar (π, η) meson is taken to be $\Lambda = 1$ GeV.

	m	Γ_{tot}	$\Gamma_{N\pi}$	Γ_{N_ρ}	$\Gamma_{\Delta\pi}$	$\Gamma_{N\eta}$	$\Gamma_{N\omega}$	J	I	l_ϕ	l_V	Λ^s_ρ
$\Delta(1232)$	1.232	0.12	0.12	0	0	0	0	3/2	3/2	p	p	0.8
$N(1720)$	1.717	0.131	0.011	0.11	0	0	0	3/2	1/2	p	p	1.0
$N(1879)$	1.879	0.498	0.13	0.217	0	0	0.151	3/2	1/2	p	p	1.1
$N(1680)$	1.684	0.139	0.096	0.011	0.031	0	0	5/2	1/2	f	p	0.9
$\Delta(1905)$	1.881	0.329	0.041	0.282	0.06	0	0	5/2	3/2	f	p	1.4
$N(2000)$	1.903	0.494	0.039	0.369	0.086	0	0	5/2	1/2	f	p	1.4
$N(1535)$	1.534	0.151	0.077	0.005	0.004	0.066	0	1/2	1/2	s	s	0.8
$\Delta(1620)$	1.672	0.153	0.014	0.044	0.0095	0	0	1/2	3/2	s	s	0.9
$N(1650)$	1.659	0.173	0.154	0.005	0.008	0.006	0	1/2	1/2	s	s	0.9
$N(2090)$	1.928	0.415	0.043	0.203	0.167	0.002	0	1/2	1/2	s	s	1.5
$N(1520)$	1.524	0.124	0.073	0.026	0.025	0	0	3/2	1/2	d	s	0.9
$\Delta(1700)$	1.762	0.598	0.081	0.046	0.471	0	0	3/2	3/2	d	s	1.3
$\Delta(1940)$	2.057	0.460	0.081	0.046	0.471	0	0	3/2	3/2	d	s	1.8
$N(2080)$	1.804	0.447	0.104	0.114	0.229	0	0	3/2	1/2	d	s	1.6

Table A.2: List of all resonances which are taken into account in our calculation. All quantities are given in GeV. Apart from mass and width into the individual decay channels, we also give spin and isospin as well as the lowest orbital angular momentum needed in pseudoscalar (ϕ) or vector (V) meson scattering on a nucleon to form the resonance. In the last row we denote the cutoff of the form factor $F(s)$ at the $\rho\, N\, R$ vertex.

	m			$\Gamma_{N\pi}$			$\Gamma_{N\rho}$			$\Gamma_{\Delta\pi}$		
$\Delta(1232)(\star)$	1.232	1.234	1.232	112	118	120	0	0	0	0	0	0
$N(1720)(\star)$	1.717	1.716	1.720	50	6	22.5	333	110	112	0	0	—
$N(1879)$	1.879	—	—	130	—	—	217	—	—	0	—	—
$N(1680)(\star)$	1.684	1.679	1.68	97	88	84.5	16	10	12	32	31	29
$\Delta(1905)(\star)$	1.881	1.873	1.905	36	22	35	258	59	> 210	3	164	< 88
$N(2000)$	1.903	—	2.0	31	—	—	369	—	—	62	—	—
$N(1535)$	1.534	1.542	1.535	77	39	67.5	4.5	2	< 6	5	16	< 12
$\Delta(1620)(\star)$	1.672	1.617	1.620	14	64	37.5	45	23	24	95	56	67.5
$N(1650)(\star)$	1.659	1.689	1.650	154	150	105	5	28	12	9	12	6
$N(2090)$	1.928	1.822	2.090	41	42	—	203	92	—	166	12	—
$N(1520)(\star)$	1.524	1.518	1.52	73	78	66	26	11	24	25	33	24
$\Delta(1700)(\star)$	1.762	1.732	1.700	84	6	45	48	1	135	467	112	135
$\Delta(1940)$	2.057	—	1.940	81	—	—	162	—	—	217	—	—
$N(2080)$	1.804	2.003	2.080	103	139	—	116	64	—	228	867	—

Table A.3: List of all resonances which are taken into account in our calculation. All masses are given in GeV, the decay widths are given in MeV. We compare the results from the analysis of Manley *et al* [89](left), Vrana *et al* [124](middle) with the values quoted in the PDG [46](right). Those resonances with a $\star$ have already been included in [107].

Appendix B

Feynman Rules and Observables

B.1 γ Matrices and σ Matrices

B.1.1 σ matrices

The σ matrices are defined as follows:

$$\sigma_x \;=\; \begin{pmatrix} 0 & 1 \\ 1 & 0 \end{pmatrix} \;,\; \sigma_y \;=\; \begin{pmatrix} 0 & -i \\ i & 0 \end{pmatrix} \;,\; \sigma_z \;=\; \begin{pmatrix} 1 & 0 \\ 0 & -1 \end{pmatrix} \quad . \tag{B.1}$$

They fulfill the following (anti)commutation relations:

$$[\sigma_i, \sigma_j] \;=\; 2\,i\,\epsilon_{ijk}\,\sigma_k \quad , \quad \{\sigma_i, \sigma_j\} \;=\; 2\,\delta_{ij} \quad .$$

Adding up both relations one gets the important formula

$$\sigma_i\,\sigma_j \;=\; \delta_{ij} + i\,\epsilon_{ijk}\,\sigma_k \quad , \tag{B.2}$$

which simplifies the calculation of traces over σ matrices. We give now some trace relations:

$$\begin{aligned} Tr\,[\mathbb{1}] &= 2 \quad , \\ Tr\,[\sigma_i] &= 0 \quad , \\ Tr\,[\sigma_i\,\sigma_j] &= 2\,\delta_{ij} \quad , \\ Tr\,[\sigma_i\,\sigma_j\,\sigma_k] &= 2\,i\,\epsilon_{ijk} \quad , \\ Tr\,[\sigma_i\,\sigma_j\,\sigma_k\,\sigma_l] &= 2\,(\delta_{ij}\delta_{kl} - \delta_{ik}\delta_{jl} + \delta_{il}\delta_{jk}) \quad . \end{aligned} \tag{B.3}$$

The totally antisymmetric three-dimensional tensor ϵ_{ijk} is defined as:

$$\epsilon_{ijk} \;=\; \begin{cases} 1 & , \text{ if } i,\, j,\, k \text{ cyclic} \\ -1 & , \text{ if } i,\, j,\, k \text{ acyclic} \\ 0 & , \text{ if any of } i,\, j,\, k \text{ are equal} \end{cases} \quad . \tag{B.4}$$

The contractions of two ϵ tensors are given by:

$$\begin{aligned} \epsilon_{ijk}\,\epsilon_{mnk} &= \delta_{im}\,\delta_{jn} - \delta_{in}\,\delta_{jm} \quad , \\ \epsilon_{ijk}\,\epsilon_{mjk} &= 2\,\delta_{im} \quad , \\ \epsilon_{ijk}\,\epsilon_{ijk} &= 6 \quad . \end{aligned}$$

B.1.2 γ matrices

The γ matrices are defined by their anticommutator:

$$\{\gamma^\mu, \gamma^\nu\} = 2\, g^{\mu\nu} \quad . \tag{B.5}$$

Two combinations of the γ matrices are of particular interest:

$$\gamma_5 = i\, \gamma^0\, \gamma^1\, \gamma^2\, \gamma^3 \tag{B.6}$$

$$\sigma_{\mu\nu} = \frac{i}{2} [\gamma^\mu\, \gamma^\nu] \quad . \tag{B.7}$$

From the definition of γ^5 it follows directly that

$$\left\{\gamma^\mu, \gamma^5\right\} = 0 \quad . \tag{B.8}$$

The hermitian conjugate of the γ matrices is defined as:

$$\gamma^{\mu\,\dagger} = \gamma_0\, \gamma^\mu\, \gamma_0 \quad , \tag{B.9}$$

from which follows that γ^0, γ^5 and $\sigma^{\mu\nu}$ are hermitian, whereas the γ^i are antihermitian. From the anticommuation relation and the definition of γ^5 follow the following trace relations for the γ matrices:

$$\begin{aligned}
Tr\,[\mathbb{1}] &= 0 \quad , \\
Tr\,[\gamma^\mu] &= 0 \quad , \\
Tr\,[\gamma^\mu\, \gamma^\nu] &= 4\, g^{\mu\nu} \quad , \\
Tr\left[\gamma^\mu\, \gamma^\nu\, \gamma^\kappa\, \gamma^\lambda\right] &= 4\, \left(g^{\mu\nu}\, g^{\kappa\lambda} - g^{\mu\kappa}\, g^{\nu\lambda} + g^{\mu\lambda}\, g^{\nu\kappa}\right) \quad , \\
Tr\,[\text{any odd number of } \gamma\text{'s}] &= 0 \quad , \\
Tr\left[\gamma^5\right] &= 0 \quad , \\
Tr\left[\gamma^\mu\, \gamma^\nu\, \gamma^5\right] &= 0 \quad , \\
Tr\left[\gamma^\mu\, \gamma^\nu\, \gamma^\kappa\, \gamma^\lambda\, \gamma^5\right] &= -4\, i\, \epsilon^{\mu\nu\kappa\lambda} \quad .
\end{aligned} \tag{B.10}$$

Throughout this work we will stick to the Dirac representation of the γ matrices, in which they read:

$$\gamma_0 = \begin{pmatrix} \mathbb{1} & 0 \\ 0 & -\mathbb{1} \end{pmatrix} \quad , \quad \gamma_i = \begin{pmatrix} 0 & \sigma_i \\ -\sigma_i & 0 \end{pmatrix} \quad , \quad \gamma_5 = \begin{pmatrix} 0 & \mathbb{1} \\ \mathbb{1} & 0 \end{pmatrix} \quad . \tag{B.11}$$

In analogy to the three-dimensional case one can define a four-dimensional totally antisymmetric tensor $\epsilon_{\mu\nu\kappa\lambda}$ by:

$$\epsilon_{\mu\nu\kappa\lambda} = \begin{cases} 1 & , \text{ if } \mu,\, \nu, \kappa,\, \lambda \text{ cyclic} \\ -1 & , \text{ if } \mu,\, \nu, \kappa,\, \lambda \text{ acyclic} \\ 0 & , \text{ if any of } \mu,\, \nu, \kappa,\, \lambda \text{ are equal} \end{cases} \quad . \tag{B.12}$$

B.2 Spin-$\frac{1}{2}$ Spinors

The spinor $u_s(p)$ is a solution of the free Dirac equation:

$$\begin{aligned} (\not{p} - m)\, u_s(p) &= 0 \\ \bar{u}_s(p)\, (\not{p} - m) &= 0 \quad , \end{aligned} \tag{B.13}$$

where $\bar{u}_s(p)$ is defined by:

$$\bar{u}_s(p) = u_s^\dagger(p)\, \gamma^0 \quad .$$

By solving the free Dirac equation, the explicit form of $u_s(p)$ is found to be:

$$u_s(p) = \sqrt{E_p + m} \begin{pmatrix} \chi_s \\ \frac{\boldsymbol{\sigma}\,\mathbf{p}}{E_p + m}\, \chi_s \end{pmatrix} \quad , \tag{B.14}$$

where χ_s is the Pauli spinor and E_p denotes the *on-shell* energy $\sqrt{m^2 + \mathbf{p}^2}$. This implies that for a resonance with pole mass m_R but invariant mass $\sqrt{p^2}$ one has $E_p = \sqrt{p^2 + \mathbf{p}^2}$ and $m = \sqrt{p^2}$. The normalization and the completeness relation of the spinors read:

$$\begin{aligned} \bar{u}_r(p)\, u_s(p) &= 2\, m\, \delta_{r\,s} \\ \sum_s u_s(p)\, \bar{u}_s(p) &= \not{p} + m \qquad \text{(on-shell)} \\ \sum_s u_s(p)\, \bar{u}_s(p) &= \not{p} + \sqrt{p^2} \qquad \text{(off-shell)} \quad . \end{aligned} \tag{B.15}$$

Projectors onto states with spin-$\frac{1}{2}$ are readily constructed. The Dirac equation suggests the following form for *on-shell* states

$$P_{1/2} = \frac{\not{p} + m}{2\, m} \quad , \tag{B.16}$$

whereas for *off-shell* states with invariant mass $\sqrt{p^2} \neq m$ one finds:

$$P_{1/2} = \frac{\not{p} + \sqrt{p^2}}{2\, \sqrt{p^2}} \quad . \tag{B.17}$$

B.3 Polarization Vectors

Free massive spin-1 particles are described by the Proca equation

$$\begin{aligned} \partial_\mu\, V^{\mu\nu} + m_V^2\, V^\nu &= 0 \\ \text{where} \qquad V^{\mu\nu} &= \partial^\mu V^\nu - \partial^\nu V^\mu \quad . \end{aligned} \tag{B.18}$$

This implies 4-transversality of the free spin-1 fields:

$$\partial_\mu\, V^\mu = 0 \quad .$$

For a particle moving along the z axis, the three-transverse polarization vectors ϵ_μ^T are determined by the condition $\mathbf{q}\,\boldsymbol{\epsilon}^{\,T} = 0$. They read:

$$\epsilon_{\mu,1}^T \;=\; \frac{1}{\sqrt{2}}\,(0,1,i,0) \quad , \quad \epsilon_{\mu,2}^T \;=\; \frac{1}{\sqrt{2}}\,(0,1,-i,0) \quad .$$

The corresponding vectors for a particle moving along a different direction are obtained by a Lorenz transformation. The three-longitudinal polarization vector ϵ_μ^L can be written down in a covariant way:

$$\epsilon_\mu^L(q) \;=\; \sqrt{\frac{q^2}{(n.q)^2 - n^2 q^2}}\left(n_\mu - q_\mu\,\frac{n.q}{q^2}\right) \;=\; \frac{1}{\sqrt{q^2}}\;(-|\vec{q}|, q_0\,\vec{e}_{\vec{q}}) \quad ,$$

where in the last line the special choice $n_\mu = (m_N, 0)$ was used. This choice is motivated by the fact that we will be interested in the polarization of vector particles with respect to nuclear matter, which is typically represented by n_μ. Note that a proper definition of $\epsilon_\mu^L(q)$ is only possible for time-like four-momenta q_μ.The polarization vectors are orthogonal to each other and normalized to -1:

$$\epsilon^{\lambda,\,\mu}\,\epsilon_\mu^{\lambda',\star} \;=\; -\delta^{\lambda\,\lambda'} \quad .$$

With help of the polarization vectors one can construct the 4-transverse projector $P_{\mu\nu}^T$:

$$\sum_\lambda \epsilon_\mu^{\lambda,\star}\,\epsilon_\nu^\lambda \;=\; -g_{\mu\nu} + \frac{q_\mu\,q_\nu}{q^2} \;=\; -P_{\mu\nu}^T(q) \quad .$$

One may also define a 4-longitudinal projector $P_{\mu\nu}^L$, such that in the vacuum one gets two projectors:

$$P_{\mu\nu}^L(q) \;=\; \frac{q_\mu\,q_\nu}{q^2} \quad . \tag{B.19}$$

Note that only $P_{\mu\nu}^T(q)$ is current conserving, i.e. $q^\mu\,P_{\mu\nu}^T(q) = 0$. The projectors have the properties:

$$\begin{aligned} P_{\mu\alpha}^T(q)\,P_\nu^{\alpha\,T}(q) &= P_{\mu\nu}^T(q) \\ P_{\mu\alpha}^L(q)\,P_\nu^{\alpha\,L}(q) &= P_{\mu\nu}^L(q) \\ P_{\mu\alpha}^T(q)\,P_\nu^{\alpha\,L}(q) &= 0 \quad . \end{aligned} \tag{B.20}$$

For the trace of both projectors one fins:

$$Tr\left[P_{\mu\nu}^T\right] \;=\; 3 \quad , \quad Tr\left[P_{\mu\nu}^L\right] \;=\; 1 \quad .$$

By summing only over the transverse or longitudinal polarization, one obtains the corresponding projectors $T_{\mu\nu}(q)$ and $L_{\mu\nu}(q)$, which read in a covariant notation:

$$\begin{aligned} L_{\mu\nu}(q) &= -\frac{q^2}{(n.q)^2 - n^2 q^2}\left(n_\mu - q_\mu\,\frac{n.q}{q^2}\right)\left(n_\nu - q_\nu\,\frac{n.q}{q^2}\right) \\ T_{\mu\nu}(q) &= P_{\mu\nu}^T(q) - L_{\mu\nu}(q) \quad . \end{aligned} \tag{B.21}$$

One can easily check that they fulfill the usual projector properties such as

$$L_{\mu\nu}\, T^{\nu}{}_{\alpha} \;=\; 0 \quad , \quad L_{\mu\nu}\, L^{\nu}{}_{\alpha} \;=\; L_{\mu\alpha} \quad .$$

Furthermore, one has

$$Tr\,[L_{\mu\nu}] \;=\; 1 \quad , \quad Tr\,[T_{\mu\nu}] \;=\; 2 \quad .$$

The propagator of a massive spin-1 field is given by:

$$\begin{aligned} -\,i\,\mathcal{D}_{\mu\nu}(q) \;&=\; \frac{g_{\mu\nu} - q_\mu q_\nu/m^2}{q^2 - m^2} \\ &=\; \frac{P^T_{\mu\nu}}{q^2 - m^2 + i\epsilon} - \frac{1}{m^2}\frac{q_\mu q_\nu}{q^2} \quad , \end{aligned} \tag{B.22}$$

where in the second line we have indicated that away from the mass shell also four-longitudinal components are propagated.

B.4 Spin-$\frac{3}{2}$ Spinors

Spin-$\frac{3}{2}$ fields result from the coupling of spin-1 and spin-$\frac{1}{2}$ fields. They carry both Lorentz- and Dirac indices:

$$u^{\mu}_{s}(k) \;=\; \sum_{r,m} \left(\frac{3}{2}, s|\frac{1}{2}, r\,;\,1, m\right) u_r(k)\,\epsilon^{\mu}_{m}(k) \quad , \tag{B.23}$$

where $u_r(k)$ and ϵ_m are spin-$\frac{1}{2}$ spinor and spin-1 polarization vector, respectively. Plugging in the Clebsch-Gordan coefficients, this leads to the following explicit form of the spinors:

$$\begin{aligned} u^{\mu}_{\pm\frac{3}{2}}(k) \;&=\; u_{\pm\frac{1}{2}}(k)\,\epsilon^{\mu}_{\pm 1}(k) \\ u^{\mu}_{\pm\frac{1}{2}}(k) \;&=\; \sqrt{\frac{1}{3}}\,u_{\mp\frac{1}{2}}(k)\,\epsilon^{\mu}_{\pm 1}(k) + \sqrt{\frac{2}{3}}\,u_{\pm\frac{1}{2}}(k)\,\epsilon^{\mu}_{0}(k) \quad . \end{aligned}$$

For a spin-$\frac{3}{2}$ particle of mass m propagating along the z axis, the spinor may be written down in the following way:

$$u^{\mu}_{s}(k) \;=\; \sqrt{E_k + m}\begin{pmatrix} \mathbb{1} \\ \frac{\boldsymbol{\sigma}\,\mathbf{k}}{E_k + m} \end{pmatrix} S^{\mu}\,\chi_s \quad , \tag{B.24}$$

where χ_s denotes the spin states:

$$\chi_{+\frac{3}{2}} = \begin{pmatrix} 1 \\ 0 \\ 0 \\ 0 \end{pmatrix} \quad , \quad \chi_{+\frac{1}{2}} = \begin{pmatrix} 0 \\ 1 \\ 0 \\ 0 \end{pmatrix} \quad , \quad \chi_{-\frac{1}{2}} = \begin{pmatrix} 0 \\ 0 \\ 1 \\ 0 \end{pmatrix} \quad , \quad \chi_{-\frac{3}{2}} = \begin{pmatrix} 0 \\ 0 \\ 0 \\ 1 \end{pmatrix}$$

and the S^μ are coupling matrices containing the Clebsch-Gordan coefficients for the coupling $1 \otimes \frac{1}{2} = \frac{3}{2}$:

$$S_0 = \frac{k}{m} \begin{pmatrix} 0 & \sqrt{2/3} & 0 & 0 \\ 0 & 0 & \sqrt{2/3} & 0 \end{pmatrix} \quad , \quad S_1 = \begin{pmatrix} -\sqrt{1/2} & 0 & \sqrt{1/6} & 0 \\ 0 & -\sqrt{1/6} & 0 & \sqrt{1/2} \end{pmatrix}$$

$$S_2 = i \begin{pmatrix} \sqrt{1/2} & 0 & \sqrt{1/6} & 0 \\ 0 & \sqrt{1/6} & 0 & \sqrt{1/2} \end{pmatrix} \quad , \quad S_3 = \frac{E}{k} S_0 \tag{B.25}$$

As in the case of spin-$\frac{1}{2}$ fields, the adjungated spinor is defined as:

$$\bar{u}_s(k)^\mu \;=\; u_s^{\mu\,\dagger}(k)\,\gamma^0 \quad .$$

The spinors $u_s^\mu(p)$ are subject to the Rarita-Schwinger equations:

$$\begin{aligned} (\not{k} - m)\, u_s^\mu(k) &= 0 \\ k_\mu\, u_s^\mu(k) &= 0 \\ \gamma_\mu\, u_s^\mu(k) &= 0 \quad . \end{aligned} \tag{B.26}$$

Upon realizing that the matrix $\not{k}$ acts on the spin-$\frac{1}{2}$ component of $u_s^\mu(k)$ and k_μ on the spin-1 part, which is four-transversal, the first two equations follow directly from Eqs. B.23 and B.24. Note also, that the second constraint is fulfilled also for *off-shell* states.

Spin-1 and spin-$\frac{1}{2}$ fields can not only be coupled to form a total spin of $\frac{3}{2}$, but they may also form spin-$\frac{1}{2}$ states. As it turns out, these spin-$\frac{1}{2}$ modes show up in the *off-shell* part of the spin-$\frac{3}{2}$ propagator $\mathcal{G}^{\mu\nu}(k)$:

$$\begin{aligned} i\,\mathcal{G}^{\mu\nu}(k) &= \frac{\not{k} + m}{k^2 - m^2} \left(g^{\mu\nu} - \frac{1}{3}\,\gamma^\mu\,\gamma^\nu - \frac{2}{3\,m^2} k^\mu\,k^\nu + \frac{1}{3\,m}\,(k^\mu\,\gamma^\nu - k^\nu\,\gamma^\mu) \right) \\ &= \frac{\not{k} + m}{k^2 - m^2}\, P_{3/2}^{\mu\nu} - \frac{2}{3\,m^2}(\not{k} + m)\, P_{22}^{\mu\nu} + \frac{1}{\sqrt{3}\,m}(P_{12}^{\mu\nu} + P_{21}^{\mu\nu}) \quad . \end{aligned} \tag{B.27}$$

Here the spin-$\frac{3}{2}$ projector $P_{32}^{\mu\nu}$ as well as the projectors $P_{22}^{\mu\nu}$, $P_{12}^{\mu\nu}$ and $P_{21}^{\mu\nu}$ have been introduced. The latter project onto the spin-$\frac{1}{2}$ part of the theory. These projectors are given by:

$$\begin{aligned} P_{22}^{\mu\nu} &= \frac{k^\mu\,k^\nu}{k^2} \\ P_{11}^{\mu\nu} &= \frac{1}{3}\gamma^\mu\gamma^\nu - \frac{k^\mu k^\nu}{k^2} + \frac{1}{3\,k^2}\,(\not{k}\gamma^\mu k^\nu + k^\mu\gamma^\nu\not{k}) \\ P_{21}^{\mu\nu} &= \frac{1}{\sqrt{3}k^2}\,(k^\mu k^\nu - \not{k}\gamma^\mu k^\nu) \\ P_{12}^{\mu\nu} &= \frac{1}{\sqrt{3}k^2}\,(\not{k}k^\mu\gamma^\nu - k^\mu k^\nu) \\ P_{32}^{\mu\nu} &= g^{\mu\nu} - \frac{1}{3}\gamma^\mu\gamma^\nu - \frac{1}{3k^2}\,(\not{k}\gamma^\mu k^\nu + k^\mu\gamma^\nu\not{k}) \quad . \end{aligned} \tag{B.28}$$

The fact that away from the mass shell modes with a different are propagated is akin to the situation for spin-1 fields, see Section B.3. Whereas the meaning of $P_{32}^{\mu\nu}$ is obvious, the projectors onto the spin-$\frac{1}{2}$ subspace need some discussion. Due to Eq. B.23 and the transversality condition $k_\mu\,\epsilon^\mu = 0$, $P_{22}^{\mu\nu}$ can be identified as a projector onto states defined by $0 \oplus \frac{1}{2} = \frac{1}{2}$. This also elucidates the role of $P_{11}^{\mu\nu}$. Since the projectors fulfill the completeness relation

$$P_{3/2}^{\mu\nu} + P_{11}^{\mu\nu} + P_{22}^{\mu\nu} = g^{\mu\nu} \quad , \tag{B.29}$$

$P_{11}^{\mu\nu}$ projects onto those states for which $1 \oplus \frac{1}{2} = \frac{1}{2}$. The Rarita-Schwinger spinors obey a completeness relation:

$$\sum_r u_r^\mu(k)\,\bar{u}_r^\nu(k) \;=\; -(\not{k} + m)\left(g^{\mu\nu} - \frac{1}{3}\,\gamma^\mu\,\gamma^\nu - \frac{2}{3\,m^2}k^\mu\,k^\nu + \frac{1}{3\,m}\,(k^\mu\,\gamma^\nu - k^\nu\,\gamma^\mu)\right) \quad ,$$

which for *on-shell* states with $k^2 = m^2$ can be rewritten as:

$$\sum_r u_r^\mu(k)\,\bar{u}_r^\nu(k) \;=\; -(\not{k} + m)\,P_{3/2}^{\mu\nu}(k) \;=\; \Lambda^{\mu\nu} \quad . \tag{B.30}$$

Here the relation $(\not{p} + \sqrt{p^2})\sqrt{p^2} = \sqrt{p^2}(\not{p} + \sqrt{p^2})$ was used.

B.5 Feynman Rules

Non Interacting Theory

- spin-0 propagator:
  For each internal scalar boson line assign a factor

$$\mathcal{D}(q) \;=\; \frac{i}{q^2 - m^2 + i\,\epsilon}$$

- spin-1 propagator:
  For each internal vector boson line assign a factor

$$\mathcal{D}^{\mu\nu}(q) \;=\; i\,\frac{g^{\mu\nu} - q^\mu\,q^\nu/m^2}{q^2 - m^2 + i\,\epsilon}$$

- spin-$\frac{1}{2}$ propagator:
  For each internal spin-$\frac{1}{2}$ line assign a factor

$$\mathcal{G}(p) \;=\; \frac{i}{\not{p} - m}$$

- spin-$\frac{3}{2}$ propagator:
  For each internal spin-$\frac{3}{2}$ line assign a factor

$$\mathcal{G}^{\mu\nu}(k) \;=\; -i\frac{\not{k} + m}{k^2 - m^2 + i\,\epsilon}\left(g^{\mu\nu} - \frac{1}{3}\,\gamma^\mu\,\gamma^\nu - \frac{2}{3\,m^2}k^\mu\,k^\nu + \frac{1}{3\,m}\,(k^\mu\,\gamma^\nu - k^\nu\,\gamma^\mu)\right)$$

- external spin-$\frac{1}{2}$-particle with spin projection s:

$$u_s(p) \quad , \quad \text{if in initial state} \quad , \quad \bar{u}_s(p) \ , \ \text{if in final state}$$

- external vector meson with polarization λ:

$$\epsilon_\mu^\lambda(p) \quad , \quad \text{if in initial state} \quad , \quad \epsilon_\mu^{\lambda\star}(p) \ , \ \text{if in final state}$$

- for each vertex an additional factor of $(-i)$
- for each incoming (outgoing) momentum a factor $+(-)\, i\, q_\mu$
- for each loop assign a factor $\displaystyle\int \frac{d^4p}{(2\pi)^4}$
- if two fermions are in the same loop, multiply with an additional factor of (-1)

With these rules one obtains $i\,\mathcal{M}$, $-i\,\Pi$ and $-i\,\Sigma$.

Interacting Theory

In an interacting theory, the propagators are modified by self energy contributions. We use the following expressions for the propagators of an interacting theory:

- spin-0 propagator:
  For each internal scalar boson line assign a factor

$$\mathcal{D}(q) \;=\; \frac{i}{q^2 - m^2 - \Pi(q)}$$

- spin-1 propagator:
  For each internal vector boson line assign a factor

$$\mathcal{D}^{\mu\nu}(q) \;=\; i\,\frac{g^{\mu\nu} - q^\mu\, q^\nu/m^2}{q^2 - m^2 - \Pi(q)}$$

- spin-$\frac{1}{2}$ propagator:
  For each internal spin-$\frac{1}{2}$ line assign a factor

$$\mathcal{G}(p) \;=\; i\frac{\not{p} + \sqrt{p^2}}{p^2 - m^2 - \langle\Sigma(p)\rangle}$$

  The definition of $\langle\Sigma(p)\rangle$ is given in Eq. D.12.

- spin-$\frac{3}{2}$ propagator:
  For each internal spin-$\frac{3}{2}$ line assign a factor

$$\mathcal{G}^{\mu\nu}(k) \;=\; -i\frac{\not{k} + \sqrt{k^2}}{k^2 - m^2 - \langle\Sigma(k)\rangle}\left(g^{\mu\nu} - \frac{1}{3}\,\gamma^\mu\,\gamma^\nu - \frac{2}{3\,k^2}k^\mu\,k^\nu + \frac{1}{3\,\sqrt{k^2}}\,(k^\mu\,\gamma^\nu - k^\nu\,\gamma^\mu)\right)$$

  The definition of $\langle\Sigma(k)\rangle$ is given in Eq. D.17.

- Relativistic nucleon propagator

  The relativistic in-medium propagator of the nucleon accounts for the propagation of particle, hole and antiparticle states [119]:

$$\mathcal{G}_N^{med}(p) = i\frac{1}{2E(\mathbf{p})}\Bigg\{(\not{p}+m_N)\Bigg[\underbrace{\frac{1-\theta(p_F-|\mathbf{p}|)}{p_0-E(\mathbf{p})+i\epsilon}}_{\text{particle}}+\underbrace{\frac{\theta(p_F-|\mathbf{p}|)}{p_0-E(\mathbf{p})-i\epsilon}}_{\text{hole}}\Bigg] - (\not{\bar{p}}+m_N)\underbrace{\frac{1}{p_0+E(\mathbf{p})-i\epsilon}}_{\text{antiparticle}}\Bigg\} \quad , \tag{B.31}$$

  with $\not{p} = E(\mathbf{p})\gamma_0 - \mathbf{p}\boldsymbol{\gamma}$ and $\not{\bar{p}} = -E(\mathbf{p})\gamma_0 - \mathbf{p}\boldsymbol{\gamma}$.

- Non-relativistic nucleon propagator

  In a non-relativistic framework the in-medium propagator reduces to the propagation of particle and hole states [33]:

$$\mathcal{G}_N^{med}(p) = i\frac{1-\theta(p_F-|\mathbf{p}|)}{p_0-E(\mathbf{p})+i\epsilon}+\frac{\theta(p_F-|\mathbf{p}|)}{p_0-E(\mathbf{p})-i\epsilon} \quad . \tag{B.32}$$

B.6 Observables

In this Section we give explicit expressions for some often used relations:

- The cm momentum of the decay products in a reaction $a \leftrightarrow b+c$ is given by:

$$\begin{aligned} p_{cm}^2 &= \frac{(m_a^2-(m_b+m_c)^2)(m_a^2-(m_b-m_c)^2)}{4m_a^2} \\ &= \frac{m_a^2-m_b^2+m_c^2}{4m_a^2}-m_c^2 \quad , \end{aligned} \tag{B.33}$$

  where the second representation is useful if one of the decay products has a space like 4-momentum. Closely related to p_{cm} is p_{lab}, which is the momentum of particle c if particle b is at rest. By equating the invariant energy s of particles b and c, one obtains:

$$\begin{aligned} m_b^2+m_c^2+2m_bE_c &= s = (E_b^{cm}+E_c^{cm})^2 \\ &\Rightarrow \\ q_{cm}^2 &= \frac{m_N^2}{s}p_{lab}^2 \quad . \end{aligned} \tag{B.34}$$

- The Lorentz invariant two-body phase space Φ_2 can be integrated out and one obtains in the cm frame:

$$\begin{aligned} \Phi_2 &= \int d\Phi_2 = \frac{1}{4\pi}\frac{p_{cm}}{\sqrt{s}} \\ d\Phi_2 &= \frac{d^3p_b}{(2\pi)^3}\frac{1}{2E_b}\frac{d^3p_c}{(2\pi)^3}\frac{1}{2\sqrt{s}}(2\pi)^4\,\delta^{(4)}(p_a-p_b-p_c) \end{aligned} \tag{B.35}$$

where p_b and p_c denote the 4-momenta of the two particles in the final state, p_{cm} is as defined above and $\sqrt{s}$ stands for the the total energy of the system in the cm frame.

- The differential cross section for a reaction of the type $a + b \to c + d$ is given by:

$$d\sigma = \frac{1}{2E_a\, 2E_b\, |v_a - v_b|} |\mathcal{M}_{a+b\to c+d}|^2\, d\Phi_2 \tag{B.36}$$

The first factor represents the flux and can be evaluated to yield:

$$\begin{aligned} \frac{1}{2E_a\, 2E_b\, |v_a - v_b|} &= \frac{1}{4m_b\, |p_{a\,lab}|} \\ &= \frac{1}{4\sqrt{s}\, p_{cm}} \end{aligned}$$

- The decay width Γ follows from the following formula:

$$\begin{aligned} \Gamma &= \frac{1}{2\, E_a} \int d\Phi_2\, |\mathcal{M}_{a\to b+c}|^2 \\ &= \frac{1}{2\, E_a}\, |\mathcal{M}_{a\to b+c}|^2\, \frac{p_{cm}}{4\,\sqrt{s}} \quad . \end{aligned} \tag{B.37}$$

The last transformation is possible when one averages over the spin of the decaying particle, otherwise the squared matrix element depends on the angle. In the rest frame of the decaying particle, one has $E_a \to \sqrt{s}$.

- The optical theorem relates the total cross section to the forward scattering amplitude:

$$\sigma = \frac{1}{2\sqrt{s}\, p_{cm}} \mathcal{M}_{\text{forward}} \quad . \tag{B.38}$$

Appendix C

Lagrangians and Traces

C.1 Relativistic

In this Section we will write down the relativistic Lagrangians used for the description of the coupling of baryon resonances to nucleons and pseudoscalar mesons φ or vector mesons/photons V^μ. The guiding principle in writing down these interaction terms is that they are Lorentz invariant and gauge invariant and respect parity conservation.

C.1.1 Lagrangian

We assume the following coupling of a resonance with the quantum numbers J^π (spin J and parity π) to the φN channel:

$$\begin{aligned} \mathcal{L}_{RN\varphi} &= \frac{f}{m_\varphi}\,\bar{\psi}_R\,\gamma^\mu \left\{ \begin{array}{c} i\,\gamma^5 \\ \mathbb{1} \end{array} \right\} \psi_N\,\partial_\mu\,\varphi \qquad \text{for} \quad J^\pi = \tfrac{1}{2}^\pm \\ \mathcal{L}_{RN\varphi} &= \frac{f}{m_\varphi}\,\bar{\psi}^\mu_R \left\{ \begin{array}{c} \mathbb{1} \\ i\,\gamma^5 \end{array} \right\} \psi_N\,\partial_\mu\,\varphi \qquad \text{for} \quad J^\pi = \tfrac{3}{2}^\pm \end{aligned} \tag{C.1}$$

The standard coupling of a resonance with the quantum numbers J^π for spin J and parity π to the $V\,N$ channel reads:

$$\begin{aligned} \mathcal{L}_{RNV} &= \frac{f}{m_V}\,\bar{\psi}_R\,\sigma^{\mu\nu} \left\{ \begin{array}{c} \mathbb{1} \\ i\,\gamma^5 \end{array} \right\} \psi_N\,\partial_\mu\,V_\nu \qquad \text{for} \quad J^\pi = \tfrac{1}{2}^\pm \\ \mathcal{L}_{RNV} &= \frac{f}{m_V}\,\bar{\psi}^\mu_R\,\gamma^\nu \left\{ \begin{array}{c} i\,\gamma^5 \\ \mathbb{1} \end{array} \right\} \psi_N\,V_{\mu\nu} \qquad \text{for} \quad J^\pi = \tfrac{3}{2}^\pm \end{aligned} \tag{C.2}$$

In Eq. C.1 the coupling of pseudoscalar mesons to the nucleon current is already contained in the coupling to a resonance with quantum numbers $J^\pi = \frac{1}{2}^+$. The interaction of vector mesons with the nucleon current is determined by the Lagrangian:

$$\mathcal{L} = g_V \left(\bar{\psi}_N\,\gamma^\mu\,\psi_N\,V_\mu + \frac{\kappa_V}{2\,m_N}\bar{\psi}_N\,\sigma^{\mu\nu}\psi_N\,V_{\mu\nu} \right) \quad , \tag{C.3}$$

and for the $NN\varphi$ coupling we pseudovector coupling

$$\mathcal{L} = \frac{f}{m_\varphi}\bar{\psi}_N\,i\,\gamma_5\,\gamma^\mu\,\psi_N\,\partial_\mu\,\varphi \quad . \tag{C.4}$$

C.1.2 Traces

In this work the Lagrangians are used to find analytic expressions for the decay width of a resonance and to calculate the meson-nucleon forward scattering amplitude. In both cases one needs to calculate a trace which is of the generic form

$$\begin{aligned} \Omega^{\varphi}_{1/2} &= Tr\left[\mathcal{V}\,(\not{k}+\sqrt{k^2})\,\mathcal{V}^{\dagger}\,(\not{p}+m_N)\right] \\ \Omega^{\varphi}_{3/2} &= Tr\left[\mathcal{V}_{\mu}\,\Lambda^{\mu\nu}(k)\,\mathcal{V}^{\nu\,\dagger}\,(\not{p}+m_N)\right] \quad . \end{aligned} \tag{C.5}$$

for pseudoscalar mesons and

$$\begin{aligned} \Omega^{T/L}_{1/2} &= P^{T/L}_{\mu\nu}\,Tr\left[\mathcal{V}^{\mu}\,(\not{k}+\sqrt{k^2})\,\mathcal{V}^{\nu\,\dagger}\,(\not{p}+m_N)\right] \\ \Omega^{T/L}_{3/2} &= P^{T/L}_{\mu\nu}\,Tr\left[\mathcal{V}^{\mu}_{\alpha}\,\Lambda^{\alpha\beta}(k)\,\mathcal{V}^{\nu\,\dagger}_{\beta}\,(\not{p}\ \ +m_N)\right] \quad . \end{aligned} \tag{C.6}$$

for vector mesons. The operator $\Lambda^{\mu\nu}(k)$ has been introduced in Eq. B.30. The vertex factors $\mathcal{V}$ are obtained from the above Lagrangians Eqs. C.1 and C.2. To be more specific, we give $\mathcal{V}$ for the coupling a $J^{\pi}=\frac{1}{2}^{+}$ resonance to a pseudoscalar meson and to a vector meson:

$$\begin{aligned} \mathcal{V} &= \gamma^{\mu}\,i\,\gamma^{5}\,q_{\mu} && \text{pseudoscalar meson} \\ \mathcal{V}^{\nu} &= \sigma^{\mu\nu}\,q_{\mu} && \text{vector meson} \end{aligned} \tag{C.7}$$

We display results for these traces in Table C.1 as obtained in the cm frame of the resonance and in the rest frame of the nucleon.

The upper (lower) sign refers to resonances with positive (negative) parity. Here q_0 and $\mathbf{q}$ denote energy and three-momentum of the meson, $\sqrt{s}$ the invariant mass of the meson-nucleon system. The center-of-mass quantities $\mathbf{q}_{cm}$, $q_{0,cm}$ and E_N^{cm} are the 3-momentum and energy of the nucleon in the rest frame of the resonance. The transition from laboratory frame to center-of-mass frame is straightforward, if one realizes that $\mathbf{q}=\mathbf{q}_{cm}\,\dfrac{\sqrt{s}}{m_N}$ and $q_0+m_N=\dfrac{\sqrt{s}}{m_N}E_N^{cm}$.

C.2 Non Relativistic

In this Section we describe how the non-relativistic interactions derive from the relativistic ones. The idea behind the non-relativistic reduction is the following: think of an amplitude involving a spin-$\frac{1}{2}$ resonance, a nucleon and a meson. It will be of the generic form:

$$\mathcal{M}_{ss'} = \mathcal{N}_R\mathcal{N}_N\left(\chi_s^{\dagger},\frac{\boldsymbol{\sigma}\cdot\mathbf{k}}{E_R+m_R}\,\chi_s^{\dagger}\right)\begin{pmatrix}\Gamma_{11} & \Gamma_{12}\\ \Gamma_{21} & \Gamma_{22}\end{pmatrix}\begin{pmatrix}\chi'_s\\ \dfrac{\boldsymbol{\sigma}\cdot\mathbf{p_N}}{E_N+m_N}\,\chi'_s\end{pmatrix} \tag{C.8}$$

Here $\mathcal{N}_R$ and $\mathcal{N}_N$ denote the normalization factors $\sqrt{E_R+m_R}$ and $\sqrt{E_N+m_N}$ arising from the relativistic spinors (cf. Appendix B.2). The Γ_{ij} are 2×2 matrices and χ is a two-component Pauli spinor. By writing out the matrix product, one produces an expansion

$\mathbf{\Omega^{\varphi}_{1/2}}$	lab	$4\,m_N\,(q^2(m_N+q_0\mp\sqrt{s})+2\,\mathbf{q}^2\,m_N)$
	cm	$4\,\sqrt{s}\,\left(q^2\,(E_N^{cm}\mp m_N)+2\,\sqrt{s}\,\mathbf{q}_{cm}^2\right)$
$\mathbf{\Omega^{\varphi}_{3/2}}$	lab	$\frac{8}{3}\,\frac{m_N^3}{s}\,\mathbf{q}^2\,(m_N+q_0\pm\sqrt{s})$
	cm	$\frac{8}{3}\,\sqrt{s}\,\mathbf{q}_{cm}^2\,(E_N^{cm}\pm m_N)$
$\mathbf{\Omega^{T}_{1/2}}$	lab	$\Omega^L_{1/2}+8\,m_N^2\,\mathbf{q}^2$
	cm	$\Omega^L_{1/2}+8\,s\,\mathbf{q}_{cm}^2$
$\mathbf{\Omega^{L}_{1/2}}$	lab	$4\,m_N\,q^2\,(m_N+q_0\mp\sqrt{s})$
	cm	$4\,\sqrt{s}\,q^2\,(E_N^{cm}\mp m_N)$
$\mathbf{\Omega^{T}_{3/2}}$	lab	$\Omega^L_{3/2}+\frac{8}{3}\,m_N^2\,\mathbf{q}^2\,\left(1+\frac{m_N\,q_0+m_N^2}{s}\right)$
	cm	$\Omega^L_{3/2}+\frac{8}{3}\,s\,\mathbf{q}_{cm}^2\,\left(1+\frac{E_N^{cm}}{\sqrt{s}}\right)$
$\mathbf{\Omega^{L}_{3/2}}$	lab	$\frac{8}{3}\,m_N\,q^2\,(m_N+q_0\mp\sqrt{s})$
	cm	$\frac{8}{3}\,\sqrt{s}\,q^2\,(E_N^{cm}\mp m_N)$

Table C.1: Results for the relativistic traces Ω as appearing in the calculation of the resonance decay width and the meson self energy. Further explanations are given in the text.

in p_N/E_N and in k/E_R:

$$\mathcal{M}_{ss'} = \mathcal{N}_R\mathcal{N}_N\,\chi_s^\dagger\left(\Gamma_{11}+\Gamma_{12}\,\frac{\boldsymbol{\sigma}\cdot\mathbf{p_N}}{E_N+m_N}+\frac{\boldsymbol{\sigma}\cdot\mathbf{k}}{E_R+m_R}\,\Gamma_{21}+\right.$$
$$\left.+\frac{\boldsymbol{\sigma}\cdot\mathbf{k}}{E_R+m_R}\,\Gamma_{22}\,\frac{\boldsymbol{\sigma}\cdot\mathbf{p_N}}{E_N+m_N}\right)\chi_{s'}\quad . \tag{C.9}$$

Keeping only the first non-vanishing term of this series then yields the non-relativistic form of the amplitude. Only Γ_{11} and Γ_{12} contribute, if the resonance is assumed to be at rest.

We illustrate the procedure for the case of a pseudoscalar meson coupling to a resonance

with $J^\pi = \frac{1}{2}^+$. In the rest frame of the resonance the amplitude reads:

$$\begin{aligned}
\mathcal{M}_{ss'} &= \bar{u}_s\,\gamma^\mu\,\gamma^5\,u_{s'}\,q_\mu \\
&= \mathcal{N}_R\mathcal{N}_N\,\left(\chi_s^\dagger,0\right)\,\gamma^0\,\gamma^\mu\,\gamma^5\,\left(\begin{array}{c}\chi_{s'}\\ \dfrac{\boldsymbol{\sigma}\cdot\mathbf{p_N}}{E_N+m_N}\,\chi_{s'}\end{array}\right)\,q_\mu \\
&= \mathcal{N}_R\mathcal{N}_N\,\left(\chi_s^\dagger,0\right)\,\left[\gamma^5\,q_0+\left(\begin{array}{cc}\boldsymbol{\sigma} & 0\\ 0 & \boldsymbol{\sigma}\end{array}\right)\mathbf{q}\right]\left(\begin{array}{c}\chi_{s'}\\ \dfrac{\boldsymbol{\sigma}\cdot\mathbf{p_N}}{E_N+m_N}\,\chi_{s'}\end{array}\right) \qquad \text{(C.10)}\\
&= \mathcal{N}_R\mathcal{N}_N\,\chi_s^\dagger\,\left[\frac{\boldsymbol{\sigma}\cdot\mathbf{p_N}}{E_N+m_N}q_0+\boldsymbol{\sigma}\cdot\,\mathbf{q}\right]\,\chi_{s'} \\
&\approx \sqrt{2\,m_R}\,\sqrt{2\,m_N}\,\chi_s^\dagger\,\boldsymbol{\sigma}\cdot\,\mathbf{q}\,\chi_{s'} \quad .
\end{aligned}$$

The only approximation in the above transformations has been done in the last line, where the term p_N/m_N was neglected, in agreement with the non-relativistic scheme.

Spin-$\frac{3}{2}$ resonances are handled in much the same way. The treatment of the Rarita-Schwinger spinors follows directly from Eq. B.24. To be explicit, we consider the case of a pion coupling to a resonance with $J^\pi = \frac{3}{2}^+$:

$$\begin{aligned}
\mathcal{M}_{ss'} &= \bar{u}_s\,S^{\mu\,\dagger}\,u_{s'}\,q_\mu \\
&= \mathcal{N}_R\mathcal{N}_N\,\left(\chi_s^\dagger,0\right)\,\mathbf{S}^\dagger\,\left(\begin{array}{c}\chi_{s'}\\ \dfrac{\boldsymbol{\sigma}\cdot\mathbf{p_N}}{E_N+m_N}\,\chi_{s'}\end{array}\right)\mathbf{q} \qquad \text{(C.11)}\\
&\approx \mathcal{N}_R\mathcal{N}_N\,\chi_s^\dagger\,\mathbf{S}^\dagger\cdot\mathbf{q}\chi_{s'} \quad .
\end{aligned}$$

By going from the first to the second line we made use of $S^0 = 0$ for spin-$\frac{3}{2}$ particles at rest. The matrix $\mathbf{S}$ denotes the spin-$\frac{3}{2}$ transition operator, as given in Eq. B.25. This is one of the cases where the non-relativistic reduction can be done without any approximations.

As mentioned before, we have so far assumed that the non-relativistic reduction is performed in the rest frame of the resonance. This is, however, not mandatory and one might as well choose the rest frame of nuclear matter with $p_N = (m_N, \mathbf{0})$. The leading contribution proportional to Γ_{11} will formally look the same since it arises from the upper, momentum independent, component of the spinor. However, energy and momentum of the meson are then to be taken in the rest frame of nuclear matter.

A note concerning calculation techniques in the spin-$\frac{3}{2}$ sector is in order now. In the calculation of Ω_φ and $\Omega_{T/L}$ one encounters a completeness relation over the non-relativistic spin-$\frac{3}{2}$ states:

$$\begin{aligned}
P^{ij}_{3/2} &= \sum_r u^i_r\,u^{j\,\dagger}_r \;=\; \sum_r S^i_{r,s}\,\chi_s\,\chi^\dagger_{s'}\,S^{j\,\dagger}_{r,s'} \qquad \text{(C.12)}\\
&= \delta^{ij} - \frac{1}{3}\,\sigma^i\,\sigma^j \quad .
\end{aligned}$$

We do not derive the last step explicitly, since it can be found in many references [33, 38]. This result is quite intuitive though if one compares it with the relativistic expression for the spin-$\frac{3}{2}$ projector in Eq. B.28. Taking the limit $\mathbf{k} \to 0$ and keeping only the 2×2 matrix

in the upper left corner, one recovers the result from Eq. C.12. Similarly, one can define a projector onto spin-$\frac{1}{2}$ states:

$$P^{ij}_{1/2} \;=\; \frac{1}{3}\,\sigma^i\,\sigma^j \quad , \tag{C.13}$$

which is the non-relativistic analogon to $P^{\mu\nu}_{11}$ in Eq. B.28.

Not present in our relativistic formulation are the couplings to spin-$\frac{5}{2}$ resonances, owing to the rather involved formalism required. The construction of a non-relativistic spin-$\frac{5}{2}$ state is less complicated. It can be generated by the coupling of two spin-1 states with one spin-$\frac{1}{2}$ state:

$$u^{ij}_r \;=\; \sum_{s,\lambda,\lambda',\kappa} \left(\tfrac{5}{2}, r|2\kappa;\, \tfrac{1}{2}s\right) (2\kappa|1\lambda;\, 1\lambda')\; \epsilon^i_\lambda\, \epsilon^j_{\lambda'}\, \chi_s \quad .$$

Note the analogy to the construction of spin-$\frac{3}{2}$ states in Eq. B.23. The spin-$\frac{5}{2}$ states carries only vector indices since in the rest frame the 0-th components of the polarization vector vanish. The corresponding projector onto spin-$\frac{5}{2}$ states reads [38]:

$$\begin{aligned} P^{ij,kl}_{5/2} \;=\; & \frac{1}{2}(\delta_{ik}\delta_{jl} + \delta_{il}\delta_{jk}) - \frac{1}{5}\,\delta_{ij}\delta_{kl} - \\ & -\frac{1}{10}\,(\delta_{ik}\,\sigma_j\,\sigma_l + \delta_{il}\,\sigma_j\,\sigma_k + \delta_{jk}\,\sigma_i\,\sigma_l + \delta_{jl}\,\sigma_i\,\sigma_k) \quad . \end{aligned} \tag{C.14}$$

C.2.1 Lagrangian

The non-relativistic Lagrangians presented here are derived from the relativistic ones as given in Eqs. C.1 and C.2.

The Lagrangian describing the coupling to a pseudoscalar meson and a nucleon reads:

$$\begin{aligned} \mathcal{L}_{RN\varphi} \;&=\; i\,\frac{f}{m_\varphi}\psi^\dagger_R\,\sigma_k\,\psi_N\,\partial_k\,\varphi && \text{for} \quad J^\pi = \tfrac{1}{2}^+ \\ &=\; \frac{f}{m_\varphi}\psi^\dagger_R\,\psi_N\,\partial_0\,\varphi && \text{for} \quad J^\pi = \tfrac{1}{2}^- \\ \mathcal{L}_{RN\varphi} \;&=\; \frac{f}{m_\varphi}\,\psi^\dagger_R\,S^\dagger_k\,\psi_N\,\partial_k\,\varphi && \text{for} \quad J^\pi = \tfrac{3}{2}^+ \\ &=\; i\,\frac{f}{2\,m_N\,m_\varphi}\,\psi^\dagger_R\,S^\dagger_k\,\sigma_l\,(\partial_l\,\psi_N)\,\partial_k\,\varphi && \text{for} \quad J^\pi = \tfrac{3}{2}^- \\ \mathcal{L}_{RN\varphi} \;&=\; \frac{f}{m_\varphi}\,\psi^\dagger_R\,R_{i\,j}\,\sigma_k\psi_N\,\partial_i\,\partial_j\,\partial_k\,\varphi && \text{for} \quad J^\pi = \tfrac{5}{2}^+ \end{aligned} \tag{C.15}$$

The coupling to vector mesons and nucleons is described by:

$$\begin{aligned}
\mathcal{L}_{RN\rho} &= \frac{f}{m_V}\,\psi_R^\dagger\,\sigma_j\,\psi_N\,\epsilon_{jkl}\,\partial_k\,\rho_l && \text{for} \quad J^\pi = \tfrac{1}{2}^+ \\
&= i\,\frac{f}{m_V}\,\psi_R^\dagger \sigma_k\,\psi_N\,\left(\partial_k\,\rho_0 - \partial_0\,\rho_k\right) && \text{for} \quad J^\pi = \tfrac{1}{2}^- \\
\mathcal{L}_{RN\rho} &= i\,\frac{f}{m_V}\,\psi_R^\dagger\,S_j^\dagger\,\psi_N\,\epsilon_{jkl}\,\partial_k\,\rho_l && \text{for} \quad J^\pi = \tfrac{3}{2}^+ \\
&= \frac{f}{m_V}\,\psi_R^\dagger\,S_k^\dagger\,\psi_N\,\left(\partial_k\,\rho_0 - \partial_0\,\rho_k\right) && \text{for} \quad J^\pi = \tfrac{3}{2}^- \\
\mathcal{L}_{RN\rho} &= \frac{f}{m_V}\psi_R^\dagger\,R_{ij}\,\psi_N \partial_j\,\rho_i^T && \text{for} \quad J^\pi = \tfrac{5}{2}^+
\end{aligned} \tag{C.16}$$

In the last line the notion ρ_i^T is meant to imply that only transversely polarized vector particles couple to spin-$\frac{5}{2}$ resonances.

The non-relativistic coupling of pseudoscalar mesons and vector mesons is taken to be:

$$\begin{aligned}
\mathcal{L}_{NN\varphi} &= i\,\frac{f}{m_\varphi}\,\psi_N^\dagger\,\sigma_k\,\psi_N\,\partial_k\,\varphi \\
\mathcal{L}_{NN\rho} &= \frac{f}{m_\rho}\,\psi_N^\dagger\,\sigma_j\,\psi_N\,\epsilon_{jkl}\,\partial_k\,\rho_l \quad .
\end{aligned} \tag{C.17}$$

We close this Section by writing down the Lagrangian from the coupling of baryon resonances to the $\Delta\pi$ channel which are needed for the parametrization of $\Gamma_{\Delta\pi}$, see Eq. 3.19 in Chapter 3. For spin-$\frac{1}{2}$ resonances the coupling to this channel can be read off the non-relativistic Lagrangians of Eq. C.15. For spin-$\frac{3}{2}$ states one finds:

$$\begin{aligned}
\mathcal{L}_{R\Delta\pi} &= \frac{f}{m_\Delta}\psi_R^\dagger\,S_k^\dagger\,S_k\;\psi_\Delta\,\pi && \text{for} \quad J^\pi = \tfrac{3}{2}^- \quad . \\
\mathcal{L}_{R\Delta\pi} &= \frac{f}{m_\Delta}\psi_R^\dagger\,S_i^\dagger\,S_j\;\psi_\Delta \epsilon_{ijk}\partial_k\,\pi && \text{for} \quad J^\pi = \tfrac{3}{2}^+ \quad .
\end{aligned} \tag{C.18}$$

For the coupling of spin-$\frac{1}{2}$ resonances the appropriate Lagrangians of Eq. C.15 can be applied.

C.2.2 Traces

In analogy to the relativistic case, we give now results for the traces Ω^φ and $\Omega^{T/L}$. The results are given in Table C.2. Energy q_0 and momentum $\mathbf{q}$ of the meson are taken either in the cm-frame of the rest frame of nuclear matter. In the calculations we replace $m_R \to \sqrt{k^2}$. In Table C.3 we give results for the traces generated by the contact interactions describing short-range correlations.

$\mathbf{\Omega^{\varphi}_{1/2}}$	$\pi=+1$	$8\,m_N\,m_R\,\mathbf{q}^2$	$\mathbf{\Omega^{\varphi}_{3/2}}$	$\pi=+1$	$\frac{16}{3}\,m_N\,m_R\,\mathbf{q}^2$
	$\pi=-1$	$8\,m_N\,m_R\,q_0^2$		$\pi=-1$	$\frac{16}{3}\,m_N\,m_R\,\frac{\mathbf{q}^4}{4\,m_N^2}$
$\mathbf{\Omega^{\varphi}_{5/2}}$	$\pi=+1$	$\frac{16}{5}\,m_N\,m_R\,\mathbf{q}^2$			
$\mathbf{\Omega^{T}_{1/2}}$	$\pi=+1$	$8\,m_N\,m_R\,\mathbf{q}^2$	$\mathbf{\Omega^{T}_{3/2}}$	$\pi=+1$	$\frac{16}{3}\,m_N\,m_R\,\mathbf{q}^2$
	$\pi=-1$	$8\,m_N\,m_R\,\mathbf{q_0}^2$		$\pi=-1$	$\frac{16}{3}\,m_N\,m_R\,\mathbf{q_0}^2$
$\mathbf{\Omega^{L}_{1/2}}$	$\pi=+1$	0	$\mathbf{\Omega^{L}_{3/2}}$	$\pi=+1$	0
	$\pi=-1$	$8\,m_N\,m_R\,q^2$		$\pi=-1$	$\frac{16}{3}\,m_N\,m_R\,q^2$
$\mathbf{\Omega^{T}_{5/2}}$	$\pi=+1$	$\frac{12}{5}\,m_N\,m_R\,\mathbf{q}^2$			
$\mathbf{\Omega^{\Delta}}$	$\pi=+1$	$\frac{80}{9}\,m_\Delta\,m_R\,\mathbf{q}^2$			
	$\pi=-1$	$16\,m_\Delta\,m_R$			

Table C.2: Non-relativistic traces for the resonance decay and the meson self energy.

$\mathbf{\Omega^{\varphi,red}_{1/2}}$	$\pi=+1$	$8\,m_N\,m_R$	$\mathbf{\Omega^{,red}_{3/2}}$	$\pi=+1$	$\frac{16}{3}\,m_N\,m_R$
	$\pi=-1$	$8\,m_N\,m_R$		$\pi=-1$	$\frac{16}{3}\,m_N\,m_R\,\frac{\mathbf{q}^2}{4\,m_N^2}$
$\mathbf{\Omega^{T,red}_{1/2}}$	$\pi=+1$	$8\,m_N\,m_R$	$\mathbf{\Omega^{T,red}_{3/2}}$	$\pi=+1$	$\frac{16}{3}\,m_N\,m_R$
	$\pi=-1$	$8\,m_N\,m_R$		$\pi=-1$	$\frac{16}{3}\,m_N\,m_R$
$\mathbf{\Omega^{L,red}_{1/2}}$	$\pi=+1$	0	$\mathbf{\Omega^{L,red}_{3/2}}$	$\pi=+1$	0
	$\pi=-1$	$8\,m_N\,m_R$		$\pi=-1$	$\frac{16}{3}\,m_N\,m_R$
$\mathbf{\Omega^{T,red}_{5/2}}$	$\pi=+1$	$\frac{12}{5}\,m_N\,m_R$			

Table C.3: Reduced traces Ω^{red}, which arise from the contact interactions.

Appendix D

Self-energy and Dyson-Schwinger equation

In this Appendix we discuss the construction of the propagator in an interacting theory. It is based on two ingredients: a self energy summarizing the effects of the interactions and the Dyson-Schwinger equation which expresses the full propagator in terms of the self energy. In the first part of this Appendix we discuss the Dyson-Schwinger equation and the matrix structures arising for propagator and self energy for fields with spin. In the second part we will be concerned about how to calculate the self energy. There we concentrate on the calculation of the imaginary part. A detailed discussion of the real part can in found Appendix E.

D.1 Dyson-Schwinger Equation

In the absence of interactions the propagator of a scalar field with mass M_0 is given by [106]:

$$\mathcal{D}_0(q^2) \;=\; \frac{1}{q^2 - M_0^2} \quad . \tag{D.1}$$

Interactions of the particle give rise to the self energy $\Pi(q^2)$, which leads to corrections of the propagator $\mathcal{D}_0(q^2)$. For energies above the threshold for 2-body decay, $\Pi(q^2)$ has both a real and an imaginary part. In lowest order perturbation theory, the propagator then reads:

$$\mathcal{D}_1(q^2) \;=\; \mathcal{D}_0(q^2)\,\Pi(q^2)\,\mathcal{D}_0(q^2) \quad . \tag{D.2}$$

Such an approximation is useful whenever the particle is only weakly interacting and the self energy is small, for example in QED [106]. For strongly interacting systems, it is appropriate to perform a partial resummation of the self energy insertion $\Pi(q^2)$. The resulting geometric series is readily summed up:

$$\begin{aligned} \mathcal{D}(q^2) &= \mathcal{D}_0(q^2) + \mathcal{D}_0(q^2)\,\Pi(q^2)\,\mathcal{D}(q^2) \\ &= \frac{\mathcal{D}_0(q^2)}{1 - \mathcal{D}_0(q^2)\,\Pi(q^2)} \\ &= \frac{1}{q^2 - M_0^2 - \Pi(q^2)} \quad . \end{aligned} \tag{D.3}$$

This equation is easily interpreted: as a consequence of the interactions the bare particle mass M_0 is shifted by $\mathcal{R}\mathrm{e}\,\Pi(q^2)$. The physical mass M is the solution of the GAP equation:

$$q^2 - M_0^2 - \mathcal{R}\mathrm{e}\,\Pi(q^2) \;=\; 0 \quad . \tag{D.4}$$

The effect of a mass shift follows only after a complete resummation has been done and can not be simulated by taking into account only a finite number of terms in Eq. D.3. For energies where $\mathcal{I}\mathrm{m}\,\Pi(q^2)$ is non vanishing, the particle has a finite lifetime, or by the uncertainty principle, its dispersion relation is not sharp anymore.

D.1.1 Fields with Spin

In this Section the more complicated case of a field carrying an external spin index is considered. Think, for example, of a spin-1 particle, characterized by a polarization vector $\epsilon^\mu(q)$ or a spin-$\frac{1}{2}$ particle, described by a spinor $u_s(q)$. Then the propagator of the field and the self energy are matrices in Dirac space (spin-$\frac{1}{2}$ fields), Lorentz space (spin-1 fields) or in both spaces (spin-$\frac{3}{2}$ fields), thus complicating the solution of the Dyson-Schwinger equation. We will also discuss how the structure of propagator and self energy gets more involved in the presence of a medium.

Spin-1

For a spin-1 particle with four-momentum q_μ, the self energy tensor carries two external Lorentz indices. It depends on the four-vectors q_μ and, in the medium, on n_μ, which characterizes the medium. It follows that the most general Lorentz structure of the self energy is given by:

$$\Pi_{\mu\nu}(q,n) \;=\; g_{\mu\nu}\,\Pi_1(q,n) + q_\mu\,q_\nu\,\Pi_2(q,n) + n_\mu\,n_\nu\,\Pi_3(q,n) + n_\mu\,q_\nu\,\Pi_4(q,n) \quad . \tag{D.5}$$

Imposing current conservation $q^\mu\,\Pi_{\mu\nu} = 0$ simplifies the above structure [106, 44] since only certain combinations of p_μ and n_μ are allowed. These are the tensors $P^T_{\mu\nu}(q)$, $T_{\mu\nu}(q)$ and $L_{\mu\nu}(q)$, which have been introduced in detail in Section B.3. They allow for a decomposition of the self energy tensor $\Pi_{\mu\nu}$:

$$\begin{aligned} \Pi_{\mu\nu}(q) &= P^T_{\mu\nu}(q)\,\Pi_{vac}(q) && \text{(Vacuum)} \\ \Pi_{\mu\nu}(q) &= T_{\mu\nu}(q)\,\Pi^T(q) + L_{\mu\nu}(q)\,\Pi^L(q) && \text{(Medium)} \end{aligned} \quad . \tag{D.6}$$

The argument n_μ has been dropped here since throughout this work we will assume that $n_\mu = (m_N, \mathbf{0})$. In order to obtain the sought after scalar component of the self energy, the self energy tensor is contracted with the appropriate projector:

$$\begin{aligned} \Pi_{vac}(q) &= \tfrac{1}{3} P^T_{\mu\nu}\,\Pi^{\mu\nu}(q) && \text{(four-transverse)} \\ \Pi^T(q) &= \tfrac{1}{2} T_{\mu\nu}\,\Pi^{\mu\nu}(q) && \text{(three-transverse)} \\ \Pi^L(q) &= L_{\mu\nu}\,\Pi^{\mu\nu}(q) && \text{(three-longitudinal)} \end{aligned} \quad . \tag{D.7}$$

With these projectors the solution of the Dyson-Schwinger equation becomes trivial. Let α denote (a) the 4-transverse channel (vacuum) or (b) the either the 3-transverse and

the 3-longitudinal channels (medium). The Dyson-Schwinger, which is initially a matrix equation, reduces then into separate scalar equations for each channel α. In first order in the self energy one obtains for the propagator $\mathcal{D}_1^{\mu\nu}(q)$:

$$\begin{aligned} P_\alpha^{\nu\mu}\,\mathcal{D}_1^{\mu\nu}(q^2) &= Tr\,[P_\alpha]\;D_\alpha^1 \\ &= P_\alpha^{\nu\mu}\,\mathcal{D}_0^{\mu\kappa}(q^2)\,\Pi^{\kappa\lambda}(q^2)\mathcal{D}_0^{\lambda\nu}(q^2) \\ &= P_\alpha^{\nu\mu}\sum_{\beta,\gamma,\delta} P_\beta^{\mu\kappa}\,P_\gamma^{\kappa\lambda}\,P_\delta^{\lambda\nu}\,\mathcal{D}_{0,\beta}(q^2)\,\Pi_\gamma(q^2)\,\mathcal{D}_{0,\delta}(q^2) \\ &= Tr\,[P_\alpha]\;\mathcal{D}_{0,\alpha}(q^2)\,\Pi_\alpha(q^2)\,\mathcal{D}_{0,\alpha}(q^2) \end{aligned} \tag{D.8}$$

Here α, β, γ, δ stand for the various polarization channels and μ, ν, κ, λ denote Lorentz indices. This procedure can evidently be followed through step by step of the expansion of the full propagator, leading to the result:

$$D_\alpha(q^2) = \frac{1}{q^2 - M_0^2 - \Pi_\alpha(q^2)} \quad . \tag{D.9}$$

This has the same form as the Dyson-Schwinger equation for a scalar particle and shows that the propagator has the same decomposition as the self energy.

In the Sections D.2 and D.3 we will show how one can calculate the imaginary part of the self energy. The real part is then obtained by a dispersion relations. Further details concerning the dispersion relations are presented in Chapter 3.1 and in Appendix E.2.

Spin-$\frac{1}{2}$

For spin-$\frac{1}{2}$ states self energy and propagator are matrices in Dirac space. In vacuum the self energy of a spin-$\frac{1}{2}$ particle is written down as:

$$\Sigma(k) = \not{k}\, I_1(k) + I_2(k) \quad . \tag{D.10}$$

The scalar quantities I_1 and I_2 are obtained by appropriate traces:

$$I_1(k) = \frac{1}{4\,k^2}\,Tr\,[\not{k}\,\Sigma(k)] \quad , \quad I_2(k) = \frac{1}{4}\,Tr\,[\Sigma(k)] \quad . \tag{D.11}$$

In terms of these self energies the vacuum propagator $\mathcal{G}_F(k)$ reads:

$$\mathcal{G}_F(k) = \frac{1}{\not{k} - M - \Sigma(k)} = \frac{\not{k}(1-I_1) + (M+I_2)}{k^2(1-I_1)^2 - (M+I_2)^2} \quad .$$

In this work we will not keep the full matrix structure of propagator and self energy and make some simplifications instead. The exact self energy is replaced by a scalar averaged quantity, which results from averaging $\Sigma(k)$ over the spins:

$$\begin{aligned} \langle\Sigma(k)\rangle &= \frac{1}{2}\sum_s \bar{u}_s(k)\,\Sigma(k)\,u_s(k) \\ &= \frac{1}{2}\,Tr\left[(\not{k} + \sqrt{k^2})\,\Sigma(k)\right] \quad . \end{aligned} \tag{D.12}$$

We will show in Sections D.2 and D.3 how the imaginary part of the self energy can be calculated. The real part of the self energy is obtained via a dispersion relation from

$\langle\Sigma(k)\rangle$. For a detailed discussion see Chapter 3.2 and Appendix E.2. According to Eqs. B.16 and B.17, this expression may be viewed as the projection of the self energy $\Sigma(k)$ onto spin-$\frac{1}{2}$ states. This also explains the prefactor $\frac{1}{2}$.

It is interesting that $\langle\Sigma(k)\rangle$ consists of nearly the same combination of I_1 and I_2 as found in the denominator of the full propagator Eq. D.12, when quadratic terms in the self energy are discarded. Comparison with Eq. D.12 shows that the denominator reads:

$$2\,\mathcal{I}\mathrm{m}\,(k^2\,I_1(k) - I_1(k)^2 + M\,I_2(k) + I_2(k)^2) \;\approx\; 2\,\mathcal{I}\mathrm{m}\,(k^2\,I_1(k) + M\,I_2(k)) \quad \text{(D.13)}$$

as compared to what is obtained from Eq. D.12

$$2\,\mathcal{I}\mathrm{m}\left(k^2\,I_1(k) + \sqrt{k^2}\,I_2(k)\right) \quad . \quad \text{(D.14)}$$

Clearly, for on-shell particles both expressions are identical. But off-shell the multiplying I_2 is replaced by $M \to \sqrt{k^2}$. For the propagator we take the following form:

$$\mathcal{G}_F(k) \;=\; \frac{\not{k} + \sqrt{k^2}}{k^2 - M^2 - \langle\Sigma(k)\rangle} \quad . \quad \text{(D.15)}$$

The appearance $\sqrt{k^2}$ instead of M in the numerator is motivated in Chapter5, Section 5.2.4.

In nuclear matter one has in principle to consider one more independent structure in the self energy:

$$\Sigma(k) \;=\; \not{k}\,I_1(k) + I_2(k) + \not{n}\,I_3(k) \quad . \quad \text{(D.16)}$$

Since we average out the Dirac structure of self energy and propagator, we do not need to worry about this complication.

Spin-$\frac{3}{2}$

The self energy of a spin-$\frac{3}{2}$ field has a rather involved structure, owing to the fact that is a matrix in both Dirac and Lorentz space and a full decomposition of the self energy is very complicated already in the vacuum [66]. In analogy to the spin-$\frac{1}{2}$ states we therefore consider an averaged self energy of the form:

$$\mathcal{I}\mathrm{m}\,\langle\Sigma(k)\rangle \;=\; \frac{1}{4}\mathcal{I}\mathrm{m}\,Tr\left[(\not{k} + \sqrt{k^2})\,P^{\mu\nu}_{3/2}(k)\,\Sigma_{\mu\nu}(k)\right] \quad , \quad \text{(D.17)}$$

and as in the case of spin-$\frac{1}{2}$ states we obtain the real part of the self energy by a dispersion relation over $\mathcal{I}\mathrm{m}\,\langle\Sigma(k)\rangle$. The full propagator of the spin-$\frac{3}{2}$ field is cast into the form:

$$\mathcal{G}^{\mu\nu}_F(k) \;=\; \frac{\not{k} + \sqrt{k^2}}{k^2 - M^2 - \langle\Sigma(k)\rangle}\,P^{\mu\nu}_{3/2}(k) \quad , \quad \text{(D.18)}$$

where the replacement $M \to \sqrt{k^2}$ is explained in Chapter 5, Section 5.2.4.

D.2 Imaginary part of a self energy I

The imaginary part of a self energy diagram can be calculated in two different ways. The first one is to consider the discontinuity of the self energy across the branch cut on the positive real axis. This leads to the formulation of Cutkosky's cutting rules [106]. An alternative way is to consider the coupling to all intermediate states and calculate the corresponding squared matrix element. This corresponds to a evaluation of the width Γ, which is directly related to the imaginary part of the self energy.

D.2.1 Cutkosky's cutting rules

Cutkosky's cutting rules state the following. If one

- considers all possible cuts through propagator lines in a Feynman diagram that allow the particles to be on shell
- replaces each propagator corresponding to a stable particle according to $\dfrac{1}{p^2 - M^2 + i\,\epsilon} \to -2\pi i\,\delta(p^2 - M^2)$
- replaces each propagator corresponding to a broad particle by its spectral function according to $\dfrac{1}{p^2 - M^2 - \Pi} \to -2\pi i\,\mathcal{A}$
- sums over all cuts

then one obtains the discontinuity $Disc(\Pi) = 2i\,\mathcal{I}\mathrm{m}\,\Pi$.

We want to discuss this recipe now for a simple example, namely the self energy of a particle ϕ_1 interacting with particles ϕ_2 and ϕ_3:

$$\mathcal{L} \;=\; \lambda\,\phi_1\phi_2\phi_3 \quad . \tag{D.19}$$

According to the Feynman rules, see Appendix B, the self energy of particle 1 reads:

$$-i\Pi_1(q) \;=\; (i\lambda)^2 \int \frac{d^4p}{(2\pi)^4} \frac{i}{p^2 - m_2^2 + i\epsilon}\, \frac{i}{(q-p)^2 - m_3^2 + i\epsilon}$$

Applying the cutting rules one obtains for the imaginary part of the self energy:

$$\begin{aligned}
\mathcal{I}\mathrm{m}\,\Pi_1(q) \qquad &= \qquad -\frac{\lambda^2}{2} \int \frac{d^4p}{(2\pi)^4} (-2\pi)^2 \delta(p^2 - m_2^2)\,\delta((q-p)^2 - m_3^2) \\
&\overset{\text{in RF of 1}}{=} \quad -\frac{\lambda^2}{2} \int \frac{d^3p}{(2\pi)^2} \delta((\sqrt{q^2} - E_2(p))^2 - p^2 - m_3^2) \frac{1}{2E_2(p)} \\
&= \qquad -\frac{\lambda^2}{2}\,\frac{1}{\pi}\,\frac{p^2}{2E_2(p)}\,\frac{E_2(p)}{2\sqrt{q^2}\,p} \\
&= \qquad -\frac{p}{8\pi\sqrt{q^2}}\,\lambda^2 \quad .
\end{aligned}$$

By RF we denote the rest frame of particle ϕ_1. Note that p is the cm momentum of particles ϕ_2 and ϕ_3 and $\sqrt{q^2}$ is the invariant mass of particle ϕ_1.

D.2.2 Direct Calculation of Γ

We now aim at a direct calculation of $\mathcal{I}\mathrm{m}\,\Pi$. To this end we consider the decay width Γ, which is given by (see Eq. B.37 in Appendix B.6) :

$$\Gamma(q) \;=\; \frac{p}{8\pi q_0\sqrt{q^2}}\frac{1}{2j+1}|\mathcal{M}|^2 \quad , \tag{D.20}$$

where p is the cm momentum of the decay particles, q^2 is the squared invariant mass of the decaying particle, j its spin and $\mathcal{M}$ is the decay amplitude. By q_0 the energy of the decaying particle is denoted. In the rest frame of the decaying particle $q_0 = \sqrt{q^2}$. Applying this to the above situation with the matrix element determined by Eq. D.19, we find $|\mathcal{M}|^2 = \lambda^2$ and $j = 0$, such that

$$\Gamma(q) \;=\; \frac{p}{8\pi\sqrt{q^2}q_0}\,\lambda^2 \quad . \tag{D.21}$$

It follows a relation between decay width and imaginary part of the self energy:

$$\mathcal{I}\mathrm{m}\,\Pi(q) \;=\; -q_0\,\Gamma(q) \quad . \tag{D.22}$$

Note that the self energy is a Lorentz scalar, whereas the width transforms such that the product $q_0\,\Gamma$ is Lorentz invariant. In Chapter 3 we give explicit expressions for the vacuum self energies of ρ meson and baryon resonances.

D.3 Imaginary part of a self energy II

In this Section we calculate the imaginary part of the self energy in a slightly different way. The idea is to rewrite the Feynman propagator in terms of the retarded/advanced propagators and the quantities $D^{</>}$: Based on the Eqs. E.21, E.29 and E.49 and using the relation

$$sgn(p_0-\mu) \;=\; 1-2\,\theta(\mu-p_0) \;=\; -1+2\,\theta(p_0-\mu) \tag{D.23}$$

we can rewrite meson and nucleon propagator as

$$D^F(q) \;=\; D^+(q)+2\,i\,\pi\,\theta(-q_0)\,\mathcal{A}(q) \;=\; D^-(q)-2\,i\,\pi\,\theta(q_0)\,\mathcal{A}(q)$$

$$\mathcal{G}^F(p) \;=\; \mathcal{G}^+(p)+2\,i\,\pi\,\theta(\mu-p_0)\,\rho(p) \;=\; \mathcal{G}^-(p)-2\,i\,\pi\,\theta(p_0-\mu)\,\rho(p) \quad .$$

As we will see, the resulting terms have a more transparent analytic structure and they allow for a straightforward calculation of the imaginary part of the self energy. As an example, we calculate the self energy of a baryon resonance in the medium by decomposing the Feynman propagator according to Eqs. E.18 and E.36:

$$\begin{aligned}
\Sigma^F(k) \;&=\; i\int\frac{d^4p}{(2\pi)^4}\,D^F(k-p)\,\mathcal{G}^F(p)\,\Omega \\
&=\; i\int\frac{d^4p}{(2\pi)^4}\,\left[D^-(k-p)-2\,i\,\pi\,\theta(k_0-p_0)\mathcal{A}(k-p)\right] \\
&\qquad\qquad \left[\mathcal{G}^+(p)+2\,i\,\pi\,\theta(\mu-p_0)\rho\right]\,\Omega \\
&=\; i\int\frac{d^4p}{(2\pi)^4}\,\left[2\,i\,\pi\,\theta(\mu-p_0)\,D^-(k-p)\,\rho(p)-2\,i\,\pi\,\theta(k_0-p_0)\,\mathcal{G}^+(p)\right. \\
&\qquad\qquad \left.\times\,\mathcal{A}(k-p)+\,4\,\pi^2\,\theta(k_0-p_0)\,\theta(\mu-p_0)\,\mathcal{A}(k_0-p_0)\,\rho(p)\right]\,\Omega \quad .
\end{aligned} \tag{D.24}$$

Here Ω is a trace from the spin summation at the resonance-nucleon-meson vertices. The term involving the product of D^- and $\mathcal{G}^+$

$$\int \frac{d^4p}{(2\pi)^4} \mathcal{G}^+(p)\, D^-(k-p) \tag{D.25}$$

vanishes since the poles of $\mathcal{G}^+(p)$ and $D^-(k-p)$ are located in the same half plane and therefore the dp_0 integration vanishes. The remaining terms do not contain products of propagators and $\mathcal{I}\mathrm{m}\,\Sigma^F$ is readily found. Additional factors from isospin and and coupling constants are suppressed. The imaginary part of the self energy is now found to be:

$$\begin{aligned} \mathcal{I}\mathrm{m}\,\Sigma^F(k) &= \int \frac{d^4p}{(2\pi)^3} \left[-\theta(\mu-p_0)\,\mathcal{I}\mathrm{m}\,D^-(k-p)\,\rho(p) + \right. \\ &\qquad \theta(k_0-p_0)\,\mathcal{I}\mathrm{m}\,\mathcal{G}^+(p)\,\mathcal{A}(k_0-p_0) + \\ &\qquad \left. 2\,\pi\,\theta(k_0-p_0)\,\theta(\mu-p_0)\,\mathcal{A}(k_0-p_0)\,\rho(p)\right]\,\Omega \\ &= \int \frac{d^4p}{8\,\pi^2} \mathcal{A}(k-p)\,\rho(p)\,\left[-2\,\theta(p_0-k_0)\,\theta(\mu-p_0) - \right. \\ &\qquad \left. 2\,\theta(k_0-p_0)\,\theta(p_0-\mu)\right]\,\Omega \quad . \end{aligned} \tag{D.26}$$

The second term is the usual decay of resonance with energy $k_0 > p_0$ into a meson of positive energy and a nucleon above the Fermi sea. Apart from the Pauli correction – represented by the term $\theta(p_0-\mu)$ – this term is already present in the vacuum. The first term, however, is (partly) new and describes a physical process where a nucleon decays forming a resonance of positive energy, which is far off shell since its energy $k_0 < \mu$, and a meson. In the vacuum $\mu = 0$ and the first term just reflects the symmetry with respect to k_0 of the imaginary part of the Feynman self energy as expected from the discussion in Appendix E.2. In the practical calculations we omit the first term. It is zero around the resonance peak and may only influence the resonance region via the dispersion relation used to determine the real part of the self energy. For completeness we mention that by using Cutkosky's rules one would have obtained the same result: the first terms originates from the hole part of the nucleon propagator and the second term from its particle part.

Appendix E

Analytic Structure of the Propagator

Aim of this Appendix is the study of the analytic properties of propagator and self energy. Apart from the Feynman or causal propagator, we introduce also the retarded propagator $\mathcal{D}^+$ and self energy Π^+. In the first Section we will discuss the so called Källen-Lehmann representation for the propagator of bosons and fermions. In particular, the constraints on the spin-$\frac{1}{2}$ propagator arising from this representation are discussed in some detail. The second Section deals with dispersion relations and sum rules for the imaginary part of the retarded propagator, the spectral function. Also the relation between Feynman and retarded propagator is studied.

E.1 Källen-Lehmann

E.1.1 Scalar Particles

The Feynman propagator of a non-interacting scalar particle of mass M is defined as [106, 16]

$$\begin{aligned} \mathcal{D}_F(p^2) &= -i \int d^4x\, e^{i\,p\,x}\, \langle 0|\mathcal{T}\phi(x)\phi(0)|0\rangle \\ &= \frac{1}{p^2 - M^2 + i\epsilon} \quad . \end{aligned} \tag{E.1}$$

In an interacting theory one has to consider the possibility of intermediate multi-particle states. These may be either bound or continuous states. Therefore the analytic structure of the Feynman propagator $\mathcal{D}_F$ becomes more complicated: rather than a single pole at the on-shell point with strength 1, there will be various poles originating from the single-particle and (possibly) from bound states as well as a branch cut starting at the threshold energy for the formation of multi-particle states. This behaviour is summarized in the *Källen-Lehmann* spectral representation of the propagator:

$$\begin{aligned} \mathcal{D}_F(p^2) &= -i \int d^4x\, e^{i\,p\,x}\, \langle \Omega|\mathcal{T}\phi(x)\phi(0)|\Omega\rangle \\ &= \frac{Z}{p^2 - M^2 + i\epsilon} + \int\limits_{4\,M^2}^{\infty} dk^2 \rho(k^2)\, \frac{1}{p^2 - k^2 + i\,\epsilon} \quad . \end{aligned} \tag{E.2}$$

Here as well as in the remainder of this chapter, the contributions of bound states have been suppressed. A detailed derivation of this famous representation can be found in many text books on quantum field theory, see for example [106, 16].

The quantity $\rho(k)$ is determined by the following matrix element [16]:

$$\rho(k) \;=\; (2\,\pi)^3 \sum_{\lambda} \delta(k^2 - k_n^2) |\, \langle \Omega |\, \phi(0)\, | n \rangle \,|^2 \quad , \tag{E.3}$$

where $|n\rangle$ represents a single- or multi particle state of mass m_n^2. Since particle number is conserved, a normalization condition is fulfilled:

$$Z + \int\limits_{4\,M^2}^{\infty} dk^2 \rho(k^2) \;=\; 1 \quad , \tag{E.4}$$

implying that the strength of the one-particle state is less than unity. We will prove this sumrule in Section E.2.

E.1.2 Spin-$\frac{1}{2}$ and spin-$\frac{3}{2}$ fields

For fields which carry spin, the Källen-Lehmann representation has a more involved structure. Let us discuss in some detail the case of a spin 1/2 field. Again we follow closely the arguments presented in [16]. As it is demonstrated there, symmetry under Lorentz- and parity transformations allows to write the propagator $\mathcal{G}_F(p^2)$ as an integral over two scalar functions:

$$\mathcal{G}_F(p^2) \;=\; \int\limits_0^{\infty} dk^2 \left[\not{p}\, \rho_1(k^2) + \rho_2(k2) \right] \frac{1}{p^2 - k^2 + i\,\epsilon} \quad . \tag{E.5}$$

This result is not surprising: from Lorentz invariance one expects a scalar term and a term multiplying γ_μ, which is to be contracted with the only available four-vector. Parity conservation rules out terms $\propto \gamma^5$. Of some importance for the discussion of the meson-nucleon forward scattering amplitude are some properties of ρ_1 and ρ_2 (see discussion in Section 5.2.4), which we therefore quote and prove now. They are taken from [16]:

(1)	$\rho_1(k^2)$ and $\rho_2(k^2)$ are both real
(2)	$\rho_1(k^2) \geq 0$
(3)	$\sqrt{k^2}\,\rho_1(k^2) - \rho_2(k^2) \geq 0$

(E.6)

The proofs will rely on two representations of $\rho_{\alpha\,\beta}(k^2)$:

$$\rho_{\alpha\,\beta}(k^2) \;=\; (2\,\pi)^2 \sum_n \delta^4(k_n - k)\; \langle \Omega | \psi_\alpha(0) | n \rangle\; \left\langle n | \bar{\psi}_\beta(0) | \Omega \right\rangle \tag{E.7}$$

$$\rho_{\alpha\,\beta}(k^2) \;=\; \rho_1\, \not{k} + \rho_2\, \delta_{\alpha\,\beta} \tag{E.8}$$

Also, the rule for constructing the hermitian conjugate of any Dirac-matrix Γ_μ will be used [16, 41]:

$$\Gamma_\mu^\dagger \;=\; \gamma^0\,\Gamma_\mu\,\gamma^0 \tag{E.9}$$

Proof 1:

$$\begin{aligned}
\rho^\star_{\alpha\,\beta} &\overset{E.7}{=} (2\,\pi)^2 \sum_n \delta^4(k_n - k)\;\langle\Omega|\psi_\alpha(0)|n\rangle^\star\;\left\langle n|\bar\psi_\beta(0)|\Omega\right\rangle^\star \\
&= (2\,\pi)^2 \sum_n \delta^4(k_n - k)\;\left\langle n|\bar\psi_\mu(0)|\Omega\right\rangle\;\gamma^0_{\mu\alpha}\,\gamma^0_{\beta\nu}\,\langle\Omega|\psi_\nu(0)|n\rangle \\
&= \gamma^0_{\beta\nu}\,\rho_{\nu\mu}\,\gamma^0_{\mu\alpha} \\
&= \left[\gamma^0\,\rho\,\gamma^0\right] \\
&\overset{E.8}{=} \rho_1\,\not{k}^\star + \rho_2\,\delta_{\alpha\beta}
\end{aligned}$$

Proof 2: Here we consider $Tr\left[\rho\,\gamma^0\right]$ for both expressions E.7 and E.8:

$$\begin{aligned}
Tr\left[\gamma^0\,\rho\right] &\overset{E.8}{=} 4\,k_0\,\rho_1 \\
&\overset{E.7}{=} (2\,\pi)^2 \sum_n \delta^4(k_n - k)\;\langle\Omega|\psi_\alpha(0)|n\rangle\;\left\langle n|\bar\psi_\beta(0)|\Omega\right\rangle\;\gamma^0_{\beta\alpha} \\
&= (2\,\pi)^2 \sum_n \delta^4(k_n - k)\;\langle\Omega|\psi_\alpha(0)|n\rangle\;\left\langle n|\psi^\dagger_\alpha(0)|\Omega\right\rangle \\
&= (2\,\pi)^2 \sum_n \delta^4(k_n - k)\;|\,\langle\Omega|\psi_\alpha(0)|n\rangle\,|^2 \\
&\geq 0 \quad .
\end{aligned}$$

Since $k_0 > 0$ this implies that $\rho_1 > 0$ as well. Repeating the same steps, but tracing with the unit matrix rather than γ^0 in order to project onto ρ_2, one realizes that ρ_2 may be negative. This is interesting, as one might have been (incorrectly) tempted to interpret ρ_2 as being related to some sort of scalar spectral function.

Proof 3: This time we consider the operator $(i\not{\nabla} - m)\,\psi$, where $m = \sqrt{k^2}$ and build its absolute square:

$$\begin{aligned}
0 \;\leq\; & (2\,\pi)^2 \sum_n \delta^4(k_n - k)\;\langle\Omega|(i\not{\nabla} - m)_{\alpha\mu}\psi_\mu(0)|n\rangle\;\times \\
&\qquad\qquad \times\left\langle n|\,[(i\not{\nabla} - m)_{\alpha\nu}\,\psi_\nu(0)]^\dagger\,|\Omega\right\rangle \\
= \;& (2\,\pi)^2 \sum_n \delta^4(k_n - k)\,(i\not{\nabla} - m)_{\alpha\mu}\;\langle\Omega|\psi_\mu(0)|n\rangle\;\times \\
&\qquad\qquad \times\left\langle n|\psi_\nu(0)^\dagger|\Omega\right\rangle\;[(i\not{\nabla} - m)_{\alpha\nu}]^\dagger \\
= \;& (2\,\pi)^2 \sum_n \delta^4(k_n - k)\,(i\not{\nabla} - m)_{\alpha\mu}\;\langle\Omega|\psi_\mu(0)|n\rangle\;\times \\
&\qquad\qquad \times\left\langle n|\bar\psi_\nu(0)|\Omega\right\rangle\left[(i\not{\nabla} - m)\,\gamma^0\right]_{\nu\alpha} \\
= \;& Tr\left[(\not{k} - m)\rho(k^2)(\not{k} - m)\gamma_0\right] \\
= \;& 8\,k_0\,\sqrt{k^2}\,(\sqrt{k^2}\,\rho_1(k^2) - \rho_2(k^2)) \quad .
\end{aligned}$$

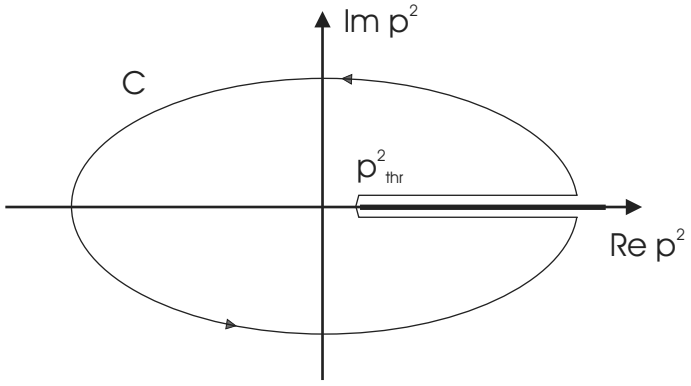

Figure E.1: Contour leading to the Källen Lehmann representation of any two point function.

Since $k_0 \geq 0$, the desired relation is proved. Note that the steps leading to the second and fourth line in the above calculation are based on the Lorenz-invariance of the field operator ψ, which manifests itself in the relation

$$[P^\mu, \psi(x)] \;=\; -i\,\frac{\partial \psi(x)}{\partial x_\mu} \quad . \tag{E.10}$$

In analogy to the scalar case, one can write down a normalization condition for the function $\rho_1(k^2)$:

$$\int\limits_{M^2_{min}}^{\infty} dk^2 \rho_1(k^2) \;=\; 1 \quad . \tag{E.11}$$

The relativistic propagator of spin-$\frac{3}{2}$ fields contains additional Lorentz indices. Therefore the most general decomposition of the propagator similar to that of Eq. E.5 is a formidable task [66, 27]. As mentioned in Subsection D.1.1, we assume that self energy and propagator are proportional to the projector $P^{\mu\nu}_{3/2}$, Eq. B.28. Then the Lorentz structure is simplified and in direct analogy to the spin-$\frac{1}{2}$ case one can write down:

$$\mathcal{G}^{\mu\nu}_F(p^2) \;=\; \int\limits_0^{\infty} dk^2 \left[\not{p}\,\rho_1(k^2) + \rho_2(k^2)\right] \frac{1}{p^2 - k^2 + i\,\epsilon}\, P^{\mu\nu}_{3/2}(k^2) \quad . \tag{E.12}$$

E.1.3 Dispersion Relation

In Fig. E.1 we show the analytic structure of the propagator in the complex p^2 plane, see also [106]. For invariant masses larger than p^2_{thr}, the propagator develops a branch cut. Using the identity [106]

$$\mathcal{I}\mathrm{m}\,\mathcal{D}_F(p^2 + i\,\epsilon) \;=\; -\mathcal{I}\mathrm{m}\,\mathcal{D}_F(p^2 - i\,\epsilon) \quad , \tag{E.13}$$

one sees that the discontinuity across this branch cut is given by:

$$Disc\,\mathcal{D}_F(p^2) \;=\; 2\,i\,\mathcal{I}\mathrm{m}\,\mathcal{D}_F(p^2 + i\,\epsilon) \quad . \tag{E.14}$$

Since $\mathcal{D}_F(p^2)$ is an analytic function of p^2 everywhere else in the complex p^2-plane, the value of $\mathcal{D}_F(p^2)$ is determined by $Disc\,\mathcal{D}_F(p^2)$ along the branch cut via a dispersion relation:

$$\mathcal{D}_F(p^2) \;=\; \int\limits_{k^2_{thr}}^{\infty}\frac{dk^2}{\pi}\,\frac{\mathcal{I}\mathrm{m}\,\mathcal{D}_F(k^2)}{k^2-p^2-i\,\epsilon} \quad\Rightarrow\quad \mathcal{R}\mathrm{e}\,\mathcal{D}_F(p^2) \;=\; \mathcal{P}\int\limits_{k^2_{thr}}^{\infty}\frac{dk^2}{\pi}\,\frac{\mathcal{I}\mathrm{m}\,\mathcal{D}_F(k^2)}{k^2-p^2} \quad . \tag{E.15}$$

Note that a dispersion relation is also suggested from the Lehmann representation. Dispersion relations hold also for the self-energies of mesons and baryon resonances, $\Pi(p^2)$ and $\Sigma(p^2)$ respectively, since the propagator is constructed from the self energies:

$$\mathcal{R}\mathrm{e}\,\Pi(p^2) \;=\; \mathcal{P}\int\limits_{k^2_{thr}}^{\infty}\frac{dk^2}{\pi}\,\frac{\mathcal{I}\mathrm{m}\,\Pi(k^2)}{k^2-p^2} \quad .$$

This relation is very useful for the calculation of the real part of loop diagrams. The imaginary part of the self-energy can be readily calculated using Cutkosky's cutting rules, see Appendix D. The principal value integral can then be obtained numerically. If the dispersion integral does not converge, one needs to employ a subtracted dispersion relation. The basic idea is not to consider the value of $\mathcal{R}\mathrm{e}\,\Pi(p^2)$, but rather the difference to some reference value taken at q^2:

$$\begin{aligned}\mathcal{R}\mathrm{e}\,\Pi(p^2)-\mathcal{R}\mathrm{e}\,\Pi(q^2) \;&=\; \mathcal{P}\int\limits_{k^2_{thr}}^{\infty}\frac{dk^2}{\pi}\,\frac{\mathcal{I}\mathrm{m}\,\Pi(k^2)}{k^2-p^2}-\mathcal{P}\int\limits_{k^2_{thr}}^{\infty}\frac{dk^2}{\pi}\,\frac{\mathcal{I}\mathrm{m}\,\Pi(k^2)}{k^2-q^2} \\ &=\; (q^2-p^2)\,\mathcal{P}\int\limits_{k^2_{thr}}^{\infty}\frac{dk^2}{\pi}\,\frac{\mathcal{I}\mathrm{m}\,\Pi(k^2)}{(k^2-p^2)(k^2-q^2)} \quad .\end{aligned} \tag{E.16}$$

The high energy contribution is now suppressed by a relative factor of $1/k^2$, which improves the convergence of the integral and reduces the sensitivity on the high-energy behaviour of the imaginary part, which is hard to control within a hadronic theory. However, the price to pay is that the subtraction constant $\mathcal{R}\mathrm{e}\,\Pi(q^2)$ is a priori unknown and needs to be fixed by additional requirements. An example of that we have seen in Chapter 3, where the real part of the ρ vacuum self energy was fixed using gauge invariance and the condition that the photon remains massless.

E.2 Field Operators

In the previous Section we have discussed the Lehmann representation of the propagator of mesons and baryons in the vacuum. Apart from discussing some properties of the strength function ρ_1 and ρ_2, this also lead us to write down a dispersion relation connecting the imaginary and real part of self energy and propagator. However, the arguments brought forward in the previous Section are not easily extended into the nuclear medium. As explained in Section 5.2.1, in a medium propagator and self energy depend on the energy p_0 and momentum $|\mathbf{p}|$ independently and a discussion of their analytic properties in terms of the invariant mass p^2 – as done in the Lehmann picture – can not be exhaustive.

We will now formulate the analytic properties of the propagator in terms of field operators. This way we can derive dispersion relations for the retarded propagator, explain the sum rules Eqs. E.4 and E.11 as well as discuss the relation between retarded and Feynman propagators. For the self energies the same relations must hold. This becomes clear when one expresses the propagator in terms of self energies, e.g.

$$D(p) \;=\; \frac{1}{p^2 - m^2 - \Pi(p)} \quad . \tag{E.17}$$

Then the symmetries of $\mathcal{R}\mathrm{e}\, D/\mathcal{I}\mathrm{m}\, D$ can only be satisfied if the self energies $\mathcal{R}\mathrm{e}\,\Pi/\mathcal{I}\mathrm{m}\,\Pi$ possess the same symmetry.

E.2.1 Bosons

Let us define the following quantities $D^<$, $D^>$, D^+, D^- and D^F:

$$\begin{aligned}
D^>(x,y) &= -i\,\big\langle \phi(x)\,\phi^\dagger(y)\big\rangle \quad , \quad D^<(x,y) \;=\; -i\,\big\langle \phi^\dagger(y)\,\phi(x)\big\rangle \\
D^+(x,y) &= -i\,\theta(x_0-y_0)\,\big\langle \big[\phi(x),\phi^\dagger(y)\big]\big\rangle \\
&= \theta(x_0-y_0)\,\langle\, D^>(x,y) - D^<(x,y)\rangle \\
D^-(x,y) &= -i\,\theta(y_0-x_0)\,\big\langle \big[\phi^\dagger(y),\phi(x)\big]\big\rangle \\
&= \theta(y_0-x_0)\,\langle D^<(x,y) - D^>(x,y)\rangle \\
D^F(x,y) &= -i\,\big\langle \big[\theta(x_0-y_0)\,\phi(x)\,\phi^\dagger(y) + \theta(y_0-x_0)\,\phi^\dagger(y)\,\phi(x)\big]\big\rangle \\
&= D^+(x,y) + D^<(x,y) \;=\; D^-(x,y) + D^>(x,y) \quad .
\end{aligned} \tag{E.18}$$

Here D^F is the Feynman propagator, D^+ is the retarded propagator and D^- is the advanced propagator. The quantities $D^>$ and $D^<$ have been introduced for notational convenience at this place. Note the behaviour of $D^<$ and $D^>$ under complex conjugation:

$$D^{<\,\dagger}(x,y) \;=\; -D^<(y,x) \quad , \quad D^{>\,\dagger}(x,y) \;=\; -D^>(y,x) \quad . \tag{E.19}$$

In the following we are going to use that the ground state $|G\rangle$ both of nuclear matter and the vacuum is invariant under translations and allows for the transformation:

$$\begin{aligned}
\big\langle G|\phi(-x)\,\phi^\dagger(0)|G\big\rangle &= \big\langle G|\mathcal{T}^{-1}\phi(-x)\mathcal{T}\mathcal{T}^{-1}\phi^\dagger(0)\mathcal{T}|G\big\rangle \\
&= \big\langle G|\phi(0)\,\phi^\dagger(x)|G\big\rangle \quad .
\end{aligned} \tag{E.20}$$

The operator $\mathcal{T}$ generates translations.

Next we calculate the imaginary part of the retarded propagator in momentum space:

$$\begin{aligned}
\mathcal{I}\mathrm{m}\, D^+(p) &= \frac{1}{2i}\,\big(D^+(p) - D^{+\star}(p)\big) \\
&= -\frac{i}{2}\left\{\int d^4x\, e^{ipx}\,\theta(x_0)\,[D^>(x,0) - D^<(x,0)] + \int d^4x e^{-ipx}\,\theta(x_0)\,[D^>(0,x) - D^<(0,x)]\right\} \\
&= -\frac{i}{2}\int d^4x e^{ipx}\left\{\theta(x_0)\,[D^>(x,0) - D^<(x,0)] + \theta(-x_0)\,[D^>(0,-x) - D^<(0,-x)]\right\} \\
&= -\frac{i}{2}\int d^4x e^{ipx}\left\{\theta(x_0)\,[D^>(x,0) - D^<(x,0)] + \theta(-x_0)\,[D^>(x,0) - D^<(x,0)]\right\} \\
&= -\frac{i}{2}\int d^4x\, e^{ipx}\,\big[D^>(x,0) - D^<(x,0)\big] \;=\; -\frac{1}{2}\int d^4x\, e^{ipx}\,\big\langle \big[\phi(x),\phi^\dagger(0)\big]\big\rangle \quad .
\end{aligned} \tag{E.21}$$

The spectral function $\mathcal{A}(p)$ is defined as the imaginary part of the retarded propagator:

$$\mathcal{A}(p) \;=\; -\frac{1}{\pi}\mathcal{I}\mathrm{m}\, D^+(p) \;=\; \frac{1}{2\pi}\int d^4x\, e^{ipx}\,\left\langle\left[\phi(x),\phi^\dagger(0)\right]\right\rangle \quad . \tag{E.22}$$

Properties of D^+

In this part we prove three properties of D^+:

$$\boxed{\begin{array}{rcll} \displaystyle\int_{-\infty}^{\infty} dp_0\, p_0\, \mathcal{A}(p^2) & = & 1 & \text{normalization} \\ \mathcal{A}(p_0,\mathbf{p}) & = & -\mathcal{A}(-p_0,\mathbf{p}) & \text{antisymmetry} \\ \mathcal{R}\mathrm{e}\, D^+(p) & = & \mathcal{P}\displaystyle\int_0^{\infty} dq_0^2\,\frac{\mathcal{A}(q_0,\mathbf{p})}{p_0^2-q_0^2} & \text{dispersion relation} \end{array}} \tag{E.23}$$

- **Normalization**
  The proof of the normalization of $\mathcal{A}$ relies on basic commutator relations. Let us introduce the conjugated momentum $\pi(x)$ as [106]:

$$\begin{aligned} \pi(x) &= \frac{\partial\mathcal{L}}{\partial(\partial_{x_0}\phi(x))} \\ &= \partial_{x_0}\phi^\dagger(x) \\ [\phi(\mathbf{x},t),\pi(\mathbf{y},t)] &= \left[\phi^\dagger(\mathbf{x},t),\pi^\dagger(\mathbf{y},t)\right] \;=\; i\,\delta^3(\mathbf{x}-\mathbf{y}) \quad . \end{aligned} \tag{E.24}$$

  This allows to write down the following normalization condition for $\mathcal{A}$:

$$\begin{aligned} \int_{-\infty}^{\infty} dp_0\, p_0\, \mathcal{A}(p^2) &= \frac{1}{2\pi}\int_{-\infty}^{\infty} dp_0\, d^4x\, e^{-i\,\mathbf{p}\,\mathbf{x}}\frac{1}{i}\left(\partial_{x_0}e^{i\,p_0\,x_0}\right)\left\langle[\phi(x),\phi^\dagger(0)]\right\rangle \\ &= \frac{1}{2\pi}\int_{-\infty}^{\infty} d^4x\, e^{-i\,\mathbf{p}\,\mathbf{x}}\frac{1}{i}\left(\partial_{x_0}2\,\pi\,\delta(x_0)\right)\left\langle[\phi(x),\phi^\dagger(0)]\right\rangle \\ &= i\int_{-\infty}^{\infty} d^4x\, e^{-i\,\mathbf{p}\,\mathbf{x}}\delta(x_0)\,\partial_{x_0}\left\langle[\phi(x),\phi^\dagger(0)]\right\rangle \\ &= i\int_{-\infty}^{\infty} d^3x\, e^{-i\,\mathbf{p}\,\mathbf{x}}\left\langle[\pi^\dagger(\mathbf{x}),\phi^\dagger(\mathbf{0})]\right\rangle \\ &= 1 \quad . \end{aligned} \tag{E.25}$$

- **Antisymmetry**
  The proof of the antisymmetry in the energy hinges on the invariance of the ground

state under isospin transformations. This is fulfilled in the vacuum and in isospin symmetric nuclear matter, but not in asymmetric nuclear matter. An isospin rotation transforms a boson into its own antiparticle and one finds for the expectation value of two fields [106, 16]:

$$\left\langle \phi(x)\,\phi^\dagger(0)\right\rangle \;\Rightarrow\; \left\langle \phi^\dagger(x)\,\phi(0)\right\rangle \quad . \tag{E.26}$$

This allows to relate $\mathcal{A}(p)$ and $\mathcal{A}(-p)$:

$$\begin{aligned}
\mathcal{A}(p) &= \frac{1}{2\pi}\int d^4x\, e^{ipx}\,\left\langle\left[\phi(x),\phi^\dagger(0)\right]\right\rangle \\
\mathcal{A}(-p) &= \frac{1}{2\pi}\int d^4x\, e^{-ipx}\,\left\langle\left[\phi(x),\phi^\dagger(0)\right]\right\rangle \\
&= \frac{1}{2\pi}\int d^4x\, e^{ipx}\,\left\langle\left[\phi(0),\phi^\dagger(x)\right]\right\rangle \;=\; -\mathcal{A}(p) \\
&\Rightarrow\; \mathcal{A}(p_0,\mathbf{p}) \;=\; -\mathcal{A}(-p_0,\mathbf{p}) \quad .
\end{aligned} \tag{E.27}$$

where the third line follows from the rotational invariance of the vacuum and the nuclear medium. It follows that in asymmetric nuclear matter the spectral function $\mathcal{A}(p)$ of charged mesons is not antisymmetric in the energy. Since neutral bosons are described by real fields with $\phi(x)=\phi^\dagger(x)$, one does not need to invoke invariance under isospin transformations to relate $\mathcal{A}(p)$ and $\mathcal{A}(-p)$ here and the spectral function of neutral bosons is antisymmetric in the energy also in asymmetric nuclear matter.

- **Dispersion Relation** The real part of the retarded propagator is related to $\mathcal{A}$ via a dispersion relation:

$$\begin{aligned}
\mathcal{R}\mathrm{e}\, D^+(p) &= \frac{1}{2}\left(D^+(p)+D^+(p)^\star\right) \\
&= \frac{1}{2}\int d^4x\, e^{ipx}\,\left[\theta(x_0)-\theta(-x_0)\right]\left[D^>(x,0)-D^<(x,0)\right] \\
&= \frac{1}{2}\int d^4x\, e^{ipx}\,\left[\theta(x_0)-\theta(-x_0)\right]\int\frac{d^4q}{(2\pi)^4}\,e^{-iqx}\,\left[D^>(q)-D^<(q)\right] \\
&= \frac{1}{2\,i}\int dx_0\,\left[\theta(x_0)-\theta(-x_0)\right]\int dq_0\, e^{i(p_0-q_0)x_0}\,\mathcal{A}(q_0,\mathbf{p}) \\
&= \frac{1}{2\,i}\int dq_0\,\mathcal{A}(q_0,\mathbf{p})\,i\,\left[\frac{1}{p_0-q_0+i\,\epsilon}+\frac{1}{p_0-q_0-i\,\epsilon}\right] \\
&= \mathcal{P}\int dq_0\,\frac{\mathcal{A}(q_0,\mathbf{p})}{p_0-q_0} \;=\; \mathcal{P}\int_0^\infty dq_0^2\,\frac{\mathcal{A}(q_0,\mathbf{p})}{p_0^2-q_0^2} \quad ,
\end{aligned} \tag{E.28}$$

where the last step follows from the antisymmetry of $\mathcal{A}$.

This dispersion relation holds both in the vacuum and in the nuclear medium. The retarded propagator can only be analytic if the retarded self energy is analytic as well and a dispersion relation must hold for the self energy. Also, the antisymmetry of the spectral

function translates directly into the self energy. Therefore we can write:

$$\mathcal{R}\mathrm{e}\,\Pi^+(p_0,\mathbf{p}) \;=\; -\mathcal{P}\int_0^\infty \frac{dq_0^2}{\pi}\,\frac{\mathcal{I}\mathrm{m}\,\Pi^+(q_0,\mathbf{p})}{p_0^2-q_0^2} \quad .$$

Having derived relations for the retarded self energy and propagator and can now address the issue up to which extent they are valid for the Feynman propagator and self energy as well. To this end we establish some relations between D^F and D^+.

Relation between D^+ and D^F

We prove the following two relations between D^+ and D^F:

$$\boxed{\begin{aligned} \mathcal{R}\mathrm{e}\,D^F(p) &= \mathcal{R}\mathrm{e}\,D^+(p) \qquad (1)\\ \mathcal{I}\mathrm{m}\,D^F(p) &= -(1+2\,n_B)\mathcal{A}(p) \qquad (2)\end{aligned}} \tag{E.29}$$

We start by calculating the imaginary part of $D^<(p)$. With Eq. E.19 and using the translational invariance of the ground state one gets:

$$\begin{aligned} \mathcal{I}\mathrm{m}\,D^<(p) &= -\frac{i}{2}\int d^4x\,\left\{e^{ipx}D^<(x,0)\;+\;e^{-ipx}D^<(0,x)\right\} \\ &= -i\,D^<(p) \quad . \end{aligned} \tag{E.30}$$

This implies that $\mathcal{R}\mathrm{e}\,D^<(p)=0$. The same relation holds for $D^>(p)$.

- **Real Part**
  With help of Eqs. E.18 and E.30, it follows immediately that:

$$\mathcal{R}\mathrm{e}\,D^F(p) \;=\; \mathcal{R}\mathrm{e}\,D^+(p) \tag{E.31}$$

- **Imaginary Part**
  Eqs. E.18, E.21 and E.30 allow to express $\mathcal{I}\mathrm{m}\,D^F(p)$ as:

$$\begin{aligned} \mathcal{I}\mathrm{m}\,D^F(p) &= \mathcal{I}\mathrm{m}\,D^+(p)+\mathcal{I}\mathrm{m}\,D^<(p) \\ &= -\frac{i}{2}\,\left(D^>(p)+D^<(p)\right) \quad . \end{aligned}$$

  This equation can be used to relate $\mathcal{I}\mathrm{m}\,D^F(p)$ and the spectral function $\mathcal{A}$. To this end we need to introduce the KMS relation which is discussed for example in [45, 59, 68, 91]:

$$D^>(p) \;=\; e^{\beta\,(p_0-\mu)}\,D^<(p) \quad . \tag{E.32}$$

  The KMS relation together with Eq. E.21 allows to express $D^>$, $D^<$ and $\mathcal{I}\mathrm{m}\,D^F$ via the spectral function $\mathcal{A}$ as:

$$\begin{aligned} D^<(p) &= -\,2\,i\,\pi\,n_B\,\mathcal{A}(p) \\ D^>(p) &= -\,2\,i\,\pi\,(1+n_B)\,\mathcal{A}(p) \\ \mathcal{I}\mathrm{m}\,D^F(p) &= -\,(1+2\,n_B)\,\pi\,\mathcal{A}(p) \quad , \end{aligned} \tag{E.33}$$

where the distribution function n_B for bosons is defined as:

$$n_B(p_0) \;=\; \frac{1}{e^{\beta(p_0-\mu)}-1} \quad . \tag{E.34}$$

Throughout this work we consider the case of zero temperature and symmetric nuclear matter. Then the meson chemical potential μ vanishes and we find the following simple relation:

$$\mathcal{I}\mathrm{m}\, D^F(p) \;=\; -\,\mathrm{sgn}(p_0)\,\pi\,\mathcal{A}(p) \quad . \tag{E.35}$$

Thus for bosons the real parts of retarded and Feynman propagator (and therefore also the self energy) are identical. Furthermore, for positive energies retarded and Feynman quantities are the same. As a consequence we can calculate the real part of the Feynman self energy in the following way: for positive energies, we use Cutkosky's cutting rules to obtain the imaginary part of the Feynman self energy. Then we make implicitly use of the antisymmetry of the retarded self energy and use the dispersion relation Eq. E.28 to obtain the real part of the self energy.

E.2.2 Fermions

In analogy to bosons Eq. E.18, one can introduce the following four quantities for fermions:

$$\begin{aligned}
\mathcal{G}^{>}(x,y) &= i\,\big\langle \psi(x)\,\bar\psi(y)\big\rangle \quad , \quad \mathcal{G}^{<}(x,y) \;=\; -i\,\big\langle \bar\psi(y)\,\psi(x)\big\rangle \\
\mathcal{G}^{+}(x,y) &= -i\,\theta(x_0-y_0)\,\big\langle\big\{\psi(x),\bar\psi(y)\big\}\big\rangle \\
&= \theta(x_0-y_0)\,\big\langle \mathcal{G}^{>}(x,y)-\mathcal{G}^{<}(x,y)\big\rangle \qquad . \\
\mathcal{G}^{F}(x,y) &= -i\,\big\langle\big[\theta(x_0-y_0)\,\psi(x)\,\bar\psi(y)-\theta(y_0-x_0)\,\bar\psi(y)\,\psi(x)\big]\big\rangle \\
&= \mathcal{G}^{+}(x,y)+\mathcal{G}^{<}(x,y)
\end{aligned} \tag{E.36}$$

Under complex conjugation one has:

$$\big[S^{<}(x,y)\,\gamma_0\big]^\dagger \;=\; \big[i\,\big\langle\psi^\dagger(y)\,\psi(x)\big\rangle\big]^\dagger \;=\; -\,\gamma_0\,S^{<}(y,x) \quad . \tag{E.37}$$

For the Dirac propagators – having a complicated matrix structure – the imaginary part is defined via the hermitian conjugate rather than the complex conjugate [16, 41]:

$$\mathcal{R}\mathrm{e}\,\mathcal{G}(p) \;=\; \frac{1}{2}\,\big(\mathcal{G}(p)+\gamma_0\,\mathcal{G}^\dagger(p)\,\gamma_0\big) \quad , \quad \mathcal{I}\mathrm{m}\,\mathcal{G}(p) \;=\; \frac{1}{2i}\,\big(\mathcal{G}(p)-\gamma_0\,\mathcal{G}^\dagger(p)\,\gamma_0\big) \tag{E.38}$$

This definition of the imaginary part of the propagator produces

$$\mathcal{I}\mathrm{m}\,\mathcal{G}(p) \;=\; \mathcal{I}\mathrm{m}\,\big(\mathcal{G}_1(p)\,\not{p}+\mathcal{G}_2(p)\big) \;=\; \mathcal{I}\mathrm{m}\,\mathcal{G}_1(p)\,\not{p}+\mathcal{I}\mathrm{m}\,\mathcal{G}_2(p) \quad . \tag{E.39}$$

Again, we introduce the spectral function via the imaginary part of the propagator:

$$\begin{aligned}
\mathcal{I}\mathrm{m}\,\mathcal{G}^{+}(p) &= -\pi\,\mathcal{A}(p) \\
\mathcal{A}_{\alpha\beta}(p) &= \frac{1}{2\pi}\int d^4x e^{ipx}\,\big\langle\big\{\psi_\alpha(x),\bar\psi_\beta(0)\big\}\big\rangle \quad .
\end{aligned} \tag{E.40}$$

of which according to the Lehmann representation Eq. E.5 in the vacuum only two independent components, $\mathcal{A}_1$ and $\mathcal{A}_2$ exist, which are related to ρ_1 and ρ_2:

$$\begin{aligned} \mathcal{A}_1 &= Tr\left[\gamma_0 \mathcal{A}\right] = -\frac{1}{\pi} Tr\left[\gamma_0 \mathcal{I}\mathrm{m}\, \mathcal{G}^+\right] = 4\, p_0\, \rho_1(p^2)\, \mathrm{sgn}(\mathrm{p_0}) \\ \mathcal{A}_2 &= Tr\left[\mathcal{A}\right] = -\frac{1}{\pi} Tr\left[\mathcal{I}\mathrm{m}\, \mathcal{G}^+\right] = 4\, \rho_2(p^2)\, \mathrm{sgn}(\mathrm{p_0}) \quad . \end{aligned} \tag{E.41}$$

In the nuclear medium one can build a third independent quantity by tracing the spectral function with γ_i. We do not discuss this in more detail since in our actual calculations we do not decompose the propagator into its individual Dirac components.

Properties of $\mathcal{R}\mathrm{e}\, \mathcal{G}^+$

With these definitions one obtains similar relations as for the bosons Eq. E.23:

$$\begin{array}{lcll} \displaystyle\int_{-\infty}^{+\infty} \frac{dp_0}{4}\, \mathcal{A}_1 & = & 1 & \text{normalization} \\ \mathcal{A}_1(p_0, \mathbf{p}) & = & \mathcal{A}_1(-p_0, \mathbf{p}) & \text{symmetry of } \mathcal{A}_1 \\ \mathcal{A}_2(p_0, \mathbf{p}) & = & -\mathcal{A}_2(-p_0, \mathbf{p}) & \text{antisymmetry of } \mathcal{A}_2 \\ \mathcal{R}\mathrm{e}\, \mathcal{G}^+(p) & = & \mathcal{P} \displaystyle\int_{-\infty}^{+\infty} dq_0\, \frac{\mathcal{A}(q_0, \mathbf{p})}{p_0 - q_0} & \text{dispersion relation} \end{array} \tag{E.42}$$

- **Normalization**
  The proof of the normalization of $\mathcal{A}_1$ makes use of the anticommutator relation of fermion fields [106, 16]

  $$\left\{\psi_\alpha(\mathbf{x}, t)\, ,\, \psi^\dagger_\beta(\mathbf{y}, t)\right\} = \delta^3(\mathbf{x} - \mathbf{y})\, \delta_{\alpha\,\beta} \quad , \tag{E.43}$$

  which allows to formulate a normalization integral for $\mathcal{A}_1$:

  $$\begin{aligned} \int \frac{dp_0}{4}\, \mathcal{A}_1 &= \int \frac{dp_0}{8\pi}\, d^4x\, e^{ipx} \left\{\psi_\alpha(x)\, ,\, \psi^\dagger_\alpha(0)\right\} \\ &= \frac{1}{4} \int d^3x \left\{\psi_\alpha(\mathbf{x})\, ,\, \psi^\dagger_\alpha(\mathbf{0})\right\} \\ &= 1 \quad . \end{aligned} \tag{E.44}$$

  This derivation also indicates that no sum rule exists for $\mathcal{A}_2$, since ψ and $\bar{\psi}$ are not related by an anticommutator.

- **Symmetry of $\mathcal{A}_1$**

We will now discuss the symmetry of $\mathcal{A}_1$. Let us therefore study the behaviour under the transformation $p \to -p$:

$$\begin{aligned} \mathcal{A}_1(p) &= \frac{1}{2\pi}\int d^4x e^{ipx}\,\left\{\psi(x),\psi^\dagger(0)\right\} \\ \mathcal{A}_1(-p) &= \frac{1}{2\pi}\int d^4x e^{ipx}\,\left\{\psi(0),\psi^\dagger(x)\right\} \end{aligned} \tag{E.45}$$

In order to relate both expressions we make use of the transformation properties of the fields ψ and $\bar{\psi}$ under charge conjugation [16]:

$$\begin{aligned} \mathcal{C}\,\psi_\alpha\,\mathcal{C}^{-1} &= C_{\alpha\beta}\,\bar{\psi}_\beta \\ \mathcal{C}\,\bar{\psi}_\alpha\,\mathcal{C}^{-1} &= -\psi_\beta\,C^{-1}_{\beta\alpha} \\ C &= i\,\gamma_2\,\gamma_0 \;=\; -C^{-1} \quad . \end{aligned} \tag{E.46}$$

After doing some algebra one finds that under charge conjugation the expectation value behaves in the following way:

$$\left\langle\psi(x)_\alpha\,\psi^\dagger(0)_\alpha\right\rangle \;\to\; \left\langle\psi^\dagger(x)_\alpha\,\psi(0)_\alpha\right\rangle \tag{E.47}$$

This implies that $\mathcal{A}_1$ is symmetric under $p \to -p$ and therefore, due to the rotational invariance of the ground state, under $p_0 \to -p_0$. This argument holds only in the vacuum, since nuclear matter is not invariant under charge conjugation which transforms particles into antiparticles. The difference between fermions and bosons is that for the latter isospin and charge conjugation have the same effect on the ground state expectation values.

- **Antisymmetry of $\mathcal{A}_2$**

  Let us now turn to $\mathcal{A}_2$:

$$\begin{aligned} \mathcal{A}_2(p) &= \frac{1}{2\pi}\int d^4x e^{ipx}\,\left\{\psi(x),\bar{\psi}(0)\right\} \\ \mathcal{A}_2(-p) &= \frac{1}{2\pi}\int d^4x e^{ipx}\,\left\{\psi(0),\bar{\psi}(x)\right\} \quad . \end{aligned}$$

  Under charge conjugation one finds:

$$\left\langle\psi(x)_\alpha\,\bar{\psi}(0)_\alpha\right\rangle \;\to\; -\left\langle\bar{\psi}(x)_\alpha\,\psi(0)_\alpha\right\rangle \quad ,$$

  and $\mathcal{A}_2$ is antisymmetric in the energy.

- **Dispersion Relation** The dispersion relation is derived in steps which are analogous to those for the bosons.

Note that the symmetry of $\mathcal{A}_1$ and $\mathcal{A}_2$ under $p_0 \to -p_0$ implies that both ρ_1 and ρ_2 are symmetric. In the vacuum one can therefore rewrite the dispersion relation Eq. E.42 and the sum rule in terms of an integral over positive energies only:

$$\begin{aligned} Tr\left[\gamma_0\,\mathcal{R}\mathrm{e}\,\mathcal{G}^+(p)\right] &= 4\,p_0\,\mathcal{P}\int dq_0^2\frac{\rho_1(q_0^2)}{q_0^2-p_0^2} \\ Tr\left[\mathcal{R}\mathrm{e}\,\mathcal{G}^+(p)\right] &= 4\,\mathcal{P}\int dq_0^2\frac{\rho_2(q_0^2)}{q_0^2-p_0^2} \\ \int dp_0^2\,\rho_1(p_0^2) &= 1 \quad . \end{aligned} \tag{E.48}$$

These results are expected from Eqs. E.5 and E.11.

Relation between $\mathcal{R}\mathrm{e}\,\mathcal{G}^+$ and $\mathcal{R}\mathrm{e}\,\mathcal{G}^F$

For fermions there exist similar relations between Feynman and retarded propagator as for bosons:

$$\boxed{\begin{array}{rcll} \mathcal{R}\mathrm{e}\,\mathcal{G}^F(p) & = & \mathcal{R}\mathrm{e}\,\mathcal{G}^+(p) & \text{real part} \\ \mathcal{I}\mathrm{m}\,\mathcal{G}^F(p) & = & -\,\mathrm{sgn}(\mathrm{p}_0-\mu)\,\mathcal{A}(\mathrm{p}) & \text{imaginary part} \end{array}} \tag{E.49}$$

We will now prove these properties.

- **Real Part**

  The proof follows along the same lines as for bosons, i. e. one makes use of the relation $\mathcal{R}\mathrm{e}\,\mathcal{G}^<(p)=0$.

- **Imaginary Part**

  The imaginary part of the Feynman propagator can be expressed as (compare also Eq. E.32):

  $$\mathcal{I}\mathrm{m}\,\mathcal{G}^F(p) \;=\; \frac{i}{2}\,(\mathcal{G}^>(p)+\mathcal{G}^<(p))$$

  To build a relationship between $\mathcal{I}\mathrm{m}\,\mathcal{G}^F$ and $\mathcal{A}$, again the KMS relation [45, 59, 68, 91] is needed (cf. Eq. E.32):

  $$\mathcal{G}^>(p) \;=\; -e^{\beta(p_0-\mu)}\,\mathcal{G}^<(p) \quad , \tag{E.50}$$

  which allows to write down the following relations:

  $$\begin{array}{rcl} \mathcal{G}^<(p) & = & 2\,i\,\pi\,n_F\,\mathcal{A}(p) \\ \mathcal{G}^>(p) & = & -2\,i\,\pi\,(1-n_F)\,\mathcal{A}(p) \\ \mathcal{I}\mathrm{m}\,\mathcal{G}^F(p) & = & -\,(1-2\,n_F)\,\pi\,\mathcal{A}(p) \quad , \end{array} \tag{E.51}$$

  where n_F is the Fermi distribution function:

  $$\begin{array}{rcl} n_F(p) & = & \dfrac{1}{e^{\beta\,(p_0-\mu)}+1} \\ & \overset{T\to 0}{\to} & \theta(p_0-\mu) \quad . \end{array} \tag{E.52}$$

  In a nuclear medium with a finite baryo-chemical potential the relation between Feynman and retarded propagator is therefore different than for bosons and one arrives at the result Eq. E.49.

As far as the calculation of the self energy is concerned, we obtain the following results: in the vacuum the symmetry in p_0 can be exploited and the real part of the self energy can be obtained by a dispersion integral over positive energies only. Note in particular that the averaged self energy $\langle\Sigma\rangle$, Eq. D.12 in Chapter D.1.1, follows also from a dispersion relation as is clear from Eq. E.48. In the medium, however, in principle a calculation of the self energy for all energies is necessary, since the symmetry in the energy is not given any more.

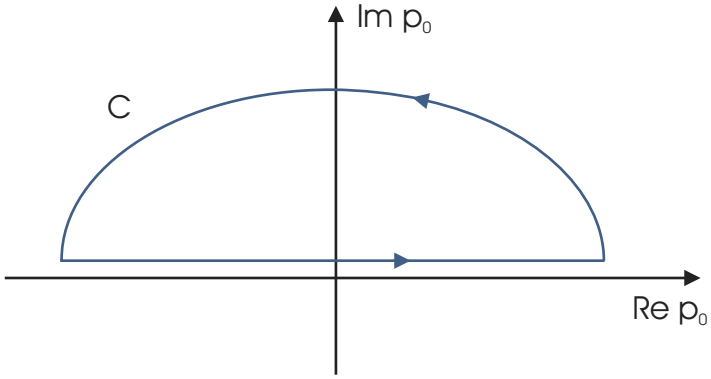

Figure E.2: Contour of the integration leading to the normalization of $\mathcal{A}$.

E.2.3 Normalization and Constraints on the Self Energy

The sum rules for bosons Eq. E.23 and fermions Eq. E.42 can alternatively be derived by directly integrating the spectral function (see also [77]):

$$\mathcal{A}(p) \;=\; -\frac{1}{\pi}\,\mathcal{I}\mathrm{m}\,\frac{1}{q^2 - M^2 - \Pi^+} \quad . \tag{E.53}$$

There one utilizes the fact that $\mathcal{D}^+$ is an analytic function in the upper half plane and that therefore any closed loop integral must vanish:

$$\begin{aligned} \int_C dp_0\, p_0\, \mathcal{A}(p) \;&=\; 0 \\ &\Rightarrow \\ \int_{-\infty}^{\infty} dp_0\, p_0\, \mathcal{A}(p) \;&=\; \lim_{p_0\to\infty} \mathcal{I}\mathrm{m}\,\frac{1}{\pi}\int_0^{\pi} i d\phi \frac{(p_0\, e^{i\,\phi})^2}{(p_0\, e^{i\,\phi})^2 - M^2 - \Pi^+} \;=\; 1 \quad . \end{aligned} \tag{E.54}$$

The contour C is sketched in Fig. E.2.3. Note that a variable transformation $p_0 \to p_0\, e^{i\phi}$ with $dp_0 = p_0\, e^{i\,\phi}\, i\, d\phi$ has been performed.

We want to point out explicitly that the derivation of Eq. E.54 imposes a constraint on the high energy behaviour of the self energy Π^+. For large energies, Π^+ has to grow slower than p_0^2 so that the self energy can be neglected in the limit $p_0 \to \infty$. The high energy behaviour of the imaginary part of the self energy is governed by the matrix elements $\mathcal{M}$:

$$\mathcal{I}\mathrm{m}\,\Pi(q_0 \to \infty) \;\to\; |\mathcal{M}|^2\,\frac{p_{cm}}{p_0} \quad , \tag{E.55}$$

where p_{cm} is the three-momentum of the decay products and the factor $\frac{p_{cm}}{p_0}$ approaches a constant for large energies. The matrix element contains typically a momentum dependence of the form p_{cm}^{2l}, where the orbital angular momentum l depends on the quantum numbers of the involved particles. It follows that without form factor the imaginary part of the self energy rises as a function of the energy which is in conflict with the constraint the self energy has to grow slower than p_0^2. This is a justification for the introduction of form factors cutting off the contribution at large energies such as those employed throughout this work.

Bibliography

[1] Photoproduction of meson and baryon resonances at energies up to 5.8 GeV.
Phys. Rev., 175:1669–1696, 1968.

[2] R. A. Adelseck, C. Bennhold, and L. E. Wright.
Kaon photoproduction operator for use in nuclear physics.
Phys. Rev., C32:1681–1692, 1985.

[3] G. Agakishiev et al.
Enhanced production of low mass electron pairs in 200 GeV/u S - Au collisions at the CERN SPS.
Phys. Rev. Lett., 75:1272–1275, 1995.

[4] G. Agakishiev et al.
Low-mass e^+e^- pair production in 158 A GeV Pb Au collisions at the CERN SPS, its dependence on multiplicity and transverse momentum.
Phys. Lett., B422:405–412, 1998.

[5] S. R. Amendolia et al.
A measurement of the pion charge radius.
Phys. Lett., B146:116, 1984.

[6] Richard A. Arndt, Igor I. Strakovsky, Ron L. Workman, and Marcello M. Pavan.
Updated analysis of pi N elastic scattering data to 2.1 GeV: The Baryon spectrum.
Phys. Rev., C52:2120–2130, 1995.

[7] P. Arve and J. Helgesson.
The NN^{-1}, π and ΔN^{-1} Δ decay modes in the nuclear medium.
Nucl. Phys., A572:600–620, 1994.

[8] Baldini, A. et. al.
Landolt-Börnstein, Vol. 1/12 a.
Springer, Berlin, 1987.

[9] L. M. Barkov et al.
Electromagnetic pion form factor in the time-like region.
Nucl. Phys., B256:365–384, 1985.

[10] H. W. Barz and B. Kampfer.
The role of three-body collisions in phi meson production processes near threshold.
Nucl. Phys., A683:594–604, 2001.

[11] C. J. Batty, E. Friedman, and A. Gal.
Strong interaction physics from hadronic atoms.
Phys. Rept., 287:385–445, 1997.

[12] M. Benmerrouche, R. M. Davidson, and N. C. Mukhopadhyay.
Problems of describing spin 3/2 baryon resonances in the effective lagrangian theory.
Phys. Rev., C39:2339–2348, 1989.

[13] V. Bernard, Norbert Kaiser, and Ulf-G. Meissner.
Chiral dynamics in nucleons and nuclei.
Int. J. Mod. Phys., E4:193–346, 1995.

[14] N. Bianchi et al.
Measurement of the total cross-section for U^{238} photofission in the nucleon resonance region.
Phys. Lett., B299:219–222, 1993.

[15] N. Bianchi et al.
Total hadronic photoabsorption cross section on nuclei in the nucleon resonance region.
Phys. Rev., C54:1688–1699, 1996.

[16] James D. Bjorken and Sidney D. Drell.
Relativistic Quantum Fields.
Mc Graw-Hill, New York, 1965.

[17] M. Brack, D. O. Riska, and W. Weise.
Pionic disintegration of the deuteron.
Nucl. Phys., A287:425–450, 1977.

[18] E. L. Bratkovskaya et al.
Anisotropy of dilepton emission from nucleon-nucleon interactions.
Phys. Lett., B348:325–330, 1995.

[19] E. L. Bratkovskaya, O. V. Teryaev, and V. D. Toneev.
Anisotropy of dilepton emission from nuclear collisions.
Phys. Lett., B348:283–289, 1995.

[20] A. D. Brody et al.
Experimental results on the reactions $\pi^- p \to \pi\pi N$ in the center-of-mass energy range 1400 MeV to 2000 Mev.
Phys. Rev., D4:2693, 1971.

[21] G. E. Brown and Mannque Rho.
Scaling effective Lagrangians in a dense medium.
Phys. Rev. Lett., 66:2720–2723, 1991.

[22] D. V. Bugg.
Collision broadening of resonances.
Nucl. Phys., B88:381, 1975.

[23] Volker D. Burkert.
Probing the structure of nucleons in the resonance region.
nucl-th/0005033.

[24] D. Cabrera, E. Oset, and M. J. Vicente Vacas.
Chiral approach to the rho meson in nuclear matter.
Nucl. Phys., A705:90–118, 2002.

[25] Simon Capstick and Winston Roberts.
Quasi two-body decays of nonstrange baryons.
Phys. Rev., D49:4570–4586, 1994.

[26] H. C. Chiang, E. Oset, and L. C. Liu.
The width of bound eta in nuclei.
Phys. Rev., C44:738–746, 1991.

[27] F. de Jong and R. Malfliet.
Covariant description of the delta in nuclear matter.
Phys. Rev., C46:2567–2581, 1992.

[28] J. Dolbeau, F. A. Triantis, M. Neveu, and F. Cadiet.
Energy independent partial wave analysis of the reaction $\pi^{\pm}p \to N\pi\pi$ in the center-of-mass energy range 1.36 GeV - 1.76 GeV.
Nucl. Phys., B108:365, 1976.

[29] C. Dover, J. Hüfner, and R. H. Lemmer.
Pions in nuclear matter - an approach to the pion-nucleus optical potential.
Ann. Phys., 66:248–292, 1971.

[30] M. Effenberger.
Eigenschaften von Hadronen in Kernmaterie in einem vereinheitlichten Transportmodell.
Phd Thesis, 1999.

[31] M. Effenberger, E. L. Bratkovskaya, W. Cassing, and U. Mosel.
e^+e^- pairs from $\pi^- A$ reactions reexamined.
Phys. Rev., C60:027601, 1999.

[32] M. Effenberger, A. Hombach, S. Teis, and U. Mosel.
Photoabsorption on nuclei.
Nucl. Phys., A613:353–370, 1997.

[33] T. Ericson and W. Weise.
Pions and Nuclei.
Clarendon Press, Oxford, 1988.

[34] Amand Faessler, C. Fuchs, M. I. Krivoruchenko, and B. V. Martemyanov.
Dilepton production in proton proton collisions at bevalac energies.
J. Phys., G29:603–624, 2003.

[35] T. Feuster and U. Mosel.
A unitary model for meson nucleon scattering.
Phys. Rev., C58:457–488, 1998.

[36] T. Feuster and U. Mosel.
Photon and meson induced reactions on the nucleon.
Phys. Rev., C59:460–491, 1999.

[37] B. Friman, M. Lutz, and G. Wolf.
From meson nucleon scattering to vector mesons in nuclear matter.
nucl-th/0003012.

[38] B. Friman and H. J. Pirner.
P-wave polarization of the rho meson and the dilepton spectrum in dense matter.

Nucl. Phys., A617:496–509, 1997.

[39] Bengt Friman.
Vector meson propagation in dense matter.
nucl-th/981053.

[40] Bengt Friman and Madeleine Soyeur.
Photoproduction of vector mesons off nucleons near threshold.
Nucl. Phys., A600:477–490, 1996.

[41] Frank Fromel, Stefan Leupold, and Ulrich Mosel.
Spectral function of quarks in quark matter.
Phys. Rev., C67:015206, 2003.

[42] Frank Froemel, Horst Lenske, and Ulrich Mosel.
Short-Range Correlations in Nuclear Matter at Finite Temperatures and High Densities.
Nucl. Phys., A723:544-556, 2003.

[43] T. Frommhold et al.
Photofission of U^{235} and U^{238} at intermediate energies: Absolute cross-sections and fragment mass distributions.
Z. Phys., A350:249–261, 1994.

[44] Charles Gale and Joseph Kapusta.
Vector dominance model at finite temperature.
Nucl. Phys., B357:65–89, 1991.

[45] Carsten Greiner and Stefan Leupold.
Stochastic interpretation of Kadanoff-Baym equations and their relation to Langevin processes.
Annals Phys., 270:328–390, 1998.

[46] K. Hagiwara et al.
Review of particle physics.
Phys. Rev., D66:010001, 2002.

[47] Tetsuo Hatsuda and Su Houng Lee.
QCD sum rules for vector mesons in nuclear medium.
Phys. Rev., C46:34–38, 1992.

[48] R. S. Hayano, S. Hirenzaki, and A. Gillitzer.
Formation of eta mesic nuclei using the recoilless (d, He^3) reaction.
Eur. Phys. J., A6:99–105, 1999.

[49] Johan Helgesson and Jorgen Randrup.
Spin - isospin modes in heavy ion collisions. 1: Nuclear matter at finite temperatures.
Ann. Phys., 244:12–66, 1995.

[50] P. A. Henning and H. Umezawa.
The delta - hole model at finite temperature.
Nucl. Phys., A571:617–644, 1994.

[51] D. Herndon et al.
A partial wave analysis of the reaction $\pi N \to \pi\pi N$ in the center-of-mass energy range 1300 MeV - 2000 MeV.

Phys. Rev., D11:3183, 1975.

[52] M. Herrmann, B. L. Friman, and W. Nörenberg.
Properties of rho mesons in nuclear matter.
Nucl. Phys., A560:411–436, 1993.

[53] D. Hirata, H. Toki, T. Watabe, I. Tanihata, and B. V. Carlson.
Relativistic hartree theory for nuclei far from the stability line.
Phys. Rev., C44:1467–1475, 1991.

[54] M. Hirata, J. H. Koch, E. J. Moniz, and F. Lenz.
Isobar hole doorway states and πO^{16} scattering.
Annals Phys., 120:205–248, 1979.

[55] Michihiro Hirata, Nobuhiko Katagiri, Kazuyuki Ochi, and Takashi Takaki.
Nuclear photoabsorption at photon energies between 300 mev and 850 mev.
Phys. Rev., C66:014612, 2002.

[56] T. Inoue and E. Oset.
Eta in the nuclear medium within a chiral unitary approach.
Nucl. Phys., A710:354–370, 2002.

[57] T. Inoue, E. Oset, and M. J. Vicente Vacas.
Chiral unitary approach to s-wave meson baryon scattering in the strangeness $S = 0$ sector.
Phys. Rev., C65:035204, 2002.

[58] B. K. Jain, J. T. Londergan, and G. E. Walker.
$(p, p' \pi^+)$ reaction at energies below 1 GeV.
Phys. Rev., C37:1564–1586, 1988.

[59] L. P. Kadanoff and G. Baym.
Quantum Statistical Mechanics.
Benjamin, New York, 1962.

[60] J. I. Kapusta and Edward V. Shuryak.
Weinberg type sum rules at zero and finite temperature.
Phys. Rev., D49:4694–4704, 1994.

[61] Hung-Chong Kim, S. Schramm, and Su Houng Lee.
Delta decay in the nuclear medium.
Phys. Rev., C56:1582–1587, 1997.

[62] F. Klingl, Norbert Kaiser, and W. Weise.
Current correlation functions, QCD sum rules and vector mesons in baryonic matter.
Nucl. Phys., A624:527–563, 1997.

[63] Volker Koch.
K^--proton scattering and the Lambda(1405) in dense matter.
Phys. Lett., B337:7–13, 1994.

[64] Volker Koch.
Aspects of chiral symmetry.
Int. J. Mod. Phys., E6:203–250, 1997.

[65] L. A. Kondratyuk, M. I. Krivoruchenko, N. Bianchi, E. De Sanctis, and V. Muccifora.
Suppression of nucleon resonances in the total photoabsorption on nuclei.
Nucl. Phys., A579:453–471, 1994.

[66] C. L. Korpa.
Complete spin structure of the pion nucleon loop delta self-energy.
Heavy Ion Phys., 5:77–84, 1997.

[67] C. L. Korpa and M. F. M. Lutz.
Self consistent and covariant propagation of pions, nucleon and isobar resonances in cold nuclear matter.
nucl-th/0306063.

[68] Ryogo Kubo.
Statistical mechanical theory of irreversible processes. 1. General theory and simple applications in magnetic and conduction problems.
J. Phys. Soc. Jap., 12:570–586, 1957.

[69] G. A. Lalazissis, J. Konig, and P. Ring.
A new parameterization for the lagrangian density of relativistic mean field theory.
Phys. Rev., C55:540–543, 1997.

[70] W. Langgärtner et al.
Direct observation of a rho decay of the $D_{13}(1520)$ baryon resonance.
Phys. Rev. Lett., 87:052001, 2001.

[71] A. B. Larionov and U. Mosel.
The n n –¿ n delta cross-section in nuclear matter.
nucl-th/0307035.

[72] S. J. Lee et al.
Relativistic hartree calculations for axially deformed nuclei.
Phys. Rev. Lett., 57:2916–2919, 1986.

[73] J. Lehr, M. Effenberger, and U. Mosel.
Electron and photon induced reactions on nuclei in the nucleon resonance region.
Nucl. Phys., A671:503–531, 2000.

[74] J. Lehr, M. Post, and U. Mosel.
In-medium modifications of the $S_{11}(1535)$ resonance and eta photoproduction.
Phys. Rev., C68, 2003.

[75] L. B. Leinson and A. Perez.
Relativistic short-range correlation effects on the pion dynamics in nuclear matter.
nucl-th/0307025.

[76] B. Lenkeit et al.
Recent results from Pb Au collisions at 158 GeV/c per nucleon obtained with the CERES spectrometer.
Nucl. Phys., A661:23–32, 1999.

[77] Stefan Leupold.
Towards a test particle description of transport processes for states with continuous mass spectra.
Nucl. Phys., A672:475–500, 2000.

[78] Stefan Leupold, Wolfram Peters, and Ulrich Mosel.
What QCD sum rules tell about the rho meson.
Nucl. Phys., A628:311–324, 1998.

[79] G. Q. Li, R. Machleidt, and R. Brockmann.
Properties of dense nuclear and neutron matter with relativistic nucleon-nucleon interactions.
Phys. Rev., C45:2782–2794, 1992.

[80] R. Longacre et al.
$N^\star$ resonance parameters and K matrix fits to the reactions $\pi N \to \Delta\pi + \rho N + \epsilon N$.
Phys. Lett., B55:415, 1975.

[81] M. Lutz, A. Steiner, and W. Weise.
Kaons in baryonic matter.
Nucl. Phys., A574:755–787, 1994.

[82] M. F. M. Lutz.
Migdal's short range correlations in a covariant model.
Phys. Lett., B552:159–164, 2003.

[83] M. F. M. Lutz and C. L. Korpa.
Self consistent propagation of hyperons and antikaons in nuclear matter based on relativistic chiral SU(3) dynamics.
Nucl. Phys., A700:309–329, 2002.

[84] M. F. M. Lutz, G. Wolf, and B. Friman.
Scattering of vector mesons off nucleons.
Nucl. Phys., A706:431–496, 2002.

[85] Matthias F. M. Lutz, Bengt Friman, and Madeleine Soyeur.
Quantum interference of ρ_0 and ω mesons in the $\pi N \to e^+e^-N$ reaction.
Nucl. Phys., A713:97–118, 2003.

[86] G. I. Lykasov, W. Cassing, A. Sibirtsev, and M. V. Rzyanin.
ωN final state interactions and omega-meson production from heavy-ion collisions.
Eur. Phys. J., A6:71–81, 1999.

[87] R. Machleidt, K. Holinde, and C. Elster.
The Bonn Meson Exchange Model for the nucleon nucleon interaction.
Phys. Rept., 149:1–89, 1987.

[88] R. Machleidt, K. Holinde, and C. Elster.
The Bonn meson exchange model for the nucleon nucleon interaction.
Phys. Rept., 149:1–89, 1987.

[89] D. M. Manley and E. M. Saleski.
Multichannel resonance parametrization of pi N scattering amplitudes.
Phys. Rev., D45:4002–4033, 1992.

[90] D. Mark Manley, Richard A. Arndt, Yogesh Goradia, and Vigdor L. Teplitz.
An isobar model partial wave analysis of $\pi N \to \pi\pi N$ in the center-of-mass energy range 1320 MeV to 1930 MeV.
Phys. Rev., D30:904, 1984.

[91] Paul C. Martin and Julian S. Schwinger.
Theory of many particle systems. I.
Phys. Rev., 115:1342–1373, 1959.

[92] M. Masera.
Dimuon production below mass 3.1 GeV/c^2 in p W and S W interactions at 200 A/GeV/c.
Nucl. Phys., A590:93c–102c, 1995.

[93] A. B. Migdal.
Pion fields in nuclear matter.
Rev. Mod. Phys., 50:107–172, 1978.

[94] A. B. Migdal, E. E. Saperstein, M. A. Troitsky, and D. N. Voskresensky.
Pion degrees of freedom in nuclear matter.
Phys. Rept., 192:179–437, 1990.

[95] J. C. Nacher, E. Oset, M. J. Vicente, and L. Roca.
The role of $\Delta(1700)$ excitation and ρ production in double pion photoproduction.
Nucl. Phys., A695:295–327, 2001.

[96] H. Nagahiro, D. Jido, and S. Hirenzaki.
Eta nucleus interactions and in-medium properties of $N^\star(1535)$ in chiral models.
nucl-th/0304068.

[97] H. B. O'Connell, B. C. Pearce, A. W. Thomas, and Anthony G. Williams.
Rho - omega mixing, vector meson dominance and the pion form-factor.
Prog. Part. Nucl. Phys., 39:201–252, 1997.

[98] E. Oset and L. L. Salcedo.
Delta self energy in nuclear matter.
Nucl. Phys., A468:631–652, 1987.

[99] E. Oset, H. Toki, and W. Weise.
Pionic modes of excitation in nuclei.
Phys. Rept., 83:281–380, 1982.

[100] E. Oset and W. Weise.
Isobar-hole description of pion elastic scattering and the pion-nuclear many body problem.
Nucl. Phys., A319:477–517, 1979.

[101] Vladimir Pascalutsa and Rob Timmermans.
Field theory of nucleon to higher-spin baryon transitions.
Phys. Rev., C60:042201, 1999.

[102] R. F. Peierls.
Possible mechanism for the pion-nucleon second resonance.
Phys. Rev. Lett., 6:641, 1961.

[103] G. Penner.
Vector meson production and nucleon resonance analysis in a coupled-channel approach.
Phd Thesis, 2002.

[104] G. Penner and U. Mosel.
Vector meson production and nucleon resonance analysis in a coupled channel approach for energies $m_N < \sqrt{s} < 2$ GeV. I: Pion induced results and hadronic parameters.
Phys. Rev., C66:055211, 2002.

[105] G. Penner and U. Mosel.
Vector meson production and nucleon resonance analysis in a coupled channel approach for energies $m_N < \sqrt{s} < 2$ GeV. II: Photon induced results.
Phys. Rev., C66:055212, 2002.

[106] Michael E. Peskin and Daniel V. Schroeder.
An Introduction to Quantum Field Theory.
Addison-Wesley Publishing Company, Reading, Massachusetts, 1995.

[107] W. Peters, M. Post, H. Lenske, S. Leupold, and U. Mosel.
The spectral function of the rho meson in nuclear matter.
Nucl. Phys., A632:109–127, 1998.

[108] M. Post, S. Leupold, and U. Mosel.
Hadronic spectral funtions in nuclear matter.
nucl-th/0309085.

[109] M. Post, S. Leupold, and U. Mosel.
The rho spectral function in a relativistic resonance model.
Nucl. Phys., A689:753–783, 2001.

[110] M. Post and U. Mosel.
Coupling of baryon resonances to the n omega channel.
Nucl. Phys., A688:808–822, 2001.

[111] R. Rapp, G. Chanfray, and J. Wambach.
Rho meson propagation and dilepton enhancement in hot hadronic matter.
Nucl. Phys., A617:472–495, 1997.

[112] R. Rapp, M. Urban, M. Buballa, and J. Wambach.
A microscopic calculation of photoabsorption cross sections on protons and nuclei.
Phys. Lett., B417:1–6, 1998.

[113] R. Rapp and J. Wambach.
Chiral symmetry restoration and dileptons in relativistic heavy-ion collisions.
Adv. Nucl. Phys., 25:1, 2000.

[114] D. O. Riska and G. E. Brown.
Nucleon resonance transition couplings to vector mesons.
Nucl. Phys., A679:577–596, 2001.

[115] M. Roebig-Landau et al.
Near threshold photoproduction of eta mesons from complex nuclei.
Phys. Lett., B373:45–50, 1996.

[116] J. J. Sakurai.
Advanced Quantum Mechanics.
Addison-Wesley, Reading, Massachusetts, 1967.

[117] L. L. Salcedo, K. Holinde, E. Oset, and C. Schutz.
A Lorentz-Lorenz effect for the pion s-wave selfenergy in pionic atoms.
Phys. Lett., B353:1–6, 1995.

[118] M. Schäfer, H. C. Donges, A. Engel, and U. Mosel.
Dilepton production in nucleon-nucleon interactions.
Nucl. Phys., A575:429–448, 1994.

[119] Brian D. Serot and John Dirk Walecka.
The relativistic many-body problem.
Adv. Nucl. Phys., 16:1–327, 1986.

[120] Mikhail A. Shifman, A. I. Vainshtein, and Valentin I. Zakharov.
Qcd and resonance physics. sum rules.
Nucl. Phys., B147:385–447, 1979.

[121] B. Ter Haar and R. Malfliet.
Nucleons, mesons and Deltas in nuclear matter. A relativistic Dirac-Brueckner approach.
Phys. Rept., 149:207–286, 1987.

[122] M. Urban, M. Buballa, R. Rapp, and J. Wambach.
Momentum dependence of the pion cloud for rho mesons in nuclear matter.
Nucl. Phys., A641:433–460, 1998.

[123] L. Van Daele, A. Yu. Korchin, D. Van Neck, O. Scholten, and M. Waroquier.
Coherent compton scattering on light nuclei in the delta resonance region.
Phys. Rev., C65:014613, 2002.

[124] T. P. Vrana, S. A. Dytman, and T. S. H. Lee.
Baryon resonance extraction from pi N data using a unitary multichannel model.
Phys. Rept., 328:181–236, 2000.

[125] T. Waas and W. Weise.
S-wave interactions of anti-K and eta mesons in nuclear matter.
Nucl. Phys., A625:287–306, 1997.

[126] K. Wehrberger and R. Wittman.
Pauli blocking for effective deltas in nuclear matter.
Nucl. Phys., A513:603–620, 1990.

[127] T. Weidmann, E. L. Bratkovskaya, W. Cassing, and U. Mosel.
e^+e^- pairs from $\pi^- A$ reactions.
Phys. Rev., C59:919–927, 1999.

[128] G.M. Welke, M. Prakash, T. T. S. Kuo, S. Das Gupta, and Gale. C.
Azimuthal distributions in heavy ion collisions and the nuclear equation of state.
Phys. Rev., C38:2101–2107, 1988.

[129] Johannes P. Wessels et al.
Latest results from CERES/NA45.
Nucl. Phys., A715:262–271, 2003.

[130] H. T. Williams.
Relativistic approach to photon nucleon scattering.
Phys. Rev., C34:1439–1445, 1986.

[131] Gyuri Wolf, Bengt Friman, and Madeleine Soyeur.
In-medium omega meson broadening and s-wave pion annihilation into e^+e^- pairs.
Nucl. Phys., A640:129–143, 1998.

[132] Lin-hua Xia, Philip J. Siemens, and Madeleine Soyeur.
Selfconsistent couplings of pions and Δ - hole states in nuclear matter.
Nucl. Phys., A578:493–510, 1994.

[133] T. Yorita et al.
Observation of $S_{11}(1535)$ resonance in nuclear medium via the $C^{12}(\gamma, \eta)$ reaction.
Phys. Lett., B476:226–232, 2000.

[134] Qiang Zhao, Zhen-ping Li, and C. Bennhold.
Omega and rho photoproduction with an effective quark model Lagrangian.
Phys. Lett., B436:42–48, 1998.

[135] Qiang Zhao, Zhen-ping Li, and C. Bennhold.
Vector meson photoproduction with an effective Lagrangian in the quark model.
Phys. Rev., C58:2393–2413, 1998.

Deutsche Zusammenfassung

Ziel dieser Arbeit ist eine Beschreibung der Eigenschaften von Baryon-Resonanzen und Mesonen in Kernmaterie. Die Frage, ob und wie sich Masse und Breite von Hadronen in einem nuklearen Medium ändern, ist aus zweierlei Gründen von Interesse: Erstens sind in einer Vielzahl von Experimenten Hinweise auf Mediummodifikationen von Hadronen gefunden worden. Weiterhin besteht ein Konsensus, daß die Änderung von hadronischen Eigenschaften in einem Medium in Zusammenhang steht mit der (teilweisen) Restaurierung einer der grundlegenden Symmetrien der Quantenchromodynamik (QCD), nämlich der chiralen Symmetrie. Wir werden nun diese beiden Punkte ausführen, bevor wir Aufbau und Ergebnisse unseres Modells erläutern.

Wir beginnen mit einem Überblick der zum jetztigen Zeitpunkt bekannten experimentellen Hinweise auf Änderungen von hadronischen Eigenschaften in Kernmaterie. Von besonderem Interesse ist das ρ Meson, welches in Dileptonen zerfallen kann. Diese transportieren aufgrund ihrer geringen Endzustandswechselwirkungen Informationen aus dichten und/oder heißen Umgebungen. Zu vielen Diskussionen Anlass gegeben haben aus Schwerionenkollisionen extrahierte Dileptonenspektren. Im Vakuum zeigen diese Spektren aufgrund der direkten Kopplung $\rho \to e^+e^-$ einen deutlichen Peak bei der invarianten Masse des ρ Mesons. Experimente der NA45/CERES Kolloboration [3, 4, 129, 76] und der HELIOS Kolloboration [92] scheinen darauf hinzudeuten, daß bei endlichen Temperaturen und Dichten mehr Dileptonenpaare bei kleineren invarianten Massen erzeugt werden, was auf eine Verschiebung von spektraler Stärke des ρ Mesons hindeutet. Um diese Interpretation zu untermauern, sind weitere Schwerionenexperimente an der GSI geplant. Komplementäre Information kann aus photon- oder pioninduzierten Reaktionen am Kern gewonnen werden, wie sie an der GSI und am JLAB in Vorbereitung sind. Photonukleare Experimente spielen auch eine gewichtige Rolle bei der Untersuchung von Baryon-Resonanzen in Kernmaterie. Aufsehen haben hier Messungen zur Photoabsorption erregt, die ein nahezu vollständiges Verschwinden resonanter Strukturen im Medium suggerieren [14, 15, 43]. Besonders ausgeprägt ist dies für die $D_{13}(1520)$ Resonanz. In welchem Ausmaße dieser Effekt auf einer Verbreiterung der $D_{13}(1520)$ beruht oder auf sonstige Modifikationen der Produktionsamplitude zurückzuführen ist, ist gegenwärtig noch nicht vollständig geklärt. Photon- und pioninduzierte Kernreaktionen haben maßgeblich zur Bestimmung der Eigenschaften der $P_{33}(1232)$ Resonanz in Kernmaterie beigetragen und man glaubt heute allgemein, daß diese eine Verbreiterung von etwa 80 MeV bei normaler Kerndichte erfährt [54, 99, 98]. Aufgrund seiner dominanten Kopplung an den η N-Kanal kann auch die $S_{11}(1535)$ in photonuklearen Experimenten gut studiert werden [133, 115]. Hier legen die Daten relativ geringe Mediummodifikationen nahe. Eine Analyse der Eigenschaften von Pionen [11] und η Mesonen [48] ist mit Hilfe von mesonischen Atomen möglich. So ist für das Pion eine leichte Erhöhung der Masse von etwa $20 - 30$ MeV bestimmt worden.

Wir wenden uns nun dem Zusammenhang zwischen der Änderung von Hadroneigenschaften und der Restaurierung der chiralen Symmetrie zu. Vernachlässigt man die (kleinen) Quarkmassen, so ist die Lagrangefunktion der QCD invariant unter chiralen Transformationen. Weil man heute allgemein davon ausgeht, daß QCD die fundamentale Theorie der starken Wechselwirkung ist, würde man erwarten, daß sich diese Symmetrie durch das Existieren von Teilchenmultipletts explizit manifestiert. Da eine chirale Transformation Teilchen entgegengesetzter Parität miteinander in Beziehung setzt, würde dies implizieren, daß sogenannte chirale Partner – Teilchen mit bis auf die Parität identischen Quantenzahlen – ähnliche Massen haben. Dies ist allerdings nicht der Fall: so ist zum Beipiel das ρ Meson mit einer Masse von $m_\rho = 770$ MeV etwa 500 MeV leichter als sein chiraler Partner, das a_1 Meson. Wenn eine Symmetrie der zugrundeliegenden Lagrangefunktion nicht vom Grundzustand der Theorie geteilt wird, so spricht man von der spontanen Brechung dieser Symmetrie und das Goldstone-Theorem sagt die Existenz von masselosen Goldstone-Bosonen vorraus. Im Falle der QCD identifiziert man die außergewöhnlich leichten Mesonen π, η und K mit diesen Goldstone-Bosonen. Ein weiteres Merkmal der sponanten Symmetriebrechung ist der endliche Wert des chiralen Kondensats $\langle \bar{\psi}\,\psi \rangle = -(240\text{MeV})^3$, welches bei einer ungebrochenen Realisierung der chiralen Symmetrie verschwinden sollte.

Relevanz für die In-Medium Physik erlangt die spontane Brechung der chiralen Symmetrie, da man erwartet, daß diese oberhalb einer kritischen Temperatur und Dichte nicht mehr gebrochen ist. Dies wird beispielsweise durch Modellrechnungen der Dichte- und Temperaturabhängigkeit des chiralen Kondensats nahegelegt [113]. Die Restaurierung der chiralen Symmetrie hat direkte Auswirkungen auf die Eigenschaften von Hadronen. Insbesondere sollten die Spektralfunktionen von chiralen Partnern – etwa ρ Meson und a_1 Meson – in der restaurierten Phase gleich sein. Dieses Argument alleine läßt jedoch keine quantitativen Rückschlüsse auf die genaue Form der Spektralfunktionen dieser Mesonen in Kernmaterie zu [60, 64]. Noch komplizierter ist die Situation für Baryon-Resonanzen, wo bereits die Identifikation von chiralen Partnern nicht eindeutig ist. Eine besondere Rolle spielen die Goldstone-Bosonen, deren Masse relativ klein bleiben muß, solange man sich noch in der gebrochen Phase befindet.

Bei zwei theoretischen Zugängen, "Brown-Rho scaling" [21] und QCD Summenregeln, wird versucht, eine Beziehung zwischen den Mediummodifikationen von Kondensaten – nicht nur des chiralen Kondensats – und hadronischen Massen zu etablieren. "Brown-Rho scaling" führt – basierend auf Argumenten über die Skaleninvarianz der QCD Lagrangefunktion – zu einer direkten Relation zwischen chiralem Kondensat und hadronischen Massen und sagt für alle Hadronen eine Absenkung der Masse von etwa 20% bei normaler Kerndichte vorraus. Obwohl von großem Einfluß auf die theoretische und experimentelle Suche nach Mediummodifikationen, wird das "Brown-Rho scaling" bis heute sehr kontrovers diskutiert. Die QCD Summenregeln benutzen eine Dispersionsrelation, um Quark- und Gluonkondensate mit einem Integral über hadronische Spektralfunktionen in Verbindung zu setzen [106, 120]. Sie sind bisher in erster Linie für Mesonen eingesetzt worden und sagen für das ρ Meson eine Absenkung an spektraler Stärke vorraus [62, 47]. Allerdings können sie keine Aussagen über die detaillierte Form der Spektralfunktion machen und sind daher insbesondere als Konsistenzcheck für hadronische Rechnungen nützlich [78].

Die bisherige Diskussion sollte verdeutlichen, daß eine modellunabhängige quantitative Bestimmung der Mediumeigenschaften von Hadronen nicht möglich ist. Wenn man also an einer detaillierten Beschreibung interessiert ist, muß man auf eine hadronische

Modellierung zurückgreifen. Medium-Modifikationen werden dann mittels einer komplexen Selbstenergie beschrieben, die bei kleinen Dichten über das Niedrig-Dichte Theorem [29] durch die Hadron-Nukleon Streuamplitude festgelegt ist. Um ein hadronisches Modell auch bei höheren Dichten anwenden zu können, ist es im allgemeinen notwendig, Korrekturen zur Niedrig-Dichte Näherung vorzunehmen und beispielsweise Effekte des Pauli-Prinzips oder von 3-Körperprozessen zu berücksichtigen. In welchem Ausmaße ein solchermaßen konstruiertes hadronisches Modell Effekte der Restaurierung der chiralen Symmetrie wiedegeben kann, ist eine offene Frage. Unstrittig ist allerdings, daß als Grundlage für weiterführende Diskussionen ein solides hadronisches Vielteilchenmodell entwickelt werden muß.

In dieser Arbeit wird ein solches hadronisches Modell vorgestellt. Zielsetzung ist die gleichzeitige Beschreibung von möglichst vielen Hadronen in Kernmaterie. Ein solcher Zugang erlaubt es, das Modell an den zahlreichen zuvor erwähnten Mediummodifikationen zu testen. Im Vergleich zu einem Modell, welches sich auf die Beschreibung von wenigen Teilchen beschränkt, beinhaltet ein solcher Zugang zwei Vorteile: Zum einen stellt man so sicher, daß die wichtigsten physikalischen Prozesse in den Rechnungen enthalten sind. Um ein konkretes Beipsiel zu geben, die Beschreibung der recht gut bekannten Eigenschaften der $P_{33}(1232)$ Resonanz in Kernmaterie erfordert die Einbeziehung von kurzreichweitigen Wechselwirkungen, die sich dann auch für die anderen Baryonresonanzen als wichtig erwiesen haben. Allerdings hätten wir die Notwendigkeit solcher Korrekturen nicht erkannt, wenn wir die $P_{33}(1232)$ nicht in unserem Modell beschrieben hätten. Ein weiterer Vorteil einer gekoppelten Analyse besteht darin, daß man sensitiv wird auf die Art und Weise, wie sich die Mediummodifikationen eines Hadrons auf die Eigenschaften der anderen Hadronen übertragen. Als Illustration dienen die In-Medium Eigenschaften von ρ Meson und $D_{13}(1520)$ Resonanz: Wir haben bereits erwähnt, daß die Dileptonenspektren eine Massenabsenkung des ρ Mesons suggerieren und Photoabsorptionsdaten eine Verbreiterung der $D_{13}(1520)$ Resonanz. Diese Phänomene können auf natürliche Art und Weise miteinander in Verbindung gebracht werden, wenn man eine Kopplung der $D_{13}(1520)$ an den $N\rho$ Kanal zuläßt. Aus Phasenraumargumenten folgt dann, daß eine Massenabsenkung des ρ Mesons automatisch eine Verbreiterung der $D_{13}(1520)$ nach sich zieht. Auch das optische Potential des η Mesons und die In-Mediumeigenschaften der $S_{11}(1535)$ Resonanz stehen direkt miteinander in Beziehung.

Unser Modell ist wie folgt aufgebaut. Die Selbstenergie der Mesonen wird bestimmt durch die Anregung von Teilchen-Loch Zuständen. Diese Mechanismen erzeugen ein kompliziertes mesonisches Spektrum mit zahlreichen Peakstrukturen. Im folgenden Schritt werden die so erzeugten Propagatoren der Mesonen zur Berechnung der Selbstenergie der Baryon-Resonanzen herrangezogen. Dies führt zu einem Selbstkonsistenzproblem, da nun die Selbstenergie der Mesonen von der Selbstenergie der Baryonen abhängt, welche wiederum implizit durch die mesonische Selbstenergie bestimmt ist. Dieses Selbstkonsistenzproblem wird iterativ gelöst. Effektiv werden durch die Iterationen Hadron-Nukleon Streuprozesse von höherer Ordnung in der Dichte erzeugt. Wir berücksichtigen die Mesonen π, η and ρ sowie alle Baryon-Resonanzen, welche an diese Mesonen koppeln. Explizite Resultate geben wir für alle Mesonen sowie die Resonanzen $P_{33}(1232)$, $D_{13}(1520)$ und $S_{11}(1535)$.

Die Wechselwirkung zwischen Nukleonen, Mesonen und Baryon-Resonanzen wird beschrieben durch Lagrangefunktionen, welche grundlegende Symmetrien wie Eichinvarianz und Paritätserhaltung respektieren. Der Imaginärteil der Selbstenergien von Mesonen und Resonanzen wird gemäß der von Cutkosky formulierten Regeln berechnet. Der Realteil

folgt dann aus Dispersionsrelationen. Durch dieses Vorgehen ist garantiert, daß die Spektralfunktionen normiert sind. Weiterhin berücksichtigen wir Effekte von kurzreichweitigen Termen in der Resonanz-Nukleon Wechselwirkung. Während diese für Resonanzen mit positiver Parität bereits wohl studiert sind, besteht ein neuer Aspekt dieser Arbeit in der konsistenten Formulierung solcher Wechselwirkungen für Resonanzen mit negativer Parität.

Wir diskutieren nun die Ergebnisse unserer Rechnungen. Für das ρ Meson finden wir starke Modifikationen durch seine Kopplung an den $D_{13}(1520)N^{-1}$ Zustand, welcher einen zusätzlichen Peak in der Spektralfunktion des ρ Mesons bei kleinen invarianten Massen verursacht. Dieser Peak ist am stärksten ausgeprägt bei kleinen Impulsen des ρ Mesons. Bei größeren Impulsen ist die relative Wichtigkeit der $D_{13}(1520)$ reduziert und die Kopplung an andere Resonanzen größerer Masse wird wichtiger. Als Resultat finden wir bei diesen Impulsen eine relativ stark verbreiterte Spektralfunktion für ein transversales ρ Meson. Ein longitudinales ρ Meson zeigt ein deutlich anderes Verhalten bei größeren Impulsen, hier ist die Modifikation nur sehr schwach ausgeprägt. Durch die Iterationen wird die Spektralfunktion bei kleinen Impulsen deutlich modifiziert, was auf die starke Verbreiterung der $D_{13}(1520)$ zurückzuführen ist. Wir haben geprüft, inwiefern die Ergebnisse sensitiv sind im Hinblick auf kurzreichweitige Wechselwirkungen und Unsicherheiten in den Kopplungskonstanten. In beiden Fällen finden wir nur recht geringe Korrekturen. Eine Berechnung der Dileptonenrate legt nahe, daß unser Modell zumindest qualitativ die beoachtete Verschiebung im Dileptonenspektrum erklären kann.

Die Spektralfunktion des Pions wird dominiert duch die Kopplung an Nukleonen und das $P_{33}(1232)$. Dies führt im Bereich mittlerer Impulse zwischen $0.3 - 0.6$ GeV zu einer Ausprägung von drei Peaks, während bei kleineren und grösseren Impulsen der Einfluß der Teilchen-Lochanregungen nicht so groß ist. Weder die Einbeziehung weiterer Resonanzen noch die Iterationen beeinflussen die Ergebnisse maßgeblich. Das η Meson wird durch seine Kopplung an das $S_{11}(1535)$ dominiert. Dies führt bei kleinen Impulsen zu einer attraktiven Wechselwirkung, während bei größeren Impulsen die Wechselwirkung repulsiv wird. Das optische Potential des η Mesons zeigt in unserem Modell einen relativ großen attraktiven Realteil, während der Imaginärteil recht klein ist. Dies läßt darauf hoffen, daß η-mesische Atome experimentell erzeugt werden könnten.

Die In-Medium Eigenschaften des $P_{33}(1232)$ werden von unserem Modell zufriedenstellend wiedergegeben und wir sind zuversichtlich, daß die wesentlichen physikalischen Mechanismen in unserem Modell berücksichtigt werden. Für die $D_{13}(1520)$ Resonanz finden wir durch ihre Kopplung an den ρN Kanal eine sehr starke Verbreiterung. Im Gegensatz zum ρ Meson sind hier die Unsicherheiten in der Kopplungskonstanten und Effekte von kurzreichweitigen Wechselwirkungen sehr wichtig für die quantitativen Ergebnisse. Während durch den ρN Kanal eine Verbreiterung von bis zu 250 MeV generiert wird, sind die Effekte durch den πN Kanal relativ klein. Auch hier spielen kurzreichweitige Korrelationen eine gewisse Rolle, insbesondere aber sind die Ergebnisse sensitiv auf die Wahl des Formfaktors. Auf der anderen Seite sind die Modifikationen der $S_{11}(1535)$ Resonanz nur sehr klein. Die Kopplung an πN und ηN spielt so gut wie keine Rolle. Nur der ρN Kanal führt zu einer kleinen Verbreiterung, die hauptsächlich auf die Kopplung an die $D_{13}(1520)$ zurückzuführen ist. Bei kleinen Impulsen führt das Pauli-Prinzip zu einer merklichen Reduktion der totalen Breite, was einen gewissen Einfluß auf die optische Potential des η Mesons hat.

Wir haben weiterhin einige allgemeine Aspekte unseres Modells untersucht. So haben wir ausführlich diskutiert, daß relativistische Korrekturen zur nichtrelativistischen Reduk-

tion nur geringfügige Änderungen für die Selbstenergie des ρ Mesons hervorrufen, solange die nichtrelativistische Reduktion konsistent durchgeführt wird. Dieses Resultat übertragt sich direkt auf die übrigen betrachteten Mesonen und Baryon-Resonanzen. Wir haben außerdem die Gültigkeit der Niedrig-Dichte Näherung untersucht. Hier verliert diese Näherung für das $D_{13}(1520)$ ihre Gültigkeit schon bei Dichten $\approx 0.4\,\rho_0$. Auch für die Mesonen π und ρ ist die Niedrig-Dichte Näherung nur begrenzt anwendbar. Für Systeme, die durch schwächere Kopplungen charakterisiert sind – wie z. B. η Meson und $S_{11}(1535)$ –, hat sie jedoch einen größeren Gültigkeitsbereich. Die Anwendung von Dispersionsrelationen zur Erzeugung von normierten Spektralfunktionen ist zwar prinzipiell wichtig, führt aber in den meisten Fällen nur zu relativ geringen Modifikationen der Ergebnisse. Am stärksten ausgeprägt ist der Einfluß auf die Selbstenergien der Baryon-Resonanzen im Vakuum.

Wir haben weiterhin den Einfluß von Mean-Field Potentialen auf unsere Ergebnisse studiert. Die gefundenen Effekte sind relativ groß, was sich auf die großen skalaren Potentiale zurückführen läßt. Diese führen zu einer substantiellen Reduktion der Normierung der Spinoren von Nukleonen und Resonanzen und folglich sind die gefundenen Verbreiterungen der Resonanzen deutlich kleiner. Allerdings ist diese Analyse mit erheblichen Unsicherheiten die Größe der Mean-Field Potentiale für die Baryon-Resonanzen betreffend behaftet, so daß man keine definitiven Schlußfolgerungen treffen kann.

Etwas losgelöst von dem bis jetzt diskutieren Modell haben wir die In-Mediumeigenschaften des ω Mesons im Rahmen eines Resonanzmodells studiert. Da experimentelle Information über die Kopplung des ω Mesons an Resonanzen relativ rar ist, haben wir im Rahmen einer Vektormesondominanz-Analyse diese Kopplung aus den relativ gut bekannten elektromagnetischen Helizitätsamplituden extrahiert. Die resultierenden Kopplungskonstanten sind relativ klein, so daß sich keine Peakstrukturen ausbilden können. Insgesamt finden wir eine leichte Verschiebung des ω Mesons hin zu größeren invarianten Massen, kombiniert mit einer Verbreiterung von etwa 40 MeV.

Danksagung

An dieser Stelle möchte ich all denen meinen Dank aussprechen, die mit Rat und Tat zum Gelingen dieser Arbeit beigetragen haben.

An erster Stelle ist Prof. Dr. Ulrich Mosel zu nennen. Mit vielen kritischen Fragen und Anregungen hat er den Fortgang der Arbeit maßgeblich mitbestimmt, mir aber gleichzeitig viele Freiräume für eigene Ideen eingeräumt. Seiner wohlwollenden Förderung verdanke ich außerdem die Teilnahme an zahlreichen Konferenzn und Workshops sowie einen 4-wöchigen Aufenthalt am Lawrence Berkeley National Laboratory in Berkeley, California.

Ein besonderes Dankeschön geht an Dr. Stefan Leupold, von dem ich in unzähligen Diskussionen sehr viel von dem lernen konnte, was in diese Arbeit eingeflossen ist. Er stand während all der Jahre unserer Zusammenarbeit stets Rede und Antwort auf all meine möglichen und unmöglichen Fragen und Ideen. Ebenfalls genossen habe ich zahlreiche Diskussionen mit Dr. Alexei Larionov, Prof. Dr. Carsten Greiner und Prof. Dr. Horst Lenske.

I had the pleasure of sharing my office with various people. Here I would like to single out the last two of them, Dr. Gregor Penner and Dr. Luis Alvarez Ruso. With both of them I enjoyed many fruiful and stimulating disucssions about physics and – just as importantly – countless exchanges on more worldly affairs.

Dr. Jürgen Lehr, Gunnar Martens und Thomas Falter waren (fast) immer leicht davon zu überzeugen, Papier und Bleistift zugunsten einer ausgiebigen Analyse solch wichtiger Themen wie den aktuellen Spiegel-Online Headlines beiseite zu legen. Insbesondere im heißen Sommer des Jahres 2003 hat dies maßgeblich zu meiner Abkühlung beigetragen. Mit Jürgen hatte ich darüber hinausgehend auch zahlreiche weniger profane Diskussionen über das "low density limit and beyond".

Sämtlichen Mitgliedern der Computer-Crew, mit denen ich zeitlichen Überlapp hatte, gilt mein Dank für Aufrechterhaltung und Ausbau eines funktionsfähigen Computersystems. Ausdrücklich hervorheben möchte ich Frank Frömel für seine prompte, freundliche und äußerst kompetente Hilfestellung bei etlichen nichtigen und manchmal auch weniger nichtigen Problemen.

All den anderen hier nicht namentlich erwähnten Mitgliedern des Instituts danke ich für die Aufrechterhaltung eines rauhen, aber herzlichen Institutsklimas.

Elke Jung und Christiane Pausch standen mir bei der Bearbeitung von Reiseanträgen, Leihscheinen und ähnlichen bürokratischen Ärgernissen stets hilfreich zur Seite, wofür ich mich ausdrücklich bei Ihnen bedanken möchte.

Meinen Eltern möchte ich nicht nur für ihre große Spendierfreudigkeit während meines gesamten Studiums danken, sondern auch für viele aufmunternde und manchmal kritische Bemerkungen auf dem langen Weg ins Ziel.

A special thankyou is reserved for my wife Michelle for providing a completely different and very enjoyable counterpoint to my daily struggles at the institute. Her moral support – in particular at the last stage of completing this work – made many things a whole lot easier for me.